TARGETING DNA REPAIR AND THE DNA DAMAGE RESPONSE: BEYOND THE STANDARD PI3 KINASE-LIKE KINASES

EDITED BY: John J. Turchi, Michael Weinfeld, Katherine Pawelczak and Peter McHugh

PUBLISHED IN: Frontiers in Oncology

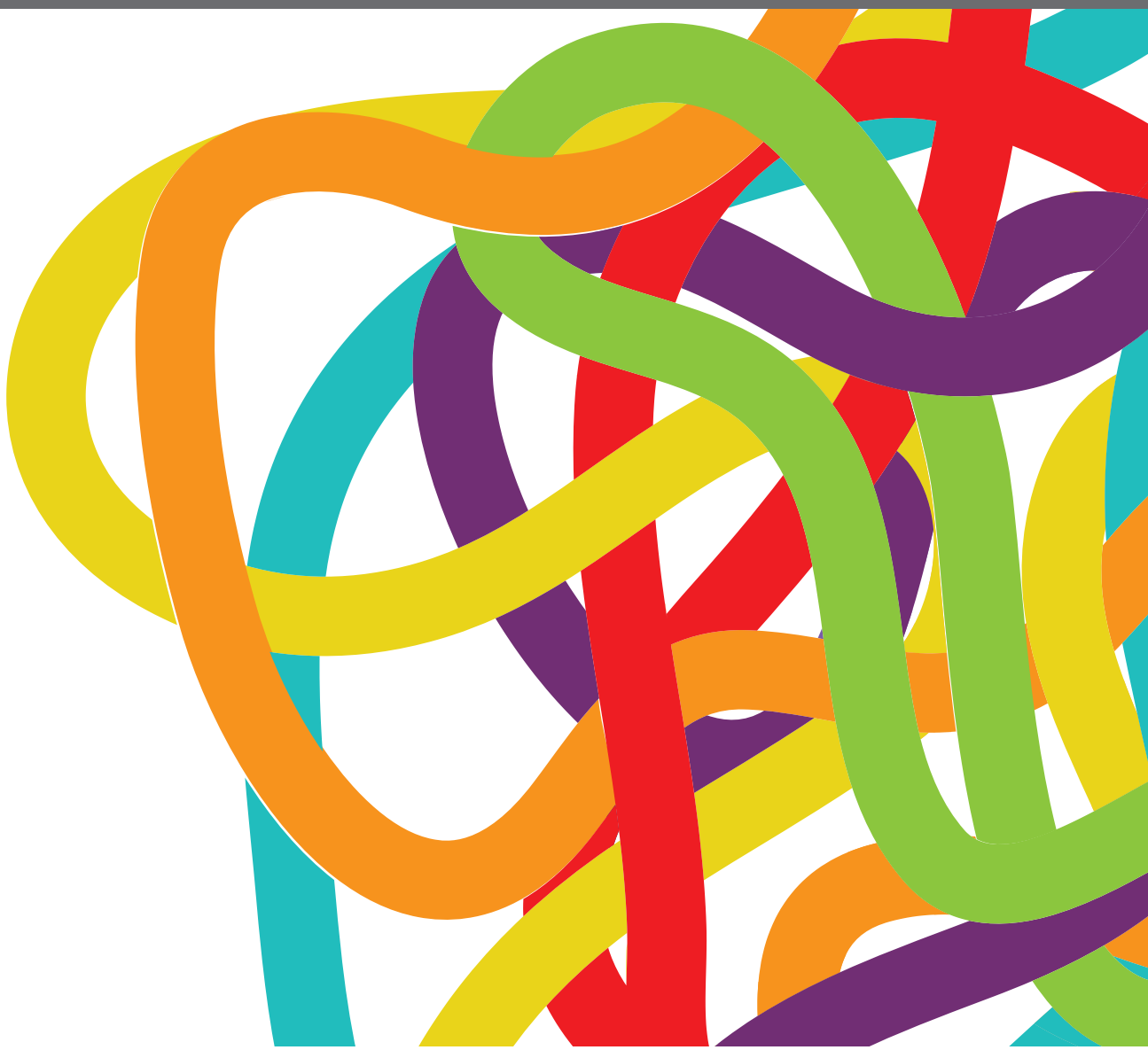

frontiers Research Topics

ISSN 1664-8714
ISBN 978-2-83250-464-2
DOI 10.3389/978-2-83250-464-2

About Frontiers

Frontiers is more than just an open-access publisher of scholarly articles: it is a pioneering approach to the world of academia, radically improving the way scholarly research is managed. The grand vision of Frontiers is a world where all people have an equal opportunity to seek, share and generate knowledge. Frontiers provides immediate and permanent online open access to all its publications, but this alone is not enough to realize our grand goals.

Frontiers Journal Series

The Frontiers Journal Series is a multi-tier and interdisciplinary set of open-access, online journals, promising a paradigm shift from the current review, selection and dissemination processes in academic publishing. All Frontiers journals are driven by researchers for researchers; therefore, they constitute a service to the scholarly community. At the same time, the Frontiers Journal Series operates on a revolutionary invention, the tiered publishing system, initially addressing specific communities of scholars, and gradually climbing up to broader public understanding, thus serving the interests of the lay society, too.

Dedication to Quality

Each Frontiers article is a landmark of the highest quality, thanks to genuinely collaborative interactions between authors and review editors, who include some of the world's best academicians. Research must be certified by peers before entering a stream of knowledge that may eventually reach the public - and shape society; therefore, Frontiers only applies the most rigorous and unbiased reviews.
Frontiers revolutionizes research publishing by freely delivering the most outstanding research, evaluated with no bias from both the academic and social point of view. By applying the most advanced information technologies, Frontiers is catapulting scholarly publishing into a new generation.

What are Frontiers Research Topics?

Frontiers Research Topics are very popular trademarks of the Frontiers Journals Series: they are collections of at least ten articles, all centered on a particular subject. With their unique mix of varied contributions from Original Research to Review Articles, Frontiers Research Topics unify the most influential researchers, the latest key findings and historical advances in a hot research area! Find out more on how to host your own Frontiers Research Topic or contribute to one as an author by contacting the Frontiers Editorial Office: frontiersin.org/about/contact

TARGETING DNA REPAIR AND THE DNA DAMAGE RESPONSE: BEYOND THE STANDARD PI3 KINASE-LIKE KINASES

Topic Editors:
John J. Turchi, Indiana University Bloomington, United States
Michael Weinfeld, University of Alberta, Canada
Katherine Pawelczak, NERx Biosciences, United States
Peter McHugh, University of Oxford, United Kingdom

Citation: Turchi, J. J., Weinfeld, M., Pawelczak, K., McHugh, P., eds. (2022). Targeting DNA Repair and the DNA Damage Response: Beyond the Standard PI3 Kinase-like Kinases. Lausanne: Frontiers Media SA.
doi: 10.3389/978-2-83250-464-2

Table of Contents

frontiers | Frontiers in Oncology

TYPE Editorial
PUBLISHED 27 September 2022
DOI 10.3389/fonc.2022.1023500

OPEN ACCESS

EDITED AND REVIEWED BY
Massimo Broggini,
Mario Negri Pharmacological Research Institute (IRCCS), Italy

*CORRESPONDENCE
John J. Turchi
jturchi@iu.edu

SPECIALTY SECTION
This article was submitted to Cancer Molecular Targets and Therapeutics, a section of the journal Frontiers in Oncology

RECEIVED 19 August 2022
ACCEPTED 13 September 2022
PUBLISHED 27 September 2022

CITATION
Turchi JJ, Pawelczak KS, Weinfeld M and McHugh PJ (2022) Editorial: Targeting DNA repair and the DNA damage response: Beyond the standard PI3 kinase-like kinases. *Front. Oncol.* 12:1023500. doi: 10.3389/fonc.2022.1023500

Editorial: Targeting DNA repair and the DNA damage response: Beyond the standard PI3 kinase-like kinases

John J. Turchi[1]*, Katherine S. Pawelczak[2], Michael Weinfeld[3] and Peter J. McHugh[4]

[1]Department of Medicine, Indiana University School of Medicine, Indianapolis, IN, United States, [2]NERx Biosciences, Indianapolis, IN, United States, [3]Department of Oncology, Cross Cancer Institute, University of Alberta, Edmonton, AB, Canada, [4]Department of Oncology, MRC Weatherall Institute of Molecular Medicine, University of Oxford, Oxford, United Kingdom

KEYWORDS

DNA damage response (DDR), cancer therapy, small molecule inhibitor, DNA repair, synthetic lethality, drug discovery

Editorial on the Research Topic

Targeting DNA repair and the DNA damage response: Beyond the standard PI3 kinase-like kinases

Targeting DNA repair pathways and the DNA damage response (DDR) for cancer therapy has gained increased attention since the advent of PARP inhibitors and the demonstration of their clinical utility in BRCA-deficient cancers (1). In the subsequent 15 years, a major focus has been on development of kinase inhibitors targeting the PI3 kinase-related kinases (PIKKs) DNA-PK, ATM and ATR, to target genome stability and DNA replication stress inherent to many cancers, and there are excellent reviews of these efforts (2). In this collection we move beyond the standard PIKKS and present a series of primary research articles and focused reviews on non-PIKK targets and pathways within the DDR and DNA repair space. These represent the future of novel agents and targets and hold considerable potential to not only delineate mechanisms of basic molecular processes in DDR and repair but also as potential targets and therapeutics for the treatment of cancer. Figure 1 highlights the breadth of targets and below we provide a brief summary of the review articles and primary research papers that make up this collection.

The review by Kelm et al. notes a variety of reasons for targeting proteins beyond the PIKKs: (i) their potential involvement in the repair of mitochondrial DNA as well as nuclear DNA; (ii) their role in protecting telomeres; (iii) the potential to expand the range of clinically beneficial synthetic lethal relationships; and (iv) the stimulation of the innate immune response when DNA repair is inhibited. The small molecule inhibitors detailed within this review target proteins in each of the four double strand break (DSB) repair pathways including Ku70/80, Artemis, DNA Ligase IV, PNKP, MRN complex, RPA,

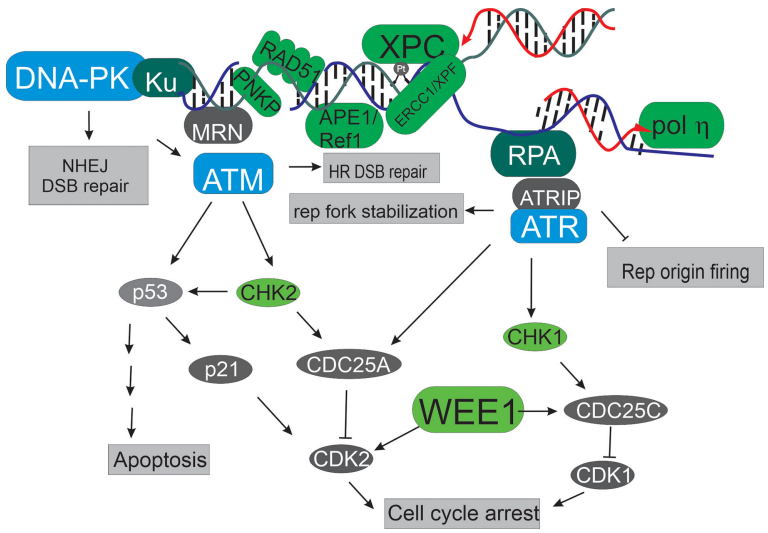

FIGURE 1
Targets in the DNA damage response and DNA repair pathways. The PIKKs, depicted in blue occupy central roles in the DDR. Beyond these targets, additional kinases are viable and interesting including Wee1, and the checkpoint kinases CHK1 and 2 (depicted in light green). Upstream of all these events are a series of proteins that often interact with DNA to fulfill their roles in the DDR and DNA repair (depicted in dark green). These include MRN, ERCC1/XPF, RPA and Ku that sense different DNA structures. Other potential targets include those that detect altered chemistry like APE1, and XPC (depicted in light green). A number of viable targets are involved in specific DNA metabolic events including Metnase, pol η, and Rad51.

RAD51, RAD52, ERCC1-XPF, helicases, and DNA polymerase θ. For most of the compounds described, inhibition is based on either direct inhibition of enzymatic activity or disruption of protein-DNA or protein-protein interactions. While most of the inhibitors have IC_{50} values in the micromolar range, and therefore require further development, a few, such as the arylpyrazolone carboxylic acid-based Ku inhibitors (based on DNA-PK kinase activity) and the DNA polymerase θ inhibitor ART558, have IC50 values in the low nanomolar range. ART4215 (an undisclosed) derivative of ART558 is now undergoing Phase 1/2 clinical trials as a monotherapy or in combination with the PARP inhibitor talazoparib in patients with advanced or metastatic solid tumors, exhibiting the high potential benefit for such agents in a clinical setting.

Targeting DNA binding proteins

Small molecule inhibitors of the RAD51 protein were initially described over a decade ago (3) and while useful tool compounds for research in some cases, translation to the clinic has been limited to compounds that target the Rad51 pathway through an unknown mechanism. In this collection, Gu et al. describe a novel class of compounds targeting Rad51 and present evidence for a direct Rad51 interaction and modulation of the cellular homologous recombination (HR) pathway. Intriguing evidence of single agent anticancer activity and in combinations in cell culture models will ultimately need to be verified *in vivo* to enable translation to the clinic.

Upstream of Rad51 in HR and ATR in the DDR lies Replication protein A (RPA), a trimeric factor that binds single-stranded DNA with high affinity, protecting these regions from nucleolytic degradation during DNA replication, repair and recombination, but also simultaneously controlling these processes through specific interactions with the actors involved. Interfering with the role of RPA in ssDNA protection has, therefore, the potential to perturb the DDR and leave ssDNA vulnerable to lethal degradation; consistently prior genetic studies imply that RPA 'exhaustion' can be lethal in cancer cells. VanderVere-Carozza et al. have previously developed a series of molecules that block RPA association with ssDNA (RPAi). In the current issue, they explore the selectivity of these compounds, demonstrate cellular toxicity across a range of cancer cells lines and show that stressed replication forks undergo degradation in the presence of RPAi. Moreover, RPAi synergy with therapeutically relevant DNA damaging agents are reported, as are antitumor effects in mouse xenograft models.

Metnase, whose name reflects a dual role as a methyltransferase and nuclease, is a factor produced through gene fusion and only found in primates. As reviewed by Nickoloff et al. Metnase plays a role in multiple DNA transactions, including in DSB repair processes, promoting NHEJ, where both the methyltransferase and nuclease domains

contribute to its activity. Roles for Metnase in combating tumor replicative stress and a role mediating resistance to Topoisomerase II poisons also argue for the development of Metnase inhibitors. Nickoloff et al. also discuss the potential of EEPD1 structure-selective endonuclease inhibition in cancer. This factor plays a role in processing damaged replication forks and in promoting HR, and a case can be made for EEPD1 inhibition to target tumor vulnerabilities in the DDR and inherent replication stress, as well as a strategy for enhancing tumor chemosensitivity.

Targeting kinases outside the PIKK family

Continuing with the theme of non-PIKK related targets, Bukhari et al. review the state-of-the-art in Wee1 inhibition. Wee1 is a tyrosine kinase originally identified by virtue of its key role in regulating the timing of *S. pombe* cell entry into mitosis, by phosphorylating and restraining the activity of CDK1. The role of Wee1 extends to the G2/M DNA damage checkpoint, and because many cancer cells harbor defects in the G1 checkpoint they become highly dependent upon the G2/M checkpoint – when the G2/M checkpoint is perturbed in such cells they will often enter a (terminal) mitotic catastrophe. Targeting Wee1 is also a potentially attractive therapeutic strategy due to emerging evidence regarding synthetic lethal interactions with DNA damage response regulators and because of potential synergies with radio- and chemotherapeutics. Bukhari et al. also describe the dozens of Wee1 inhibitor clinical trials performed to date, which suggest some promising results.

The checkpoint kinases have also been the subject of intense study with a number of inhibitors discovered over the years. Vaughan et al. in a primary research article identified the DDR and specifically Chk1 and 2 proteins as vulnerabilities in TCS-2 mutant renal cancers. This work highlights the complexity of pathway crosstalk and utility of chemical biology screening to elucidate previously unknown interactions. Impressive *in vivo* data are presented that demonstrate that abrogation of Chk1/2 activity with the dual AZD inhibitors results in prolonged tumor stasis and a reduction of cysts common in mTOR-driven disease. The question of whether specific Chk1 or Chk2 inhibitors recapitulate the results with the dual inhibitor remains but offer intriguing possibilities for these complex diseases.

Polynucleotide kinase/phosphatase (PNKP) is another very interesting kinase target but is responsible for phosphorylating DNA 5'-termini as opposed to proteins. This kinase activity along with intrinsic DNA 3'-phosphatase activity of PNKP is critical in the repair of DNA strand breaks to prepare DNA termini for ligation. This is especially important in the context of IR- induced DNA damage, where chemical modification of both bases and sugars often give rise to termini that are unable to be ligated. In this collection Sadat et al. describe a novel polysubstituted imidopiperidine PNKP 3'-phosphatase inhibitor encapsulated in a novel nano-particle formulation. Extensive analyses presented indicate excellent pharmacokinetics, biodistribution and *in vivo* efficacy. The *in vivo* experiments conducted in a colorectal tumor xenograft model demonstrate convincing radiosensitization and effective tumor reduction in the nano-particle formulation compared to the free-soluble drug, an effect that was demonstrated to be a function of enhanced bio-distribution and tumor uptake. Together these data position PNKP as a viable druggable target that is poised for further translation to clinical utility in treating cancer.

Novel targets within the NER and BER pathways

Moving beyond DSB repair and kinases to nucleotide excision repair (NER) and base excision repair (BER) and crosslink repair, the manuscript by Weilbeer et al. presents additional *in silico* screening of a previously reported ERCC1-XPF inhibitor that focused on modifications of a specific side chain, resulting in a substantial increase in potency. The structure selective endonuclease ERCC1-XPF plays a role in repairing damage induced by crosslinking agents like platinum-based chemotherapies and ionizing radiation, and inhibition of its biological activity has the potential to potently sensitize cells to DNA damaging based therapies. The compounds discovered disrupt the protein-protein interaction required for heterodimerization, presenting an innovative mechanism of action for inhibition of ERCC1-XPF endonuclease activity. A lead hit was further evaluated and shown to sensitize cells to UV irradiation, cyclophosphamide crosslinking and ionizing radiation, further suggesting the potential for therapeutic applications with this family of novel inhibitors.

Nasrallah et al. examine the role that XPC may play in hematologic and non-dermatologic solid tumors. They point out that in addition to its canonical participation in the NER pathway, data strongly indicate XPC's involvement in the BER, double strand break repair and interstrand crosslink repair pathways, possibly serving as a global DNA damage sensor. The authors go on to discuss the evidence associating XPC mutations, single-nucleotide polymorphisms and epigenetic alterations with elevated risk of malignancies as well as clinical response to chemotherapy. Based on these observations the authors recommend further investigation of XPC's potential as a prognostic and/or predictive biomarker.

Continuing the BER theme, Mijit et al. investigated the influence of RelA (nuclear factor NF-κB p65 subunit) on the response of Kras-mutated pancreatic ductal adenocarcinoma (PDAC) cells to inhibitors of the redox function of Ref-1 (also known as the DNA repair endonuclease, APE1). While the BER activity of APE1 is targetable, the redox function has been shown

to be important for cancer survival. They observed that RelA deficiency rendered the PDAC cells more resistant to the Ref-1 inhibitors. Furthermore, Ref-1 inhibition led to a marked reduction in IL-8, FOSB, and c-Jun, but this required the presence of active RelA. Their data indicate a critical role for RelA in redox homeostasis of Kras-mutated PDAC cells with implications for therapy targeting PDAC drug resistance.

Targeting DNA damage tolerance pathways

While repair of DNA damage has garnered considerable attention, tolerance of damage remains an important component of how cells respond and cope with genetic abnormalities. Ler and Carty present a comprehensive review of DNA damage tolerance and the implication for carcinogenesis and opportunities for impinging on this pathway to treat cancer. The two main tolerance pathways discussed include translesion synthesis catalyzed by the by-pass polymerases and homology directed tolerance. The discussion of pathway choice offers unique insights into how cells coordinate the response to damage in relation to tolerance. Existing small molecule inhibitors of translesion polymerases are also reviewed and highlight the opportunities to disrupt this pathway to subvert cancer growth and resistance.

Drug development work targeting DNA repair associated polymerases is a rapidly growing field, and POLH represents a novel target within this family that has clinical promise due to its intriguing biological role in translesion synthesis that result in cellular resistance to damage from agents such as UV light and cisplatin. The work described by Wilson et al. presents a fragment-based drug development (FBDD) approach that utilizes a crystallization screen, resulting in novel x-ray crystal structures of small drug-like compounds bound to POLH. This emerging methodology and subsequent structural data have the potential to drive the rapid discovery and development of novel drug-like molecules, and may be particularly useful in developing drugs targeting complex enzymes like those in the polymerase families.

Clearly, the DDR space remains incredibly active in both discovery, preclinical and clinical development, with over 35 ongoing clinical trials spanning a variety of agents and targets. Importantly, there is an expanding wealth of knowledge regarding novel targets, therapeutic combinations and genetic alterations that are ripe for exploitation to impact the treatment of cancer with DDR targeted therapies. The long and circuitous route to clinical success of PARP inhibitors has provided a solid framework by which to pursue and evaluate the current and future DDR targeted agents, not least in the appropriate design of clinical trials. These experiences should remind us to not lose site of the underlying biology nor be swept up by the latest wave of success. The clinical reality is that the majority of those diagnosed with cancer will succumb to the disease. Only by pursuing the discovery and development of novel therapeutic strategies and targets can we expand the armamentarium to better equip our medical oncologist colleagues to impact the lives of cancer patients.

Author contributions

JT, KP, MW and PM participated in the preparation of the initial manuscript draft and the final product. All authors contributed to the article and approved the submitted version.

Funding

This work was supported by Cancer Research UK Program Award A24759 and MRC grant MR/X000192/1 to PM and NIH awards R01CA257430 and R01CA247370 to JT.

Conflict of interest

Author KP was employed by NERx Biosciences.

The remaining authors declare that the research was conducted in the absence of any commercial or financial relationships that could be construed as a potential conflict of interest.

Publisher's note

References

1. Mateo J, Lord CJ, Serra V, Tutt A, Balmana J, Castroviejo-Bermejo M, et al. A decade of clinical development of PARP inhibitors in perspective. *Ann Oncol* (2019) 30:1437–47. doi: 10.1093/annonc/mdz192

2. Cheng B, Pan W, Xing Y, Xiao Y, Chen J, Xu Z. Recent advances in DDR (DNA damage response) inhibitors for cancer therapy. *Eur J Med Chem* (2022) 230:114109. doi: 10.1016/j.ejmech.2022.114109

3. Demeyer A, Benhelli-Mokrani H, Chenais B, Weigel P, Fleury F. Inhibiting homologous recombination by targeting RAD51 protein. *Biochim Biophys Acta Rev Cancer* (2021) 1876:188597. doi: 10.1016/j.bbcan.2021.188597

frontiers in Oncology

ORIGINAL RESEARCH
published: 20 September 2021
doi: 10.3389/fonc.2021.733700

Targeting DNA Homologous Repair Proficiency With Concomitant Topoisomerase II and c-Abl Inhibition

*Arafat Siddiqui[1], Manuela Tumiati[2], Alia Joko[3], Jouko Sandholm[4], Pia Roering[1], Sofia Aakko[1], Reetta Vainionpää[5], Katja Kaipio[1], Kaisa Huhtinen[1], Liisa Kauppi[2], Johanna Tuomela[1] and Sakari Hietanen[6]**

[1] Institute of Biomedicine, University of Turku, Turku, Finland, [2] ONCOSYS, Research Programs Unit, University of Helsinki, Helsinki, Finland, [3] Department of Biology, Åbo Akademi University, Turku, Finland, [4] Turku Bioscience Centre, University of Turku and Åbo Akademi University, Turku, Finland, [5] Laboratory of Genetics, HUS Diagnostic Center, Helsinki University Hospital, Helsinki, Finland, [6] Turku University Hospital, FICAN West Cancer Centre, Turku, Finland

OPEN ACCESS

Edited by:
John Turchi,
Indiana University Bloomington, United States

Reviewed by:
Pamela L. Mendoza-Munoz, Indiana University, Purdue University Indianapolis, United States
Lindsey Mayo, Purdue University Indianapolis, United States

***Correspondence:**
Sakari Hietanen
sakari.hietanen@utu.fi

Specialty section:
This article was submitted to Cancer Molecular Targets and Therapeutics, a section of the journal Frontiers in Oncology

Received: 30 June 2021
Accepted: 27 August 2021
Published: 20 September 2021

Citation:
Siddiqui A, Tumiati M, Joko A, Sandholm J, Roering P, Aakko S, Vainionpää R, Kaipio K, Huhtinen K, Kauppi L, Tuomela J and Hietanen S (2021) Targeting DNA Homologous Repair Proficiency With Concomitant Topoisomerase II and c-Abl Inhibition. Front. Oncol. 11:733700. doi: 10.3389/fonc.2021.733700

Critical DNA repair pathways become deranged during cancer development. This vulnerability may be exploited with DNA-targeting chemotherapy. Topoisomerase II inhibitors induce double-strand breaks which, if not repaired, are detrimental to the cell. This repair process requires high-fidelity functional homologous recombination (HR) or error-prone non-homologous end joining (NHEJ). If either of these pathways is defective, a compensatory pathway may rescue the cells and induce treatment resistance. Consistently, HR proficiency, either inherent or acquired during the course of the disease, enables tumor cells competent to repair the DNA damage, which is a major problem for chemotherapy in general. In this context, c-Abl is a protein tyrosine kinase that is involved in DNA damage-induced stress. We used a low-dose topoisomerase II inhibitor mitoxantrone to induce DNA damage which caused a transient cell cycle delay but allowed eventual passage through this checkpoint in most cells. We show that the percentage of HR and NHEJ efficient HeLa cells decreased more than 50% by combining c-Abl inhibitor imatinib with mitoxantrone. This inhibition of DNA repair caused more than 87% of cells in G2/M arrest and a significant increase in apoptosis. To validate the effect of the combination treatment, we tested it on commercial and patient-derived cell lines in high-grade serous ovarian cancer (HGSOC), where chemotherapy resistance correlates with HR proficiency and is a major clinical problem. Results obtained with HR-proficient and deficient HGSOC cell lines show a 50–85% increase of sensitivity by the combination treatment. Our data raise the possibility of successful targeting of treatment-resistant HR-proficient cancers.

Keywords: DNA repair, cell cycle arrest, c-Abl, imatinib, mitoxantrone

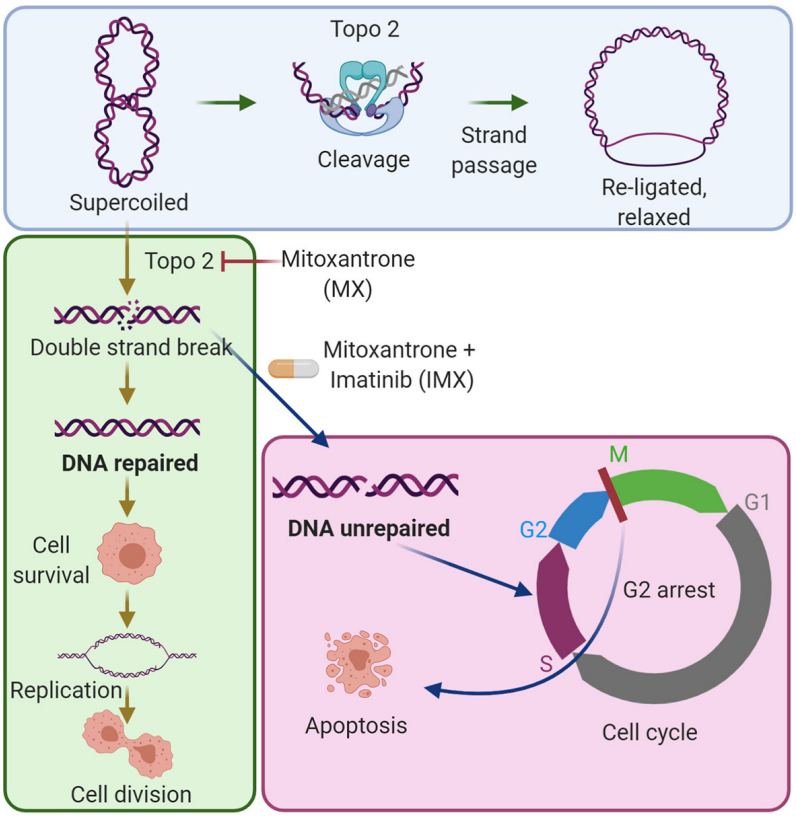

GRAPHICAL ABSTRACT | The combination of imatinib with low-dose mitoxantrone inhibits DNA repair in cancer cells. The blue area shows the established mechanism of the type II topoisomerase (Topo 2) enzyme in DNA synthesis. The green area shows that low-dose mitoxantrone inhibits Topo 2 and causes DNA double-strand breaks, which can be repaired by cancer cells, and by this, the cells can survive the damage. The magenta area shows that the combination of imatinib with mitoxantrone prevents DNA repair, causes G2/M cell cycle arrest, and induces apoptosis.

INTRODUCTION

DNA damage repair (DDR) plays a critical role in the maintenance of genomic stability. An appropriate response to genotoxic drugs is required for cancer cell survival. Targeting this response has become an active area of research in the field of developing new cancer therapies. DNA damage alerts surveillance networks that stall cell cycle, allowing time for DNA repair. High in the hierarchy of these pathways lie the activities of ATM and ATR, which belong to the phosphatidylinositol 3-kinase-related protein kinase family (1–3). DNA repair involves mainly six pathways, including mismatch repair, homologous recombination repair, non-homologous end joining, trans-lesion DNA synthesis, base excision repair, and nucleotide excision (4). The most common pathways to repair double-stranded breaks (DSBs) are non-homologous end joining (NHEJ) and homologous recombination (HR). NHEJ is error-prone and active throughout the cell cycle, whereas HR is a high-fidelity repair mechanism limited to the S and G2 phases of the cell cycle after genotoxic stress (5).

Induction of genotoxic stress response is one of the hallmarks of chemotherapy. However, resistance to genotoxic chemotherapies is a problem in HR-proficient (HRP) cancers. HRP cancers can repair the damage, resulting in treatment resistance (6). This is a very common case in high-grade serous ovarian cancer (HGSOC), which is the most lethal gynecological cancer and is mostly treated by surgery together with platinum-based therapy. However, HGSOC becomes resistant to platinum-based therapy and most patients relapse within 2 years (7). In contrast, HR-deficient (HRD) cancers are usually sensitive to treatment. Recent pivotal clinical studies have shown that Poly (ADP-ribose) polymerase (PARP) inhibitors have dramatically improved in the prognosis of HRD cancers (8–10). However, HRD cancers can also regain partial HR function, making them resistant to these inhibitors (11, 12). This development closely correlates with HR-proficiency and makes HGSOC a difficult-to-treat disease. There is an unmet clinical need for treatment that can abrogate HR-proficiency.

Type II topoisomerases are essential for resolving DNA tangles and supercoils during replication. They cut both daughter strands while simultaneously passing another duplex

DNA through the break, and then rejoin the broken strands (8). Failure in strand separation leads to cell death, which is the mechanistic principle behind the use of topoisomerase II inhibitors as a chemotherapeutic. Topoisomerase II inhibitors have been successfully used in cancer therapy for over 30 years but they display considerable tissue toxicity. Mitoxantrone (MX) is a topoisomerase II inhibitor that leads to accumulation of DNA crosslinks as well as single- and double-strand breaks. In DNA damage repair by HR, the c-Abl proto-oncoprotein has a direct role, where it phosphorylates RAD51 at Tyr-315 (13). Once in the nucleus, the phosphorylated RAD51 co-localizes with BRCA1 at DSB sites. Activation of c-Abl at the G1-S transition ensures DNA repair capability when replication progresses into S phase (14, 15). It has been reported that c-Abl activity increases in three cases. First, c-Abl is activated in an ATM-dependent manner as response to DNA damage following genotoxic stress (16). Second, in chronic myeloid leukemia, c-Abl is constitutively active due to its fusion with breakpoint cluster region protein (BCR), promoting DNA repair (17, 18). Third, overexpression of wild type c-Abl may occur in solid tumors in non-stressed conditions, such as in aggressive types of breast cancer and non-small cell lung cancer (19).

Here, we show that combining low dose topoisomerase II inhibitor mitoxantrone with c-Abl inhibitor imatinib (IM) effectively impairs DNA repair in both HR-deficient and -proficient cells. We validated the findings in HGSOC cells, where HR proficiency is a key problem in both chemotherapy resistance and PARP inhibitor resistance.

MATERIALS AND METHODS

Cell Lines and Cytotoxic Drugs

HeLa cell line was used as a 2D cancer cell model for microarray analysis and DNA-repair assay. FUCCI-HeLa was used for functional validation of G2/M arrest. BRCA1-wt MDA-MB-231 and BRCA1-mutant HCC-1937 cell lines were used to perform other *in vitro* assays (**Supplementary Table S1**).

We used total 13 patient-derived and conventional HGSOC cell lines to validate cytotoxicity of MX *versus* IMX. Patient-derived cell lines include M022p, M022i, M048i, H002, and OC002. Commercial cell lines include COV318, CaOV3, OVCAR3, OVCAR4, OVCAR5, COV362, Kuramochi, and OVCAR8 (**Supplementary Tables S1, S2**). Patient-derived cell lines were developed from tissue and ascites specimen, which were collected from consented high-grade serous ovarian cancer (HGSOC) patients at Department of obstetrics & gynaecology, Turku University Hospital (TYKS) as described previously (20). Tissue samples and clinical information were collected from four patients diagnosed with stage III or IV as described earlier. Treatment-naïve ascites was collected during diagnostic laparoscopy (cell line OC002). Patients considered primarily inoperable received three cycles of neoadjuvant chemotherapy (NACT), and new samples were taken during interval debulking surgery (cell lines M022i, M048i, and H002i). Ascites samples (cell lines OC002, M022i, and H002i) were gradient centrifuged with Histopaque-1077 concentrate the cancer cells and plated. Omentum tumor sample (cell line M048i) was minced into approximately 1 mm^3 pieces and plated on six-well plates. The stromal and immune cells were grown out by passaging approximately five times. SBS3 is considered as strong predictor of defective HR-based repair (21). Functional HR-score was also performed for all cell lines (22). All cell lines were grown in either DMEM or RPMI-1640 with additional supplements under standard cell culture condition (**Supplementary Table S3**). DMSO (0.1%), mitoxantrone, and imatinib mesylate were used as treatments (**Supplementary Table S4**).

Microarray Analysis

Total RNA from triplicate treatments of 5 μM IM, 0.8 μM MX, or their combinations for 30 h was extracted using Trizol and further purified with RNeasy RNA isolation kit according to manufacturer's instructions (**Supplementary Table S4**). The quality of RNA was controlled before hybridization, and one low quality sample (MX) was excluded from the analysis. The analysis was done on an Illumina HumanRafSeq-8v2 chip containing 22184 transcripts. Quantile normalisation method was applied after hybridization to remove non-biological variation. Data similarity between replicates was confirmed with Pearson coefficient metrics and Principal Component Analysis. Treatment group comparisons were performed with R-language limma package.

Pathway Enrichment Analysis

Gene Set Enrichment Analysis (GSEA v. 4.0.3) ref) was performed using GOPB_AllPathways_no_GO_ie as reference gene set:

(http://download.baderlab.org/EM_Genesets/current_release/Human/symbol/)

A total of 1000 gene permutations (term size from 15 to 300) were used to generate a null distribution of enrichment score (ES), and then each pathway will attain normalization ES (NES). FDR Q-value (false discovery rate) <0.1 and p value < 0.01 were considered significant. Volcano plots of each full data set were generated with Galaxy server (23). The functional network was constructed with the GSEA data fed into Cytoscape v. 3.8.0, where both up- and downregulated pathways can be visualized simultaneously (24). Most significant pathway nodes were filtered with Diffusion plugin.

Cell Viability and IC_{50} Measurement

Cells (2500–5000 cells per well) were grown in 96-well plates for 24 h prior to drug treatment. IC_{50} values of MX with and without IM were determined using CCK-8 kit (**Supplementary Table S4**). The MX dose started from 4000 nM and was followed by 50% serial dilutions to lower doses until 0.0 nM of MX. In all groups, we used constant 5 μM IM. DMSO (0.1%) was used as a vehicle control. Relative absorbance at 450 nm was measured after 72 h treatment. The IC_{50} value was obtained by non-linear regression analysis using Graph Pad Prism 8.4.2 (GraphPad Software, San Diego, USA). Additional cell viability experiments were performed to confirm the IC_{50} values. Cells were treated with vehicle, IM, MX, and IM+MX (IMX) for 72 h followed by CCK8-

assay and optical density measurement, as described earlier. Based on these measurements, working drug concentrations were determined for individual cell lines, and these were used throughout the study, as follows: 34 nM MX and 5 μM IM for HeLa and FUCCI-HeLa, 103.5 nM MX and 5 μM IM for MDA-MB-231, and 9 nM MX and 5 μM IM for HCC-1937.

Live Cell Imaging

Vehicle or indicated concentrations of drugs were added to cells (2500–5000 cells per well in a 96-well plate). Cells were imaged at 5 min to 1 h intervals for 5–10 days using IncuCyte S3 imaging system (Essen Bioscience, Michigan, USA) with a 20x objective. IncuCyte 2019B Rev2 software (Essen BioScience Michigan, USA) was used to calculate mean confluences (three parallel wells per treatment) from phase contrast images. For FUCCI-HeLa cells, fluorescence channels were used. Representative wells were selected for time-lapse movies, which were built with ImageJ ver 1.47d (25).

Flow Cytometry

All flow cytometry experiments were performed on a BD LSRFortessa™ flow cytometer (BD Biosciences). Flowing Software 2.5.1 (Mr Perttu Terho, Turku Bioscience Centre, Turku, Finland) and FlowJo ver 10 (Tree Star Inc) were used for analysis.

Nuclear Fractionation for RAD51 Measurement

HeLa cells (200,000 cells per well were seeded on six-well plates and incubated overnight) were treated with 0.1% DMSO, 5 μM IM, 34 nM MX, and IMX for 24 h. Then, cells were subjected to nuclear fractionation followed by staining with rabbit α-RAD51 primary antibody and donkey anti-rabbit IgG-AlexaFluor 488 secondary antibody (**Supplementary Tables S4, S5**). Samples were analyzed by flow cytometry. In addition to nuclear fractions, whole cell samples were analyzed to validate the fractionation process where whole cell population had different position than nuclear population in FSC/SSC plot.

Cell Cycle Analysis With EdU and FUCCI-HeLa Cells

Assay kit was used to assess the treatment effect on cell cycle of HeLa, MDA-MB-231, and HCC-1937 cells. Cells (200,000) per well were seeded on six-well plates followed by overnight incubation. Cells were treated for 24–72 h with 0.1% DMSO, 5 μM IM, and individual doses of MX and IMX per cell lines. The samples were analyzed by flow cytometry.

FUCCI-HeLa cells were seeded at 20,000 per well in 24-well plates. After 24 h of treatment with vehicle, 5 μM IM, 34 nM MX, or 5 μM IM + 34 nM MX (IMX), cell pellets were collected and fixed with fixation buffer followed by flow cytometry analysis (**Supplementary Table S4**).

RNA Interference and Western Blot Analysis

FlexiTube siRNA BRCA1 (5 nmol) and 0.3 ml Lipofectamine were used to silence BRCA1 in MDA-MB-231 and FUCCI-HeLa cell lines. For Western blot, cells were lysed in RIPA buffer supplemented with protease inhibitor. Protein concentrations were determined with BCA method. 30 μg protein was loaded on SDS-PAGE gels and transferred to nitrocellulose membranes. The membranes were incubated with BRCA1 antibody (**Supplementary Tables S4, S5**). Detection was done with Odyssey Imager (LI-COR Biosciences). After image acquisition, the obtained images were analyzed using Image Studio Lite (Version 5.0).

Immunocytochemistry (ICC)

Cells were seeded on coverslips and treated with vehicle or indicated doses of MX, IM, and IMX. After 8 h or 24 h, cells were fixed with 2% buffered PFA for 10 min, permeabilized for 20 min in 0.2% Triton X-100/PBS, and washed thrice with 1% BSA/0.05% Tween/PBS. To reduce unspecific signal, cells were blocked in 1% BSA/10% Normal Donkey Serum/PBS for 30 min and then incubated overnight at +4°C with the following primary antibodies: α-γH2Ax, α-RAD51, α-cleaved Caspase-3, and actin. Cells were subsequently washed thrice with 1% BSA/0.05% Tween/PBS and incubated for 1 h at room temperature with fluorescently labeled secondary antibodies. Nuclei were counterstained with Hoechst 33342. Stained coverslips were mounted with ProlongGold. Images were acquired with a Nikon 90i Eclipse microscope (10x) and analyzed with the NIS Elements software. MDA-MB-231 (BRCA1-wt and silenced) cells were stained with α-γH2Ax and RAD51 antibodies. HeLa and HCC-1937 cells were stained with α-γH2Ax and α-cleaved Caspase-3 antibodies (**Supplementary Tables S4, S5**).

DNA Double Strand Break Repair Assay

HeLa cells with pDRGFP (HR plasmid construct) and pimEJ5GFP (NHEJ plasmid construct) were transfected with pCBASceI, a I-SceI endonuclease expression vector with a mammalian promoter to introduce a DSB at a genomic I-SceI site of DNA repair plasmid constructs. Cells were grown for 4 days followed by flow cytometry analysis with Alexa Fluor 488 and mCherry channel. mCherry was used as a transfection control, pcDNA3-EGFP was an EGFP control, and HPRT was a negative control (26). Colony that posed superior amount of EGFP signal was chosen for next experiments with drug treatments. The transfections of pCBASceI, mCherry2-C1, and all other control plasmids were done. For the experiment with drug treatments, 300,000 HeLa cells per well were plated on six-well plates on day 1, followed by pCBASceI and control transfections on day 2 and drug treatment on day 3. Additionally, the repair assay was also analysed with live imaging with phase contrast and GFP channel (**Supplementary Tables S4, S6**).

Apoptosis Assay

Total 100,000–200,000 cells were seeded per well in six-well plates, followed by drug treatment with vehicle, 5 μM IM, MX, and IMX. MX concentrations were 34 nM for HeLa, 103.5 nM for MDA-MB-231, and 9 nM for HCC-1937. Next, cells were incubated for 48 h. Cell pellets were collected and stained according to the kit protocol (**Supplementary Table S4**). Samples were then run with a flow cytometer. The data was analyzed with Flowing Software 2.5.1 (Mr Perttu Terho, Turku Bioscience Centre, Turku, Finland).

Validation of Cytotoxicity of IMX *Versus* MX in Patient-Derived and Commercial HGSOC Cell Lines

Patient-derived cell lines including M022p, M022i, M048i, H002, and OC002 were plated with a seeding density of 5000–8000 per well in 96-wells plate. M022p, M022i, H002 and OC002 required the use of basement membrane matrix prior to plating (**Supplementary Table S18**). Dose preparation by serial dilution and IC_{50} measurement were done as mentioned before (see 2.4). Similar experimental design was applied to conventional cell lines including COV318, CaOV3, OVCAR3, OVCAR4, OVCAR5, COV362, Kuramochi, and OVCAR8.

Statistical Analysis for Data Interpretation

Graph Pad Prism 6 was used in all experiments where P value of less than 0.05 was considered statistically significant. One-way ANOVA (Sidak's multiple comparisons) was used to analyze more than two groups, and unpaired t-test was used to analyze only two groups in cell viability assay. Non-linear fit regression analysis (log inhibitor *vs*. response, extra sum-of-squares F-test) was performed to determine the IC_{50} value.

RESULTS

Gene Set Enrichment Analysis (GSEA) Showed That IM Downregulates Pathways Related to DNA Repair in MX-Stressed Cells

We previously found that c-Abl inhibition after MX results in increased DNA cometing indicative of elevated DNA damage and massive cell death in cancer cells. Previously, we showed that inhibition of possible other IM substrates like c-kit and PDGF receptor kinase by AG1296 did not have any effect on cell viability. Moreover, c-Abl knockdown diminished the effect of IM in combination with MX in HeLa cells indicating its' central role in IMX treatment (27). Thereby, we proposed the effect of IMX is due to inhibition of c-Abl in combination with topoisomerase II inhibition. Here, we show the mechanism in detail and therefore used HeLa cell line as model in RNA expression analyses. The primary objective of the microarray analyses was to determine the effect of c-Abl inhibition by IM in replicative stress conditions.

When IM was added to the vehicle, some gene pathways were enriched (**Figure 1A**) but the changes in individual gene levels were so subtle that only a few genes passed the threshold level of 1.5-fold increase and $p < 0.05$ (**Figure 1B**). The ATM-ATR pathway is central to the maintenance of genome integrity, and as an example, we depict the expression of leading edge genes of ATR pathway in both IM and IM+MX (IMX)-treated cells (**Figures 1B, D**). In the global expression analysis, only MX and IMX treatments resulted in significant up- or downregulation of genes, in contrast to IM (**Figures 1B–D**).

GSEA analysis can detect subtle enrichment signals. The hundreds of pathways depicted in **Figure 1A** were clustered and visualized with Cytoscape (**Figure 2**). Compared to control, MX treatment yielded positive pathways which clustered in 'metabolic pathways', 'stress-activated pathways', and 'mitochondrial pathway' related to apoptosis, to mention the most significant.

Conversely, pathways regulating 'chromatid separation and mRNA cytoplasmic translation' were downregulated (data not shown). None of the stress-related pathways were detected in IM-treated samples. However, IM combined with MX (IMX) produced a new array of enriched pathways. The stress-signaling pathways, such as 'interferon signaling, and p38 MAP-kinase stress cascade' were also upregulated in IMX versus control as well as in IMX *vs*. MX. Similarly, 'apoptosis and oxidative stress' and 'stress-induced senescence' pathways were enriched in the upregulated phenotype. Several pathways were linked to 'chromatin silencing and transcription repression'. Most notably, pathways related to HR and DNA repair were downregulated. Additionally, pathways involved in mitosis, like 'microtubule organization', 'spindle formation', 'DNA replication maintenance', 'D-loop structure resolution', 'kinetochore amplification', and 'G1/S and mitotic metaphase/anaphase transitions' were downregulated (**Figure 2** and **Supplementary Tables S7, S8**).

At the DNA damage sensor site, Reactome terms 'recruitment and ATM-mediated phosphorylation of repair and signaling proteins at DNA double strand breaks' and 'DNA double-strand break response' were upregulated in IMX *vs*. MX (**Figure 2**). 'Non-homologous end joining' was among the upregulated nodes in IMX *vs*. Control (FDR = 0.099), but did not reach the 0.1 FDR threshold in IMX *vs*. MX comparison. Pathways related to G1/S transition and especially G2/M were also downregulated.

Taken together, the transcriptome data suggest that addition of IM to non-stressed HeLa cells has very little, if any, effect on the pathway regulation, whereas the effect on MX-stressed cells is profound, especially for DNA repair. Defective genome maintenance can lead to many of the consequences seen in the pathway enrichment analysis and necessitates further, direct functional scrutiny.

IM Reduces IC_{50} of MX in Cancer Cells

In the microarray experiments, we used 0.8 μM MX, 5 μM IM and the combinations as initial drug concentrations for HeLa cells. For all subsequent functional analyses, MX IC_{50} values were determined for the cell lines used (HeLa, MDA-MB-231, and HCC-1937) (**Figure 3**). We also used FUCCI-HeLa for which HeLa IC_{50} was utilized. HeLa, FUCCI-HeLa, and MDA-MB-231 cells were validated by panel sequencing of HR-related genes to exclude possible alterations in other DNA repair pathways at the DNA level (data not shown). The HCC-1937 cell line is BRCA1-mutated (28, 29). In line with our previous studies with cervical and vulvar cancer cell lines (27), IM treatment alone did not reduce cell viability. We found that 5 μM IM significantly reduced viability of MX-treated HeLa, MDA-MB-231, and HCC-1937 cells regardless of their HR status (**Figure 3** and **Supplementary Figure S9**). IMX (5 μM IM + 34 nM MX) showed similar effect as 92.5 nM MX in HeLa cells, 5 μM IM + 103.5 nM MX showed similar effect as 707 nM MX in MDA-MB-231 cells, and 5 μM IM + 9 nM MX showed similar effect as 136 nM MX in HCC-1937 cells.

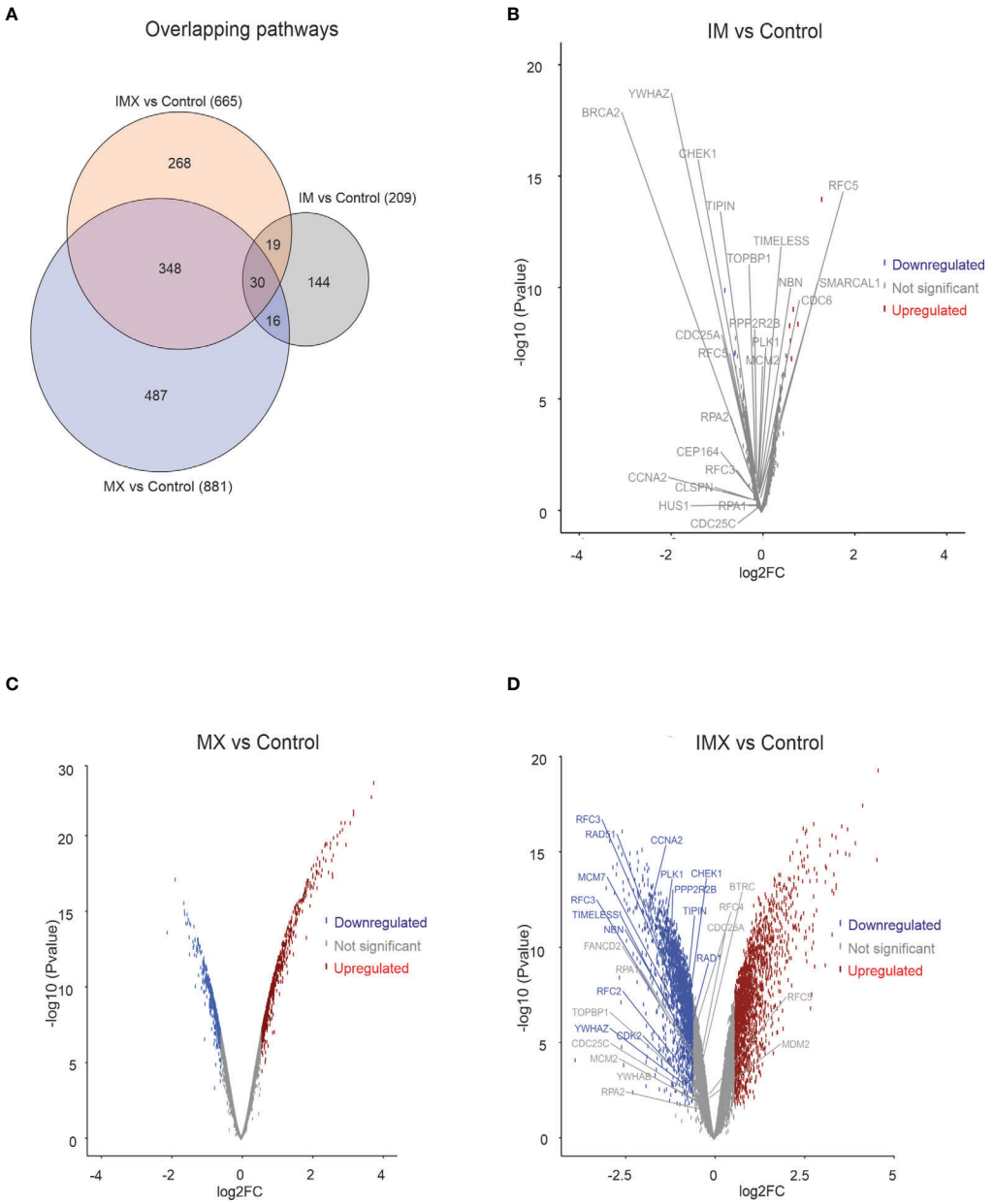

FIGURE 1 | Transcriptome analysis in HeLa cell line. HeLa cells were treated with either imatinib (IM), mitoxantrone (MX), or IM + MX (IMX). The hybridization set consisting of 18196 differentially expressed genes was run against 18425 gene sets in a gene set enrichment analysis platform (GSEA). **(A)** Euler diagram showing the overlapping pathways. FDR q-value of 0.1 was used as a threshold. **(B–D)** Volcano plots of whole probe set with log2 fold change of 0.58 (FC = 1.5) of differentially expressed genes. Their significance values p = 0.01 were used as threshold. Red dots represent upregulated and blue dots downregulated genes. Dots below threshold are greyed. ATR pathway was downregulated in both IM *vs*. C and IMX *vs*. C, and the leading edge genes are separately depicted. None of the leading edge genes in IM-treated cells reached the threshold.

Imatinib Increases DNA Damage But Reduces Nuclear RAD51 Levels

Pathway analysis (**Figure 2**) revealed that IMX treatment resulted in upregulation of the DSB response but downregulation of homology-directed recombination repair pathways (**Figure 2**). We tested whether these putative changes were directly detectable in drug-treated cells. To this end, we used flow cytometry (**Figure 4A**) and immunocytochemistry (**Supplementary Figures S10–S12**). The expression of γH2AX, a marker for DNA damage, increased after MX treatment, and IMX caused a more pronounced increase of DNA damage. IM alone did not show significant effect compared to vehicle (**Figure 4B** and **Supplementary Figures S10–S13**).

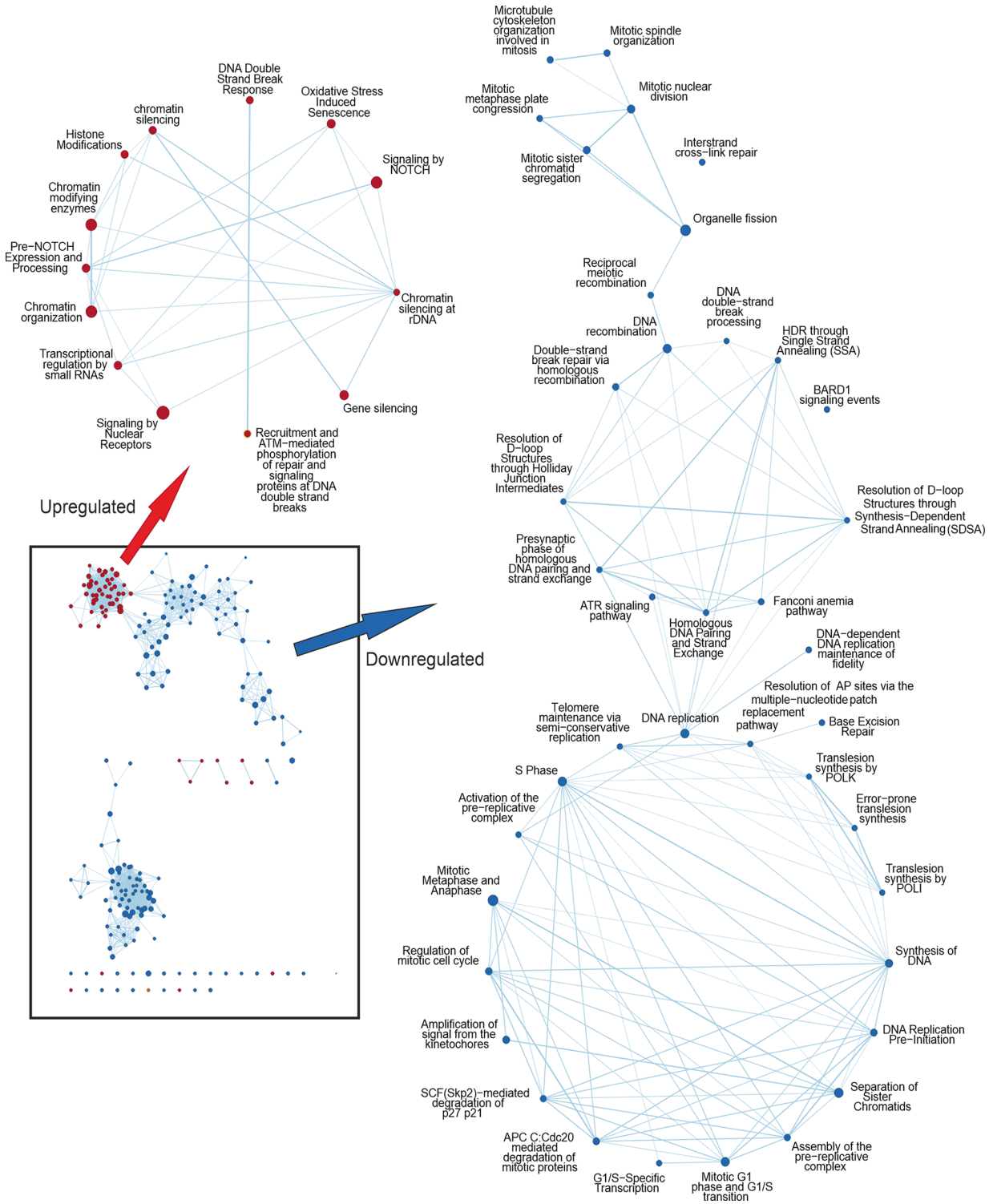

FIGURE 2 | Cytoscape network analysis of the enriched pathways in IMX compared to MX indicating the effect of IM. Upregulated nodes in IMX are shown in red and downregulated nodes in blue. Lower left box represents the most significant nodes. Arrows depict the magnification of nodes filtered with diffusion algorithm. Pathways related to DNA damage response are upregulated, whereas pathways related to cell cycle progression and mitosis are downregulated. In the middle cluster of the downregulated nodes are pathways related to homologous recombination and ATR signalling.

We further studied RAD51 expression as a proxy for HR-mediated DNA repair. Isolated HeLa cell nuclei were analyzed using flow cytometry after 24 h of drug treatment (30). MX-induced stress resulted in increase in RAD51 levels, indicative of augmented HR. However, further increase in DSBs after IMX treatment did not result in a corresponding accumulation of nuclear RAD51 levels, but instead a clear attenuation of the signal at 24 h after treatment (**Figure 4A**). This suggests that IMX prevented nuclear localization of RAD51.

Similarly, using indirect immunofluorescence, we observed a marked increase in RAD51 signal after MX treatment, but diminished amount of RAD51 foci in IMX-treated MDA-MB-231 cells (**Supplementary Figure S11**). When BRCA1 was silenced with siRNA, IMX increased γH2AX levels and reduced RAD51 levels (**Supplementary Figure S12**). This suggests that c-Abl may directly facilitate RAD51 activity independently of BRCA1 after DNA damage, in line with previous studies.

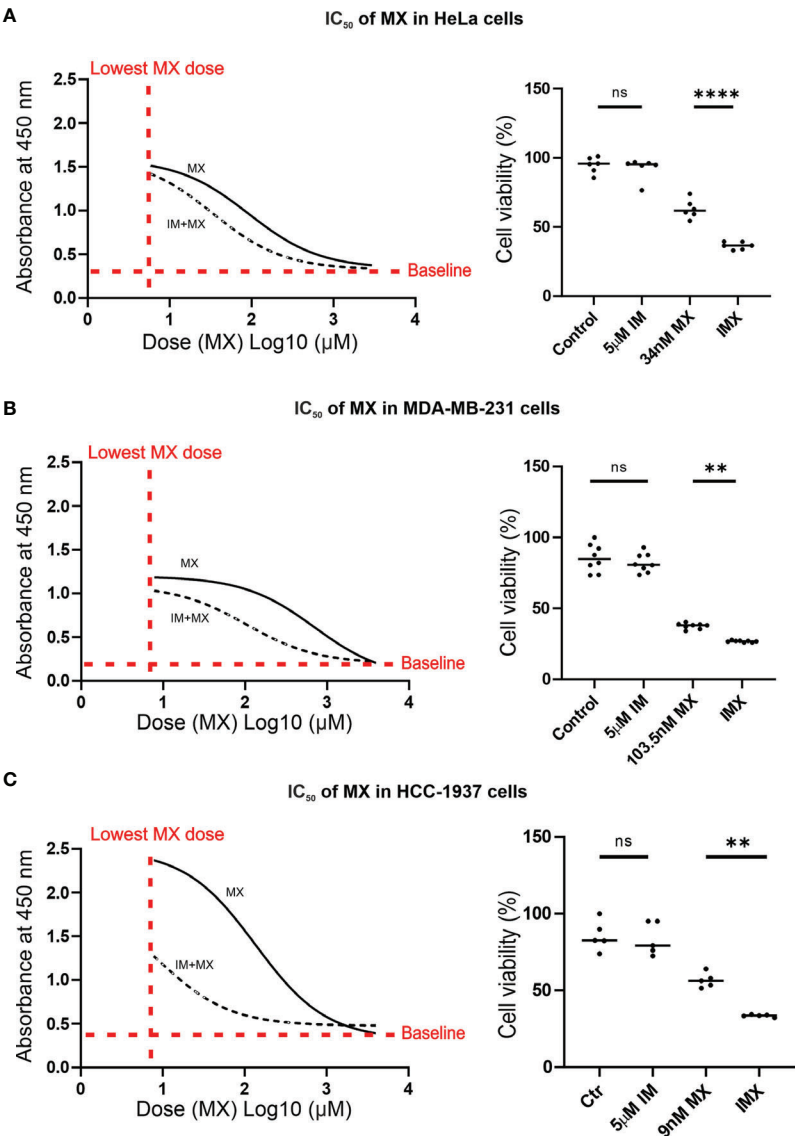

FIGURE 3 | IM reduces IC50 of MX in cancer cells. In A–C, the non-linear plots show dose *vs*. response curves where X-axis presents dose (MX) Log10 (μM) and Y-axis represents absorbance at 450 nm, which is proportional to the amount of viable cells ($p < 0.05$). The column scatter plots represent median cell viability (%), where the effect of MX combined with 5 μM IM (IMX) is compared to 0.1% DMSO (control), 5 μM IM, and MX (ordinary one-way ANOVA: $p < 0.05$). **(A)** In HeLa cells, IC_{50} of MX was 92.5 nM (95% confidence interval (CI): 63–136.5), and IC_{50} of MX combined with 5 μM IM (IMX) was 34 nM (95% CI: 25–46). **(B)** In MDA-MB-231 cells, IC_{50} of MX was 707 nM (95% CI: 542.5–921) and IC_{50} of MX with 5 μM IM (IMX) was 103.5 nM (95% CI: 86–124). **(C)** In HCC-1937 cells, IC_{50} of MX was 136 nM (95% CI: 104.5–176) and $IC_{50\ of}$ MX with 5 μM IM (IMX) was 9 nM (95% CI: 5–16). **p<0.005, ****p<0.0001; ns, non-significant.

HR and NHEJ Are Suppressed by Imatinib After DNA Damage

To study DNA repair, we used two HeLa cell lines that contain HR or NHEJ reporter cassettes expressing GFP when DNA repair occurs (**Figure S14**). The baseline HR efficiency of HeLa cells was 0.03 and the baseline NHEJ efficiency of HeLa cells was 0.12, four times higher than HR (**Supplementary Figure S15**). Treatment with IM alone did not alter DNA repair activity (**Figure 4C**). In **Figure 4C**, vehicle and 5 μM IM treatment lines overlap suggesting no difference in HR or NHEJ capacity of the cells in the absence of stress. In contrast, GFP signal was lower and fewer cells were positive with IMX compared to MX (**Figures 4C, D**). Thus, IM significantly suppressed both HR and NHEJ in MX-damaged cells. The findings in the DNA repair reporter assays are consistent with the GSEA data and with the observed RAD51 data, as RAD51 is responsible for the actual recombination step in HR (**Figure 4A**). Interestingly, in line with this, our microarray data suggested that expression of the PRKDC gene, encoding a critical NHEJ component DNA-PK, was 2.3-fold downregulated in IMX-treated cells compared to vehicle ($p = 2.7 \times 10^{-6}$, FDR adj. $p = 1.8 \times 10^{-5}$).

We further followed the temporal and functional course of DNA repair in MX-treated HeLa cells by time-lapse microscopy for 7 days. GFP-expressing cells with a HR reporter cassette underwent normal bipolar cell division in the presence of MX (**Supplementary Video S17**). After cell division, these cells entered G1 normally, which is consistent with flow cytometry analysis, where a distinct G1 population was present after MX treatment (**Figure 5**). For the GFP-expressing cells with a NHEJ reporter cassette, normal metaphase was observed after MX treatment. There, cells were able to employ NHEJ and normal cell division ensued (**Supplementary Video S17**).

Collectively, this suggests that IM impairs both HR and NHEJ-mediated repair of DNA damage in cells with topoisomerase II inhibition-induced replication stress.

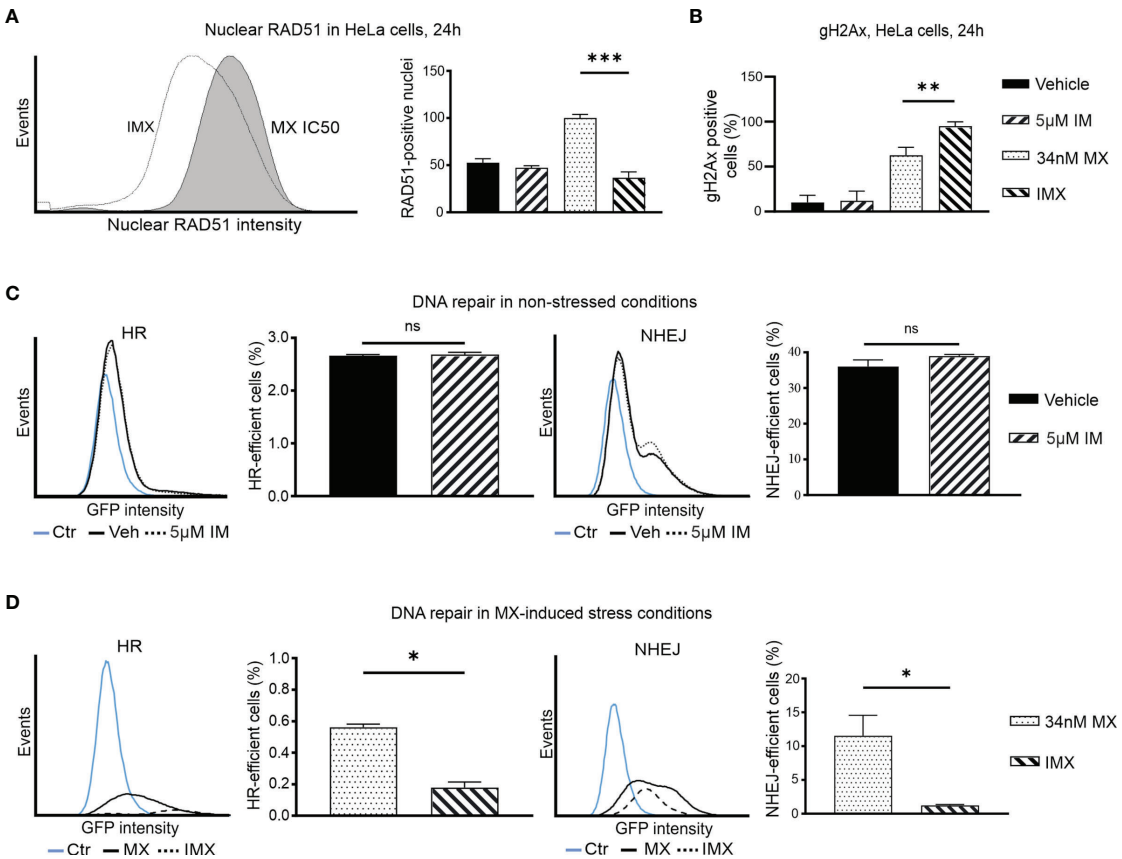

FIGURE 4 | IM decreases nuclear RAD51 level after DNA-damage and blocks DNA repair in cancer cells. **(A)** Histogram shows nuclear RAD51 intensity under 34 nM MX and 5 μM IM + 34 nM MX (IMX) treatment. The bar chart shows percent of nuclear RAD51 population after different treatments (95% CI of difference for MX *vs*. IMX: 47.49–82.51 where p = 0.0004, ordinary one-way ANOVA). **(B)** Bar chart shows percentage of γH2Ax-positive cells (95% CI of difference for MX *vs*. IMX: -54.26 to -10.56 where p = 0.0063, Ordinary one-way ANOVA). **(C)** The histograms show HR and NHEJ repair signal intensity, and bar chart shows percent of HR and NHEJ-efficient cells (corrected against transfection efficiency) after IM treatment in non-stressed conditions (95% CI of difference for HR: 5 μM IM *vs*. vehicle: -0.1189–0.1662 where p = 0.5499, NHEJ: 5 μM IM *vs*. vehicle: -2.764–8.630 where p = 0.1571, two-tailed, unpaired t-test). **(D)** The histograms show HR and NHEJ repair signal intensity, and bar chart shows percent of HR and NHEJ-efficient cells (corrected against transfection efficiency) after IM treatment in MX-induced stress conditions (95% CI of difference for HR: 5 μM IM *vs*. vehicle: -0.5037 to -0.2601 where p = 0.0054; NHEJ: MX *vs*. IMX: -19.49 to -1.139 where p = 0.0402, two-tailed, unpaired t-test). *p<0.05, **p<0.005, ***p=0.0001; ns, non-significant.

Imatinib Induces G2/M Arrest and Apoptosis in MX-Treated Cancer Cells

According to pathway analysis, IMX treatment downregulates pathways such as 'S-phase', 'synthesis of DNA', 'G2/M transition', 'G1/S transition', and 'mitotic cell cycle'. For functional validation, we studied cell cycle using FUCCI-HeLa cells. The fusion protein mKO-Ctd1, expressed in G1, confers cells in this phase red fluorescence, while mAG-Geminin, expressed throughout S-M phase, produces green fluorescence. Cells transitioning from G1 to S show yellow fluorescence, while right after cell division no fluorescence can be detected (31). After MX treatment, these cells were able to enter mitosis after prolonged G2 (**Supplementary Video S18**). Flow cytometry data showed no G2/M arrest after MX treatment (**Figure 5A**). In sharp contrast, with IMX there was a delay in G1/S progression and a population of FUCCI-HeLa cells with red fluorescence accumulated in G1 for 6–8 h (**Figure 5B**). Eventually, cells exited from G1, entered S phase, and finally the entire cell population accumulated in G2/M phase with green fluorescence and larger nuclear size (data not shown). Moreover, cells which accumulated in G2/M phase did not enter mitosis, and eventually died over the 7-day observation period. The complete G2/M block was verified by flow cytometry (**Figure 5A**).

In addition, G2/M arrest was also seen in MDA-MB-231 and HCC-1937 cells after IMX treatment (**Supplementary Figure S16**). According to time-lapse microscopy, apoptosis followed by G2/M arrest was the hallmark of IMX effect, which implies that IMX-treated cells were unable to repair DNA damage (**Supplementary Video S18**). There was also a statistically significant increase in the apoptotic cell population in HeLa, MDA-MB-231, and HCC-1937 cell lines after IMX treatment (**Figure 6**). Although there was upregulation of 'oxidative stress-

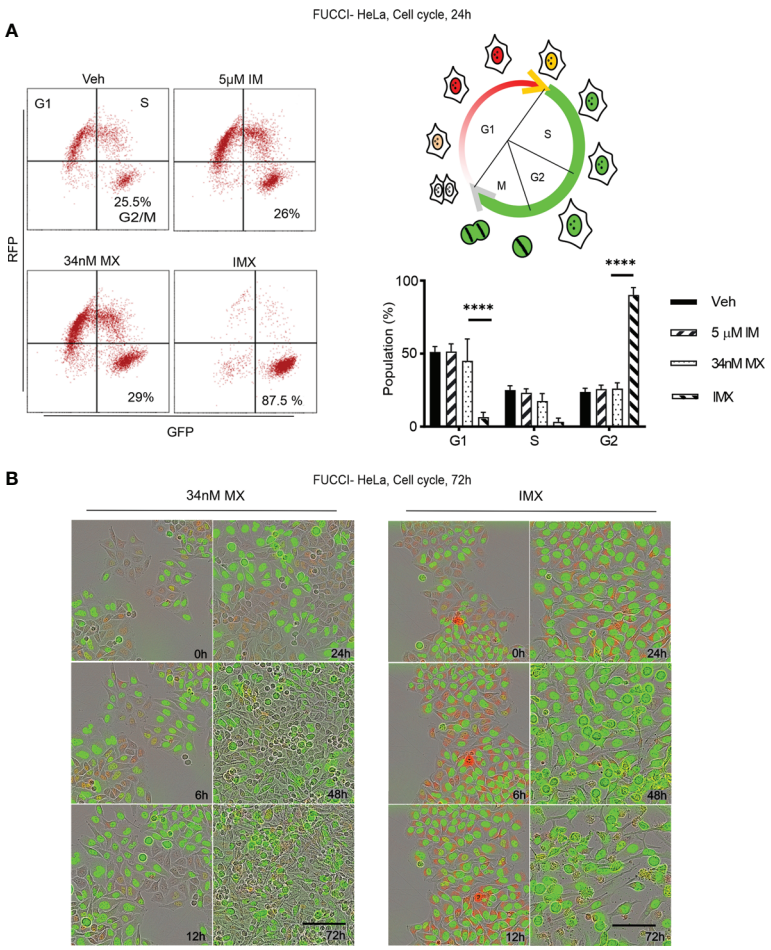

FIGURE 5 | c-Abl inhibition in combination with MX causes complete G2 arrest in FUCCI-HeLa cells. **(A)** Flow cytometry data on FUCCI-HeLa cells in different cell cycle phases. The representative dot plots show cell cycle after different treatments where lower right quadrant shows G2/M population. The picture demonstrates cell cycle in terms of FUCCI system where newly divided daughter cells have no color, G1 cells show red fluorescence, G1-S transition shows yellow fluorescence, and S/G2/M shows green fluorescence. G2/M population was separated from S in FACS analysis. Bar chart shows percent of population in each phase (95% CI of difference for G0/G1 phase: MX *vs*. IMX is 21.88–55.45 where $p < 0.0001$; G2/M phase: MX *vs*. IMX is -82.89 to -45.35 where $p < 0.0001$, 2 way ANOVA). **(B)** Representative images of FUCCI-HeLa cells in 5 time points after 34 nM MX or IMX treatments. Scale bar = 50 μm. ****$p<0.0001$.

induced senescence' after IMX treatment in micro-array analysis (**Figure 2**), we observed that cancer cells die predominantly by apoptosis after G2/M arrest.

Imatinib Significantly Reduces Viability of Patient-Derived and Commercial HGSOC Cells After MX Irrespective of Their HR Status

HR proficiency is a clinical problem that is centrally linked to development of resistance to treatments. Therefore, we wanted to test if the effect on cytotoxicity in different adenocarcinomas and squamous cell cancers is also applicable to HGSOC.

We validated the effect of c-Abl inhibition on MX-induced lethality in five patient-derived and eight commercial HGSOC cell lines. **Supplementary Tables S19, S20** show that all the HGSOC cell lines have known HR-status. Cell viability assay was conducted to determine the IC_{50} of MX (± IM). These cell lines were not sensitive to IM. Therefore, there is no IC_{50} for IM.

M022p, M022i, M048i, and H002 are patient-derived HRP HGSOC cells. M022p is obtained from laparoscopy at diagnosis. M022i, M048i, and H002 are obtained from patients during interval surgery after three courses of neoadjuvant chemotherapy treatment. OC002 is HRD cell line obtained from patient with primary laparoscopy at diagnosis (**Supplementary Table S19**). IC_{50} data shows that IM decreased IC_{50} MX-dose by 74.5%, 56%, 83%, and 59.5% in M022p, M022i, M048i, and H002 cell lines, respectively. In OC002 cells, MX-dose decreased by 72% after IM combination (**Supplementary Table S19**). We also tested HRP HGSOC commercial cell lines COV318, CaOV3, OVCAR3, OVCAR4, and OVCAR5. CaOV3, which has known platinum resistance, was unexpectedly the most sensitive to MX (**Supplementary Table S20**). In contrast, COV318 with known platinum resistance, was the least sensitive to MX among all HRP cell lines (**Figure 7** and **Supplementary Table S20**). Additionally, we studied COV362, Kuramochi and OVCAR8 HRD cell lines. Kuramochi was the least sensitive to MX though it has been reported to be platinum sensitive (**Supplementary Table S20**). In all these cell lines regardless of HR-status, neoadjuvant chemotherapy, or platinum-sensitivity, IM significantly reduced the IC_{50} dose of MX. The results also show that the previously reported platinum sensitivities do not directly correlate with mitoxantrone toxicities.

DISCUSSION

During carcinogenesis, neoplastic cells often lose a critical DDR pathway. This is an Achilles heel of cancers with high replication stress, which has been exploited with radiation therapy and DNA-targeting chemotherapy (32). Examples of the latter include

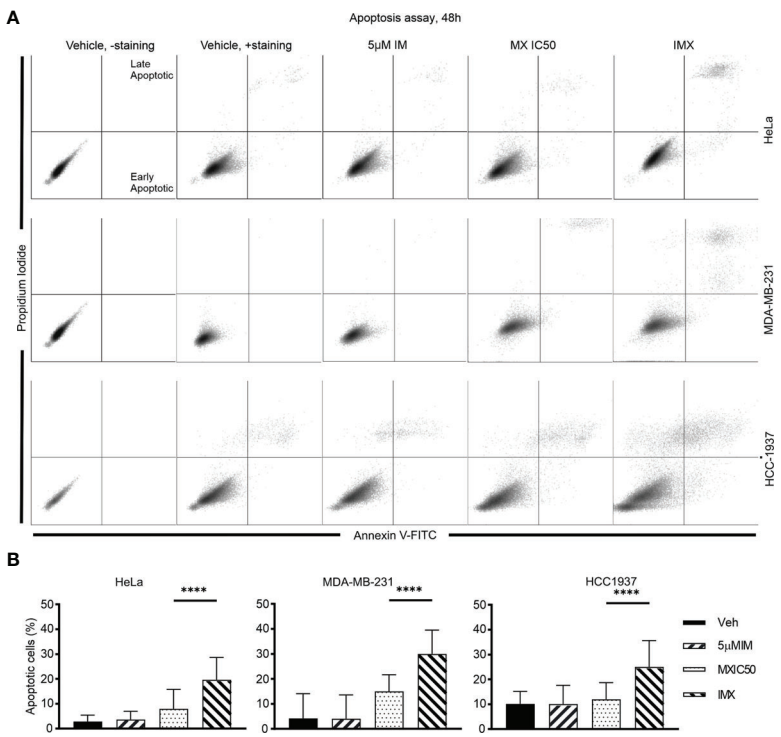

FIGURE 6 | IM induced apoptosis in HeLa, MDA-MB-231, and HCC-1937 cells after DNA damage. **(A)** The dot plots show distribution of early and late apoptotic populations in different cell lines. Annexin V-positive cells in the lower right quadrant are early apoptotic. Double-positive population in the upper right quadrant is late apoptotic/necrotic. The percentages of both early and late apoptotic populations are calculated as total percent of apoptotic population. **(B)** The bar chart shows the percent of apoptotic cells in total population under different treatments in different cell lines. ****p<0.0001.

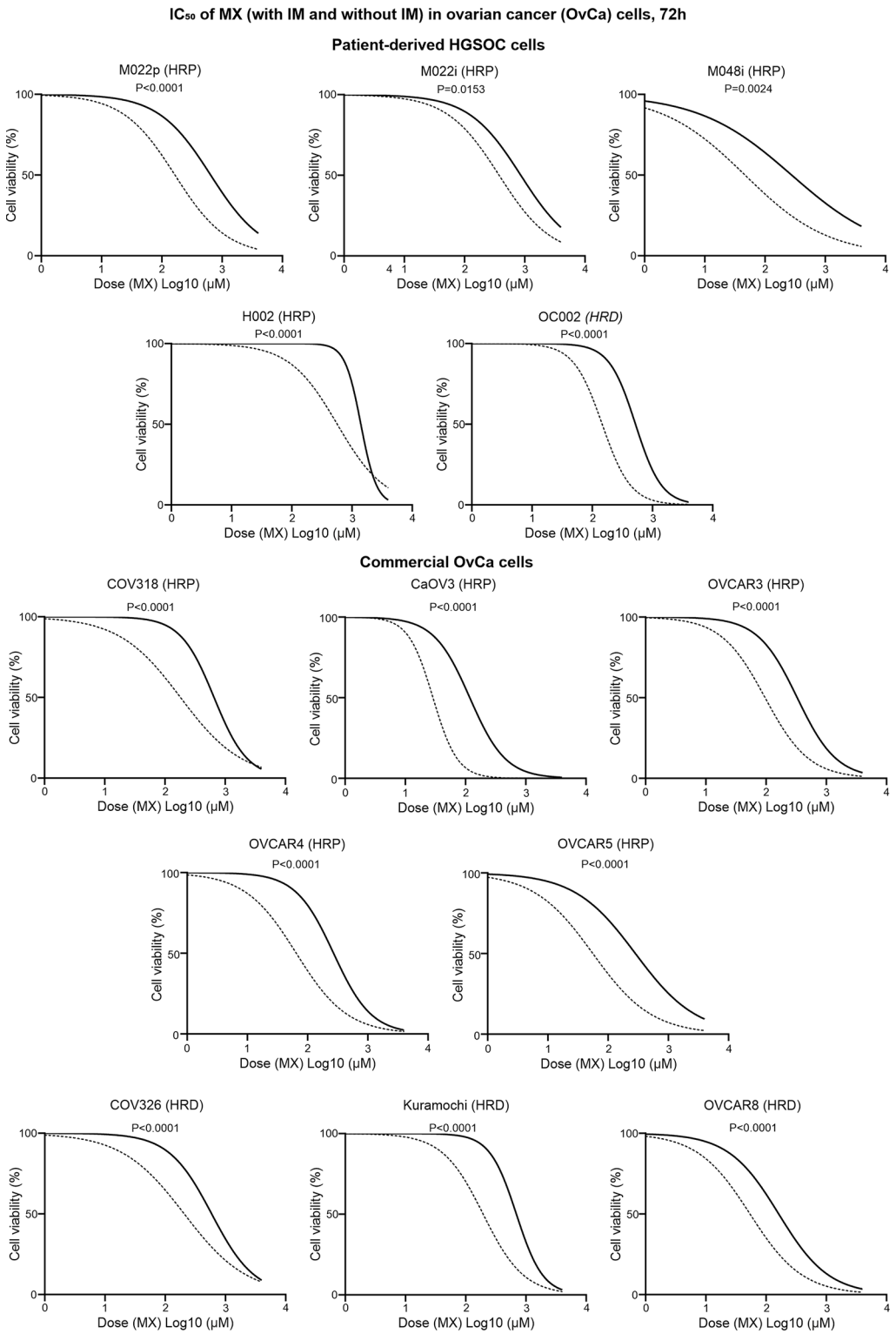

FIGURE 7 | IC_{50} values of MX and IMX in ovarian cancer cell lines after 72 h of treatment. The cell lines include five patient-derived HGSOC cell lines (M022p, M022i, M048i, H002, and OC002) and eight commercial HGSOC cell lines (COV318, CaOV3, OVCAR3, OVCAR4, OVCAR5, COV326, Kuramochi, and OVCAR8) with known HR status (either HRP or HRD). The non-linear regression plots show log (inhibitor) *vs*. normalized response-variable slope where black solid line is MX-only (without IM) and dotted line is MX with 5 μm IM.

topoisomerase I and II inhibitors that prevent decatenation and resealing of chromosomal breaks inducing unresolved DSBs during replication (33, 34). DSBs are detrimental to the cell due to the need of accurate chromosome segregation during mitosis, but importantly also due to persistent DDR signalling. DSBs activate DDR *via* ATM-dependent manner to delay cell cycle progression to facilitate repair. Successful high-fidelity DSB repair involves HR. HR defects, e.g., due to inactivating mutations in *BRCA1* and *BRCA2* genes, are exploited in ovarian and breast cancer treatment, where single strand repair inhibitors (PARP inhibitors) as post-chemotherapy maintenance treatment show high efficacy in the HR-deficient subpopulation of patients. In contrast, HR-proficient tumours are usually resistant to PARP inhibitors and to chemotherapy in general (35, 36). Here, we show that HR can be blocked with simultaneous treatment of mitoxantrone and imatinib.

In this study, we used γH2AX as a marker for DNA damage and found increased nuclear signal after MX treatment, which was further augmented with IM in all tested cell lines, regardless of their BRCA1 status. We studied the pathway-level effects of DSB accumulation in HeLa cells at the global transcriptomic level with useful hints for further mechanistic analyses which is consistent with Peng and co-workers who showed that HR deficiency and protein expression levels closely correlated with changes at the transcriptional level (37). We found that c-Abl inhibition after MX treatment downregulated several DNA repair pathways, most notably those related to HR. In the network analysis, these nodes were connected to downregulation of cell cycle transition in G2/M and mitosis. Limited availability of dNTPs causes replication fork stalling (38). We found deoxyribonucleotide triphosphate (dNTP) synthesis among the downregulated pathways, providing a potential explanation for replication stress. Collectively, gene expression analysis suggested broad impairment of DNA repair in response to IMX, which we studied in more detail.

There is a constitutive interaction between the PXXP motif in the C-terminus of BRCA1 and the SH3 domain of c-Abl (16). This type of interaction is disrupted in an ATM-dependent manner after irradiation, followed by increased c-Abl kinase activity. In addition, c-Abl facilitates the progression of HR by activating RAD51, and allows its translocation into the nucleus after DNA damage (13, 39, 40). In the present study, we found that MX increased nuclear RAD51 levels in BRCA1-wt HeLa and MDA-MB-231 cells. However, RAD51 levels were significantly higher under MX treatment compared to vehicle even after BRCA1 silencing. Adding IM to MX significantly reduced nuclear RAD51 expression in Hela, BRCA1-wt MDA-MB-231, and BRCA1-silenced MDA-MB-231 cells. These findings suggest that the effects of concurrent inhibition of c-Abl and topoisomerase II are independent of BRCA1 status and depict a major role for c-Abl in DNA repair in these cancer cells. Moreover, BRCA1 is considered as negative regulator of c-Abl. BRCA1-mutant cancer cell line HCC-1937 has a constitutively high c-Abl kinase activity (16). This suggests a dependency on c-Abl, which is supported by the finding that HCC-1937 was the cell line most sensitive to IMX, with a 15-fold decrease in IC_{50} compared to MX.

The aforementioned findings are supported by gene expression data showing downregulated HR in response to IMX. Correspondingly, in a direct HR reporter assay, significantly reduced HR was observed in IMX-treated HeLa cells. The other major DSB repair pathway, NHEJ, does not rely on the presence of the replicated sister chromatid (41). We therefore asked whether loss of HR could be compensated by NHEJ. The fusion form of c-Abl (BCR-Abl) upregulated NHEJ in chronic myeloid leukaemia after irradiation suggesting that IM may reduce NHEJ (17). The regulation of NHEJ by c-Abl in solid cancers remains poorly understood. In this study, we found that IM reduces NHEJ capacity in HeLa cells.

Of note, HeLa cells used in the experiments express HPV18 E6 which binds and degrades tumor suppressor p53, and still show dramatic stabilization of p53 with a 4-fold reporter activation in IMX (27). Our previous study also showed that p53 reactivation is possible after treatment despite destabilization by E6 (42, 43). By transcriptome profiling in this study, we also detected a 4.5-fold increase in *CDKN1A* (p21) which is transcriptionally regulated by p53. The ATM response pathway which directly phosphorylates p53 was upregulated in GSEA after IMX treatment. In addition, ATM kinase is a major physiological mediator of H2AX phosphorylation in response to DSBs, producing γH2AX, and this was highly elevated in IMX-treated cell lines. Taken together, our findings indicate that the DNA damage sensor site is working in these cells, but the effector part of the downstream kinase cascade is tilted towards DDR inhibition, persistent cell cycle arrest, and eventual death. The previous study showed that loss of c-Abl may cause senescence in mouse embryonic fibroblasts (44). We also observed upregulation of 'oxidative stress-induced senescence' in microarray data but the apoptosis assay and time-lapse microscopy suggests predominant death of cancer cells *via* apoptosis after G2/M arrest.

Inactivating *BRCA1* and *BRCA2* mutations result in HR dysfunction that occurs in 50% of HGSOC (35). Though BRCA1/2-deficient cancers are sensitive to platinum-based therapy, secondary *BRCA1/2* mutations are also responsible for acquired resistance to cisplatin in ovarian carcinomas (45, 46). In BRCA-mutated tumors, synthetic lethality can be induced by PARP inhibitors (47). PARP inhibitor efficacy relies heavily on tumor HR deficiency, and PARP inhibitors have limited or no activity in tumors with functional HR (36). So ideally, inducing HR deficiency in resistant tumors would make them sensitive to DNA-damaging chemotherapy and to PARP inhibitors. This was achieved in HRP epithelial ovarian cancer, which is sensitive to PARP inhibitors when combined with PI3K inhibitor alpelisib that inhibits HR (48). Interestingly, PI3K is downstream to Abl in the HR pathway (49, 50). In the present study, we used MDA-MB-231 cell line with different BRCA1 statuses to assess whether the IMX treatment outcome is dependent on the function of this protein which is essential for HR. Neither cell viability, cell cycle distribution, γH2Ax expression, nor nuclear RAD51 levels were different in parental MDA-MB-231 cells with intact BRCA1, compared to BRCA1-silenced cells after IMX treatment. We also observed that IMX has similar cytotoxic effect on cell viability of

HeLa, MDA-MB-231, HCC-1937, and 13 HGSOC cell lines, which are squamous cell and adenocarcinoma. Among these cell lines, in addition to HeLa and MDA-MB-231, 11 cancer cell lines have functional BRCA1 and HR. We used three commercial BRCA1-mutant HRD HGSOC cell lines, which may have high c-Abl activity similar to HCC-1937 (16). HeLa was used as a cancer cell model for DNA repair assays. Other *in vitro* assays were performed in MDA-MB-231 and HeLa, where IMX caused reduction of nuclear RAD51 and HR-proficiency. It is likely that same mechanism is responsible for the lethality of IMX on HRP HGSOC cell lines where similar cytotoxicity was achieved. In HeLa cells we showed that IMX-treated cells have reduced NHEJ-capacity. As it is known that HRD cancer cells mostly rely on NHEJ, IMX may also work *via* this mechanism in HRD HGSOC cells. Moreover, our data suggested that IMX is lethal to HGSOC cell lines, both patient-derived and commercial, regardless of their HR-status and platinum-sensitivity.

Despite the therapeutic success of PARP inhibitors in HRD cancers, several other DDR targets have gained interest. For example, inhibitors of ATR, ATM, DNA-PK, CHK1 and 2, and WEE1 are in clinical trials. Efficacy of single-agent use is dependent on and often hampered by the tumors' proficiency to deal with different forms of DNA damage. Adding chemotherapy to these compounds, or combining them with different DDR inhibitors may increase toxicity substantially (51). Although we do not know the potential clinical toxicity of the present IMX combination, it is noteworthy that the cell lines here or in our previous report were rather inert to IM in non-stressed condition. The finding that IM increases the therapeutic index of MX 3- to 15-fold suggests that the concentration of this compound can be reduced several fold, resulting potentially to fewer side effects of which cardiomyopathy can lead to severe consequences in long term use (52). In this respect, it is reassuring that even a long-term administration of IM to chronic myeloid leukemia patients does not cause unacceptable cumulative or late toxic effects (53). We also have previously tested IMX in normal low-passage fibroblasts and found that IM did not alter the proliferation of these cells when combined with MX, suggesting that malignant cells are more vulnerable to IMX than normal cells (27).

Overall, our results demonstrate that c-Abl inhibition increases the effect of topoisomerase II inhibitor MX. Moreover, the data indicate that both HR and NHEJ are suppressed by this dual inhibition, potentially opening up a possibility for better efficacy even in hard-to-treat HR-proficient cancers.

CONCLUSIONS

This study provides evidence that concomitant c-Abl and topoisomerase II inhibition suppresses HR-mediated DSB repair. Additionally, the combination treatment may also suppress NHEJ-mediated DSB repair, leading to G2 arrest, and eventually apoptosis of cancer cells. We also demonstrate that addition of IM to MX significantly increases the therapeutic index of MX and shows strong synergy in killing of patient-derived HGSOC cell lines, independent of BRCA1 status.

DATA AVAILABILITY STATEMENT

The datasets presented in this study can be found in online repositories. The names of the repository/repositories and accession number(s) can be found below: https://www.ebi.ac.uk/arrayexpress/, E-MTAB-9475.

AUTHOR CONTRIBUTIONS

AS and SH conceived the project and designed experiments. AS carried out experiments, analysis, and interpretation of data and prepared original draft. MT conducted immunofluorescence experiment. AJ conducted FUCCI-HeLa cell cycle assay with FACS. JS and SA visualized data and provided technical guidance to AS. RV performed DNA sequencing. KK and PR developed, maintained, and provided patient-derived HGSOC cell lines for conducting assays. SH, LK, MT, SA, and KH revised the manuscript. All authors reviewed the article. SH, AS, and JS finalized the manuscript. All authors contributed to the article and approved the submitted version.

FUNDING

This work was funded by the Finnish Cancer Foundation and the Sigrid Jusélius Foundation (grants to LK) and the Academy of Finland (grant number 314338 to SH, 308375 to JT, and 314394 to LK).

ACKNOWLEDGMENTS

Cell Imaging and Cytometry unit (Turku Bioscience Centre) and Biocenter Finland are acknowledged for the microscopy and flow cytometry instrumentation. The authors thank Reija Venho and Asta Laiho for technical assistance in microarray analyses. The authors also thank Dr. Imtiaz Khuda and Dr. Ubaid Ullah for giving valuable comments on manuscript. In memory of adjunct professor Johanna Tuomela who dedicated her research investigating cancer.

SUPPLEMENTARY MATERIAL

The Supplementary Material for this article can be found online at: https://www.frontiersin.org/articles/10.3389/fonc.2021.733700/full#supplementary-material

REFERENCES

1. Canman CE, Lim DS, Cimprich KA, Taya Y, Tamai K, Sakaguchi K, et al. Activation of the ATM Kinase by Ionizing Radiation and Phosphorylation of P53. *Sci (80-)* (1998) 281:1677–9. doi: 10.1126/science.281.5383.1677
2. Bakkenist CJ, Kastan MB. DNA Damage Activates ATM Through Intermolecular Autophosphorylation and Dimer Dissociation. *Nature* (2003) 421:499–506. doi: 10.1038/nature01368
3. Cliby WA, Roberts CJ, Cimprich KA, Stringer CM, Lamb JR, Schreiber SL, et al. Overexpression of a kinase-inactive ATR protein causes sensitivity to DNA-damaging agents and defects in cell cycle checkpoints. *EMBO J* (1998) 17:159–69. doi: 10.1093/emboj/17.1.159
4. Ragu S, Matos-Rodrigues G, Lopez BS. Replication Stress, DNA Damage, Inflammatory Cytokines and Innate Immune Response. *Genes (Basel)* (2020) 11:409. doi: 10.3390/genes11040409
5. Trenner A, Sartori AA. Harnessing DNA Double-Strand Break Repair for Cancer Treatment. *Front Oncol* (2019) 9:1388. doi: 10.3389/fonc.2019.01388
6. Lheureux S, Mirza M, Coleman R. The DNA Repair Pathway as a Target for Novel Drugs in Gynecologic Cancers. *J Clin Oncol* (2019) 37:2449–59. doi: 10.1200/JCO.19.00347
7. Matulonis UA, Sood AK, Fallowfield L, Howitt BE, Sehouli J, Karlan BY. Ovarian Cancer. *Nat Rev Dis Prim* (2016) 2:16061. doi: 10.1038/nrdp.2016.61
8. Bryant HE, Schultz N, Thomas HD, Parker KM, Flower D, Lopez E, et al. Specific Killing of BRCA2-Deficient Tumours With Inhibitors of Poly(ADP-Ribose) Polymerase. *Nature* (2005) 434:913–7. doi: 10.1038/nature03443
9. Farmer H, McCabe H, Lord CJ, Tutt AHJ, Johnson DA, Richardson TB, et al. Targeting the DNA Repair Defect in BRCA Mutant Cells as a Therapeutic Strategy. *Nature* (2005) 434:917–21. doi: 10.1038/nature03445
10. Fong PC, Boss DS, Yap TA, Tutt A, Wu P, Mergui-Roelvink M, et al. Inhibition of Poly(ADP-Ribose) Polymerase in Tumors From. *BRCA Mutat Carriers N Engl J Med* (2009) 361:123–34. doi: 10.1056/NEJMoa0900212
11. Kondrashova O, Nguyen M, Shield-Artin K, Tinker AV, Teng NN, Harrell MI, et al. Secondary Somatic Mutations Restoring RAD51C and RAD51D Associated With Acquired Resistance to the PARP Inhibitor Rucaparib in High-Grade Ovarian Carcinoma. *Cancer Discov* (2017) 19:20. doi: 10.1158/2159-8290.CD-17-0419
12. Quigley D, Alumkal JJ, Wyatt AW, Kothari V, Foye A, Lloyd P, et al. Analysis of Circulating Cell-Free DnA Identifi Es Multiclonal Heterogeneity of BRCA2 Reversion Mutations Associated With Resistance to PARP Inhibitors. *Cancer Discovery* (2017) 999–1005. doi: 10.1158/2159-8290.CD-17-0146
13. Takizawa Y, Kinebuchi T, Kagawa W, Yokoyama S, Shibata T, Kurumizaka H. Mutational Analyses of the Human Rad51-Tyr315 Residue, a Site for Phosphorylation in Leukaemia Cells. *Genes to Cells* (2004) 9:781–90. doi: 10.1111/j.1365-2443.2004.00772.x
14. Welch PJ, Wang JYJ. A C-Terminal Protein-Binding Domain in the Retinoblastoma Protein Regulates Nuclear C-Abl Tyrosine Kinase in the Cell Cycle. *Cell* (1993) 75:779–90. doi: 10.1016/0092-8674(93)90497-E
15. Welch PJ, Wang JYJ. Abrogation of Retinoblastoma Protein Function by C-Abl Through Tyrosine Kinase-Dependent and -Independent Mechanisms. *Mol Cell Biol* (1995) 15:5542–51. doi: 10.1128/MCB.15.10.5542
16. Foray N, Marot D, Randrianarison V, Venezia ND, Picard D, Perricaudet M, et al. Constitutive Association of BRCA1 and C-Abl and Its ATM-Dependent Disruption After Irradiation. *Mol Cell Biol* (2002) 22:4020–32. doi: 10.1128/MCB.22.12.4020-4032.2002
17. Salles D, Mencalha AL, Ireno IC, Wiesmüller L, Abdelhay E. BCR-ABL Stimulates Mutagenic Homologous DNA Double-Strand Break Repair *via* the DNA-End-Processing Factor CtIP. *Carcinogenesis* (2011) 32:27–34. doi: 10.1093/carcin/bgq216
18. Slupianek A, Schmutte C, Tombline G, Nieborowska-Skorska M, Hoser G, Nowicki MO, et al. BCR/ABL Regulates Mammalian RecA Homologs, Resulting in Drug Resistance. *Mol Cell* (2001) 8:795–806. doi: 10.1016/S1097-2765(01)00357-4
19. Blanchard Z, Mullins N, Ellipeddi P, Lage JM, McKinney S, El-Etriby R, et al. Geminin Overexpression Promotes Imatinib Sensitive Breast Cancer: A Novel Treatment Approach for Aggressive Breast Cancers, Including a Subset of Triple Negative. *PloS One* (2014) 9:1–18. doi: 10.1371/journal.pone.0095663
20. Kaipio K, Chen P, Roering P, Huhtinen K, Mikkonen P, Östling P, et al. ALDH1A1-Related Stemness in High-Grade Serous Ovarian Cancer is a Negative Prognostic Indicator But Potentially Targetable by EGFR/mTOR-PI3K/aurora Kinase Inhibitors. *J Pathol* (2020) 250:159–69. doi: 10.1002/path.5356
21. Alexandrov LB, Kim J, Haradhvala NJ, Huang MN, Tian Ng AW, Wu Y, et al. The Repertoire of Mutational Signatures in Human Cancer. *Nature* (2020) 578:94–101. doi: 10.1038/s41586-020-1943-3
22. Tumiati M, Hietanen S, Hynninen J, Pietilä E, Färkkilä A, Kaipio K, et al. Precision Medicine and Imaging A Functional Homologous Recombination Assay Predicts Primary Chemotherapy Response and Long-Term Survival in Ovarian Cancer Patients. *Clin Cancer Res* (2018) 24:4482–93. doi: 10.1158/1078-0432.CCR-17-3770
23. Blankenberg D, Chilton J, Coraor N. Galaxy External Display Applications: Closing a Dataflow Interoperability Loop. *Nat Methods* (2020) 17:123–4. doi: 10.1038/s41592-019-0727-x
24. Shannon P, Markiel A, Ozier O, Baliga NS, Wang JT, Ramage D, et al. Cytoscape: A Software Environment for Integrated Models of Biomolecular Interaction Networks. *Genome Res* (2003) 13:2498–504. doi: 10.1101/gr.1239303
25. Schneider CA, Rasband WS, Eliceiri KW. NIH Image to ImageJ: 25 Years of Image Analysis. *Nat Methods* (2012) 9:671–5. doi: 10.1038/nmeth.2089
26. Seluanov A, Mao Z, Gorbunova V. Analysis of DNA Double-Strand Break (DSB) Repair in Mammalian Cells. *J Vis Exp* (2010) (43):e2002. doi: 10.3791/2002
27. Alpay K, Farshchian M, Tuomela J, Sandholm J, Aittokallio K, Siljamäki E, et al. Inhibition of C-Abl Kinase Activity Renders Cancer Cells Highly Sensitive to Mitoxantrone. *PloS One* (2014) 9. doi: 10.1371/journal.pone.0105526
28. Arun B, Akar U, Gutierrez-Barrera AM, Hortobagyi GN, Ozpolat B. The PARP Inhibitor AZD2281 (Olaparib) Induces Autophagy/Mitophagy in BRCA1 and BRCA2 Mutant Breast Cancer Cells. *Int J Oncol* (2015) 47:262–8. doi: 10.3892/ijo.2015.3003
29. Sobhian B, Shao G, Lilli DR, Culhane AC, Moreau LA, Xia B, et al. RAP80 Targets BRCA1 to Specific Ubiquitin Structures at DNA Damage Sites. *Science* (2007) 316:1198–202. doi: 10.1126/science.1139516
30. Rosner M, Schipany K, Hengstschläger M. Merging High-Quality Biochemical Fractionation With a Refined Flow Cytometry Approach to Monitor Nucleocytoplasmic Protein Expression Throughout the Unperturbed Mammalian Cell Cycle. *Nat Protoc* (2013) 8:602–26. doi: 10.1038/nprot.2013.011
31. Sakaue-Sawano A, Kurokawa H, Morimura T, Hanyu A, Hama H, Osawa H, et al. Visualizing Spatiotemporal Dynamics of Multicellular Cell-Cycle Progression. *Cell* (2008) 132:487–98. doi: 10.1016/j.cell.2007.12.033
32. Lheureux S, Cristea MC, Bruce JP, Garg S, Cabanero M, Mantia-Smaldone G, et al. Adavosertib Plus Gemcitabine for Platinum-Resistant or Platinum-Refractory Recurrent Ovarian Cancer: A Double-Blind, Randomised, Placebo-Controlled, Phase 2 Trial. *Lancet* (2021) 397:281–92. doi: 10.1016/S0140-6736(20)32554-X
33. Delgado JL, Hsieh CM, Chan NL, Hiasa H. Topoisomerases as Anticancer Targets. *Biochem J* (2018) 475:373–98. doi: 10.1042/BCJ20160583
34. Evison BJ, Sleebs BE, Watson KG, Phillips DR, Cutts SM. Mitoxantrone, More Than Just Another Topoisomerase II Poison. *Med Res Rev* (2016) 36(2):248–99. doi: 10.1002/med
35. Gourley C, Balmaña J, Ledermann JA, Serra V, Dent R, Loibl S, et al. Moving From Poly (ADP-Ribose) Polymerase Inhibition to Targeting DNA Repair and DNA Damage Response in Cancer Therapy. *J Clin Oncol* (2019) 37:2257–69. doi: 10.1200/JCO.18.02050
36. Konstantinopoulos PA, Ceccaldi R, Shapiro GI, D'andrea AD. Homologous Recombination Deficiency: Exploiting the Fundamental Vulnerability of Ovarian Cancer. *Cancer Discov* (2015) 5:1137–54. doi: 10.1158/2159-8290.CD-15-0714
37. Peng G, Lin CCJ, Mo W, Dai H, Park YY, Kim SM, et al. Genome-Wide Transcriptome Profiling of Homologous Recombination DNA Repair. *Nat Commun* (2014) 5:1–11. doi: 10.1038/ncomms4361
38. Técher H, Koundrioukoff S, Nicolas A, Debatisse M. The Impact of Replication Stress on Replication Dynamics and DNA Damage in Vertebrate Cells. *Nat Rev Genet* (2017) 18:535–50. doi: 10.1038/nrg.2017.46
39. Chen G, Yuan SSF, Liu W, Xu Y, Trujillo K, Song B, et al. Radiation-Induced Assembly of Rad51 and Rad52 Recombination Complex Requires ATM and C-Abl. *J Biol Chem* (1999) 274:12748–52. doi: 10.1074/jbc.274.18.12748

40. Yuan ZM, Huang Y, Ishiko T, Nakada S, Utsugisawa T, Kharbanda S, et al. Regulation of Rad51 Function by C-Abl in Response to DNA Damage. *J Biol Chem* (1998) 273:3799–802. doi: 10.1074/jbc.273.7.3799
41. O'Connor MJ. Targeting the DNA Damage Response in Cancer. *Mol Cell* (2015) 60:547–60. doi: 10.1016/J.MOLCEL.2015.10.040
42. Hietanen S, Lain S, Krausz E, Blattner C, Lane DP. Activation of P53 in Cervical Carcinoma Cells by Small Molecules. *Proc Natl Acad Sci* (2000) 97:8501–6. doi: 10.1073/PNAS.97.15.8501
43. Koivusalo R, Krausz E, Ruotsalainen P, Helenius H, Hietanen S. Chemoradiation of Cervical Cancer Cells: Targeting Human Papillomavirus E6 and P53 Leads to Either Augmented or Attenuated Apoptosis Depending on the Platinum Carrier Ligand 1. *Cancer Res* (2002) 62:7364–71.
44. Zhang M, Li L, Wang Z, Liu H, Hou J, Zhang M, et al. A Role for C-Abl in Cell Senescence and Spontaneous Immortalization. *Age (Omaha)* (2013) 35:1251. doi: 10.1007/S11357-012-9452-4
45. Swisher EM, Sakai W, Karlan BY, Wurz K, Urban N, Taniguchi T. Secondary BRCA1 Mutations in BRCA1-Mutated Ovarian Carcinomas With Platinum Resistance. *Cancer Res* (2008) 68:2581–6. doi: 10.1158/0008-5472.CAN-08-0088
46. Sakai W, Swisher EM, Karlan BY, Agarwal MK, Higgins J, Friedman C, et al. Secondary Mutations as a Mechanism of Cisplatin Resistance in BRCA2-Mutated Cancers. *Nature* (2008) 451:1116–20. doi: 10.1038/nature06633
47. Liu JF, Barry WT, Birrer M, Lee J-M, Buckanovich RJ, Fleming GF, et al. Overall Survival and Updated Progression-Free Survival Outcomes in a Randomized Phase II Study of Combination Cediranib and Olaparib *Versus* Olaparib in Relapsed Platinum-Sensitive Ovarian Cancer. *Evid an early on-therapy biomark response patients Adv melanoma Treat anti-PD-1* (2019) 30:551–7. doi: 10.1093/annonc/mdz018
48. Konstantinopoulos PA, Barry WT, Birrer M, Westin SN, Cadoo KA, Shapiro GI, et al. Olaparib and α-Specific PI3K Inhibitor Alpelisib for Patients With Epithelial Ovarian Cancer: A Dose-Escalation and Dose-Expansion Phase 1b Trial. *Lancet Oncol* (2019) 20:570–80. doi: 10.1016/S1470-2045(18)30905-7
49. Zhou Y, Feng Z, Cao F, Liu X, Xia X, Yu C-H. Abl-Mediated PI3K Activation Regulates Macrophage Podosome Formation. *J Cell Sci* (2020) 133:jcs234385. doi: 10.1242/jcs.234385
50. Kharas MG, Fruman DA. *ABL Oncogenes and Phosphoinositide 3-Kinase: Mechanism of Activation and Downstream Effectors* (2005). Available at: www.aacrjournals.org (Accessed April 15, 2021).
51. Pilié PG, Tang C, Mills GB, Yap TA. State-Of-the-Art Strategies for Targeting the DNA Damage Response in Cancer. *Nat Rev Clin Oncol* (2019) 16:81–104. doi: 10.1038/s41571-018-0114-z
52. Kingwell E, Koch M, Leung B, Isserow S, Geddes J, Rieckmann P, et al. Cardiotoxicity and Other Adverse Events Associated With Mitoxantrone Treatment for MS. *Neurology* (2010) 74:1822–6. doi: 10.1212/WNL.0b013e3181e0f7e6
53. Hochhaus A, Larson RA, Guilhot F, Radich JP, Branford S, Hughes TP, et al. Long-Term Outcomes of Imatinib Treatment for Chronic Myeloid Leukemia. *N Engl J Med* (2017) 376:917–27. doi: 10.1056/NEJMoa1609324

Conflict of Interest: The authors declare that the research was conducted in the absence of any commercial or financial relationships that could be construed as a potential conflict of interest.

Publisher's Note: All claims expressed in this article are solely those of the authors and do not necessarily represent those of their affiliated organizations, or those of the publisher, the editors and the reviewers. Any product that may be evaluated in this article, or claim that may be made by its manufacturer, is not guaranteed or endorsed by the publisher.

frontiers in Oncology

ORIGINAL RESEARCH
published: 19 November 2021
doi: 10.3389/fonc.2021.778925

Early Drug Discovery and Development of Novel Cancer Therapeutics Targeting DNA Polymerase Eta (POLH)

*David M. Wilson 3rd[1,2], Matthew A. J. Duncton[1], Caleb Chang[3], Christie Lee Luo[3], Taxiarchis M. Georgiadis[1], Patricia Pellicena[1], Ashley M. Deacon[1], Yang Gao[3] and Debanu Das[1]**

[1] XPose Therapeutics, Inc., San Carlos, CA, United States, [2] Biomedical Research Institute, Hasselt University, Diepenbeek, Belgium & Boost Scientific, Heusden-Zolder, Belgium, [3] Department of BioSciences, Rice University, Houston, TX, United States

Polymerase eta (or Pol η or POLH) is a specialized DNA polymerase that is able to bypass certain blocking lesions, such as those generated by ultraviolet radiation (UVR) or cisplatin, and is deployed to replication foci for translesion synthesis as part of the DNA damage response (DDR). Inherited defects in the gene encoding POLH (a.k.a., XPV) are associated with the rare, sun-sensitive, cancer-prone disorder, xeroderma pigmentosum, owing to the enzyme's ability to accurately bypass UVR-induced thymine dimers. In standard-of-care cancer therapies involving platinum-based clinical agents, e.g., cisplatin or oxaliplatin, POLH can bypass platinum-DNA adducts, negating benefits of the treatment and enabling drug resistance. POLH inhibition can sensitize cells to platinum-based chemotherapies, and the polymerase has also been implicated in resistance to nucleoside analogs, such as gemcitabine. POLH overexpression has been linked to the development of chemoresistance in several cancers, including lung, ovarian, and bladder. Co-inhibition of POLH and the ATR serine/threonine kinase, another DDR protein, causes synthetic lethality in a range of cancers, reinforcing that POLH is an emerging target for the development of novel oncology therapeutics. Using a fragment-based drug discovery approach in combination with an optimized crystallization screen, we have solved the first X-ray crystal structures of small novel drug-like compounds, i.e., fragments, bound to POLH, as starting points for the design of POLH inhibitors. The intrinsic molecular resolution afforded by the method can be quickly exploited in fragment growth and elaboration as well as analog scoping and scaffold hopping using medicinal and computational chemistry to advance hits to lead. An initial small round of medicinal chemistry has resulted in inhibitors with a range of functional activity in an *in vitro* biochemical assay, leading to the rapid identification of an inhibitor to advance to subsequent rounds of chemistry to generate a lead compound. Importantly, our chemical matter is different from the traditional nucleoside analog-based approaches for targeting DNA polymerases.

Keywords: fragment-based drug discovery (FBDD), structure-based drug discovery (SBDD), X-ray crystallography, cancer therapeutics, DNA damage response (DDR), polymerases, Pol eta, POLH

OPEN ACCESS

Edited by:
Katherine Pawelczak, NERx Biosciences, United States

Reviewed by:
Diana Ainembabazi, Indiana University–Purdue University Indianapolis, United States
Navnath Gavande, Wayne State University, United States

***Correspondence:**
Debanu Das
info@xposetx.com

Specialty section:
This article was submitted to Cancer Molecular Targets and Therapeutics, a section of the journal Frontiers in Oncology

Received: *17 September 2021*
Accepted: *27 October 2021*
Published: *19 November 2021*

Citation:
Wilson DM 3rd, Duncton MAJ, Chang C, Lee Luo C, Georgiadis TM, Pellicena P, Deacon AM, Gao Y and Das D (2021) Early Drug Discovery and Development of Novel Cancer Therapeutics Targeting DNA Polymerase Eta (POLH). Front. Oncol. 11:778925. doi: 10.3389/fonc.2021.778925

INTRODUCTION

Cancer will directly affect the lives of over one-third of the population, with the process of carcinogenesis involving (at least) six biological phenomenon/hallmarks (1): sustaining proliferative signaling, evading growth suppressors, resisting cell death, enabling replicative immortality, inducing angiogenesis, and activating invasion and metastasis. Many of these hallmarks, if not all, can be fostered by genomic instability that arises due to excessive DNA damage or defects in DNA damage response (DDR) components. The upregulation of certain DDR pathways is also a compensatory mechanism employed by cancer cells to adapt to the elevated background levels of DNA damage imparted by their rapid cell division and increased metabolism (2) or to survive treatment-related DNA-damaging agents, like certain forms of chemotherapy and radiotherapy (3, 4). The recognition that these intrinsic changes in the DDR (i.e., sporadic inactivation or upregulation) offer therapeutic opportunities has led to advances in cancer treatment efficacy. Most notably, the discovery that homologous recombination repair (HRR)-defective breast and ovarian cancers are uniquely sensitive to poly (ADP-ribose) polymerase (PARP) inhibitors *via* a mechanism broadly referred to as synthetic lethality (SL) has led to improved drug design/application and better outcomes for many of these cancer-affected individuals (5). Thus, further development of DDR inhibitors to combat both intrinsic and acquired drug resistance presents an enormous therapeutic opportunity that could widen the repertoire of initial treatment options and re-sensitize cells to therapies that have failed due to upregulation of DDR pathways. Two primary therapeutic approaches involving DDR targeting could include: combinatorial treatments that involve anticancer genotoxic agents and SL, a phenomenon that as mentioned above exploits a sporadic DDR defect to achieve cancer-specific cell death. Here, we provide results on our early drug discovery efforts around the identification and development of novel inhibitors targeting human DNA polymerase eta (Pol η or POLH).

DDR is an intricate system involving damage recognition, cell cycle regulation, DNA repair, and cell fate determination, playing a significant role in cancer etiology and therapy. POLH, a.k.a., xeroderma pigmentosum variant (XPV) protein, is a translesion DNA polymerase that is a member of the Y family of polymerases (6, 7). The enzyme exhibits low fidelity on undamaged DNA, yet accurately copies ultraviolet (UV) light-induced dithymine cyclobutane pyrimidine dimers (CPDs) by inserting A-A opposite the lesion. In addition to UV-induced DNA damage, POLH has been shown to bypass cisplatin adducts, as well as oxaliplatin adducts (8–14). Additional studies suggest that POLH may also play an important role in oxidative stress resistance, likely by carrying out translesion synthesis (TLS) (15, 16) of bulky oxidative base lesions, such as cyclopurines (17–19).

Consistent with the known biochemistry, elevated POLH expression correlates with reduced cisplatin sensitivity in models of lung and bladder cancer (8). Strategic downregulation of POLH in these cases re-sensitizes cancer cells to cisplatin treatment, supporting targeting of the polymerase in certain situations of acquired drug resistance. Suppression of POLH expression also enhances cisplatin-induced apoptosis of cancer stem cells isolated from both ovarian cancer cell lines and primary tumors (10). Furthermore, studies indicate that POLH is a predictive factor of treatment response and survival of metastatic gastric adenocarcinoma patients receiving oxaliplatin-based first-line chemotherapy (20). In addition to its well-established role in platin drug resistance, preclinical studies indicate that POLH-deficient cells are 3-fold more sensitive to the nucleoside analogs β-D-arabinofuranosylcytosine and gemcitabine, and even more sensitive (10-fold) to gemcitabine/cisplatin combination treatment (21), a commonly used clinical regimen for treating a wide spectrum of cancers, including bladder, pancreatic, ovarian, cervical, and non-small cell lung. Additional investigations have revealed that co-inhibition of POLH and ATR, a protein central to the replicative stress response, offers a SL approach for the treatment of a range of cancer types (22, 23). Notably, ATR inhibitors are progressing well in the clinic (24, 25), and ATR haploinsufficiency, arising due to somatic mutations in one allele, is frequent in certain cancers (26), presenting therapeutic opportunities for POLH inhibition. Despite the promise of targeting POLH in anticancer therapies, clinical inhibitors have yet to be developed.

It is worth emphasizing that polymerases are validated targets in several clinical paradigms. For example, one of the most important polymerases against which medicines have been made is the DNA polymerase of HIV-1 (i.e., the reverse transcriptase, RT), the main target of antiretroviral therapies involving both nucleotide and non-nucleotide inhibitors (NRTIs and NNRTIs). In this context, it is intriguing that POLH has also been recently found to be a human RT, although the precise biological role of this biochemical function is still unclear (27). Other examples include the development of inhibitors against viral RNA polymerases (RdRp), such as the drug remdesivir (28), which was first developed as an Ebola Virus RdRp inhibitor (29) and is now being pursued in SARS-CoV-2 (30), as well as the clinically-approved anti-Hepatitis C NSB5 polymerase drug sofosbuvir (31). In addition to PARP (see above), POLQ (DNA polymerase theta), an enzyme involved in double strand break repair, is another DDR polymerase of current interest in the design of new oncology therapeutics (32), including in a SL paradigm involving BRCA1/2 mutations.

With the value in targeting DNA polymerases in general and POLH in particular, specifically in the context of new oncology therapeutics, it is not surprising that some attempts have been made in this direction. Previous work on developing POLH inhibitors focused on compounds derived from N-aryl-substituted indole barbituric acid (IBA), indole thiobarbituric acid (ITBA), and indole quinuclidine scaffolds (9, 33), which are predicted to interfere with template DNA orientation. However, these compounds have yet to advance further, and our assessment based on information available is that could be due to: (i) precise target engagement/hit validation is unknown due to absence of crystal structures, preventing further interaction-based optimization, and/or (ii) suitability of these compounds for further chemistry tractability/optimization.

To overcome the bottleneck of lack of information regarding target engagement of an identified inhibitor, our approach integrates ABS-OneStep (Accelero Biostructures, CA), a fragment-based drug discovery (FBDD) approach that uses high-throughput X-ray crystallographic screening of small molecule fragment libraries for hit generation (34). This strategy, coupled with iterative structure-guided optimization/structure-based drug discovery (SBDD), facilitates the rational development of novel therapeutics, namely small molecule inhibitors or target ligands in a targeted protein degradation approach involving a proteolysis-targeting chimera. Here, we report on the first high resolution crystal structures of POLH bound to distinct fragments that reveal direct target engagement, binding site, binding pose and protein-ligand interactions; and describe functional activity of our hits.

MATERIALS AND METHODS

Protein Expression and Purification

Wild-type human POLH (residues 1–432) was cloned into a modified pET28p vector with a N-terminal 6-histidine tag and a PreScission Protease cleavage site. For protein expression, this POLH plasmid was transformed into BL21 DE3 *E. coli* cells. When the optical density of the *E. coli* cells reached 0.8, isopropyl ß-D-1-thiogalactopyranoside (IPTG) was added to a final concentration of 1 μM IPTG. After 20 hrs (16°C) of induction, the cell paste was collected *via* centrifugation and resuspended in a buffer that contained 20 mM Tris (pH 7.5), 1 M NaCl, 20 mM imidazole, and 5 mM ß-mercaptoethanol (BME). After sonication, POLH was loaded onto a HisTrap HP column (GE Healthcare), which was pre-equilibrated with a buffer that contained 20 mM Tris (pH 7.5), 1 M NaCl, 20 mM imidazole, and 5 mM BME. The column was washed with 300 mL of buffer to remove nonspecific bound proteins and was eluted with buffer that contained 20 mM Tris (pH 7.5), 1 M NaCl, 300 mM imidazole, and 3 mM dithiothreitol (DTT). The eluted POLH was incubated with PreScission Protease to cleave the N-terminal 6-histidine-tag. Subsequently, POLH was buffer-exchanged and desalted to 20 mM 2-(N-morpholino)ethanesulfonic acid (MES) (pH 6.0), 250 mM KCl, 10% glycerol, 0.1 mM ethylenediaminetetraacetic acid (EDTA), and 3 mM DTT and was loaded onto a MonoS 10/100 column (GE Healthcare). Protein was eluted with an increasing salt (KCl) gradient. Finally, POLH was purified with a Superdex 200 10/300 GL column (GE Healthcare) with a buffer that contained 20 mM Tris (pH 7.5), 450 mM KCl, and 3 mM DTT.

Hit Generation by High-Throughput X-Ray Crystallography-Based Screening of Fragment Library

Hit generation by screening a diverse fragment library and the crystal structures of their binding sites in a single step was performed by using the ABS-OneStep platform (Accelero Biostructures, CA) (34). Briefly, crystals of the apo binary POLH-DNA complex were reproduced (18) and the crystallization optimized to generate several hundred crystals of relatively uniform quality for library screening directly by ultra-high throughput X-ray crystallography. Approximately 300 crystals of the POLH-DNA complex were then used to screen the ABS-Real300 (Accelero Biostructures) 300-fragment library, one fragment at a time. A total of approximately 300 individual X-ray diffraction data sets were collected at SSRL on beamline 9-2 using the BLU-ICE (35) data collection environment. The data sets were collected at 100 K, using a Pilatus 6M detector (Dectris). The data were processed with data processing and structure determination pipelines within the ABS-OneStep platform using XDS (36) and CCP4 (37), with structure determination performed by molecular replacement using our 1.5Å resolution apo POLH-DNA binary complex as the search template.

DNA Synthesis Assay for Screening Inhibitors

POLH biochemical assays testing nucleotide incorporation activity were performed as previously described (38). The reaction mixture contained 3 nM POLH, 200 nM DNA, 50 μM dNTP, 150 mM KCl, 45 mM Tris (pH 7.5), 5 mM $MgCl_2$, 10 mM DTT, 0.1 mg/mL bovine serum albumin, 5% glycerol, and 10% DMSO, and 0.01-20 mM inhibitory compound. Initial tests and next phase assays were executed using DNA template (5'-GAG TCA TGT TTA CGC TAG GCA C-3') and 5'-fluorescein-labeled primer (5'-GTGCCTAGCGTAA-3'). Reactions were conducted at 37°C for 5 min and were stopped by adding formamide quench buffer to the final concentrations of 40% formamide, 50 mM EDTA (pH 8.0), 0.1 mg/ml xylene cyanol, and 0.1 mg/ml bromophenol. After heating to 97°C for 5 min and immediately placing it on ice, reaction products were resolved on 22.5% polyacrylamide urea gels. The gels were visualized by a Sapphire Biomolecular Imager and quantified using the built-in software. Visual representation of the acquired data was rendered in Graph Prism. For the initial inhibitor tests, each compound was assayed for any inhibitory effect on POLH nucleotide incorporation activity at different concentrations (0.01, 0.1, and 1 mM for the first batch and 0.2, 2, and 20 mM for a second batch). The gels were visualized and quantified by a Sapphire Biomolecular Imager using the built-in software.

For the compounds that exhibited signs of inhibition, each compound was serially diluted and added to a reaction mixture to a final concentration of 0.01- 20 mM. The reaction mixture contained 3 nM POLH, 200 nM DNA, 50 μM dATP, 150 mM KCl, 45 mM Tris (pH 7.5), 5 mM $MgCl_2$, 10 mM DTT, 0.1 mg/mL bovine serum albumin, 5% glycerol, and 10% DMSO. Assays were performed and examined similarly as in the initial test. Quantification of IC50 and fitting was executed by Graph Prism.

RESULTS

Determination of Apo POLH-DNA Binary Complex Crystal Structure

Crystals of the apo binary POLH-DNA complex were reproduced (18), and we generated several hundred crystals of

relatively uniform quality for library screening directly by ultra-high throughput X-ray crystallography (see below). During the optimization process, we obtained the highest resolution crystal structure of a POLH-DNA binary complex to date, at 1.5Å resolution, which was refined to a crystallographic R/R_{free} of 13.0/19.0% (**Figure 1**). This structure revealed details of water-mediated interactions in the binary complex that we can utilize for our structure-guided inhibitor optimization (**Figure 2**), and provided us with a very high resolution binary complex structure to use as our template for crystal structure determination by molecular replacement of fragment-bound crystal structures.

Fragment Hit Generation and Hit Elaboration for Hit-to-Lead Development

Hit identification was achieved in a single step using ABS-OneStep, which combines fragment-based screening with X-ray crystallography. Using approximately 300 crystals of the POLH-DNA binary complex and screening a diverse, unbiased, 300-fragment library, one fragment at a time, produced four hits, resulting in a hit rate of 1.3%. A total of approximately 300 individual X-ray diffraction data sets were collected, processed, and crystal structures determined. All crystallographic data sets were approximately in the ~1.7-2.2 Å resolution range with reasonable crystallographic R/R_{free} values. A screening schematic for hit generation and a representative hit (XPTx-0267) from a 1.7 Å crystal structure is shown in a partial view interacting with POLH (**Figure 3**). Due to intellectual property considerations, high resolution details of compound engagement with POLH or specifics of the fragment growth cannot be shown at this time.

Inhibitor Validation by Biochemical Assays

Fragment hits from the screen were subjected to fragment growth strategies, such as alternating the functional groups, analog growth, and scaffold hopping, by our in-house medicinal chemistry team. An initial limited iteration of fragment elaboration led to the selection of 40 compounds for testing in an *in vitro* nucleotide incorporation (POLH) biochemical assay as previously described (38). The assay was performed in two steps: an initial pass at detecting functional activity at either 0.01, 0.1, and 1 mM of the compound; or 0.2, 2, and 20 mM for a second batch of the compounds (**Figure 4**), followed by a more detailed pass at different compound concentrations to determine IC50 and Hill slopes. About 15 of the 40 compounds subjected to the first step were advanced to the second step for detailed measurements (**Figure 5**). In these follow-up studies, we obtained one compound with a submillimolar IC50 (230 μM), about eight compounds with IC50 ~1-5 mM, and one compound with an IC50 of ~8 mM; all had Hill slopes of ~0.8-2.4. Having in hand a set of compounds displaying varied inhibition levels provides alternative starting points and/or development paths. Based on the initial profiling, our approach quickly led to the identification of our lead compound, XPTx-0289, with an IC50 of 230 μM (**Figure 6**), with additional backup compounds also being identified.

DISCUSSION

FBDD holds immense promise in the development of target-specific novel and active chemical matter, as demonstrated by the advancement of several medicines to the clinic. Our FBDD strategy has quickly produced functional compounds from weak hits identified in our initial library screens, irrespective of where the compounds were on the potency spectrum from weak to strong. Indeed, we have shown for two of our targets, POLH (herein) and apurinic/apyrimidinic endonuclease 1

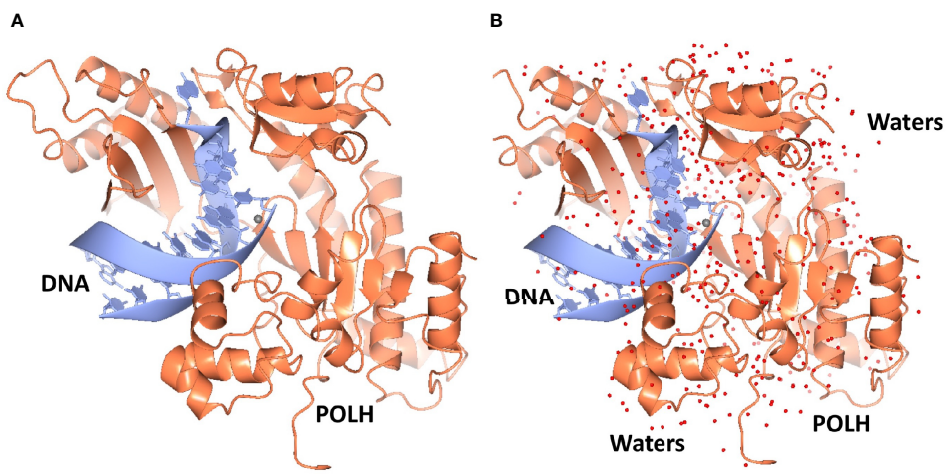

FIGURE 1 | **(A)** Ribbon representation of the highest resolution 1.5Å crystal structure of the POLH-DNA binary complex. **(B)** Determination of water structure (red spheres) revealing details of water-mediated interactions, to aid structure-based drug discovery efforts on POLH.

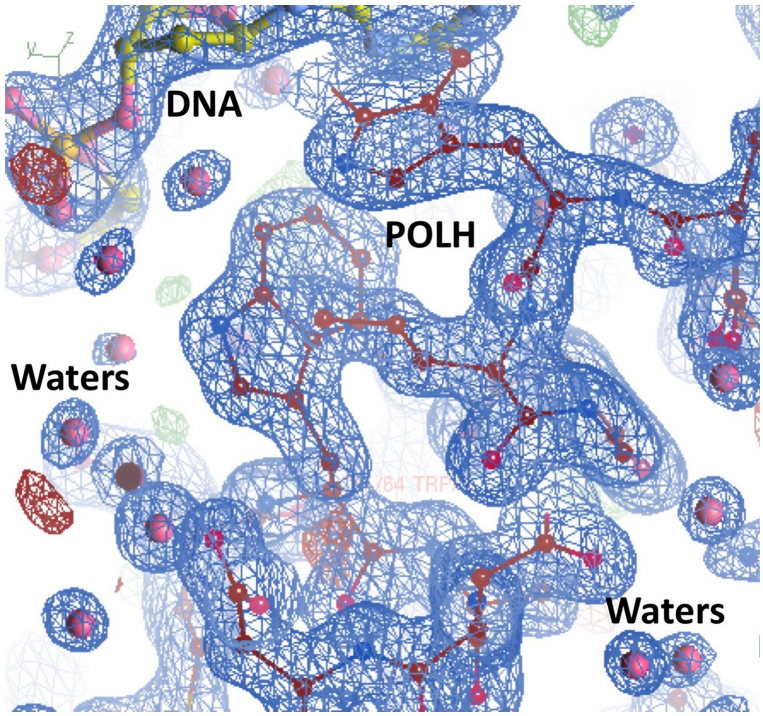

FIGURE 2 | Highest resolution 1.5Å crystal structure of the POLH-DNA binary complex with R/R_{free} 13.0/19.0% in a 2fo-fc electron density map at 1.0σ map contour, revealing details of water-mediated interactions, in aid of our structure-based drug discovery efforts on POLH.

(APE1; see more below), where biochemical assays could not detect functional activity of the original fragments, that from a single/initial round of fragment growth and expansion, we can rapidly facilitate hit-to-lead conversion using just the empirical knowledge intrinsic to the crystal structures. While library screening by biophysical assays like SPR (Surface Plasmon Resonance) and NMR (Nuclear Magnetic Resonance) are better than biochemical assays at detecting protein-fragment interactions during library screening, they do not provide information on binding site, binding pose, or protein-ligand interactions. Biophysical assays also do not separate hits into orthosteric or allosteric site binders or reveal potentially new binding hotspots. By integrating a method with the widest detection range (i.e., X-ray crystallography), the FBDD approach allows one not to miss relevant chemical matter during screening and facilitates rapid hit-to-lead optimization efforts *via* a structure-guided approach.

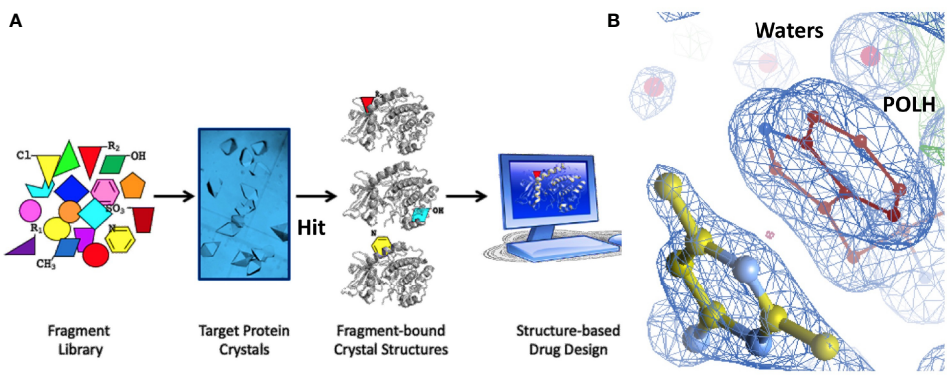

FIGURE 3 | **(A)** Schematic of our approach to hit generation by screening fragment libraries directly by X-ray crystallography in a primary screen. **(B)** 1.7Å crystal structure of a POLH-DNA-Hit ternary complex with R/R_{free} 16.7/20.7% in a 2fo-fc electron density map at 1. 5σ map contour.

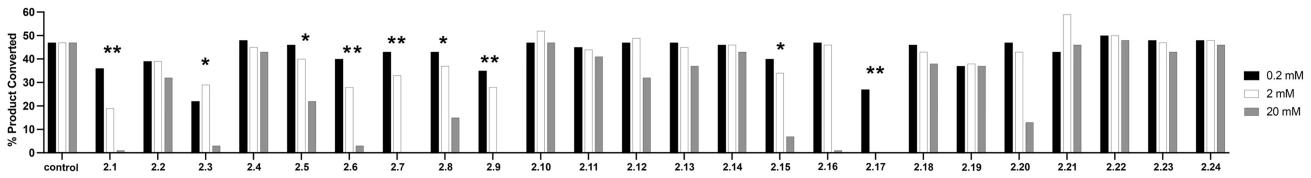

FIGURE 4 | Initial pass at detecting functional activity in an *in vitro* assay for DNA synthesis. ** Represents compounds that had a 20% drop in product conversion at both 20 mM and 2 mM, * represents compounds that had a 20% drop in product conversion at only 20 mM.

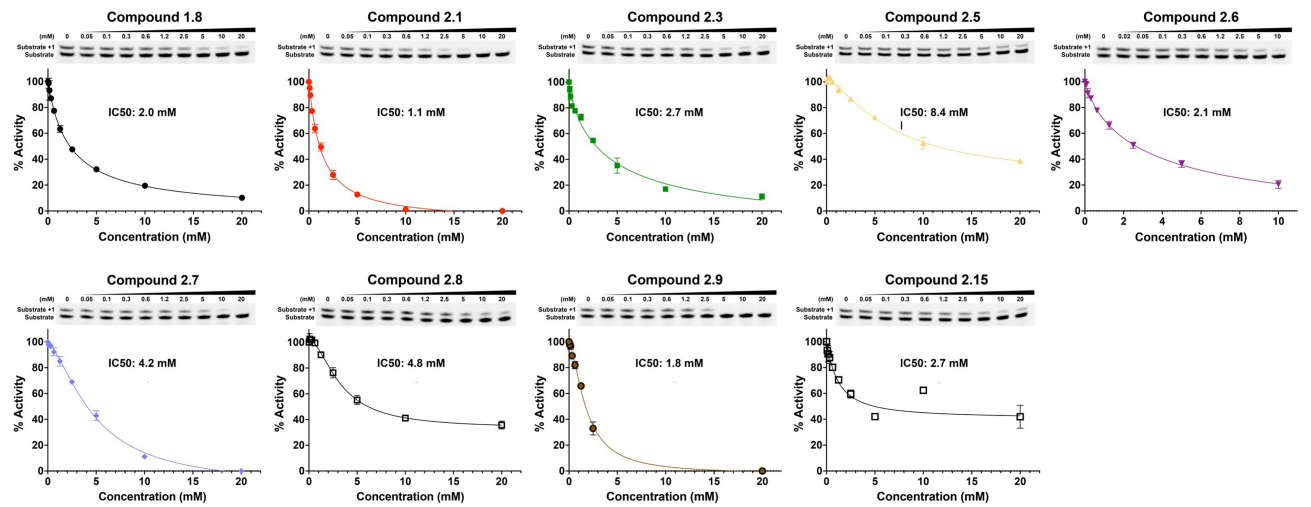

FIGURE 5 | IC50 determination for some representative compounds an *in vitro* assay for DNA synthesis.

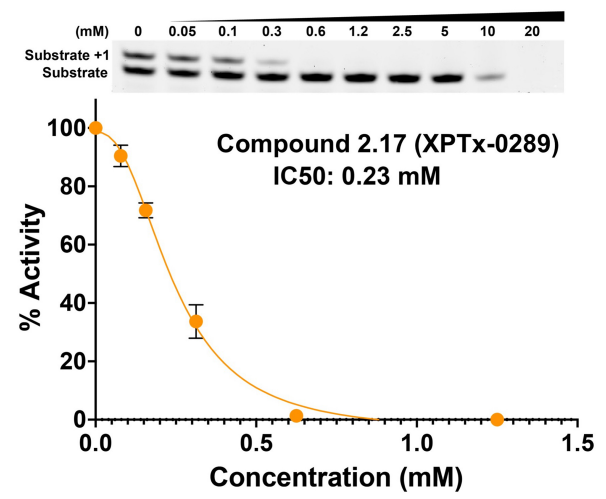

FIGURE 6 | Concentration-dependent inhibition of DNA synthesis by compound XPTx-0289.

While the measured potencies for XPTx-0289 (IC50 230 μM) and XPTx-0267 (2 mM) may appear low, such values, and even weaker, are typical for starting hits in FBDD projects. For instance, recent examples of programs successfully advancing fragments with initial low potencies (>2 mM Kd or IC50) include inhibitors against Cyclophilin D (39), Mycobacterium tuberculosis InhA (40), and WDR5-Myc (41). For our DDR target APE1, we now have in hand a lead inhibitor with a Ki of 350 nM (IC50 ~500 nM) after a single round of fragment expansions encompassing ~200 compounds based on the starting hit from a similar crystallography-based primary screen using ABS-OneStep (34). Notably, in our APE1 effort, the original fragment hit had undetectable activity as an inhibitor of APE1 AP site cleavage activity in a standard biochemical assay. The rapid advancement of an initial hit to significantly improved congener inhibitors demonstrates the power of our platform to rapidly execute hit-to-lead campaigns for the development of target-specific inhibitors. Indeed, XPTx-0289 is now ready to advance to lead generation in a hit-to-lead campaign, in conjunction with cellular TLS and co-inhibition assays.

DATA AVAILABILITY STATEMENT

The datasets presented in this article are not readily available because of intellectual property considerations. Requests to access the datasets should be directed to info@xposetx.com.

AUTHOR CONTRIBUTIONS

DD and AD contributed POLH-DNA binary complex crystallization, library screening for hit generation and X-ray crystallography, and structure analyses. MD and TG contributed to hit expansions and fragment elaborations. CC, CL, and YG contributed to POLH protein and binary complex production, and biochemical assays. DD, AD, MD, PP, DW, TG, CC, and YG contributed to the interpretation of results and critical review of the manuscript. DW, DD, CC, and YG contributed to writing the manuscript. All authors contributed to the article and approved the submitted version.

FUNDING

Research included in this publication was supported by the National Center For Advancing Translational Sciences of the NIH under Award Number R43 TR001736, and the National Institute of General Medical Sciences of the NIH under Award Number R44 GM132796, to Accelero Biostructures Inc.; National Cancer Institute of the NIH under Award Number R43 CA254552 to XPose Therapeutics, Inc.; and Cancer Prevention & Research Institute of Texas (CPRIT) Award RR190046 and Welch Foundation Grant Number C-2033-20200401 to YG. CC was supported by a fellowship from the Houston Area Molecular Biophysics Program (NIH Grant No. T32 GM008280, Program Director Dr. Theodore Wensel).

ACKNOWLEDGMENTS

Synchrotron X-ray diffraction data collection and data processing was performed by Accelero Biostructures, Inc., California. Synchrotron data was collected at Stanford Synchrotron Radiation Lightsource (SSRL), SLAC National Accelerator Laboratory, Menlo Park, California. Use of the Stanford Synchrotron Radiation Lightsource (SSRL), SLAC National Accelerator Laboratory, is supported by the U.S. Department of Energy, Office of Science, Office of Basic Energy Sciences under Contract No. DE-AC02-76SF00515. The SSRL Structural Molecular Biology Program is supported by the DOE Office of Biological and Environmental Research, and by the National Institutes of Health, National Institute of General Medical Sciences (P41 GM103393). The contents of this publication are solely the responsibility of the authors and do not necessarily represent the official views of NIGMS or NIH.

REFERENCES

1. Hanahan D, Weinberg RA. Hallmarks of Cancer: The Next Generation. *Cell* (2011) 144(5):646–745. doi: 10.1016/j.cell.2011.02.013
2. O'Connor MJ. Targeting the DNA Damage Response in Cancer. *Mol Cell* (2015) 60(4):547–60. doi: 10.1016/j.molcel.2015.10.040
3. Madhusudan S, Hickson ID. DNA Repair Inhibition: A Selective Tumour Targeting Strategy. *Trends Mol Med* (2005) 11(11):503–11. doi: 10.1016/j.molmed.2005.09.004
4. Helleday T, Petermann E, Lundin C, Hodgson B, Sharma RA. DNA Repair Pathways as Targets for Cancer Therapy. *Nat Rev Cancer* (2008) 8(3):193–204. doi: 10.1038/nrc2342
5. Slade D. PARP and PARG Inhibitors in Cancer Treatment. *Genes Dev* (2020) 34(5-6):360–94. doi: 10.1101/gad.334516.119
6. Saha P, Mandal T, Talukdar AD, Kumar D, Kumar S, Tripathi SP, et al. DNA Polymerase Eta: A Potential Pharmacological Target for Cancer Therapy. *J Cell Physiol* (2020) 236:4106–20. doi: 10.1002/jcp.30155
7. Yang W. An Overview of Y-Family DNA Polymerases and a Case Study of Human DNA Polymerase η. *Biochemistry* (2014) 53(17):2793–803. doi: 10.1021/bi500019s
8. Zhang J, Sun W, Ren C, Kong X, Yan W, Chen X. A PolH Transcript With a Short 3'utr Enhances PolH Expression and Mediates Cisplatin Resistance. *Cancer Res* (2019) 79(14):3714–245. doi: 10.1158/0008-5472.CAN-18-3928
9. Zafar MK, Maddukuri L, Ketkar A, Penthala NR, Reed MR, Eddy S, et al. A Small-Molecule Inhibitor of Human DNA Polymerase η Potentiates the Effects of Cisplatin in Tumor Cells. *Biochemistry* (2018) 57(7):1262–73. doi: 10.1021/acs.biochem.7b01176
10. Srivastava AK, Han C, Zhao R, Cui T, Dai Y, Mao C, et al. Enhanced Expression of DNA Polymerase Eta Contributes to Cisplatin Resistance of Ovarian Cancer Stem Cells. *Proc Natl Acad Sci USA* (2015) 112(14):4411–6. doi: 10.1073/pnas.1421365112
11. Alt A, Lammens K, Chiocchini C, Lammens A, Carsten Pieck J, Kuch D, et al. Bypass of DNA Lesions Generated During Anticancer Treatment With Cisplatin by DNA Polymerase Eta. *Science* (2007) 318(5852):967–70. doi: 10.1126/science.1148242
12. Albertella MR, Green CM, Lehmann AR, O'Connor MJ. A Role for Polymerase Eta in the Cellular Tolerance to Cisplatin-Induced Damage. *Cancer Res* (2005) 65(21):9799–98065. doi: 10.1158/0008-5472.CAN-05-1095
13. Bassett E, King NM, Bryant MF, Hector S, Pendyala L, Chaney SG, et al. The Role of DNA Polymerase Eta in Translesion Synthesis Past Platinum-DNA Adducts in Human Fibroblasts. *Cancer Res* (2004) 64(18):6469–75. doi: 10.1158/0008-5472.CAN-04-1328
14. Vaisman A, Masutani C, Hanaoka F, Chaney SG. Efficient Translesion Replication Past Oxaliplatin and Cisplatin GpG Adducts by Human DNA Polymerase Eta. *Biochemistry* (2000) 39(16):4575–805. doi: 10.1021/bi000130k
15. Wilkinson NA, Mnuskin KS, Ashton NW, Woodgate R. Ubiquitin and Ubiquitin-Like Proteins Are Essential Regulators of DNA Damage Bypass. *Cancers* (2020) 12(10):2848. doi: 10.3390/cancers12102848
16. Yang W, Gao Y. Translesion and Repair DNA Polymerases: Diverse Structure and Mechanism. *Annu Rev Biochem* (2018) 87:239–61. doi: 10.1146/annurev-biochem-062917-012405
17. Yao R, Shi L, Wu C, Qiao W, Liu L, Wu J. Lsm12 Mediates Deubiquitination of DNA Polymerase η To Help Saccharomyces Cerevisiae Resist Oxidative Stress. *Appl Environ Microbiol* (2019) 85(1):e01988–18. doi: 10.1128/AEM.01988-18
18. Weng PJ, Gao Y, Gregory MT, Wang P, Wang Y, Yang W. Bypassing a 8,5'-Cyclo-2'-Deoxyadenosine Lesion by Human DNA Polymerase η at Atomic Resolution. *Proc Natl Acad Sci USA* (2018) 115(42):10660–655. doi: 10.1073/pnas.1812856115
19. Kuraoka I, Robins P, Masutani C, Hanaoka F, Gasparutto D, Cadet J, et al. Oxygen Free Radical Damage to DNA. Translesion Synthesis by Human DNA Polymerase Eta and Resistance to Exonuclease Action at Cyclopurine

Deoxynucleoside Residues. *J Biol Chem* (2001) 276(52):49283–88. doi: 10.1074/jbc.M107779200
20. Teng KY, Qiu MZ, Li ZH, Luo HY, Zeng ZL, Luo RZ, et al. DNA Polymerase η Protein Expression Predicts Treatment Response and Survival of Metastatic Gastric Adenocarcinoma Patients Treated With Oxaliplatin-Based Chemotherapy. *J Trans Med* (2010) 8:126. doi: 10.1186/1479-5876-8-126
21. Zhou W, Chen YW, Liu X, Chu P, Loria S, Wang Y, et al. Expression of DNA Translesion Synthesis Polymerase η in Head and Neck Squamous Cell Cancer Predicts Resistance to Gemcitabine and Cisplatin-Based Chemotherapy. *PLoS One* (2013) 8(12):e83978. doi: 10.1371/journal.pone.0083978
22. Barnes RP, Tsao WC, Moldovan GL, Eckert KA. DNA Polymerase Eta Prevents Tumor Cell-Cycle Arrest and Cell Death During Recovery From Replication Stress. *Cancer Res* (2018) 78(23):6549–605. doi: 10.1158/0008-5472.CAN-17-3931
23. Li XQ, Ren J, Chen P, Chen YJ, Wu M, Yan Wu, et al. Co-Inhibition of Pol η and ATR Sensitizes Cisplatin-Resistant Non-Small Cell Lung Cancer Cells to Cisplatin by Impeding DNA Damage Repair. *Acta Pharmacologica Sin* (2018) 39(8):1359–72. doi: 10.1038/aps.2017.187
24. Gorecki L, Andrs M, Korabecny J. Clinical Candidates Targeting the ATR-CHK1-WEE1 Axis in Cancer. *Cancers* (2021) 13(4):795. doi: 10.3390/cancers13040795
25. Barnieh FM, Loadman PM, Falconer RA. Progress Towards a Clinically-Successful ATR Inhibitor for Cancer Therapy. *Curr Res Pharmacol Drug Discov* (2021) 2:100017. doi: 10.1016/j.crphar.2021.100017
26. Menoyo A, Alazzouzi H, Espín E, Armengol M, Yamamoto H, Schwartz S Jr. Somatic Mutations in the DNA Damage-Response Genes ATR and CHK1 in Sporadic Stomach Tumors With Microsatellite Instability. *Cancer Res* (2001) 61(21):7727–30.
27. Su Y, Ghodke PP, Egli M, Li L, Wang Y, Guengerich FP. Human DNA Polymerase η Has Reverse Transcriptase Activity in Cellular Environments. *J Biol Chem* (2019) 294(15):6073–815. doi: 10.1074/jbc.RA119.007925
28. Yin W, Mao C, Luan X, Shen DD, Shen Q, Su X, et al. Structural Basis for Inhibition of the RNA-Dependent RNA Polymerase From SARS-CoV-2 by Remdesivir. *Science* (2020) 368(6498):1499–504. doi: 10.1126/science.abc1560
29. Tchesnokov EP, Feng JY, Porter DP, Götte M. Mechanism of Inhibition of Ebola Virus RNA-Dependent RNA Polymerase by Remdesivir. *Viruses* (2019) 11(4). doi: 10.3390/v11040326
30. Chien M, Anderson TK, Jockusch S, Tao C, Li X, Kumar S, et al. Nucleotide Analogues as Inhibitors of SARS-CoV-2 Polymerase, A Key Drug Target for COVID-19. *J Proteome Res* (2020) 19:4690–7. doi: 10.1021/acs.jproteome.0c00392
31. Lawitz E, Jacobson IM, Nelson DR, Zeuzem S, Sulkowski MS, Esteban R, et al. Development of Sofosbuvir for the Treatment of Hepatitis C Virus Infection. *Ann NY Acad Sci* (2015) 1358:56–67. doi: 10.1111/nyas.12832
32. Schrempf A, Slyskova J, Loizou JI. Targeting the DNA Repair Enzyme Polymerase θ in Cancer Therapy. *Trends Cancer Res* (2021) 7(2):98–1115. doi: 10.1016/j.trecan.2020.09.007
33. Coggins GE, Maddukuri L, Penthala NR, Hartman JH, Eddy S, Ketkar A, et al. N-Aroyl Indole Thiobarbituric Acids as Inhibitors of DNA Repair and Replication Stress Response Polymerases. *ACS Chem Biol* (2013) 8(8):1722–9. doi: 10.1021/cb400305r
34. Wilson DM3rd, Deacon AM, Duncton MAJ, Pellicena P, Georgiadis MM, Yeh AP, et al. Fragment- and Structure-Based Drug Discovery for Developing Therapeutic Agents Targeting the DNA Damage Response. *Prog Biophysics Mol Biol* (2020) 163:130–42. doi: 10.1016/j.pbiomolbio.2020.10.005
35. McPhillips TM, McPhillips SE, Chiu HJ, Cohen AE, Deacon AM, Ellis PJ, et al. Blu-Ice and the Distributed Control System: Software for Data Acquisition and Instrument Control at Macromolecular Crystallography Beamlines. *J Synchrotron Radiat* (2002) 9(Pt 6):401–6. doi: 10.1107/S0909049502015170
36. Kabsch W. XDS. *Acta Crystallographica Section D Biol Crystallogr* (2010) 66 (Pt 2):125–32. doi: 10.1107/S0907444909047337
37. Winn MD, Ballard CC, Cowtan KD, Dodson EJ, Emsley P, Evans PR, et al. Overview of the CCP4 Suite and Current Developments. *Acta Crystallographica Section D Biol Crystallogr* (2011) 67(Pt 4):235–42. doi: 10.1107/S0907444910045749
38. Samara NL, Gao Y, Wu J, Yang W. Detection of Reaction Intermediates in Mg^{2+}-Dependent DNA Synthesis and RNA Degradation by Time-Resolved X-Ray Crystallography. *Methods Enzymology* (2017) 592:283–327. doi: 10.1016/bs.mie.2017.03.022
39. Grädler U, Schwarz D, Blaesse M, Leuthner B, Johnson TL, Bernard F, et al. Discovery of Novel Cyclophilin D Inhibitors Starting From Three Dimensional Fragments With Millimolar Potencies. *Bioorganic Medicinal Chem Lett* (2019) 29(23):126717. doi: 10.1016/j.bmcl.2019.126717
40. Sabbah M, Mendes V, Vistal RG, Dias DMG, Záhorszká M, Mikušová K, et al. Fragment-Based Design of Mycobacterium Tuberculosis InhA Inhibitors. *J Medicinal Chem* (2020) 63(9):4749–61. doi: 10.1021/acs.jmedchem.0c00007
41. Chacón Simon S, Wang F, Thomas LR, Phan J, Zhao B, Olejniczak ET, et al. Discovery of WD Repeat-Containing Protein 5 (WDR5)-MYC Inhibitors Using Fragment-Based Methods and Structure-Based Design. *J Medicinal Chem* (2020) 63(8):4315–33. doi: 10.1021/acs.jmedchem.0c00224

Conflict of Interest: Authors DW, MD, TG, PP, AD and DD receive compensation, including stock-based awards from XPose Therapeutics, Inc.

The remaining authors declare that the research was conducted in the absence of any commercial or financial relationships that could be construed as a potential conflict of interest.

The authors declare that this study received funding from XPose Therapeutics, Inc. and Accelero Biostructures, Inc. The funders had the following involvement in the study: study design, data collection and analysis, decision to publish, or preparation of the manuscript.

Publisher's Note: All claims expressed in this article are solely those of the authors and do not necessarily represent those of their affiliated organizations, or those of the publisher, the editors and the reviewers. Any product that may be evaluated in this article, or claim that may be made by its manufacturer, is not guaranteed or endorsed by the publisher.

frontiers in Oncology

ORIGINAL RESEARCH
published: 23 December 2021
doi: 10.3389/fonc.2021.772920

Nano-Delivery of a Novel Inhibitor of Polynucleotide Kinase/Phosphatase (PNKP) for Targeted Sensitization of Colorectal Cancer to Radiation-Induced DNA Damage

Sams M. A. Sadat[1], Melinda Wuest[2], Igor M. Paiva[1], Sirazum Munira[1], Nasim Sarrami[1], Forughalsadat Sanaee[1], Xiaoyan Yang[2], Marco Paladino[3], Ziyad Binkhathlan[1,4], Feridoun Karimi-Busheri[2], Gary R. Martin[5], Frank R. Jirik[5,6], David Murray[2], Armin M. Gamper[2], Dennis G. Hall[3], Michael Weinfeld[2] and Afsaneh Lavasanifar[1,7]**

[1] Faculty of Pharmacy and Pharmaceutical Sciences, University of Alberta, Edmonton, AB, Canada, [2] Department of Oncology, Cross Cancer Institute, Faculty of Medicine and Dentistry, University of Alberta, Edmonton, AB, Canada, [3] Department of Chemistry, Faculty of Science, University of Alberta, Edmonton, AB, Canada, [4] Department of Pharmaceutics, College of Pharmacy, King Saud University, Riyadh, Saudi Arabia, [5] Department of Biochemistry and Molecular Biology, University of Calgary, Calgary, AB, Canada, [6] Department of Medicine, University of Calgary, Calgary, AB, Canada, [7] Department of Chemical and Material Engineering, University of Alberta, Edmonton, AB, Canada

Inhibition of the DNA repair enzyme polynucleotide kinase/phosphatase (PNKP) increases the sensitivity of cancer cells to DNA damage by ionizing radiation (IR). We have developed a novel inhibitor of PNKP, i.e., A83B4C63, as a potential radio-sensitizer for the treatment of solid tumors. Systemic delivery of A83B4C63, however, may sensitize both cancer and normal cells to DNA damaging therapeutics. Preferential delivery of A83B4C63 to solid tumors by nanoparticles (NP) was proposed to reduce potential side effects of this PNKP inhibitor to normal tissue, particularly when combined with DNA damaging therapies. Here, we investigated the radio-sensitizing activity of A83B4C63 encapsulated in NPs (NP/A83) based on methoxy poly(ethylene oxide)-*b*-poly(α-benzyl carboxylate-ε-caprolactone) (mPEO-*b*-PBCL) or solubilized with the aid of Cremophor EL: Ethanol (CE/A83) in human HCT116 colorectal cancer (CRC) models. Levels of γ-H2AX were measured and the biodistribution of CE/A83 and NP/A83 administered intravenously was determined in subcutaneous HCT116 CRC xenografts. The radio-sensitization effect of A83B4C63 was measured following fractionated tumor irradiation using an image-guided Small Animal Radiation Research Platform (SARRP), with 24 h pre-administration of CE/A83 and NP/A83 to Luc^+/HCT116 bearing mice. Therapeutic effects were analyzed by monitoring tumor growth and functional imaging using Positron Emission Tomography (PET) and [^{18}F]-fluoro-3'-deoxy-3'-L:-fluorothymidine ([^{18}F]FLT) as a radiotracer for cell proliferation. The results showed an increased persistence of DNA damage in cells treated with a combination of CE/A83 or NP/A83 and IR compared to those only exposed to IR. Significantly higher tumor growth delay in mice treated with a combination of IR and NP/A83 than those treated with IR plus CE/A83 was observed. [^{18}F]FLT PET displayed

OPEN ACCESS

Edited by:
Jason Luke Parsons, University of Liverpool, United Kingdom

Reviewed by:
Gabrielle Grundy, University of Liverpool, United Kingdom
Mikio Shimada, Tokyo Institute of Technology, Japan
Mark A Hill, University of Oxford, United Kingdom

***Correspondence:**
Afsaneh Lavasanifar
afsaneh@ualberta.ca
Michael Weinfeld
mweinfel@ualberta.ca

Specialty section:
This article was submitted to Cancer Molecular Targets and Therapeutics, a section of the journal Frontiers in Oncology

Received: *09 September 2021*
Accepted: *24 November 2021*
Published: *23 December 2021*

Citation:
Sadat SMA, Wuest M, Paiva IM, Munira S, Sarrami N, Sanaee F, Yang X, Paladino M, Binkhathlan Z, Karimi-Busheri F, Martin GR, Jirik FR, Murray D, Gamper AM, Hall DG, Weinfeld M and Lavasanifar A (2021) Nano-Delivery of a Novel Inhibitor of Polynucleotide Kinase/Phosphatase (PNKP) for Targeted Sensitization of Colorectal Cancer to Radiation-Induced DNA Damage. Front. Oncol. 11:772920. doi: 10.3389/fonc.2021.772920

significant functional changes for tumor proliferation for the drug-loaded NP. This observation was attributed to the higher A83B4C63 levels in the tumors for NP/A83-treated mice compared to those treated with CE/A83. Overall, the results demonstrated a potential for A83B4C63-loaded NP as a novel radio-sensitizer for the treatment of CRC.

Keywords: DNA repair, DNA damage, PNKP, radio-sensitization, colorectal cancer, ionizing radiation, nanoparticle, combination therapy

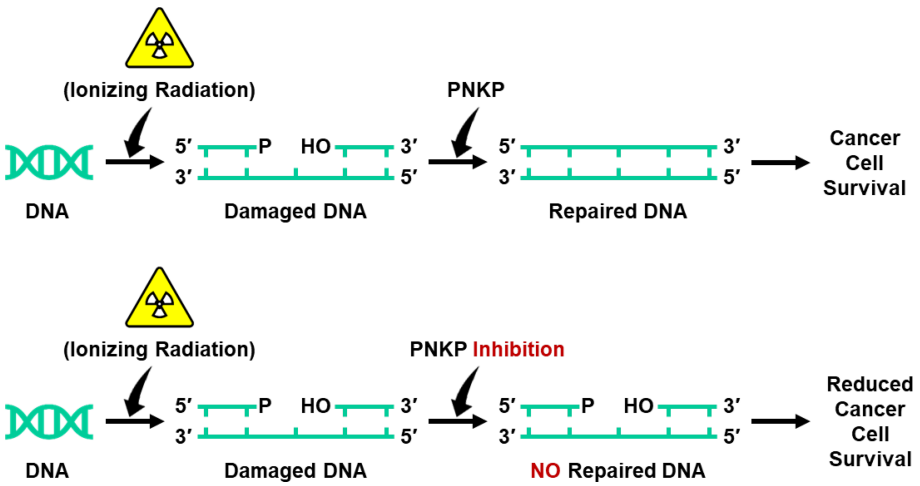

GRAPHICAL ABSTRACT |

INTRODUCTION

Colorectal cancer (CRC) is the second most common cause of cancer death globally (1) and its incidence is expected to increase by 33% by 2028 (2). Clinical outcomes from the conventional treatment options in CRC appear to depend on the location as well as molecular features of individual tumors (3). Thus, the best treatment decisions must be individualized for patients (4–6). Surgery is a very common option for most CRC patients (7). Adjunctive chemotherapy or ionizing radiation (IR) is often accompanied before or after surgery. Although IR is not a preferred option to treat colon cancer, it is fairly common in rectal cancer (7). Radiation therapy, often with neoadjuvant chemotherapy, is considered to help in shrinking the localized CRC tumors before surgery (8, 9). Radiation therapy may also be used to eradicate cancer cells that may have been left behind with the resection boundary after the surgery (10).

Inherent or acquired cellular resistance mechanisms in CRC cells can undermine the effectiveness of IR, eventually leading to cancer recurrence in CRC patients (11–13). IR generates DNA strand breaks. However, the intracellular capacity to repair damaged DNA is one of the major causes of resistance to IR (12, 14). Inhibition of DNA repair is considered a promising approach to improve the sensitivity of cancer cells to IR, thus, different DNA repair enzymes have been validated as therapeutic targets for radiosensitization in various cancers (15–22).

Human polynucleotide kinase-phosphatase (PNKP) is identified as a key enzyme involved in DNA repair following damage by IR or topoisomerase I inhibitors (e.g. irinotecan) in many types of cancer including CRC (23–26). PNKP phosphorylates DNA 5'-termini and dephosphorylates DNA 3'-termini, which allows DNA polymerases and ligases to rejoin the damaged strands of the DNA. The validity of PNKP as a therapeutic target in sensitizing cancer cells to topoisomerase I inhibitors and IR, has been previously shown by our research team and others (26–30). Through RNAi screening, we made the exciting discovery that the deficiency of a tumor suppressor protein, i.e., phosphatase and TENsin homolog (PTEN), makes cancer cells even more sensitive to the PNKP inhibition (31, 32).

Abbreviations: AUC, area under the curve; $CDCl_3$, deuterated chloroform; CE, cremophor EL: ethanol; CE/A83, A83B4C63-solubilized cremophor EL: ethanol formulation; C_{max}, peak plasma concentration; CRC, colorectal cancer; DLS, dynamic light scattering; DMEM/F12, dulbecco's modified eagle medium and F12; DNA, deoxy ribonucleic acid; HLB, hydrophilic-lipophilic balance; IR, ionizing radiation; IV, intravenous; IVIS®, *in vivo* imaging systems; Kp, tissue to plasma ratio; MAP, maximum a posteriori; mPEO, methoxy polyethylene oxide; mPEO-*b*-PBCL, methoxy poly(ethylene oxide)-*b*-poly(α-benzyl carboxylate-ϵ-caprolactone); MRT, mean residence time; MW, molecular weight; NP, nanoparticle; NP/A83, A83B4C63-encapsulated mPEO-*b*-PBCL nanoparticle; PARP, poly (ADP-ribose) polymerase; PDI, polydispersity index; PET, positron emission tomography; PNKP, polynucleotide kinase/phosphatase; PTEN, phosphatase and TENsin homolog deleted on chromosome 10; ROI, regions of interest; SARRP, small animal radiation research platform; SUV, standardized uptake values; TEM, transmission electron microscopy; T_{max}, peak plasma concentration time; TV, tumor volume.

This has inspired the development of small molecule inhibitors of PNKP by our research team.

A83B4C63 is a second generation polysubstituted imidopiperidine small molecule inhibitor of PNKP with IC_{50} and K_D values in the low micro and nanomolar range, respectively (33). The water-solubility of A83B4C63 is <1 mM and its log D value is ~4.16, which makes this compound a non-ideal candidate for the drug development process. To overcome the limitation of poor water-solubility, and at the same time reduce the access and radio/chemo-sensitizing effects of A83B4C63 in normal tissues, we have developed NP formulations of this compound, which were based on methoxy poly(ethylene oxide)-poly(α-benzyl carboxylate-ε;-caprolactone) (mPEO-*b*-PBCL). Passive targeting of solid tumors by NPs is attributed to the presence of leaky vasculature as well as impaired drainage of the lymphatic system at the tumor site (34–42). The nanocarriers of appropriate size (below 200 nm) and specific surface properties can extravasate from the leaky vasculature at the tumor sites, while the impaired lymphatic drainage prevents their rapid removal out of the tumor microenvironment (43, 44). This phenomenon, which is known as the enhanced permeation and retention (EPR) effect, is believed to play a key role in preferential distribution of nanocarriers in solid tumors compared to many normal tissues (45–48). In a recent study, we have shown that polymeric micellar NPs (PMNPs), formed through self-assembly of poly(ethylene oxide)-blockpoly(α-benzyl carboxylate-ϵ-caprolactone) (PEO-*b*-PBCL) containing methoxy-PEO (mPEO) or acetal-PEO (acPEO), and radiolabeled with ^{64}Cu resulted in a 3-fold increased measurable accumulation into subcutaneous HCT116 tumors (perhaps due to the EPR effect) versus muscle tissue as determined with PET (49).

In our previous studies, the nano-formulation of A83B4C63 was shown to effectively reduce the viability of PTEN-deficient CRC, as monotherapy (33). The mPEO-*b*-PBCL based NPs of A83B4C63 were also shown to sensitize CRC cells to IR and irinotecan, *in vitro* (24). *In vivo*, the NPs of A83B4C63 were tolerated better than conventional formulations of this compound and showed significantly enhanced delivery and activity of incorporated A83B4C63 in PTEN-deficient HCT116 xenografts in mice. The objective of the current study was to assess the therapeutic effect of conventional versus mPEO-*b*-PBCL nano-formulations of A83B4C63 for sensitization of wild type CRC models to IR, both *in vitro* and *in vivo*.

MATERIALS AND METHODS

Materials

Methoxy polyethylene oxide (mPEO) (average molecular weight of 5000 g/mol), Cremophor EL: Ethanol (CE), and all research grade organic solvents were purchased from Sigma (St. Louis, MO, USA). α-Benzyl carboxylate-ε-caprolactone monomer was synthesized by Alberta Research Chemicals Inc. (Edmonton, AB, Canada). Stannous octoate was purchased from MP Biomedicals Inc. (Tuttlingen, Germany).

Synthesis of A83B4C63 and PEO-*b*-PBCL Copolymer

The polysubstituted imidopiperidine compound, A83B4C63, was synthesized using a three-component aza[4 + 2]/allylboration reaction and purified to homogeneity *via* reverse-phase HPLC as previously described (50). The structure of the compound was confirmed by NMR, infrared spectroscopy, and LC-MS as previously reported (24).

The mPEO-*b*-PBCL block copolymer with 26 degree of polymerization (DP), i.e., the number of repeating units in a polymer chain, for the PBCL block was synthesized by ring-opening polymerization of α-benzyl carboxylate-ε-caprolactone using mPEO (MW: 5000 g/mol) as an initiator and stannous octoate as catalyst according to the method described previously (24, 51) (**Figure 1**). The synthesized copolymers were characterized for their average molecular weights by ^1H NMR (600 MHz Avance III - Bruker, East Milton, ON, Canada) using deuterated chloroform ($CDCl_3$) as solvent and tetramethylsilane as an internal reference standard.

Formulation and Characterization of A83B4C63-Encapsulated mPEO-*b*-PBCL NPs Versus A83B4C63 Solubilized With the Aid of CE

A83B4C63-encapsulated mPEO-*b*-PBCL NPs (NP/A83) were prepared as previously described (24). In brief, 10 mg A83B4C63 and 30 mg mPEO-*b*-PBCL polymer were completely dissolved in 1 mL of acetone. Then, the organic phase was transferred dropwise to 10 mL aqueous phase and left overnight with continuous stirring with a magnetic bar in a fume hood to completely evaporate the organic solvent. The unencapsulated A83B4C63 was removed by centrifugation at 11600 × g for 5 min to obtain NP/A83. The NP/A83 solution was then transferred into Amicon Ultra-15 centrifugal filter tubes (molecular weight cut-off, 100 kDa; Millipore, ON, Canada) and centrifuged at 11600 × g for 20 min at 4°C in order to concentrate as required. CE/A83 formulation was prepared by previously described method (33). In brief, 2 mg of A83B4C63 drug was dissolved in 400 µL of 100% ethanol to prepare the oil phase using a water bath sonicator until the drug was completely dissolved. Then, 400 µL of CE solution was added into it and vortexed for 2-3 min. The oil phase was poured in water phase (5% dextrose in double distilled water) to emulsify the solubilized drug in the form of NP (**Figure S1**) and was purified using a 0.22 µm syringe filter. The average size and polydispersity index (PDI) of the NP and CE formulations were measured by dynamic light scattering (DLS) using a Malvern Zetasizer 3000 (Malvern Instruments Ltd, Malvern, UK). A83B4C63 loading and encapsulation efficiency were measured and analyzed using a Varian Prostar 210 HPLC system. Reversed phase chromatography was carried out with a Microsorb-MV 5 µm C18-100 Å column (4.6 mm × 250 mm) with 20 µL of sample injected and eluted under isocratic conditions with a solution of 0.1% trifluroacetic acid/acetonitrile (1:1 v/v) at a flow rate of 0.7 mL/min at room temperature. Detection was performed at 280 nm wavelength

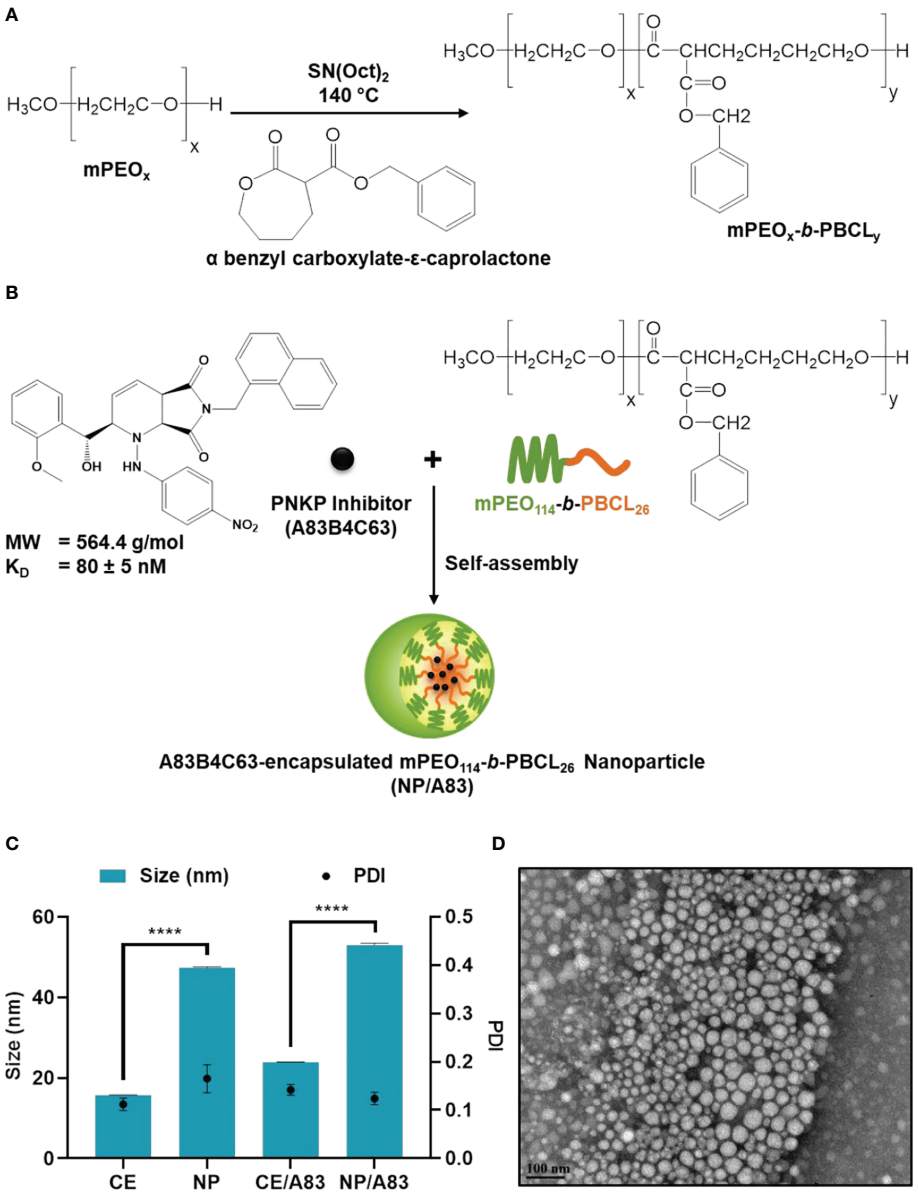

FIGURE 1 | Chemical structure of **(A)** methoxy poly(ethylene oxide)-*b*-poly(α-benzyl carboxylate-ε-caprolactone or mPEO-*b*-PBCL and **(B)** illustration of encapsulation process of 2-[hydroxy(2-methoxyphenyl)methyl]-6-(naphthalene-1-ylmethyl)-1-[(4-nitrophenyl)amino]-2H, 4aH, 7aH-pyrrolo[3,4-b]pyridine-5,7-dione or A83B4C63. **(C)** Physicochemical characterization of water-soluble CE, empty NP, A83B4C63-solubilized (CE/A83), and A83B4C63-encapsulated mPEO-*b*-PBCL (NP/A83) formulations (n = 10). Hydrodynamic diameter and polydispersity index (PDI) of NP/A83 micelles in aqueous medium were obtained using dynamic light scattering (DLS). **(D)** TEM image of A83B4C63-encapsulated micellar formulation (NP/A83) in aqueous medium. The TEM image was obtained at a magnification of 110,000X at 75 kV. The bar in the bottom left corner of the image indicates a scale of 100 nm. Data from three independent experiments were compared by two-way ANOVA multiple comparison test following Tukey's method. (****p ≤ 0.0001). The TEM image displayed is a representative of at least three independent experiments.

for A83B4C63 using a Varian 335 Photodiode Array HPLC detector (Varian Inc., Palo Alto, CA, USA). In this study, A83B4C63 control was solubilized with DMSO for all *in vitro* experiments, while for *in vivo* experiments, A83B4C63 was dissolved with the aid of CE (CE/A83). Finally, the A83B4C63 loading and loading efficiency were calculated according to the following equations:

$$\text{A83B4C63 loading (\%)} = \frac{\text{Weight of the encapsulated A83B4C63 in NPs}}{\text{Total weight of the polymer in NPs}} \times 100$$

$$\text{A83B4C63 encapsulation efficiency (\%)} = \frac{\text{Weight of the encapsulated A83B4C63}}{\text{Initial weight of the A83B4C63 added}} \times 100$$

Transmission Electron Microscopy (TEM)

The morphology of self-assembled structures under study was investigated by TEM using a Morgagni TEM (Field Emission Inc., Hillsboro, OR, USA) with Gatan digital camera (Gatan, Pleasanton, CA, USA). In brief, 20 µL of micellar solution with a polymer concentration of 0.25 mg/mL or Cremophor EL at a concentration of 0.2 mg/mL was placed on a copper-coated grid. The grid was held horizontally for 1-2 min to allow the colloidal particles to settle down. The excess fluid was removed by filter paper. The copper-coated grids holding the aqueous samples were then negatively stained by 2% phosphotungstic acid. After 2 min, the excess fluid was removed by filter paper and the grid was loaded into the TEM for image analysis.

Cell Lines

Wild type HCT116 cells were obtained from the American Type Culture Collection and luciferase positive Luc^+/HCT116 cells were generated as previously described (52). Cells were routinely cultured at 37°C in 5% CO_2 in a humidified incubator in a 1:1 mixture of Dulbecco's modified Eagle medium and F12 (DMEM/F12) supplemented with 10% FBS, 50 U/mL penicillin, 50 mg/mL streptomycin, 2 mmol/L L-glutamine, 0.1 mmol/L nonessential amino acids, and 1 mmol/L sodium pyruvate. All culture supplements were purchased from Invitrogen (Burlington, ON, Canada).

Microscopic Study for γ-H2AX Evaluations

1×10^5 wild type HCT116 cells were seeded onto each glass coverslip in a 35-mm Petri dish and incubated overnight to attach. The cells were then pretreated with the nano-formulations for 24 h prior to 3 Gy γ-irradiation. Irradiation was carried out at room temperature at a dose rate of 0.66 Gy/min. After irradiation, the cells were incubated for two time points up to 6 h. After the incubation, the cells were fixed with 4% paraformaldehyde in PBS for 20 min, then permeabilized, and blocked with 1% BSA in 1 x PBS/0.1% Tween 20 for 20 min. After 3 washes with 1 x PBST, anti-phospho-histone H2A.X (Ser139) antibody (catalog# 05-636, Millipore, Temecula, CA, USA) at 1:4000 dilution was applied to the cells and incubated for 1 h at room temperature. The cells were washed three times with 1 x PBST and then incubated with Alexa Fluor 488 goat anti-mouse secondary antibody (catalog# A11059, Life Technologies, Carlsbad, CA, USA) at a 1:200 dilution in 0.1% BSA/1 x PBST for 1 h in the dark. After washing the cells, the coverslips were mounted on the slides with DAPI-containing mounting media (53) (Molecular Probes, Eugene, Oregon, USA) at 1 µg/mL concentration. Images were taken with an Axio Imager Z2 microscope (Carl Zeiss, Jena, Germany) using MetaMorph 7 and MetaXpress 6 software (Molecular Devices, San Jose, CA, USA) to image and quantify foci.

Western Blot

Western blot was used to assess the level of cleaved caspase 3/7 and PARP induced by A83B4C63 as free drug (CE/A83) and NP (NP/A83) formulation in HCT116 cells with or without radiation. Initially, 1.5 million cells were plated. Then, cells were treated with CE/A83 and NP/A83, or vehicles alone, at an A83B4C63 concentration of 10 µM, or equivalent drug free CE and NP levels. After 24 h incubation with A83 formulations or vehicle controls, cells were exposed to a fixed dose of radiation (4 Gy) using a ^{60}Co Gamma irradiator (AECL, Chalk River, ON, Canada). The cells were harvested at either 1 or 4 h after exposure to IR. Each experiment was performed in triplicate.

Protein extracts for western blot analysis were prepared using commercial RIPA lysis buffer (ThermoFisher Scientific, Mississauga, ON, Canada) supplemented with a cocktail of protease inhibitors (Millipore Sigma, Mississauga, ON, Canada). Protein concentrations were measured using the BCA assay kit (Pierce/ThermoFisher Scientific, Mississauga, ON, Canada) according to the manufacturer's protocol. Equal concentrations of protein were separated by SDS-PAGE and transferred to nitrocellulose membranes. After blocking with 5% skimmed milk in TBST (50 mM Tris-HCl, pH 7.4, 150 mM NaCl, and 0.1% Tween 20), the blots were incubated with the respective primary antibodies (caspase-3 catalog# 9662S, caspase-7 catalog# 9492S, PARP catalog# 9542S) and secondary antibody (HRP-linked anti-rabbit IgG cat# 7074S) purchased from Cell Signaling Technology (Whitby, ON, Canada). The protein bands were detected using an enhanced chemiluminescence (ECL) based system (Pierce/ThermoFisher Scientific, Mississauga, ON, Canada) and quantified by densitometric analysis using ImageJ software.

Xenograft Models

NIH-III nude mice were purchased from Charles River Laboratories (Wilmington, MA, USA). All animal studies were conducted in accordance with the guidelines of the Canadian Council on Animal Care and with approval from the local Animal Care Committee of the Cross Cancer Institute (Edmonton, AB, Canada). The HCT116 and Luc^+/HCT116 xenograft tumor mouse models were generated by subcutaneous injection of 0.5×10^6 cells in a 100 µL mixture of culture media and matrigel matrix (Corning, MA, USA) (1:1 v/v) in the right flank or left shoulder of 4 - 6 week-old female NIH-III nude mice. The CRC cell implanted mice were routinely monitored for tumor growth and signs of sickness. Animals reaching early endpoints as set in our animal protocol were euthanized. All animals were euthanized at day-22 following the tumor inoculation.

In Vivo Anticancer Activity of Combination Therapies

This study was performed on Luc^+/HCT116 xenografts developed as described above. When the tumor volume reached 80 to 150 mm^3, mice were randomly assigned into test groups receiving empty NP without IR (n = 6), or empty NP (n = 6), CE/A83 (n = 6), and NP/A83 (n = 7) formulations of A83B4C63 with a fractionated radiation dose of 3 x 5 Gy q.a.d. The treatments (empty NPs, PNKP inhibitor A83B4C63 alone or

CE/A83, A83B4C63-encapsulated NPs (NP/A83) were started on day 0. On day -2 (2 days before starting the treatments), tumor sizes were measured with a digital slide caliper and by bioluminescence using an *in vivo* imaging system (IVIS®). All drugs were given *via* intravenous (IV) injection *via* tail vein and administered on days 0, 2, and 4. The IV A83B4C63 dose was 25 mg/kg, which was injected three times one day apart. Mice received three fractionated radiation doses of 5 Gy every alternative day. The excipient dose, i.e., empty NP in control groups was selected equivalent to their amounts in the NP/A83 test group. The length (L) and width (W) of the tumor were measured two times per week and the tumor volume (TV) was calculated using the formula $TV = (L \times W^2)/2$. The measurements continued until day 22 (since the day of tumor inoculation) when all mice were euthanized.

The fractionated radiation therapy using a daily dose of 5 Gy was started on day 1 and given 3x including days 3 and 5. Radiation therapy was administered using the image-guided small-animal radiation research platform (SARRP; Xstrahl Inc. Suwanee, GA, USA) Mice were placed ventrally onto the bed of the SARRP and immobilized with continuous isoflurane with anesthesia. A cone beam computed tomography (CT) scan was acquired first for each mouse and used for radiation therapy planning per mouse using integrated Muriplan/Murislice® software (Xstrahl Medical & Life Sciences, Camberley, UK). The radiation target volume was defined as the tumor volume contoured from the cone beam CT scan and the isocenter defined in the center of the tumor volume and radiation doses were calculated. After therapy planning, the radiation therapy to the target tumor area was delivered using a 0.15 mm copper filter with 220 kVp X-rays and 13 mA using and two opposing dorsal beams at 45 to 60 degrees and minus 45 to 60 degrees and a 10 mm x 10 mm square-shaped collimator at a dose rate of 0.042 Gy/sec and an exposure time of 60 s per beam. The collimator size was big enough to completely cover tumor tissue for the applied irradiation.

In Vivo Imaging Systems (IVIS®) for Evaluating Anticancer Activity of CE/A83 and NP/A83 With or Without Radiation

The animals inoculated with Luc^+/HCT116 and treated as described above were also imaged for the expression of luciferase to follow their tumor growth. For the optical imaging, mice were subcutaneously injected with the XenoLight D-Luciferin - K+ salt bioluminescent substrate (PerkinElmer, UK) at a dose of 10 µL/g of body weight before the luciferase detection. Mice were anesthetized and placed in the dark chamber of a IVIS® LUMINA XMRS optical imaging systems (PerkinElmer, Waltham, MA, USA) for whole-body animal imaging and the emitted photons were quantified and analyzed using Living Image® Software (PerkinElmer, Waltham, MA, USA). Imaging of live animals was performed twice a week.

PET Imaging

Luc^+/HCT116 tumor-bearing female NIH-III nude mice from the radiation therapy study (as described above) were analyzed on days 10-12 after last treatment for tumor proliferation using Positron Emission Tomography (PET). Mice were anesthetized by isoflurane (100% O_2). A needle catheter was placed into the tail vein of these mice and 3 - 6 MBq of [^{18}F]FLT in 100 to 150 µL saline were injected. [^{18}F]FLT was synthesized at the cyclotron research facility of the Cross Cancer Institute according to the previously described procedure (54) using 5-O-(4,4-dimethoxytrityl)-2,3-anhydrothymidine (ABX GmbH, Radeberg, Germany) as the synthesis precursor. Radioactivity in the injection solution in a 0.5 mL insulin syringe was determined using a dose calibrator (AtomlabTM 300, Biodex Medical Systems, Shirley, NY, USA). After radiotracer injection, mice were allowed to regain consciousness for about 40 to 45 min before anesthetizing them again. They were immobilized in prone position into the center field of view of a preclinical INVEON® PET scanner (Siemens Preclinical Solutions, Knoxville, TN, USA). Acquisition data were collected in three-dimensional list mode for 10 min, reaching ~60 min post injection. Static PET images were reconstructed using a maximum *a posteriori* (MAP) algorithm. Image files were further processed using the ROVER v2.0.51 software (ABX GmbH, Radeberg, Germany). Masks defining three-dimensional regions of interest (ROI) over tumor tissue were defined and ROI's were analyzed with 50% threshold of radioactivity uptake. Mean standardized uptake values [SUV_{mean} = (measured radioactivity in the ROI/mL tumor tissue)/(total injected radioactivity/mouse body weight)] were calculated for each ROI.

Biodistribution of CE/A83 and NP/A83 Formulations in HCT116 Tumor-Bearing Mice

The biodistribution profiles of A83B4C63 in CE and NP forms were assessed in wild type HCT116 tumor-bearing NIH-III mice. Tumor-bearing mice were developed as described above, except for the use of HCT116 cells instead of Luc^+/HCT116. When the tumor volume reached 1200 to 1500 mm^3, mice were randomly assigned and grouped into three test groups (n = 3). The test groups received CE/A83 or its NP form three times, one day apart at an IV dose of 25 mg/kg. The control mice received empty NPs. 4, 24, and 48 h after the last injection, all mice were euthanized, and blood, excised tumors and other organs including brain, heart, lung, liver, kidney, and spleen were collected to define drug levels using an LC/MS/MS method of quantification as previously described (33). In brief, all snap-frozen dissected tumor tissues were weighed and homogenized with an ice-cooled solution of acetonitrile/water (50:50 v/v) using an electric hand homogenizer. The collected whole blood samples of the mice were centrifuged at 2000 × g for 5 min at 4°C to separate the plasma. Tissue homogenate samples were centrifuged at 2000 × g for 15 min at 4°C. To 250 µL of plasma/homogenized tissues 1000 µL cold acetonitrile was added. The mixture was vortexed for 5 min and then the samples were centrifuged at 2000 × g for 20 min. The solutions were separated and transferred to clean tubes and evaporated to dryness.

An Agilent 1100 HPLC system coupled to a Waters Quattro Micro triple quadrupole mass spectrometer (Waters, Milford, MA, USA) and attached to an Agilent Poroshell 120 SB- C18 2.7-micron LC column with dimensions of 2.1 mm x 50 mm was used. The column was heated to 35°C. The mobile phase consisted of water with 0.1% formic acid (A) and acetonitrile with 0.1% formic acid (B). A gradient elution was programmed to commence with 20% B for post-injection followed by a gradual increase in 3 min of B to 95%. The composition was maintained for 3 min when it was gradually decreased back to 20% of B in 0.1 min. The flow rate was 0.3 mL/min and 2 μL of sample was injected. Standard curves were linear over the range of 1 - 1000 ng/mL ($r^2 > 0.99$; coefficient of variation < 20%). The lowest limit of quantification was set at 1 ng/mL. The mass spectrometer was operated in positive mode with capillary voltage at 3.2 kV, source temperature at 120°C, desolvation temperature at 275°C, and desolvation gas flow at 800 L/h. Instrumental control and data analysis were performed using MassLynx software (Waters, Milford, MA, USA).

Propranolol dissolved in the solution of acetonitrile/water with 50:50 v/v ratios was used as an internal standard. The dried residues in sample vials were reconstituted with 100 μL of internal standard solution with vigorous vortexing before placing into the auto-sampler of the LC/MS/MS (Waters Quattro Micro ± ES MS Triple Quadrupole, Milford, MA, USA) fitted with an Agilent Technology: Poroshell 120 SB-C18 2.1x50 mm, 2.7-micron column. The mobile phase consisted of 50:50 v/v ratios of water with 0.1% formic acid and acetonitrile with 0.1% formic acid.

The terminal elimination rate constant was estimated from the log-linear portion of the plasma concentration - time curves. Because of the destructive sampling procedure used for the collection of blood and tissues from different animals at each time point, the area under the plasma/tissue curve (AUC) was estimated using the trapezoidal rule from the average plasma concentrations at different time points and the variance of AUC was estimated using Bailer's method based on the standard error of the mean (SEM). The ratio of tissue concentration at each time point to that of plasma (Kp) was also calculated and reported.

Statistical Analysis

GraphPad Prism 9 software (La Jolla, CA, USA) was used for statistical analysis. Significance of differences between groups was assessed using one-way and two-way ANOVA followed by Tukey's *post-hoc* test, where appropriate. If a significant difference was found among the groups, median ranks between pairs of groups were compared using the Mann-Whitney U test. A value of $p \leq 0.05$ was considered as statistically significant in all experiments.

For biodistribution experiment, the AUC of plasma or tissue versus time curves were obtained using the approach outlined by Bailer (55). Pairwise comparisons of the AUC were performed at $\alpha = 0.05$. The critical value of Z (Zcrit) for the two-sided test after Bonferroni adjustment was 2.24 (56), and the observed value of Z (Zobs) was calculated as previously described (57, 58). When Zobs values are greater than Zcrit, the difference between AUCs was considered statistically significant.

RESULTS

Physicochemical Characterization

The ^{1}H NMR spectra and peak assignments of mPEO-*b*-PBCL (**Figure 1A**) and A83B4C63 (**Figure 1B**) were previously reported (24, 51, 59–61). According to the calculations based on the ^{1}H NMR spectra, the DP was 26 for PBCL block in mPEO-*b*-PBCL copolymers. A83B4C63 encapsulation into the mPEO-*b*-PBCL micellar NPs was performed following a simple one-step self-assembly nanoprecipitation method (**Figure 1B**). 21.97 ± 0.65% loading and 70.28 ± 3.47% encapsulation efficiency were measured when A83B4C63-encapsulated mPEO-*b*-PBCL NPs (NP/A83) were prepared at a 1:3 w/w A83B4C63:mPEO-*b*-PBCL ratio. The NP/A83 were ~60 nm in diameter on average and showed a low polydispersity index (PDI), i.e., < 0.25, indicating the uniformity of the nanocarrier population in terms of diameter (**Figure 1C**). After A83B4C63-solubilization by CE formulation, the average size of CE/A83 micelles was < 35 nm in diameter, which was significantly lower (****$p \leq 0.0001$) than that of NP/A83. However, no significant difference was measured for the PDI values obtained from CE/A83 and NP/A83. The diameter of the empty carriers from both formulation types i.e, NP, CE, were significantly lower (*$p \leq 0.05$) than their drug-encapsulated counterparts. As shown in **Figure 1D**, the TEM image confirmed the formation of spherical NP/A83 micelles with uniform size. In the TEM image, a similar distribution pattern in the micellar population having a clear boundary was observed that also indicated the low aggregation tendency among the formed micelles.

Mechanistic Evaluations

Upright microscopic evaluations were performed to assess the DNA damage following treatment of cells with a combination of PNKP inhibitor and a fixed dose of IR (3 Gy). **Figure 2A** shows the wide-field fluorescence images of the γ-H2AX-positive cells treated with CE/A83 and NP/A83. Here, we studied the temporal and spatial distribution of the foci of the phosphorylated form of the histone protein H2AX (γ-H2AX) that is known to be modified, upon γ-irradiation, by kinases activated by double-strand breaks in cellular DNA. Qualitative analysis based on the microscopic images of the distribution of foci in each cell indicated greater clustering of DNA damage by radiation in cells when they were pre-treated with A83B4C63 delivered by either CE or NP formulations. Quantitative analysis using the MetaXpress 6 software was performed to quantify the number of foci in each cell. A significantly higher number of γ-H2AX-positive foci was observed 40 min after γ-irradiation in NP/A83-pretreated cells than in CE/A83 pretreated and untreated (radiation alone) groups. The difference observed at 40 min is likely related to the inhibition of repair by A83B4C63 treatment. The number of foci decreased at 6 h post γ-irradiation for both A83B4C63 formulations. Significantly higher foci numbers post γ-irradiation in cells pretreated with either CE/A83 or NP/A83 compared to cells without drug demonstrated the proof of concept for the radio-sensitizing activity of our PNKP inhibitor, i.e., A83B4C63.

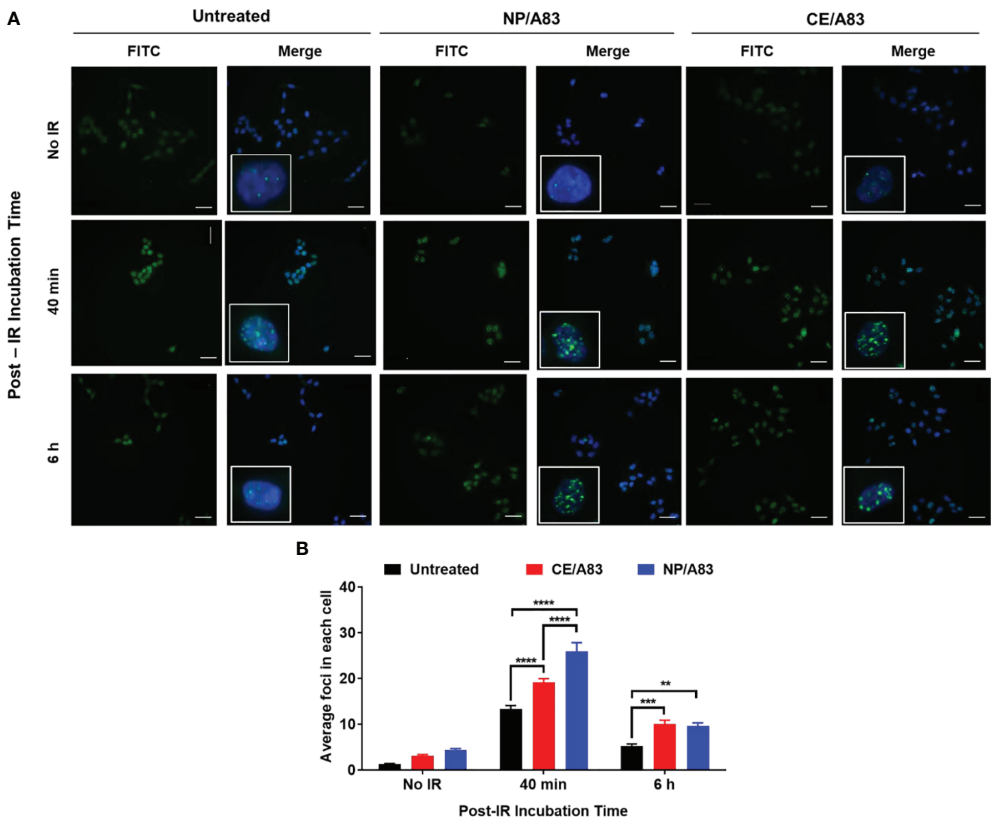

FIGURE 2 | Formation and repair of double strand breaks of DNA analyzed by γ-H2AX foci formation (H2A.X Ser139) in HCT116 cells. **(A)** Representative images of γ-H2AX (green) foci and nuclei (blue) were counterstained with DAPI. Inset figures show typical γ-H2AX foci in individual cells. **(B)** Quantitative analysis for the number of foci in each treated cell. 24 h prior to 3 Gy γ-irradiation, cells on the coverslips were treated with 10 μM CE/A83 and NP/A83. At 40 min or 6 h after irradiation, cells were fixed, permeabilized, and stained for foci to be visualized under the microscope. MetaXpress 6 software was used to take images and to quantify the number of foci in each cell. Data from three independent experiments were compared by two-way ANOVA multiple comparison test following Tukey's method. Differences were considered significant if (**$p \leq 0.01$, ***$p \leq 0.001$, and ****$p \leq 0.0001$). Micrographs displayed are representative of at least three independent experiments; scale bar = 40 μm.

We also analyzed the induction of cleaved PARP, cleaved caspase-7, and cleaved caspase-3 expressions following treatment by A83B4C63 with and without radiation. Both CE/A83 and NP/A83 formulations slightly induced the level of cleaved PARP, cleaved caspase-7 and cleaved caspase-3, but the level of induction was low, suggesting that apoptosis does not play a major role in the cellular response to radiation with or without the repair inhibitor (**Figure S2**).

In Vivo Radio-Sensitizing Activity of CE/A83 and NP/A83 in Wild Type HCT116 Xenografted Mice

To explore the radio-sensitizing anticancer activity of intravenously administered CE/A83 and NP/A83 at a dose of 25 mg/kg three times a week in mice bearing Luc^{+}/HCT116 xenografts, all mice were inoculated with 0.5 million cells 10 days (day -10) before the treatment schedule as shown in **Figure 3A**. According to the experimental design (**Figure 3A**), the tumor-bearing control mice received empty NPs in isotonic 5% dextrose. Mice receiving systemic empty NPs plus IR were also used as a control group. To investigate the anticancer activity for this combination treatment approach, we conducted both digital slide caliper measurement and bioluminescence live imaging to monitor the growth of xenograft tumors in the mice.

As shown in **Figure 3B**, the mice receiving empty NP with no IR exhibited rapid CRC tumor growth compared to other treatment groups that received IR. IR induced a growth delay, but mice receiving empty NP plus IR or CE/A83 plus IR still showed moderate tumor size increases. However, NP/A83 plus IR demonstrated the slowest tumor growth among the treatment groups. **Figure 3C** represents the average tumor volumes obtained from the treated groups on day 12 post first IV injection. A highly significant growth delay in the xenografted tumors was observed for the mice receiving NP/A83 plus IR compared to the control (empty NP without IR).

As shown in **Figure 3C**, the decrease in the average size of excised tumors from NP/A83-treated mice matched the average tumor volumes obtained from either slide caliper or bioluminescence measurements. At the day of termination

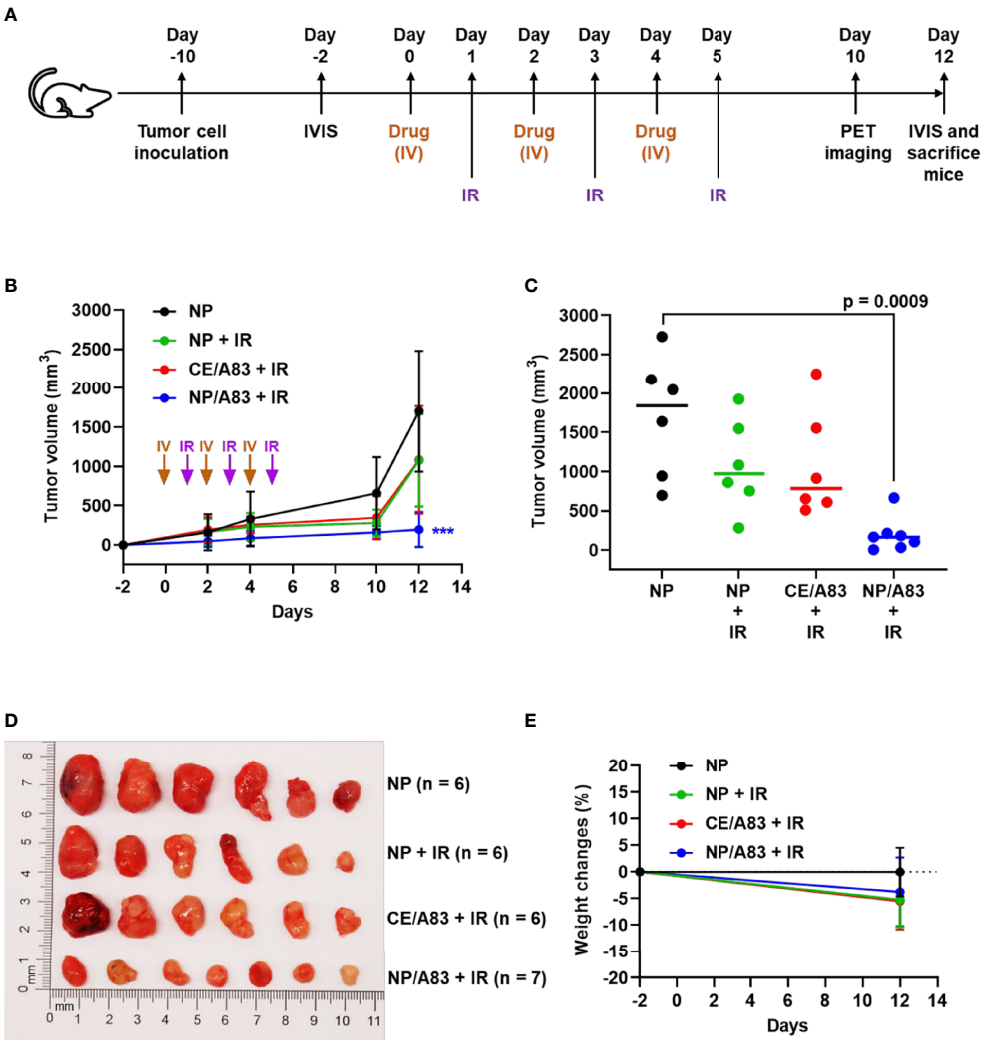

FIGURE 3 | **(A)** Schematic experimental design for evaluating the anticancer activity of A83B4C63 as CE and NP formulations in female NIH-III nude mice following IV administration (n = 6 or 7). Colorectal Luc$^+$/HCT116 cells were inoculated and grown as subcutaneous tumor xenografts in the right flank of the mice. When tumors became palpable based on the tumor measurement by calipers the treatments started. The *in vivo* live imaging system (IVIS®) was also used before and after treatment to follow tumor growth. A total of 25 mice were divided into 4 groups (6 + 6 + 6 + 7), which were intravenously injected with (i) control empty NPs, (ii) control empty NP plus 3 x 5 Gy IR, (iii) CE/A83 (A83B4C63 formulated with the aid of CE) plus 3 x 5 Gy IR, and (iv) NP/A83 (A83B4C63-encapsulated $mPEO_{114}$-*b*-$PBCL_{26}$ micelles) plus 3 x 5 Gy IR three times with a one day interval at a dose of 25 mg/kg. **(B)** Average tumor volume growth curves for mice in each treatment group for Luc$^+$/HCT116 CRC xenograft. **(C)** The average tumor volumes obtained from the treated groups on day-12 post injection. Using digital calipers, the length (L) and width (W) of the tumor mass were measured 2 times per week and the tumor volume (TV) was calculated according to the following formula, $TV = (L \times W^2)/2$. **(D)** Images of representative tumors from **(B)**. **(E)** The average percentage for the change in body weight of mice bearing Luc$^+$/HCT116 xenografts. Differences were considered significant if (***P < 0.001).

(day 12), the average tumor volumes reached 1706.02 ± 773.80, 1076.45 ± 586.78, and 1082.72 ± 685.81 mm^3 (n = 6), in the mice treated with empty NP, empty NP plus IR, and CE/A83 plus IR, respectively, whereas the tumor volumes remained as low as 196.56 ± 221.01 mm^3 (n = 7) in mice treated with IV NP/A83 plus IR. The overall results clearly showed the *in vivo* radio-sensitizing activity of A83B4C63 in its NP formulation in wild type Luc$^+$/HCT116 CRC xenografts in mice, which was in contrast to no statistically significant activity for the CE formulation of this PNKP inhibitor compared to control groups receiving empty NPs with or without IR ($p > 0.05$). **Figure 3D** also shows the images of excised tumors from the mice of all treatment groups at the termination day. These data verified the results of tumor growth measurement by the digital slide calipers (and IVIS®, see below). The measured mean body weight variation of the mice receiving systemic treatments were within a 20% margin (**Figure 3E**) and did not show any statistical difference irrespective of the treatment groups.

To further evaluate the radio-sensitizing anticancer activity of A83B4C63, tumor growth in mice was also detected by *in vivo*

bioluminescence imaging. Based on the average radiance for bioluminescence of Luc$^+$/HCT116 cells in mice (**Figure 4A**), NP/A83 pretreatment with fractionated IR dose of 3 x 5 Gy was found to delay the tumor growth significantly when compared to the other treatment groups. At day 12 (**Figure 4B**), the quantitative analysis exhibited a significant difference in average radiance in the NP/A83-pretreated group ($*p \leq 0.05$, two-way ANOVA) in comparison to that of other pretreatment groups, including the empty NP, empty NP plus IR, and CE/A83 plus IR cohorts. Therefore, the radiance for bioluminescence of Luc$^+$/HCT116 xenografts in the respective treatment groups of mice showed a similar pattern in tumor growth to that observed by slide caliper measurements. When comparison was made between the day -2 (2 days prior to starting treatments) and day 12 (termination day), significant increases in luciferase-tagged cancer cells (bioluminescence) were found for all treatment groups except NP/A83-treated mice, which did not show any difference in the bioluminescence of xenografts from day -2 to day 12. The data validated the anti-tumoral activity of systemic NP/A83 administration in the HCT116 CRC xenograft model as a novel radio-sensitizing nanomedicine.

PET Imaging of HCT116 CRC Xenograft Mice

Figure 5 summarizes results from the non-invasive PET imaging experiments using [^{18}F]FLT to determine the tumor proliferation

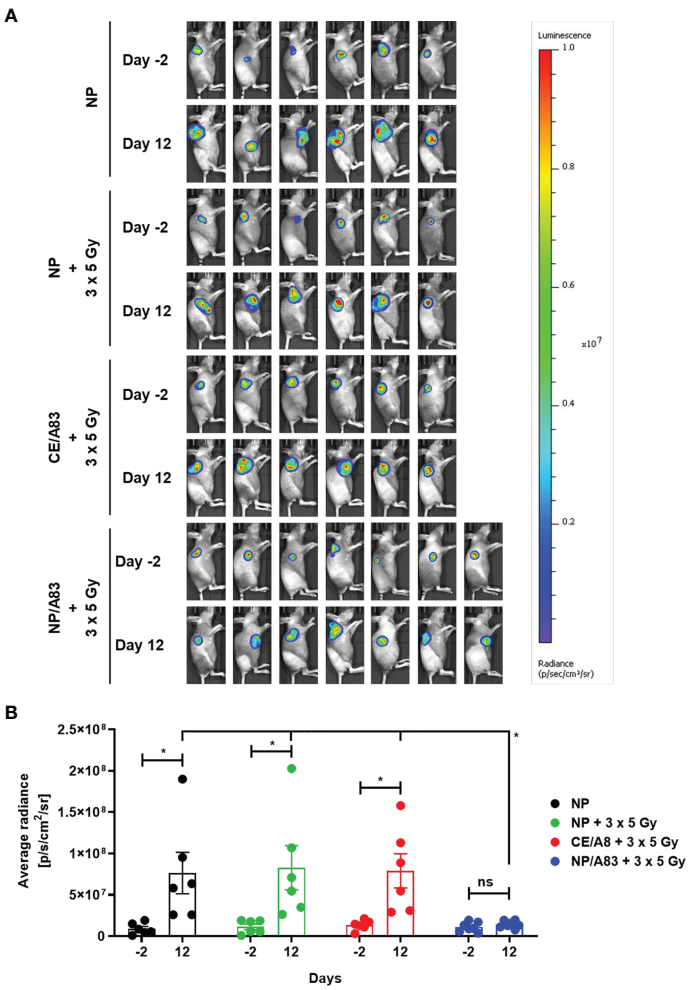

FIGURE 4 | **(A)** Representative bioluminescence images from the tumor-bearing mice on days-2 and 12 for evaluating the radio-sensitizing anticancer activity of A83B4C63 as CE and NP formulations in female NIH-III nude mice following IV administration (n = 6 or 7). 0.5 × 10^6 colorectal Luc$^+$/HCT116 cells were inoculated and grown as subcutaneous tumor xenografts in the right flank of the female athymic NIH-III nude mice. When tumors became palpable, a total of 25 mice were randomly assigned into 4 groups (6 + 6 + 6 + 7), which were intravenously injected with (i) control empty NPs, (ii) control empty NP plus 3 x 5 Gy IR, (iii) CE/A83 (A83B4C63 formulated with the aid of CE) plus 3 x 5 Gy IR, and (iv) NP/A83 (A83B4C63-encapsulated mPEO$_{114}$-*b*-PBCL$_{26}$ micelles) plus 3 x 5 Gy IR three times with a one day interval at a dose of 25 mg/kg. The mice were imaged for luciferase intensity 2 days before the treatment started. Radiation therapy was administered using an image-guided SARRP platform. **(B)** Quantitative analysis for the average radiance (photons per s per cm^2 per square) bioluminescence signal for the four treatment groups of mice on day -2 (2 days prior to start treatment) and day 12 (termination day). To show tumor growth, the tumor radiance at day -2 (two days before treatment) is subtracted from tumor radiance at day 12 from the same mouse. Differences were considered significant if $*p \leq 0.05$. ns stands for not significant.

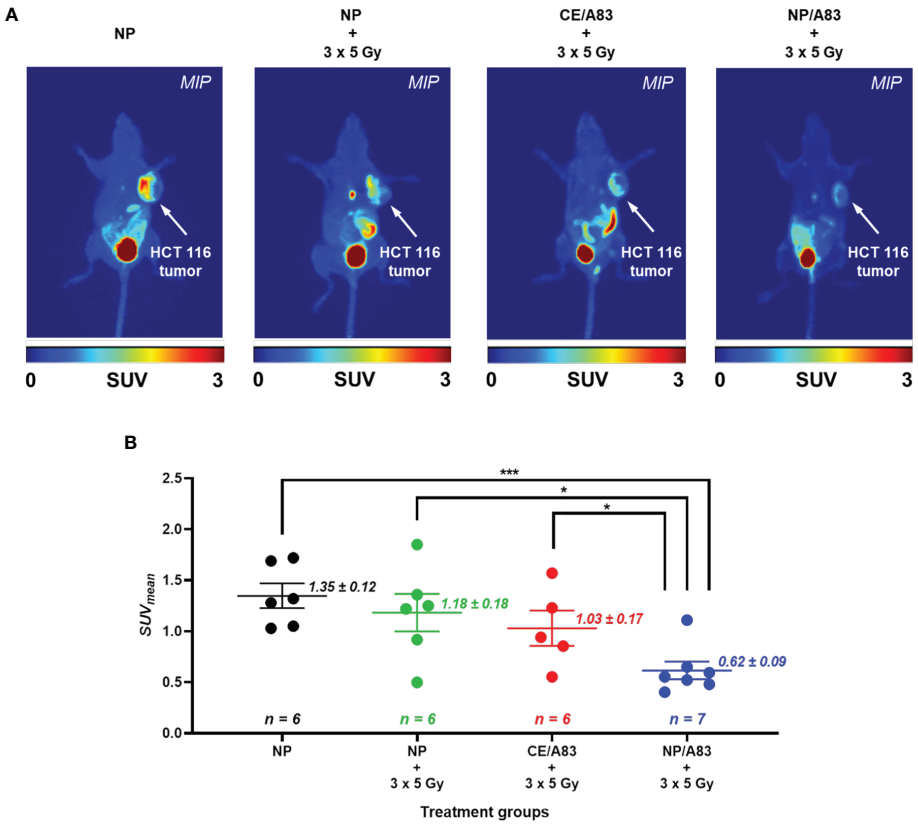

FIGURE 5 | **(A)** Static [^{18}F]FLT-PET images after 60 min post injection of female athymic NIH-III nude mice (one representative image from each treatment group) post treatment (day 10) with empty NP, CE/A83, and NP/A83 with a fractionated 3 x 5 Gy dose of radiation. The control mice received empty NP without radiation. The white arrows indicate the xenograft CRC. **(B)** The quantitative data for the analyzed SUV_{mean} values of the [^{18}F]FLT tumor uptake. Differences were considered significant if $^{*}p \leq 0.05$, and $^{***}p \leq 0.001$ following two-way ANOVA followed by Tukey's method. Data are shown as mean ± SEM from n experiments.

in vivo in highly multiplying cancer cells in the HCT116 xenografts to determine the radio-sensitizing activity of A83B4C63 formulations in these tumors. In line with the results of caliper and bioluminescence measurements, administration of NP/A83 at 25 mg/kg dose plus IR led to a significant reduction of [^{18}F]FLT uptake in the HCT116 xenografts. This contrasted with CE/A83 plus IR that did not show any significant reduction of [^{18}F]FLT uptake when compared to the control receiving empty NPs plus IR. Following tumor uptake levels of [^{18}F]FLT were determined as mean standardized uptake values (SUV_{mean}) ± SEM: 1.35 ± 0.12, 1.18 ± 0.18, 1.03 ± 0.17 (all n = 6) and 0.62 ± 0.09 (n = 7), for empty NP, empty NP plus IR, CE/A83 plus IR, and NP/A83 plus IR, respectively. When compared for significant differences as shown in **Figure 5B**, the NP/A83 plus 3 x 5 Gy IR-treated mice group displayed a significantly lower SUV_{mean} value than that of empty NP without IR at α level of 0.001. The difference in SUV_{mean} value for mice that received NP/A83 plus IR was significantly lower than for the mice that received empty NPs or CE/A83 plus IR ($^{*}p < 0.05$). However, no significant differences were observed between the NP plus IR and CE/A83 plus IR treatment groups.

Biodistribution Profile of CE and NP Formulations of A83B4C63

Figure 6 and **Table 1** represent the plasma or tissue concentration versus times profile, as well as tissue to plasma ratio of A83B4C63 formulations and their AUC following IV administration of the above formulations at a dose of 25 mg/kg three times in mice bearing HCT116 tumors (**Figure 6A**). As shown in **Figure 6B**, the concentration of A83B4C63 obtained by CE/A83 formulation fell below the limit of detection after 24 h while NP/A83 formulation yielded plasma drug concentrations ($^{****}p \leq 0.0001$) significantly above the detection limits for up to 48 h. The concentration of A83B4C63 obtained by NP/A83 formulation was significantly higher at 24 h ($^{*}p \leq 0.05$) and 48 h ($^{****}p \leq 0.0001$) when compared with that of CE/A83. This resulted in a significantly higher plasma AUC level for the mice that received NP/A83 (34246.64 ± 3710.36) treatment to those that received CE/A83 (21078.86 ± 1534.31) ($^{*}p \leq 0.05$, student's t-test).

Biodistribution data (**Table 1**) showed significantly higher AUC values for NP/A83 than for CE/A83 in tumor and liver, while the AUC of NP/A83 was lower in kidney compared

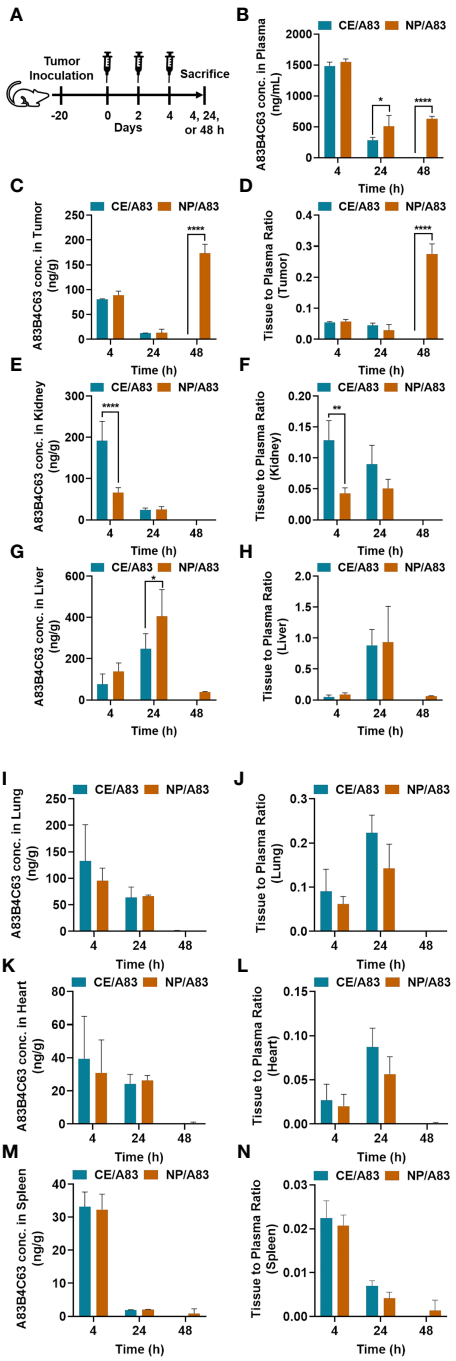

FIGURE 6 | **(A)** The experimental schedule for determining the bio-fate of A83B4C63 intravenously delivered *via* CE and NP formulations in CRC tumor-bearing mice. **(B–N)** The biodistribution profile of A83B4C63 in wild-type HCT116 CRC xenograft bearing NIH-III female nude mice (n = 3) 4, 24, and 48 h after tail vein administration of CE/A83 and NP/A83 formulations. Mice were inoculated with HCT116 CRC cells. 21 days following tumor cell inoculation, the mice received CE/A83 and NP/A83 formulations intravenously at a dose of 25 mg/kg three times with a one-day interval. The control mice received empty NPs, equivalent to the amounts used in the test groups. 4, 24, and 48 h after the last IV injection, all mice were euthanized to collect blood plasma by cardiac puncture. Then, tumors and other organs including kidney, liver, lung, heart, and spleen were collected, snap frozen in liquid nitrogen, and stored at -80°C for later use. Drug concentration was quantified using LC/MS/MS (mean ± SD). **(B)** A83B4C63 plasma concentration versus time curves of CE/A83 and NP/A83 formulations in HCT116 xenograft tumor-bearing mice. **(C**, **E**, **G**, **I**, **K**, **M)** represent A83B4C63 concentrations obtained from the excised tumor, kidney, liver, lung, heart, and spleen, respectively, after administration of CE/A8 and NP/A83. **(D**, **F**, **H**, **J**, **L**, **N)** represents the ratio of tissues (tumor, kidney, liver, lung, heart, and spleen, respectively) to plasma concentration of CE/A83 and NP/A83-treated xenograft mice. Differences were considered significant if $^{*}p \leq 0.05$, $^{**}p \leq 0.01$, and $^{****}p \leq 0.0001$ following two-way ANOVA followed by Tukey's test.

TABLE 1 | Calculated area under the curve (AUC) for plasma concentrations of CE/A83 and NP/A83 formulations in HCT116 tumor-bearing mice until 48 h time point post drug administration.

Specimens	Formulations	AUC ± SEM (ng.h/mL or g)
Plasma	CE/A83	21078.86 ± 1534.31
	NP/A83	34246.64 ± 3710.36*
Tumor	CE/A83	1071.11 ± 21.00
	NP/A83	3254.89 ± 259.94*
Kidney	CE/A83	2455.59 ± 374.71*
	NP/A83	1211.89 ± 177.67
Liver	CE/A83	6198.00 ± 2032.99
	NP/A83	10773.38 ± 3161.52*
Lung	CE/A83	2740.85 ± 695.96
	NP/A83	2409.93 ± 249.46
Heart	CE/A83	931.07 ± 188.99
	NP/A83	894.02 ± 161.52
Spleen	CE/A83	374.87 ± 45.43
	NP/A83	376.25 ± 49.65

*Significant differences between CE/A83 and NP/A83 were distinguished by *p < 0.05 (n = 3) according to student's t-test.*

to CE/A83 (*$p \leq 0.5$, student's t-test). However, no significant differences were observed between these treatment groups in lung, heart, and spleen (**Figures 6E–M**).

A83B4C63 concentrations in excised tumors from the mice were also measured and the results are shown in **Figures 6C, D**. The results showed tumor accumulation of A83B4C63 delivered by NP/A83 formulation at 48 h post injection, whereas the detected concentrations of A83B4C63 in CE/A83-treated xenografts were below the limit of detection at this time point. Calculation of tumor to plasma concentration ratio for the two formulations showed a significant increase at 48 h for the NP formulation as well.

Notably, CE/A83 formulation resulted in significantly higher accumulation of A83B4C63 in the kidney at 4 h post dose time point compared to that of NP/A83 (****$p \leq 0.0001$) (**Figure 6E**). Similarly, the kidney to plasma ratio (Kp value) yielded a significantly higher ratio for A83B4C63 in the kidney of mice treated with CE/A83 (**$p \leq 0.01$) compared to that of NP/A83-treated mice. In contrast, the obtained A83B4C63 concentration was significantly higher in the liver samples (**Figures 6G, H**) of NP/A83-treated mice than that of CE/A83-treated mice at 24 h (*$p \leq 0.05$) post dose, only. However, no significant difference was observed in liver to plasma ratio between CE/A83 and NP/A83 treatment groups.

DISCUSSION

Human PNKP phosphorylates DNA 5′-termini and dephosphorylates DNA 3′-termini, allowing DNA polymerases and ligases to rejoin the strands, and therefore plays a key role in both single- and double-strand break repair (30). PNKP has been identified as a potential therapeutic target in different types of cancer, as depletion of PNKP in cancer cells or tumor xenografts has shown a synthetic lethal partnership with the loss of the tumor suppressor protein PTEN (24, 33). Moreover, the downregulation of PNKP by siRNA or its inhibition by small molecule inhibitors have been shown to sensitize cancer cells to IR and to topoisomerase I inhibitors (24–26, 31, 32).

We have identified new small molecule inhibitors of PNKP. Our initial attention was on inhibition of the DNA 3′-phosphatase activity of PNKP, with a polysubstituted imidopiperidine, A12B4C3, identified as the first hit (31, 32). At a non-cytotoxic dose, A12B4C3 effectively sensitized human lung cancer A549 cells to IR and camptothecin. However, it failed to further sensitize the cancer cells that were already depleted of PNKP by shRNA, providing strong evidence for PNKP as the druggable target of A12B4C3 (25). The Reilly group showed that A12B4C3 sensitizes human myeloid leukemia cells to radio-immunotherapy providing more evidence for the promise of PNKP inhibitors as radio-sensitizers (62, 63).

PNKP inhibitors render tumors more susceptible to DNA damage by IR or topoisomerase I inhibitors but may act similarly on normal cells leading to intolerable toxicities in patients. To overcome the problem of non-specificity for cancer and, at the same time, to enhance the solubility of PNKP inhibitors for *in vivo* administration, we have developed NP formulations of a second generation polysubstituted imidopiperidine, named A83B4C63. Nanocarriers can significantly improve the therapeutic index of anticancer agents (43, 44). Nanocarriers are small enough to enter leaky blood vessels in solid tumors, but not normal blood vessels (64). Lymphatic function in tumors is impaired, thus nanocarriers are not drained effectively and accumulate in the tumor (65–67). NPs have the capacity to deliver higher quantities of drugs to targets and can be actively targeted to tumor cells (48). Nanocarriers of conventional anticancer agents (e.g., doxorubicin, paclitaxel, and irinotecan) have already found their way into the clinic (68, 69).

At a concentration range of 1-10 μM, both free and encapsulated A83B4C63 in PEO-*b*-PBCL NPs were effective in reducing the viability of PTEN$^{-/-}$ HCT116 cells but did not affect wild-type (WT) or HCT116/PTEN$^{+/+}$ cell viability (24, 33). Our previous study has also shown the success of PEO-*b*-PBCL NP formulations of A83B4C63 as monotherapeutic in the selective inhibition of tumor growth in PTEN-deficient HCT116 tumor xenografts, due to synthetic lethality in this cancer model (33). This contrasted with the CE formulations of this drug candidate that did not show anticancer activity in HCT116/PTEN$^{-/-}$ tumor xenografts when compared to mice receiving 5% dextrose. The current study focused on *in vitro* and *in vivo* evaluation of NP versus CE formulations of A83B4C63 in sensitization of HCT116/PTEN$^{+/+}$ tumors to IR. Radiation therapy is commonly used to treat rectal cancer (7, 70). In colon cancer, radiation therapy, is mostly used as a neoadjuvant therapy before surgery or as an adjuvant therapy after or during surgery to further eradicate cancerous cells (8–10). Radiation therapy is also used in metastatic CRC, where cancer has spread to liver or lung (22).

The NP/A83 formulation can successfully be reproduced and showed an average particle size of < 60 nm with low PDI,

consistent with our previous reports (24, 33). The NP/A83 formulation enhanced the solubility of A83B4C63 in water to a level over 6.5 mg/mL, enabling administration of the compound to mice at the desired therapeutic doses (71). Comparisons were made with a conventional CE-based solubilizing formulation of A83B4C63. CE is a well-known water-soluble nanocarrier for cyclosporin A and paclitaxel (72–74). However, CE is associated with acute or chronic side-effects (e.g. anaphylaxis, nephro- and neurotoxicity) (75, 76) and is also known to interfere with the pharmacokinetics of several drugs (77–83).

In vitro studies on HCT116 cells revealed the activity of A83B4C63 either as CE or NP formulation in delaying DNA repair and enhancing DNA damage persistence. This was evidenced through the measurement of γ-H2AX foci formation, which showed an increase in foci numbers upon co-treatment of cells with IR plus both A83B4C63 formulations compared to the IR treatment alone (**Figure 2**). The A83B4C63 formulations on their own, without IR, did not cause any significant rise in the level of γ-H2AX foci at the dose applied here, reflecting the lack of DNA damage induced by A83B4C63 alone.

For the *in vivo* studies, a relatively low fractionated dose (3 x 5 Gy) of IR was used to avoid potential side-effects on normal tissues surrounding the irradiated site (84). The treatment groups were shown to be safe and well-tolerated as there was no evidence for any toxicity symptoms, such as weight reduction in mice during and after the treatments. The HCT116 xenografts showed significant tumor growth delay when NP/A83 treatment was combined with the fractionated dose of IR. This observation was similar to our findings of the anticancer effect of A83B4C63 as a synthetic lethal mono-therapeutic in PTEN-deficient HCT116 xenografts, in which only NP/A83 and not CE/A83 was shown to be an effective anticancer agent. The activity of NP/A83 as a radio-sensitizer was confirmed through the analysis of three different tumor parameters: classical tumor volume measurements using slide calipers (**Figure 3**), optical imaging of LUC^+ tumors (**Figure 4**) and functional PET imaging using [^{18}F]FLT (**Figure 5**) to measure proliferation of tumor cells in live animals. Collectively these data validated the intravenously administered NP/A83 as a more effective radio-sensitizer than CE/A83 in CRC xenografts in mice. The data showed the overall lower effectiveness of the CE/A83 formulation in radio-sensitizing activity, *in vivo*. In addition, the data confirmed that [^{18}F]FLT PET could be used as a non-invasive functional imaging tool to detect and monitor therapeutic effects of NP/A83 in a translational clinical setting.

To shed some light on the reason behind the superior activity of NP/A83 over CE/A83 *in vivo*, we investigated the biodistribution profile of A83B4C63 in HCT116 CRC tumor-bearing mice following a similar administration schedule as used in the anticancer activity study. A83B4C63 is a new investigational drug and the effect of CE on its pharmacokinetic profile is not known. Our data on the biodistribution of NP/A83 versus CE/A83 formulations at 4, 24, and 48 h post last injection, revealed an interesting pattern (**Figure 6**): In plasma, following the administration of the CE formulation, A83B4C63 was eliminated rapidly, and no detectable drug levels were identified at the 48 h time point. The NP/A83, on the other hand, enhanced the resident time of A83B4C63 in plasma. This profile coincided with a delayed accumulation of A83B4C63 in tumor tissue 48 h following the last dose. Accordingly, a significant enhancement in the AUC of A83B4C63 in tumor tissue for the NP over CE formulation was achieved. This pattern contrasted with the distribution profile of NP versus CE formulations of A83B4C63 in normal tissues, where a decline in drug levels for both formulations was seen from 24 to 48 h. Among the normal tissues, liver was the only organ that showed significantly higher AUC for the NP formulation of A83B4C63. On the other hand, the AUC of NP formulations of A83B4C63 showed reduction in kidneys compared to the CE formulation. The reason for the delayed accumulation of A83B4C63 by its NP formulation in HCT116 xenografts is not clear and needs further investigation. Nevertheless, a sustained inhibition of PNKP resulting from higher accumulation of its nano-formulation in tumor xenografts along with a continuous release of the drug in the tumor site might have been responsible for the higher activity of NP/A83 over CE/A83, *in vivo*. The delayed distribution of NP/A83 in tumor tissue may provide opportunities for the optimization of intervals between chemo or radiation co-treatments with NP/A83, which will be explored in future. In this regard, assessing the variation in the concentration of NP/A83 in the tumor between injections would also be of immense interest.

CONCLUSIONS

In summary, our data demonstrated that the PNKP inhibitor, A83B4C63 loaded into mPEO-*b*-PBCL nanocarriers leads to additional radio-sensitizing effects in a CRC model, as analyzed both *in vitro* and *in vivo*. The present data provide a strong case for potential benefit of nanotechnology in the formulation of drug candidates for clinical development during the drug development process which can be monitored with non-invasive imaging methodologies through their translational path.

DATA AVAILABILITY STATEMENT

The raw data supporting the conclusions of this article will be made available by the authors, without undue reservation.

ETHICS STATEMENT

All animal studies were conducted in accordance with the guidelines of the Canadian Council on Animal Care and with approval from the local Animal Care Committee of the Cross Cancer Institute and University of Alberta (Edmonton, AB, Canada).

AUTHOR CONTRIBUTIONS

SS has been responsible for the design and completion of all studies in this manuscript. He has prepared the first draft of the manuscript. MWu has assisted in the conduction of *in vivo* radiation studies and edited the manuscript. IP, SM, NS, FS, and ZB have provided assistance in the biodistribution studies. XY has provided assistance in fluorescent microscopy measurements. GM, FJ, DM, and AG provided feedback on *in vivo* studies and edited the manuscript. MP has synthesized A83B4C63. DH has supervised the synthesis of A83B4C63 and edited the manuscript. MWe and AL have supervised the study and edited the manuscript. All authors contributed to the article and approved the submitted version.

FUNDING

This work was supported by grants funded by the Canadian Institutes of Health Research (MOP 15385) to MWe and (159757 and 178028) to AL, the Alberta Cancer Foundation Transformative Program Project (26603) to DH, FJ, AL, and MWe. Funding from Nanomedicine Innovation Network (NMIN) grant (2019-T1-06) to DH, MWe, and AL is also acknowledged.

ACKNOWLEDGMENTS

We thank Dr. Mary Hitt in Faculty of Medicine and Dentistry (University of Alberta) for their advice and technical assistance. We also thank Hao Fu for support in the HPLC analysis and purification of compound A83B4C63. The authors thank Floyd Baker, David Clendening, and Blake Lazurko from the Edmonton Radiopharmaceutical Center for ^{18}F production on a TR-19 cyclotron (Advanced Cyclotron Systems Inc, Vancouver, BC, Canada); Cody Bergman from the Dept. of Oncology at the University of Alberta for performing the radiosynthesis of [^{18}F] FLT as well as Dan McGinn from the Vivarium of the Cross Cancer Institute for support with the animal work. SS acknowledges funding from Alberta Innovates and CIHR Fellowships. SM and NS acknowledge funding from NSERC CREATE training PoND program. The SARRP device was purchased with funding awarded to DM from the Canadian Foundation for Innovation, Alberta Economic Development and Trade, and the Alberta Cancer Foundation.

SUPPLEMENTARY MATERIAL

The Supplementary Material for this article can be found online at: https://www.frontiersin.org/articles/10.3389/fonc.2021.772920/full#supplementary-material

Supplementary Figure 1 | (A) Chemical structure of Cremophor EL used in CE/A83 formulation. **(B)** TEM image of CE/A83.

Supplementary Figure 2 | (A) Representative western blot detection of cleaved PARP, cleaved caspase-7, and cleaved caspase-3 in HCT116 CRC cells pretreated with or without PNKP inhibitor (either CE/A83 or NP/A83 formulation). β-actin was used as a loading control. The conditions for all sample preparations and western blots were the same. The statistical analysis for the protein levels of **(B)** cleaved PARP, **(C)** cleaved caspase-7, and **(D)** cleaved caspase-3 was performed after normalization to β-actin. Differences were considered significant if $^{*}p \leq 0.05$, $^{**}p \leq 0.01$, $^{***}p \leq 0.001$, and $^{****}p \leq 0.0001$ following two-way ANOVA followed by Tukey's method. Data are expressed as mean ± SD (n = 3).

REFERENCES

1. Bray F, Ferlay J, Soerjomataram I, Siegel RL, TorreL A, Jemal A. Global Cancer Statistics 2018: GLOBOCAN Estimates of Incidence and Mortality Worldwide for 36 Cancers in 185 Countries. *CA: A Cancer J Clin* (2018) 68 (6):394–424. doi: 10.3322/caac.21492
2. Høydahl Ø, Edna T-H, Xanthoulis A, Lydersen S, Endreseth BH. Long-term trends in colorectal cancer: incidence, localization, and presentation. *BMC Cancer* (2020) 20:1077. doi: 10.1186/s12885-020-07582-x
3. Murphy CC, Harlan LC, Lund JL, Lynch CF, Geiger AM. Patterns of Colorectal Cancer Care in the United States: 1990-2010. *J Natl Cancer Inst* (2015) 107(10):1–11. doi: 10.1093/jnci/djv198
4. Kennedy RH, Francis EA, Wharton R, Blazeby JM, Quirke P, West NP, et al. Multicenter Randomized Controlled Trial of Conventional Versus Laparoscopic Surgery for Colorectal Cancer Within an Enhanced Recovery Programme: Enrol. *J Clin Oncol* (2014) 32(17):1804–11. doi: 10.1200/JCO.2013.54.3694
5. Koopman M, Antonini NF, Douma J, Wals J, Honkoop AH, Erdkamp FL, et al. Sequential Versus Combination Chemotherapy With Capecitabine, Irinotecan, and Oxaliplatin in Advanced Colorectal Cancer (CAIRO): A Phase III Randomised Controlled Trial. *Lancet* (2007) 370(9582):135–42. doi: 10.1016/S0140-6736(07)61086-1
6. Seymour MT, Maughan TS, Ledermann JA, Topham C, James R, Gwyther SJ, et al. Different Strategies of Sequential and Combination Chemotherapy for Patients With Poor Prognosis Advanced Colorectal Cancer (MRC FOCUS): A Randomised Controlled Trial. *Lancet* (2007) 370(9582):143–52. doi: 10.1016/S0140-6736(07)61087-3
7. Siegel RL, Miller KD, Goding Sauer A, Fedewa SA, Butterly LF, Anderson JC, et al. Colorectal Cancer Statistics, 2020. *CA: A Cancer J Clin* (2020) 70(3):145–64. doi: 10.3322/caac.21601
8. Overgaard M, Overgaard J, Sell A. Dose-Response Relationship for Radiation Therapy of Recurrent, Residual, and Primarily Inoperable Colorectal Cancer. *Radiother Oncol* (1984) 1(3):217–25. doi: 10.1016/S0167-8140(84)80003-1
9. Higgins GA Jr, Conn JH, Jordan PH, Humphrey EW, Roswit B, Keehn RJ. Preoperative Radiotherapy for Colorectal Cancer. *Ann Surg* (1975) 181 (5):624–31. doi: 10.1097/00000658-197505000-00017
10. Wolpin BM, Meyerhardt JA, Mamon HJ, Mayer RJ. Adjuvant Treatment of Colorectal Cancer. *CA: A Cancer J Clin* (2007) 57(3):168–85. doi: 10.3322/canjclin.57.3.168
11. Glimelius B, Grönberg H, Järhult J, Wallgren A, Cavallin-ståhl E. A Systematic Overview of Radiation Therapy Effects in Rectal Cancer. *Acta Oncol* (2003) 42 (5-6):476–92. doi: 10.1080/02841860310012301
12. Klein C, Dokic I, Mairani A, Mein S, Brons S, Häring P, et al. Overcoming Hypoxia-Induced Tumor Radioresistance in Non-Small Cell Lung Cancer by Targeting DNA-Dependent Protein Kinase in Combination With Carbon Ion Irradiation. *Radiat Oncol* (2017) 12(1):208. doi: 10.1186/s13014-017-0939-0
13. Dariya B, Aliya S, Merchant N, Alam A, Nagaraju GP. Colorectal Cancer Biology, Diagnosis, and Therapeutic Approaches. *Crit Rev Oncog* (2020) 25 (2):71–94. doi: 10.1615/CritRevOncog.2020035067
14. Falk M. Nanodiamonds and Nanoparticles as Tumor Cell Radiosensitizers-Promising Results But an Obscure Mechanism of Action. *Ann Trans Med* (2017) 5(1):18–8. doi: 10.21037/atm.2016.12.62

15. Brown JS, O'Carrigan B, Jackson SP, Yap TA. Targeting DNA Repair in Cancer: Beyond PARP Inhibitors. *Cancer Discov* (2017) 7(1):20–37. doi: 10.1158/2159-8290.CD-16-0860
16. Ledermann J, Harter P, Gourley C, Friedlander M, Vergote L, Rustin G, et al. Olaparib Maintenance Therapy in Patients With Platinum-Sensitive Relapsed Serous Ovarian Cancer: A Preplanned Retrospective Analysis of Outcomes by BRCA Status in a Randomised Phase 2 Trial. *Lancet Oncol* (2014) 15(8):852–61. doi: 10.1016/S1470-2045(14)70228-1
17. Lee JM, Ledermann JA, Kohn EC. PARP Inhibitors for BRCA1/2 Mutation-Associated and BRCA-Like Malignancies. *Ann Oncol* (2014) 25(1):32–40. doi: 10.1093/annonc/mdt384
18. Hunter JE, Willmore E, Irving JA, Hostomsky Z, Veuger SJ, Durkacz BW. Nf-κb Mediates Radio-Sensitization by the PARP-1 Inhibitor, AG-014699. *Oncogene* (2012) 31(2):251–64. doi: 10.1038/onc.2011.229
19. Lagunas-Rangel FA, Bermúdez-Cruz RM. Natural Compounds That Target DNA Repair Pathways and Their Therapeutic Potential to Counteract Cancer Cells. *Front Oncol* (2020) 10:598174. doi: 10.3389/fonc.2020.598174
20. Gupta P, Saha B, Chattopadhyay S, Patro BS. Pharmacological Targeting of Differential DNA Repair, Radio-Sensitizes WRN-Deficient Cancer Cells In Vitro and In Vivo. *Biochem Pharmacol* (2021) 186:114450. doi: 10.1016/j.bcp.2021.114450
21. Wilson A, Menon V, Khan Z, Alam A, Litovchick L, Yakovlev V. Nitric Oxide-Donor/PARP-Inhibitor Combination: A New Approach for Sensitization to Ionizing Radiation. *Redox Biol* (2019) 24:101169. doi: 10.1016/j.redox.2019.101169
22. George TJ, Franke AJ, Chakravarthy AB, Das P, Dasari A, El-Rayes BF, et al. National Cancer Institute (NCI) State of the Science: Targeted Radiosensitizers in Colorectal Cancer. *Cancer* (2019) 125(16):2732–46. doi: 10.1002/cncr.32150
23. Abbotts R, Thompson N, Madhusudan S. DNA Repair in Cancer: Emerging Targets for Personalized Therapy. *Cancer Manag Res* (2014) 6:77–92. doi: 10.2147/CMAR.S50497
24. Shire Z, Vakili MR, Morgan TDR, Hall DG, Lavasanifar A, Weinfeld M. Nanoencapsulation of Novel Inhibitors of PNKP for Selective Sensitization to Ionizing Radiation and Irinotecan and Induction of Synthetic Lethality. *Mol Pharm* (2018) 15(6):2316–26. doi: 10.1021/acs.molpharmaceut.8b00169
25. Bernstein NK, Karimi-Busheri F, Rasouli-Nia A, Mani R, Dianov G, Glover JN, Weinfeld M. Polynucleotide Kinase as a Potential Target for Enhancing Cytotoxicity by Ionizing Radiation and Topoisomerase I Inhibitors. *Anticancer Agents Med Chem* (2008) 8(4):358–67. doi: 10.2174/187152008784220311
26. Bernstein NK, Williams RS, Rakovszky ML, Cui D, Green R, Karimi-Busheri F, et al. The Molecular Architecture of the Mammalian DNA Repair Enzyme, Polynucleotide Kinase. *Mol Cell* (2005) 17(5):657–70. doi: 10.1016/j.molcel.2005.02.012
27. Chappell C, Hanakahi LA, Karimi-Busheri F, Weinfeld M, West SC. Involvement of Human Polynucleotide Kinase in Double-Strand Break Repair by Non-Homologous End Joining. *EMBO J* (2002) 21(11):2827–32. doi: 10.1093/emboj/21.11.2827
28. Karimi-Busheri F, Daly G, Robins P, Canas B, Pappin DJ, Sgouros J, et al. Molecular Characterization of a Human DNA Kinase. *J Biol Chem* (1999) 274 (34):24187–94. doi: 10.1074/jbc.274.34.24187
29. Rasouli-Nia A, Karimi-Busheri F, Weinfeld M. Stable Down-Regulation of Human Polynucleotide Kinase Enhances Spontaneous Mutation Frequency and Sensitizes Cells to Genotoxic Agents. *Proc Natl Acad Sci USA* (2004) 101 (18):6905–10. doi: 10.1073/pnas.0400099101
30. Weinfeld M, Mani RS, Abdou I, Aceytuno RD, Glover JN. Tidying Up Loose Ends: The Role of Polynucleotide Kinase/Phosphatase in DNA Strand Break Repair. *Trends Biochem Sci* (2011) 36(5):262–71. doi: 10.1016/j.tibs.2011.01.006
31. Freschauf GK, Karimi-Busheri F, Ulaczyk-Lesanko A, Mereniuk TR, Ahrens A, Koshy JM, et al. Identification of a Small Molecule Inhibitor of the Human DNA Repair Enzyme Polynucleotide Kinase/Phosphatase. *Cancer Res* (2009) 69(19):7739–46. doi: 10.1158/0008-5472.CAN-09-1805
32. Freschauf GK, Mani RS, Mereniuk TR, Fanta M, Virgen CA, Dianov GL, et al. Mechanism of Action of an Imidopiperidine Inhibitor of Human Polynucleotide Kinase/Phosphatase. *J Biol Chem* (2010) 285(4):2351–60. doi: 10.1074/jbc.M109.055764
33. Sadat SMA, Paiva IM, Shire Z, Sanaee F, Morgan TDR, Paladino M, et al. A Synthetically Lethal Nanomedicine Delivering Novel Inhibitors of Polynucleotide Kinase 3'-Phosphatase (PNKP) for Targeted Therapy of PTEN-Deficient Colorectal Cancer. *J Control Release* (2021) 334:335–52. doi: 10.1016/j.jconrel.2021.04.034
34. Koizumi F, Kitagawa M, Negishi T, Onda T, Matsumoto S, Hamaguchi T, et al. Novel SN-38-Incorporating Polymeric Micelles, NK012, Eradicate Vascular Endothelial Growth Factor-Secreting Bulky Tumors. *Cancer Res* (2006) 66(20):10048–56. doi: 10.1158/0008-5472.CAN-06-1605
35. Matsumura Y, Kataoka K. Preclinical and Clinical Studies of Anticancer Agent-Incorporating Polymer Micelles. *Cancer Sci* (2009) 100(4):572–9. doi: 10.1111/j.1349-7006.2009.01103.x
36. Dawidczyk CM, Kim C, Park JH, Russell LM, Lee KH, Pomper MG, et al. State-Of-the-Art in Design Rules for Drug Delivery Platforms: Lessons Learned From FDA-Approved Nanomedicines. *J Control Release* (2014) 187:133–44. doi: 10.1016/j.jconrel.2014.05.036
37. Estanqueiro M, Amaral H, Conceicao J, Sousa Lobo JM. Nanotechnological Carriers for Cancer Chemotherapy: The State of the Art. *Colloids Surf B Biointerfaces* (2015) 126:631–48. doi: 10.1016/j.colsurfb.2014.12.041
38. Pérez-Herrero E, Fernández-Medarde A. Advanced Targeted Therapies in Cancer: Drug Nanocarriers, the Future of Chemotherapy. *Eur J Pharm Biopharm* (2015) 93:52–79. doi: 10.1016/j.ejpb.2015.03.018
39. Peer D, Karp Jm, Hong S, Farokhzad OC, Margalit R, Langer R. Nanocarriers as an Emerging Platform for Cancer Therapy. *Nat Nanotechnol* (2007) 2 (12):751–60. doi: 10.1038/nnano.2007.387
40. Adams ML, Lavasanifar A, Kwon GS. Amphiphilic Block Copolymers for Drug Delivery. *J Pharm Sci* (2003) 92(7):1343–55. doi: 10.1002/jps.10397
41. Torchilin VP. Multifunctional, Stimuli-Sensitive Nanoparticulate Systems for Drug Delivery. *Nat Rev Drug Discov* (2014) 13(11):813–27. doi: 10.1038/nrd4333
42. Houdaihed L, Evans JC, Allen C. Overcoming the Road Blocks: Advancement of Block Copolymer Micelles for Cancer Therapy in the Clinic. *Mol Pharm* (2017) 14(8):2503–17. doi: 10.1021/acs.molpharmaceut.7b00188
43. Matsumura Y, Maeda H. A New Concept for Macromolecular Therapeutics in Cancer Chemotherapy: Mechanism of Tumoritropic Accumulation of Proteins and the Antitumor Agent Smancs. *Cancer Res* (1986) 46(12 Pt 1):6387–92.
44. Noguchi Y, Wu zj, Duncan R, Strohalm J, Ulbrich K, Akaike T. Early Phase Tumor Accumulation of Macromolecules: A Great Difference in Clearance Rate Between Tumor and Normal Tissues. *Jpn J Cancer Res* (1998) 89(3):307–14. doi: 10.1111/j.1349-7006.1998.tb00563.x
45. Kobayashi H, Choyke PL. Super Enhanced Permeability and Retention (SUPR) Effects in Tumors Following Near Infrared Photoimmunotherapy. *Nanoscale* (2016) 8(25):12504–9. doi: 10.1039/C5NR05552K
46. Chen L, Zang F, Wu H, Li J, Xie J, Ma M, et al. Using Pegylated Magnetic Nanoparticles to Describe the EPR Effect in Tumor for Predicting Therapeutic Efficacy of Micelle Drugs. *Nanoscale* (2018) 10(4):1788–97. doi: 10.1039/C7NR08319J
47. Aliabadi HM, Shahin M, Brocks DR, Lavasanifar A. Disposition of Drugs in Block Copolymer Micelle Delivery Systems: From Discovery to Recovery. *Clin Pharmacokinet* (2008) 47(10):619–34. doi: 10.2165/00003088-200847100-00001
48. Malam Y, Loizidou M, Seifalian AM. Liposomes and Nanoparticles: Nanosized Vehicles for Drug Delivery in Cancer. *Trends Pharmacol Sci* (2009) 30(11):592–9. doi: 10.1016/j.tips.2009.08.004
49. Paiva I, Mattingly S, Wuest M, Leier S, Vakili MR, Weinfeld M, et al. Synthesis and Analysis of (64)Cu-Labeled GE11-Modified Polymeric Micellar Nanoparticles for EGFR-Targeted Molecular Imaging in a Colorectal Cancer Model. *Mol Pharm* (2020) 17(5):1470–81. doi: 10.1021/acs.molpharmaceut.9b01043
50. Touré BB, Hoveyda HR, Tailor J, Ulaczyk-Lesanko A, Hall DG. A three-component reaction for diversity-oriented synthesis of polysubstituted piperidines: solution and solid-phase optimization of the first tandem aza[4 +2]/allylboration. *Chemistry* (2003) 9:466–74. doi: 10.1002/chem.200390049
51. Garg SM, Vakili MR, Lavasanifar A. Polymeric Micelles Based on Poly (Ethylene Oxide) and α-Carbon Substituted Poly(ε-Caprolactone): An In Vitro Study on the Effect of Core Forming Block on Polymeric Micellar Stability, Biocompatibility, and Immunogenicity. *Colloids Surfaces B: Biointerfaces* (2015) 132:161–70. doi: 10.1016/j.colsurfb.2015.05.015

52. Bondareva A, Bondareva A, Downey CM, Ayres F, Liu W, Boyd SK, et al. The Lysyl Oxidase Inhibitor, Beta-Aminopropionitrile, Diminishes the Metastatic Colonization Potential of Circulating Breast Cancer Cells. *PloS One* (2009) 4 (5):e5620.
53. Harlow E, Lane D. *Using Antibodies: A Laboratory Manual/Ed Harlow, David Lane*. Cold Spring Harbor, N.Y: Cold Spring Harbor Laboratory Press (1999).
54. Machulla HJ, Blocher A, Kuntzsch M, Piert M, Wei R, Grierson JR. Simplified Labeling Approach for Synthesizing 3′-Deoxy-3′-[18f]Fluorothymidine ([18f] FLT). *J Radioanalytical Nucl Chem* (2000) 243(3):843–6. doi: 10.1023/A:1010684101509
55. Bailer AJ. Testing for the equality of area under the curves when using destructive measurement techniques. *J Pharmacokinet Biopharm* (1988) 16:303–9.
56. Miller RG. Regression Techniques. In: RG Miller, editor. *Simultaneous Statistical Inference*. New York, NY: Springer New York (1981). p. 109–28.
57. Yuan J. Estimation of variance for AUC in animal studies. *J Pharm Sci* (1993) 82:761–3. doi: 10.1111/j.1476-5381.2010.00759.x
58. Mehvar R, Robinson MA, Reynolds JM. Molecular weight dependent tissue accumulation of dextrans: *in vivo* studies in rats. *J Pharm Sci* (1994) 83:1495–9. doi: 10.1002/jps.2600831024
59. Yu S, Piao H, Gao Y, Xu C, Tian Y, Wang L. Total Synthesis of Camptothecin and SN-38. *J Org Chem* (2012) 77(1):713–7. doi: 10.1021/jo201974f
60. Liu Y, Vakili MR, Paiva IM, Weinfeld M, Lavasanifar A. Comparison of Two Self-Assembled Macromolecular Prodrug Micelles With Different Conjugate Positions of SN38 for Enhancing Antitumor Activity. *Int J Nanomed* (2015) 10:2295–311. doi: 10.2147/IJN.S77957
61. Sadat SMA, Vakili MR, Paiva IM, Weinfeld M, Lavasanifar A. Development of Self-Associating SN-38-Conjugated Poly(Ethylene Oxide)-Poly(Ester) Micelles for Colorectal Cancer Therapy. *Pharmaceutics* (2020) 12(11):1033. doi: 10.3390/pharmaceutics12111033
62. Zereshkian A, Leyton JV, Cai Z, Bergstrom D, Weinfeld M, Reilly RM. The Human Polynucleotide Kinase/Phosphatase (Hpnkp) Inhibitor A12B4C3 Radiosensitizes Human Myeloid Leukemia Cells to Auger Electron-Emitting Anti-CD123 ^{111}in-NLS-7g3 Radioimmunoconjugates. *Nucl Med Biol* (2014) 41(5):377–83. doi: 10.1016/j.nucmedbio.2014.02.003
63. Srivastava P, Sarma A, Chaturvedi CM. Targeting DNA Repair With PNKP Inhibition Sensitizes Radioresistant Prostate Cancer Cells to High LET Radiation. *PloS One* (2018) 13(1):e0190516. doi: 10.1371/journal.pone.0190516
64. Bazak R, Houri M, Achy SE, Hussein W, Refaat T. Passive Targeting of Nanoparticles to Cancer: A Comprehensive Review of the Literature. *Mol Clin Oncol* (2014) 2(6):904–8. doi: 10.3892/mco.2014.356
65. Zhang H, Jiang Y, Ni X, Chen L, Wu M, Liu J. Glycyrrhetinic Acid-Modified Norcantharidin Nanoparticles for Active Targeted Therapy of Hepatocellular Carcinoma. *J BioMed Nanotechnol* (2018) 14(1):114–26. doi: 10.1166/jbn.2018.2467
66. Xia Y, Wu X, Zhao J, Zhao J, Li Z, Ren W. Three Dimensional Plasmonic Assemblies of Aunps With an Overall Size of Sub-200 Nm for Chemo-Photothermal Synergistic Therapy of Breast Cancer. *Nanoscale* (2016) 8 (44):18682–92. doi: 10.1039/C6NR07172D
67. Xu Z, Liu S, Kang Y, Wang M. Glutathione- and Ph-Responsive Nonporous Silica Prodrug Nanoparticles for Controlled Release and Cancer Therapy. *Nanoscale* (2015) 7(13):5859–68. doi: 10.1039/C5NR00297D
68. Green MR, Manikhas GM, Orlov S, Afanasyev B, Makhson AM, Bhar P, et al. Abraxane, a Novel Cremophor-Free, Albumin-Bound Particle Form of Paclitaxel for the Treatment of Advanced Non-Small-Cell Lung Cancer. *Ann Oncol* (2006) 17(8):1263–8. doi: 10.1093/annonc/mdl104
69. Wu D, Si M, Xue HY, Wong HL. Nanomedicine Applications in the Treatment of Breast Cancer: Current State of the Art. *Int J Nanomed* (2017) 12:5879–92. doi: 10.2147/IJN.S123437
70. Siegel RL, Miller KD, Fedewa SA, Ahnen DJ, Meester RGS, Barzi A, et al. Colorectal Cancer Statistics, 2017. *CA Cancer J Clin* (2017) 67(3):177–93. doi: 10.3322/caac.21395
71. Kalepu S, Nekkanti V. Insoluble Drug Delivery Strategies: Review of Recent Advances and Business Prospects. *Acta Pharm Sin B* (2015) 5(5):442–53. doi: 10.1016/j.apsb.2015.07.003
72. Ran Y, Zhao L, Xu Q, Yalkowsky SH. Solubilization of Cyclosporin a. *AAPS PharmSciTech* (2001) 2(1):E2. doi: 10.1208/pt020102
73. Gelderblom H, Verweij J, Nooter K, Sparreboom A. Cremophor EL: The Drawbacks and Advantages of Vehicle Selection for Drug Formulation. *Eur J Cancer* (2001) 37(13):1590–8. doi: 10.1016/S0959-8049(01)00171-X
74. Gelderblom H, Loos WJ, Verweij J, van der Burg ME, de Jonge MJ, Brouwer E, et al. Modulation of Cisplatin Pharmacodynamics by Cremophor EL: Experimental and Clinical Studies. *Eur J Cancer* (2002) 38(1):205–13. doi: 10.1016/S0959-8049(01)00348-3
75. Weiss RB, Donehower C, Wiernik PH, Ohnuma T, Gralla RJ, Trump DL, et al. Hypersensitivity Reactions From Taxol. *J Clin Oncol* (1990) 8(7):1263–8. doi: 10.1200/JCO.1990.8.7.1263
76. Sparreboom A, van Tellingen O, Nooijen WJ, Beijnen JH. Nonlinear Pharmacokinetics of Paclitaxel in Mice Results From the Pharmaceutical Vehicle Cremophor EL. *Cancer Res* (1996) 56(9):2112–5.
77. de Jonge ME, Huitema AD, Schellens JH, Rodenhuis S, Beijnen JH. Population Pharmacokinetics of Orally Administered Paclitaxel Formulated in Cremophor EL. *Br J Clin Pharmacol* (2005) 59(3):325–34. doi: 10.1111/j.1365-2125.2004.02325.x
78. Sykes E, Woodburn K, Decker D, Kessel D. Effects of Cremophor EL on Distribution of Taxol to Serum Lipoproteins. *Br J Cancer* (1994) 70(3):401–4. doi: 10.1038/bjc.1994.317
79. Ellis AG, Webster LK. Inhibition of Paclitaxel Elimination in the Isolated Perfused Rat Liver by Cremophor EL. *Cancer Chemother Pharmacol* (1999) 43 (1):13–8. doi: 10.1007/s002800050857
80. Gianni L, Gianni L, Vigano L, Locatelli A, Capri G, Giani A, et al. Human Pharmacokinetic Characterization and In Vitro Study of the Interaction Between Doxorubicin and Paclitaxel in Patients With Breast Cancer. *J Clin Oncol* (1997) 15(5):1906–15. doi: 10.1200/JCO.1997.15.5.1906
81. Scripture CD, Figg WD, Sparreboom A. Paclitaxel Chemotherapy: From Empiricism to a Mechanism-Based Formulation Strategy. *Ther Clin Risk Manag* (2005) 1(2):107–14. doi: 10.2147/tcrm.1.2.107.62910
82. Henningsson A, Marsh S, Loos WJ, Karlsson MO, Garsa A, Mross K, et al. Association of CYP2C8, CYP3A4, CYP3A5, and ABCB1 Polymorphisms With the Pharmacokinetics of Paclitaxel. *Clin Cancer Res* (2005) 11 (22):8097–104. doi: 10.1158/1078-0432.CCR-05-1152
83. Fransson MN, Green H, Litton JE, Friberg LE. Influence of Cremophor EL and Genetic Polymorphisms on the Pharmacokinetics of Paclitaxel and Its Metabolites Using a Mechanism-Based Model. *Drug Metab Dispos* (2011) 39(2):247–55. doi: 10.1124/dmd.110.035394
84. Wu M, Liu J, Hu C, Li D, Yang J, Wu Z, et al. Olaparib Nanoparticles Potentiated Radiosensitization Effects on Lung Cancer. *Int J Nanomed* (2018) 13:8461–72. doi: 10.2147/IJN.S181546

Conflict of Interest: The authors declare the following competing financial interest(s): Material in this manuscript has been included in recent US patent applications. AL is Vice-President of Meros Polymers which has the license to mPEO-b-PBCL polymer used in this manuscript.

Publisher's Note: All claims expressed in this article are solely those of the authors and do not necessarily represent those of their affiliated organizations, or those of the publisher, the editors and the reviewers. Any product that may be evaluated in this article, or claim that may be made by its manufacturer, is not guaranteed or endorsed by the publisher.

frontiers in Oncology

MINI REVIEW
published: 07 January 2022
doi: 10.3389/fonc.2021.768685

HBI-8000, HUYABIO Lead Clinical Program, Is a Selective Histone Deacetylase Inhibitor With Therapeutic Benefits in Leukemia and in Solid Tumors

Farbod Shojaei, Bob Goodenow, Gloria Lee, Fairooz Kabbinavar and Mireille Gillings*

HUYABIO International LLC, San Diego, CA, United States

HBI-8000 is a small molecule inhibitor of class I HDACs and has been approved for the treatment of PTCL, ATL and, in combination with exemestane, in a subpopulation of breast cancer. Given the roles of HDACs in normal and cancerous cells, there are currently multiple clinical trials, by HUYABIO International, to test the efficacy of HBI-8000 in monotherapy or in combination settings in leukemias and in solid tumors. The current review is focused on the applications of HDACi HBI-8000 in cancer therapy and its potential in combination with DDR agents.

Keywords: HBI-8000, HDACs, oncology, clinical, MOA, tumor immunology

OPEN ACCESS

Edited by:
Katherine Pawelczak,
NERx Biosciences, United States

Reviewed by:
Ramiro Vázquez,
Italian Institute of Technology (IIT), Italy
Nawar Al Nasrallah,
Indiana University Bloomington, United States

****Correspondence:***
Farbod Shojaei
fshojaei@huyabio.com

Specialty section:
This article was submitted to Cancer Molecular Targets and Therapeutics, a section of the journal Frontiers in Oncology

Received: *01 September 2021*
Accepted: *15 December 2021*
Published: *07 January 2022*

Citation:
Shojaei F, Goodenow B, Lee G, Kabbinavar F and Gillings M (2022) HBI-8000, HUYABIO Lead Clinical Program, Is a Selective Histone Deacetylase Inhibitor With Therapeutic Benefits in Leukemia and in Solid Tumors. Front. Oncol. 11:768685. doi: 10.3389/fonc.2021.768685

INTRODUCTION

HDACs and their role in physiological or disease status have been extensively studied (1). HBI-8000 (also known as CS055, tucidinostat, chidamide, Epidaza® or Hiyasta®) is an orally bioavailable small molecule inhibitor of histone deacetylases (HDACs) targeting the catalytic pocket of class I HDACs. Biochemical analysis revealed that HBI-8000 selectively inhibits HDAC1, 2, 3 (class I) and HDAC10 (class II) (2). As an epigenetic modulator, inhibition of HDACs by HBI-8000 affects the expression of multiple downstream genes involved in cancer cell survival and proliferation, thereby suppressing tumor growth and invasiveness (3). HBI-8000 (**Figure 1**) was originally discovered and developed by Chipscreen Biosciences (Shenzhen, China). HBI-8000 showed reasonable safety and tolerability in the IND enabling studies, and was approved in 2014 by the China National Medical Products Administration for the treatment of relapsed/refractory peripheral T cell lymphoma (PTCL) (5). Additionally, HBI-8000 was approved in 2019 in combination with aromatase inhibitors for the treatment of breast cancer (locally advanced or metastatic) (6).

Abbreviations: AE, Adverse event; AITL, Angioimmunoblastic T-cell lymphoma; ALCL, Anaplastic large cell lymphoma; ALK, Anaplastic lymphoma kinase; AML, Acute myeloid leukemia; ATL, Adult T cell lymphoma/leukemia; CCR4 CC, chemokine receptor 4; CFDA, China Food and Drug Administration; CPI, Checkpoint inhibitor; CI, Confidence interval; DDR, DNA Damage response; DNMT, DNA methyl transferase; EATL, Enteropathy-associated T-cell lymphoma; ER, Estrogen receptor; HR, Hormone receptor; NLRP3, Nucleotide-binding oligomerization domain, leucine rich repeat and pyrin domain containing 3; NSCLC, Non-small cell lung cancer; ORR, Objective response rate; OS, Overall survival; P, Placebo; PFS, Progression-free survival; PTCL, Peripheral T cell lymphoma; PTCL, NOS PTCL Not otherwise specified; R/R, Relapsed or refractory; RCC, Renal cell carcinoma; TE, Tucidinostat plus exemestane.

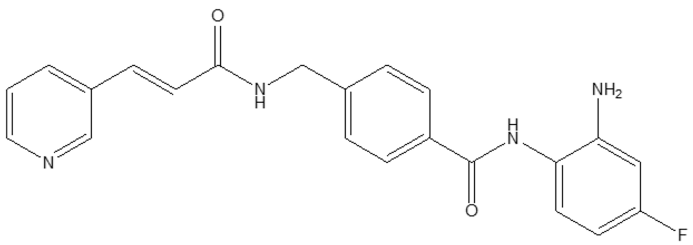

FIGURE 1 | HBI-8000 molecular structure N-(2-Amino-4-fluorophenyl)-4-[N-[(E)-3-(3-pyridyl) acryloyl]aminomethyl] benzamide (C22H19FN4O2; MW 390.41) (4).

HUYABIO International LLC (HUYABIO, San Diego, CA, USA) successfully licensed the rights to develop and commercialize HBI-8000 globally outside of China. HUYABIO initiated HBI-8000 clinical trials in relapsed/refractory adult T cell lymphoma/leukemia (R/R ATL) in Japan as monotherapy and later in combination with nivolumab in solid tumors in the USA. **Table 1** contains list of all the major clinical trials and indications sponsored by HUYABIO International.

HBI-8000 IN MONOTHERAPY

PTCL in China

PTCL is a subset of non-Hodgkin's lymphoma (NHL) comprised of the heterogenous populations of T-cells and NK cells (7). There are approximately 50000 patients diagnosed with PTCL in China each year. There is currently no first-line therapy in PTCL mainly due to limited number of patients and lack of randomized clinical trials. The main treatment options include stem cell transplantation and high-dose chemotherapy (5). Recent FDA approval of HDAC inhibitors [romidepsin (8) and belinostat (9)] in USA provided new treatment avenues for R/R PTCL patients. Similarly, chidamide was initially tested in China in R/R PTCL patients and in an open-label, single arm Phase II study with ORR being the primary endpoint (10). Out of 83 patients enrolled in the study, 79 were eligible to receive the therapy based on PTCL diagnosis. Patients were treated with chidamide at 30 mg BIW for 3 weeks and continued to receive the therapy till cancer progression. The ORR was 28% while the median OS and PFS were 21.4 and 2.1 months, respectively [4, 9]. The most notable AEs (≥ grade 3) were neutropenia (11%), leucopenia (13%) and thrombocytopenia (22%). These data led to approval of chidamide as an orphan drug by for R/R PTCL CFDA in 2014 (10).

R/R ATL in Japan

The safety and efficacy of HBI-8000 in PTCL in China (10) led to HUYABIO-sponsored registration studies in Japan following a Phase 1 trial in NHL (HBI-8000-201). These two registration studies were in PTCL (HBI-8000-203) and in refractory recurrent T-cell lymphoma ATL (HBI-8000-210).

ATL is a cancer of human mature T cells caused by infection with human T-cell lymphotropic virus 1 and is clinically divided into smothering, unfavorable chronic, lymphoma, and acute subtypes (11). According to the data provided by the Japan Ministry of Health, Labor, and Welfare, there are nearly 2000 ATL patients in Japan, 700–1000 of whom die from the disease each year (12). Aggressive ATL has a 3-year survival rate of only 25%. Conventional therapy includes chemotherapy, allogeneic hematopoietic stem cell transplantation, interferon-α treatment, and anti-CC chemokine receptor 4 antibody (mogamulizumab) therapy. The majority of ATL patients, however, develop resistance (relapse or refractory) to the above therapies, further emphasizing the need to develop novel approaches to treat ATL.

In 2016, Hasegawa and colleagues isolated ATL cells from relapsed patients and performed a cell viability assay with HBI-8000. The results of their investigation demonstrated induction of apoptosis in relapsed ATL cells treated with HBI-8000 and with a mean IC50 of 4.35 μM (3). Additionally, treatment with HBI-8000 resulted in the upregulation tumor suppressor genes such as p53 and p21 as an additional mechanism targeting ATL

TABLE 1 | HBI-8000 clinical trials.

Trial	Phase	Indication	Mono/Combo	Place	Clinical Trial Number	Status
HBI-8000-101	Phase I	All	Mono	USA		Completed
HBI-8000-201	Phase I	NHL	Mono	Japan	NCT02697552	Completed
HBI-8000-210	Phase II	R/R ATL	Mono	Japan	NCT02955589	Completed; JNDA accepted
HBI-8000-203	NDA	PTCL	Mono	Japan	NCT02953652	JNDA submitted
HBI-8000-302	Phase Ib/II	Melanoma, RCC, NSCLC	Combo	USA	NCT02718066	Ongoing, not recruiting
HBI-8000-303	Phase III	Melanoma	Combo	Global (Ex-China)	NCT04674683	Trial initiated
HBI-8000-304	Phase I FE and DDI	Healthy Volunteers	Mono	USA		Completed

NHL, non-Hodgkin's lymphoma; R/R ATL, relapsed/refractory adult T-cell leukemia/lymphoma; R/R PTCL, relapsed/refractory peripheral T-cell lymphoma; RCC, renal cell carcinoma; NSCLC, non-small cell lung cancer; JNDA, Japan new drug application; FE, food effect; DDI, drug-drug interaction.

cells (3). Gene expression studies identified the upregulation of Bim, a pro-apoptotic factor, and NLRP3 inflammasomes, confirming the role of HBI-8000 in the induction of apoptosis in ATL cells (3). Additionally, cell cycle analysis in ATL-treated primary cells showed induction of cell cycle arrest in G1 and accumulation of cell in sub-G1 phase indicative of delay in cell cycle progression and potentially cell proliferation (3). When histone acetylation was measured, it was found that exposure to HBI-8000 increased H3 and H4 histone acetylation in the ATL cells, thus confirming HBI-8000 target engagement.

Consistent with the preclinical observations, in a clinical trial twenty-three patients were treated with HBI-8000 orally twice weekly (BIW), ORR was 30.4% [95% confidence interval (CI) 13.2–52.9%]. Median progression free survival (PFS) was 1.7 months (95% CI 0.8–7.4), median duration of response (DOR) was seven months (95% CI 3–9), and median OS was 12.1 months (95% CI 2.1–18.0) (13). All patients experienced adverse events (AEs), predominantly hematologic and gastrointestinal. Incidence of grade ≥3 AEs was 78.3%; most were laboratory abnormalities (decreases in platelets, neutrophils, white blood cells, and anemia). HBI-8000 was well tolerated with expected toxicities that could be managed with supportive care and dose modifications. Results from this clinical trial led to the granting of an orphan disease designation to HBI-8000 for R/R ATL and a marketing approval by PMDA (Pharmaceuticals and Medical Devices Agency) in Japan and under the brand name of Hiyasta®.

Additionally, HBI-8000 (chidamide) was approved in China as the treatment for r/r PTCL, under the brand name of Epidaza®. In the registration study, and in 79 patients receiving chidamide, the ORR was 28% (22 of 79) including 14% (11 of 79) with complete response/unconfirmed complete response (CR/CRu). Median progression-free survival and overall survival were 2.1 and 21.4 months, respectively. ATL patients tended to have higher ORR (50%) and CR/CRu rate (40%), as well as more durable responses to chidamide treatment. Most adverse events (AEs) were grade 1 or 2, and grade ≥ 3 that occurred in ≥10% patients were thrombocytopenia (22%), leucopenia (13%) and neutropenia (11%), respectively (10). Similarly, in the registration study in patients with r/r PTCL conducted in Japan and in South Korea, in the intent to treatment analysis in a total of 55 patients, the median PFS was 24.1 weeks, median DOR was 50.1 weeks and median OS was 99.1 weeks. Among the 46 patients, evaluable for objective response according to protocol criteria, ORR was 45.7% (21/46 [95% CI: 30.9, 61.0]). ORRs in PTCL subtypes were PTCL-NOS 35.3% (12/34); AITL 87.5% (7/8); ALCL, ALK 33.3% (1/3) and EATL 100.0% (1/1) respectively. All 55 dosed patients experienced adverse events. Most frequent AEs were hematological such as thrombocytopenia and neutropenia, followed by non-hematological AEs such as diarrhea and decreased appetite. AEs led to study drug interruption or dose reduction were observed in 72.7% (40/55) and led to the treatment discontinuation in 32.7% (18/55), respectively. The incidence of Grade ≥3 AEs was 83.6% and most AEs were asymptomatic laboratory abnormalities. HUYABIO submitted the results from this study to PMDA and received regulatory approval in Japan in November 2021.

HBI-8000 IN COMBINATION THERAPY

Combination With Exemestane in HR+ Breast Cancer Patients (ACE Trial)

Preclinical studies indicated that HDAC inhibitors may sensitize resistant breast cancer cell lines to treatment with aromatase inhibitors through reduction of expression and stability of HER2 (14). ERs (estrogen receptor) transcriptional expression is regulated by a balance between recruitment of coactivators (causing transcriptional activation) such as HATs (histone acetyl transferases) (15) vs. recruitment of corepressors (downregulating suppression of transcription) such as HDACs (16). Therefore role of HDAC inhibitors in inhibiting activation of corepressors, leading to continuous expression of ER, suggested a potential therapeutic benefit for HDAC inhibitors in breast cancer in the clinic (17).

In addition to successful trials as monotherapy in subsets of leukemia patients, HBI-8000 was tested in combination with exemestane [steroidal aromatase inhibitor (18)] in post-menopausal HR+ breast cancer patients (6). In a randomized double-blind placebo control Phase III ACE trial, 365 patients were enrolled and assigned to tucidinostat (30 mg BIW) plus exemestane at 25 mg/kg qd (TE; n=244) or placebo (P; n=121) group. Patients were followed up for a median of 13.9 months, PFS was 7.4 vs. 3.8 months in the TE vs. P group respectively, and HR was 0.75 (6). The most common AE (grade 3 or 4) was neutropenia (51% in TE vs. 2% in P), thrombocytopenia (27% in TE vs 2% in P) and leucopenia (19% in TE vs 2% in P). The above data led to CFDA approval of tucidinostat in combination with exemestane in HR+ breast cancer (6).

Combination With Checkpoint Inhibitors in Solid Tumors

Recently CPIs have established themselves as the mainstay in cancer therapy. They have significantly improved treatment outcome in a subset of cancer patients and demonstrated the role of anti-tumor immunity in tumor progression and aggressiveness (19). However, similar to other anti-cancer agents, patients are either primarily refractory or develop resistance to CPI therapy over the course of treatment. Among the many factors involved in the development of resistance, epigenetic inhibitors have recently attracted increased attention, demonstrating a direct impact on the activity of tumor infiltrating immune cells *via* mechanisms such as i) induction of the activity of antigen-presenting cells and human leukocyte antigen expression, ii) reinvigoration of exhausted T cells, iii) upregulation of the expression of programmed death-ligand 1 (PD-L1) in cancer cells, and iv) modulating Treg cell activity in the tumor microenvironment (20). A recent study by Freeman and colleagues at Harvard University suggested that PD-L1 acetylation status determines its nuclear translocation and is necessary for anti-PD1 activity (21). PD-L1 is initially acetylated

by p300 and subsequent deacetylation by HDAC2 determines PD-L1 nuclear translocation. Pharmacologic inhibition of HDAC2 with a selective HDAC2 inhibitor (santacruzamate A), but not of HDAC6, blocks PD-L1 nuclear translocation and induces the expression of immune-related genes involved in boosting anti-tumor immunity (21). Consistently, targeting HDAC2 using small interference RNA or CRISPR-Cas9 recapitulates the pharmacologic inhibition (21). As mentioned in the introduction, HDAC2 is one of the main targets of HBI-8000, providing further evidence that HDAC2 plays a role in the induction of tumor immunity in the tumor microenvironment. Additionally, p53 acetylation showed to play an important role in PD-1 transcription in cancer cells resulting in their growth inhibition independent of the role of PD-1 in the immune system explaining a synergy between HDAC inhibitors and p53 in tumor growth suppression (22). Therefore, HDAC inhibitors appear to play an important role in targeting solid tumors by induction of tumor immunity and directly by acetylation of key components of cancer cells survival.

We tested the efficacy of HBI-8000 in combination with anti-PD1, anti-PD-L1 or anti-CTLA4 monoclonal antibodies in multiple preclinical tumor models (e.g. MC38, CT26, and A20) to investigate its activity in tumor immunity. Compared to single agent CPI monotherapy, HBI-8000 significantly inhibited tumor growth when combined with the above antibodies (23). Mechanistic analysis of tumors using nanoString gene expression showed upregulation of genes responsible for dendritic cell activity, natural killer cells, and cytotoxic T cells in HBI-8000 monotherapy and in combination groups (23). Interestingly, expression of this group of genes was downregulated in the anti-PD1 monotherapy group, further confirming role of HBI-8000 in the induction of activity of key components of tumor immunity (23). Thus, it appears that HBI-8000 plays an important role in converting the tumor microenvironment from cold (immunosuppressive) to hot when combined with CPIs.

The above observations further motivated HUYABIO to initiate a clinical study (HBI-8000-302) to test the safety and efficacy of HBI-8000 (oral, 30 mg, biweekly) in combination with the standard dose of nivolumab (Opdivo®, BMS Pharmaceuticals) in patients with melanoma, non-small cell lung cancer, and renal cell carcinoma. Safety analyses showed that the combination was well tolerated. Furthermore, the efficacy observed in the melanoma patients who were naïve to CPI based therapy was encouraging and showed a PFS of 36.9 months vs. 5.7 months for nivolumab monotherapy using publicly available data (24). Furthermore, the overall objective response rate was 69.4%, with 4% complete response and the disease control rate was 94.4% among 36 patients evaluable for objective response. After a median follow-up of 10.8 months among the 38 patients receiving any amount of HBI-8000, the PFS was 36.9 months based on the intent-to-treat analysis. These observations, albeit preliminary, compared favorably with nivolumab monotherapy in this patient population.

The clinical data from Study HBI-8000-302 corroborated the preclinical findings, consisted with the expected role of HBI-8000 in anti-tumor immunity in melanoma patients. HUYABIO is currently conducting the global Phase III program (HBI-8000-303) in several countries around the world.

HDACs AND DNA DAMAGE RESPONSE

Independent of HBI-8000 studies, Miller et al., investigated role of HDACs in DDR (DNA damage response) and showed localization of HDACs 1&2 at DNA damage sites causing a reduction in acetylated H3K56 and H4K16 in cell lines treated with laser micro-irradiation (25). Treatment with an HDACi (sodium butyrate) blocked localization of HDAC 1&2 at the DNA damage sites. Depletion of both HDACs 1&2 but not HDAC3 resulted in hyperacetylation of H3K56 and H4K16 in human cancer cell lines. The HDAC 1&2 depleted cells were more sensitive to DDR signaling as measured by γH2AX and showed significant defect in repair mechanisms (26). Overall, these investigations indicated a significant role for HDACs 1&2 in DDR and suggested an additional mechanism for anti-tumor activity of inhibitors of HDAC 1&2 such as HBI-8000. Furthermore, combination of Vorinostat [a pan HDAC inhibitor (27)] and AZD1775 [targeting Wee1, a cell cycle checkpoint molecule (28)] showed synergy in tumor growth inhibition in a preclinical model of AML and *via* induction of DNA damage and premature entry into mitosis (29). These data further indicate an important role for HDAC inhibitors in future combination therapies with DNA damage agents in certain subset of cancer patients.

DISCUSSION

Epigenetics plays an important role in regulating gene expression in normal and cancerous cells. Epigenetic factors (such as HDACs and DNMTs) have long been studied for their role in tumor progression. Given the ubiquitous expression of epigenetic factors in many cell types in TME and pending cancer type, epigenetic modulators may affect tumor growth *via* several mechanisms mainly induction of apoptosis, promotion of tumor immunity and interference with DDR. Overall, available preclinical and clinical data suggest HBI-8000 play significant roles in cancer therapy, either as monotherapy in ATL and PTCL or in combination with mainstay treatment, such as immune CPIs or aromatase inhibitors, in solid tumors. Recent studies on detailed molecular mechanisms of epigenetic factors along with biomarker identification for patient stratification may support application of epigenetic modulators such as HBI-8000 in combination therapy with other anti-cancer modalities.

AUTHORS CONTRIBUTIONS

FS wrote the first of the manuscript, all authors (FS, BG, GL, FK, and MG) contributed in editing and revising the manuscript in preparation to generate the final version.

REFERENCES

1. McClure JJ, Li X, Chou CJ. Advances and Challenges of HDAC Inhibitors in Cancer Therapeutics. *Adv Cancer Res* (2018) 138:183–211. doi: 10.1016/bs.acr.2018.02.006
2. Ning ZQ, Li ZB, Newman MJ, Shan S, Wang XH, Pan DS, et al. Chidamide (CS055/HBI-8000): A New Histone Deacetylase Inhibitor of the Benzamide Class With Antitumor Activity and the Ability to Enhance Immune Cell-Mediated Tumor Cell Cytotoxicity. *Cancer Chemother Pharmacol* (2012) 69:901–9. doi: 10.1007/s00280-011-1766-x
3. Hasegawa H, Bissonnette RP, Gillings M, Sasaki D, Taniguchi H, Kitanosono H, et al. Induction of Apoptosis by HBI-8000 in Adult T-Cell Leukemia/Lymphoma is Associated With Activation of Bim and NLRP3. *Cancer Sci* (2016) 107:1124–33. doi: 10.1111/cas.12971
4. Lu X-P, Xie A, Shi L, Li B, Ning Z, Shan S, et al. *Benzamide Derivatives as Histone Deacetylase Inhibitors With Potent Differentation And Ant-Proliferation Activity*. United States Patent US 7.550,490 B2 (Jun. 23, 2009).
5. Lu X, Ning Z, Li Z, Cao H, Wang X. Development of Chidamide for Peripheral T-Cell Lymphoma, the First Orphan Drug Approved in China. *Intractable Rare Dis Res* (2016) 5:185–91. doi: 10.5582/irdr.2016.01024
6. Jiang Z, Li W, Hu X, Zhang Q, Sun T, Cui S, et al. Tucidinostat Plus Exemestane for Postmenopausal Patients With Advanced, Hormone Receptor-Positive Breast Cancer (ACE): A Randomised, Double-Blind, Placebo-Controlled, Phase 3 Trial. *Lancet Oncol* (2019) 20:806–15. doi: 10.1016/S1470-2045(19)30164-0
7. Armitage JO, Vose JM, Weisenburger DD. Towards Understanding the Peripheral T-Cell Lymphomas. *Ann Oncol* (2004) 15:1447–9. doi: 10.1093/annonc/mdh409
8. Coiffier B, Pro B, Prince HM, Foss F, Sokol L, Greenwood M, et al. Results From a Pivotal, Open-Label, Phase II Study of Romidepsin in Relapsed or Refractory Peripheral T-Cell Lymphoma After Prior Systemic Therapy. *J Clin Oncol* (2012) 30:631–6. doi: 10.1200/JCO.2011.37.4223
9. O'Connor OA, Horwitz S, Masszi T, Van Hoof A, Brown P, Doorduijn J, et al. Belinostat in Patients With Relapsed or Refractory Peripheral T-Cell Lymphoma: Results of the Pivotal Phase II BELIEF (CLN-19) Study. *J Clin Oncol* (2015) 33:2492–9. doi: 10.1200/JCO.2014.59.2782
10. Shi Y, Dong M, Hong X, Zhang W, Feng J, Zhu J, et al. Results From a Multicenter, Open-Label, Pivotal Phase II Study of Chidamide in Relapsed or Refractory Peripheral T-Cell Lymphoma. *Ann Oncol* (2015) 26:1766–71. doi: 10.1093/annonc/mdv237
11. Sabattini E, Bacci F, Sagramoso C, Pileri SA. WHO Classification of Tumours of Haematopoietic and Lymphoid Tissues in 2008: An Overview. *Pathologica* (2010) 102:83–7.
12. Katsuya H, Ishitsuka K, Utsunomiya A, Hanada S, Eto T, Moriuchi Y, et al. Treatment and Survival Among 1594 Patients With ATL. *Blood* (2015) 126:2570–7. doi: 10.1182/blood-2015-03-632489
13. Tsukasaki K, Hermine O, Bazarbachi A, Ratner L, Ramos JC, Harrington WJr., et al. Definition, Prognostic Factors, Treatment, and Response Criteria of Adult T-Cell Leukemia-Lymphoma: A Proposal From an International Consensus Meeting. *J Clin Oncol* (2009) 27:453–9. doi: 10.1200/JCO.2008.18.2428
14. Sabnis GJ, Goloubeva OG, Kazi AA, Shah P, Brodie AH. HDAC Inhibitor Entinostat Restores Responsiveness of Letrozole-Resistant MCF-7Ca Xenografts to Aromatase Inhibitors Through Modulation of Her-2. *Mol Cancer Ther* (2013) 12:2804–16. doi: 10.1158/1535-7163.MCT-13-0345
15. Kim MY, Hsiao SJ, Kraus WL. A Role for Coactivators and Histone Acetylation in Estrogen Receptor Alpha-Mediated Transcription Initiation. *EMBO J* (2001) 20:6084–94. doi: 10.1093/emboj/20.21.6084
16. Mazumdar A, Wang RA, Mishra SK, Adam L, Bagheri-Yarmand R, Mandal M, et al. Transcriptional Repression of Oestrogen Receptor by Metastasis-Associated Protein 1 Corepressor. *Nat Cell Biol* (2001) 3:30–7. doi: 10.1038/35050532
17. Jang ER, Lim SJ, Lee ES, Jeong G, Kim TY, Bang YJ, et al. The Histone Deacetylase Inhibitor Trichostatin a Sensitizes Estrogen Receptor Alpha-Negative Breast Cancer Cells to Tamoxifen. *Oncogene* (2004) 23:1724–36. doi: 10.1038/sj.onc.1207315
18. Giudici D, Ornati G, Briatico G, Buzzetti F, Lombardi P, di Salle E. 6-Methylenandrosta-1,4-Diene-3,17-Dione (FCE 24304): A New Irreversible Aromatase Inhibitor. *J Steroid Biochem* (1988) 30:391–4. doi: 10.1016/0022-4731(88)90129-X
19. Kawakami Y OS, Sayem MA, Tsukamoto N, Yaguchi T. Immune-Resistant Mechanisms in Cancer Immunotherapy. *Int J Clin Oncol* (2020). doi: 10.1007/s10147-019-01611-x
20. Barrero MJ. Epigenetic Strategies to Boost Cancer Immunotherapies. *Int J Mol Sci* (2017) 18. doi: 10.3390/ijms18061108
21. Gao Y, Nihira NT, Bu X, Chu C, Zhang J, Kolodziejczyk A, et al. Acetylation-Dependent Regulation of PD-L1 Nuclear Translocation Dictates the Efficacy of Anti-PD-1 Immunotherapy. *Nat Cell Biol* (2020) 22:1064–75. doi: 10.1038/s41556-020-0562-4
22. Cao Z, Kon N, Liu Y, Xu W, Wen J, Yao H, et al. An Unexpected Role for P53 in Regulating Cancer Cell-Intrinsic PD-1 by Acetylation. *Sci Adv* (2021) 7. doi: 10.1126/sciadv.abf4148
23. Bissonnette RP, Cesario RM, Goodenow B, Shojaei F, Gillings M. The Epigenetic Immunomodulator, HBI-8000, Enhances the Response and Reverses Resistance to Checkpoint Inhibitors. *BMC Cancer* (2021) 21:969. doi: 10.1186/s12885-021-08702-x
24. Arheden A, Skalenius J, Bjursten S, Stierner U, Ny L, Levin M, et al. Real-World Data on PD-1 Inhibitor Therapy in Metastatic Melanoma. *Acta Oncol* (2019) 58:962–6. doi: 10.1080/0284186X.2019.1620966
25. Miller KM, Tjeertes JV, Coates J, Legube G, Polo SE, Britton S, et al. Human HDAC1 and HDAC2 Function in the DNA-Damage Response to Promote DNA Nonhomologous End-Joining. *Nat Struct Mol Biol* (2010) 17:1144–51. doi: 10.1038/nsmb.1899
26. Mah LJ, El-Osta A, Karagiannis TC. Gammah2ax: A Sensitive Molecular Marker of DNA Damage and Repair. *Leukemia* (2010) 24:679–86. doi: 10.1038/leu.2010.6
27. Grant S, Easley C, Kirkpatrick P. Vorinostat. *Nat Rev Drug Discov* (2007) 6:21–2. doi: 10.1038/nrd2227
28. Do K, Doroshow JH, Kummar S. Wee1 Kinase as a Target for Cancer Therapy. *Cell Cycle* (2013) 12:3159–64. doi: 10.4161/cc.26062
29. Zhou L, Zhang Y, Chen S, Kmieciak M, Leng Y, Lin H, et al. A Regimen Combining the Wee1 Inhibitor AZD1775 With HDAC Inhibitors Targets Human Acute Myeloid Leukemia Cells Harboring Various Genetic Mutations. *Leukemia* (2015) 29:807–18. doi: 10.1038/leu.2014.296

Conflict of Interest: All authors were employed by HUYABIO International LLC.

frontiers in Oncology

MINI REVIEW
published: 28 January 2022
doi: 10.3389/fonc.2022.808757

Metnase and EEPD1: DNA Repair Functions and Potential Targets in Cancer Therapy

Jac A. Nickoloff[1], Neelam Sharma[1], Lynn Taylor[1], Sage J. Allen[1], Suk-Hee Lee[2] and Robert Hromas[3]*

[1] Department of Environmental and Radiological Health Sciences, Colorado State University, Fort Collins, CO, United States, [2] Department of Biochemistry & Molecular Biology, Indiana University School of Medicine, Indianapolis, IN, United States, [3] Division of Hematology and Medical Oncology, Department of Medicine and the Mays Cancer Center, University of Texas Health Science Center, San Antonio, TX, United States

Cells respond to DNA damage by activating signaling and DNA repair systems, described as the DNA damage response (DDR). Clarifying DDR pathways and their dysregulation in cancer are important for understanding cancer etiology, how cancer cells exploit the DDR to survive endogenous and treatment-related stress, and to identify DDR targets as therapeutic targets. Cancer is often treated with genotoxic chemicals and/or ionizing radiation. These agents are cytotoxic because they induce DNA double-strand breaks (DSBs) directly, or indirectly by inducing replication stress which causes replication fork collapse to DSBs. EEPD1 and Metnase are structure-specific nucleases, and Metnase is also a protein methyl transferase that methylates histone H3 and itself. EEPD1 and Metnase promote repair of frank, two-ended DSBs, and both promote the timely and accurate restart of replication forks that have collapsed to single-ended DSBs. In addition to its roles in HR, Metnase also promotes DSB repair by classical non-homologous recombination, and chromosome decatenation mediated by TopoIIα. Although mutations in Metnase and EEPD1 are not common in cancer, both proteins are frequently overexpressed, which may help tumor cells manage oncogenic stress or confer resistance to therapeutics. Here we focus on Metnase and EEPD1 DNA repair pathways, and discuss opportunities for targeting these pathways to enhance cancer therapy.

Keywords: DNA repair, DNA double-strand breaks, genome instability, homologous recombination, non-homologous end-joining, chromosome decatenation, DNA damage

OPEN ACCESS

Edited by:
Peter McHugh, University of Oxford, United Kingdom

Reviewed by:
Edward Ayson Motea, Indiana University-Purdue University Indianapolis, United States
Jeremy Stark, Beckman Research Institute, City of Hope, United States

****Correspondence:***
Jac A. Nickoloff
J.Nickoloff@colostate.edu

Specialty section:
This article was submitted to Cancer Molecular Targets and Therapeutics, a section of the journal Frontiers in Oncology

Received: *03 November 2021*
Accepted: *12 January 2022*
Published: *28 January 2022*

Citation:
Nickoloff JA, Sharma N, Taylor L, Allen SJ, Lee S-H and Hromas R (2022) Metnase and EEPD1: DNA Repair Functions and Potential Targets in Cancer Therapy. Front. Oncol. 12:808757. doi: 10.3389/fonc.2022.808757

INTRODUCTION

DNA damage is a constant threat to genome integrity and numerous DNA damage sensing, signaling, and repair systems help manage these threats, collectively called the DNA damage response (DDR). DNA damage arises spontaneously due to DNA lability, reactive oxygen species generated during oxidative metabolism, activity of various nucleases such as RAG1/2, AID/APOBEC deaminases, and mis-incorporated ribonucleotides (1–7). Exogenous sources of DNA damage comprise physical agents including non-ionizing and ionizing radiation (UV light, X-rays,

γ-rays, charged particles), and DNA-reactive chemicals such as alkylating agents and others used as cancer chemotherapeutics (8–11). DNA lesions include ring-opened bases, adducts, inter- and intra-strand crosslinks, protein-DNA crosslinks, and single- and double-strand breaks (DSBs). DSBs are among the most dangerous lesions as they can lead to deleterious mutations (including deletions and insertions), genome rearrangements, and cell death if mis-repaired or unrepaired. The DDR is critical for maintaining genome stability and preventing cancer. The often-altered DDR in cancer cells can thwart the action of anti-tumor chemo- and radiotherapeutics, thus DDR factors are important therapeutic targets (12–14).

DSB sensors and signal transducers include three phosphatidyl inositol 3' kinase-related kinases (PIKKs), DNA-PKcs, ATM and ATR, and other regulatory factors such as 53BP1, Ku70/Ku80, MRE11-RAD50-NBS1 (MRN), BRCA1, and RIF1 (15). SIRT6, a chromatin-associated protein of the SIRT family of NAD^+-dependent deacylases and ADP-ribosylases, was recently shown to sense DSBs, promote recruitment of ATM and DSB repair proteins, and promote phosphorylation of histone H2AX (γH2AX) in megabase-pair chromatin domains flanking DSBs (16). PIKK signals can arrest the cell cycle and promote repair, or activate apoptosis of heavily damaged cells (17). Apoptotic signaling by p53 or other checkpoint factors is often dysregulated in cancer, and this promotes tumor cell survival despite significant damage due to endogenous and exogenous stress, i.e., oncogenic stress or genotoxic therapeutics, respectively (18, 19).

Some DSBs, such as those induced directly by radiation, described as 'frank' or 'two-ended' DSBs, are repaired by at least four pathways. The two major DSB repair pathways in mammalian cells are classical non-homologous end-joining (cNHEJ) and homologous recombination (HR) (**Figure 1A**). cNHEJ is an error-prone, template-free pathway mediated by Ku70/Ku80, DNA-PKcs, Artemis, DNA polymerases (Pol) μ and λ, XLF, XRCC4, and DNA ligase IV. cNHEJ typically results in small (<20 bp) deletions or short (1-2 bp) insertions (20), but it also mediates translocations if broken ends from different chromosomes are joined (21). HR is generally accurate as it uses a homologous sequence (usually the sister chromatid) as a repair template. 'Misuse' of non-sister templates, such as homologous chromosomes or repetitive elements, causes small- and large-scale genome alterations including local loss of heterozygosity by gene conversion, arm-level loss of heterozygosity by inter-homolog crossovers, deletions, inversions, and translocations that are cancer hallmarks (22–24). HR is mediated by RAD51, assisted by BRCA1/2, RAD52, RAD54/B, five RAD51 paralogs (XRCC2, XRCC3, RAD51B, RAD51C, and RAD51D), and the Fanconi anemia proteins (25, 26). End resection is the key determinant of cNHEJ vs. HR pathway choice, regulated by anti-resection factors 53BP1 and RIF1, pro-resection factors BRCA1 and CtIP, and mediated by MRE11, EXO1, and DNA2-BLM (27–32). cNHEJ and HR are backed up by error-prone, alternative NHEJ (aNHEJ) and by single-strand annealing (SSA) (33–36) (**Figure 1B**). aNHEJ requires limited end resection to expose 1-16 nt microhomologies flanking the DSB, although aNHEJ can efficiently join ends with longer ssDNA tails (~50-75 nt) (37, 38). SSA requires more extensive resection to expose long, homologous repeats that are annealed by RAD52 (34); SSA resection tracts >25 kbp have been observed in yeast (39).

A distinct type of DSB arises when replication forks are remodeled or collapse to single-ended DSBs (seDSBs) through fork encounters with single-strand breaks, fork regression to a four-way junction (chicken foot), or when stressed forks are cleaved by structure-specific endonucleases MUS81 or EEPD1 (40–43) (**Figures 1C, D**). An important distinction between frank, two-ended DSBs and seDSBs is that the latter pose significant risk of large deletions or translocations, if repaired by cNHEJ or aNHEJ. Despite these risks, stressed forks are frequently processed to seDSBs by fork regression or fork cleavage (40, 44, 45). Cells have seveal other options to complete DNA replication in the face of replication stress, including rescue of stressed forks by an adjacent fork, translesion synthesis, repriming, and template switching, however, these pathways also pose risks to genome integrity (46–48). Cells prevent genome rearrangements due to misrepair of seDSBs by resecting seDSB ends, which blocks cNHEJ and promotes accurate, HR-mediated fork restart (**Figures 1C, D**) (47). Many of the same HR factors that mediate HR repair of frank DSBs also mediate HR repair of seDSBs to accurately restart collapsed forks. Of note, end resection is critical for HR repair in both repair contexts (26, 47).

Several structure-specific nucleases have been implicated in replication stress responses. The 3' nuclease MUS81 (with EME1 and EME2 cofactors) cleaves Holiday junction intermediates arising during DSB repair by HR, and stressed replication forks (**Figure 1D**) (40, 41, 49–53). EEPD1 is a 5' nuclease that cleaves stressed replication forks, complementing the 3' activity of MUS81 (**Figure 1D**) (42, 43). SLX1, with the SLX4 scaffold protein, cleaves branched DNA structures such as replication forks *in vitro*, but there is no direct evidence that SLX1 cleaves stalled forks *in vivo* (54, 55). Metnase is structure-specific nuclease that promotes restart of stressed replication forks, but Metnase doesn't cleave stressed replication forks *in vivo*, and may instead process flaps or other branched structures that arise during HR-mediated fork restart (43). Here, we focus on EEPD1 and Metnase roles in DSB repair, replication stress checkpoint activation, restart of stressed forks, and cellular resistance to DNA damaging agents. These topics are discussed with respect to their potential roles in cancer etiology and as therapeutic targets.

METNASE: A PROTEIN METHYLTRANSFERASE AND STRUCTURE-SPECIFIC ENDONUCLEASE THAT PROMOTES DNA REPAIR IN ALL CYCLE PHASES

Metnase was originally called SETMAR to reflect its SET and *Mariner* lineage (56), but it was renamed Metnase to emphasize its protein methylase and nuclease activities (57). Metnase arose ~50 Mya in monkeys when an Hsmar1 (*Mariner*) transposon

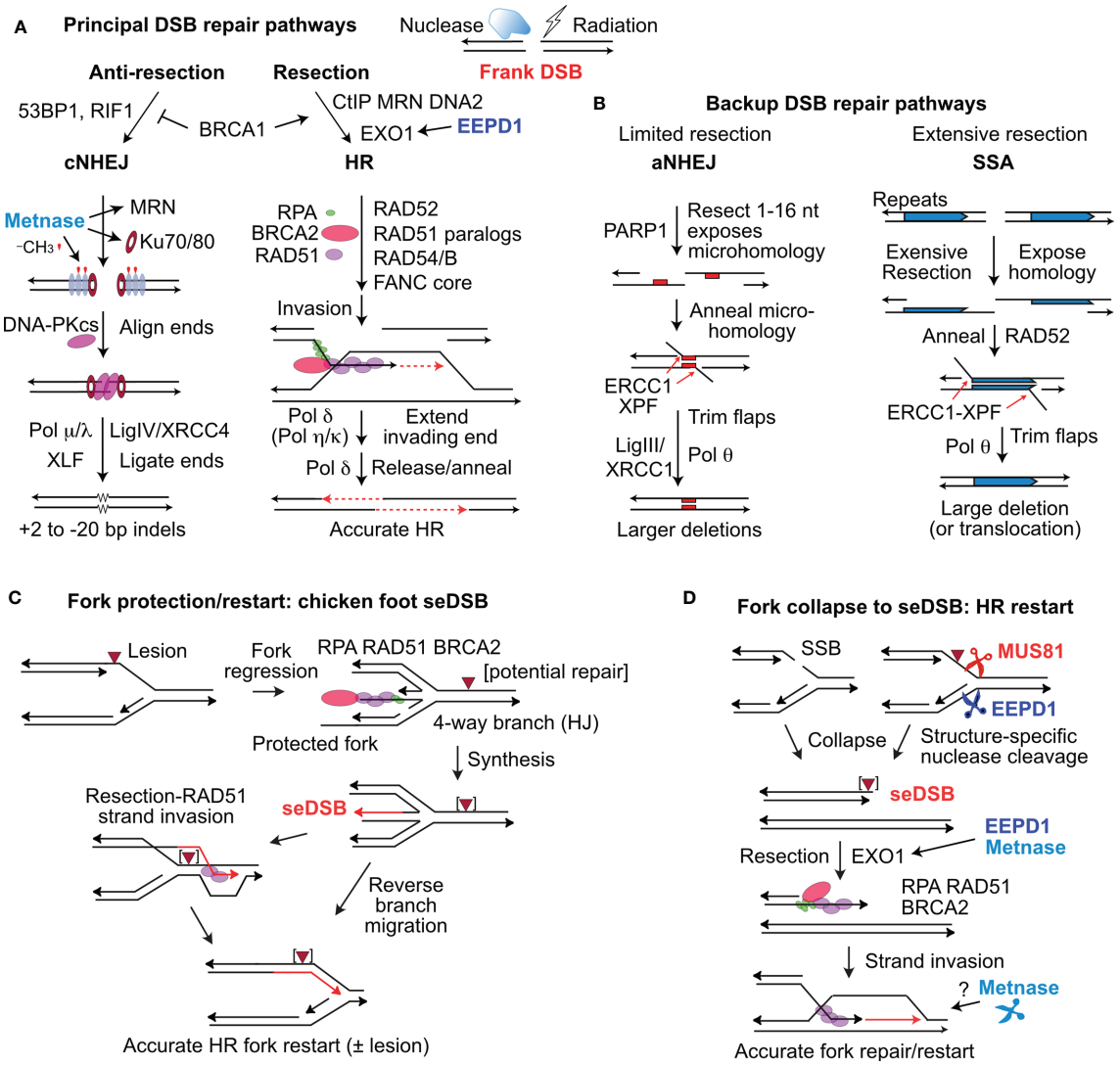

FIGURE 1 | Repair of frank DSBs and seDSBs at collapsed replication forks. **(A)** Nucleases and ionizing radiation create frank, two-ended DSBs processed mainly by cNHEJ and HR regulated by factors that suppress resection (53BP1, RIF1) and those that promote resection (CtIP, MRN, DNA2, and EXO1), controlled by BRCA1. EEPD1 promotes resection through interactions with EXO1. Metnase promotes cNHEJ by methylating histone H3 (red symbols) in nucleosomes (grey ovals) near the DSB, and by promoting recruitment/retention of Ku and MRN. DNA-PKcs interacts with Ku and DNA ends to align ends and promote ligation by DNA ligase IV and other factors. Resected ends are repaired by HR by RAD51 loaded onto resected DNA, mediated by many factors including RPA and BRCA2. RAD51-ssDNA invades homologous duplex DNA and the end is extended (red, dashed arrows), and then released to pair with the second resected end. Gap filling and ligation completes accurate HR repair. **(B)** aNHEJ and SSA are backup repair pathways. aNHEJ results in larger deletions as ends are aligned at 1-6 nt microhomologies (red rectangles) flanking the DSB exposed by limited resection. 3' flaps are trimmed by ERCC1-XPF and Ligase III-XRCC1 and Pol θ complete repair that results in loss of one microhomology and intervening sequences. SSA is analogous to aNHEJ but requires extensive resection to expose repeated sequences that anneal in a RAD52-dependent reaction. SSA between linked repeats (shown) deletes one repeat and the intervening sequence; SSA between non-linked repeats results in translocations (not shown). **(C)** Forks stalled at blocking lesions can regress to a 4-way branched (chicken foot) structure similar to a Holiday junction (HJ). Extension of the leading nascent strand using the lagging nascent strand as template allows the leading strand to bypass the lesion in the leading template strand. The regressed fork can be restored to a functional fork by reverse branch migration, or by RAD51-mediated strand invasion beyond the blocking lesion. **(D)** Forks may collapse to seDSBs by encountering a single-strand nick, or blocked forks may be cleaved by MUS81 or EEPD1. Resection of the seDSB by EXO1 is promoted by both EEPD1 and Metnase, allowing RAD51-mediated HR to reestablish the fork. Metnase nuclease doesn't cleave forks, but it may promote HR-mediated fork restart by processing late HR intermediates.

integrated downstream of a SET (protein methylase) gene related to human G9a and *Drosophila* Su(var)3-9 and trithorax genes (58), followed by local sequence changes to create the Metnase fusion protein (56) (**Figure 2A**). The crystal structure of the Metnase nuclease domain was solved (59) (**Figure 2B**). Unlike the 200 divergent, non-functional Hsmar1 remnants in the human genome, the Metnase nuclease domain is full length and highly conserved based on an Hsmar1 consensus sequence. This suggests

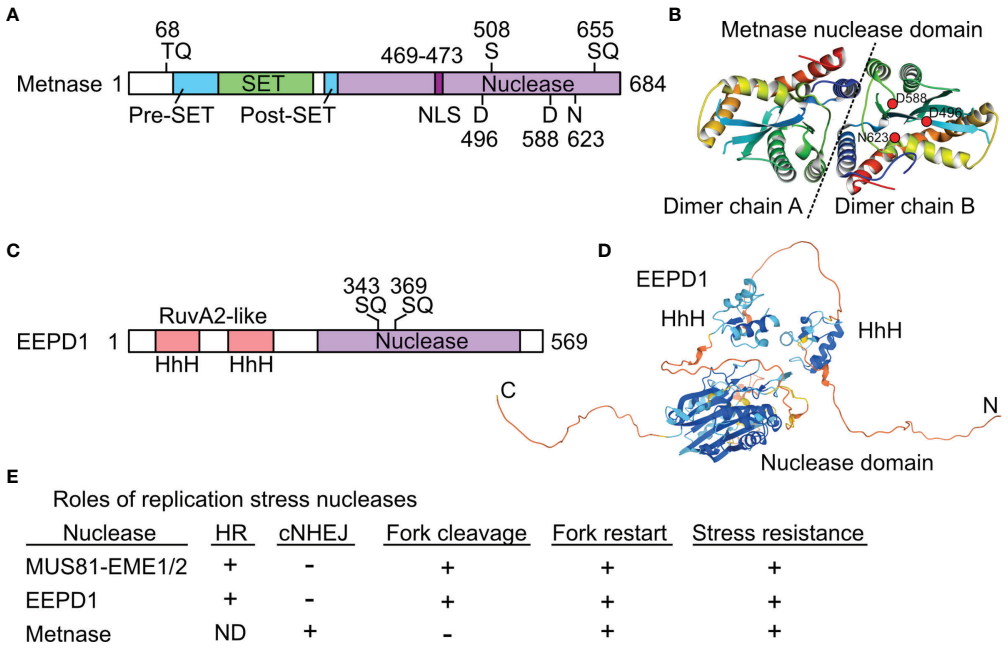

E

Roles of replication stress nucleases

Nuclease	HR	cNHEJ	Fork cleavage	Fork restart	Stress resistance
MUS81-EME1/2	+	-	+	+	+
EEPD1	+	-	+	+	+
Metnase	ND	+	-	+	+

FIGURE 2 | Structures and roles of replication stress nucleases. **(A)** Metnase is a fusion of SET and nuclease domains. Two S/TQ sites (potential PIKK targets) are indicated, along with the DDN nuclease motif. S508 is phosphorylated by Chk1. **(B)** Crystal structure of Metnase nuclease domains shown as a dimer (separated by dashed line), as solved by the Georgiadis lab (59); image from the Protein Data Bank Japan (60) using the Molmil molecular structure viewer (61). Positions of DDN core nuclease residues are indicated in dimer chain B by red dots. **(C)** EEPD1 has two helix-hairpin-helix (HhH) domains related to prokaryotic RuvA2, a component of RuvAB that mediates Holliday junction branch migration. Two potential PIKK target SQ sites are indicated. **(D)** Predicted EEPD1 structure showing HhH and nuclease domains with intervening non-structured regions; image from AlphaFold (62). **(E)** Summary of known functions of three replication stress nucleases. ND, not determined; +, promotes process; -, not involved in indicated process. See text for further details.

the fusion protein had selective benefits, although the consensus DDD/DDE nuclease active site residues shifted to $D_{496}D_{588}N_{623}$ in Metnase (58). Both WT (DDN) Metnase and a DDD reconstruction stimulate Hsmar1 transposition *in vitro*, and Metnase binds to Hsmar1 transposon terminal inverted repeat (TIR) sequences (63). Metnase retains only one of two TIRs required for transposition (56), so it cannot mobilize itself.

Initial analysis of Metnase functions demonstrated that it promotes integration of transfected plasmid DNA, cNHEJ, and resistance to ionizing radiation, and that it methylates histone H3 K4 and K36 residues *in vitro*, well-known marks of open chromatin (57). The helix-turn-helix (HtH) motif within the nuclease domain is required for specific binding to TIRs, yet Metnase has non-sequence-specific endonuclease activity that is HtH-independent, but eliminated by a D496A mutation (64) [Note: here we use the aa sequence of the dominant variant, which has 13 more aa than the variant in early publications; thus, D496A is denoted D483A in Roman et al. and other early reports]. Metnase interacts with PSO4 (also known as PRPF19), which functions in transcription-coupled nucleotide excision repair and pre-mRNA splicing (65). PSO4 recruits Metnase to DSBs to promote plasmid DNA integration (65). Metnase also stimulates lentiviral DNA integration (66), consistent with roles in cNHEJ.

Both the Metnase SET and nuclease activities enhance cNHEJ. WT Metnase added to cell extracts promotes cNHEJ, but this activity is eliminated by a nuclease-dead D496A mutation (67), and strongly suppressed by DDD and DDE (Hsmar1-like) versions (68); thus DDN_{623} plays a key role in cNHEJ. Inactivation of the SET domain also abrogates Metnase stimulation of cNHEJ (57). Metnase promotes the efficiency and accuracy of cNHEJ through its interaction with DNA ligase IV (69). Chromosome translocations are often mediated by aNHEJ, and Metnase suppresses translocations by promoting the competing cNHEJ pathway (70). Chromatin immunoprecipitation revealed that Metnase promotes cNHEJ by di-methylating histone H3 K36 in narrow (~2 nucleosome) regions flanking DSBs (71). This contrasts with the far larger γH2AX domains, which extend >1 Mbp from DSBs (~7000 nucleosomes) (72). Importantly, di-methyl H3 K36 near DSBs promotes recruitment and/or retention of early cNHEJ factors Ku70 and NBS1, components of the DNA-PK and MRN complexes, respectively (71). H3 K36 di-methylation is also enhanced at radiation-induced DSBs (71). In cells, DNA repair operates within a chromatin environment, and by the mid-2000s it had been established that chromatin remodeling involving nucleosome eviction by the INO80 complex promotes DSB repair in yeast (73–75); this is also true in mammalian cells (76). The discovery that Metnase promotes cNHEJ by modifying histone H3 adjacent to DSBs was the first suggestion of a histone code for DNA repair (71), analogous to the prototypical histone code for transcription regulation (77).

Metnase also interacts with TopoIIα, which mediates chromosome decatenation of replicated chromosomes before segregation in mitosis. This interaction promotes TopoIIα activity *in vivo* and this activity is suppressed by Metnase automethylation of K495, suggesting that tumors may exploit Metnase to gain resistance to chemotherapeutics that target TopoIIα (78). Indeed, Metnase promotes resistance to the TopoIIα poisons etoposide, doxorubicin, and ICRF-193 in acute myeloid leukemia and breast cancer cells (79, 80). TopoIIα poisons block TopoIIα by binding near its DNA binding site (81). Apparently, Metnase binds this region as well, blocking access and thereby conferring resistance to TopoIIα poisons. Neoamphimedine is a TopoIIα inhibitor derived from a marine sponge that binds near the TopoIIα ATPase domain and thus acts by a different mechanism than traditional TopoIIα poisons. Importantly, Metnase and neoamphimedine bind to distinct regions of TopoIIα, thus Metnase does not confer resistance to neoamphimedine (82).

Metnase SET and nuclease domains play important roles in replication stress responses. siRNA depletion of Metnase delays restart of replication forks stalled by nucleotide depletion with hydroxyurea (HU), and sensitizes cells to HU and several other replication stress agents (83). Fork restart is accelerated by overexpression of Metnase, but this effect is abrogated by defects in the Metnase nuclease or SET domains (68, 84). As noted above, MUS81 and EEPD1 cleave stalled replication forks to promote fork restart *via* HR. Although Metnase accelerates replication fork restart *in vivo*, and cleaves branched structures (including replication forks) *in vitro* (68), Metnase does not cleave stalled forks *in vivo* (43). This raises the possibility that Metnase nuclease promotes fork restart by cleaving flap or other structures that arise during HR-mediated fork restart. Metnase methylation targets during replication fork restart are unknown, but Metnase may methylate histones near stalled forks (43), as it does near DSBs (71). Metnase plays another important role in replication fork restart by HR. Recall that seDSBs at cleaved replication forks must be resected to allow RPA and then RAD51 to bind to 3' ssDNA tails, which invade sister chromatids to reestablish a functional replication fork (**Figure 1D**). Metnase interacts with EXO1 to promote resection, suppressing cNHEJ of seDSBs and promoting HR-mediated fork restart (85). Metnase is phosphorylated on S508 by Chk1 in response to replication stress; unlike WT Metnase, an S508A mutant does not stimulate cNHEJ, nor does it associate with chromatin in response to replication stress (86). Interestingly, the S508A mutant accelerates replication fork restart more than WT Metnase, suggesting Metnase and Chk1 function in a regulatory feedback loop to coordinate DNA repair and replication stress responses (86). It is intriguing that Metnase promotes cNHEJ of frank DSBs, but suppresses cNHEJ at seDSBs by promoting EXO1 resection at collapsed forks to facilitate HR-mediated fork restart. The lack of cNHEJ activity at seDSBs is reminiscent of the lack of cNHEJ activity by Ku/DNA-PKcs present at telomeres (87). Note that Metnase promotes cNHEJ, a critical function in G1 cells that are largely incapable of HR, it promotes HR-mediated fork restart in S phase, it promotes chromosome decatenation in G2/M phases, and it regulates DNA damage checkpoint signaling. Thus, Metnase augments DNA repair and DDR signaling throughout the cell cycle.

EEPD1: A STRUCTURE-SPECIFIC NUCLEASE THAT PROMOTES HR REPAIR OF DSBs AND STRESSED REPLICATION FORKS

EEPD1 was first characterized in 2015. EEPD1 has DNA binding domains with helix-hairpin-helix motifs related to RuvA2, and a DNase I-like nuclease domain (**Figure 2C**). A crystal structure for EEPD1 is not available; a predicted AlphaFold structure (62) is shown in **Figure 2D**. Defects in EEPD1 confer sensitivity to genotoxins, and cause cytogenetic aberrations and cell death by mitotic catastrophe (42, 43). EEPD1 is recruited to and promotes restart of stalled replication forks, and it enhances resection of frank DSBs and seDSBs, thereby suppressing cNHEJ and promoting accurate repair by HR (42). Like Metnase, EEPD1 promotes resection of broken ends through interactions with EXO1, and the resection defects in EEPD1-defective cells prevent ssDNA formation and subsequent activation of ATR and Chk1 (42, 88), indicating that EEPD1 is important for both DSB repair and DNA damage checkpoint signaling. EEPD1 has critical roles during rapid cell proliferation in vertebrate embryonic development (89), highlighting the importance of HR in maintaining genome stability during this sensitive developmental phase. Unlike Metnase, EEPD1 directly cleaves stalled replication forks, similar to MUS81 (42, 43). However, EEPD1 is a 5' nuclease and MUS81 is a 3' nuclease. It appears that MUS81, which evolved >1500 Mya in early eukaryotes, was joined by the complementary EEPD1 nuclease in chordates/early vertebrates ~450 Mya. EEPD1 may have been selected to ensure accurate replication of expanding genomes (90) with the consequent increase in replication stress. It is possible that 5' cleavage of stalled forks by EEPD1 is superior to 3' cleavage by MUS81 because MUS81 cleaves the leading strand, forcing strand invasion into the lagging (Okazaki) strand which may be delayed until Okazaki fragments mature, and/or further resection occurs to permit HR-mediated fork restart (43). Fork restart timing is important because persistent stalled forks may be restructured into toxic HR intermediates (47, 91), and even short delays in fork restart correlate with increased sensitivity to replication stress and increased genome instability (42, 68, 84, 89). EEPD1 and Metnase both promote HR-mediated fork restart by promoting EXO1 resection of seDSBs, and EEPD1 promotes repair of frank DSBs by HR whereas Metnase promotes frank DSB repair by cNHEJ; there is no evidence that Metnase influences frank DSB repair by HR. The partially overlapping roles of Metnase, MUS81, and EEPD1 in DSB repair and replication stress responses are summarized in **Figure 2E**.

METNASE AND EEPD1 IN CANCER ETIOLOGY AND AS POTENTIAL THERAPEUTIC TARGETS

Given their roles in DNA repair, damage signaling, and genome stabilization, it's possible that defects in Metnase or EEPD1

might predispose to cancer, similar to other DDR factors like BRCA1, BRCA2, and ATM (92). However, no gain or loss of function mutations in Metnase or EEPD1 have yet been verified in cancers; if they exist, they are likely to be rare. Because tumor cells experience considerable stress, i.e., oncogenic stress and DNA damage from therapeutics (93), DDR factors are often overexpressed in cancer. Both Metnase and EEPD1 are frequently overexpressed in breast, brain, cervix, colon, head and neck, kidney, skin, lung, prostate, and uterine cancers; Metnase is also overexpressed in some liver cancers (94). Because these proteins promote tumor cell survival in response to DNA damage by radiation and genotoxic chemotherapeutics, direct inhibition of their nuclease activities, or the Metnase SET activity, may augment traditional chemo- or radiotherapy. Inhibiting Metnase or EEPD1 may be most beneficial for patients whose tumors overexpress these proteins.

There are many cell-based and *in vitro* biochemical assays available to monitor specific Metnase and EEPD1 activities. Defects or inhibition of these proteins uniformly cause sensitivity to genotoxins (42, 57, 83), hence drug screens can be performed using rapid cell survival/proliferation assays (95). If screening for specific nuclease inhibitors, *in vitro* assays with model branched DNA substrates (64, 67), and traditional or automated comet assays (42, 43, 96) are also attractive options. Once a candidate drug is identified, mechanistic insights can be obtained with more time-consuming approaches such as fork restart, chromosome aberration, mitotic catastrophe, and DDR signaling assays.

Current evidence suggests several promising therapeutic approaches. The widely used antibiotic ciprofloxacin inhibits Metnase nuclease and enhances cisplatin sensitivity of A549 lung tumor cells and tumor xenografts in mice (97). TopoIIα poisons are used to treat a variety of tumor types, and tumors that overexpress Metnase may be better controlled with higher doses of traditional TopoIIα poisons (79, 80), or by use of alternative inhibitors (82). Because the Metnase SET activity is important for both cNHEJ and replication fork restart, a specific Metnase SET inhibitor may augment therapeutics that induce frank DSBs and/or replication-associated seDSBs. Although no Metnase SET inhibitors are available, specific SET inhibitors are being developed to treat cancer (98, 99).

Breast and other tumors with BRCA1 or BRCA2 defects are HR-deficient and show synthetic lethality with PARP1 inhibitors, owing to increased replication stress and defective HR-mediated fork restart (100). Inhibition or downregulation of MUS81 also causes synthetic lethality in BRCA2-deficient cells (101). BRCA1, BRCA2, and PALB2 defects are synthetically lethal with RAD52 defects (102, 103), and we found that this lethality depends on EEPD1 (104). Thus, targeting RAD52 may enhance treatment of BRCA-deficient tumors, but co-inhibition of RAD52 and EEPD1 would likely be self-defeating, enhancing tumor cell survival and potentially enhancing tumor progression by allowing severely damaged cells to survive.

Finally, because most cancer therapeutics cause replication stress, combining these agents with inhibitors that target one or more replication stress proteins may improve treatment efficacy. DDR factors including ATR and ATM are being targeted to augment radio- and chemotherapy (105–107). Novel combination therapies targeting upstream PIKKs and/or downstream replication stress nucleases MUS81, EEPD1 or Metnase, may be effective anti-cancer treatments on their own, or when combined with genotoxic chemo- and radiotherapeutics.

AUTHOR CONTRIBUTIONS

JN, NS, LT, SA, S-HL, and RH wrote the manuscript and JN prepared the figures. All authors contributed to the article and approved the submitted version.

FUNDING

The Nickoloff lab was supported by NIH R01 GM084020 and American Lung Association grant LCD-686552. The Lee lab was supported by NIH R01 CA152367. The Hromas lab was supported by NIH R01 CA205224.

REFERENCES

1. Chatterji M, Tsai CL, Schatz DG. New Concepts in the Regulation of an Ancient Reaction: Transposition by RAG1/RAG2. *Immunol Rev* (2004) 200:261–71. doi: 10.1111/j.0105-2896.2004.00167.x
2. Ciccia A, Elledge SJ. The DNA Damage Response: Making It Safe to Play With Knives. *Mol Cell* (2010) 40:179–204. doi: 10.1016/j.molcel.2010.09.019
3. Meroni A, Mentegari E, Crespan E, Muzi-Falconi M, Lazzaro F, Podesta A. The Incorporation of Ribonucleotides Induces Structural and Conformational Changes in DNA. *Biophys J* (2017) 113:1373–82. doi: 10.1016/j.bpj.2017.07.013
4. Tubbs A, Nussenzweig A. Endogenous DNA Damage as a Source of Genomic Instability in Cancer. *Cell* (2017) 168:644–56. doi: 10.1016/j.cell.2017.01.002
5. Petljak M, Maciejowski J. Molecular Origins of APOBEC-Associated Mutations in Cancer. *DNA Repair* (2020) 94:102905. doi: 10.1016/j.dnarep.2020.102905
6. Juan CA, Perez de la Lastra JM, Plou FJ, Perez-Lebena E. The Chemistry of Reactive Oxygen Species (ROS) Revisited: Outlining Their Role in Biological Macromolecules (DNA, Lipids and Proteins) and Induced Pathologies. *Int J Mol Sci* (2021) 22:4642. doi: 10.3390/ijms22094642
7. Sarmiento-Salinas FL, Perez-Gonzalez A, Acosta-Casique A, Ix-Ballote A, Diaz A, Trevino S, et al. Reactive Oxygen Species: Role in Carcinogenesis, Cancer Cell Signaling and Tumor Progression. *Life Sci* (2021) 284:119942. doi: 10.1016/j.lfs.2021.119942
8. Ward JF. Complexity of Damage Produced by Ionizing Radiation. *Cold Spring Harb Symp Quant Biol* (2000) 65:377–82. doi: 10.1101/sqb.2000.65.377
9. Fu D, Calvo JA, Samson LD. Balancing Repair and Tolerance of DNA Damage Caused by Alkylating Agents. *Nat Rev Cancer* (2012) 12:104–20. doi: 10.1038/nrc3185
10. Swift LH, Golsteyn RM. Genotoxic Anti-Cancer Agents and Their Relationship to DNA Damage, Mitosis, and Checkpoint Adaptation in Proliferating Cancer Cells. *Int J Mol Sci* (2014) 15:3403–31. doi: 10.3390/ijms15033403

11. Roy S. Impact of UV Radiation on Genome Stability and Human Health. *Adv Exp Med Biol* (2017) 996:207–19. doi: 10.1007/978-3-319-56017-5_17
12. Desai A, Yan Y, Gerson SL. Advances in Therapeutic Targeting of the DNA Damage Response in Cancer. *DNA Repair* (2018) 66-67:24–9. doi: 10.1016/j.dnarep.2018.04.004
13. Pilie PG, Tang C, Mills GB, Yap TA. State-Of-the-Art Strategies for Targeting the DNA Damage Response in Cancer. *Nat Rev Clin Oncol* (2019) 16:81–104. doi: 10.1038/s41571-018-0114-z
14. Nickoloff JA, Taylor L, Sharma N, Kato TA. Exploiting DNA Repair Pathways for Tumor Sensitization, Mitigation of Resistance, and Normal Tissue Protection in Radiotherapy. *Cancer Drug Res* (2020) 4:244–63. doi: 10.20517/cdr.2020.89
15. Blackford AN, Jackson SP. ATM, ATR, and DNA-PK: The Trinity at the Heart of the DNA Damage Response. *Mol Cell* (2017) 66:801–17. doi: 10.1016/j.molcel.2017.05.015
16. Onn L, Portillo M, Ilic S, Cleitman G, Stein D, Kaluski S, et al. SIRT6 Is a DNA Double-Strand Break Sensor. *Elife* (2020) 9:e51636. doi: 10.7554/eLife.51636
17. Tang Y, Luo J, Zhang W, Gu W. Tip60-Dependent Acetylation of P53 Modulates the Decision Between Cell-Cycle Arrest and Apoptosis. *Mol Cell* (2006) 24:827–39. doi: 10.1016/j.molcel.2006.11.021
18. Chang L, Graham PH, Hao J, Ni J, Bucci J, Cozzi PJ, et al. PI3K/Akt/mTOR Pathway Inhibitors Enhance Radiosensitivity in Radioresistant Prostate Cancer Cells Through Inducing Apoptosis, Reducing Autophagy, Suppressing NHEJ and HR Repair Pathways. *Cell Death Dis* (2014) 5:e1437. doi: 10.1038/cddis.2014.415
19. Chen J. The Cell-Cycle Arrest and Apoptotic Functions of P53 in Tumor Initiation and Progression. *Cold Spring Harb Perspect Med* (2016) 6:a026104. doi: 10.1101/cshperspect.a026104
20. Chang HHY, Pannunzio NR, Adachi N, Lieber MR. Non-Homologous DNA End Joining and Alternative Pathways to Double-Strand Break Repair. *Nat Rev Mol Cell Biol* (2017) 18:495–506. doi: 10.1038/nrm.2017.48
21. Lieber MR, Gu J, Lu H, Shimazaki N, Tsai AG. Nonhomologous DNA End Joining (NHEJ) and Chromosomal Translocations in Humans. *Subcell Biochem* (2010) 50:279–96. doi: 10.1007/978-90-481-3471-7_14
22. Nickoloff JA. Paths From DNA Damage and Signaling to Genome Rearrangements *via* Homologous Recombination. *Mutat Res* (2017) 806:64–74. doi: 10.1016/j.mrfmmm.2017.07.008
23. Piazza A, Heyer WD. Homologous Recombination and the Formation of Complex Genomic Rearrangements. *Trends Cell Biol* (2019) 29:135–49. doi: 10.1016/j.tcb.2018.10.006
24. Polleys EJ, Freudenreich CH. Homologous Recombination Within Repetitive DNA. *Curr Opin Genet Dev* (2021) 71:143–53. doi: 10.1016/j.gde.2021.08.005
25. Michl J, Zimmer J, Tarsounas M. Interplay Between Fanconi Anemia and Homologous Recombination Pathways in Genome Integrity. *EMBO J* (2016) 35:909–23. doi: 10.15252/embj.201693860
26. Wright WD, Shah SS, Heyer WD. Homologous Recombination and the Repair of DNA Double-Strand Breaks. *J Biol Chem* (2018) 293:10524–35. doi: 10.1074/jbc.TM118.000372
27. Zimmermann M, Lottersberger F, Buonomo SB, Sfeir A, De Lange T. 53BP1 Regulates DSB Repair Using Rif1 to Control 5' End Resection. *Science* (2013) 339:700–4. doi: 10.1126/science.1231573
28. Sturzenegger A, Burdova K, Kanagaraj R, Levikova M, Pinto C, Cejka P, et al. DNA2 Cooperates With the WRN and BLM RecQ Helicases to Mediate Long-Range DNA End Resection in Human Cells. *J Biol Chem* (2014) 289:27314–26. doi: 10.1074/jbc.M114.578823
29. Symington LS. Mechanism and Regulation of DNA End Resection in Eukaryotes. *Crit Rev Biochem Mol Biol* (2016) 51:195–212. doi: 10.3109/10409238.2016.1172552
30. Mirman Z, Lottersberger F, Takai H, Kibe T, Gong Y, Takai K, et al. 53bp1-RIF1-Shieldin Counteracts DSB Resection Through CST- and Pol α-Dependent Fill-in. *Nature* (2018) 560:112–6. doi: 10.1038/s41586-018-0324-7
31. Densham RM, Morris JR. Moving Mountains-The BRCA1 Promotion of DNA Resection. *Front Mol Biosci* (2019) 6:79. doi: 10.3389/fmolb.2019.00079
32. Zhao F, Kim W, Kloeber JA, Lou Z. DNA End Resection and Its Role in DNA Replication and DSB Repair Choice in Mammalian Cells. *Exp Mol Med* (2020) 52:1705–14. doi: 10.1038/s12276-020-00519-1
33. Iliakis G, Murmann T, Soni A. Alternative End-Joining Repair Pathways Are the Ultimate Backup for Abrogated Classical non-Homologous End-Joining and Homologous Recombination Repair: Implications for the Formation of Chromosome Translocations. *Mutat Res Genet Toxicol Environ Mutagen* (2015) 793:166–75. doi: 10.1016/j.mrgentox.2015.07.001
34. Bhargava R, Onyango DO, Stark JM. Regulation of Single-Strand Annealing and Its Role in Genome Maintenance. *Trends Genet* (2016) 32:566–75. doi: 10.1016/j.tig.2016.06.007
35. Hromas R, Williamson E, Lee SH, Nickoloff J. Preventing the Chromosomal Translocations That Cause Cancer. *Trans Am Clin Climatol Assoc* (2016) 127:176–95.
36. Seol JH, Shim EY, Lee SE. Microhomology-Mediated End Joining: Good, Bad and Ugly. *Mutat Res* (2018) 809:81–7. doi: 10.1016/j.mrfmmm.2017.07.002
37. Sfeir A, Symington LS. Microhomology-Mediated End Joining: A Back-Up Survival Mechanism or Dedicated Pathway? *Trends Biochem Sci* (2015) 40:701–14. doi: 10.1016/j.tibs.2015.08.006
38. Wyatt DW, Feng W, Conlin MP, Yousefzadeh MJ, Roberts SA, Mieczkowski P, et al. Essential Roles for Polymerase Theta-Mediated End Joining in the Repair of Chromosome Breaks. *Mol Cell* (2016) 63:662–73. doi: 10.1016/j.molcel.2016.06.020
39. Vaze MB, Pellicioli A, Lee SE, Ira G, Liberi G, Arbel-Eden A, et al. Recovery From Checkpoint-Mediated Arrest After Repair of a Double-Strand Break Requires Srs2 Helicase. *Mol Cell* (2002) 10:373–85. doi: 10.1016/S1097-2765(02)00593-2
40. Pepe A, West SC. MUS81-EME2 Promotes Replication Fork Restart. *Cell Rep* (2014) 7:1048–55. doi: 10.1016/j.celrep.2014.04.007
41. Sarbajna S, Davies D, West SC. Roles of SLX1-SLX4, MUS81-EME1, and GEN1 in Avoiding Genome Instability and Mitotic Catastrophe. *Genes Dev* (2014) 28:1124–36. doi: 10.1101/gad.238303.114
42. Wu Y, Lee SH, Williamson EA, Reinert BL, Cho JH, Xia F, et al. EEPD1 Rescues Stressed Replication Forks and Maintains Genome Stability by Promoting End Resection and Homologous Recombination Repair. *PloS Genet* (2015) 11:e1005675. doi: 10.1371/journal.pgen.1005675
43. Sharma N, Speed MC, Allen CP, Maranon DG, Williamson E, Singh S, et al. Distinct Roles of Structure-Specific Endonucleases EEPD1 and Metnase in Replication Stress Responses. *NAR Cancer* (2020) 2:zcaa008. doi: 10.1093/narcan/zcaa008
44. Zellweger R, Dalcher D, Mutreja K, Berti M, Schmid JA, Herrador R, et al. Rad51-Mediated Replication Fork Reversal Is a Global Response to Genotoxic Treatments in Human Cells. *J Cell Biol* (2015) 208:563–79. doi: 10.1083/jcb.201406099
45. Meng X, Zhao X. Replication Fork Regression and Its Regulation. *FEMS Yeast Res* (2017) 17:fow110. doi: 10.1093/femsyr/fow110
46. Conti BA, Smogorzewska A. Mechanisms of Direct Replication Restart at Stressed Replisomes. *DNA Repair* (2020) 95:102947. doi: 10.1016/j.dnarep.2020.102947
47. Nickoloff JA, Sharma N, Taylor L, Allen SJ, Hromas R. The Safe Path at the Fork: Ensuring Replication-Associated DNA Double-Strand Breaks Are Repaired by Homologous Recombination. *Front Genet* (2021) 12:748033. doi: 10.3389/fgene.2021.748033
48. Tye S, Ronson GE, Morris JR. A Fork in the Road: Where Homologous Recombination and Stalled Replication Fork Protection Part Ways. *Semin Cell Dev Biol* (2021) 113:14–26. doi: 10.1016/j.semcdb.2020.07.004
49. Doe CL, Ahn JS, Dixon J, Whitby MC. Mus81-Eme1 and Rqh1 Involvement in Processing Stalled and Collapsed Replication Forks. *J Biol Chem* (2002) 277:32753–9. doi: 10.1074/jbc.M202120200
50. Dehe PM, Coulon S, Scaglione S, Shanahan P, Takedachi A, Wohlschlegel JA, et al. Regulation of Mus81-Eme1 Holliday Junction Resolvase in Response to DNA Damage. *Nat Struct Mol Biol* (2013) 20:598–603. doi: 10.1038/nsmb.2550
51. Wyatt HD, Sarbajna S, Matos J, West SC. Coordinated Actions of SLX1-SLX4 and MUS81-EME1 for Holliday Junction Resolution in Human Cells. *Mol Cell* (2013) 52:234–47. doi: 10.1016/j.molcel.2013.08.035

52. Amangyeld T, Shin YK, Lee M, Kwon B, Seo YS. Human MUS81-EME2 Can Cleave a Variety of DNA Structures Including Intact Holliday Junction and Nicked Duplex. *Nucleic Acids Res* (2014) 42:5846–62. doi: 10.1093/nar/gku237
53. Calzetta NL, Gonzalez Besteiro MA, Gottifredi V. Mus81-Eme1-Dependent Aberrant Processing of DNA Replication Intermediates in Mitosis Impairs Genome Integrity. *Sci Adv* (2020) 6:eabc8257. doi: 10.1126/sciadv.abc8257
54. Falquet B, Rass U. Structure-Specific Endonucleases and the Resolution of Chromosome Underreplication. *Genes* (2019) 10:232–54. doi: 10.3390/genes10030232
55. Xu X, Wang M, Sun J, Yu Z, Li G, Yang N, et al. Structure Specific DNA Recognition by the SLX1-SLX4 Endonuclease Complex. *Nucleic Acids Res* (2021) 49:7740–52. doi: 10.1093/nar/gkab542
56. Cordaux R, Udit S, Batzer MA, Feschotte C. Birth of a Chimeric Primate Gene by Capture of the Transposase Gene From a Mobile Element. *Proc Natl Acad Sci USA* (2006) 103:8101–6. doi: 10.1073/pnas.0601161103
57. Lee SH, Oshige M, Durant ST, Rasila KK, Williamson EA, Ramsey H, et al. The SET Domain Protein Metnase Mediates Foreign DNA Integration and Links Integration to Nonhomologous End-Joining Repair. *Proc Natl Acad Sci USA* (2005) 102:18075–80. doi: 10.1073/pnas.0503676102
58. Robertson HM, Zumpano KL. Molecular Evolution of an Ancient Mariner Transposon, Hsmar1, in the Human Genome. *Gene* (1997) 205:203–17. doi: 10.1016/S0378-1119(97)00472-1
59. Goodwin KD, He H, Imasaki T, Lee SH, Georgiadis MM. Crystal Structure of the Human Hsmar1-Derived Transposase Domain in the DNA Repair Enzyme Metnase. *Biochemistry* (2010) 49:5705–13. doi: 10.1021/bi100171x
60. Kinjo AR, Bekker GJ, Suzuki H, Tsuchiya Y, Kawabata T, Ikegawa Y, et al. Protein Data Bank Japan (PDBj): Updated User Interfaces, Resource Description Framework, Analysis Tools for Large Structures. *Nucleic Acids Res* (2017) 45:D282–8. doi: 10.1093/nar/gkw962
61. Bekker GJ, Nakamura H, Kinjo AR. Molmil: A Molecular Viewer for the PDB and Beyond. *J Cheminform* (2016) 8:42. doi: 10.1186/s13321-016-0155-1
62. Jumper J, Evans R, Pritzel A, Green T, Figurnov M, Ronneberger O, et al. Highly Accurate Protein Structure Prediction With AlphaFold. *Nature* (2021) 596:583–9. doi: 10.1038/s41586-021-03819-2
63. Liu D, Bischerour J, Siddique A, Buisine N, Bigot Y, Chalmers R. The Human SETMAR Protein Preserves Most of the Activities of the Ancestral Hsmar1 Transposase. *Mol Cell Biol* (2007) 27:1125–32. doi: 10.1128/MCB.01899-06
64. Roman Y, Oshige M, Lee Y-J, Goodwin K, Georgiadis MM, Hromas RA, et al. Biochemical Characterization of a SET and Transposase Fusion Protein, Metnase (SETMAR) for its DNA Binding and DNA Cleavage Activity. *Biochemistry* (2007) 46:11369–76. doi: 10.1021/bi7005477
65. Beck BD, Park SJ, Lee YJ, Roman Y, Hromas RA, Lee SH. Human PSO4 Is a Metnase (SETMAR) Binding Partner That Regulates Metnase Function in DNA Repair. *J Biol Chem* (2008) 283(14):9023–30, 9023-9030. doi: 10.1074/jbc.M800150200
66. Williamson EA, Farrington J, Martinez L, Ness S, O'rourke J, Lee SH, et al. Expression Levels of the Human DNA Repair Protein Metnase Influence Lentiviral Genomic Integration. *Biochimie* (2008) 90:1422–6. doi: 10.1016/j.biochi.2008.05.010
67. Beck BD, Lee SS, Williamson E, Hromas RA, Lee SH. Biochemical Characterization of Metnase's Endonuclease Activity and Its Role in NHEJ Repair. *Biochemistry* (2011) 50:4360–70. doi: 10.1021/bi200333k
68. Kim H-S, Chen Q, Kim S-K, Nickoloff JA, Hromas R, Georgiadis MM, et al. The DDN Catalytic Motif Is Required for Metnase Functions in NHEJ Repair and Replication Restart. *J Biol Chem* (2014) 289:10930–8. doi: 10.1074/jbc.M113.533216
69. Hromas R, Wray J, Lee SH, Martinez L, Farrington J, Corwin LK, et al. The Human Set and Transposase Domain Protein Metnase Interacts With DNA Ligase IV and Enhances the Efficiency and Accuracy of Non-Homologous End-Joining. *DNA Repair* (2008) 7:1927–37. doi: 10.1016/j.dnarep.2008.08.002
70. Wray J, Williamson EA, Farrington J, Chester S, Kwan L, Weinstock D, et al. The Transposase Domain Protein Metnase/SETMAR Suppresses Chromosomal Translocations. *Cancer Genet Cytogenet* (2010) 200:184–90. doi: 10.1016/j.cancergencyto.2010.04.011
71. Fnu S, Williamson EA, De Haro LP, Brenneman M, Wray J, Shaheen M, et al. Methylation of Histone H3 Lysine 36 Enhances DNA Repair by Nonhomologous End-Joining. *Proc Natl Acad Sci USA* (2011) 108:540–5. doi: 10.1073/pnas.1013571108
72. Clouaire T, Rocher V, Lashgari A, Arnould C, Aguirrebengoa M, Biernacka A, et al. Comprehensive Mapping of Histone Modifications at DNA Double-Strand Breaks Deciphers Repair Pathway Chromatin Signatures. *Mol Cell* (2018) 72:250–262 e256. doi: 10.1016/j.molcel.2018.08.020
73. Morrison AJ, Highland J, Krogan NJ, Arbel-Eden A, Greenblatt JF, Haber JE, et al. INO80 and γ-H2AX Interaction Links ATP-Dependent Chromatin Remodeling to DNA Damage Repair. *Cell* (2004) 119:767–75. doi: 10.1016/j.cell.2004.11.037
74. Tsukuda T, Fleming AB, Nickoloff JA, Osley MA. Chromatin Remodeling at a DNA Double-Strand Break Site in Saccharomyces Cerevisiae. *Nature* (2005) 438:379–83. doi: 10.1038/nature04148
75. Tsukuda T, Lo YC, Krishna S, Sterk R, Osley MA, Nickoloff JA. INO80-Dependent Chromatin Remodeling Regulates Early and Late Stages of Mitotic Homologous Recombination. *DNA Repair* (2009) 8:360–9. doi: 10.1016/j.dnarep.2008.11.014
76. Wu S, Shi Y, Mulligan P, Gay F, Landry J, Liu H, et al. A YY1-INO80 Complex Regulates Genomic Stability Through Homologous Recombination-Based Repair. *Nat Struct Mol Biol* (2007) 14:1165–72. doi: 10.1038/nsmb1332
77. Strahl BD, Allis CD. The Language of Covalent Histone Modifications. *Nature* (2000) 403:41–5. doi: 10.1038/47412
78. Williamson EA, Rasila KK, Corwin LK, Wray J, Beck BD, Severns V, et al. The SET and Transposase Domain Protein Metnase Enhances Chromosome Decatenation: Regulation by Automethylation. *Nucleic Acids Res* (2008) 36:5822–31. doi: 10.1093/nar/gkn560
79. Wray J, Williamson EA, Fnu S, Lee S-H, Libby E, Willman CL, et al. Metnase Mediates Chromosome Decatenation in Acute Leukemia Cells. *Blood* (2009) 114:1852–8. doi: 10.1182/blood-2008-08-175760
80. Wray J, Williamson EA, Royce M, Shaheen M, Beck BD, Lee SH, et al. Metnase Mediates Resistance to Topoisomerase II Inhibitors in Breast Cancer Cells. *PloS One* (2009) 4:e5323. doi: 10.1371/journal.pone.0005323
81. Classen S, Olland S, Berger JM. Structure of the Topoisomerase II ATPase Region and its Mechanism of Inhibition by the Chemotherapeutic Agent ICRF-187. *Proc Natl Acad Sci USA* (2003) 100:10629–34. doi: 10.1073/pnas.1832879100
82. Ponder J, Yoo BH, Adedoyin AD, Li Q, Ashley AK, Amerin CL, et al. Neoamphimedine Circumvents Metnase-Enhanced DNA Topoisomerase IIα Activity Through ATP-Competitive Inhibition. *Marine Drugs* (2011) 9:2397–408. doi: 10.3390/md9112397
83. De Haro LP, Wray J, Williamson EA, Durant ST, Corwin L, Gentry AC, et al. Metnase Promotes Restart and Repair of Stalled and Collapsed Replication Forks. *Nucleic Acids Res* (2010) 38:5681–91. doi: 10.1093/nar/gkq339
84. Kim HS, Kim SK, Hromas R, Lee SH. The SET Domain Is Essential for Metnase Functions in Replication Restart and the 5' End of SS-Overhang Cleavage. *PloS One* (2015) 10:e0139418. doi: 10.1371/journal.pone.0139418
85. Kim HS, Williamson EA, Nickoloff JA, Hromas RA, Lee SH. Metnase Mediates Loading of Exonuclease 1 Onto Single-Strand Overhang DNA for End Resection at Stalled Replication Forks. *J Biol Chem* (2016) 292:1414–25. doi: 10.1074/jbc.M116.745646
86. Hromas R, Williamson E, Fnu S, Lee Y-J, Park S-J, Beck BD, et al. Chk1 Phosphorylation of Metnase Enhances DNA Repair But Inhibits Replication Fork Restart. *Oncogene* (2012) 31:4245–54. doi: 10.1038/onc.2011.586
87. Sui J, Zhang S, Chen BPC. DNA-Dependent Protein Kinase in Telomere Maintenance and Protection. *Cell Mol Biol Lett* (2020) 25:2. doi: 10.1186/s11658-020-0199-0
88. Kim HS, Nickoloff JA, Wu Y, Williamson EA, Sidhu GS, Reinert BL, et al. Endonuclease EEPD1 Is a Gatekeeper for Repair of Stressed Replication Forks. *J Biol Chem* (2017) 292:2795–804. doi: 10.1074/jbc.M116.758235
89. Chun C, Wu Y, Lee SH, Williamson EA, Reinert BL, Jaiswal AS, et al. The Homologous Recombination Component EEPD1 Is Required for Genome Stability in Response to Developmental Stress of Vertebrate Embryogenesis. *Cell Cycle* (2016) 15:957–62. doi: 10.1080/15384101.2016.1151585
90. Panopoulou G, Hennig S, Groth D, Krause A, Poustka AJ, Herwig R, et al. New Evidence for Genome-Wide Duplications at the Origin of Vertebrates Using an Amphioxus Gene Set and Completed Animal Genomes. *Genome Res* (2003) 13:1056–66. doi: 10.1101/gr.874803

91. Fabre F, Chan A, Heyer WD, Gangloff S. Alternate Pathways Involving Sgs1/Top3, Mus81/ Mms4, and Srs2 Prevent Formation of Toxic Recombination Intermediates From Single-Stranded Gaps Created by DNA Replication. *Proc Natl Acad Sci USA* (2002) 99:16887–92. doi: 10.1073/pnas.252652399
92. Jeggo PA, Pearl LH, Carr AM. DNA Repair, Genome Stability and Cancer: A Historical Perspective. *Nat Rev Cancer* (2016) 16:35–42. doi: 10.1038/nrc.2015.4
93. Kotsantis P, Petermann E, Boulton SJ. Mechanisms of Oncogene-Induced Replication Stress: Jigsaw Falling Into Place. *Cancer Discov* (2018) 8:537–55. doi: 10.1158/2159-8290.CD-17-1461
94. Park SJ, Yoon BH, Kim SK, Kim SY. GENT2: An Updated Gene Expression Database for Normal and Tumor Tissues. *BMC Med Genomics* (2019) 12:101. doi: 10.1186/s12920-019-0514-7
95. Adan A, Kiraz Y, Baran Y. Cell Proliferation and Cytotoxicity Assays. *Curr Pharm Biotechnol* (2016) 17:1213–21. doi: 10.2174/1389201017666160808160513
96. Weingeist DM, Ge J, Wood DK, Mutamba JT, Huang Q, Rowland EA, et al. Single-Cell Microarray Enables High-Throughput Evaluation of DNA Double-Strand Breaks and DNA Repair Inhibitors. *Cell Cycle* (2013) 12:907–15. doi: 10.4161/cc.23880
97. Williamson EA, Damiani L, Leitao A, Hu C, Hathaway H, Oprea T, et al. Targeting the Transposase Domain of the DNA Repair Component Metnase to Enhance Chemotherapy. *Cancer Res* (2012) 72:6200–8. doi: 10.1158/0008-5472.CAN-12-0313
98. Kaniskan HU, Konze KD, Jin J. Selective Inhibitors of Protein Methyltransferases. *J Med Chem* (2015) 58:1596–629. doi: 10.1021/jm501234a
99. Butler KV, Ma A, Yu W, Li F, Tempel W, Babault N, et al. Structure-Based Design of a Covalent Inhibitor of the SET Domain-Containing Protein 8 (SETD8) Lysine Methyltransferase. *J Med Chem* (2016) 59:9881–9. doi: 10.1021/acs.jmedchem.6b01244
100. Puigvert JC, Sanjiv K, Helleday T. Targeting DNA Repair, DNA Metabolism and Replication Stress as Anti-Cancer Strategies. *FEBS J* (2016) 283:232–45. doi: 10.1111/febs.13574
101. Lai X, Broderick R, Bergoglio V, Zimmer J, Badie S, Niedzwiedz W, et al. MUS81 Nuclease Activity Is Essential for Replication Stress Tolerance and Chromosome Segregation in BRCA2-Deficient Cells. *Nat Commun* (2017) 8:15983. doi: 10.1038/ncomms15983
102. Feng Z, Scott SP, Bussen W, Sharma GG, Guo G, Pandita TK, et al. Rad52 Inactivation Is Synthetically Lethal With BRCA2 Deficiency. *Proc Natl Acad Sci USA* (2011) 108:686–91. doi: 10.1073/pnas.1010959107
103. Lok BH, Carley AC, Tchang B, Powell SN. RAD52 Inactivation Is Synthetically Lethal With Deficiencies in BRCA1 and PALB2 in Addition to BRCA2 Through RAD51-Mediated Homologous Recombination. *Oncogene* (2013) 32:3552–8. doi: 10.1038/onc.2012.391
104. Hromas R, Kim HS, Sidhu G, Williamson EA, Jaiswal A, Totterdale TA, et al. The Endonuclease EEPD1 Mediates Synthetic Lethality in RAD52-Depleted BRCA1-Mutant Breast Cancer Cells. *Breast Cancer Res* (2017) 19:122. doi: 10.1186/s13058-017-0912-8
105. Jackson SP, Helleday T. Drugging DNA Repair. *Science* (2016) 352:1178–9. doi: 10.1126/science.aab0958
106. Carrassa L, Damia G. DNA Damage Response Inhibitors: Mechanisms and Potential Applications in Cancer Therapy. *Cancer Treat Rev* (2017) 60:139–51. doi: 10.1016/j.ctrv.2017.08.013
107. Nickoloff JA, Taylor L, Sharma N, Kato TA. Exploiting DNA Repair Pathways for Tumor Sensitization, Mitigation of Resistance, and Normal Tissue Protection in Radiotherapy. *Cancer Drug Resist* (2021) 4:244–63. doi: 10.20517/cdr.2020.89

Conflict of Interest: The authors declare that the research was conducted in the absence of any commercial or financial relationships that could be construed as a potential conflict of interest.

The reviewer EM declared a shared affiliation, with one of the authors, S-HL, to the handling editor at the time of the review.

Publisher's Note: All claims expressed in this article are solely those of the authors and do not necessarily represent those of their affiliated organizations, or those of the publisher, the editors and the reviewers. Any product that may be evaluated in this article, or claim that may be made by its manufacturer, is not guaranteed or endorsed by the publisher.

frontiers in Oncology

REVIEW
published: 07 February 2022
doi: 10.3389/fonc.2021.822500

DNA Damage Tolerance Pathways in Human Cells: A Potential Therapeutic Target

Ashlynn Ai Li Ler[1†] *and Michael P. Carty*[1,2*]

[1] *Biochemistry, School of Biological and Chemical Sciences, The National University of Ireland (NUI) Galway, Galway, Ireland,* [2] *DNA Damage Response Laboratory, Centre for Chromosome Biology, NUI Galway, Galway, Ireland*

OPEN ACCESS

Edited by:
John Turchi, Indiana University Bloomington, United States

Reviewed by:
Christine Canman, University of Michigan, United States
Youri I. Pavlov, University of Nebraska Medical Center, United States

***Correspondence:**
Michael P. Carty
michael.carty@nuigalway.ie

†Present address:
Ashlynn Ai Li Ler, National University of Singapore, Yong Loo Lin School of Medicine, Singapore, Singapore

Specialty section:
This article was submitted to Cancer Molecular Targets and Therapeutics, a section of the journal Frontiers in Oncology

Received: *25 November 2021*
Accepted: *30 December 2021*
Published: *07 February 2022*

Citation:
Ler AAL and Carty MP (2022) DNA Damage Tolerance Pathways in Human Cells: A Potential Therapeutic Target. Front. Oncol. 11:822500. doi: 10.3389/fonc.2021.822500

DNA lesions arising from both exogenous and endogenous sources occur frequently in DNA. During DNA replication, the presence of unrepaired DNA damage in the template can arrest replication fork progression, leading to fork collapse, double-strand break formation, and to genome instability. To facilitate completion of replication and prevent the generation of strand breaks, DNA damage tolerance (DDT) pathways play a key role in allowing replication to proceed in the presence of lesions in the template. The two main DDT pathways are translesion synthesis (TLS), which involves the recruitment of specialized TLS polymerases to the site of replication arrest to bypass lesions, and homology-directed damage tolerance, which includes the template switching and fork reversal pathways. With some exceptions, lesion bypass by TLS polymerases is a source of mutagenesis, potentially contributing to the development of cancer. The capacity of TLS polymerases to bypass replication-blocking lesions induced by anti-cancer drugs such as cisplatin can also contribute to tumor chemoresistance. On the other hand, during homology-directed DDT the nascent sister strand is transiently utilised as a template for replication, allowing for error-free lesion bypass. Given the role of DNA damage tolerance pathways in replication, mutagenesis and chemoresistance, a more complete understanding of these pathways can provide avenues for therapeutic exploitation. A number of small molecule inhibitors of TLS polymerase activity have been identified that show synergy with conventional chemotherapeutic agents in killing cancer cells. In this review, we will summarize the major DDT pathways, explore the relationship between damage tolerance and carcinogenesis, and discuss the potential of targeting TLS polymerases as a therapeutic approach.

Keywords: DNA damage, DNA damage tolerance pathways, DNA replication, translesion synthesis (TLS), TLS inhibitors, cancer therapeutics

INTRODUCTION

It is estimated that up to 50,000 DNA lesions can occur per cell in a single day, an average of around 2,000 DNA lesions per cell per hour (1). While the majority of DNA damage is removed by repair pathways, including nucleotide excision repair and base excision repair, prior to cells entering S-phase, lesions can remain in the DNA template during DNA replication. The main DNA polymerases that carry out genomic DNA replication, polymerase δ (Pol δ) on the lagging strand and polymerase ϵ (Pol ϵ) on the leading strand, can both be blocked by DNA damage in the template strand, leading to replication fork stalling, fork collapse, chromosome breakage and genomic instability. To resolve this problem, DNA damage tolerance (DDT) pathways that allow replication of damaged DNA to continue while reducing genomic instability, are present in virtually all organisms (1–4).

THE MAIN DNA DAMAGE TOLERANCE PATHWAYS IN EUKARYOTES

There are two main DDT pathways described in eukaryotic cells, namely (i) translesion synthesis (TLS) and (ii) homology-directed DDT (**Figure 1**). TLS involves the recruitment of specialized TLS DNA polymerases to the arrested replication fork to facilitate lesion bypass, which can take place either directly at the replication fork, or behind the fork by repriming DNA synthesis at daughter strand gaps (DSGs) (**Figure 1**) (5). In response to DNA damage, monoubiquitination of the clamp protein proliferating cell nuclear antigen (PCNA) results in recruitment of the specialized TLS polymerases required to bypass the DNA lesion. Lesion bypass takes place either directly at the site of the arrested fork, or during gap-filling subsequent to replication restart away from the lesion site (6, 7) (**Figure 1**). However, despite some exceptions discussed below, bypass by TLS polymerases contributes to mutagenesis owing to the tendency for base misincorporation opposite lesions (7–9). In fact, the error-prone nature of TLS polymerases has been implicated both in the development of cancer and in promoting chemoresistance in cancer cells (10–12). Hence, TLS is considered an error-prone DDT pathway (13).

In addition to TLS, damage tolerance can also take place through homology-directed DDT, which consists of two pathways, fork reversal (FR) and template switching (TS) (**Figure 1**) (5). Both FR and TS are initiated through the polyubiquitination of PCNA, and involve a temporary switch from the damaged template strand to using the newly-synthesized copy of the complementary strand on a homologous sister chromatid as the template for DNA synthesis. Because an undamaged template is copied, FR and TS are error-free lesion bypass pathways (5). Fork reversal involves formation of a 'chicken foot'-like DNA structure, allowing the replisome on the arrested nascent strand to gain access to the homologous sister template (14, 15) (**Figure 1**). In contrast, TS occurs following repriming at DSGs generated at lesion sites behind the replication fork (16, 17). TS involves strand invasion, where the newly-synthesized strand from the homologous sister chromatid transiently serves as a template for nascent strand synthesis to allow the replication machinery to bypass the lesion (13, 18) (**Figure 1**).

On a biochemical level, the process of damage tolerance is complex, requiring multiple proteins. While these proteins are potential targets for development of novel cancer therapeutics, a more complete understanding of the molecular genetics, cell biology and biochemistry of damage tolerance is necessary to advance this potential. The present review provides an overview of the main DDT pathways in human cells, and discusses recent advances in targeting these pathways to develop cancer therapeutics.

Initiation of DNA Damage Tolerance (DDT)

Both the TLS and TS pathways share common initial steps. Stalling of the replicative DNA polymerase at a DNA lesion site together with ongoing helicase activity at the replication fork generates a region of single-stranded DNA (ssDNA) on the template strand which is bound by replication protein A (RPA). The ssDNA-RPA complex recruits ATRIP, and activates the ataxia telangiectasia and RAD3-related protein (ATR)-dependent replication checkpoint (18–20). At the same time, the chromatin remodelling protein INO80 binds to the stalled replication fork (18, 21–23). This, in conjunction with the RPA-ssDNA complex facilitates the recruitment of the RAD18 E3 ubiquitin ligase to the site of DNA damage (18, 23–26). At the lesion site, RAD18 recruits the E2 ligase RAD6, leading to the formation of the E2-E3 ubiquitinase (18, 25, 27–30) which monoubiquitinates PCNA on K164 (18, 25, 31–33). Monoubiquitination can be facilitated by other E3 ligases such as ring finger protein 8 (RNF8) in conjunction with the E2 ligase, Ubiquitin-conjugating Enzyme H5c (UbcH5c) (34). At this step, the two DDT pathways diverge, with monoubiquitination of PCNA on K164 resulting in the induction of TLS, while polyubiquitination at K164 leads to homology-directed DDT (**Figure 2**).

Translesion Synthesis

Following monoubiquitination of PCNA, one or more TLS polymerases are recruited to the stalled replication fork. Human TLS polymerases comprise proteins belonging to 4 families: the Y-family (Rev 1, Pol η, Pol ι and Pol κ), the A-family (Pol θ), the B-family (Pol ζ) and the archaeo-eukaryotic primase (AEP) family (PrimPol) (6, 35–38). In Y-family TLS

Abbreviations: ATR, ataxia telangiectasia and RAD3-related protein; ATRIP, ATR-interacting protein; DDT, DNA damage tolerance; FA, Fanconi anemia; FR, fork reversal; HTLF, helicase-like transcription factor; PARP, Poly(ADP-ribose) polymerase; PCNA, proliferating cell nuclear antigen; PIP, PCNA-interacting peptide; PPI, protein-protein interactions; Rev1-CT, Rev1 C-terminal; RIR, Rev1-interacting region; RPA, Replication protein A; SHPRH, SNF2 histone linker PHD RING helicase; SMARCAL1, SWI/SNF-related matrix associated actin-dependent regulator of chromatin subfamily A-like protein 1; SPARTAN, SprT-like domain at the N-terminus; ssDNA, single-stranded DNA; TLS, translesion synthesis; TLSi, translesion synthesis inhibitor; TS, template switching; UBM, ubiquitin-binding motif; UBZ, ubiquitin-binding zinc finger; USP1, ubiquitin carboxyl-terminal hydroxylase 1; USP7, ubiquitin carboxyl-terminal hydroxylase 7; XP-V, xeroderma pigmentosum variant; ZRANB3, Translocase zinc finger RANBP2 type –containing 3.

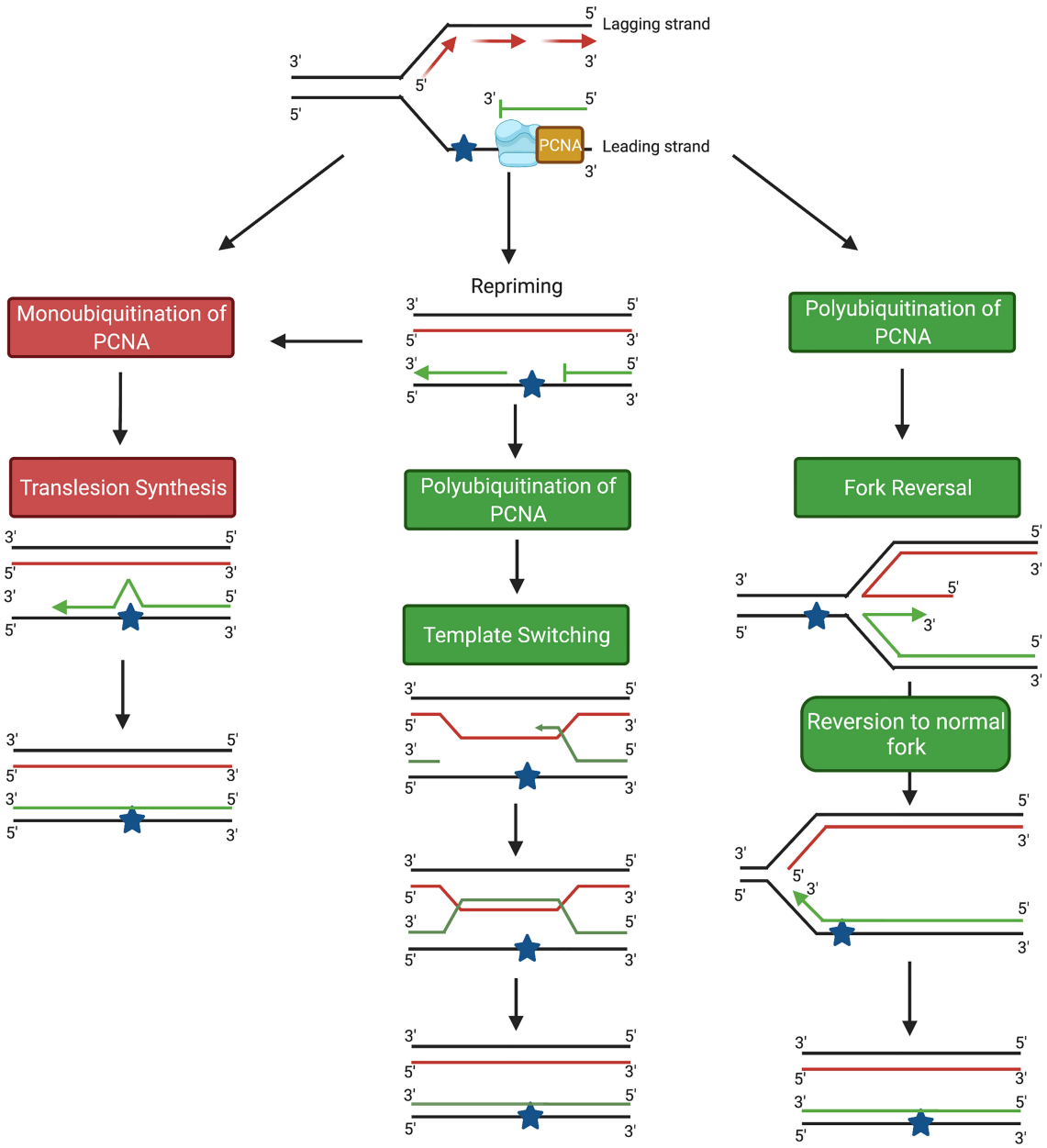

FIGURE 1 | Schematic diagram showing the main DDT pathways in eukaryotic cells. TLS pathways are highlighted in red; homology-based damage tolerance pathways are highlighted in green. Image generated with BioRender.com.

polymerases, the active site that catalyses lesion bypass is located within the conserved N-terminal domain (39, 40), while the variable C-terminal region facilitates recruitment of the protein to stalled forks (39, 40). Y-family TLS polymerases can bind directly to K164-ubiquitinated PCNA through ubiquitin-binding zinc fingers (UBZ) found in Pol η and κ, or to ubiquitin-binding motifs (UBM) present in Pol ι and Rev1 (39). The PCNA-interacting peptide (PIP) boxes on Pol ι, η and κ, and the BRCA1 C-terminus (BRCT) domain in the N-terminal of Rev1, also facilitate the binding of TLS polymerases to PCNA (39, 41, 42).

TLS generally occurs by either a 'one-polymerase' mechanism or a 'multiple-polymerase' mechanism (35). Upon replication fork stalling in the presence of DNA damage, the replicative polymerase (δ or ϵ) is replaced by a TLS polymerase. Following this step, in the one-polymerase mechanism, a single TLS polymerase inserts nucleotides at the lesion site and continues to extend the replicated DNA strand past the lesion site, and is then replaced again by the replicative polymerase (35). The multiple-polymerase mechanism usually involves two TLS polymerases working in concert, such that one polymerase

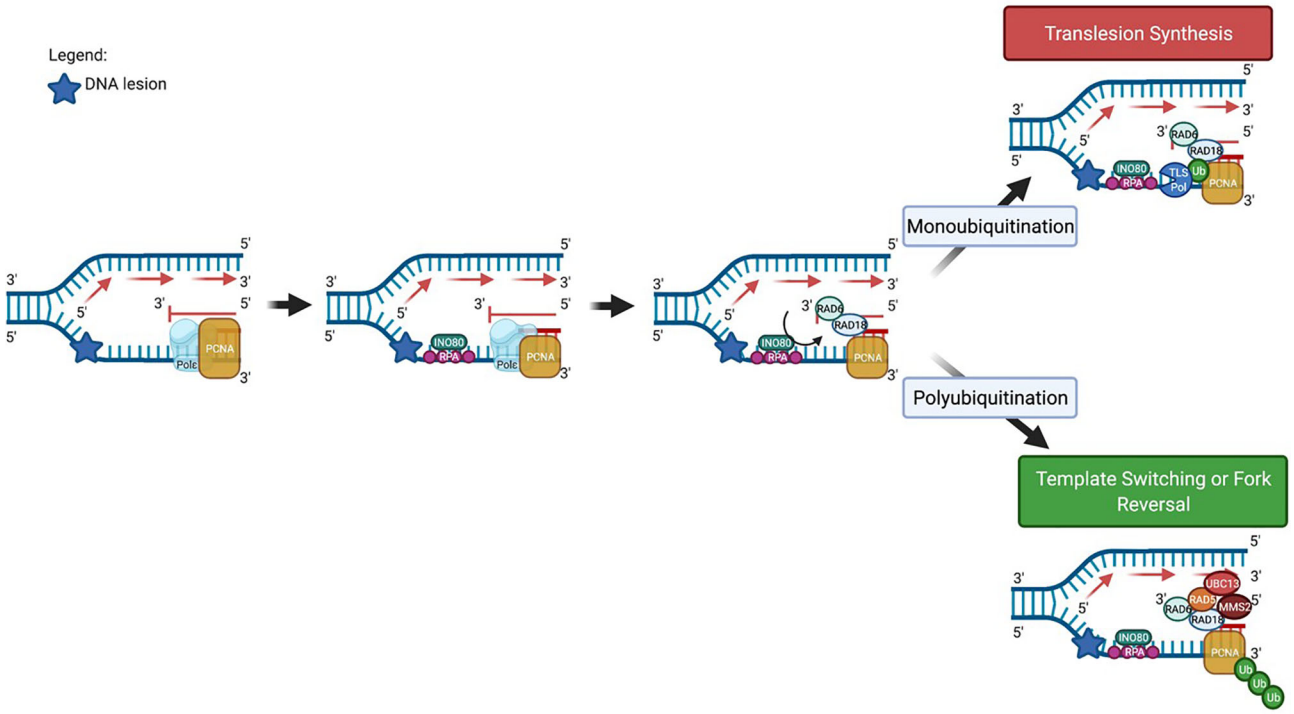

FIGURE 2 | Schematic diagram showing key proteins involved in the initial steps of DNA damage tolerance pathway activation at an arrested replication fork. PCNA, proliferating cell nuclear antigen; RPA, replication protein A; UBC13, Ubiquitin-conjugating enzyme E2 13; MMS2, Ubiquitin-conjugating enzyme variant MMS2. Image generated with BioRender.com.

inserts a nucleotide opposite the lesion site, while the other extends the primer beyond the lesion site (35, 40, 43). Rev1 incorporates a single dCTP opposite a lesion site, but does not carry out subsequent polymerization (44–48). During bypass by *S. cerevisiae* Rev1, the lesion on the template strand is flipped into an extra-helical position and stabilised inside a hydrophobic pocket of Rev1, where it remains during incorporation of the incoming cytosine (49). The R324 side-chain of Rev1 displaces the DNA lesion, acting as an alternative template for Watson-Crick base pairing with the incoming cytosine (49). Following phosphodiester bond formation coupled with the hydrolysis of pyrophosphate, hydrogen bonding between the cytosine and R324 is broken (49). Rev1 then dissociates from the DNA and the lesion is reincorporated into the double helix (49).

Y-family DNA polymerases are characterised by a more open active site that can accommodate altered bases, and by the absence of 3'->5' proofreading exonuclease activity (9, 40, 50, 51). For example, the active site of human Pol η can accommodate the two covalently-linked thymine bases in a UV-induced *cis-syn* thymine-thymine CPD lesion (50, 51). A β-strand in the little finger (LF) domain of the protein provides a molecular splint that stabilises the newly-synthesized double-stranded DNA into a B-form structure, preventing CPD-induced duplex distortion and frameshift formation, which facilitates efficient and accurate Pol η-mediated bypass of thymine-thymine CPDs (40, 50, 51).

As noted above, the capacity of TLS polymerases to accommodate altered bases in the active site, and the absence of 3' to 5' exonuclease activity facilitate lesion bypass (**Table 1**). Bypass is often at the cost of replication fidelity (70). The accuracy of TLS polymerases is lesion-dependent, such that specific TLS polymerases are more accurate than others when encountering particular lesions (70). For example, Pol θ predominantly incorporates the correct base when replicating across a 1,N^6-ethenodeoxyadenosine lesion in human cells (66). However, Pol θ also plays an important role in the error-prone bypass of UV-induced *cis-syn* thymine-thymine CPDs and (6–4) PP lesions (66). By preventing the collapse of arrested replication forks and thereby reducing genome instability, error-prone lesion bypass by Pol θ protects against UV-induced skin cancer in mice (66). The overall fidelity of lesion bypass during TLS results from a combination of the biochemical properties of the individual TLS polymerases, the affinity of the polymerases for the lesion, as well as the sequence context of the lesion (9, 71).

Homology-Directed DDT

In addition to the error-prone TLS pathway, lesion bypass during S-phase can occur through the error-free homology-directed DDT pathways, FR and TS. Error-free DNA damage tolerance requires PCNA polyubiquitination, mediated by the recruitment of one of the yeast RAD5 homologues, SNF2 histone linker PHD RING helicase (SHPRH) or helicase-like transcription factor

TABLE 1 | Examples of lesion bypass by human TLS polymerases.

TLS polymerase	Gene Name	Lesions bypassed
Rev1	*REV1*	UV-induced lesions (52) 8-oxoguanine (8-oxoG) (53) Trans-anti-benzo[a]pyrene-N 2-dG (53) 1,N 6-ethenoadenine adducts (53)
Pol η	*POLH*	UV-induced lesions, particularly T-T CPDs (54) *N*-2-acetylaminofluorene (AAF)-modified guanine (54) Cisplatin-induced guanine-guanine intrastrand adducts (54) 8-oxoG (55) Abasic sites (56)
Pol ι	*POLI*	N2-guanine adduct (57) 5-hydroxycytosine (5-OHC) (58) 5-hydroxyuracil (5-OHU) (58) 5,6-dihydrouracil (5,6-DHU) (58) 8-oxoG (58) T-T (6–4) PP (59)
Pol κ	*POLK*	Thymine glycol (60) Benzo[a]pyrene-guanine adducts (BP-G) (61) 8-oxo-dG (62) Acetylaminofluorene-modified G (62) Abasic site (63)
Pol θ	*POLQ*	Abasic sites (64) Thymine glycols (65) 1,N 6-ethenoadenine adducts (66) UV-induced lesions (66)
Pol ζ	*REV3*	T-T (6–4) PP (67, 68) CPD (68) Extender polymerase for numerous lesions
PrimPol	*PRIMPOL*	AP site (69)

UV, ultraviolet; CPD: cyclobutane pyrimidine dimers; T-T 6-4 PP, thymine-thymine 6-4 photoproducts; XP-V, xeroderma pigmentosum variant; AP site, apyrimidinic/apurinic site.

(HLTF), to the RAD6/RAD18 complex (2). In the FR pathway, remodeling of the stalled replication fork into the characteristic 'chicken-foot' structure (**Figure 1**) is initiated by the recruitment of the helicase protein SMARCAL1, which binds directly to ssDNA and removes bound RPA (5, 72–74). Following the removal of RPA, translocase zinc finger RANBP2-type containing 3 (ZRANB3) then promotes further fork reversal (5, 75–77). Binding of the Fanconi anemia complementation group M (FANCM) helicase to the protein-DNA complex leads to the formation of a four-way junction (78, 79). The reversed fork is stabilized by BRCA1, BRCA2 and RAD51, which bind to the exposed ends of the nascent leading and lagging strands and prevent MRE-11-mediated exonucleolytic degradation (5, 80–83). Following successful lesion bypass, regression of the reversed fork from a four-way junction into the original three-way junction (**Figure 1**) is catalysed by RecQ-like helicase (RECQ1), Werner syndrome RECQ-like helicase (WRN) and DNA replication helicase/nuclease 2 (DNA2) (5, 84, 85).

In the TS pathway (**Figure 1**), following polyubiquitination of PCNA, the 9-1-1 complex binds to the 5' end of the gap on the nascent DNA strand and recruits exonuclease 1 (EXO1) (18, 86). A RAD51-ssDNA presynaptic filament, stabilized by RAD55/RAD57, then forms on the ssDNA region of the template strand (87–89). ATP-dependent DNA helicase SRS2 (SRS2) disrupts the nucleofilament and opposes the action of RAD55/RAD57; the balance between these processes determines the overall stability of the RAD51-ssDNA presynaptic filament (18, 90, 91). The nucleofilament, with RAD52 and RAD54, carries out both the homology search and strand invasion of the sister chromatid (18, 89, 92). After complementary base-pairing between the invading strand and the homologous template, DNA pol δ is recruited and continues DNA replication, generating a D-loop and subsequently a sister-chromatid junction (SCJ) (18, 89, 93–95). D-loop formation is negatively regulated by SRS2 (18, 96). Finally, the slow growth suppressor 1 (SGS1)/DNA topoisomerase 3 (TOP3)/RECQ-mediated genome instability protein 1 (RMI1) complex pries the SCJ apart, regenerating the normal double-helical DNA structure (16, 18, 97, 98) (**Figure 1**).

Regulation of DDT Pathway Choice

The type of PCNA ubiquitination plays a key role in the choice of DDT pathway between either TLS or homology-directed DDT (5, 9, 99). PCNA monoubiquitination leads to TLS, while polyubiquitination results in the initiation of homology-directed DDT. The overall level of ubiquitinated PCNA is also regulated by ubiquitin-specific processing protease 7 (USP7), by the USP1/upstream activation factor (UAF1) complex, and by enhanced level of genomic instability 1 (ELG1) (99–103). Following UV irradiation, USP1 undergoes auto-cleavage and degradation, increasing the level of modified PCNA (104). It has been proposed that the extent of replication arrest is a factor in determining the type of PCNA ubiquitination, such that prolonged replication arrest leads to polyubiquitination of PCNA molecules that remain bound at the arrest site, promoting a switch to homology-directed DDT (99). Alternatively, homology-directed DDT could be activated first where HLTF is recruited together with the RAD6/RAD18 complex, resulting in the immediate polyubiquitination of PCNA (99). In addition to ubiquitination, PCNA undergoes other related modifications. Protein inhibitor of STAT (PIAS1 and PIAS4)-mediated SUMOylation of PCNA on K164 promotes template switching rather than TLS (105). After TLS is completed, monoubiquitinated PCNA is modified by the addition of interferon-stimulated gene 15 (ISG15) molecules, leading to recruitment of USP10 and PCNA deubiquitination (99, 106, 107). Understanding the interplay between PCNA modification and the choice of DNA damage tolerance pathway is an important area for further study.

Regulation of TLS

Since TLS polymerases are generally error-prone it is critical that TLS activity is tightly regulated. The main points of regulation of TLS involve the interactions between TLS polymerases, accessory proteins, RAD18 and PCNA (108). CHK1 and CLASPIN are essential for binding of RAD18 to chromatin (18, 109). SIVA1, TIMELESS and HLTF play important roles in PCNA monoubiquitination (18, 109–111), while protein with SprT-like domain at the N-terminus (SPARTAN) is crucial both for binding of RAD18 to chromatin and for monoubiquitination of PCNA (112, 113).

Regulation of the TLS pathway also occurs at the level of the individual polymerases, where TLS polymerases undergo post-translational modification including ubiquitination,

SUMOylation and phosphorylation (as shown in **Table 2** for human Pol η). In the absence of DNA damage in the template, or when DNA lesions have been bypassed, TLS polymerases are monoubiquitinated, switching the protein from an open conformation, where the C-terminal ubiquitin-binding domain is available to interact with monoubiquitinated PCNA, to a closed conformation, where this domain is bound in *cis* to ubiquitin and is unable to interact with PCNA (128). For human Pol η, in the closed conformation ubiquitination of one of the four lysines K682, K686, K694 and K709 results in interaction between the ubiquitin moiety and the UBZ domain of the polymerase which competes with ubiquitinated PCNA for UBZ binding, thereby abrogating the PCNA interaction (118, 128). Following UV-induced DNA damage in non-small cell lung and colon carcinoma cell lines, ubiquitinated Pol η is polyubiquitinated by mouse double minute 2 homologue (MDM2) resulting in degradation by the proteasome by 24 hours post-irradiation (121, 128). The other Y family TLS polymerases Rev 1, Pol ι and Pol κ are also ubiquitinated (51, 128). In addition to ubiquitination, Pol η undergoes SUMOylation (126, 127). PIAS1-dependent SUMOylation on K163 targets Pol η to difficult-to-replicate regions of the genome such as fragile sites even in the absence of exogenous DNA damage (127). Following completion of TLS, SUMOylation of Pol η on multiple lysine residues prevents ongoing interaction with ubiquitinated PCNA, leading to SUMO-targeted ubiquitin ligase (STUbL)-mediated ubiquitination of Pol η and its' exclusion from damage sites (127).

TLS polymerase activity is also modulated by phosphorylation. Pol η is phosphorylated at a number of sites in the C-terminus by protein kinases including ATR, CDK2 and PKC. Following DNA damage, ATR-mediated phosphorylation of Pol η on serine 601 (114) releases it from sequestration by Pol δ-interacting protein of 38 kDa (PDIP38), freeing Pol η to bind to monoubiquitinated PCNA (115). This links ATR activation by replication arrest-induced single-stranded DNA, with recruitment of TLS polymerases to the arrested fork (115). Pol η is additionally phosphorylated by PKC on S587 and T617 (129), and on serine 687 by CDK2, which increases the stability of the polymerase in late-S and G2/M (125).

In addition to post-translational modification of specific proteins, TLS is regulated at the transcriptional level. Following DNA damage, *POLH* expression is p53-dependent (130), while *POLK* expression is regulated by the aryl hydrocarbon receptor (AhR) (131, 132). A recent report shows that TLS is negatively regulated by Pumilio RNA Binding Family Member 1 (PUM1), a protein that mediates mRNA decay (133). miRNAs have also been identified which modulate expression of DNA damage tolerance proteins. Examples include MiR-145 and miR-630 which downregulate RAD18 expression, and miR-93 and miR-619 which downregulate Pol η expression (39, 134). Furthermore, alternative polyadenylation of the *POLH* mRNA transcript in lung and bladder cancer cells generates three transcripts having 3'-UTR sequences of 427, 2516 or 6245 nucleotides, respectively (135). Of note, miR-619 only targets the longer transcript, while the shortest transcript is resistant to miR-619, and is responsible for increased Pol η expression and cisplatin resistance in cancer cell lines (135).

Regulation of Homology-Directed DDT

Interplay between fork-protective and fork-degradative factors plays a key role in modulating fork reversal (104). BRCA1, BRCA2 and RAD51 shield the nascent DNA strands at the reversed fork from degradation by the exonuclease action of MRE-11 (5, 80, 81). WRN helicase interacting protein 1 (WRNIP1) also protects reversed forks from structure-specific endonuclease subunit SLX4 (SLX4)-mediated fork cleavage and subsequent DNA2-mediated fork degradation (136–138). The interaction of polyubiquitinated PCNA with ZRANB3 slows fork progression, promoting fork reversal through the translocase

TABLE 2 | Proteins regulating Pol η function in TLS.

Regulatory protein	Function
ATR	Phosphorylates Pol η on serine 601 and releases it from PDIP38 (114, 115)
NBS1	Binds to RAD18 and facilitates recruitment of Pol η to DNA damage sites (18, 116, 117)
SIVA1	Binds to PCNA to facilitate RAD18 recruitment and Pol η focus formation (18, 110)
SPARTAN	Binds to RAD18 and prevents its removal from DNA (18, 112, 113)
HLTF	Required for recruitment of Pol η (18, 111)
PirH2	Facilitates monoubiquitination of Pol η (39, 118, 119)
USP7	Deubiquitinates Pol η and allows it to bind to PCNA to initiate TLS (39, 120)
MDM2	Polyubiquitinates Pol η and marks it for degradation (39, 121)
PAF15	Removal of ubiquitinated PAF15 allows PCNA to bind to Pol η (39, 122); terminates TLS by removing Pol η from PCNA (39)
PARP10	Facilitates monoubiquitination of PCNA (39, 123)
CHK1, CLASPIN and TIMELESS	Promote binding of RAD18 to PCNA (39, 109)
SART3	Facilitates the binding of RPA to ssDNA and the interaction between Pol η and RAD18 (39, 124)
CDK2	Phosphorylates Pol η and increases its stability (39, 125)
PIAS1	SUMOylates Pol η at K163 to promote recruitment to replication forks (126); SUMOylates Pol η at multiple sites to target it for removal from PCNA (127)
STUbL	Extracts Pol η from DNA damage sites (127)

SPARTAN, Protein with SprT-like domain at the N terminus; HLTF, helicase-like transcription factor; PirH2, p-53 induced RING-H2 protein; USP7, ubiquitin carboxyl-terminal hydroxylase 7; MDM2, mouse double minute 2 homologue; PAF15, PCNA-associated factor 15; PARP10, poly (ADP-ribose) polymerase 10; SART3, squamous cell carcinoma antigen recognized by T Cells 3; CDK, cyclin-dependent kinase; PIAS1, Protein Inhibitor of Activated STAT 1.

activity of ZRANB3 (75, 76). Recruitment of SMARCAL1 to the stalled fork is regulated by ATR-mediated phosphorylation, thereby limiting the extent of fork reversal (136, 139). Poly (ADP-ribose) polymerase 1 (PARP1) modulates fork reversal and fork restart by inhibiting RECQ1 helicase, and prolongs FR by preventing RECQ1-mediated regression of reversed forks to three-way junctions (15, 85, 136).

Template switching is regulated at a number of points including PCNA polyubiquitination, the formation of the RAD51-ssDNA presynaptic filament and SCJ formation [reviewed in (18)]. The chromatin remodeling protein INO80, and the human Rad5 orthologues, HLTF and SHPRH are important for PCNA polyubiquitination (140). Chromatin remodeling by INO80 facilitates the addition of K63-linked polyubiquitin chains to PCNA by HLTF and SHRPH (5, 23, 141–143). The stability of the RAD51-ssDNA filament involved in homology searching is negatively regulated by SRS2 (18, 144, 145), while exonuclease 1 (EXO1), INO80 and high mobility group protein 1 (HMO1) facilitate SCJ formation (18, 23, 89, 146).

DNA DAMAGE TOLERANCE AND CARCINOGENESIS

The role of TLS in preventing cancer is clearly demonstrated in the sun-sensitive skin cancer-prone disease xeroderma pigmentosum variant (XP-V), where the absence of Pol η as a result of inactivating mutations in *POLH* (147, 148) leads to prolonged replication arrest at the sites of UV-induced lesions in the template. In the absence of error-free bypass of UV-induced CPDs by Pol η in XP-V cells, error-prone lesion bypass is carried out by polymerases including Pol ι and Pol ζ, resulting in increased mutagenesis that contributes to skin carcinogenesis in XP-V patients (9, 149). However, error-prone TLS can also play an anti-carcinogenic role. As noted, error-prone bypass of UV-induced lesions by Pol θ protects against skin cancer in mice, by allowing ongoing DNA synthesis to proceed thereby preventing strand break formation and the resulting genomic rearrangements (66). As a source of spontaneous mutagenesis, low-fidelity TLS polymerases may play a role in driving carcinogenesis. Y-family TLS polymerases in particular have been implicated as a source of somatic mutations in tumors (150). For example, Pol η mutational signatures are found in the genome of cancer cells from patients with malignant B-cell lymphoma and chronic lymphocytic leukemia (151).

Polymorphisms in genes encoding TLS polymerases are also associated with increased cancer risk. Polymorphisms in *REV1* and *POLI*, leading to single amino acid substitutions in Rev1 and Pol ι, were associated with increased risk of squamous cell carcinoma and adenocarcinoma, respectively (152), while *POLH* polymorphisms are associated with increased risk of malignant melanoma (153). In addition to polymorphic variants, sequencing of tumor DNA has revealed somatic mutations in TLS polymerase genes in a number of tumor types (10, 154). While the functional significance of most of these mutations remains to be determined experimentally, mutations in TLS genes that affect protein function could in principle lead to genome instability and contribute to tumor development, or alter the response of tumor cells to chemotherapeutic DNA damaging agents (10).

TLS polymerases are overexpressed in a number of different cancers. It has been proposed that overexpression of TLS polymerases can facilitate error-prone replication and adaptation of the cancer cells to targeted therapy (155). For example, expression of TLS polymerases ι, κ, λ, μ and Rev1 was upregulated in colorectal cancer cells following treatment with inhibitors of B-RAF or EGFR signalling (155). However, whether increased levels of TLS polymerases directly contribute to the acquisition of adaptive mutations requires further investigation. In non-small-cell lung tumors increased expression of Pol η is associated with poorer prognosis (156, 157), while increased expression of Pol ι is associated with oesophageal squamous cell cancer and directly correlates with the degree of metastasis (158). Pol ι expression also correlates with the grade of bladder tumors (159), while high expression of Pol κ in glioblastoma tumors is associated with poor prognosis (160).

From the perspective of cancer treatment, TLS can increase the tolerance of cancer cells to DNA damage induced by chemotherapeutic anti-cancer agents, thus promoting cancer cell survival, and increasing the mutational burden as result of error-prone lesion bypass. Pol κ plays a role in the response to the alkylating agent temozolomide used in the treatment of glioblastoma. Increased expression of Pol κ enhanced the resistance of human glioblastoma cell lines to temozolomide while down-regulation sensitised the cells to the drug (135). Pol η can bypass cisplatin-induced intrastrand lesions (161–163), and also plays a role in interstrand crosslink repair (164, 165). Human cells lacking Pol η are more sensitive to platinum-based chemotherapeutic agents (162, 163, 166–168). Overexpression of Pol η and Pol ζ contributes to cisplatin resistance in ovarian cancer stem cells and human glioma cells (169, 170). It was recently shown that PrimPol enhances survival of cisplatin-treated BRCA-deficient human ovarian cancer and osteosarcoma cells (171). PrimPol promotes repriming by reinitiating DNA synthesis downstream of blocking lesions in the template, thereby preventing fork reversal and degradation (171). In addition to promoting resistance to direct DNA-damaging agents, TLS polymerase levels also affect the response to signalling pathway inhibitors. Pol κ increased the resistance of melanoma cells to the B-RAF inhibitor vemurafenib (70). Although the mechanisms of TLS polymerase overexpression in cancer cells remain to be elucidated, overexpression of Pol κ is regulated through activation of the aryl hydrocarbon receptor (AhR) by the endogenous tryptophan-derived ligand kyneurin, as well as by DNA damaging agents such as benzo[a]pyrene (B[a]P) (131, 132, 172, 173). In the case of Pol η, expression is regulated in a p53-dependent manner after exposure of cells to DNA damage (130).

Other than DNA polymerases, alterations to regulatory proteins that play a role in TLS may also contribute to cancer development. For example, *RAD18* deletions were identified in 5% of pancreatic tumors and 11% of renal cell carcinoma tumors

examined (174). Increased expression of RAD18 in a variety of human cancer cell lines (including H1299 non-small cell lung carcinoma cells, H157 and H650 adenocarcinoma cells and U2OS osteosarcoma cells) leads to excessive activation of the TLS pathway, contributing significantly to hypermutability (150). RAD18 protein levels can be increased by upregulation of melanoma antigen-A4 (MAGE-A4), which binds to and stabilises RAD18, activating the TLS pathway (175). The RAD5 ortholog HLTF, important in PCNA polyubiquitination, is downregulated through promoter methylation in colon cancer cell lines and in primary tumors (176).

DDT PATHWAYS AS THERAPEUTIC TARGETS

Given the role of DNA damage tolerance pathways in driving chemoresistance, there is potential to sensitize cancer cells to chemotherapy by inhibiting these pathways (177). To date, the major focus has been on identification of TLS inhibitors. A number of inhibitors of TLS-mediated lesion bypass have been reported (**Table 3**) and are discussed below. The inhibitors fall broadly into two categories: (i) inhibitors that directly interfere with TLS polymerase catalytic function and (ii) inhibitors that interfere with protein-protein interactions (PPIs) to inhibit TLS indirectly.

Direct Inhibitors of TLS Polymerases

In recent years, several TLS polymerase inhibitors have been reported (187). Examples include indole thiobarbituric acid (ITBA) and its' derivatives (185, 186). ITBA binds directly to the finger and LF domains of Pol η, which may prevent the polymerase from binding to ssDNA and interfere with nucleotide incorporation (186). The ITBA derivative ITBA-12 inhibits Pol η and Pol κ activity (186), while ITBA-16 and ITBA-19, containing N-1-naphthoyl and N-2-naphthoyl Ar-substituents have increased specificity towards Pol η (186). The ITBA derivative, PNR-7-02 which binds to the little finger domain and inhibits Pol η function, acts synergistically with cisplatin to kill chronic myeloid leukaemia and ovarian cancer cell lines (185). An indole-aminoguanidine analogue, IAG-10, binds human Pol κ preventing the N-clasp domain from holding the LF domain in place, triggering a conformational change that decreases the contact between the protein and the DNA template (190). IAG-10 synergises with temozolomide to kill glioblastoma cell lines in culture (190). This supports the concept that direct inhibitors of TLS polymerases can increase the cytotoxic effects of conventional chemotherapeutic agents (190).

In addition to the identification of novel compounds that inhibit TLS polymerases, certain existing small molecules in clinical use have been reported to inhibit TLS. These include candesartan cilexetil, used clinically as an angiotensin-II receptor antagonist in the treatment of hypertension (191); manoalide, a phospholipase A2 inhibitor with both analgesic and anti-inflammatory properties (192), and MK-886, a leukotriene antagonist (193). Candesartan cilexetil, manoalide and MK-886 were shown to inhibit the *in vitro* activity of purified human Pol κ on undamaged DNA templates and to inhibit bypass of a γ-HOPdG lesion by Pol κ (178). Candesartan cilexetil, but not the other two compounds, sensitised Pol η-deficient XP-V cells to UV radiation (178). The fungal-derived molecules 3-O-methylfunicone, and Penicilliols A and B have been identified by screening for natural products that inhibit TLS polymerases (183). 3-O-methylfunicone, isolated from an Australian sea salt fungal strain, inhibits Y-polymerases κ, ι and η (183), competing directly with the DNA template-primer for interaction with the DNA binding domain of Pol κ (183). 3-O-methylfunicone decreased the growth of two cervical carcinoma and colon carcinoma cell lines, while having little effect on the growth and proliferation of normal human cells (183). Penicilliols A and B, isolated from a strain of *Penicillium daleae*, also inhibit mammalian Y-family polymerases, in particular Pol ι (184).

Recent reports (188, 189) demonstrating that novel inhibitors of human Pol θ synergise with HR-deficiency or resistance to PARP inhibition to kill cancer cells provides strong support for the strategy of targeting specialised DNA polymerases in cancer

TABLE 3 | Inhibitors of TLS polymerases.

Inhibitor	TLS polymerase(s)	Effect on cancer cells
Candesartan cilexetil	Pol η, Pol ι, Pol κ	Sensitises XP-V cells to UV radiation (178)
Manoalide; MK-886	Pol κ	Inhibit Pol κ *in vitro* but do not sensitise XP-V cells to UV radiation (178)
Cholesterol hemisuccinate	Pol η, Pol ι, Pol κ	Not reported (179)
Penta-1,2,3,4,6-O-galloyl-*beta*-D-glucose	Pol η, Pol ι, Pol κ	Not reported (180)
Pinophilins A and B	Pol η, Pol ι, Pol κ	Inhibit proliferation of cancer cell lines (181)
β-Sitosteryl (6'-O-linoleoyl)-glucoside	Pol η, Pol ι, Pol κ	Not reported (182)
3-O-methylfunicone	Pol ι, Pol κ	Inhibits cervical and colon carcinoma cell growth; sensitises cervical carcinoma cells to UV radiation (183)
Penicilliols A and B	Pol η, Pol ι, Pol κ	Not reported (184)
PNR-7-02	Rev 1, Pol η	Sensitises chronic myeloid leukaemia and ovarian cancer cell lines to cisplatin (185)
IAG-10	Pol κ	Sensitises glioblastoma cell lines to temozolomide (186)
JH-RE-06	Rev1	Sensitises melanoma cells to cisplatin; reduces melanoma tumor volume in mouse model (177, 187)
Novobiocin	Pol θ	Synthetic lethality with olaparib in HR-deficient ovarian cancer cells; tumor regression in mouse model (188)
ART558; ART812	Pol θ	Synthetic lethality with olaparib in HR-deficient colon cancer cells; inhibition of HR-deficient tumor xenografts in rat model (189)

therapy. The Pol θ inhibitors include the antibiotic novobiocin (188) and the synthetic small molecule allosteric inhibitor ART558 (189). When used in conjunction with PARP inhibitors, Pol θ inhibitors induce synthetic lethality in HR-deficient cancer cells. PARP is required for repair of single strand breaks and inhibition of PARP-dependent single-strand break repair increases the level of double-strand breaks in the genome. Novobiocin synergistically increased the cytotoxic effects of the PARP inhibitors rucaparib and olaparib in BRCA1-deficient human retinal pigment epithelial cells and ovarian cancer cell lines, respectively (188). In mouse studies, novobiocin sensitized tumors arising from PARPi-resistant ovarian carcinoma cells to treatment with olaparib, resulting in tumor regression (188). The novel small molecule ART558 induced synthetic lethality in PARPi-resistant BRCA2-deficient human colon cancer cells treated with olaparib (189). ART812, a more bioavailable derivative of ART558, inhibits tumor xenograft growth in a rat model (189). Mechanistically, the cytotoxic effects of the Pol θ inhibitors are synergistic with HR-deficiency and PARP inhibitor resistance due to the effect of the molecules on Pol θ activity in the Theta-mediated end-joining pathway of DNA double-strand break repair (188, 189).

Inhibitors of TLS Polymerase PPIs

Protein-protein interactions (PPIs) play a critical role in lesion bypass. PPIs include the key interactions between Ub-PCNA and TLS polymerases, as well as interactions between inserter and extender TLS polymerases, for example between Rev1 and other TLS polymerases, and between the Rev7 and Rev3 subunits of the Pol ζ complex. A number of PPI inhibitors have been developed based on detailed structural information on the interaction domains of the target proteins (194).

Inhibitors of Interactions Between PCNA and TLS Polymerases

Indirect inhibitors of TLS can inhibit the recruitment of TLS polymerases to PCNA, thereby preventing lesion bypass. Small molecule inhibitors of the PCNA/PIP-box interaction compete with the PIP-box sequence of TLS polymerases for binding to PCNA during the initiation phase of TLS. The compound 3,3',5-triiodothyronine (T3) and its synthetic derivative T2 amino alcohol (T2AA) were reported to inhibit the PCNA/PIP-box PPI (195). T2AA and its analogues suppressed TLS in NER-deficient human cells, decreased cell division in osteosarcoma cells treated with cisplatin (196), and inhibited interstrand DNA cross-link (ICL) repair, slowing proliferation of cervical cancer cells (196). Consistent with the importance of the PCNA-PIP box interaction, a novel compound which specifically targets the L126 to Y133 region of the PIP-interaction loop of PCNA sensitises cancer cells to cisplatin (197). Other inhibitors of the PCNA/TLS polymerase interaction specifically prevent the recruitment of Rev1 to PCNA. One small molecule inhibitor, compound 1, binds Rev1 directly *via* the UBM2 motif and prevents interaction with K164-ubiquitinated PCNA (198). Compound 1 increased the cytotoxicity of both 4-hydroxycyclophosphamide and cisplatin by up to 10-fold in cultured cells (198).

Inhibitors of PPIs Between Inserter and Extender Polymerases

Inhibitors of essential PPIs between inserter and extender TLS polymerases have also been identified that suppress TLS and enhance the cytotoxicity of chemotherapeutic agents. Among these are small molecule inhibitors of the interaction between the C-terminal domain of Rev1 (Rev1-CT) and the Rev1-interacting region (RIR) of other Y-family TLS polymerases. Two such compounds, 4 and 5, have been reported (199) that bind to the Rev1-CT, preventing the recruitment of Pol ζ to Rev1, and sensitising fibrosarcoma cell lines to cisplatin and to UV radiation. Both compounds decreased the level of cisplatin-induced *HPRT* gene mutations, indicating the molecules can attenuate the mutagenicity associated with error-prone replication of platinum-induced DNA lesions (199). Additional derivatives have been developed that also compete with TLS polymerases for binding to the Rev1-CT domain, and increase the cytotoxicity of cisplatin (200, 201). Of note, inhibition of the Rev1-CT/RIR interaction was synergistic with the ATM and ATR inhibitor VE-821 and the Wee1 inhibitor MK-1775, leading to the formation of daughter strand gaps (DSGs) in replicating DNA, and sensitising bone osteosarcoma and colon cancer cells to these agents (201). Consistent with this, Pol η-deficient cells are significantly more sensitive to ATR inhibitors than normal cells (129, 202, 203). Since daughter strand gaps can also result from replication stress in oncogene-mutated cancer cells, it is proposed that in addition to direct lesion bypass, TLS polymerases contribute to cancer cell survival by carrying out DNA synthesis at DSGs. This limits the accumulation of single-stranded DNA in the genome (201), a process termed gap suppression (201). TLS inhibitors could therefore be used to achieve synthetic lethality in combination with cell cycle checkpoint inhibitors that induce DSGs, such as inhibitors of ATR and Wee1 (201).

Aside from inhibitors that interrupt Rev1-CT-RIR interactions, a small molecule inhibitor that disrupts the interaction between Rev1 and the Rev7 subunit of Pol ζ has also been identified. In both human and mouse cell lines, JH-RE-06, a small molecule that binds to the C-terminal domain of Rev1 and blocks interaction with the Rev7 subunit of Pol ζ, sensitised melanoma cells to cisplatin, and reduced drug-induced mutagenesis (204). Combination treatment with JH-RE-06 and cisplatin reduced tumor volume and improved survival in a mouse xenograft model of A375 melanoma cells, demonstrating the potential of targeting key PPIs as a therapeutic strategy (204, 205). Treatment of fibrosarcoma and melanoma cells with JH-RE-06 leads to senescence following cisplatin-induced DNA damage (204, 205). The impact of chemical inhibition of Pol ζ activity on overall genome stability should also be considered, since genetic ablation of *REV3L* encoding the catalytic subunit of Pol ζ increased genome instability in *REV3L*-null mouse embryo fibroblasts (206), and contributed to development of lymphomas and mammary tumors in mice where *REV3L* was conditionally deleted (207).

Recent evidence indicates that the interaction between Rev7 and Rev3 proteins required to form active Pol ζ is actively regulated in cells (208). The ATPase thyroid receptor-

interacting protein 13, (TRIP13), modulates the conformation of Rev7, preventing both its' interaction with Rev3 to form of active Pol ζ which is required for TLS, and interaction with the Shieldin complex which activates NHEJ (208). TRIP13 therefore mediates pathway choice, promoting error-free HDR over mutagenic TLS or NHEJ (208). TRIP13 overexpression correlates with BRCA1-deficiency in breast cancer cells and contributes to chemoresistance towards PARP inhibitors (208). The interaction of Rev7 with the Shieldin complex and with Rev3 is also inhibited by expression of the p31^{comet} HORMA-like protein (209, 210), identifying Rev7 as a key modulator of pathway choice after DNA damage. Overall, inhibition of key interactions between TLS polymerases and partner proteins represents a promising approach to sensitising cancer cells to chemotherapy.

Inhibitors of TLS Regulators

While targeting the catalytic activity and protein-protein interactions of TLS polymerases has been shown to be effective in overcoming chemoresistance in cancer cells, there may also be potential in targeting upstream regulators of TLS to inhibit the action of multiple TLS polymerases for therapeutic effect. For example, targeting the TLS pathway regulator RAD6 and PCNA monoubiquitination could be a more potent method to inhibit TLS than targeting individual TLS polymerases. However, the effects of inhibiting RAD6 on cytotoxicity and genome stability after DNA damage should be directly compared with the effects of targeting individual TLS polymerases using specific inhibitors. Inhibition of RAD6 by a small-molecule inhibitor, SMI#9, attenuated cisplatin resistance in triple-negative breast cancer cells, and enhanced the cytotoxicity of oxaliplatin towards the oxaliplatin-resistant colorectal carcinoma cell line HCT116-OxR (211, 212). Co-administration of SMI#9 with cisplatin decreased the growth of tumors arising from triple-negative breast cancer cells and lymph node metastasis (211). Molecules that modulate the extent of PCNA monoubiquitination and therefore the recruitment of TLS polymerases to DNA damage sites have also been described. C11 and G8, two inhibitors of the protein kinase AKT, inhibit damage-induced PCNA monoubiquitination and show synthetic lethality with UV-irradiation in *BRCA1*-deficient triple-negative breast cancer and colon cancer cell lines (213). The specific targets of AKT that modulate PCNA monoubiquitination are of interest (213).

Additional potential targets for inhibition of TLS include the USP1/UAF1 deubiquitinase complex. Two small molecule USP1/UAF1 inhibitors, pimozide and GW7647, enhanced the cytotoxicity of cisplatin and decreased cell division in non-small cell lung cancer cell lines (214). A third USP1/UAF1 inhibitor, ML323, was found to increase the cytotoxic effect of cisplatin on osteosarcoma and non-small cell lung cancer cells (215). As well as affecting TLS, USP1/UAF1 inhibitors increase cisplatin sensitivity by disrupting deubiquitination of the FANCD2/FANCI complex, preventing repair of drug-induced interstrand adducts by the FA crosslink repair pathway (215–217). The level of the chaperone protein Hsp90 is also important in the stability of TLS polymerases, including Rev1 (218) and Pol η (219). Tanespimycin (17-AAG), which promotes proteasomal degradation of Hsp90, decreased the amount of Rev1 in human prostate and bone osteosarcoma cancer cells (218), and downregulated the recruitment of Rev 1 to sites of UV-induced DNA damage in the nucleus (218). The proteasome inhibitors, lactacystin and MG-132, prevented the reduction in Rev1 levels induced by 17-AAG (218), indicating that Hsp90 normally protects Rev1 from proteasomal degradation. Following UV-induced DNA damage, Pol η undergoes direct PIAS1-mediated poly-SUMOylation upon recruitment to PCNA. The protein is then modified by SUMO-targeted ubiquitin ligases (STUbLs), which is crucial for clearance of the polymerase from damage sites following lesion bypass. Targeting the human STUbLs RNF4 and RNF11 could potentially enhance the turnover rate of mutagenic TLS polymerases and decrease lesion bypass in cancer cells (127). Given the extensive ubiquitination of proteins involved in DNA damage tolerance, the response to general inhibitors of the proteasome is complex. Of interest, it has been reported that the proteasome inhibitors MG-132, lactacystin, and MG-262 inhibited TLS in human cancer cell lines, but not in normal cells (220), indicating that targeting the degradation of specific proteins could represent another approach to modulation of the DNA damage tolerance pathway in cancer cells.

Other Approaches to TLS Inhibition

Alternative approaches of TLS inhibition include the use of novel non-natural nucleotides to inhibit bypass synthesis, and down-regulation of DDT protein expression using miRNAs. Two synthetic nucleotide analogues, 5-nitro-indolyl-2′deoxyriboside triphosphate (5-NITP) and 5-phenyl-indolyl-2′deoxyriboside triphosphate (5-PhITP), are preferentially incorporated opposite abasic sites during DNA replication, while resisting both excision by proofreading exonuclease activity and subsequent elongation, preventing further DNA replication past the damage sites (221). TLS polymerases, specifically Pol η and Pol ι, preferentially inserted 5-NITP over dATP opposite temozolomide-induced abasic sites, preventing lesion bypass at the damage sites (222). The synthetic nucleoside potentiated the cytotoxic effects of temozolomide in glioblastoma cancer cell lines, and led to tumor regression in mouse models of tumor growth (222).

Identification of miRNAs that regulate expression of key genes represents another potential mechanism of DDT inhibition. For example, miR-96 regulates expression of *RAD51* and *REV1* (223). Knockdown of *REV1* expression using miR-96 contributed to cisplatin sensitization in bone osteosarcoma cells with intact HR repair, as well as in *BRCA1*-deficient breast cancer and *BRCA2*-deficient ovarian cancer cell lines with compromised HR pathways (223). Direct inhibition of *RAD51* and *REV1* expression by overexpression of miR-96 ultimately slowed growth of tumors from triple-negative breast cancer cells in mice (223).

FUTURE PERSPECTIVES

There is increasing evidence that inhibition of DNA damage tolerance pathways can sensitize cancer cells to conventional chemotherapeutic agents. Ongoing research into the molecular basis of DNA damage tolerance will provide opportunities for further advances. The factors that influence pathway choice in specific circumstances require further investigation. For the TLS

pathway, understanding the contribution of individual DNA polymerases to lesion bypass in cancer and normal cells will be important, and will further inform the design of specific inhibitors that target polymerases or accessory proteins. In addition to polymerases, other DDT proteins could also represent therapeutic targets, using agents that directly block protein function, or interfere with specific PPIs that are essential for DNA damage tolerance. The major focus to date has been on inhibition of TLS, but given the recent advances in elucidating the genetics and biochemistry of fork reversal and template switching, there is potential to identify new inhibitors targeting these pathways. The risk of directing replication intermediates into other more error-prone pathways, increasing genetic instability and further contributing to the development of resistant cancer cells, also has to be considered in this context. Further challenges include the development of specific inhibitors, proving that cellular phenotypes are due to inhibition of the proposed target, and demonstrating clinical utility for small molecule inhibitors. Ongoing research will advance the potential to target DNA tolerance pathways as a therapeutic approach for cancer.

CONCLUSION

DDT pathways are critical to allow cells to tolerate DNA lesions and facilitate the completion of DNA replication. However, imbalances in these pathways in cancer cells can lead to significant mutagenesis, contributing to chemoresistance and increased cancer cell survival. Considering the evidence that inhibiting DDT pathways can sensitize cancer cells to chemotherapy, more research into novel therapeutics in this area could eventually lead to the development of a new class of cancer therapeutic agents that enhance the response to treatment with conventional chemotherapy.

AUTHOR CONTRIBUTIONS

AL wrote the initial draft of the review and MC revised and edited the review. Both authors approved the final version.

FUNDING

Open access publication fees were supported by the Discipline of Biochemistry, The National University of Ireland Galway.

ACKNOWLEDGMENTS

The authors apologise to colleagues for any work not cited in this review.

REFERENCES

1. Livneh Z, Cohen IS, Paz-Elizur T, Davidovsky D, Carmi D, Swain U, et al. High-Resolution Genomic Assays Provide Insight Into the Division of Labor Between TLS and HDR in Mammalian Replication of Damaged DNA. *DNA Repair* (2016) 44:59–67. doi: 10.1016/j.dnarep.2016.05.007
2. Xu X, Blackwell S, Lin A, Li F, Qin Z, Xiao W. Error-Free DNA-Damage Tolerance in Saccharomyces Cerevisiae. *Mutat Research/Reviews Mutat Res* (2015) 764:43–50. doi: 10.1016/j.mrrev.2015.02.001
3. Ulrich H. Conservation of DNA Damage Tolerance Pathways From Yeast to Humans. *Biochem Soc Trans* (2007) 35(5):1334–7. doi: 10.1042/BST0351334
4. Kunz BA, Xiao W. DNA Damage Tolerance in Plants *via* Translesion Synthesis. *Genes Genomes Genomics* (2007) 1(1):89–99.
5. Pilzecker B, Buoninfante OA, Jacobs H. DNA Damage Tolerance in Stem Cells, Ageing, Mutagenesis, Disease and Cancer Therapy. *Nucleic Acids Res* (2019) 47(14):7163–81. doi: 10.1093/nar/gkz531
6. Yang W. An Overview of Y-Family DNA Polymerases and a Case Study of Human DNA Polymerase η. *Biochemistry* (2014) 53(17):2793–803. doi: 10.1021/bi500019s
7. Makarova AV, Burgers PM. Eukaryotic DNA Polymerase ζ. *DNA Repair* (2015) 29:47–55. doi: 10.1016/j.dnarep.2015.02.012
8. Waters LS, Minesinger BK, Wiltrout ME, D'Souza S, Woodruff RV, Walker GC. Eukaryotic Translesion Polymerases and Their Roles and Regulation in DNA Damage Tolerance. *Microbiol Mol Biol Rev* (2009) 73(1):134–54. doi: 10.1128/MMBR.00034-08
9. McCulloch SD, Kunkel TA. The Fidelity of DNA Synthesis by Eukaryotic Replicative and Translesion Synthesis Polymerases. *Cell Res* (2008) 18 (1):148–61. doi: 10.1038/cr.2008.4
10. Makridakis N, Reichardt J. Translesion DNA Polymerases and Cancer. *Front Genet* (2012) 3:174. doi: 10.3389/fgene.2012.00174
11. Basu A, Broyde S, Iwai S, Kisker C. DNA Damage, Mutagenesis, and DNA Repair. *J Nucleic Acids* (2010) 182894.
12. Knobel PA, Marti TM. Translesion DNA Synthesis in the Context of Cancer Research. *Cancer Cell Int* (2011) 11(1):1–19. doi: 10.1186/1475-2867-11-39
13. Branzei D, Psakhye I. DNA Damage Tolerance. *Curr Opin Cell Biol* (2016) 40:137–44. doi: 10.1016/j.ceb.2016.03.015
14. Sogo JM, Lopes M, Foiani M. Fork Reversal and ssDNA Accumulation at Stalled Replication Forks Owing to Checkpoint Defects. *Science* (2002) 297 (5581):599–602. doi: 10.1126/science.1074023
15. Chaudhuri AR, Hashimoto Y, Herrador R, Neelsen KJ, Fachinetti D, Bermejo R, et al. Topoisomerase I Poisoning Results in PARP-Mediated Replication Fork Reversal. *Nat Struct Mol Biol* (2012) 19(4):417–23. doi: 10.1038/nsmb.2258
16. Giannattasio M, Zwicky K, Follonier C, Foiani M, Lopes M, Branzei D. Visualization of Recombination-Mediated Damage Bypass by Template Switching. *Nat Struct Mol Biol* (2014) 21(10):884–92. doi: 10.1038/nsmb.2888
17. Fumasoni M, Zwicky K, Vanoli F, Lopes M, Branzei D. Error-Free DNA Damage Tolerance and Sister Chromatid Proximity During DNA Replication Rely on the Polα/Primase/Ctf4 Complex. *Mol Cell* (2015) 57 (5):812–23. doi: 10.1016/j.molcel.2014.12.038
18. Bi X. Mechanism of DNA Damage Tolerance. *World J Biol Chem* (2015) 6 (3):48–56. doi: 10.4331/wjbc.v6.i3.48
19. Binz SK, Sheehan AM, Wold MS. Replication Protein A Phosphorylation and the Cellular Response to DNA Damage. *DNA repair* (2004) 3(8-9):1015–24. doi: 10.1016/j.dnarep.2004.03.028
20. Ünsal-Kaçmaz K, Makhov AM, Griffith JD, Sancar A. Preferential Binding of ATR Protein to UV-Damaged DNA. *Proc Natl Acad Sci* (2002) 99(10):6673–8. doi: 10.1073/pnas.102167799
21. Papamichos-Chronakis M, Peterson CL. The Ino80 Chromatin-Remodeling Enzyme Regulates Replisome Function and Stability. *Nat Struct Mol Biol* (2008) 15(4):338–45. doi: 10.1038/nsmb.1413
22. Shimada K, Oma Y, Schleker T, Kugou K, Ohta K, Harata M, et al. Ino80 Chromatin Remodeling Complex Promotes Recovery of Stalled Replication Forks. *Curr Biol* (2008) 18(8):566–75. doi: 10.1016/j.cub.2008.03.049

23. Falbo KB, Alabert C, Katou Y, Wu S, Han J, Wehr T, et al. Involvement of a Chromatin Remodeling Complex in Damage Tolerance During DNA Replication. *Nat Struct Mol Biol* (2009) 16(11):1167–72. doi: 10.1038/nsmb.1686
24. Huttner D, Ulrich HD. Cooperation of Replication Protein A With the Ubiquitin Ligase Rad18 in DNA Damage Bypass. *Cell Cycle* (2008) 7 (23):3629–33. doi: 10.4161/cc.7.23.7166
25. Hedglin M, Benkovic SJ. Regulation of Rad6/Rad18 Activity During DNA Damage Tolerance. *Annu Rev Biophysics* (2015) 44:207–28. doi: 10.1146/annurev-biophys-060414-033841
26. Hedglin M, Aitha M, Pedley A, Benkovic SJ. Replication Protein A Dynamically Regulates Monoubiquitination of Proliferating Cell Nuclear Antigen. *J Biol Chem* (2019) 294(13):5157–68. doi: 10.1074/jbc.RA118.005297
27. Notenboom V, Hibbert RG, van Rossum-Fikkert SE, Olsen JV, Mann M, Sixma TK. Functional Characterization of Rad18 Domains for Rad6, Ubiquitin, DNA Binding and PCNA Modification. *Nucleic Acids Res* (2007) 35(17):5819–30. doi: 10.1093/nar/gkm615
28. Ulrich HD, Jentsch S. Two RING Finger Proteins Mediate Cooperation Between Ubiquitin-Conjugating Enzymes in DNA Repair. *EMBO J* (2000) 19(13):3388–97. doi: 10.1093/emboj/19.13.3388
29. Bailly V, Lamb J, Sung P, Prakash S, Prakash L. Specific Complex Formation Between Yeast RAD6 and RAD18 Proteins: A Potential Mechanism for Targeting RAD6 Ubiquitin-Conjugating Activity to DNA Damage Sites. *Genes Dev* (1994) 8(7):811–20. doi: 10.1101/gad.8.7.811
30. Bailly V, Lauder S, Prakash S, Prakash L. Yeast DNA Repair Proteins Rad6 and Rad18 Form a Heterodimer That has Ubiquitin Conjugating, DNA Binding, and ATP Hydrolytic Activities. *J Biol Chem* (1997) 272(37):23360–5. doi: 10.1074/jbc.272.37.23360
31. Finley D, Ulrich HD, Sommer T, Kaiser P. The Ubiquitin–Proteasome System of Saccharomyces Cerevisiae. *Genetics* (2012) 192(2):319–60. doi: 10.1534/genetics.112.140467
32. Hoege C, Pfander B, Moldovan G-L, Pyrowolakis G, Jentsch S. RAD6-Dependent DNA Repair is Linked to Modification of PCNA by Ubiquitin and SUMO. *Nature* (2002) 419(6903):135–41. doi: 10.1038/nature00991
33. Yoon J-H, Prakash S, Prakash L. Requirement of Rad18 Protein for Replication Through DNA Lesions in Mouse and Human Cells. *Proc Natl Acad Sci* (2012) 109(20):7799–804. doi: 10.1073/pnas.1204105109
34. Zhang S, Chea J, Meng X, Zhou Y, Lee EY, Lee MY. PCNA is Ubiquitinated by RNF8. *Cell Cycle* (2008) 7(21):3399–404. doi: 10.4161/cc.7.21.6949
35. Quinet A, Lerner LK, Martins DJ, Menck CF. Filling Gaps in Translesion DNA Synthesis in Human Cells. *Mutat Research/Genetic Toxicol Environ Mutagenesis* (2018) 836:127–42. doi: 10.1016/j.mrgentox.2018.02.004
36. Lehmann AR, Niimi A, Ogi T, Brown S, Sabbioneda S, Wing JF, et al. Translesion Synthesis: Y-Family Polymerases and the Polymerase Switch. *DNA Repair* (2007) 6(7):891–9. doi: 10.1016/j.dnarep.2007.02.003
37. Guo C, Kosarek-Stancel JN, Tang T-S, Friedberg EC. Y-Family DNA Polymerases in Mammalian Cells. *Cell Mol Life Sci* (2009) 66(14):2363–81. doi: 10.1007/s00018-009-0024-4
38. Friedberg EC, Wagner R, Radman M. Specialized DNA Polymerases, Cellular Survival, and the Genesis of Mutations. *Science* (2002) 296 (5573):1627–30. doi: 10.1126/science.1070236
39. Ma X, Tang TS, Guo C. Regulation of Translesion DNA Synthesis in Mammalian Cells. *Environ Mol Mutagen* (2020) 61(7):680–92. doi: 10.1002/em.22359
40. Yang W, Gao Y. Translesion and Repair DNA Polymerases: Diverse Structure and Mechanism. *Annu Rev Biochem* (2018) 87:239–61. doi: 10.1146/annurev-biochem-062917-012405
41. Guo C, Sonoda E, Tang T-S, Parker JL, Bielen AB, Takeda S, et al. REV1 Protein Interacts With PCNA: Significance of the REV1 BRCT Domain *In Vitro* and In Vivo. *Mol Cell* (2006) 23(2):265–71. doi: 10.1016/j.molcel.2006.05.038
42. Pustovalova Y, Maciejewski MW, Korzhnev DM. NMR Mapping of PCNA Interaction With Translesion Synthesis DNA Polymerase Rev1 Mediated by Rev1-BRCT Domain. *J Mol Biol* (2013) 425(17):3091–105. doi: 10.1016/j.jmb.2013.05.029
43. Livneh Z, Shachar S. Multiple Two-Polymerase Mechanisms in Mammalian Translesion DNA Synthesis. *Cell Cycle* (2010) 9(4):729–35. doi: 10.4161/cc.9.4.10727
44. Yoon J-H, Park J, Conde J, Wakamiya M, Prakash L, Prakash S. Rev1 Promotes Replication Through UV Lesions in Conjunction With DNA Polymerases η, ι, and κ But Not DNA Polymerase ζ. *Genes Dev* (2015) 29 (24):2588–602. doi: 10.1101/gad.272229.115
45. Pustovalova Y, Magalhães MT, D'Souza S, Rizzo AA, Korza G, Walker GC, et al. Interaction Between the Rev1 C-Terminal Domain and the PolD3 Subunit of Polζ Suggests a Mechanism of Polymerase Exchange Upon Rev1/Polζ-Dependent Translesion Synthesis. *Biochemistry* (2016) 55(13):2043–53. doi: 10.1021/acs.biochem.5b01282
46. Kikuchi S, Hara K, Shimizu T, Sato M, Hashimoto H. Structural Basis of Recruitment of DNA Polymerase ζ by Interaction Between REV1 and REV7 Proteins. *J Biol Chem* (2012) 287(40):33847–52. doi: 10.1074/jbc.M112.396838
47. Pozhidaeva A, Pustovalova Y, D'Souza S, Bezsonova I, Walker GC, Korzhnev DM. NMR Structure and Dynamics of the C-Terminal Domain From Human Rev1 and its Complex With Rev1 Interacting Region of DNA Polymerase η. *Biochemistry* (2012) 51(27):5506–20. doi: 10.1021/bi300566z
48. Washington MT, Minko IG, Johnson RE, Haracska L, Harris TM, Lloyd RS, et al. Efficient and Error-Free Replication Past a Minor-Groove N2-Guanine Adduct by the Sequential Action of Yeast Rev1 and DNA Polymerase ζ. *Mol Cell Biol* (2004) 24(16):6900–6. doi: 10.1128/MCB.24.16.6900-6906.2004
49. Weaver TM, Cortez LM, Khoang TH, Washington MT, Agarwal PK, Freudenthal BD. Visualizing Rev1 Catalyze Protein-Template DNA Synthesis. *Proc Natl Acad Sci* (2020) 117(41):25494–504. doi: 10.1073/pnas.2010484117
50. Biertümpfel C, Zhao Y, Kondo Y, Ramón-Maiques S, Gregory M, Lee JY, et al. Structure and Mechanism of Human DNA Polymerase η. *Nature* (2010) 465(7301):1044–8. doi: 10.1038/nature09196
51. Sale JE, Lehmann AR, Woodgate R. Y-Family DNA Polymerases and Their Role in Tolerance of Cellular DNA Damage. *Nat Rev Mol Cell Biol* (2012) 13 (3):141–52. doi: 10.1038/nrm3289
52. Quinet A, Martins DJ, Vessoni AT, Biard D, Sarasin A, Stary A, et al. Translesion Synthesis Mechanisms Depend on the Nature of DNA Damage in UV-Irradiated Human Cells. *Nucleic Acids Res* (2016) 44(12):5717–31. doi: 10.1093/nar/gkw280
53. Zhang Y, Wu X, Rechkoblit O, Geacintov NE, Taylor J-S, Wang Z. Response of Human REV1 to Different DNA Damage: Preferential dCMP Insertion Opposite the Lesion. *Nucleic Acids Res* (2002) 30(7):1630–8. doi: 10.1093/nar/30.7.1630
54. Masutani C, Kusumoto R, Iwai S, Hanaoka F. Mechanisms of Accurate Translesion Synthesis by Human DNA Polymerase η. *EMBO J* (2000) 19 (12):3100–9. doi: 10.1093/emboj/19.12.3100
55. Haracska L, Yu S-L, Johnson RE, Prakash L, Prakash S. Efficient and Accurate Replication in the Presence of 7, 8-Dihydro-8-Oxoguanine by DNA Polymerase η. *Nat Genet* (2000) 25(4):458–61. doi: 10.1038/78169
56. Choi J-Y, Lim S, Kim E-J, Jo A, Guengerich FP. Translesion Synthesis Across Abasic Lesions by Human B-Family and Y-Family DNA Polymerases α, δ, η, ι, κ, and REV1. *J Mol Biol* (2010) 404(1):34–44. doi: 10.1016/j.jmb.2010.09.015
57. Choi J-Y, Guengerich FP. Kinetic Evidence for Inefficient and Error-Prone Bypass Across Bulky N2-Guanine DNA Adducts by Human DNA Polymerase ι. *J Biol Chem* (2006) 281(18):12315–24. doi: 10.1074/jbc.M600112200
58. Vaisman A, Woodgate R. Unique Misinsertion Specificity of Polι may Decrease the Mutagenic Potential of Deaminated Cytosines. *EMBO J* (2001) 20(22):6520–9. doi: 10.1093/emboj/20.22.6520
59. Vaisman A, Frank EG, Iwai S, Ohashi E, Ohmori H, Hanaoka F, et al. Sequence Context-Dependent Replication of DNA Templates Containing UV-Induced Lesions by Human DNA Polymerase ι. *DNA Repair* (2003) 2 (9):991–1006. doi: 10.1016/S1568-7864(03)00094-6
60. Fischhaber PL, Gerlach VL, Feaver WJ, Hatahet Z, Wallace SS, Friedberg EC. Human DNA Polymerase κ Bypasses and Extends Beyond Thymine Glycols During Translesion Synthesis *In Vitro*, Preferentially Incorporating Correct Nucleotides. *J Biol Chem* (2002) 277(40):37604–11. doi: 10.1074/jbc.M206027200
61. Ogi T, Shinkai Y, Tanaka K, Ohmori H. Polκ Protects Mammalian Cells Against the Lethal and Mutagenic Effects of Benzo [a] Pyrene. *Proc Natl Acad Sci* (2002) 99(24):15548–53. doi: 10.1073/pnas.222377899

62. Zhang Y, Yuan F, Wu X, Wang M, Rechkoblit O, Taylor J-S, et al. Error-Free and Error-Prone Lesion Bypass by Human DNA Polymerase κ In Vitro. *Nucleic Acids Res* (2000) 28(21):4138–46. doi: 10.1093/nar/28.21.4138
63. Ohashi E, Ogi T, Kusumoto R, Iwai S, Masutani C, Hanaoka F, et al. Error-Prone Bypass of Certain DNA Lesions by the Human DNA Polymerase κ. *Genes Dev* (2000) 14(13):1589–94. doi: 10.1101/gad.14.13.1589
64. Seki M, Masutani C, Yang LW, Schuffert A, Iwai S, Bahar I, et al. High-Efficiency Bypass of DNA Damage by Human DNA Polymerase Q. *EMBO J* (2004) 23(22):4484–94. doi: 10.1038/sj.emboj.7600424
65. Yoon J-H, Choudhury JR, Park J, Prakash S, Prakash L. A Role for DNA Polymerase θ in Promoting Replication Through Oxidative DNA Lesion, Thymine Glycol, in Human Cells. *J Biol Chem* (2014) 289(19):13177–85. doi: 10.1074/jbc.M114.556977
66. Yoon J-H, McArthur MJ, Park J, Basu D, Wakamiya M, Prakash L, et al. Error-Prone Replication Through UV Lesions by DNA Polymerase θ Protects Against Skin Cancers. *Cell* (2019) 176(6):1295–309.e15. doi: 10.1016/j.cell.2019.01.023
67. Yoon J-H, Prakash L, Prakash S. Error-Free Replicative Bypass of (6–4) Photoproducts by DNA Polymerase ζ in Mouse and Human Cells. *Genes Dev* (2010) 24(2):123–8. doi: 10.1101/gad.1872810
68. Yoon J-H, Basu D, Sellamuthu K, Johnson RE, Prakash S, Prakash L. A Novel Role of DNA Polymerase λ in Translesion Synthesis in Conjunction With DNA Polymerase ζ. *Life Sci alliance* (2021) 4(4). doi: 10.26508/lsa.202000900
69. García-Gómez S, Reyes A, Martínez-Jiménez MI, Chocrón ES, Mourón S, Terrados G, et al. PrimPol, an Archaic Primase/Polymerase Operating in Human Cells. *Mol Cell* (2013) 52(4):541–53. doi: 10.1016/j.molcel.2013.09.025
70. Temprine K, Campbell NR, Huang R, Langdon EM, Simon-Vermot T, Mehta K, et al. Regulation of the Error-Prone DNA Polymerase Polκ by Oncogenic Signaling and its Contribution to Drug Resistance. *Sci Signaling* (2020) 13(629). doi: 10.1126/scisignal.aau1453
71. Chatterjee N, Walker GC. Mechanisms of DNA Damage, Repair, and Mutagenesis. *Environ Mol Mutagenesis* (2017) 58(5):235–63. doi: 10.1002/em.22087
72. Yusufzai T, Kadonaga JT. HARP is an ATP-Driven Annealing Helicase. *Science* (2008) 322(5902):748–50. doi: 10.1126/science.1161233
73. Poole LA, Cortez D. Functions of SMARCAL1, ZRANB3, and HLTF in Maintaining Genome Stability. *Crit Rev Biochem Mol Biol* (2017) 52(6):696–714. doi: 10.1080/10409238.2017.1380597
74. Bétous R, Mason AC, Rambo RP, Bansbach CE, Badu-Nkansah A, Sirbu BM, et al. SMARCAL1 Catalyzes Fork Regression and Holliday Junction Migration to Maintain Genome Stability During DNA Replication. *Genes Dev* (2012) 26(2):151–62. doi: 10.1101/gad.178459.111
75. Vujanovic M, Krietsch J, Raso MC, Terraneo N, Zellweger R, Schmid JA, et al. Replication Fork Slowing and Reversal Upon DNA Damage Require PCNA Polyubiquitination and ZRANB3 DNA Translocase Activity. *Mol Cell* (2017) 67(5):882–90.e5. doi: 10.1016/j.molcel.2017.08.010
76. Ciccia A, Nimonkar AV, Hu Y, Hajdu I, Achar YJ, Izhar L, et al. Polyubiquitinated PCNA Recruits the ZRANB3 Translocase to Maintain Genomic Integrity After Replication Stress. *Mol Cell* (2012) 47(3):396–409. doi: 10.1016/j.molcel.2012.05.024
77. Tian T, Bu M, Chen X, Ding L, Yang Y, Han J, et al. The ZATT-TOP2A-PICH Axis Drives Extensive Replication Fork Reversal to Promote Genome Stability. *Mol Cell* (2021) 81(1):198–211.e6. doi: 10.1016/j.molcel.2020.11.007
78. Gari K, Décaillet C, Delannoy M, Wu L, Constantinou A. Remodeling of DNA Replication Structures by the Branch Point Translocase FANCM. *Proc Natl Acad Sci* (2008) 105(42):16107–12. doi: 10.1073/pnas.0804777105
79. Gari K, Décaillet C, Stasiak AZ, Stasiak A, Constantinou A. The Fanconi Anemia Protein FANCM can Promote Branch Migration of Holliday Junctions and Replication Forks. *Mol Cell* (2008) 29(1):141–8. doi: 10.1016/j.molcel.2007.11.032
80. Lemaçon D, Jackson J, Quinet A, Brickner J, Li S. MRE11 and EXO1 Nucleases Degrade Reversed Forks and Elicit MUS81-Dependent Fork Rescue in BRCA2-Deficient Cells. *Nat Commun* (2017) 8:860. doi: 10.1038/s41467-017-01180-5
81. Kolinjivadi AM, Sannino V, De Antoni A, Zadorozhny K, Kilkenny M, Técher H, et al. Smarcal1-Mediated Fork Reversal Triggers Mre11-Dependent Degradation of Nascent DNA in the Absence of Brca2 and Stable Rad51 Nucleofilaments. *Mol Cell* (2017) 67(5):867–81.e7. doi: 10.1016/j.molcel.2017.07.001
82. Mijic S, Zellweger R, Chappidi N, Berti M, Jacobs K, Mutreja K, et al. Replication Fork Reversal Triggers Fork Degradation in BRCA2-Defective Cells. *Nat Commun* (2017) 8(1):1–11. doi: 10.1038/s41467-017-01164-5
83. Mason JM, Chan Y-L, Weichselbaum RW, Bishop DK. Non-Enzymatic Roles of Human RAD51 at Stalled Replication Forks. *Nat Commun* (2019) 10(1):1–11. doi: 10.1038/s41467-019-12297-0
84. Quinet A, Lemaçon D, Vindigni A. Replication Fork Reversal: Players and Guardians. *Mol Cell* (2017) 68(5):830–3. doi: 10.1016/j.molcel.2017.11.022
85. Berti M, Chaudhuri AR, Thangavel S, Gomathinayagam S, Kenig S, Vujanovic M, et al. Human RECQ1 Promotes Restart of Replication Forks Reversed by DNA Topoisomerase I Inhibition. *Nat Struct Mol Biol* (2013) 20(3):347–54. doi: 10.1038/nsmb.2501
86. Karras GI, Fumasoni M, Sienski G, Vanoli F, Branzei D, Jentsch S. Noncanonical Role of the 9-1-1 Clamp in the Error-Free DNA Damage Tolerance Pathway. *Mol Cell* (2013) 49(3):536–46. doi: 10.1016/j.molcel.2012.11.016
87. Liu J, Renault L, Veaute X, Fabre F, Stahlberg H, Heyer W-D. Rad51 Paralogues Rad55–Rad57 Balance the Antirecombinase Srs2 in Rad51 Filament Formation. *Nature* (2011) 479(7372):245–8. doi: 10.1038/nature10522
88. Godin S, Wier A, Kabbinavar F, Bratton-Palmer DS, Ghodke H, Van Houten B, et al. The Shu Complex Interacts With Rad51 Through the Rad51 Paralogues Rad55–Rad57 to Mediate Error-Free Recombination. *Nucleic Acids Res* (2013) 41(8):4525–34. doi: 10.1093/nar/gkt138
89. Vanoli F, Fumasoni M, Szakal B, Maloisel L, Branzei D. Replication and Recombination Factors Contributing to Recombination-Dependent Bypass of DNA Lesions by Template Switch. *PloS Genet* (2010) 6(11):e1001205. doi: 10.1371/journal.pgen.1001205
90. Bernstein KA, Reid RJ, Sunjevaric I, Demuth K, Burgess RC, Rothstein R. The Shu Complex, Which Contains Rad51 Paralogues, Promotes DNA Repair Through Inhibition of the Srs2 Anti-Recombinase. *Mol Biol Cell* (2011) 22(9):1599–607. doi: 10.1091/mbc.e10-08-0691
91. Sasanuma H, Tawaramoto M, Lao J, Hosaka H, Sanda E, Suzuki M, et al. A New Protein Complex Promoting the Assembly of Rad51 Filaments. *Nat Commun* (2013) 4:1676. doi: 10.1038/ncomms2678
92. Zhang H, Lawrence CW. The Error-Free Component of the RAD6/RAD18 DNA Damage Tolerance Pathway of Budding Yeast Employs Sister-Strand Recombination. *Proc Natl Acad Sci* (2005) 102(44):15954–9. doi: 10.1073/pnas.0504586102
93. Branzei D. Ubiquitin Family Modifications and Template Switching. *FEBS Lett* (2011) 585(18):2810–7. doi: 10.1016/j.febslet.2011.04.053
94. San Filippo J, Sung P, Klein H. Mechanism of Eukaryotic Homologous Recombination. *Annu Rev Biochem* (2008) 77:229–57. doi: 10.1146/annurev.biochem.77.061306.125255
95. Symington LS. Role of RAD52 Epistasis Group Genes in Homologous Recombination and Double-Strand Break Repair. *Microbiol Mol Biol Rev* (2002) 66(4):630–70. doi: 10.1128/MMBR.66.4.630-670.2002
96. Burkovics P, Sebesta M, Sisakova A, Plault N, Szukacsov V, Robert T, et al. Srs2 Mediates PCNA-SUMO-Dependent Inhibition of DNA Repair Synthesis. *EMBO J* (2013) 32(5):742–55. doi: 10.1038/emboj.2013.9
97. Cejka P, Plank JL, Dombrowski CC, Kowalczykowski SC. Decatenation of DNA by the S. Cerevisiae Sgs1-Top3-Rmi1 and RPA Complex: A Mechanism for Disentangling Chromosomes. *Mol Cell* (2012) 47(6):886–96. doi: 10.1016/j.molcel.2012.06.032
98. Bernstein KA, Shor E, Sunjevaric I, Fumasoni M, Burgess RC, Foiani M, et al. Sgs1 Function in the Repair of DNA Replication Intermediates Is Separable From its Role in Homologous Recombinational Repair. *EMBO J* (2009) 28(7):915–25. doi: 10.1038/emboj.2009.28
99. Masuda Y, Masutani C. Spatiotemporal Regulation of PCNA Ubiquitination in Damage Tolerance Pathways. *Crit Rev Biochem Mol Biol* (2019) 54(5):418–42. doi: 10.1080/10409238.2019.1687420
100. Kashiwaba S-I, Kanao R, Masuda Y, Kusumoto-Matsuo R, Hanaoka F, Masutani C. USP7 is a Suppressor of PCNA Ubiquitination and Oxidative-Stress-Induced Mutagenesis in Human Cells. *Cell Rep* (2015) 13(10):2072–80. doi: 10.1016/j.celrep.2015.11.014

101. Cohn MA, Kowal P, Yang K, Haas W, Huang TT, Gygi SP, et al. A UAF1-Containing Multisubunit Protein Complex Regulates the Fanconi Anemia Pathway. *Mol Cell* (2007) 28(5):786–97. doi: 10.1016/j.molcel.2007.09.031
102. Kim JM, Parmar K, Huang M, Weinstock DM, Ruit CA, Kutok JL, et al. Inactivation of Murine Usp1 Results in Genomic Instability and a Fanconi Anemia Phenotype. *Dev Cell* (2009) 16(2):314–20. doi: 10.1016/j.devcel.2009.01.001
103. Lee K-Y, Yang K, Cohn MA, Sikdar N, D'Andrea AD, Myung K. Human ELG1 Regulates the Level of Ubiquitinated Proliferating Cell Nuclear Antigen (PCNA) Through Its Interactions With PCNA and USP1. *J Biol Chem* (2010) 285(14):10362–9. doi: 10.1074/jbc.M109.092544
104. Huang TT, Nijman SM, Mirchandani KD, Galardy PJ, Cohn MA, Haas W, et al. Regulation of Monoubiquitinated PCNA by DUB Autocleavage. *Nat Cell Biol* (2006) 8(4):341–7. doi: 10.1038/ncb1378
105. Mohiuddin M, Evans TJ, Rahman MM, Keka IS, Tsuda M, Sasanuma H, et al. SUMOylation of PCNA by PIAS1 and PIAS4 Promotes Template Switch in the Chicken and Human B Cell Lines. *Proc Natl Acad Sci* (2018) 115(50):12793–8. doi: 10.1073/pnas.1716349115
106. Park JM, Yang SW, Yu KR, Ka SH, Lee SW, Seol JH, et al. Modification of PCNA by ISG15 Plays a Crucial Role in Termination of Error-Prone Translesion DNA Synthesis. *Mol Cell* (2014) 54(4):626–38. doi: 10.1016/j.molcel.2014.03.031
107. Leung W, Baxley RM, Moldovan G-L, Bielinsky A-K. Mechanisms of DNA Damage Tolerance: Post-Translational Regulation of PCNA. *Genes* (2019) 10 (1):10. doi: 10.3390/genes10010010
108. Watanabe K, Tateishi S, Kawasuji M, Tsurimoto T, Inoue H, Yamaizumi M. Rad18 Guides Polη to Replication Stalling Sites Through Physical Interaction and PCNA Monoubiquitination. *EMBO J* (2004) 23(19):3886–96. doi: 10.1038/sj.emboj.7600383
109. Yang XH, Shiotani B, Classon M, Zou L. Chk1 and Claspin Potentiate PCNA Ubiquitination. *Genes Dev* (2008) 22(9):1147–52. doi: 10.1101/gad.1632808
110. Han J, Liu T, Huen MS, Hu L, Chen Z, Huang J. SIVA1 Directs the E3 Ubiquitin Ligase RAD18 for PCNA Monoubiquitination. *J Cell Biol* (2014) 205(6):811–27. doi: 10.1083/jcb.201311007
111. Lin J-R, Zeman MK, Chen J-Y, Yee M-C, Cimprich KA. SHPRH and HLTF Act in a Damage-Specific Manner to Coordinate Different Forms of Postreplication Repair and Prevent Mutagenesis. *Mol Cell* (2011) 42 (2):237–49. doi: 10.1016/j.molcel.2011.02.026
112. Centore RC, Yazinski SA, Tse A, Zou L. Spartan/C1orf124, a Reader of PCNA Ubiquitylation and a Regulator of UV-Induced DNA Damage Response. *Mol Cell* (2012) 46(5):625–35. doi: 10.1016/j.molcel.2012.05.020
113. Juhasz S, Balogh D, Hajdu I, Burkovics P, Villamil MA, Zhuang Z, et al. Characterization of Human Spartan/C1orf124, an Ubiquitin-PCNA Interacting Regulator of DNA Damage Tolerance. *Nucleic Acids Res* (2012) 40(21):10795–808. doi: 10.1093/nar/gks850
114. Göhler T, Sabbioneda S, Green CM, Lehmann AR. ATR-Mediated Phosphorylation of DNA Polymerase η Is Needed for Efficient Recovery From UV Damage. *J Cell Biol* (2011) 192(2):219–27. doi: 10.1083/jcb.201008076
115. Peddu C, Zhang S, Zhao H, Wong A, Lee EY, Lee MY, et al. Phosphorylation Alters the Properties of Pol η: Implications for Translesion Synthesis. *iScience* (2018) 6:52–67. doi: 10.1016/j.isci.2018.07.009
116. Yanagihara H, Kobayashi J, Tateishi S, Kato A, Matsuura S, Tauchi H, et al. NBS1 Recruits RAD18 *via* a RAD6-Like Domain and Regulates Pol η-Dependent Translesion DNA Synthesis. *Mol Cell* (2011) 43(5):788–97. doi: 10.1016/j.molcel.2011.07.026
117. Saito Y, Komatsu K. Functional Role of NBS1 in Radiation Damage Response and Translesion DNA Synthesis. *Biomolecules* (2015) 5(3):1990–2002. doi: 10.3390/biom5031990
118. Jung Y-S, Hakem A, Hakem R, Chen X. Pirh2 E3 Ubiquitin Ligase Monoubiquitinates DNA Polymerase Eta to Suppress Translesion DNA Synthesis. *Mol Cell Biol* (2011) 31(19):3997–4006. doi: 10.1128/MCB.05808-11
119. Jung Y-S, Liu G, Chen X. Pirh2 E3 Ubiquitin Ligase Targets DNA Polymerase Eta for 20S Proteasomal Degradation. *Mol Cell Biol* (2010) 30 (4):1041–8. doi: 10.1128/MCB.01198-09
120. Qian J, Pentz K, Zhu Q, Wang Q, He J, Srivastava AK, et al. USP7 Modulates UV-Induced PCNA Monoubiquitination by Regulating DNA Polymerase Eta Stability. *Oncogene* (2015) 34(36):4791–6. doi: 10.1038/onc.2014.394
121. Jung Y-S, Qian Y, Chen X. DNA Polymerase Eta is Targeted by Mdm2 for Polyubiquitination and Proteasomal Degradation in Response to Ultraviolet Irradiation. *DNA Repair* (2012) 11(2):177–84. doi: 10.1016/j.dnarep.2011.10.017
122. Povlsen LK, Beli P, Wagner SA, Poulsen SL, Sylvestersen KB, Poulsen JW, et al. Systems-Wide Analysis of Ubiquitylation Dynamics Reveals a Key Role for PAF15 Ubiquitylation in DNA-Damage Bypass. *Nat Cell Biol* (2012) 14 (10):1089–98. doi: 10.1038/ncb2579
123. Nicolae CM, Aho ER, Vlahos AH, Choe KN, De S, Karras GI, et al. The ADP-Ribosyltransferase PARP10/ARTD10 Interacts With Proliferating Cell Nuclear Antigen (PCNA) and Is Required for DNA Damage Tolerance. *J Biol Chem* (2014) 289(19):13627–37. doi: 10.1074/jbc.M114.556340
124. Huang M, Zhou B, Gong J, Xing L, Ma X, Wang F, et al. RNA-Splicing Factor SART3 Regulates Translesion DNA Synthesis. *Nucleic Acids Res* (2018) 46 (9):4560–74. doi: 10.1093/nar/gky220
125. Bertoletti F, Cea V, Liang CC, Lanati T, Maffia A, Avarello MDM, et al. Phosphorylation Regulates Human Polη Stability and Damage Bypass Throughout the Cell Cycle. *Nucleic Acids Res* (2017) 45(16):9441–54. doi: 10.1093/nar/gkx619
126. Despras E, Sittewelle M, Pouvelle C, Delrieu N, Cordonnier AM, Kannouche PL. Rad18-Dependent SUMOylation of Human Specialized DNA Polymerase Eta is Required to Prevent Under-Replicated DNA. *Nat Commun* (2016) 7(1):1–15. doi: 10.1038/ncomms13326
127. Guérillon C, Smedegaard S, Hendriks IA, Nielsen ML, Mailand N. Multisite SUMOylation Restrains DNA Polymerase η Interactions With DNA Damage Sites. *J Biol Chem* (2020) 295(25):8350–62. doi: 10.1074/jbc.RA120.013780
128. Cipolla L, Maffia A, Bertoletti F, Sabbioneda S. The Regulation of DNA Damage Tolerance by Ubiquitin and Ubiquitin-Like Modifiers. *Front Genet* (2016) 7:105. doi: 10.3389/fgene.2016.00105
129. Chen Y-W, Cleaver JE, Hatahet Z, Honkanen RE, Chang J-Y, Yen Y, et al. Human DNA Polymerase η Activity and Translocation Is Regulated by Phosphorylation. *Proc Natl Acad Sci* (2008) 105(43):16578–83. doi: 10.1073/pnas.0808589105
130. Lerner LK, Francisco G, Soltys DT, Rocha CR, Quinet A, Vessoni AT, et al. Predominant Role of DNA Polymerase Eta and P53-Dependent Translesion Synthesis in the Survival of Ultraviolet-Irradiated Human Cells. *Nucleic Acids Res* (2017) 45(3):1270–80. doi: 10.1093/nar/gkw1196
131. Bostian AC, Maddukuri L, Reed MR, Savenka T, Hartman JH, Davis L, et al. Kynurenine Signaling Increases DNA Polymerase Kappa Expression and Promotes Genomic Instability in Glioblastoma Cells. *Chem Res Toxicol* (2016) 29(1):101–8. doi: 10.1021/acs.chemrestox.5b00452
132. Brauze D, Rawłuszko AA. The Effect of Aryl Hydrocarbon Receptor Ligands on the Expression of Polymerase (DNA Directed) Kappa (Polκ), Polymerase RNA II (DNA Directed) Polypeptide A (PolR2a), CYP1B1 and CYP1A1 Genes in Rat Liver. *Environ Toxicol Pharmacol* (2012) 34(3):819–25. doi: 10.1016/j.etap.2012.09.004
133. Yamada T, Imamachi N, Imamura K, Taniue K, Kawamura T, Suzuki Y, et al. Systematic Analysis of Targets of Pumilio-Mediated mRNA Decay Reveals That PUM1 Repression by DNA Damage Activates Translesion Synthesis. *Cell Rep* (2020) 31(5):107542. doi: 10.1016/j.celrep.2020.107542
134. Srivastava AK, Han C, Zhao R, Cui T, Dai Y, Mao C, et al. Enhanced Expression of DNA Polymerase Eta Contributes to Cisplatin Resistance of Ovarian Cancer Stem Cells. *Proc Natl Acad Sci* (2015) 112 (14):4411–6. doi: 10.1073/pnas.1421365112
135. Zhang J, Sun W, Ren C, Kong X, Yan W, Chen X. A PolH Transcript With a Short 3′ UTR Enhances PolH Expression and Mediates Cisplatin Resistance. *Cancer Res* (2019) 79(14):3714–24. doi: 10.1158/0008-5472.CAN-18-3928
136. Neelsen KJ, Lopes M. Replication Fork Reversal in Eukaryotes: From Dead End to Dynamic Response. *Nat Rev Mol Cell Biol* (2015) 16(4):207–20. doi: 10.1038/nrm3935
137. Porebski B, Wild S, Kummer S, Scaglione S, Gaillard P-HL, Gari K. WRNIP1 Protects Reversed DNA Replication Forks From SLX4-Dependent Nucleolytic Cleavage. *iScience* (2019) 21:31–41. doi: 10.1016/j.isci.2019.10.010
138. Leuzzi G, Marabitti V, Pichierri P, Franchitto A. WRNIP 1 Protects Stalled Forks From Degradation and Promotes Fork Restart After Replication Stress. *EMBO J* (2016) 35(13):1437–51. doi: 10.15252/embj.201593265

139. Couch FB, Bansbach CE, Driscoll R, Luzwick JW, Glick GG, Bétous R, et al. ATR Phosphorylates SMARCAL1 to Prevent Replication Fork Collapse. *Genes Dev* (2013) 27(14):1610–23. doi: 10.1101/gad.214080.113
140. Unk I, Hajdú I, Blastyák A, Haracska L. Role of Yeast Rad5 and its Human Orthologs, HLTF and SHPRH in DNA Damage Tolerance. *DNA Repair* (2010) 9(3):257–67. doi: 10.1016/j.dnarep.2009.12.013
141. MacKay C, Toth R, Rouse J. Biochemical Characterisation of the SWI/SNF Family Member HLTF. *Biochem Biophys Res Commun* (2009) 390(2):187–91. doi: 10.1016/j.bbrc.2009.08.151
142. Motegi A, Sood R, Moinova H, Markowitz SD, Liu PP, Myung K. Human SHPRH Suppresses Genomic Instability Through Proliferating Cell Nuclear Antigen Polyubiquitination. *J Cell Biol* (2006) 175(5):703–8. doi: 10.1083/jcb.200606145
143. Unk I, Hajdú I, Fátyol K, Szakál B, Blastyák A, Bermudez V, et al. Human SHPRH is a Ubiquitin Ligase for Mms2–Ubc13-Dependent Polyubiquitylation of Proliferating Cell Nuclear Antigen. *Proc Natl Acad Sci* (2006) 103(48):18107–12. doi: 10.1073/pnas.0608595103
144. Veaute X, Jeusset J, Soustelle C, Kowalczykowski SC, Le Cam E, Fabre F. The Srs2 Helicase Prevents Recombination by Disrupting Rad51 Nucleoprotein Filaments. *Nature* (2003) 423(6937):309–12. doi: 10.1038/nature01585
145. Antony E, Tomko EJ, Xiao Q, Krejci L, Lohman TM, Ellenberger T. Srs2 Disassembles Rad51 Filaments by a Protein-Protein Interaction Triggering ATP Turnover and Dissociation of Rad51 From DNA. *Mol Cell* (2009) 35(1):105–15. doi: 10.1016/j.molcel.2009.05.026
146. Gonzalez-Huici V, Szakal B, Urulangodi M, Psakhye I, Castellucci F, Menolfi D, et al. DNA Bending Facilitates the Error-Free DNA Damage Tolerance Pathway and Upholds Genome Integrity. *EMBO J* (2014) 33(4):327–40. doi: 10.1002/embj.201387425
147. Masutani C, Kusumoto R, Yamada A, Dohmae N, Yokoi M, Yuasa M, et al. The XPV (Xeroderma Pigmentosum Variant) Gene Encodes Human DNA Polymerase η. *Nature* (1999) 399(6737):700–4. doi: 10.1038/21447
148. Johnson RE, Kondratick CM, Prakash S, Prakash L. Hrad30 Mutations in the Variant Form of Xeroderma Pigmentosum. *Science* (1999) 285(5425):263–5. doi: 10.1126/science.285.5425.263
149. Ziv O, Geacintov N, Nakajima S, Yasui A, Livneh Z. DNA Polymerase ζ Cooperates With Polymerases κ and ι in Translesion DNA Synthesis Across Pyrimidine Photodimers in Cells From XPV Patients. *Proc Natl Acad Sci* (2009) 106(28):11552–7. doi: 10.1073/pnas.0812548106
150. Yang Y, Gao Y, Zlatanou A, Tateishi S, Yurchenko V, Rogozin IB, et al. Diverse Roles of RAD18 and Y-Family DNA Polymerases in Tumorigenesis. *Cell Cycle* (2018) 17(7):833–43. doi: 10.1080/15384101.2018.1456296
151. Rogozin IB, Pavlov YI, Goncearenco A, De S, Lada AG, Poliakov E, et al. Mutational Signatures and Mutable Motifs in Cancer Genomes. *Briefings Bioinf* (2018) 19(6):1085–101. doi: 10.1093/bib/bbx049
152. Sakiyama T, Kohno T, Mimaki S, Ohta T, Yanagitani N, Sobue T, et al. Association of Amino Acid Substitution Polymorphisms in DNA Repair Genes TP53, POLI, REV1 and LIG4 With Lung Cancer Risk. *Int J Cancer* (2005) 114(5):730–7. doi: 10.1002/ijc.20790
153. Di Lucca J, Guedj M, Lacapère J-J, Fargnoli MC, Bourillon A, Dieudé P, et al. Variants of the Xeroderma Pigmentosum Variant Gene (POLH) are Associated With Melanoma Risk. *Eur J Cancer* (2009) 45(18):3228–36. doi: 10.1016/j.ejca.2009.04.034
154. Yadav S, Anbalagan M, Baddoo M, Chellamuthu VK, Mukhopadhyay S, Woods C, et al. Somatic Mutations in the DNA Repairome in Prostate Cancers in African Americans and Caucasians. *Oncogene* (2020) 39(21):4299–311. doi: 10.1038/s41388-020-1280-x
155. Russo M, Crisafulli G, Sogari A, Reilly NM, Arena S, Lamba S, et al. Adaptive Mutability of Colorectal Cancers in Response to Targeted Therapies. *Science* (2019) 366(6472):1473–80. doi: 10.1126/science.aav4474
156. Ceppi P, Novello S, Cambieri A, Longo M, Monica V, Iacono ML, et al. Polymerase η mRNA Expression Predicts Survival of Non–Small Cell Lung Cancer Patients Treated With Platinum-Based Chemotherapy. *Clin Cancer Res* (2009) 15(3):1039–45. doi: 10.1158/1078-0432.CCR-08-1227
157. Berdis AJ. Inhibiting DNA Polymerases as a Therapeutic Intervention Against Cancer. *Front Mol Biosci* (2017) 4:78. doi: 10.3389/fmolb.2017.00078
158. Sun H, Zou S, Zhang S, Liu B, Meng X, Li X, et al. Elevated DNA Polymerase Iota (Poli) is Involved in the Acquisition of Aggressive Phenotypes of Human Esophageal Squamous Cell Cancer. *Int J Clin Exp Pathol* (2015) 8(4):3591.
159. Yuan F, Xu Z, Yang M, Wei Q, Zhang Y, Yu J, et al. Overexpressed DNA Polymerase Iota Regulated by JNK/c-Jun Contributes to Hypermutagenesis in Bladder Cancer. *PloS One* (2013) 8(7):e69317. doi: 10.1371/journal.pone.0069317
160. Peng C, Chen Z, Wang S, Wang H-W, Qiu W, Zhao L, et al. The Error-Prone DNA Polymerase κ Promotes Temozolomide Resistance in Glioblastoma Through Rad17-Dependent Activation of ATR-Chk1 Signaling. *Cancer Res* (2016) 76(8):2340–53. doi: 10.1158/0008-5472.CAN-15-1884
161. Hicks JK, Chute CL, Paulsen MT, Ragland RL, Howlett NG, Guéranger Q, et al. Differential Roles for DNA Polymerases Eta, Zeta, and REV1 in Lesion Bypass of Intrastrand Versus Interstrand DNA Cross-Links. *Mol Cell Biol* (2010) 30(5):1217–30. doi: 10.1128/MCB.00993-09
162. Albertella MR, Green CM, Lehmann AR, O'Connor MJ. A Role for Polymerase η in the Cellular Tolerance to Cisplatin-Induced Damage. *Cancer Res* (2005) 65(21):9799–806. doi: 10.1158/0008-5472.CAN-05-1095
163. Sokol AM, Cruet-Hennequart S, Pasero P, Carty MP. DNA Polymerase η Modulates Replication Fork Progression and DNA Damage Responses in Platinum-Treated Human Cells. *Sci Rep* (2013) 3(1):1–9. doi: 10.1038/srep03277
164. Roy U, Mukherjee S, Sharma A, Frank EG, Schärer OD. The Structure and Duplex Context of DNA Interstrand Crosslinks Affects the Activity of DNA Polymerase η. *Nucleic Acids Res* (2016) 44(15):7281–91. doi: 10.1093/nar/gkw485
165. Zheng H, Wang X, Warren AJ, Legerski RJ, Nairn RS, Hamilton JW, et al. Nucleotide Excision Repair-and Polymerase η-Mediated Error-Prone Removal of Mitomycin C Interstrand Cross-Links. *Mol Cell Biol* (2003) 23(2):754–61. doi: 10.1128/MCB.23.2.754-761.2003
166. Chen Y-W, Cleaver JE, Hanaoka F, Chang C-F, Chou K-M. A Novel Role of DNA Polymerase η in Modulating Cellular Sensitivity to Chemotherapeutic Agents. *Mol Cancer Res* (2006) 4(4):257–65. doi: 10.1158/1541-7786.MCR-05-0118
167. Cruet-Hennequart S, Villalan S, Kaczmarczyk A, O'Meara E, Sokol AM, Carty MP. Characterization of the Effects of Cisplatin and Carboplatin on Cell Cycle Progression and DNA Damage Response Activation in DNA Polymerase Eta-Deficient Human Cells. *Cell Cycle* (2009) 8(18):3043–54. doi: 10.4161/cc.8.18.9624
168. Cruet-Hennequart S, Glynn MT, Murillo LS, Coyne S, Carty MP. Enhanced DNA-PK-Mediated RPA2 Hyperphosphorylation in DNA Polymerase Eta-Deficient Human Cells Treated With Cisplatin and Oxaliplatin. *DNA Repair* (2008) 7(4):582–96. doi: 10.1016/j.dnarep.2007.12.012
169. Srivastava AK, Han C, Zhao R, Cui T, Dai Y, Mao C, et al. Enhanced Expression of DNA Polymerase eta Contributes to Cisplatin Resistance of Ovarian Cancer Stem Cells. *PNAS* (2015) 112(14):4411–6. doi: 10.1073/pnas.1421365112
170. Wang H, Zhang S-Y, Wang S, Lu J, Wu W, Weng L, et al. REV3L Confers Chemoresistance to Cisplatin in Human Gliomas: The Potential of Its RNAi for Synergistic Therapy. *Neuro-Oncology* (2009) 11(6):790–802. doi: 10.1215/15228517-2009-015
171. Quinet A, Tirman S, Jackson J, Šviković S, Lemaçon D, Carvajal-Maldonado D, et al. PRIMPOL-Mediated Adaptive Response Suppresses Replication Fork Reversal in BRCA-Deficient Cells. *Mol Cell* (2020) 77(3):461–74.e9. doi: 10.1016/j.molcel.2019.10.008
172. Opitz CA, Litzenburger UM, Sahm F, Ott M, Tritschler I, Trump S, et al. An Endogenous Tumour-Promoting Ligand of the Human Aryl Hydrocarbon Receptor. *Nature* (2011) 478(7368):197–203. doi: 10.1038/nature10491
173. Cheong JE, Sun L. Targeting the IDO1/TDO2–KYN–AhR Pathway for Cancer Immunotherapy–Challenges and Opportunities. *Trends Pharmacol Sci* (2018) 39(3):307–25. doi: 10.1016/j.tips.2017.11.007
174. Buoninfante OA, Pilzecker B, Aslam MA, Zavrakidis I, van der Wiel R, van de Ven M, et al. Precision Cancer Therapy: Profiting From Tumor Specific Defects in the DNA Damage Tolerance System. *Oncotarget* (2018) 9(27):18832. doi: 10.18632/oncotarget.24777
175. Gao Y, Mutter-Rottmayer E, Greenwalt AM, Goldfarb D, Yan F, Yang Y, et al. A Neomorphic Cancer Cell-Specific Role of MAGE-A4 in Trans-Lesion Synthesis. *Nat Commun* (2016) 7(1):1–14. doi: 10.1038/ncomms12105
176. Moinova HR, Chen W-D, Shen L, Smiraglia D, Olechnowicz J, Ravi L, et al. HLTF Gene Silencing in Human Colon Cancer. *Proc Natl Acad Sci* (2002) 99(7):4562–7. doi: 10.1073/pnas.062459899

177. Yamanaka K, Chatterjee N, Hemann MT, Walker GC. Inhibition of Mutagenic Translesion Synthesis: A Possible Strategy for Improving Chemotherapy? *PloS Genet* (2017) 13(8):e1006842. doi: 10.1371/journal.pgen.1006842
178. Yamanaka K, Dorjsuren D, Eoff RL, Egli M, Maloney DJ, Jadhav A, et al. A Comprehensive Strategy to Discover Inhibitors of the Translesion Synthesis DNA Polymerase κ. *PLoS One* (2012) 7(10):1–8. doi: 10.1371/journal.pone.0045032
179. Ishimaru C, Kuriyama I, Shimazaki N, Koiwai O, Sakaguchi K, Kato I, et al. Cholesterol Hemisuccinate: A Selective Inhibitor of Family X DNA Polymerases. *Biochem Biophys Res Commun* (2007) 354(2):619–25. doi: 10.1016/j.bbrc.2007.01.034
180. Mizushina Y, Zhang J, Pugliese A, Kim S-H, Lü J. Anti-Cancer Gallotannin Penta-O-Galloyl-Beta-D-Glucose is a Nanomolar Inhibitor of Select Mammalian DNA Polymerases. *Biochem Pharmacol* (2010) 80(8):1125–32. doi: 10.1016/j.bcp.2010.06.031
181. Myobatake Y, Takeuchi T, Kuramochi K, Kuriyama I, Ishido T, Hirano K, et al. Inhibitors of Mammalian A-, B-, and Y-Family DNA Polymerases and Human Cancer Cell Proliferation. *J Natural products* (2012) 75(2):135–41. doi: 10.1021/np200523b
182. Horie S, Okuda C, Yamashita T, Watanabe K, Sato Y, Yamaguchi Y, et al. β-Sitosteryl (6'-O-Linoleoyl)-Glucoside of Soybean (Glycine Max L.) Crude Extract Inhibits Y-Family DNA Polymerases. *J oleo Sci* (2010) 59(11):621–30. doi: 10.5650/jos.59.621
183. Mizushina Y, Motoshima H, Yamaguchi Y, Takeuchi T, Hirano K, Sugawara F, et al. 3-O-Methylfunicone, a Selective Inhibitor of Mammalian Y-Family DNA Polymerases From an Australian Sea Salt Fungal Strain. *Marine Drugs* (2009) 7(4):624–39. doi: 10.3390/md7040624
184. Kimura T, Takeuchi T, Kumamoto-Yonezawa Y, Ohashi E, Ohmori H, Masutani C, et al. Penicilliols A and B, Novel Inhibitors Specific to Mammalian Y-Family DNA Polymerases. *Bioorganic medicinal Chem* (2009) 17(5):1811–6. doi: 10.1016/j.bmc.2009.01.064
185. Zafar MK, Maddukuri L, Ketkar A, Penthala NR, Reed MR, Eddy S, et al. A Small-Molecule Inhibitor of Human DNA Polymerase η Potentiates the Effects of Cisplatin in Tumor Cells. *Biochemistry* (2018) 57(7):1262–73. doi: 10.1021/acs.biochem.7b01176
186. Coggins GE, Maddukuri L, Penthala NR, Hartman JH, Eddy S, Ketkar A, et al. N-Aroyl Indole Thiobarbituric Acids as Inhibitors of DNA Repair and Replication Stress Response Polymerases. *ACS Chem Biol* (2013) 8(8):1722–9. doi: 10.1021/cb400305r
187. Saha P, Mandal T, Talukdar AD, Kumar D, Kumar S, Tripathi PP, et al. DNA Polymerase Eta: A Potential Pharmacological Target for Cancer Therapy. *J Cell Physiol* (2021) 236(6):4106–20. doi: 10.1002/jcp.30155
188. Zhou J, Gelot C, Pantelidou C, Li A, Yücel H, Davis RE, et al. A First in Class Polymerase Theta Inhibitor Selectively Targets Homologous Recombination-Deficient Tumors. *Nat Cancer* (2021) 2(6):598–620. doi: 10.1038/s43018-021-00203-x
189. Zatreanu D, Robinson HM, Alkhatib O, Boursier M, Finch H, Geo L, et al. Polθ Inhibitors Elicit BRCA-Gene Synthetic Lethality and Target PARP Inhibitor Resistance. *Nat Commun* (2021) 12(1):1–15. doi: 10.1038/s41467-021-23463-8
190. Ketkar A, Maddukuri L, Penthala NR, Reed MR, Zafar MK, Crooks PA, et al. Inhibition of Human DNA Polymerases Eta and Kappa by Indole-Derived Molecules Occurs Through Distinct Mechanisms. *ACS Chem Biol* (2019) 14(6):1337–51. doi: 10.1021/acschembio.9b00304
191. Ardiana F, Lestari ML, Indrayanto G. Candesartan Cilexetil. *Profiles Drug Substances Excipients Related Method* (2012) 37:79–112. doi: 10.1016/B978-0-12-397220-0.00003-9
192. Soriente A, De Rosa M, Scettri A, Sodano G, Terencio M, Paya M, et al. Manoalide. *Curr medicinal Chem* (1999) 6(5):415–31. doi: 10.1021/jm980027h
193. Jawien J, Gajda M, Rudling M, Mateuszuk L, Olszanecki R, Guzik T, et al. Inhibition of Five Lipoxygenase Activating Protein (FLAP) by MK-886 Decreases Atherosclerosis in Apoe/LDLR-Double Knockout Mice. *Eur J Clin Invest* (2006) 36(3):141–6. doi: 10.1111/j.1365-2362.2006.01606.x
194. Patel SM, Dash RC, Hadden MK. Translesion Synthesis Inhibitors as a New Class of Cancer Chemotherapeutics. *Expert Opin Investigational Drugs* (2021) 30(1):13–24. doi: 10.1080/13543784.2021.1850692
195. Punchihewa C, Inoue A, Hishiki A, Fujikawa Y, Connelly M, Evison B, et al. Identification of Small Molecule Proliferating Cell Nuclear Antigen (PCNA) Inhibitor That Disrupts Interactions With PIP-Box Proteins and Inhibits DNA Replication. *J Biol Chem* (2012) 287(17):14289–300. doi: 10.1074/jbc.M112.353201
196. Actis M, Inoue A, Evison B, Perry S, Punchihewa C, Fujii N. Small Molecule Inhibitors of PCNA/PIP-Box Interaction Suppress Translesion DNA Synthesis. *Bioorganic medicinal Chem* (2013) 21(7):1972–7. doi: 10.1016/j.bmc.2013.01.022
197. Gu L, Lingeman R, Yakushijin F, Sun E, Cui Q, Chao J, et al. The Anticancer Activity of a First-in-Class Small-Molecule Targeting PCNA. *Clin Cancer Res* (2018) 24(23):6053–65. doi: 10.1158/1078-0432.CCR-18-0592
198. Vanarotti M, Evison BJ, Actis ML, Inoue A, McDonald ET, Shao Y, et al. Small-Molecules That Bind to the Ubiquitin-Binding Motif of REV1 Inhibit REV1 Interaction With K164-Monoubiquitinated PCNA and Suppress DNA Damage Tolerance. *Bioorganic medicinal Chem* (2018) 26(9):2345–53. doi: 10.1016/j.bmc.2018.03.028
199. Sail V, Rizzo AA, Chatterjee N, Dash RC, Ozen Z, Walker GC, et al. Identification of Small Molecule Translesion Synthesis Inhibitors That Target the Rev1-CT/RIR Protein–Protein Interaction. *ACS Chem Biol* (2017) 12(7):1903–12. doi: 10.1021/acschembio.6b01144
200. Dash RC, Ozen Z, McCarthy KR, Chatterjee N, Harris CA, Rizzo AA, et al. Virtual Pharmacophore Screening Identifies Small-Molecule Inhibitors of the Rev1-CT/RIR Protein–Protein Interaction. *ChemMedChem* (2019) 14(17):1610–7. doi: 10.1002/cmdc.201900307
201. Nayak S, Calvo JA, Cong K, Peng M, Berthiaume E, Jackson J, et al. Inhibition of the Translesion Synthesis Polymerase REV1 Exploits Replication Gaps as a Cancer Vulnerability. *Sci Adv* (2020) 6(24):eaaz7808. doi: 10.1126/sciadv.aaz7808
202. Quinet A, Vessoni AT, Rocha CR, Gottifredi V, Biard D, Sarasin A, et al. Gap-Filling and Bypass at the Replication Fork are Both Active Mechanisms for Tolerance of Low-Dose Ultraviolet-Induced DNA Damage in the Human Genome. *DNA Repair* (2014) 14:27–38. doi: 10.1016/j.dnarep.2013.12.005
203. Barnes RP, Tsao W-C, Moldovan G-L, Eckert KA. DNA Polymerase Eta Prevents Tumor Cell-Cycle Arrest and Cell Death During Recovery From Replication Stress. *Cancer Res* (2018) 78(23):6549–60. doi: 10.1158/0008-5472.CAN-17-3931
204. Wojtaszek JL, Chatterjee N, Najeeb J, Ramos A, Lee M, Bian K, et al. A Small Molecule Targeting Mutagenic Translesion Synthesis Improves Chemotherapy. *Cell* (2019) 178(1):152–9.e11. doi: 10.1016/j.cell.2019.05.028
205. Chatterjee N, Whitman MA, Harris CA, Min SM, Jonas O, Lien EC, et al. REV1 Inhibitor JH-RE-06 Enhances Tumor Cell Response to Chemotherapy by Triggering Senescence Hallmarks. *Proc Natl Acad Sci* (2020) 117(46):28918–21. doi: 10.1073/pnas.2016064117
206. Wittschieben JP, Reshmi SC, Gollin SM, Wood RD. Loss of DNA Polymerase ζ Causes Chromosomal Instability in Mammalian Cells. *Cancer Res* (2006) 66(1):134–42. doi: 10.1158/0008-5472.CAN-05-2982
207. Wittschieben JP, Patil V, Glushets V, Robinson LJ, Kusewitt DF, Wood RD. Loss of DNA Polymerase ζ Enhances Spontaneous Tumorigenesis. *Cancer Res* (2010) 70(7):2770–8. doi: 10.1158/0008-5472.CAN-09-4267
208. Clairmont CS, Sarangi P, Ponnienselvan K, Galli LD, Csete I, Moreau L, et al. TRIP13 Regulates DNA Repair Pathway Choice Through REV7 Conformational Change. *Nat Cell Biol* (2020) 22(1):87–96. doi: 10.1038/s41556-019-0442-y
209. Alfieri C, Chang L, Barford D. Mechanism for Remodelling of the Cell Cycle Checkpoint Protein MAD2 by the ATPase Trip13. *Nature* (2018) 559(7713):274–8. doi: 10.1038/s41586-018-0281-1
210. Sarangi P, Clairmont CS, Galli LD, Moreau LA, D'Andrea AD. P31comet Promotes Homologous Recombination by Inactivating REV7 Through the TRIP13 ATPase. *Proc Natl Acad Sci* (2020) 117(43):26795–803. doi: 10.1073/pnas.2008830117
211. Sanders MA, Haynes B, Nangia-Makker P, Polin LA, Shekhar MP. Pharmacological Targeting of RAD6 Enzyme-Mediated Translesion Synthesis Overcomes Resistance to Platinum-Based Drugs. *J Biol Chem* (2017) 292(25):10347–63. doi: 10.1074/jbc.M117.792192
212. Haynes B, Gajan A, Nangia-Makker P, Shekhar MP. RAD6B is a Major Mediator of Triple Negative Breast Cancer Cisplatin Resistance: Regulation of Translesion Synthesis/Fanconi Anemia Crosstalk and BRCA1 Independence. *Biochim Biophys Acta (BBA)-Molecular Basis Dis* (2020) 1866(1):165561. doi: 10.1016/j.bbadis.2019.165561

213. Villafañez F, García IA, Carbajosa S, Pansa MF, Mansilla S, Llorens MC, et al. AKT Inhibition Impairs PCNA Ubiquitylation and Triggers Synthetic Lethality in Homologous Recombination-Deficient Cells Submitted to Replication Stress. *Oncogene* (2019) 38(22):4310–24. doi: 10.1038/s41388-019-0724-7
214. Chen J, Dexheimer TS, Ai Y, Liang Q, Villamil MA, Inglese J, et al. Selective and Cell-Active Inhibitors of the USP1/UAF1 Deubiquitinase Complex Reverse Cisplatin Resistance in Non-Small Cell Lung Cancer Cells. *Chem Biol* (2011) 18(11):1390–400. doi: 10.1016/j.chembiol.2011.08.014
215. Liang Q, Dexheimer TS, Zhang P, Rosenthal AS, Villamil MA, You C, et al. A Selective USP1–UAF1 Inhibitor Links Deubiquitination to DNA Damage Responses. *Nat Chem Biol* (2014) 10(4):298–304. doi: 10.1038/nchembio.1455
216. Kim H, D'Andrea AD. Regulation of DNA Cross-Link Repair by the Fanconi Anemia/BRCA Pathway. *Genes Dev* (2012) 26(13):1393–408. doi: 10.1101/gad.195248.112
217. Wang W. Emergence of a DNA-Damage Response Network Consisting of Fanconi Anaemia and BRCA Proteins. *Nat Rev Genet* (2007) 8(10):735–48. doi: 10.1038/nrg2159
218. Mayca Pozo F, Oda T, Sekimoto T, Murakumo Y, Masutani C, Hanaoka F, et al. Molecular Chaperone Hsp90 Regulates REV1-Mediated Mutagenesis. *Mol Cell Biol* (2011) 31(16):3396–409. doi: 10.1128/MCB.05117-11
219. Sekimoto T, Oda T, Pozo FM, Murakumo Y, Masutani C, Hanaoka F, et al. The Molecular Chaperone Hsp90 Regulates Accumulation of DNA Polymerase η at Replication Stalling Sites in UV-Irradiated Cells. *Mol Cell* (2010) 37(1):79–89. doi: 10.1016/j.molcel.2009.12.015
220. Takezawa J, Ishimi Y, Yamada K. Proteasome Inhibitors Remarkably Prevent Translesion Replication in Cancer Cells But Not Normal Cells. *Cancer Sci* (2008) 99(5):863–71. doi: 10.1111/j.1349-7006.2008.00764.x
221. Zhang X, Lee I, Berdis AJ. A Potential Chemotherapeutic Strategy for the Selective Inhibition of Promutagenic DNA Synthesis by Nonnatural Nucleotides. *Biochemistry* (2005) 44(39):13111–21. doi: 10.1021/bi050584n
222. Choi J-S, Kim CS, Berdis A. Inhibition of Translesion DNA Synthesis as a Novel Therapeutic Strategy to Treat Brain Cancer. *Cancer Res* (2018) 78 (4):1083–96. doi: 10.1158/0008-5472.CAN-17-2464
223. Wang Y, Huang J-W, Calses P, Kemp CJ, Taniguchi T. MiR-96 Downregulates REV1 and RAD51 to Promote Cellular Sensitivity to Cisplatin and PARP Inhibition. *Cancer Res* (2012) 72(16):4037–46. doi: 10.1158/0008-5472.CAN-12-0103

Conflict of Interest: The authors declare that the research was conducted in the absence of any commercial or financial relationships that could be construed as a potential conflict of interest.

Publisher's Note: All claims expressed in this article are solely those of the authors and do not necessarily represent those of their affiliated organizations, or those of the publisher, the editors and the reviewers. Any product that may be evaluated in this article, or claim that may be made by its manufacturer, is not guaranteed or endorsed by the publisher.

frontiers in Oncology

REVIEW
published: 17 February 2022
doi: 10.3389/fonc.2022.828684

Targeting the DNA Damage Response for Cancer Therapy by Inhibiting the Kinase Wee1

*Amirali B. Bukhari, Gordon K. Chan and Armin M. Gamper**

Department of Oncology, Cross Cancer Institute, University of Alberta, Edmonton, AB, Canada

Cancer cells typically heavily rely on the G2/M checkpoint to survive endogenous and exogenous DNA damage, such as genotoxic stress due to genome instability or radiation and chemotherapy. The key regulator of the G2/M checkpoint, the cyclin-dependent kinase 1 (CDK1), is tightly controlled, including by its phosphorylation state. This posttranslational modification, which is determined by the opposing activities of the phosphatase cdc25 and the kinase Wee1, allows for a more rapid response to cellular stress than *via* the synthesis or degradation of modulatory interacting proteins, such as p21 or cyclin B. Reducing Wee1 activity results in ectopic activation of CDK1 activity and drives premature entry into mitosis with unrepaired or under-replicated DNA and causing mitotic catastrophe. Here, we review efforts to use small molecule inhibitors of Wee1 for therapeutic purposes, including strategies to combine Wee1 inhibition with genotoxic agents, such as radiation therapy or drugs inducing replication stress, or inhibitors of pathways that show synthetic lethality with Wee1. Furthermore, it become increasingly clear that Wee1 inhibition can also modulate therapeutic immune responses. We will discuss the mechanisms underlying combination treatments identifying both cell intrinsic and systemic anti-tumor activities.

Keywords: kinase, DNA damage response (DDR), cell cycle, cancer therapy, Wee1, synthetic lethality

OPEN ACCESS

Edited by:
Peter McHugh,
University of Oxford, United Kingdom

Reviewed by:
Vijay Menon,
Yale University, United States
Julio Morales,
University of Oklahoma, United States

***Correspondence:**
Armin M. Gamper
gamper@ualberta.ca

Specialty section:
This article was submitted to Cancer Molecular Targets and Therapeutics, a section of the journal Frontiers in Oncology

Received: *03 December 2021*
Accepted: *21 January 2022*
Published: *17 February 2022*

Citation:
Bukhari AB, Chan GK and Gamper AM (2022) Targeting the DNA Damage Response for Cancer Therapy by Inhibiting the Kinase Wee1. Front. Oncol. 12:828684. doi: 10.3389/fonc.2022.828684

WEE1, THE CELL CYCLE, AND THE DNA DAMAGE RESPONSE

The cellular genome is exposed to insults by several endogenous (reactive oxygen species, DNA replication errors) as well as exogenous (chemical mutagens, ionizing radiation, ultraviolet light) DNA damaging factors. Ionizing radiation from cosmic radiations or medical treatments (X-ray scans or radiation therapy) can generate base lesions as well as single and double-strand DNA breaks. Additionally, cancer chemotherapeutics can intentionally induce a variety of DNA lesions, including inter- and intra-strand cross-links arising from drugs like cisplatin or Mitomycin C. To ensure safe passage of the genomic material to the next generation, all organisms have evolved mechanisms – collectively termed the DNA damage response (DDR) – to detect DNA damage and to activate a signaling cascade to promote repair, including *via* cell cycle checkpoint activation (1), or in the case of extensive DNA damage to trigger mechanisms to either permanently exit the cell cycle (senescence) or undergo programmed cell death (apoptosis), presumably preventing cells from accumulating mutations and resulting in the development of cancer.

The DNA damage response and the cell cycle are intimately linked through cell cycle checkpoints, "control mechanisms enforcing dependency in the cell cycle" (2). Of the four cell cycle checkpoints, only the spindle checkpoint in mitosis is not clearly linked to pathways activated by DNA damage. As most cells in a human are in G1 (G0) phase, the G1/S checkpoint will prevent most normal cells to enter the cell cycle after DNA damage. The pathways initiated by the apical kinases Ataxia Telangiectasia-mutated (ATM) (3, 4) and Ataxia telangiectasia and Rad3 related (ATR) (5) relay the damage signal to downstream effectors, including the tumor suppressor p53, a central node in the DNA damage response (6). These two kinases also play an important role in the S phase checkpoint (7–9), which ensuring accurate replication, and for the G2/M checkpoint (7, 10). The latter checkpoint prevents cells with damaged or under-replicated DNA to enter mitosis, an event which poses a high risk of chromosome aberrations (11). As all checkpoints are governed by cyclin-dependent kinases (CDKs), all DNA damage pathways ultimately converge on the regulation of the CDK activity. A dysregulated cell cycle is able to lead to DNA damage and genomic instability is a hallmark of cancer (12).

THE KINASE WEE1, A GATEKEEPER AT SEVERAL CELL CYCLE CHECKPOINTS

Wee1 is a tyrosine kinase originally discovered in *Schizosaccharomyces pombe* (13). Human Wee1 was subsequently discovered as a crucial regulator of the G2/M checkpoint (14). The primary structure of Wee1 is composed of an amino-terminal regulatory domain, a kinase domain, and a short C-terminal domain. The N-terminal domain coordinates signals to shuttle Wee1 into and out of the nucleus (15, 16). Wee1 contains four cyclin binding motifs, RxL1, RxL2, RxL3, and RxL4, to facilitate interaction with CDK (15) (**Figure 1A**).

The Wee kinase family comprises three serine/threonine kinases: *Wee1*, *PKMYT1*, and *Wee2*. In mammalian cells, Wee1 and PKMYT1 (protein kinase membrane-associated tyrosine/threonine 1; also known as Myt1) have a vital role in regulating the G2/M transition (17) (**Figure 1B**). Wee2 (or Wee1B) is only expressed in germ cells, where it prevents premature restart of oocyte meiosis prior to ovulation and permits metaphase II exit at fertilization (18). PKMYT1 functions as an essential component of an organelle-based cell cycle checkpoint to prevent CDK1-induced premature

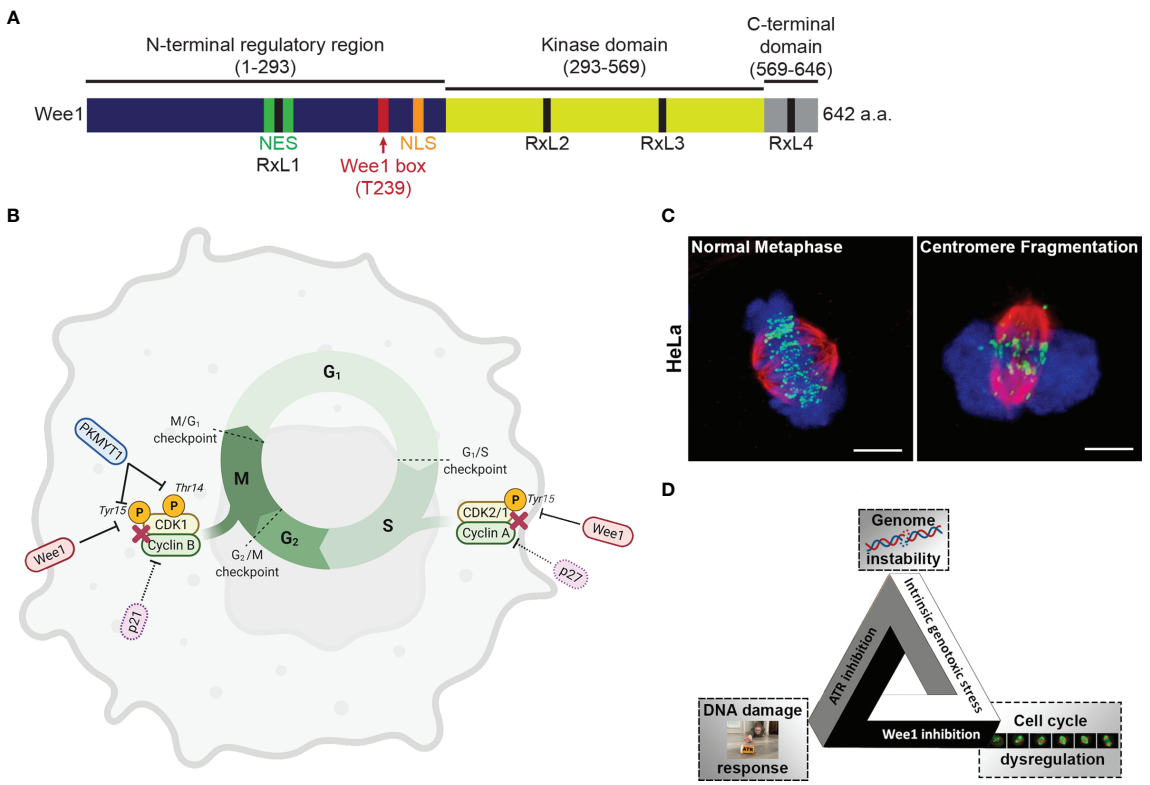

FIGURE 1 | **(A)** The 642 amino acid long protein kinase Wee1 contains a N-terminal regulatory domain (dark blue), a kinase domain (yellow green), and a short C-terminal domain (gray). The diagram also shows a nuclear localization sequence (NLS; orange), a nuclear export sequence (NES; green), a highly conserved regulatory Wee1 box (red), and four cyclin binding motifs (RxL1, RxL2, RxL3, and RxL4; black). **(B)** Regulation of the cell cycle *via* phosphorylation of Cyclin-Dependent Kinases (CDKs) by Wee1 and the related protein kinase MYT1. **(C)** Images of HeLa cells in metaphase undergoing unperturbed mitosis or centromere fragmentation due to mitotic catastrophe as a result of premature entry into mitosis. (chromosomes, blue; tubulin, red; centromeres, green) **(D)** The fateful triangle underlying the conditional synthetic lethality observed in cancer cells leading to selective killing by combined ATR and Wee1 inhibition.

fragmentation of Golgi and the endoplasmic reticulum during the G2 phase (19). PKMYT1 negatively regulates CDK1 activity by phosphorylation on both threonine 14 and tyrosine 15 (20, 21) - unlike Wee1, which only phosphorylates CDK1 on tyrosine 15 rendering CDK1 inactive (22, 23). In the absence of DNA damage, CDK1 is dephosphorylated by the Cell division cycle 25 (Cdc25c) phosphatase resulting in CDK1/cyclin B activation and initiation of mitotic events (24). In the unperturbed cell cycle Polo-like kinase 1 (PLK1) phosphorylates Wee1 at the G2/M transition, which targets Wee1 for degradation *via* the ubiquitin proteasome system (25). PLK1 also phosphorylates and activates the phosphatase cdc25 resulting in CDK1 activation (25, 26). Furthermore, Wee1 has a role in regulating replication dynamics during S phase. During S phase, initiation of replication results in the firing of many replication origins triggered by the action of DBF4-Dependent cdc7 kinase (DDK) and CDK2, the main S phase CDK (26, 27). Wee1 and cdc25 control CDK2 activity by regulating the phosphorylation status at tyrosine 15 (28). Importantly, Wee1 downregulation triggers a DNA damage response resulting in DNA replication stalling and reduced replication fork speed and causes cells to accumulate in S phase (29). It was proposed that in unperturbed cells, Wee1 protects replication forks and prevents generation of DNA damage by inhibiting the Mus81 endonuclease (29). Several studies have indicated that Wee1 levels are regulated by non-coding RNAs, which could impact cellular sensitivity to genotoxic agents (30).

Cancers often have a deregulated G1 checkpoint. As a result, they are heavily reliant on the G2/M checkpoint for survival and mitosis. Consequently, Wee1 is often highly expressed in many cancers including breast (31, 32) and lung (31) cancers, glioma (33), melanoma (34), leukemia (35, 36), osteosarcoma (37), and squamous cell carcinoma (38). As most cancer therapies aim to induce lethal amounts of DNA damage in cancer cells, Wee1 overexpression promotes cancer cell survival (and resistance) by reinforcing DNA damage checkpoints and preventing mitotic catastrophe (33). The key role of Wee1 in regulating the G2/M checkpoint in response to DNA damage has made it an attractive target for cancer therapy. Despite its appeal, to date only one selective and highly potent small molecule Wee1 inhibitor, AZD1775 (also known as Adavosertib or MK-1775) (39), has been widely reported and is being evaluated against various advanced cancers in phase I/II clinical trials either as a monotherapy (40–42) or in combination with other chemotherapies (40, 43, 44). Yet several new inhibitors are being developed or are already making it into the clinic (see below).

WEE1 INHIBITION AND MITOTIC CATASTROPHE

Mitotic catastrophe is a major mode of tumor cell death following genotoxic treatments including irradiation (45). Mitotic catastrophe is loosely defined as cell death that occurs during or following an aberrant mitosis (46, 47). While its molecular mechanism is unclear, increasing evidence points to the involvement of caspases (46, 48). Wee1 knockout and the loss of Cdk1 T14 and Y15 phosphorylation causes ectopic Cdk1 activity, uncontrolled mitotic entry and cell death (14, 49–51). Similarly, Wee1 inhibition with AZD1775 or siRNA-mediated knockdown of Wee1 results in premature mitotic entry, prolonged mitotic arrest and mitotic catastrophe (33, 52–56). Furthermore, ectopic activation of Cdk1 and activation of the Mus81 endonuclease complex in S phase results in stalled DNA replication forks and DNA damage (29, 57). The ectopic Cdk1 activity induces replication stress and fork collapse through the depletion of dNTPs and aberrant replication origin firing (58–60), as Cdk1 phosphorylation of the ribonucleotide reductase subunit RRM2 induces its ubiquitin mediated degradation during DNA synthesis resulting in a 70% drop in dNTPs (60). Since Cdk1 activity induces chromosome condensation, ectopic Cdk1 activity also promotes premature chromosome condensation (61–63), generates torsional strain to the DNA backbone and results in DNA breakage (64, 65). Centromeres are late replicating due to a lower prevalence of replication origins and are prone to breakage during premature condensation or cleavage by the Mus81 endonuclease complex (64, 66). In a process known as checkpoint adaptation, cells with damaged DNA eventually escape the S and G2 checkpoint and enter mitosis prematurely (67). Checkpoint adaptation in both lower eukaryotes and mammalian cells has been consistently linked to the Plk1 [reviewed in (68)], the kinase phosphorylating Wee1 and promotes its ubiquitin mediated degradation through the $SCF^{\beta TrCP}$ pathway (69, 70). Underlining the importance of this coordinated timing of kinases, Wee1 inhibition and subsequent premature entry into mitosis in the presence of under-replicated chromosomes can result in centromere fragmentation, a morphological marker of mitotic catastrophe (53, 71) (**Figure 1C**). Conversely, Wee1 overexpression can promote cell survival by reinforcing the DNA damage checkpoints and preventing mitotic catastrophe (33).

Wee1 inhibition by AZD1775 has been shown to induce *in vitro* and *in vivo* synergistic tumor cell killing with several DNA damaging therapies including IR (55) and chemotherapeutics like cisplatin, paclitaxel doxorubicin, 5-fluorouracil, and gemcitabine (53, 72–74). Given the role of p53 in regulating the G1 cell cycle checkpoint, treatment with AZD1775 has been reported to selectively target cancers harboring p53 mutations or loss of gene function (39, 75). Having said that, a few studies have also shown that AZD1775 sensitizes cancer cells to DNA damaging therapies independent of p53 status (76–78). Additionally, DNA damaging agents that specifically interfere with DNA synthesis and arrest cells in S-phase show high synergy with AZD1775 (59, 72). Overall, these preclinical studies support that AZD1775 has antitumor effects in a wide range of tumors both as a monotherapy and in combination with other chemotherapeutics.

WEE1 INHIBITORS IN THE CLINIC

There are 60 clinical trials listed on clinicaltrials.gov (accessed January 2022) for AZD1775 where it is being evaluated against a wide range of cancer types including breast cancer, cervical

cancer, leukemia, lung cancer, ovarian cancer, pancreatic cancer, pediatric and adult brain tumors (For a list of completed and active clinical trials with Wee1 inhibitors, see **Table 1**). Findings of phase I clinical trials show that AZD1775 is relatively well tolerated with acceptable toxicity profiles both as a single agent and in combination with other therapies (42). As a monotherapy, the maximum tolerated dose was determined as 225 mg, which was administered orally to ovarian cancer patients in five doses (2 twice per day, 1 once a day) per week over 3 weeks (42). The dose limiting toxicities included hematologic events, nausea, vomiting, and fatigue (40, 42). Interestingly, two of nine patients harboring *BRCA1* mutation recorded partial response, but unexpectedly none of the patients with documented p53 mutation exhibited a response (42). Early indications from a phase II trial evaluating AZD1775 plus carboplatin in p53 mutant ovarian cancer refractory or therapy-resistant patients show encouraging antitumor activity with one (5%) complete response and eight (38%) partial responses (43). Moreover, the overall response rate (43%) far exceeded the results that could be expected with second-line single agent treatments (11% to 21%) (43). A recent clinical trial evaluated the efficacy of AZD1775 as a monotherapy given once-daily as 5 days on and 2 days off in a 21 day cycle to patients (n = 42) with advanced solid tumors (79). The recommended phase II dose was determined as 300 mg, with most common toxicities including gastrointestinal and hematologic adverse effects. The dose-limiting toxicities included grade 4 hematologic toxicity and grade 3 fatigue (79). Six patients (14%; four ovarian and two endometrial cancers) confirmed partial response as the best response. Interestingly, one patient who progressed rapidly was found to have a Wee1 tumor mutation and potential compensatory PKMYT1 overexpression (79) (see below).

While AZD1775 is the most promising Wee1 inhibitor undergoing phase II clinical testing to date, its toxicity profile limits its use to intermittent dosing, potentially impacting clinical efficacy. Recently, Zentalis Pharmaceuticals reported the development of ZN-c3, a selective small molecule orally active bioavailable inhibitor of Wee1. Compared to AZD1775, which at higher concentrations also inhibits PLK1, a negative regulator of Wee1, ZN-c3 showed much higher selectivity for Wee1 over other kinases (80). Moreover, ZN-c3 demonstrated similar efficacy to AZD1775 *in vivo*. The expected superior safety profiles of ZN-c3 has enabled its quick transition to phase I/II clinical testing either as a monotherapy or in combination with other chemotherapies (NCT04158336). Similarly, a Wee1 inhibitor developed by Debiopharm, Debio 0123, is being tested in a phase I study (NCT03968653).

TABLE 1 | Wee1 inhibitors in clinical trials.

Study Identifier	Co-Treatment	Tumor Type	Phase	Status
Adavosertib (AZD1775) as Monotherapy				
NCT01748825	–	S	1	Complete
NCT03313557	–	S	1	Complete
NCT03668340	–	S	2	Active
NCT03315091	–	S	1	Complete
NCT02659241	–	S	1	Active
NCT03333824	–	S	1	Active
NCT02207010	–	S	0	Complete
NCT04439227	–	S/H	2	Active
NCT02593019	–	S	2	Complete
NCT04590248	–	S	2	Active
NCT03385655	–	S	2	Active
Adavosertib in combination with other cytotoxic therapies				
NCT02666950	Cytarabine	H	2	Complete
NCT01164995	Carboplatin	S	2	Active
NCT03012477	Cisplatin	S	2	Complete
NCT02101775	Gemcitabine	S	2	Active
NCT02906059	Irinotecan	S	1	Complete
NCT03330847	Olaparib	S	2	Active
NCT02341456	Carboplatin/Paclitaxel	S	1b	Complete
NCT02508246	Cisplatin/Docetaxel	S	1	Complete
NCT02194829	Gemcitabine/Paclitaxel	S	1, 2	Active
NCT03345784	Cisplatin/RT	S	1	Active
NCT02585973	Cisplatin/RT	S	1	Complete
NCT03028766	Cisplatin/RT	S	1	Complete
NCT02037230	Gemcitabine/RT	S	1, 2	Complete
NCT01849146	Temozolomide/RT	S	1	Active
Other Wee1 inhibitors in clinical testing – Zn-c3				
NCT04158336	–	S	1	Active
Other Wee1 inhibitors in clinical testing – IMP7068				
NCT04768868	–	S	1	Active
Other Wee1 inhibitors in clinical testing – Debio 0123				
NCT03968653	Carboplatin	S	1	Active

Suspended trials were not included in the list. S, solid tumors. H, hematological cancers.

Early results for ZN-c3 of the phase I dose-escalation (25 mg to 450 mg) trial (NCT04158336) reported 300 mg as the recommended phase II dose (81). Of the 16 patients with post-baseline tumor assessments, 5 patients showed indications of stable disease, and 2 patients showed partial response. Interestingly, both the partial response patients had stage IV metastatic disease (colorectal cancer and ovarian cancer, respectively) and had undergone several lines of therapy (81). Importantly, ZN-c3 was reported to have higher selectivity and better safety profiles compared to AZD1775, making it particularly well suited for combination therapies (82). Out of the 39 patients involved in the trial, 30 experienced mild to moderate symptoms like nausea, diarrhea, vomiting, and fatigue (81). In addition to this, ZN-c3 is also undergoing clinical testing in combination with other chemotherapeutics like carboplatin, doxorubicin, paclitaxel, and gemcitabine in patients with platinum-resistant ovarian cancer (NCT04516447).

Other Wee1 inhibitors in clinical trials are Debio 0123 by the French company Debiopharm and, the most recent addition, IMP7068, developed by Impact Therapeutiucs in China. Schrödinger and Nuvation Bio have preclinical compounds that might soon advance soon in the pipeline as well (SDGR2 and NUV-569, respectively).

RADIOSENSITIZATION BY WEE1 INHIBITION

The G2/M checkpoint constitutes an important safeguard for preventing cells with damaged or under-replicated DNA to enter mitosis, particularly in cancer cells which often have an abrogated G1 checkpoint due to aberrations in p53 signaling, caused e.g. by mutations in the p53 gene, viral proteins or MDM2 overexpression. It is therefore not surprising that the first described Wee1 inhibitor, (non-selective) PD0166285, was tested in combination with ionizing radiation and was found to radiosensitize, i.e. to kill more efficiently, cancer cells in a p53-dependent manner (83). Studies with AZD1775 (39), which unlike PD0166285 does not inhibit the related kinase PKMYT1 as well, confirmed that inhibition of Wee1 leads to radiosensitization of a variety of cancer cells and increased radiation-induced tumor delay in mouse models (55). Since then several studies have shown that combining ionizing radiation with inhibition of Wee1 by AZD1775 increased cell death or clonogenic death of cells derived from a variety of cancers, including of the lung, breast, prostate, esophagus, cervix, liver, brain, and pancreas (55, 84–93). Yet it is not always clear in the mentioned studies whether the cooperativity was synergistic or just additive. (Only in the former case it would be appropriate to call the effect radiosensitizing.) Importantly, several preclinical studies in mice also showed increased tumor delay when radiation was combined with Wee1 inhibition (55, 85–87, 90–93) and several clinical trials are currently examining the efficacy of AZD1775 with radiation therapy (sometimes in combination with chemotherapy). Phase I trials produced promising results (94, 95), although the combination with cisplatin prompted the need for toxicity–related dosing adjustments (95). The initial proposal that p53 status was an essential biomarker for the radiosensitization by Wee1 inhibition (55) was put into doubt by subsequent studies (89). A likely explanation is that p53 status-independent defects of the G1 checkpoint could make cancer cells reliant on the G2/M checkpoint. Indeed, cyclin E overexpression renders cancer cells sensitive to Wee1 inhibition (96). Furthermore, several other mechanisms could lead to increased replication stress in cancer cells which would synergize with radiation and Wee1 inhibitor-mediated replication stress to endanger the survival of cancer cells entering mitosis. In this regard, the exact cellular mechanisms underlying the radiosensitization by Wee1 inhibition are still to be determined. For example, is the main reason for the cooperativity due to Wee1 inhibition lowering the G2/M transition threshold or increasing replication stress on top of ionizing radiation-induced DNA damage? Wee1 inhibition also suppresses homologous recombination (97), an important repair pathway particularly for radiation-induced double strand breaks. In the G2 phase homologous recombination could repair even complex DNA damage and DNA structures resulting from stalled or collapsed replication forks. The contribution of inhibition of these Wee1 roles, as well as known and yet to be identified crosstalk with other cellular pathways [e.g. autophagy (93)], to radiosensitization is likely specific to the cell type or even to the subpopulation (given tumor heterogenicity). Of importance for the clinic – and unfortunately much less characterized - is the heterogeneity in the radiosensitization of normal cells (between cell type and between persons) by inhibitors of cell cycle regulators. Of particular concern for normal tissue complications are potential deleterious effects of combining Wee1 inhibitors and radiation on stem cells, which often rely on an intricate crosstalk between external signaling factors and the cell cycle machinery to regulate their differentiation potential (98). As tissue homeostasis is usually dependent on tissue specific stem cells, the impact of Wee1 inhibition in the clinic must also be seen in the context of the heterogeneity in the radiation response within the stem cell compartment and plasticity (reviewed in (99)). Radiosensitizers are only useful for cancer therapy if they improve the therapeutic index in the current highly conformal treatment plans in radiation oncology.

SYNTHETIC LETHALITY WITH WEE1 INHIBITION

Synthetic lethality refers to an interaction between two genes when the perturbation of either gene alone is viable but the simultaneous perturbation of both genes (gene functions) leads to cell death. A well-known example is deficiency of homologous recombination proteins BRCA1 or BRCA2 causing cancer cell sensitivity to poly (ADP-ribose) polymerase (PARP) inhibitors (100, 101). This distinctive synthetic lethality led to a strong interest in therapeutic approaches targeting cancer cells with other deficiencies in DNA damage response (DDR) pathways by

inhibition of the alternative DDR pathway. Yet as this approach only targets cells with a specific defect in the DDR, unless loss of gene function leads to the cell-of-origin or occurs early in carcinogenesis, in which case the gene defect would be in all or most tumor cells, it is bound to only affect a subset of populations within a heterogeneous tumor. For example, the loss of Ataxia Telangiectasia-mutated (ATM) frequently observed in a variety of cancers (102) is likely due to a driver mutation occurring at an early stage during lung carcinogenesis (103). It therefore is expected that most cancer cells in those tumors will be killed by targeted drugs showing high efficacy in the background of defective ATM (104). Yet except for the ATM and p53 pathways (alterations in ATM, CHEK2, p53, MDM2), the majority of driver mutations in DNA damage response and repair genes were found to be subclonal in non-small cell lung cancer (103). It is to be expected that targeting an evolutionary late occurring gene defect, even if found in the subpopulation that constitutes the bulk of the cancer cells, would lead to the selection for the subpopulation with the functional gene and treatment resistance to follow. Furthermore, even in a homogenous population with a common DDR defect resistance can arise by reactivation of the defective pathway, as was observed in some PARP inhibitor resistant breast cancers (105). *Conditional* synthetic lethality refers to synthetic lethality observed only under certain circumstances, such as genetic background or metabolic state of cells or cellular environment (106). An approach to build synthetic lethality around cancer-intrinsic characteristics has the potential to decrease the probability for the tumors to acquire resistance. In that regard, one of the most common features of cancer cells is oncogene-induced DNA damage (107, 108), often leading to levels of replication and mitotic stress not observed in normal proliferating cells. This tumor-specific property makes it an ideal selective condition to base a synthetic lethality on to achieve a favorable therapeutic index.

An example of a successful attempt to establish a fateful triangle for cancer cells in a conditional synthetic lethality approach is the combination of inhibitors of Wee1 and of the kinase Ataxia telangiectasia and Rad3 related (ATR). This multi-pronged attack takes advantage of three features of cancer cells to selectively target them: genomic instability, dysregulated cell cycle and the reliance on particular DDR pathways for survival (**Figure 1D**). In a 2008 review discussing genomic instability, a designated hallmark of cancer (12), Halazonetis, Gourgoulis, and Bartek pointed out that, based on their data and the literature on observations in many cancer cell lines and precancerous and cancerous lesions from patients, "the presence of DNA damage was a feature that could distinguish precancerous lesions and cancers from normal tissues, irrespective of their proliferation rate" (108). DNA damage (genotoxic stress) is therefore a fundamental characteristic of cancer cells, unlike some other hallmarks of cancer which, due to tumor heterogeneity, may not manifest in every tumor or every tumor cell.

ATR is an apical kinase in the DDR and is activated by replication protein A (RPA)-coated single-stranded DNA, structures that can arise from stalled replication forks or resected DNA double-strand breaks (1). Not surprisingly, ATR plays a crucial role in the response to replication stress – likely the reason for it being an essential gene (109, 110). As a result, cancer cells rely on functional ATR signaling, particularly as other DNA damage response pathways are lost (such as the p53 and/or ATM pathway). This is exemplified by the importance of ATR signaling for the survival of cancer cells to ionizing radiation (5). Unsurprisingly, ATR activity is often upregulated in cancer cells (111, 112), including in cancer stem cells (113). ATR regulates Chk1 activity by phosphorylation of Chk1 kinase at serines 317 and 345 (1). Chk1 in turn targets Cdc25, the phosphatase removing inhibitory phospho-groups from cyclin-dependent kinases (CDKs), for degradation by phosphorylation-dependent ubiquitination. Because CDKs, particularly CDK1 and CDK2, regulate entry into mitosis and replication origin firing, Chk1 activation thereby prevents cell cycle progression (114). Thus, ATR/Chk1 signaling initiated at structures containing single-stranded DNA controls the S and G2 phase cell cycle checkpoints in mammalian cells (114). Importantly, the phosphorylation state of CDKs 1 and 2 (and thus their inhibition) is regulated by the balance between the kinase activity of Wee1 (and Myt1) and the phosphatase activity of Cdc25. The observed synergistic effects of Wee1 and ATR inhibition (71, 115) on cancer cell killing are surely in grant part due to the lowering of the threshold for CDK activation by combining inhibiting the constitutive phosphorylation and preventing checkpoint activation by the ATR/CHK1/Cdc25 axis, as combined AZD1775 and AZD6738 treatment leads to mitotic catastrophe in cancer cells (71). Yet both Wee1 and ATR regulate other cellular aspects that will play a role, including their activities during replication: For example, the above mentioned role of Wee1 during S phase, including replication fork protection, as well as reportedly in timing the entry into S phase (116) are perturbed by AZD1775 and lead to substantial replication stress. ATR on the other hand, besides the many functions during unperturbed replication (117), also regulates DNA damage repair by promoting extensive DNA end-resection needed for homologous recombination (5, 118, 119). By utilizing the reversibility of Wee1 and ATR inhibition, we characterized the contributions of inactivation of each kinase and during different phases of the cell cycle, thus studying how abrogation of ATR and Wee1 activity cooperatively leads to cell death caused by mitotic defects (71). The findings are compatible with a model, where synergistic killing by ATR and Wee1 inhibitors is based on an increase in the DNA damage level while simultaneously lowering the DNA damage response capacity leading to mitotic catastrophe. This is achieved by Wee1 inhibition-induced DNA damage during replication, abrogation of ATR-mediated S phase checkpoint activation, inhibition of ATR-dependent homologous recombination, and amplified by increased entry into mitosis with defective genomes due to combined inhibition of ATR and Wee1. As high replication stress in cancer cells - due to the high level of baseline DNA damage *per se*, but also to the resulting exhaustion of factors needed for both repair and replication, such as RPA (120) – contrasts from the stress in normal cells, even in highly proliferative tissues, and cancer cells often have an

increased reliance on the G2/M checkpoint, a therapeutic window is achieved in an example of a conditional synthetic lethality.

Several studies have also investigated whether defects in specific pathways sensitize to Wee1 inhibition. A recent study in basal-like breast cancer cells suggests that loss of PTEN may be one of the strongest markers of Wee1 inhibitor sensitivity (121). This might not come as a surprise, given the role PTEN plays in replication progression and several studies showing that PTEN loss increases replication stress (122–124). A recent study also showed that HPV16 positivity sensitizes head and neck squamous cell carcinomas to Wee1 inhibition by a mechanism involving a circuit linking CDK1 and FOXM1 (125), a master transcriptional regulator of mitotic genes (126). Fitting with the scheme of vulnerability to Wee1 inhibition based on an already dysregulated cell cycle, an unbiased screen identified several S phase genes as determinants for AZD1775 sensitivity (127). Related, another screen identified defects in the Fanconi anemia pathway and in homologous recombination, mechanisms needed for effective DNA replication particularly in the background of increased DNA damage, as sensitizing to Wee1 inhibition (128). A strategy of releasing tumor cells from a cell cycle block into a phase where the cells are sensitive to Wee1 inhibition was used in a preclinical study with sarcoma. The combined sequential treatment with the CDK4/6 inhibitor Palbociclib and AZD1775 showed at least additive effects on tumor growth (129). In a model for the clinical scenario of breast cancer cells resistant to endocrine therapy and CDK4/6 inhibitors, derived long-term estrogen deprived endocrine resistant cell lines were found to be more resistant to CDK4/6 inhibitors, but more sensitive to AZD1775 or Wee1 knockdown than their parental cell lines (130). An interesting observed synergistic interaction was found between AZD1775 and A1155463 in cancer cells from a genetically engineered animal model for triple negative breast cancers (131). A1155463 is an inhibitor of the anti-apoptotic BCL-X_L protein (132). The drug combination also showed efficacy *in vivo*, but unfortunately the authors did not report the effect of the individual drugs in their mouse model (131). AZD1775 was also found to synergize with the PARP inhibitor olaparib in a xenograft model for triple negative breast cancer (133).

RESISTANCE MECHANISMS TO WEE1 INHIBITION

Obvious candidate resistance mechanisms to Wee1 inhibitors include reversal of expression profiles of genes that are the base for Wee1 inhibitor vulnerability. For example, while cyclin E overexpression sensitizes cancer cells to AZD1775, reducing cyclin E levels has the opposite effect (96). A mechanism of *acquired* AZD1775 resistance observed both *in vitro* and *in vivo* is *via* the upregulation of PKMYT1 (53). As mentioned, Wee1 and the related kinase PKMYT1 exhibit functionally redundant roles in the inhibition of CDK1/cyclin B, the mitosis promoting complex (134–136). Yet compared to Wee1, PKMYT1 is much less studied in the context of cancer biology. This might be due to reports that inhibition or knockdown of Wee1 alone is sufficient to abrogate the S- and G2/M DNA damage checkpoints and that the loss of PKMYT1 neither affects the timing of mitosis nor abrogates DNA damage checkpoints in the presence of Wee1 (56, 137–139). On the other hand, combined knockdown of Wee1 and PKMYT1 causes more HeLa cells to enter mitosis with damaged DNA compared to Wee1 knockdown alone (56), PKMYT1 knockdown enhances AZD1775 induced cell killing in cell lines derived from brain metastases (140), and PKMYT1 is essential for cell survival in a subset of glioblastoma cells that have downregulated Wee1 expression (141). The protective mechanism by PKMYT1 upregulation leading to AZD1775 resistance was found to be due to compensatory inhibition of ectopic CDK1 activity by PKMYT1, allowing cells to escape mitotic catastrophe, the mode of cell death induced by Wee1 inhibition (53).

It was proposed that cancer stem cells, which often show increased chemo- and radiation resistance compared to bulk cancer cells and due to their cellular plasticity and tumor initiating capability can lead to tumor relapse (142), could be targeted by Wee1 inhibition (143). Only a few studies have examined the efficacy of Wee1 inhibition – alone or in combination - in the eradication of cancer stem cells. Early findings that Wee1 inhibition by the unspecific inhibitor PD0166285 radiosensitizes glioma stem cells (CD133 enriched glioma neurospheres) (33) were contradicted by a study using AZD1775 (and glioma cell lines enriched for neuronal stem cells) (92). In contrast, another study found that glioma stem cells (unlike neuronal progenitor cells) were sensitive to Wee1 inhibition alone (141). Our studies in breast cancer showed that breast cancer stem cells were less sensitive to AZD1775 compared to bulk cancer cells, which could be due to reduced drug uptake or decreased reliance on Wee1 signaling. Interestingly, combined Wee1 and ATR inhibition was as toxic to cancer stem cells as to bulk breast cancer cells, potentially explaining the antimetastatic effect of the combination treatment (71). To our knowledge, this was the first report of a higher drug synergy observed in cancer stem cells compared to bulk cancer cells, compensating for the reduced sensitivity of cancer stem cells to the individual drugs. A recent study found that trastuzumab resistant breast cancer cell lines were enriched in cancer stem cells, but on average showed greater sensitive to AZD1775. AZD1775 treatment disrupted stem like properties in the tested trastuzumab resistant breast cancer cell lines (144). These studies indicate that insights into the role of Wee1 in cancer stem cell maintenance and the associated correlation with drug resistance could have a significant impact in the clinic.

As the ongoing clinical trials will provide data and samples from patients treated with AZD1775 (Adavosertib), not only will predictive biomarkers be identified, but it will also become clearer which are the preferred pathways for resistance acquisition to single agent therapies. This in turn will provide important clues for improved treatment plans with combination therapies.

WEE1 INHIBITION - BEYOND CELL-INTRINSIC CYTOTOXICITY

The interaction between tumor cells and immune cells plays a determining role not only during carcinogenesis, where the survival of transformed cells is based on immune evasion, but also in cancer therapy, where the immune system is a key factor in achieving local and systemic tumor control. Several pathways involved in both DNA damage repair/signalling and immunity indicate that the immune system and the DNA damage response (DDR) have coevolved, resulting in processes with overlapping enzymatic networks. Examples range from prokaryotic defense systems, such as the antiviral CRISPR machinery, to the complex mammalian immune stimulation and maturation processes, such as class-switch recombination. A classic case in point is the discovery in 1995 that the lack of DNA-PK caused both extreme radiosensitivity and severe combined immunodeficiency (145, 146). Since then several cellular links between proteins in the DNA damage response and immune signaling have been uncovered. Of particular interest is the stimulator of interferon genes (STING) pathway, that can be activated by cyclic GMP-AMP synthase (cGAS) binding to DNA fragments and the subsequent production of the allosteric modulator of STING, the small messenger molecule cGAMP (147). This pathway was discovered as an important defense mechanism against DNA viruses, but was later found to get activated by DNA damage in the nucleus or mitochondria as well (148, 149). Besides cGAS, which binds to the DNA backbone, STING activation by DNA fragments might also involve the recognition of DNA ends by DNAPK (150) and/or the MRN complex (151). Kinases downstream of STING, TANK binding kinase 1 and IκB kinase, induce the transcription of genes involved in the innate immune response, such as interferons, interleukins and TNF, *via* the transcription factors IRF3 and NFκB (152). Several studies have shown that exogenous and endogenous genotoxic stress can induce the expression of interferon-stimulated genes, including stress due the loss of genes involved in the DNA damage response [reviewed in (153)]. Furthermore, activation of the apical DDR kinases ATM and ATR can also lead to upregulation of PD-L1 (*via* the STAT1 and STAT3 pathway) (154) and natural killer group 2D (NKG2D) ligands (155, 156).

Besides these DNA damage-induced changes in surviving cells, therapy-induced cell death itself can have a big immunomodulatory effect. The Nomenclature Committee on Cell Death defines immunogenic cell death (ICD) as "a functionally peculiar form of regulated cell death that is sufficient to activate an adaptive immune response specific for endogenous (cellular) or exogenous (viral) antigens expressed by dying cells" (45). Besides the release of antigenic determinants, such as neoepitopes, dying tumor cells also can lead to a local release of damage-associated molecular patterns and cytokines resulting in local effects on immune cell trafficking and activation. The observation that inhibition of Wee1 increases replication stress as well as the likelihood of untimely entry into mitosis, raising the possibility of DNA structures activating the STING pathway as well as mitotic catastrophe, make Wee1 inhibition a good candidate drug to increase the antitumor immune response. This makes Wee1 inhibition especially attractive to be combined with radiation therapy, as the latter is well known to be particularly inducive to ICD and Wee1 inhibitors are, as discussed previously, also radiosensitizing (39, 89, 157). Indeed preclinical studies have shown immune stimulating effects of Wee1 inhibition in combination with irradiation (158, 159). The exact mechanisms underlying the increased anti-tumor immunity, including the extent interferon signaling is involved, are still unclear. Of note, a recent study showed that inhibition of Wee1 alone failed to induce a type I interferon response, despite increasing DNA double strand breaks, cytosolic DNA, and micronuclei – all cellular phenotypes previously correlated with STING pathway activation (160).

CONCLUSION

In conclusion, Wee1 inhibitors show great potential to make an impact in the clinic for the therapy of several cancer types. While some concerns have arisen from phase I/II clinical trials regarding potential side effects, it remains to be seen whether newer Wee1 inhibitors with supposedly higher kinase selectivity show an improved safety profile. Yet the most promising path are combination therapies allowing lower dosing of the Wee1 inhibitor than in monotherapy. Furthermore, optimization of the treatment plans, such as intermittent dosing of the Wee1 inhibitor, might improve the drug tolerance.

Regarding the kinase itself, still many questions remain to be elucidated on the biological role of Wee1, which revealed itself to be a multifaceted player during several phases of the cell cycle. Of special interest are the redundant and divergent roles of Wee1 and the related kinase PKMYT1, in normal tissues and in various cancer types.

AUTHOR CONTRIBUTIONS

AB, GC, and AG wrote and reviewed the manuscript together. All authors contributed to the article and approved the submitted version.

FUNDING

ABB is supported by Alberta Cancer Foundation's Dr. Cyril M. Kay Graduate Scholarship. GKC and AMG are funded by the Canadian Institute of Health Research and the Natural Sciences and Engineering Research Council of Canada, as well as the Cancer Research Society and Women and Children's Health Research Institute (AMG).

ACKNOWLEDGMENTS

We would like to acknowledge the many researchers who contributed to our growing knowledge of the biology of Wee1 and the DDR in general and whose work we could not cite in this non-exhaustive overview of the field. We thank members of the Chan and Gamper labs for images used in the figures, and Kenaan Ramji for help in proofreading the manuscript. We also thank Stéphanie La France for her assistance with an image used in the figure. Some illustrations were generated using BioRender.

REFERENCES

1. Ciccia A, Elledge SJ. The DNA Damage Response: Making It Safe to Play With Knives. *Mol Cell* (2010) 40(2):179–204. doi: 10.1016/j.molcel.2010.09.019
2. Hartwell LH, Weinert TA. Checkpoints: Controls That Ensure the Order of Cell Cycle Events. *Science* (1989) 246(4930):629–34. doi: 10.1126/science.2683079
3. Kastan MB, Zhan Q, el-Deiry WS, Carrier F, Jacks T, Walsh WV, et al. A Mammalian Cell Cycle Checkpoint Pathway Utilizing P53 and GADD45 Is Defective in Ataxia-Telangiectasia. *Cell* (1992) 71(4):587–97. doi: 10.1016/0092-8674(92)90593-2
4. Bakkenist CJ, Kastan MB. DNA Damage Activates ATM Through Intermolecular Autophosphorylation and Dimer Dissociation. *Nature* (2003) 421(6922):499–506. doi: 10.1038/nature01368
5. Gamper AM, Rofougaran R, Watkins SC, Greenberger JS, Beumer JH, Bakkenist CJ. ATR Kinase Activation in G1 Phase Facilitates the Repair of Ionizing Radiation-Induced DNA Damage. *Nucleic Acids Res* (2013) 41 (22):10334–44. doi: 10.1093/nar/gkt833
6. Vogelstein B, Lane D, Levine AJ. Surfing the P53 Network. *Nature* (2000) 408(6810):307–10. doi: 10.1038/35042675
7. Painter RB, Young BR. Radiosensitivity in Ataxia-Telangiectasia: A New Explanation. *Proc Natl Acad Sci USA* (1980) 77(12):7315–7. doi: 10.1073/pnas.77.12.7315
8. Hekmat-Nejad M, You Z, Yee MC, Newport JW, Cimprich KA. Xenopus ATR is a Replication-Dependent Chromatin-Binding Protein Required for the DNA Replication Checkpoint. *Curr Biol* (2000) 10(24):1565–73. doi: 10.1016/S0960-9822(00)00855-1
9. Gamper AM, Choi S, Matsumoto Y, Banerjee D, Tomkinson AE, Bakkenist CJ. ATM Protein Physically and Functionally Interacts With Proliferating Cell Nuclear Antigen to Regulate DNA Synthesis. *J Biol Chem* (2012) 287 (15):12445–54. doi: 10.1074/jbc.M112.352310
10. Cliby WA, Roberts CJ, Cimprich KA, Stringer CM, Lamb JR, Schreiber SL, et al. Overexpression of a Kinase-Inactive ATR Protein Causes Sensitivity to DNA-Damaging Agents and Defects in Cell Cycle Checkpoints. *EMBO J* (1998) 17(1):159–69. doi: 10.1093/emboj/17.1.159
11. Wilhelm T, Said M, Naim V. DNA Replication Stress and Chromosomal Instability: Dangerous Liaisons. *Genes (Basel)* (2020) 11(6):646–74. doi: 10.3390/genes11060642
12. Hanahan D, Weinberg RA. Hallmarks of Cancer: The Next Generation. *Cell* (2011) 144(5):646–74. doi: 10.1016/j.cell.2011.02.013
13. Thuriaux P, Nurse P, Carter B. Mutants Altered in the Control Co-Ordinating Cell Division With Cell Growth in the Fission Yeast Schizosaccharomyces Pombe. *Mol Gen Genet* (1978) 161(2):215–20. doi: 10.1007/BF00274190
14. Heald R, McLoughlin M, McKeon F. Human Wee1 Maintains Mitotic Timing by Protecting the Nucleus From Cytoplasmically Activated Cdc2 Kinase. *Cell* (1993) 74(3):463–74. doi: 10.1016/0092-8674(93)80048-J
15. Li C, Andrake M, Dunbrack R, Enders GH. A Bifunctional Regulatory Element in Human Somatic Wee1 Mediates Cyclin A/Cdk2 Binding and Crm1-Dependent Nuclear Export. *Mol Cell Biol* (2010) 30(1):116–30. doi: 10.1128/MCB.01876-08
16. Squire CJ, Dickson JM, Ivanovic I, Baker EN. Structure and Inhibition of the Human Cell Cycle Checkpoint Kinase, Wee1A Kinase: An Atypical Tyrosine Kinase With a Key Role in CDK1 Regulation. *Structure* (2005) 13(4):541–50. doi: 10.1016/j.str.2004.12.017
17. Schmidt M, Rohe A, Platzer C, Najjar A, Erdmann F, Sippl W. Regulation of G2/M Transition by Inhibition of WEE1 and PKMYT1 Kinases. *Molecules* (2017) 22(12). doi: 10.3390/molecules22122045
18. Oh JS, Susor A, Conti M. Protein Tyrosine Kinase Wee1B Is Essential for Metaphase II Exit in Mouse Oocytes. *Science* (2011) 332(6028):462–5. doi: 10.1126/science.1199211
19. Villeneuve J, Scarpa M, Ortega-Bellido M, Malhotra V. MEK1 Inactivates Myt1 to Regulate Golgi Membrane Fragmentation and Mitotic Entry in Mammalian Cells. *EMBO J* (2013) 32(1):72–85. doi: 10.1038/emboj.2012.329
20. Liu F, Stanton JJ, Wu Z, Piwnica-Worms H. The Human Myt1 Kinase Preferentially Phosphorylates Cdc2 on Threonine 14 and Localizes to the Endoplasmic Reticulum and Golgi Complex. *Mol Cell Biol* (1997) 17(2):571–83. doi: 10.1128/MCB.17.2.571
21. Booher RN, Holman PS, Fattaey A. Human Myt1 Is a Cell Cycle-Regulated Kinase That Inhibits Cdc2 But Not Cdk2 Activity. *J Biol Chem* (1997) 272 (35):22300–6. doi: 10.1074/jbc.272.35.22300
22. McGowan CH, Russell P. Cell Cycle Regulation of Human WEE1. *EMBO J* (1995) 14(10):2166–75. doi: 10.1002/j.1460-2075.1995.tb07210.x
23. Do K, Doroshow JH, Kummar S. Wee1 Kinase as a Target for Cancer Therapy. *Cell Cycle* (2013) 12(19):3159–64. doi: 10.4161/cc.26062
24. Donzelli M, Draetta GF. Regulating Mammalian Checkpoints Through Cdc25 Inactivation. *EMBO Rep* (2003) 4(7):671–7. doi: 10.1038/sj.embor.embor887
25. Lindqvist A, Rodriguez-Bravo V, Medema RH. The Decision to Enter Mitosis: Feedback and Redundancy in the Mitotic Entry Network. *J Cell Biol* (2009) 185(2):193–202. doi: 10.1083/jcb.200812045
26. Labib K. How do Cdc7 and Cyclin-Dependent Kinases Trigger the Initiation of Chromosome Replication in Eukaryotic Cells? *Genes Dev* (2010) 24 (12):1208–19. doi: 10.1101/gad.1933010
27. Heller RC, Kang S, Lam WM, Chen S, Chan CS, Bell SP. Eukaryotic Origin-Dependent DNA Replication *In Vitro* Reveals Sequential Action of DDK and S-CDK Kinases. *Cell* (2011) 146(1):80–91. doi: 10.1016/j.cell.2011.06.012
28. Beck H, Nahse V, Larsen MS, Groth P, Clancy T, Lees M, et al. Regulators of Cyclin-Dependent Kinases Are Crucial for Maintaining Genome Integrity in S Phase. *J Cell Biol* (2010) 188(5):629–38. doi: 10.1083/jcb.200905059
29. Dominguez-Kelly R, Martin Y, Koundrioukoff S, Tanenbaum ME, Smits VA, Medema RH, et al. Wee1 Controls Genomic Stability During Replication by Regulating the Mus81-Eme1 Endonuclease. *J Cell Biol* (2011) 194(4):567–79. doi: 10.1083/jcb.201101047
30. Aranza-Martinez A, Sanchez-Perez J, Brito-Elias L, Lopez-Camarillo C, Cantu de Leon D, Perez-Plasencia C, et al. Non-Coding RNAs Associated With Radioresistance in Triple-Negative Breast Cancer. *Front Oncol* (2021) 11:752270. doi: 10.3389/fonc.2021.752270
31. Iorns E, Lord CJ, Grigoriadis A, McDonald S, Fenwick K, Mackay A, et al. Integrated Functional, Gene Expression and Genomic Analysis for the Identification of Cancer Targets. *PloS One* (2009) 4(4):e5120. doi: 10.1371/journal.pone.0005120
32. Murrow LM, Lord CJ, Grigoriadis A, McDonald S, Fenwick K, Mackay A. Identification of WEE1 as a Potential Molecular Target in Cancer Cells by RNAi Screening of the Human Tyrosine Kinome. *Breast Cancer Res Treat* (2010) 122(2):347–57. doi: 10.1007/s10549-009-0571-2
33. Mir SE, De Witt Hamer PC, Krawczyk PM, Balaj L, Claes A, Niers JM, et al. *In Silico* Analysis of Kinase Expression Identifies WEE1 as a Gatekeeper Against Mitotic Catastrophe in Glioblastoma. *Cancer Cell* (2010) 18(3):244–57. doi: 10.1016/j.ccr.2010.08.011
34. Magnussen GI, Holm R, Emilsen E, Rosnes AK, Slipicevic A, Florenes VA. High Expression of Wee1 is Associated With Poor Disease-Free Survival in Malignant Melanoma: Potential for Targeted Therapy. *PloS One* (2012) 7(6): e38254. doi: 10.1371/journal.pone.0038254
35. Tibes R, Bogenberger JM, Chaudhuri L, Hagelstrom RT, Chow D, Buechel ME, et al. RNAi Screening of the Kinome With Cytarabine in Leukemias. *Blood* (2012) 119(12):2863–72. doi: 10.1182/blood-2011-07-367557
36. Porter CC, Kim J, Fosmire S, Gearheart CM, van Linden A, Baturin D, et al. Integrated Genomic Analyses Identify WEE1 as a Critical Mediator of Cell Fate and a Novel Therapeutic Target in Acute Myeloid Leukemia. *Leukemia* (2012) 26(6):1266–76. doi: 10.1038/leu.2011.392
37. PosthumaDeBoer J, Wurdinger T, Graat HC, van Beusechem VW, Helder MN, van Royen BJ, et al. WEE1 Inhibition Sensitizes Osteosarcoma to Radiotherapy. *BMC Cancer* (2011) 11:156. doi: 10.1186/1471-2407-11-156
38. Magnussen GI, Hellesylt E, Nesland JM, Trope CG, Florenes VA, Holm R. High Expression of Wee1 Is Associated With Malignancy in Vulvar Squamous Cell Carcinoma Patients. *BMC Cancer* (2013) 13:288. doi: 10.1186/1471-2407-13-288
39. Hirai H, Iwasawa Y, Okada M, Arai T, Nishibata T, Kobayashi M, et al. Small-Molecule Inhibition of Wee1 Kinase by MK-1775 Selectively Sensitizes P53-Deficient Tumor Cells to DNA-Damaging Agents. *Mol Cancer Ther* (2009) 8(11):2992–3000. doi: 10.1158/1535-7163.MCT-09-0463

40. Leijen S, van Geel RM, Pavlick AC, Tibes R, Rosen L, Razak AR, et al. Phase I Study Evaluating WEE1 Inhibitor AZD1775 As Monotherapy and in Combination With Gemcitabine, Cisplatin, or Carboplatin in Patients With Advanced Solid Tumors. *J Clin Oncol* (2016) 34(36):4371–80. doi: 10.1200/JCO.2016.67.5991
41. Sanai N, Li J, Boerner J, Stark K, Wu J, Kim S, et al. Phase 0 Trial of AZD1775 in First-Recurrence Glioblastoma Patients. *Clin Cancer Res* (2018) 24(16):3820–8. doi: 10.1158/1078-0432.CCR-17-3348
42. Do K, Wilsker D, Ji J, Zlott J, Freshwater T, Kinders RJ, et al. Phase I Study of Single-Agent AZD1775 (MK-1775), a Wee1 Kinase Inhibitor, in Patients With Refractory Solid Tumors. *J Clin Oncol* (2015) 33(30):3409–15. doi: 10.1200/JCO.2014.60.4009
43. Leijen S, van Geel RM, Sonke GS, de Jong D, Rosenberg EH, Marchetti S, et al. Phase II Study of WEE1 Inhibitor AZD1775 Plus Carboplatin in Patients With TP53-Mutated Ovarian Cancer Refractory or Resistant to First-Line Therapy Within 3 Months. *J Clin Oncol* (2016) 34(36):4354–61. doi: 10.1200/JCO.2016.67.5942
44. Mendez E, Rodriguez CP, Kao MC, Raju S, Diab A, Harbison RA, et al. A Phase I Clinical Trial of AZD1775 in Combination With Neoadjuvant Weekly Docetaxel and Cisplatin Before Definitive Therapy in Head and Neck Squamous Cell Carcinoma. *Clin Cancer Res* (2018) 24(12):2740–8. doi: 10.1158/1078-0432.CCR-17-3796
45. Galluzzi L, Vitale I, Aaronson SA, Abrams JM, Adam D, Agostinis P, et al. Molecular Mechanisms of Cell Death: Recommendations of the Nomenclature Committee on Cell Death 2018. *Cell Death Differ* (2018) 25 (3):486–541. doi: 10.1038/s41418-017-0012-4
46. Vakifahmetoglu H, Olsson M, Zhivotovsky B. Death Through a Tragedy: Mitotic Catastrophe. *Cell Death Differ* (2008) 15(7):1153–62. doi: 10.1038/cdd.2008.47
47. Vitale I, Galluzzi L, Castedo M, Kroemer G. Mitotic Catastrophe: A Mechanism for Avoiding Genomic Instability. *Nat Rev Mol Cell Biol* (2011) 12(6):385–92. doi: 10.1038/nrm3115
48. Galluzzi L, Vitale I, Abrams JM, Alnemri ES, Baehrecke EH, Blagosklonny MV, et al. Molecular Definitions of Cell Death Subroutines: Recommendations of the Nomenclature Committee on Cell Death 2012. *Cell Death Differ* (2012) 19(1):107–20. doi: 10.1038/cdd.2011.96
49. Duda H, Arter M, Gloggnitzer J, Teloni F, Wild P, Blanco MG, et al. A Mechanism for Controlled Breakage of Under-Replicated Chromosomes During Mitosis. *Dev Cell* (2016) 39(6):740–55. doi: 10.1016/j.devcel.2016.11.017
50. Szmyd R, Niska-Blakie J, Diril MK, Renck Nunes P, Tzelepis K, Lacroix A, et al. Premature Activation of Cdk1 Leads to Mitotic Events in S Phase and Embryonic Lethality. *Oncogene* (2019) 38(7):998–1018. doi: 10.1038/s41388-018-0464-0
51. Tominaga Y, Li C, Wang RH, Deng CX. Murine Wee1 Plays a Critical Role in Cell Cycle Regulation and Pre-Implantation Stages of Embryonic Development. *Int J Biol Sci* (2006) 2(4):161–70. doi: 10.7150/ijbs.2.161
52. De Witt Hamer PC, Mir SE, Noske D, Van Noorden CJ, Wurdinger T. WEE1 Kinase Targeting Combined With DNA-Damaging Cancer Therapy Catalyzes Mitotic Catastrophe. *Clin Cancer Res* (2011) 17(13):4200–7. doi: 10.1158/1078-0432.CCR-10-2537
53. Lewis CW, Jin Z, Macdonald D, Wei W, Qian XJ, Choi WS, et al. Prolonged Mitotic Arrest Induced by Wee1 Inhibition Sensitizes Breast Cancer Cells to Paclitaxel. *Oncotarget* (2017) 8(43):73705–22. doi: 10.18632/oncotarget.17848
54. Mak JP, Man WY, Chow JP, Ma HT, Poon RY. Pharmacological Inactivation of CHK1 and WEE1 Induces Mitotic Catastrophe in Nasopharyngeal Carcinoma Cells. *Oncotarget* (2015) 6(25):21074–84. doi: 10.18632/oncotarget.4020
55. Bridges KA, Hirai H, Buser CA, Brooks C, Liu H, Buchholz TA, et al. MK-1775, a Novel Wee1 Kinase Inhibitor, Radiosensitizes P53-Defective Human Tumor Cells. *Clin Cancer Res* (2011) 17(17):5638–48. doi: 10.1158/1078-0432.CCR-11-0650
56. Chow JP, Poon RY. The CDK1 Inhibitory Kinase MYT1 in DNA Damage Checkpoint Recovery. *Oncogene* (2013) 32(40):4778–88. doi: 10.1038/onc.2012.504
57. Alexander JL, Orr-Weaver TL. Replication Fork Instability and the Consequences of Fork Collisions From Rereplication. *Genes Dev* (2016) 30 (20):2241–52. doi: 10.1101/gad.288142.116
58. Beck H, Nahse-Kumpf V, Larsen MS, O'Hanlon KA, Patzke S, Holmberg C, et al. Cyclin-Dependent Kinase Suppression by WEE1 Kinase Protects the Genome Through Control of Replication Initiation and Nucleotide Consumption. *Mol Cell Biol* (2012) 32(20):4226–36. doi: 10.1128/MCB.00412-12
59. Hauge S, Naucke C, Hasvold G, Joel M, Rodland GE, Juzenas P, et al. Combined Inhibition of Wee1 and Chk1 Gives Synergistic DNA Damage in S-Phase Due to Distinct Regulation of CDK Activity and CDC45 Loading. *Oncotarget* (2017) 8(7):10966–79. doi: 10.18632/oncotarget.14089
60. Pfister SX, Markkanen E, Jiang Y, Sarkar S, Woodcock M, Orlando G, et al. Inhibiting WEE1 Selectively Kills Histone H3K36me3-Deficient Cancers by dNTP Starvation. *Cancer Cell* (2015) 28(5):557–68. doi: 10.1016/j.ccell.2015.09.015
61. Langan TA, Gautier J, Lohka M, Hollingsworth R, Moreno S, Nurse P, et al. Mammalian Growth-Associated H1 Histone Kinase: A Homolog of Cdc2 +/CDC28 Protein Kinases Controlling Mitotic Entry in Yeast and Frog Cells. *Mol Cell Biol* (1989) 9(9):3860–8. doi: 10.1128/mcb.9.9.3860-3868.1989
62. Peter M, Nakagawa J, Doree M, Labbe JC, Nigg EA, et al. *In Vitro* Disassembly of the Nuclear Lamina and M Phase-Specific Phosphorylation of Lamins by Cdc2 Kinase. *Cell* (1990) 61(4):591–602. doi: 10.1016/0092-8674(90)90471-P
63. Seibert M, Kruger M, Watson NA, Sen O, Daum JR, Slotman JA, et al. CDK1-Mediated Phosphorylation at H2B Serine 6 Is Required for Mitotic Chromosome Segregation. *J Cell Biol* (2019) 218(4):1164–81. doi: 10.1083/jcb.201806057
64. Beeharry N, Rattner JB, Caviston JP, Yen T. Centromere Fragmentation Is a Common Mitotic Defect of S and G2 Checkpoint Override. *Cell Cycle* (2013) 12(10):1588–97. doi: 10.4161/cc.24740
65. El Achkar E, Gerbault-Seureau M, Muleris M, Dutrillaux B, Debatisse M. Premature Condensation Induces Breaks at the Interface of Early and Late Replicating Chromosome Bands Bearing Common Fragile Sites. *Proc Natl Acad Sci USA* (2005) 102(50):18069–74. doi: 10.1073/pnas.0506497102
66. Madan K, Allen JW, Gerald PS, Latt SA. Fluorescence Analysis of Late DNA Replication in Mouse Metaphase Chromosomes Using BUdR and 33258 Hoechst. *Exp Cell Res* (1976) 99(2):438–44. doi: 10.1016/0014-4827(76)90604-2
67. Kubara PM, Kerneis-Golsteyn S, Studeny A, Lanser BB, Meijer L, Golsteyn RM. Human Cells Enter Mitosis With Damaged DNA After Treatment With Pharmacological Concentrations of Genotoxic Agents. *Biochem J* (2012) 446 (3):373–81. doi: 10.1042/BJ20120385
68. Verma N, Franchitto M, Zonfrilli A, Cialfi S, Palermo R, Talora C. DNA Damage Stress: Cui Prodest? *Int J Mol Sci* (2019) 20(5):1073. doi: 10.3390/ijms20051073
69. van Vugt MA, Bras A, Medema RH. Polo-Like Kinase-1 Controls Recovery From a G2 DNA Damage-Induced Arrest in Mammalian Cells. *Mol Cell* (2004) 15(5):799–811. doi: 10.1016/j.molcel.2004.07.015
70. Watanabe N, Arai H, Nishihara Y, Taniguchi M, Watanabe N, Hunter T, et al. M-Phase Kinases Induce Phospho-Dependent Ubiquitination of Somatic Wee1 by SCFbeta-TrCP. *Proc Natl Acad Sci USA* (2004) 101 (13):4419–24. doi: 10.1073/pnas.0307700101
71. Bukhari AB, Lewis CW, Pearce JJ, Luong D, Chan GK, Gamper AM. Inhibiting Wee1 and ATR Kinases Produces Tumor-Selective Synthetic Lethality and Suppresses Metastasis. *J Clin Invest* (2019) 129(3):1329–44. doi: 10.1172/JCI122622
72. Aarts M, Sharpe R, Garcia-Murillas I, Gevensleben H, Hurd MS, Shumway SD, et al. Forced Mitotic Entry of S-Phase Cells as a Therapeutic Strategy Induced by Inhibition of WEE1. *Cancer Discov* (2012) 2(6):524–39. doi: 10.1158/2159-8290.CD-11-0320
73. Hirai H, Arai T, Okada M, Nishibata T, Kobayashi M, Sakai N, et al. MK-1775, a Small Molecule Wee1 Inhibitor, Enhances Anti-Tumor Efficacy of Various DNA-Damaging Agents, Including 5-Fluorouracil. *Cancer Biol Ther* (2010) 9(7):514–22. doi: 10.4161/cbt.9.7.11115
74. Zheng H, Shao F, Martin S, Xu X, Deng CX. WEE1 Inhibition Targets Cell Cycle Checkpoints for Triple Negative Breast Cancers to Overcome Cisplatin Resistance. *Sci Rep* (2017) 7:43517. doi: 10.1038/srep43517
75. Rajeshkumar NV, De Oliveira E, Ottenhof N, Watters J, Brooks D, Demuth T, et al. MK-1775, a Potent Wee1 Inhibitor, Synergizes With Gemcitabine to Achieve Tumor Regressions, Selectively in P53-Deficient Pancreatic Cancer

Xenografts. *Clin Cancer Res* (2011) 17(9):2799–806. doi: 10.1158/1078-0432.CCR-10-2580
76. Van Linden AA, Baturin D, Ford JB, Fosmire SP, Gardner L, Korch C, et al. Inhibition of Wee1 Sensitizes Cancer Cells to Antimetabolite Chemotherapeutics *In Vitro* and *In Vivo*, Independent of P53 Functionality. *Mol Cancer Ther* (2013) 12(12):2675–84. doi: 10.1158/1535-7163.MCT-13-0424
77. Harris PS, Venkataraman S, Alimova I, Birks DK, Balakrishnan I, Cristiano B, et al. Integrated Genomic Analysis Identifies the Mitotic Checkpoint Kinase WEE1 as a Novel Therapeutic Target in Medulloblastoma. *Mol Cancer* (2014) 13:72. doi: 10.1186/1476-4598-13-72
78. Kreahling JM, Gemmer JY, Reed D, Letson D, Bui M. MK1775, a Selective Wee1 Inhibitor, Shows Single-Agent Antitumor Activity Against Sarcoma Cells. *Mol Cancer Ther* (2012) 11(1):174–82. doi: 10.1158/1535-7163.MCT-11-0529
79. Takebe N, Naqash AR, O'Sullivan Coyne G, Kummar S, Do K, Bruns A, et al. Safety, Antitumor Activity, and Biomarker Analysis in a Phase I Trial of the Once-Daily Wee1 Inhibitor Adavosertib (AZD1775) in Patients With Advanced Solid Tumors. *Clin Cancer Res* (2021) 27(14):3834–44. doi: 10.1158/1078-0432.CCR-21-0329
80. Huang PQ, Boren BC, Hegde SG, Liu H, Unni AK, Abraham S, et al. Discovery of ZN-C3, a Highly Potent and Selective Wee1 Inhibitor Undergoing Evaluation in Clinical Trials for the Treatment of Cancer. *J Med Chem* (2021) 64(17):13004–24. doi: 10.1021/acs.jmedchem.1c01121
81. Tolcher A, Mamdani H, Chalasani P, Meric-Bernstam F, Gazdoiu M, Makris L, et al. Abstract CT016: Clinical Activity of Single-Agent ZN-C3, an Oral WEE1 Inhibitor, in a Phase 1 Dose-Escalation Trial in Patients With Advanced Solid Tumors. *Cancer Res* (2021) 81(13 Supplement):CT016. doi: 10.1158/1538-7445.AM2021-CT016
82. Li J, Boren B, Huang PQ, Bunker KD, Doñate F, Samatar AA. Abstract 1965: Discovery of ZN-C3, a Potent Wee-1 Inhibitor With a Differentiated Pharmacologic and Kinase Selectivity Profile. *Cancer Res* (2021) 81(13 Supplement):1965. doi: 10.1158/1538-7445.AM2021-1965
83. Wang Y, Li J, Booher RN, Kraker A, Lawrence T, Leopold WR, et al. Radiosensitization of P53 Mutant Cells by PD0166285, a Novel G(2) Checkpoint Abrogator. *Cancer Res* (2001) 61(22):8211–7.
84. Gill SJ, Wijnhoven PWG, Fok JHL, Lloyd RL, Cairns J, Armenia J, et al. Radiopotentiation Profiling of Multiple Inhibitors of the DNA Damage Response for Early Clinical Development. *Mol Cancer Ther* (2021) 20 (9):1614–26. doi: 10.1158/1535-7163.MCT-20-0502
85. Yang L, Shen C, Pettit CJ, Li T, Hu AJ, Miller ED, et al. Wee1 Kinase Inhibitor AZD1775 Effectively Sensitizes Esophageal Cancer to Radiotherapy. *Clin Cancer Res* (2020) 26(14):3740–50. doi: 10.1158/1078-0432.CCR-19-3373
86. Lee YY, Cho YJ, Shin SW, Choi C, Ryu JY, Jeon HK, et al. Anti-Tumor Effects of Wee1 Kinase Inhibitor With Radiotherapy in Human Cervical Cancer. *Sci Rep* (2019) 9(1):15394. doi: 10.1038/s41598-019-51959-3
87. Parsels LA, Karnak D, Parsels JD, Zhang Q, Velez-Padilla J, Reichert ZR, et al. PARP1 Trapping and DNA Replication Stress Enhance Radiosensitization With Combined WEE1 and PARP Inhibitors. *Mol Cancer Res* (2018) 16(2):222–32. doi: 10.1158/1541-7786.MCR-17-0455
88. Richer AL, Cala JM, O'Brien K, Carson VM, Inge LJ, Whitsett TG. WEE1 Kinase Inhibitor AZD1775 Has Preclinical Efficacy in LKB1-Deficient Non-Small Cell Lung Cancer. *Cancer Res* (2017) 77(17):4663–72. doi: 10.1158/0008-5472.CAN-16-3565
89. Cuneo KC, Morgan MA, Davis MA, Parcels LA, Parcels J, Karnak D, et al. Wee1 Kinase Inhibitor AZD1775 Radiosensitizes Hepatocellular Carcinoma Regardless of TP53 Mutational Status Through Induction of Replication Stress. *Int J Radiat Oncol Biol Phys* (2016) 95(2):782–90. doi: 10.1016/j.ijrobp.2016.01.028
90. Mueller S, Hashizume R, Yang X, Kolkowitz I, Olow AK, Phillips J, et al. Targeting Wee1 for the Treatment of Pediatric High-Grade Gliomas. *Neuro Oncol* (2014) 16(3):352–60. doi: 10.1093/neuonc/not220
91. Caretti V, Hiddingh L, Lagerweij T, Schellen P, Koken PW, Hulleman E, et al. WEE1 Kinase Inhibition Enhances the Radiation Response of Diffuse Intrinsic Pontine Gliomas. *Mol Cancer Ther* (2013) 12(2):141–50. doi: 10.1158/1535-7163.MCT-12-0735
92. Sarcar B, Kahali S, Prabhu AH, Shumway SD, Xu Y, Demuth T, et al. Targeting Radiation-Induced G(2) Checkpoint Activation With the Wee-1 Inhibitor MK-1775 in Glioblastoma Cell Lines. *Mol Cancer Ther* (2011) 10 (12):2405–14. doi: 10.1158/1535-7163.MCT-11-0469
93. Suzuki M, Anko M, Ohara M, Matsumoto KI, Hasegawa S, et al. Radiation-Induced Autophagy in Human Pancreatic Cancer Cells Is Critically Dependent on G2 Checkpoint Activation: A Mechanism of Radioresistance in Pancreatic Cancer. *Int J Radiat Oncol Biol Phys* (2021) 111(1):260–71. doi: 10.1016/j.ijrobp.2021.04.001
94. Cuneo KC, Morgan MA, Sahai V, Schipper MJ, Parsels LA, Parsels JD, et al. Dose Escalation Trial of the Wee1 Inhibitor Adavosertib (AZD1775) in Combination With Gemcitabine and Radiation for Patients With Locally Advanced Pancreatic Cancer. *J Clin Oncol* (2019) 37(29):2643–50. doi: 10.1200/JCO.19.00730
95. Chera BS, Sheth SH, Patel SA, Goldin D, Douglas KE, Green RL, et al. Phase 1 Trial of Adavosertib (AZD1775) in Combination With Concurrent Radiation and Cisplatin for Intermediate-Risk and High-Risk Head and Neck Squamous Cell Carcinoma. *Cancer* (2021) 37(29):2643–50. doi: 10.1002/cncr.33789
96. Chen X, Low KH, Alexander A, Jiang Y, Karakas C, Hess KR, et al. Cyclin E Overexpression Sensitizes Triple-Negative Breast Cancer to Wee1 Kinase Inhibition. *Clin Cancer Res* (2018) 24(24):6594–610. doi: 10.1158/1078-0432.CCR-18-1446
97. Krajewska M, Heijink AM, Bisselink YJ, Seinstra RI, Sillje HH, de Vries EG, et al. Forced Activation of Cdk1 *via* Wee1 Inhibition Impairs Homologous Recombination. *Oncogene* (2013) 32(24):3001–8. doi: 10.1038/onc.2012.296
98. Liu L, Michowski W, Kolodziejczyk A, Sicinski P. The Cell Cycle in Stem Cell Proliferation, Pluripotency and Differentiation. *Nat Cell Biol* (2019) 21 (9):1060–7. doi: 10.1038/s41556-019-0384-4
99. McBride WH, Schaue D. Radiation-Induced Tissue Damage and Response. *J?Pathol* (2020) 250(5):647–55. doi: 10.1002/path.5389
100. Bryant HE, Schultz N, Thomas HD, Parker KM, Flower D, Lopez E, et al. Specific Killing of BRCA2-Deficient Tumours With Inhibitors of Poly(ADP-Ribose) Polymerase. *Nature* (2005) 434(7035):913–7. doi: 10.1038/nature03443
101. Farmer H, McCabe N, Lord CJ, Tutt AN, Johnson DA, Richardson TB, et al. Targeting the DNA Repair Defect in BRCA Mutant Cells as a Therapeutic Strategy. *Nature* (2005) 434(7035):917–21. doi: 10.1038/nature03445
102. Jette NR, Kumar M, Radhamani S, Arthur G, Goutam S, Yip S, et al. ATM-Deficient Cancers Provide New Opportunities for Precision Oncology. *Cancers (Basel)* (2020) 12(3):917–21. doi: 10.3390/cancers12030687
103. Jamal-Hanjani M, Wilson GA, McGranahan N, Birkbak NJ, Watkins TBK, Veeriah S, et al. Tracking the Evolution of Non-Small-Cell Lung Cancer. *N Engl J Med* (2017) 376(22):2109–21. doi: 10.1056/NEJMoa1616288
104. Jette NR, Radhamani S, Arthur G, Ye R, Goutam S, Bolyos A, et al. Combined Poly-ADP Ribose Polymerase and Ataxia-Telangiectasia Mutated/Rad3-Related Inhibition Targets Ataxia-Telangiectasia Mutated-Deficient Lung Cancer Cells. *Br J Cancer* (2019) 121(7):600–10. doi: 10.1038/s41416-019-0565-8
105. Fugger K, Hewitt G, West SC, Boulton SJ. Tackling PARP Inhibitor Resistance. *Trends Cancer* (2021) 7(12):1102–18. doi: 10.1016/j.trecan.2021.08.007
106. O'Neil NJ, Bailey ML, Hieter P. Synthetic Lethality and Cancer. *Nat Rev Genet* (2017) 18(10):613–23. doi: 10.1038/nrg.2017.47
107. Lecona E, Fernandez-Capetillo O. Replication Stress and Cancer: It Takes Two to Tango. *Exp Cell Res* (2014) 329(1):26–34. doi: 10.1016/j.yexcr.2014.09.019
108. Halazonetis TD, Gorgoulis VG, Bartek J. An Oncogene-Induced DNA Damage Model for Cancer Development. *Science* (2008) 319(5868):1352–5. doi: 10.1126/science.1140735
109. Brown EJ, Baltimore D. ATR Disruption Leads to Chromosomal Fragmentation and Early Embryonic Lethality. *Genes Dev* (2000) 14 (4):397–402. doi: 10.1101/gad.14.4.397
110. de Klein A, Muijtjens M, van Os R, Verhoeven Y, Smit B, Carr AM, et al. Targeted Disruption of the Cell-Cycle Checkpoint Gene ATR Leads to Early Embryonic Lethality in Mice. *Curr Biol* (2000) 10(8):479–82. doi: 10.1016/S0960-9822(00)00447-4

111. Parikh RA, Appleman LJ, Bauman JE, Sankunny M, Lewis DW, Vlad A, et al. Upregulation of the ATR-CHEK1 Pathway in Oral Squamous Cell Carcinomas. *Genes Chromosomes Cancer* (2014) 53(1):25–37. doi: 10.1002/gcc.22115
112. Abdel-Fatah TM, Middleton FK, Arora A, Agarwal D, Chen T, Moseley PM, et al. Untangling the ATR-CHEK1 Network for Prognostication, Prediction and Therapeutic Target Validation in Breast Cancer. *Mol Oncol* (2015) 9 (3):569–85. doi: 10.1016/j.molonc.2014.10.013
113. Bao S, Wu Q, McLendon RE, Hao Y, Shi Q, Hjelmeland AB, et al. Glioma Stem Cells Promote Radioresistance by Preferential Activation of the DNA Damage Response. *Nature* (2006) 444(7120):756–60. doi: 10.1038/nature05236
114. Sorensen CS, Syljuasen RG. Safeguarding Genome Integrity: The Checkpoint Kinases ATR, CHK1 and WEE1 Restrain CDK Activity During Normal DNA Replication. *Nucleic Acids Res* (2012) 40(2):477–86. doi: 10.1093/nar/gkr697
115. Jin J, Fang H, Yang F, Ji W, Guan N, Sun Z, et al. Combined Inhibition of ATR and WEE1 as a Novel Therapeutic Strategy in Triple-Negative Breast Cancer. *Neoplasia* (2018) 20(5):478–88. doi: 10.1016/j.neo.2018.03.003
116. Moiseeva TN, Qian C, Sugitani N, Osmanbeyoglu HU, Bakkenist CJ. WEE1 Kinase Inhibitor AZD1775 Induces CDK1 Kinase-Dependent Origin Firing in Unperturbed G1- and S-Phase Cells. *Proc Natl Acad Sci USA* (2019) 116 (48):23891–3. doi: 10.1073/pnas.1915108116
117. Simoneau A, Zou L. An Extending ATR-CHK1 Circuitry: The Replication Stress Response and Beyond. *Curr Opin Genet Dev* (2021) 71:92–8. doi: 10.1016/j.gde.2021.07.003
118. Kibe T, Zimmermann M, de Lange T. TPP1 Blocks an ATR-Mediated Resection Mechanism at Telomeres. *Mol Cell* (2016) 61(2):236–46. doi: 10.1016/j.molcel.2015.12.016
119. Buisson R, Niraj J, Rodrigue A, Ho CK, Kreuzer J, Foo TK, et al. Coupling of Homologous Recombination and the Checkpoint by ATR. *Mol Cell* (2017) 65(2):336–46. doi: 10.1016/j.molcel.2016.12.007
120. Toledo LI, Altmeyer M, Rask MB, Lukas C, Larsen DH, Povlsen LK, et al. ATR Prohibits Replication Catastrophe by Preventing Global Exhaustion of RPA. *Cell* (2013) 155(5):1088–103. doi: 10.1016/j.cell.2013.10.043
121. Brunner A, Suryo Rahmanto A, Johansson H, Franco M, Viiliainen J, Gazi M, et al. PTEN and DNA-PK Determine Sensitivity and Recovery in Response to WEE1 Inhibition in Human Breast Cancer. *Elife* (2020) 9:1088–103. doi: 10.7554/eLife.57894
122. He J, Kang X, Yin Y, Chao KS, Shen. WH. PTEN Regulates DNA Replication Progression and Stalled Fork Recovery. *Nat Commun* (2015) 6:7620. doi: 10.1038/ncomms8620
123. Wang G, Li Y, Wang P, Liang H, Cui M, Zhu M, et al. PTEN Regulates RPA1 and Protects DNA Replication Forks. *Cell Res* (2015) 25(11):1189–204. doi: 10.1038/cr.2015.115
124. Feng J, Liang J, Li J, Li Y, Liang H, Zhao X, et al. PTEN Controls the DNA Replication Process Through MCM2 in Response to Replicative Stress. *Cell Rep* (2015) 13(7):1295–303. doi: 10.1016/j.celrep.2015.10.016
125. Diab A, Gem H, Swanger J, Kim HY, Smith K, Zou G, et al. FOXM1 Drives HPV+ HNSCC Sensitivity to WEE1 Inhibition. *Proc Natl Acad Sci USA* (2020) 117(45):28287–96. doi: 10.1073/pnas.2013921117
126. Alvarez-Fernandez M, Medema RH. Novel Functions of FoxM1: From Molecular Mechanisms to Cancer Therapy. *Front Oncol* (2013) 3:30. doi: 10.3389/fonc.2013.00030
127. Heijink AM, Blomen VA, Bisteau X, Degener F, Matsushita FY, Kaldis P, et al. A Haploid Genetic Screen Identifies the G1/S Regulatory Machinery as a Determinant of Wee1 Inhibitor Sensitivity. *Proc Natl Acad Sci USA* (2015) 112(49):15160–5. doi: 10.1073/pnas.1505283112
128. Aarts M, Bajrami I, Herrera-Abreu MT, Elliott R, Brough R, Ashworth A, et al. Functional Genetic Screen Identifies Increased Sensitivity to WEE1 Inhibition in Cells With Defects in Fanconi Anemia and HR Pathways. *Mol Cancer Ther* (2015) 14(4):865–76. doi: 10.1158/1535-7163.MCT-14-0845
129. Francis AM, Alexander A, Liu Y, Vijayaraghavan S, Low KH, Yang D, et al. CDK4/6 Inhibitors Sensitize Rb-Positive Sarcoma Cells to Wee1 Kinase Inhibition Through Reversible Cell-Cycle Arrest. *Mol Cancer Ther* (2017) 16 (9):1751–64. doi: 10.1158/1535-7163.MCT-17-0040
130. Fallah Y, Demas DM, Jin L, He W, Shajahan-Haq AN. Targeting WEE1 Inhibits Growth of Breast Cancer Cells That Are Resistant to Endocrine Therapy and CDK4/6 Inhibitors. *Front Oncol* (2021) 11:681530. doi: 10.3389/fonc.2021.681530
131. Lamballe F, Ahmad F, Vinik Y, Castellanet O, Daian F, Muller AK, et al. Modeling Heterogeneity of Triple-Negative Breast Cancer Uncovers a Novel Combinatorial Treatment Overcoming Primary Drug Resistance. *Adv Sci (Weinh)* (2021) 8(3):2003049. doi: 10.1002/advs.202003049
132. Tao ZF, Hasvold L, Wang L, Wang X, Petros AM, Park CH, et al. Discovery of a Potent and Selective BCL-XL Inhibitor With *in Vivo* Activity. *ACS Med Chem Lett* (2014) 5(10):1088–93. doi: 10.1021/ml5001867
133. Ha DH, Min A, Kim S, Jang H, Kim SH, Kim HJ, et al. Antitumor Effect of a WEE1 Inhibitor and Potentiation of Olaparib Sensitivity by DNA Damage Response Modulation in Triple-Negative Breast Cancer. *Sci Rep* (2020) 10 (1):9930. doi: 10.1038/s41598-020-66018-5
134. Ayeni JO, Varadarajan R, Mukherjee O, Stuart DT, Sprenger F, Srayko M, et al. Dual Phosphorylation of Cdk1 Coordinates Cell Proliferation With Key Developmental Processes in Drosophila. *Genetics* (2014) 196(1):197–210. doi: 10.1534/genetics.113.156281
135. Okumura E, Fukuhara T, Yoshida H, Hanada Si S, Kozutsumi R, Mori M, et al. Akt Inhibits Myt1 in the Signalling Pathway That Leads to Meiotic G2/M-Phase Transition. *Nat Cell Biol* (2002) 4(2):111–6. doi: 10.1038/ncb741
136. Palmer A, Gavin AC, Nebreda AR. A Link Between MAP Kinase and P34 (Cdc2)/Cyclin B During Oocyte Maturation: P90(Rsk) Phosphorylates and Inactivates the P34(Cdc2) Inhibitory Kinase Myt1. *EMBO J* (1998) 17 (17):5037–47. doi: 10.1093/emboj/17.17.5037
137. Coulonval K, Kooken H, Roger PP. Coupling of T161 and T14 Phosphorylations Protects Cyclin B-CDK1 From Premature Activation. *Mol Biol Cell* (2011) 22(21):3971–85. doi: 10.1091/mbc.e11-02-0136
138. Nakajima H, Yonemura S, Murata M, Nakamura N, Piwnica-Worms H, Nishida E. Myt1 Protein Kinase Is Essential for Golgi and ER Assembly During Mitotic Exit. *J Cell Biol* (2008) 181(1):89–103. doi: 10.1083/jcb.200708176
139. Wells NJ, Watanabe N, Tokusumi T, Jiang W, Verdecia MA, Hunter T. The C-Terminal Domain of the Cdc2 Inhibitory Kinase Myt1 Interacts With Cdc2 Complexes and Is Required for Inhibition of G(2)/M Progression. *J Cell Sci* (1999) 112(Pt 19):3361–71. doi: 10.1242/jcs.112.19.3361
140. Guertin AD, Li J, Liu Y, Hurd MS, Schuller AG, Long B, et al. Preclinical Evaluation of the WEE1 Inhibitor MK-1775 as Single-Agent Anticancer Therapy. *Mol Cancer Ther* (2013) 12(8):1442–52. doi: 10.1158/1535-7163.MCT-13-0025
141. Toledo CM, Ding Y, Hoellerbauer P, Davis RJ, Basom R, Girard EJ, et al. Genome-Wide CRISPR-Cas9 Screens Reveal Loss of Redundancy Between PKMYT1 and WEE1 in Glioblastoma Stem-Like Cells. *Cell Rep* (2015) 13 (11):2425–39. doi: 10.1016/j.celrep.2015.11.021
142. Pattabiraman DR, Weinberg RA. Tackling the Cancer Stem Cells - What Challenges do They Pose? *Nat Rev Drug Discov* (2014) 13(7):497–512. doi: 10.1038/nrd4253
143. Ronco C, Martin AR, Demange L, Benhida. R. ATM, ATR, CHK1, CHK2 and WEE1 Inhibitors in Cancer and Cancer Stem Cells. *Medchemcomm* (2017) 8(2):295–319. doi: 10.1039/C6MD00439C
144. Sand A, Piacsek M, Donohoe DL, Duffin AT, Riddell GT, Sun C, et al. WEE1 Inhibitor, AZD1775, Overcomes Trastuzumab Resistance by Targeting Cancer Stem-Like Properties in HER2-Positive Breast Cancer. *Cancer Lett* (2020) 472:119–31. doi: 10.1016/j.canlet.2019.12.023
145. Kirchgessner CU, Patil CK, Evans JW, Cuomo CA, Fried LM, Carter T, et al. DNA-Dependent Kinase (P350) as a Candidate Gene for the Murine SCID Defect. *Science* (1995) 267(5201):1178–83. doi: 10.1126/science.7855601
146. Lees-Miller SP, Godbout R, Chan DW, Weinfeld M, Day RS 3rd, Barron GM, et al. Absence of P350 Subunit of DNA-Activated Protein Kinase From a Radiosensitive Human Cell Line. *Science* (1995) 267(5201):1183–5. doi: 10.1126/science.7855602
147. Decout A, Katz JD, Venkatraman S, Ablasser A. The cGAS-STING Pathway as a Therapeutic Target in Inflammatory Diseases. *Nat Rev Immunol* (2021) 21 (9):548–69. doi: 10.1038/s41577-021-00524-z
148. Harding SM, Benci JL, Irianto J, Discher DE, Minn AJ, Greenberg RA. Mitotic Progression Following DNA Damage Enables Pattern Recognition Within Micronuclei. *Nature* (2017) 548(7668):466–70. doi: 10.1038/nature23470

149. Mackenzie KJ, Carroll P, Martin CA, Murina O, Fluteau A, Simpson DJ, et al. cGAS Surveillance of Micronuclei Links Genome Instability to Innate Immunity. *Nature* (2017) 548(7668):461–5. doi: 10.1038/nature23449
150. Ferguson BJ, Mansur DS, Peters NE, Ren H, Smith GL. DNA-PK is a DNA Sensor for IRF-3-Dependent Innate Immunity. *Elife* (2012) 1:e00047. doi: 10.7554/eLife.00047
151. Kondo T, Kobayashi J, Saitoh T, Maruyama K, Ishii KJ, Barber GN, et al. DNA Damage Sensor MRE11 Recognizes Cytosolic Double-Stranded DNA and Induces Type I Interferon by Regulating STING Trafficking. *Proc Natl Acad Sci USA* (2013) 110(8):2969–74. doi: 10.1073/pnas.1222694110
152. Motwani M, Pesiridis S, Fitzgerald KA. DNA Sensing by the cGAS-STING Pathway in Health and Disease. *Nat Rev Genet* (2019) 20(11):657–74. doi: 10.1038/s41576-019-0151-1
153. Reislander T, Groelly FJ, Tarsounas M. DNA Damage and Cancer Immunotherapy: A STING in the Tale. *Mol Cell* (2020) 80(1):21–8. doi: 10.1016/j.molcel.2020.07.026
154. Sato H, Niimi A, Yasuhara T, Permata TBM, Hagiwara Y, Isono M, et al. DNA Double-Strand Break Repair Pathway Regulates PD-L1 Expression in Cancer Cells. *Nat Commun* (2017) 8(1):1751. doi: 10.1038/s41467-017-01883-9
155. Soriani A, Zingoni A, Cerboni C, Iannitto ML, Ricciardi MR, Di Gialleonardo V, et al. ATM-ATR-Dependent Up-Regulation of DNAM-1 and NKG2D Ligands on Multiple Myeloma Cells by Therapeutic Agents Results in Enhanced NK-Cell Susceptibility and Is Associated With a Senescent Phenotype. *Blood* (2009) 113 (15):3503–11. doi: 10.1182/blood-2008-08-173914
156. Gasser S, Orsulic S, Brown EJ, Raulet DH. The DNA Damage Pathway Regulates Innate Immune System Ligands of the NKG2D Receptor. *Nature* (2005) 436(7054):1186–90. doi: 10.1038/nature03884
157. Karnak D, Engelke CG, Parsels LA, Kausar T, Wei D, Robertson JR, et al. Combined Inhibition of Wee1 and PARP1/2 for Radiosensitization in Pancreatic Cancer. *Clin Cancer Res* (2014) 20(19):5085–96. doi: 10.1158/1078-0432.CCR-14-1038
158. Patel P, Sun L, Robbins Y, Clavijo PE, Friedman J, Silvin C, et al. Enhancing Direct Cytotoxicity and Response to Immune Checkpoint Blockade Following Ionizing Radiation With Wee1 Kinase Inhibition. *Oncoimmunology* (2019) 8(11):e1638207. doi: 10.1080/2162402X.2019.1638207
159. Wang B, Sun L, Yuan Z, Tao Z. Wee1 Kinase Inhibitor AZD1775 Potentiates CD8+ T Cell-Dependent Antitumour Activity *via* Dendritic Cell Activation Following a Single High Dose of Irradiation. *Med Oncol* (2020) 37(8):66. doi: 10.1007/s12032-020-01390-w
160. Wayne J, Brooks T, Landras A, Massey AJ. Targeting DNA Damage Response Pathways to Activate the STING Innate Immune Signaling Pathway in Human Cancer Cells. *FEBS J* (2021) 288(15):4507–40. doi: 10.1111/febs.15747

Conflict of Interest: The authors declare that the research was conducted in the absence of any commercial or financial relationships that could be construed as a potential conflict of interest.

Publisher's Note: All claims expressed in this article are solely those of the authors and do not necessarily represent those of their affiliated organizations, or those of the publisher, the editors and the reviewers. Any product that may be evaluated in this article, or claim that may be made by its manufacturer, is not guaranteed or endorsed by the publisher.

frontiers in Oncology

ORIGINAL RESEARCH
published: 18 February 2022
doi: 10.3389/fonc.2022.826655

In Vivo Targeting Replication Protein A for Cancer Therapy

Pamela S. VanderVere-Carozza[1], Navnath S. Gavande[1,2], Shadia I. Jalal[1], Karen E. Pollok[3], Elmira Ekinci[4], Joshua Heyza[4], Steve M. Patrick[4], Andi Masters[5], John J. Turchi[1,6] and Katherine S. Pawelczak[6]**

[1] Department of Medicine, Indiana University School of Medicine, Indianapolis, IN, United States, [2] Department of Pharmaceutical Sciences, Wayne State University College of Pharmacy and Health Sciences, Detroit, MI, United States, [3] Herman B. Wells Center for Pediatric Research, Departments of Pediatrics, Pharmacology and Toxicology, Medical and Molecular Genetics Indiana University Simon Comprehensive Cancer Center, Indianapolis, IN, United States, [4] Department of Oncology, Wayne State University School of Medicine and Barbara Ann Karmanos Cancer Institute, Detroit, MI, United States, [5] Indiana University Cancer Center, Indiana University School of Medicine, Indianapolis, IN, United States, [6] NERx BioSciences, Indianapolis, IN, United States

OPEN ACCESS

Edited by:
Shoumin Zhu, University of Miami Health System, United States

Reviewed by:
Lei Chen, Capital Medical University, China
Alvaro Galli, Pisa Research Area (CNR), Italy
Jac Nickoloff, Colorado State University, United States

***Correspondence:**
John J. Turchi
jturchi@iu.edu
Katherine S. Pawelczak
kspawelczak@NERxbiosciences.com

Specialty section:
This article was submitted to Cancer Molecular Targets and Therapeutics, a section of the journal Frontiers in Oncology

Received: *01 December 2021*
Accepted: *18 January 2022*
Published: *18 February 2022*

Citation:
VanderVere-Carozza PS, Gavande NS, Jalal SI, Pollok KE, Ekinci E, Heyza J, Patrick SM, Masters A, Turchi JJ and Pawelczak KS (2022) In Vivo Targeting Replication Protein A for Cancer Therapy. Front. Oncol. 12:826655. doi: 10.3389/fonc.2022.826655

Replication protein A (RPA) plays essential roles in DNA replication, repair, recombination, and the DNA damage response (DDR). Retrospective analysis of lung cancer patient data demonstrates high RPA expression as a negative prognostic biomarker for overall survival in smoking-related lung cancers. Similarly, relative expression of RPA is a predictive marker for response to chemotherapy. These observations are consistent with the increase in RPA expression serving as an adaptive mechanism that allows tolerance of the genotoxic stress resulting from carcinogen exposure. We have developed second-generation RPA inhibitors (RPAis) that block the RPA–DNA interaction and optimized formulation for *in vivo* analyses. Data demonstrate that unlike first-generation RPAis, second-generation molecules show increased cellular permeability and induce cell death *via* apoptosis. Second-generation RPAis elicit single-agent *in vitro* anticancer activity across a broad spectrum of cancers, and the cellular response suggests existence of a threshold before chemical RPA exhaustion induces cell death. Chemical RPA inhibition potentiates the anticancer activity of a series of DDR inhibitors and traditional DNA-damaging cancer therapeutics. Consistent with chemical RPA exhaustion, we demonstrate that the effects of RPAi on replication fork dynamics are similar to other known DDR inhibitors. An optimized formulation of RPAi NERx **329** was developed that resulted in single-agent anticancer activity in two non-small cell lung cancer models. These data demonstrate a unique mechanism of action of RPAis eliciting a state of chemical RPA exhaustion and suggest they will provide an effective therapeutic option for difficult-to-treat lung cancers.

Keywords: DNA repair inhibitors, Replication Stress Response, Replication Protein A, DNA damage response, DNA repair and cancer

INTRODUCTION

The DNA damage response (DDR) is composed of a complex network of DNA repair and cell signaling pathways that are critical toward maintaining genomic stability. Dysfunctional DDR causes damage to the genome that results in genomic instability, providing a selective advantage over normal cells and enabling rampant proliferation and survival. This genomic instability frequently arises from mutations of certain cell cycle and DDR genes, which in turn creates an increased dependency on other components of the DDR network. This reliance on specific DDR machinery can make cancer cells more vulnerable to therapies targeting DDR components. Certain drugs, like the popular poly (ADP-ribose) polymerase (PARP) inhibitors, can take advantage of targeting cancers with specific known DDR mutations and can impart therapeutic benefit through a synthetic lethality approach (1). Recent evidence also suggests that the DDR is involved in activation of the innate immune response, suggesting that DDR inhibitors combined with immunotherapy may have anticancer activity (2). Other agents targeting specific DDR signaling molecules have shown single-agent and combination activity (3).

Oncogenic replication stress (RS) coupled with DDR blockade results in local effects at the replication fork and global effects on cell cycle and signaling that ultimately result in replication catastrophe (RC) and cell death. The human single-stranded DNA (ssDNA) binding protein, replication protein A (RPA), is a critical regulator of the DDR, with depletion of active RPA or "RPA exhaustion" driving RC and cell death. RPA is the major eukaryotic ssDNA binding protein, and its level and activity are tightly regulated. High levels of ssDNA resulting from DDR inhibition can exhaust cellular RPA such that there is insufficient RPA–DNA binding capacity to engage all the ssDNA generated. The lack of RPA available to protect ssDNA then renders DNA susceptible to digestion by nucleases resulting in DNA strand breaks at replication forks, RC, and cell death (4, 5). We have targeted this crucial DNA metabolic pathway required for genome stability and maintenance *via* small molecule inhibitors (SMIs) that block the RPA–DNA interaction.

First-generation RPA inhibitors (RPAis) were developed and have been extensively characterized with respect to potency and mechanism of action (6–8). Predecessor RPAi TDRL-551 **(551)** displays *in vivo* activity in lung cancer xenograft models. In an effort to determine if lowering the RPA threshold with **551** would result in a synergy with DNA-damaging agents like platinum (Pt)-based drugs, *in vivo* efficacy studies were performed in non-small cell lung cancer (NSCLC) xenograft models. Combinatorial experiments with Pt were conducted with a reduction of both carboplatin and **551** doses to ensure a window to observe potential synergy. Single-agent activity was observed, as well as a greater than additive effect on tumor growth delay with the carboplatin–**551** combination compared to each agent alone. In addition, **551** displays *in vitro*, cellular, and *in vivo* anticancer activity and synergy with cisplatin. Despite the effectiveness of **551** in preclinical studies, certain chemical moieties of the molecule represented chemical liabilities for clinical readiness of the drug. A series of second-generation inhibitors was generated and optimized for solubility, stability, and cellular uptake (9). A morpholino derivative, NERx **329** (**329**), demonstrated enhanced solubility and cellular uptake with superior physicochemical properties. The chemical modifications resulting in ideal drug-like characteristics in the **329** molecule are expected to vastly improve cellular potency, the *in vivo* anticancer activity, and general clinical readiness of the drug. Here, we report the cellular effects and *in vivo* studies completed with **329** and introduce a novel formulation strategy that dramatically improves bioavailability of **329**.

MATERIALS AND METHODS

Replication Protein A Inhibitors

RPAis 329 and 2004 were synthesized and characterized as previously described (9).

Electrophoretic Mobility Shift Assay (EMSA)

EMSAs were performed as previously described (9). Briefly, reactions were conducted in 20 mM HEPES (pH 7.8), 1 mM DTT, 0.001% NP-40, and 50 mM NaCl. RPAis were suspended in 100% dimethlysulfoxide (DMSO), and DMSO concentration in the final reaction mixture was constant at less than 5%. Purified full-length RPA (120 ng) was incubated with the indicated RPAi or vehicle in reaction buffer for 30 min before the addition of the [^{32}]P-labeled 34-base ssDNA probe. Reactions were incubated for 5 min at room temperature, and products were separated *via* 6% native polyacrylamide gel electrophoresis. The bound and unbound fractions were quantified by phosphor-imager analysis using ImageQuant software (Molecular Dynamics, CA), and data were fit by non-linear regression using GraphPad Prism.

CCK-8 Viability Assays

Cell lines were obtained from ATCC and maintained as monolayer cultures in RPMI 1640 medium (H460) or Dulbecco's Modified Eagle's Medium (DMEM) (A549) supplemented with 10% fetal bovine serum. H460 and A549 cells were plated at 2.5×10^3 cells/well and A2780 and GCT27 cells plated at 5×10^3 cells/well in a 96-well plate and incubated for 18–24 h prior to treatments. Cells were treated with the indicated concentration of RPAi for 48 h. The vehicle (DMSO) concentration was held constant at 1%. Cell metabolism/viability was assessed by a mitochondrial metabolism assay (CCK-8) as we have described previously (10). The generation of the water-soluble formazan product by cellular dehydrogenases is proportional to the number of living cells. Following incubation with CCK-8 reagent, absorbance was measured at 450 nm with a BioTek Synergy H1 plate reader. Values were compared to those of vehicle-treated controls to determine percent viability, and the results represent the average and SEM of triplicate determinations.

Apoptosis Assay

Apoptosis induction was determined by activation of Caspases 3 and 7 using the CellEvent™ Caspase-3/7 Green Detection Reagent (Invitrogen). H460 cells were plated at 5×10^3 cells/well in black 96-well plates with clear bottoms (Costar) and incubated for 24 h prior to treatments. Cells were treated with the indicated concentration of RPAi or cisplatin for 24 h. The vehicle (DMSO) concentration was held constant at 1% for RPAi treatments. For caspase 3/7 detection, medium was removed and replaced with phosphate buffered saline (PBS) containing 5% fetal bovine serum (FBS) and 2 μM CellEvent™ Caspase-3/7 Green Detection Reagent. Cells were incubated at 37°C/5% CO_2 for 1 h, and fluorescence intensity was measured in a BioTek Synergy H1 plate reader (excitation/emission 485/528). Images were captured with an Evos FL2 Auto microscope (Invitrogen) using a 10× objective.

Cell Viability in 60 Cancer Cell Lines

In this study, 90-μl cell suspensions were seeded in 96-well plates in respective culture medium with a final cell density of 4×10^3 cells/well and incubated overnight. Here, 10× solution of **329** (top working concentration: 40 μM of test article in media with 3.16-fold serial dilutions to achieve 9 dose levels) was prepared, and 10 μl of drug solution or culture medium containing 0.5% DMSO (vehicle control) was added to the plate (triplicate for each drug concentration). Plates were incubated for 72 h at 37°C with 5% CO_2 and then measured by CellTiter-Glo assay (Promega). Briefly, plates were equilibrated at room temperature for 30 min, and 50 μl of CellTiter-Glo reagent was added to each well. Contents were mixed for 5 min on an orbital shaker to induce cell lysis, and plates were further incubated at room temperature for 20 min to stabilize the luminescent signal. Luminescence was recorded using EnVision Multi Plate Reader. Percent cell growth was calculated relative to DMSO-treated cells (vehicle control), and the data were fit using non-linear regression analysis (GraphPad PRISM) to calculate cellular IC_{50}.

DNA Fiber Analysis

Analysis of DNA replication intermediates was performed as previously described with minor modifications (11, 12). H460 cells were seeded in 6-well plates at a density of 2×10^5 cells. The following day, cells were labeled with iodo-deoxyuridine (IdU) (20 μM) for 20 min, followed by treatment with hydroxyurea (HU) (2.5 mM) for 60 min, then released into chloro-deoxyuridine (CldU) (200 μM) for 20 min, followed by treatment with ATR inhibitor (ATRi) VE-822 (2 μM, Selleckchem, S8807) for 2 h or RPAi **329** (50 μM) for 2 h. After harvesting, the cells were resuspended in PBS at a concentration of 1,000,000 cells/ml, and 2 μl of the cell suspension was mixed with 8 μl of lysis buffer (200 mM Tris-HCl pH 7.5, 50 mM EDTA, 0.5% SDS) on a Superfrost Plus microscope slide (Fisher Scientific). After 6 min of incubation, the slides were tilted at a 45-degree angle to allow cell lysates to slowly run down the slide. After air-drying, the slides were fixed in methanol:acetic acid (3:1) and stored at 4°C. DNA fibers were denatured with 2.5N HCl for 1 h, washed with PBS, and blocked with 5% BSA in PBS-T (PBS + 0.1% Tween-20) for 1 h. DNA fibers were incubated with rat anti-BrdU antibody (1:50, Abcam, ab6326) for CldU and mouse anti-BrdU antibody (1:50, BD Biosciences, 347580) for IdU in a humid chamber at 37°C for 1 h. After washing, slides were incubated with secondary antibodies anti-rat Alexa 488 (1:100) and anti-mouse Alexa 568 (1:100) at room temperature for 45 min. Excess antibodies were removed by washing with PBS-T 3 times. After air-drying, the slides were mounted onto a coverslip with mounting medium. Fiber tracts were imaged with a Nikon epifluorescence microscope using a 40× oil immersion objective, and 100 fibers for each group were analyzed in ImageJ where the ratios of CldU : IdU were compared using pixel length. Data were analyzed by ANOVA with Bonferroni test for multiple comparisons.

Combination Studies

To assess synergy, the combination index (CI) was determined as described by Chou-Talalay as we have previously described (8). Briefly, H460 cells were treated with RPAi and the indicated agent alone and in combination. The range of treatment was dependent on the IC_{50} of each agent, and the range was ¼ to 3 × IC_{50}. The data from both the single-agent treatments and the combination treatment were used to calculate the CI and plot this value as a function of the fraction of cells affected (Fa). A CI of >1 indicates antagonism between the two agents, while a CI <1 indicates synergy. A CI of 1 demonstrates an additive effect.

Pharmacokinetics

A method to quantify **329** from plasma has been developed using an internal standard, liquid–liquid extraction, and HPLC-MS/MS. Mouse plasma samples were prepared from treated mice at the indicated times frozen at -80°C until analysis. Plasma samples were thawed (20 μl) and transferred to polypropylene tubes, and the internal standard is added (20 μl of 0.1 ng/μl). Samples were diluted in 0.1 M phosphate buffer (pH = 7.4) and equal volume of methyl tertiary butyl ether. The samples were mixed and centrifuged at 12,000×g for 5 min, and the supernatant was transferred to a clean polypropylene tube. The solvent was evaporated to dryness, brought up in mobile phase analyzed by HPLC-MS/MS (ABSciex 4000). The mobile phase is delivered *via* gradient using acetonitrile and 0.1% formic acid on an Agilent Zorbax 300SB-C8 150 × 4.6 mm, 5-μm column. The mass spectrometer utilized an electrospray ionization probe run in positive mode. Multiple reaction monitoring was employed with Q1/Q3 (m/z) transitions for **329** at 718.2/128.1 and 687.3/128.1 for the internal standard. The lower limit of quantification is 0.1 ng/ml using 20 μl of plasma.

In Vivo Analyses

To assess anticancer efficacy, the hind flanks of 60 8–10-week-old Nod SCID gamma (NSG) mice were implanted with the indicated cells (~2×10^6) in Matrigel. Tumor volumes were monitored by electronic caliper measurement [tumor volumes = length × (perpendicular width)^2 × 0.5]. NSG studies were approved by the Institutional Animal Care and Use Committee at Indiana University School of Medicine. Male NSG (NOD-

scid/IL2Rg^{null}) mice (*In Vivo* Therapeutics Core Facility, IU Simon Comprehensive Cancer Center, Indianapolis, IN, USA) were used and housed in a pathogen-free facility at IUSM LARC. Mice with tumors of approximately 100 mm^3 were randomized into individual treatment arms. The indicated RPAi was formulated and administered *via* intraperitoneal injection (IP) at the indicated times. Tumor volumes were monitored biweekly as indicated, and the results are presented as the average tumor volume ± standard error of the mean for each group. The number (n) for each experiment is presented in the figure legend.

RESULTS

Retrospective Analysis of Replication Protein A Expression in Lung Cancer

Considering the model of RPA exhaustion limiting the DDR to exogenous damage and replication stress, we sought to determine how the expression of RPA impacted survival in lung cancer. We selected lung cancer, as lung epithelial cells are continuously exposed to a wide array of potentially carcinogenic agents, a situation exacerbated by smoking and second-hand smoke exposure. To assess the potential clinical utility of RPA inhibition, we performed a retrospective analysis of gene expression data in lung cancer as a function of smoking history and response to chemotherapy treatment. In current and former smokers, the data reveal that high RPA expression is a negative prognostic biomarker correlating with worse overall survival (**Figure 1A**). This difference in survival as a function of RPA expression was also observed when selecting patients who received adjuvant chemotherapy that often includes Pt-based DNA-damaging agents (**Figure 1B**). These data demonstrate that low RPA expression is predictive of a better therapeutic response. In the analysis of never smokers (**Figure 1C**), no correlation between RPA expression and survival was observed. Importantly, this patient population is a collection of heterogeneous cancer phenotypes that is characterized by a higher level of driver mutations in growth signaling pathways, and as such, these never smokers are expected to have received targeted kinase inhibitor therapy. The finding that RPA expression level does not impact survival is therefore not surprising. Collectively, these data suggest that potential genotoxic damage induced by smoke exposure induces reliance on RPA expression to protect against genotoxic stress that, if reversed, could impact survival.

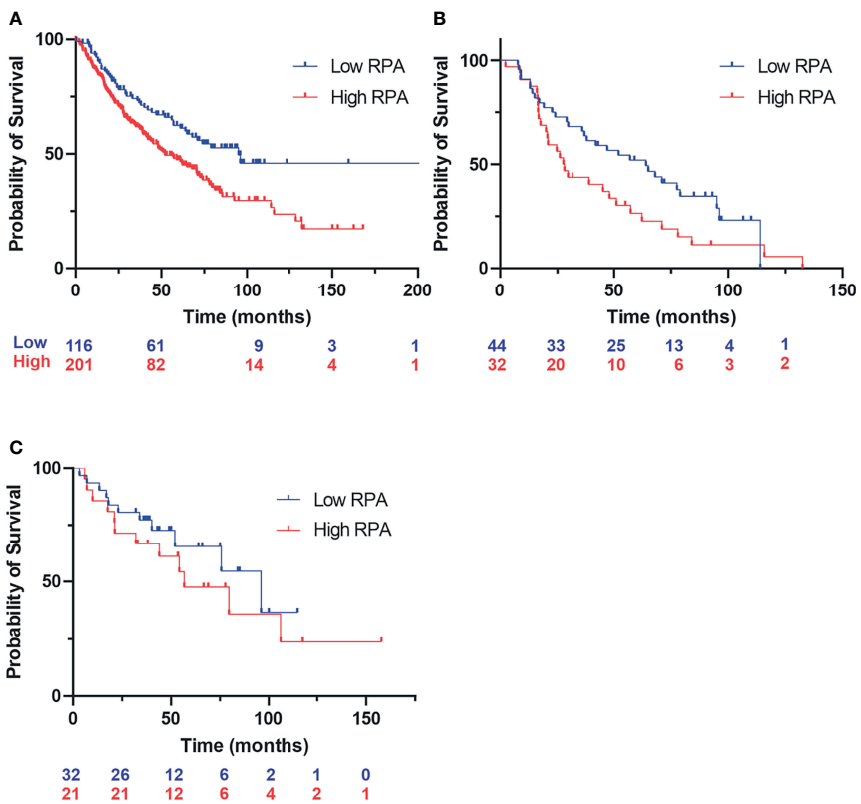

FIGURE 1 | Kaplan–Meyer retrospective analysis of overall survival as a function of replication protein A (RPA) gene expression in non-small cell lung cancer (NSCLC). Blue numbering indicates patients with low RPA expression, red numbering indicates patients with high RPA expression. Analysis represents a 500-patient cohort from the caARRAY, with optimized cutoff. **(A)** Former and current smokers. HR = 1.63 (1.17–2.28) log-rank: p = 0.0035. **(B)** Former and current smokers who received chemotherapy. HR = 1.69 (1–2.86) log-rank: p = 0.049. **(C)** Never smokers.

Chemical Inhibition of Replication Protein A and Mechanisms of Cell Death

Our previous analyses of reversible RPAis revealed both *in vitro* and *in vivo* activity, but chemical liabilities limited their broad utility in cell-based and *in vivo* assays (6, 8). We have further optimized the **551** candidate to generate candidate RPAi **329** and a derivative **2004** (**Figure 2A**) that possess potent RPA inhibitory activity *in vitro*, *in vivo*, and in cellular assays (**Figures 2B, C**). The data also show that the compounds are specific for inhibiting the RPA ssDNA interaction, as the interaction of *Escherichia coli* single strand binding protein (SSB) with ssDNA as indicated is not impacted by the RPAis. These compounds also display excellent solubility, cellular uptake, and physicochemical properties (9). As the addition of a propyl-morpholino to the oxopentoic acid moiety increased solubility and cellular uptake, we sought to assess single-agent cellular anticancer activity in the H460 NSCLC cell line (**Figure 2C**). The data demonstrate that **329** and **2004** possess potent single-agent activity compared to the **551** predecessor as assessed by CCK-8 metabolic assay.

Predecessor reversible RPAis **505** and **551** also displayed single-agent anticancer activity, although this was not accompanied by caspase activation or annexin V/PI positivity, suggesting a non-apoptotic mechanism of cell death (6). The increased cellular uptake and potency displayed by the morpholino-containing compound **329** prompted us to revisit this activity. Using the activation of caspases 3 and 7 as a readout, we demonstrate that **329** induces cell death *via* a classical apoptotic pathway (**Figure 3**), and the activation of caspases 3

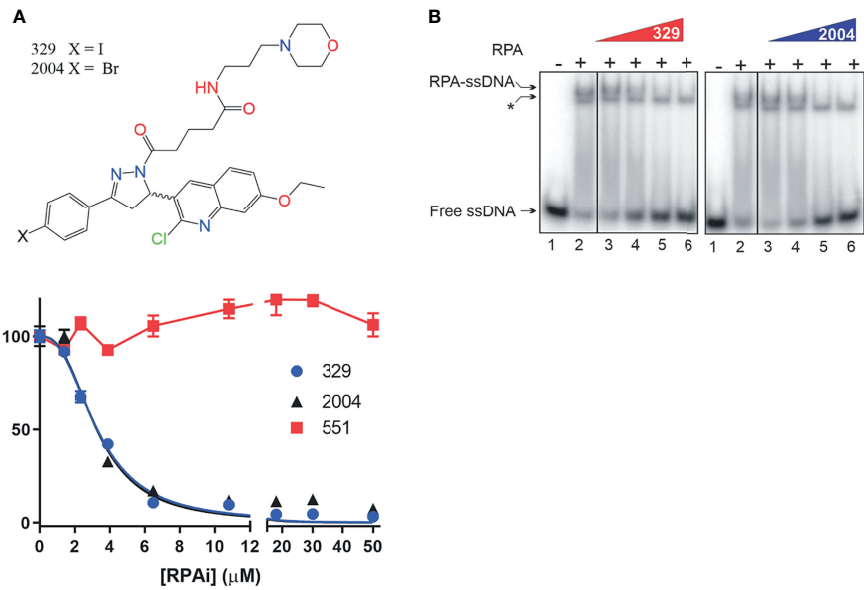

FIGURE 2 | Replication protein A inhibitor (RPAi) inhibitory activity. **(A)** Chemical structure of RPAi's **329** and **2004**. **(B)** EMSA analysis of RPA–DNA interaction inhibition by **329** and **2004**. Lanes 3–6 in each panel contain 6.25, 12.5, 25, and 50 μM of the indicated RPAi, respectively. The * indicates the position of the *Escherichia coli* SSB–single-stranded DNA (ssDNA) complex that serves as an internal specificity control. **(C)** Cell viability of H460 NSCLC cells in response to **329** and **2004**.

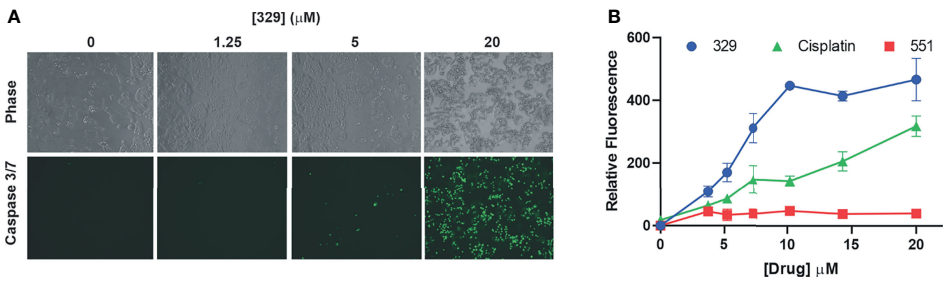

FIGURE 3 | The **329** induction of apoptotic cell death. **(A)** Analysis of caspase 3/7 activity in H460 cells following 24 h of treatment with 1% DMSO or the indicated concentrations of **329**. Fluorescence images were captured as described in the *Materials and Methods*. **(B)** Quantification of caspase 3/7 activity. Fluorescence was measured in 96-well plates using a Biotek Synergy H1 plate reader following 24-h incubation with the indicated drugs and concentrations.

and 7 clearly distinguishes it from predecessor compound **551**. Importantly, **551** does show decreased viability in clonogenic survival assays at the concentrations tested. The inability to detect caspase activity suggests that this is a distinguishing characteristic between the two (8). The titration analyses assessing apoptosis correlated with the corresponding CCK-8 viability curves and show the presence of a modest threshold. Assessment of apoptosis at 48 h was similar to 24 h in terms of the titration, though the maximum signal detected was higher, as expected.

Analyses of single-agent activity of compound **329** in 60 discrete cancer cell lines across a variety of solid tumors revealed similar findings. A range of IC_{50} values were obtained, with most falling between 5 and 10 μM and largely independent of tumor site (**Figure 4A**). Certain uterine, lung, and esophageal cancer cell lines were the most sensitive, while pancreatic adenocarcinomas tended to be more resistant. Interestingly, the Hill coefficients spanned a much larger range (**Figure 4B**), which did not necessarily correlate with the potency as measured by IC_{50}. Certain lung, muscle, ovarian, and cervical cancer lines were characterized by the lowest Hill coefficients. These data are consistent with the tumor agnostic nature of RPA inhibition and a mechanism of action involving a threshold of measurable cytotoxic sensitivity.

A further measure of altered DDR induced by RPA inhibition is the degradation of replication forks upon stalling and RPA exhaustion. We therefore assessed replication fork dynamics and nascent strand degradation using DNA fiber analysis. The treatment scheme is depicted in **Figure 5A**. We first pulse-labeled replicating DNA with IdU for 20 min. After IdU removal, replication forks were stalled by the addition of HU or left to replicate with vehicle treatment. HU was removed and replication labeled with CldU. Then, CldU cells were treated with the DDRi or vehicle. The data obtained are presented in

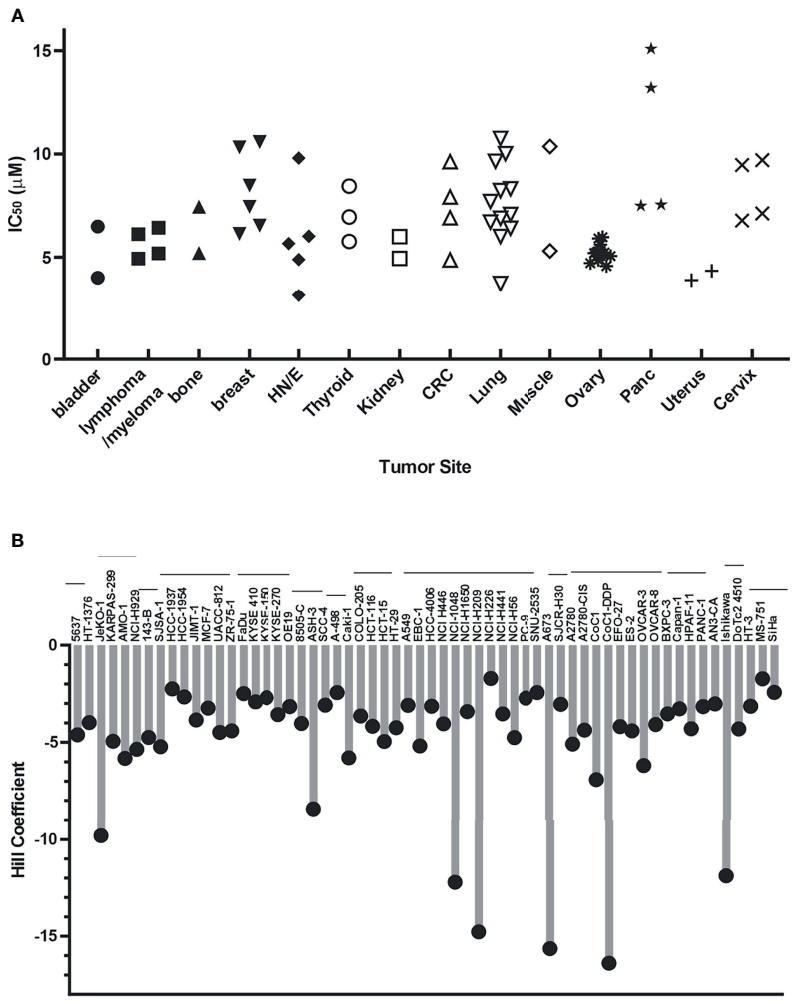

FIGURE 4 | Cellular activity of **329** in 60 cancer cell lines. Cell lines were treated with a 4-log range of replication protein A inhibitor (RPAi) **329** for 72 h. Cell viability was assessed using CellTiter-Glo luminescent viability assay. The data represent the average of triplicate treatments, and the data were fit using non-linear regression analysis to calculate cellular IC_{50}s. **(A)** IC_{50} results from each cell line grouped by tumor type. **(B)** Hill coefficients for individual cell lines. The horizontal lines above cell line names indicated the tumor sites in the order depicted in panel **(A)**.

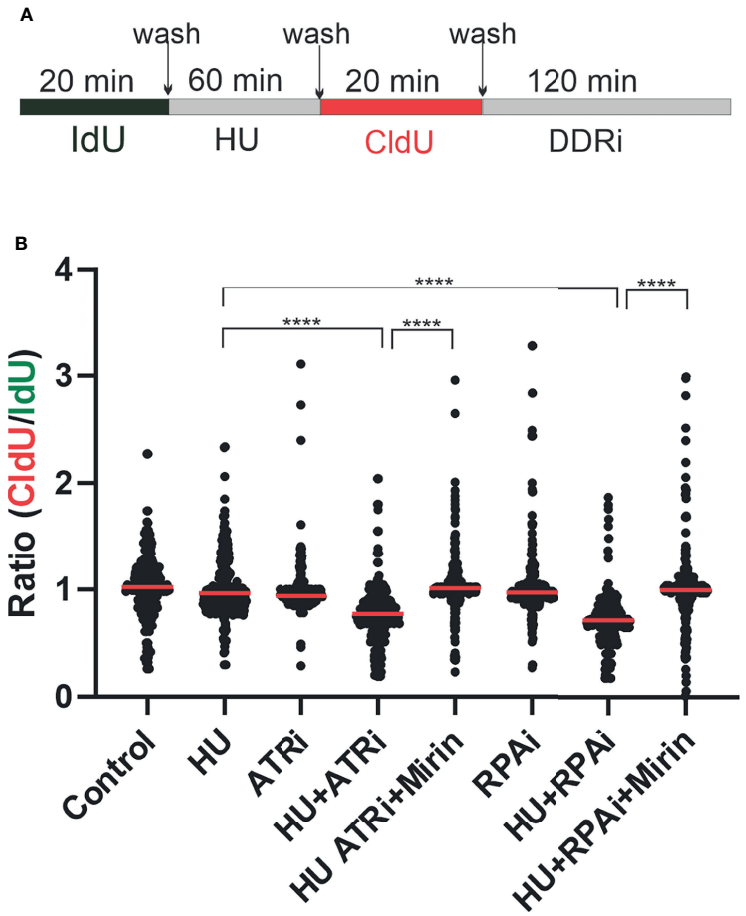

FIGURE 5 | Replication protein A inhibitor (RPAi) impact on replication fork dynamics. **(A)** Schematic depiction of experimental design. DNA was pulse-labeled with IdU for 20 min. After IdU removal, replication forks were stalled by the addition of HU or left to replicate with vehicle treatment. HU was removed, and replication was labeled with CldU. Following CldU, cells were treated with the DDRi or vehicle. **(B)** Quantification of results from DNA fiber analysis in H460 cells treated with the indicated agents. HU was used at a final concentration of 2.5 mM, the ATRi VE-822 at 2 μM, and the RPAi **329** at 50 μM. Data presented are combined from three individual experiments (100 fibers analyzed per experiment; 300 fibers total). Red bar indicates the median value of CldU/IdU. Data were analyzed by ANOVA with Bonferroni test for multiple comparisons (****$p < 0.0001$).

Figure 5B. As expected, minimal effects were observed with ATRi or RPAi alone. However, in cells that received HU and then either ATRi or RPAi, a significant decrease in CldU/IdU signal was observed. These data suggest that the addition of DDRi after fork stalling by HU results in nascent strand degradation at stalled replication forks. Importantly, this decrease observed was reversible by mirin, an inhibitor that blocks degradation of the forks. Importantly, the effect of RPAi was similar to ATRi, as expected for targets in the same pathway. These data suggest that DDR checkpoint abrogation by ATRi or RPAi and a subsequent increase in the presence of unprotected ssDNA in S-phase result in replication fork instability and nascent strand degradation.

Therapeutic Combinations

Considering RPA's role in numerous DNA metabolic processes, we determined how inhibition of RPA impacts sensitivity to a variety of DNA-damaging chemotherapeutics that induce different types of damage. Interestingly, we observe synergy, as indicated by a CI <1 at 0.5 or higher fraction of cells affected, with agents that cause replication stress, bulky lesions, and DNA double-strand breaks (**Figure 6A**), whereas no synergy was observed with paclitaxel, a non-DNA-damaging therapeutic. These results suggest that the cytotoxic effects of RPAis may be mediated by a broader effect on the DDR as opposed to suppression of individual replication and repair pathways. Considering these data, we suspected that RPA inhibition would synergize with other DDR-targeted therapeutics to block multiple pathways within the more broadly concerted DDR. We therefore assessed synergy of RPAis with a series of DDR-targeted agents that are currently in clinical trials (**Figure 6B**). The data demonstrate that modest synergy is observed with each agent in the H460 NSCLC cell model, with exception of the Wee1 inhibitor. Interestingly, we did observe modest synergy with the

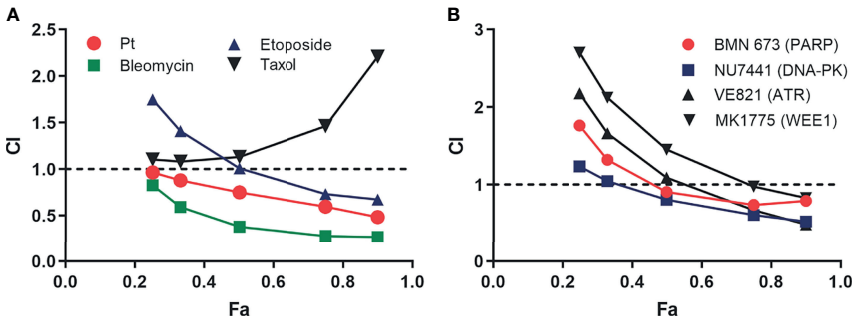

FIGURE 6 | Analysis of replication protein A inhibitor (RPAi) **329** combination treatment. **(A)** Chou-Talalay analysis of combination with chemotherapeutics. The combination index **(CI)** is plotted as a function of the fraction of cell affected (Fa) for each treatment combination of the **329. (B)** Chou-Talalay analysis of combination with DDR-targeted agents as described in panel **(A)**.

PARPi BMN637 in BRCA wild-type cells despite the relatively limited activity seen with single-agent PARPi in these cells. Not surprisingly, we have demonstrated a greater degree of synergy between RPAi and PARPi in BRCA1 null cells compared to BRCA wild-type cells (13). Interestingly, both ATR and DNA-dependent protein kinase (PK) inhibition were more effective when used in combination with RPAi treatment, suggesting that either inhibition of parallel pathways or sequential inhibition of a single pathway in the case of ATR contributes to enhanced increased anticancer activity. Wee1 inhibition however was antagonistic or additive with RPAi over the entire range of cells affected that places its activity downstream of RPA as expected.

In Vivo Analyses

Toward the goal to identify efficacious and safe RPAi **329** treatment regimens, we conducted single-agent screening in two lung cancer cell line-derived xenograft models. Predecessors to **329** and **2004**, compounds **505** and **551**, possessed modest *in vivo* activity (8). Having optimized cellular uptake and solubility *via* the addition of the propyl morpholino in **329** and **2004**, we sought to determine how these modifications impact *in vivo* anticancer activity using two NSCLC models, A549 adenocarcinoma and H460 large cell carcinoma. Analysis of toxicity revealed that safe dosing could be achieved up to 200 mg/kg with no overt toxicity when formulated as a suspension in DMSO/Tween and no significant loss in body weight similar to predecessor compounds. Assessment of kidney function also showed no differences from vehicle controls (data not shown). Interestingly, we observed only modest single-agent anticancer activity in both models with differing dosing regimens of **329** and **2004** (14). That the modest *in vivo* activity is in fact similar to that observed for the **551** predecessor compound (8) was surprising in light of the increases in RPA inhibitory activity *in vitro*, increase in cellular uptakes (9), and dramatically increased activity in tissue culture models. This result suggested that the morpholino addition to **551** to generate **329** could be negatively impacting bioavailability. Analyses of intrinsic clearance and half-life were conducted in mouse and rat microsomes (**Table 1**). Here, **329** displayed favorable rates of clearance in mouse microsomes, ~43 µl/min/mg. These values are less than the rate of 48, which is considered rapid clearance. In rat microsomes, rates of ~64 were obtained for 329 and are less than the rapid rate of 71. Half-lives of 20–40 min in mice and rats are also well within range for these *in vitro* clearance studies, suggesting that **329** was not limited by these parameters. Comparative analyses of PK parameters with **329** *vs.* **551** in the DMSO/Tween formulation revealed a significant reduction in AUC and C_{max} with **329** compared to **551** (data not shown).

Formulation of NERx 329

With favorable potency, cellular activity, plasma stability, and a clear deficit in PK, we initiated a series of studies to assess and optimize a formulation of **329** for *in vivo* bioavailability. Here, **329** solubility was assessed in a series of additives, excipients, and co-solvents to identify initial favorable vehicles (**Table 2**). The surprising result was that **329** was highly soluble in N-methylpyrilidone and displayed moderate solubility in oleic acid, propylene glycol, and PEG400. A series of different formulations were assessed. The final formulation consisted of polysorbate 80, N-methyl-2-pyrrolidone (NMP), propylene glycol, and PEG 400 (+1.1 mol. eq. HCl added as 12 M HCl),

TABLE 1 | Plasma stability and clearance.

		329
	Mouse	
$t_{1/2}$	(min)	43.9
CLint	(uL/min/mg)	31.7
	Rat	
$t_{1/2}$	(min)	21.7
CLint	(uL/min/mg)	63.8

Analyses of intrinsic clearance and half-life were conducted in mouse and rat microsomes.

TABLE 2 | Vehicle/excipient screen.

Vehicle	Solubility (mg/m l)
Water	<1
50 mM sodium acetate pH 4	<1
30% SBECD in water	<1
Oleic acid	2.4
Cremophor EL	<1
Labrasol	1.1
Propylene glycol	1.3
Polyethylene glycol 400	1.2
NMP	70.4
Polysorbate 8O	<1
Ethanol	<1

A series of additives, excipients, and co-solvents were assessed in basic formulation studies to optimize bioavailability.

and **329** was soluble up to 20 mg/ml, and 10-fold dilution in PBS was well dispersed with minimal precipitation. Fourteen-day stability assessments were conducted with this formulation, and the data demonstrate that **329** is very stable up to 40°C, while degradation was observed with extended incubations at 60° C (**Figure 7A**) Calculation of the T90, time to reduce active agent to 90%, was calculated for each temperature and extrapolated to 5°C where **329** is predicted to be stable for over 5 years and at room temperature for over 3 months (**Table 3**). Based on these data, the lead formulation is deemed stable for preparation and storage of **329** at room temperature to support *in vivo* studies.

Pharmacokinetic Analysis of 329 in Optimized Formulation

PK parameters were assessed in a series of studies in immunocompetent mice both IV and IP (**Figure 7B** and **Table 4**). Data demonstrate that IP delivery with the new formulation at 200 mg/kg is enhanced, and results showed significantly improved values including C_{max}, T_{max}, and AUC. The half-life was also well within acceptable range (9 h). However, dosing at 200 mg/kg in the new formulation resulted in increased toxicity. Considering the increased exposure as a result of drastically improved PK parameters, increased toxicity is not surprising. Interestingly, reducing the dose to 20 mg/kg results in a similar C_{max} but reduced AUC as a result of $T_{1/2}$ and T_{max} differences. IV dosing was performed to allow calculation of absolute bioavailability of 0.84 at 20 mg/kg.

TABLE 3 | Stability analysis.

Condition	t90* (days)
60°C	3.2
40°C	26
25°C	140
5°C (extrapolated)	2100

*The chemical stability of 10 mg/ml of NERx **329** in lead formulation was assessed at 25°C, 40°C, and 60°C for a period of 2 weeks.*

In Vivo Analysis of 329 in Optimized Formulation in Non-Small Cell Lung Cancer (NSCLC) Xenograft Models

The long-term goal is to move toward efficacious and safe combination therapies that include RPA inhibition. Predecessor molecules to **329** and **2004**, compounds 505 and 551, possessed modest *in vivo* activity (8). With optimized formulation for **329** and favorable PK parameters, we proceeded to *in vivo* single-agent efficacy studies in H460 large cell carcinoma and A549 adenocarcinoma xenografts. Tumor cells were implanted in NOD/SCID mice that were randomized and treated with vehicle or 20 mg/kg of **329**. Considering the rapid growth kinetics of H460, we administered **329** at 20 mg/kg daily for 5 days, with 2 days off, repeated 3 times. With this dosing strategy, a decrease in tumor volume was observed starting at day 17 (**Figure 8A**). Importantly, previous studies with **329** in a suboptimal formulation resulted in similar tumor growth delay, but with dosing completed at 200 mg/kg (data not shown). This suggests that the newly identified formulation results in single-agent activity as predicted, but that anticancer activity can be achieved using one-tenth the amount of drug. This study clearly shows that a dynamic range is possible and further demonstrates a dose response to **329** *in vivo*, particularly profound as tumor size slightly increases when animals had 2 days of recovery from drug dosing, followed by an immediate tumor reduction after dosing was resumed. Similar studies were conducted in A549 xenograft model, with IP dosing as indicated in the figure, at 40 mg/kg. The results demonstrate that mice in the treatment arm display a significant reduction in tumor growth (**Figure 8B**). This result was confirmed in the analysis of terminal tumor weight that revealed significant smaller tumors in **329**-treated mice (**Figure 8C**). Together, these data demonstrate the utility of RPAi in treating lung cancer.

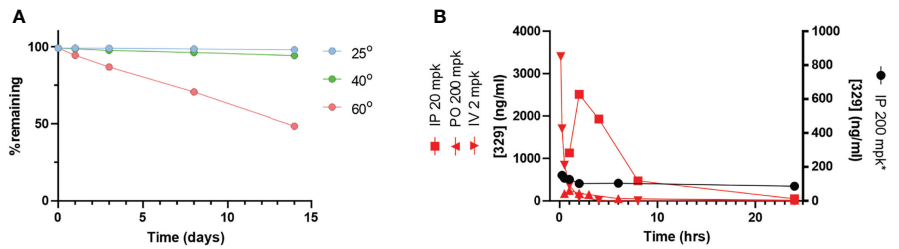

FIGURE 7 | The **329** *in vivo* analysis. **(A)** Stability analysis. Compound stability was assessed over a 14-day time period at varying temperatures as indicated. **(B)** Pharmacokinetic analysis. Time course of drug plasma concentration over 24 h following drug administration as indicated in legend.

TABLE 4 | Pharmacokinetic analysis of **329**.

Parameter	Unit	Value			
Route/Vehicle/dose	mg/kg	|IP/DMSO/200	IP/NMP/200	IP/NMP/20	IV/NMP/2
Lambda_z	1/h	0.02	0.07	0.11	0.21
t1/2	h	30.86	9.311	6.30	3.28
Tmax	h	0.25	8.00	2.00	0.50
Cmax	ng/ml	92.11	2913.57	2511.65	840.89
Clast_obs/Cmax		0.305	0.315	0.002	0.003
AUC 0-t	ng/ml*h	967.99	52010.59	16425.20	1396.47
AUC 0-inf_obs	ng/ml*h	2218.00	64333.98	16474.36	1407.62
AUC 0-t/0-inf_obs		0.44	0.81	1.00	0.99
AUMC 0-inf_obs	ng/ml*h^2	95023.52	947545.56	98489.24	1897.83
MRT 0-inf_obs	h	42.84	14.73	5.981	1.35
Vz/F_obs	(mg/kg)/(ng/ml)	4.015	0.172	0.011	0.007
Cl/F_obs	(mg/kg)/(ng/ml)/h	0.0902	0.0128	0.0012	0.0014

Drug formulated in the optimal NMP solution was assessed for IV or IP delivery at varying doses, as indicated.

Further analysis including dosing and schedule is predicted to achieve maximal anticancer activity.

DISCUSSION

The DDR is actively being pursued for cancer therapy, with phase I results being recently reported for ATRis (15). The vast majority of individual targets being developed in the DDR space are kinases, largely a function of the advances made over the past decade on developing kinase-targeted agents in the growth signaling pathways (16). Kinases, however, represent a minority of the protein components in the DDR pathway and larger replication, repair, and recombination pathways [8;25]. There are myriad opportunities to impede the DDR *via* non-kinase targeted agents (10, 17, 18). The DDR pathway is initiated by sensing DNA discontinuities, damage, or DNA structures *via* DNA binding modules associated with each kinase DNA-PK, ATM, and ATR. We have targeted these unique protein–DNA interactions with small molecules to first elucidate specific mechanisms of DDR activation that can be used to guide the development of cancer therapeutics (19–23). RPA is a complex target as a function of its roles in multiple DNA metabolic and catabolic pathways (24). Two classes of RPAis were initially discovered: (i) covalent RPA modification agents and (ii) reversible inhibitors that target the oligonucleotide/oligosaccharide binding folds (OB-folds) responsible for the RPA–DNA interaction (3). In this report using optimized reversible RPAis, we demonstrate single-agent *in vivo* activity and synergy in combination with traditional and DDR-targeted therapy. Furthermore, we probed the putative mechanism of RPAi's anticancer activity.

PARPi therapy has now been approved in 4 different solid tumors, with prostate and pancreatic joining ovarian and breast in the list of approved indications. Recent evidence on the mechanism of PARPi suggests that ssDNA and specifically lagging strand gaps contribute to PARP efficacy (25). If this mechanism is relevant, one could envision that BRCA wild-type cells would be sensitized to PARPi if the DDR was chemically inhibited. Our finding of synergy as measured by Chou-Talalay combination index analysis supports this basic finding and extends to our recent analyses in BRCA1-deficient cells that show that BRCA1-deficient cells are hypersensitive to RPAi compared to BRCA-complemented cells (26). The observation of synergy in BRCA wild-type cells suggests that RPA inhibition could impair homologous recombination repair (HRR) to create an HR phenotype that increases the potency of PARPi. The impact on HR could be in addition to the effect on the DDR. This result is consistent with our observation of synergy with both ATR and DNA-PK inhibition that can be explained by RPAi impacts on individual and parallel pathways or cross talk between the DDR signaling events. An alternative hypothesis is that another aspect of RPA involvement could explain the synergy, including an alteration in replication fork stability and restart. This is supported by the single-molecule studies that the effects of RPAi on replication dynamics are similar to those of ATRi effects that remain consistent with the dependent nature of ATR on RPA–DNA binding activity in signaling replication fork stress. It is interesting that ATR activity is impacted by ATM as well based on recent studies in both *in vitro* models and patient responses in clinical trial data. This suggests that the cross talk between the three arms of the DDR, DNA-PK, ATM, and ATR, is advantageous if not necessary for responding to replication stress or DNA damage. The ability to block the binding of RPA to ssDNA can induce differential effects depending on the RPA requirement for each pathway. For instance, the amount of RPA needed for nucleotide excision repair (NER) of cisplatin-treated cells is anticipated to be very low based on the cellular levels of cisplatin damage. Accordingly, our observation that RPAi does not impact NER-catalyzed repair is not surprising. Similarly, in normal, unperturbed DNA replication, RPAi has minimal effects on our initial assessment of replication dynamics; however, when fork stalling is induced by HU, a dramatic effect of RPAi is observed, consistent with the increase in the amount of RPA needed to address the replication stress and the limited RPA available as a function of the inhibitor.

The model of RPA threshold is consistent with our analysis of RPAi cellular activity and the tumor agnostic mechanism of action. Also consistent with these data are previous findings that RPA expression has been described as a prognostic and predictive biomarker in a small number of studies (27–29).

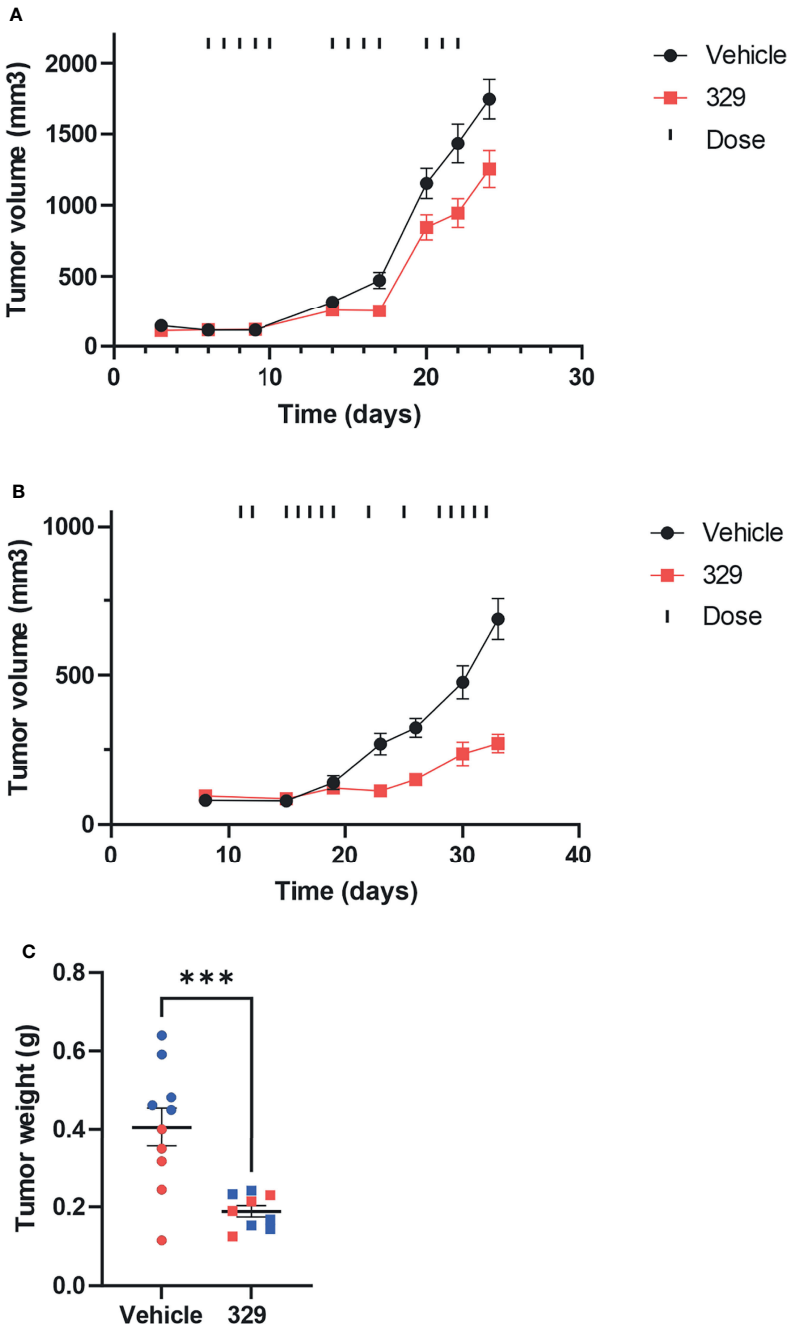

FIGURE 8 | *In vivo* analysis of anticancer activity of **329**. **(A)** Anticancer activity was assessed in human H460 NCSLC tumor xenografts in NOD/SCID mice. Mice were implanted subcutaneously on day 1 with H460 NSCLC cells, tumors were measured by calipers, and mice assigned randomly to treatment arms. Treatment with **329** was initialized at day 6 and administered *via* intraperitoneal injection (IP) once daily (20 mg/kg), as indicated (|). Tumor volumes were completed with caliper measurement biweekly. **(B)** A549 cells were implanted subcutaneously, mice were randomized, and treatment with **329** was initiated at day 11 *via* IP (40 mg/kg) and treated once daily as indicated (|). **(C)** Tumor weight from A549 cells was determined on day 32. Statistically significance differences from vehicle-treated tumors are indicated by the asterisk *$p < 0.05$; ***$p < 0.01$.

Our retrospective analysis of NSCLC confirms and extends these studies to demonstrate that RPA expression levels can be both prognostic and predictive in smoking-associated lung cancers. Its role in the DDR is likely critical to respond and protect from the myriad of genetic insults stemming from carcinogen exposure. It is therefore interesting to speculate that RPA expression or activity may also be predictive of response to other DDR-targeted therapeutics.

Recent advances in kinase-targeted agents and immuno-oncology (IO) therapy have changed many treatment paradigms for lung cancer. The discovery of driver mutations and chromosomal rearrangements in NSCLC has resulted in the availability of molecularly targeted agents for 40% of NSCLC (30), including EGFR tyrosine kinase inhibitors (TKIs) and ALK TKIs. Despite these targeted therapeutic advances, the clinical reality is that over 60% of NSCLC patients will continue to receive the common chemotherapy, Pt-based agent, as part of their therapy. Lung epithelial cells are exposed to a variety of carcinogens that can be dramatically increased in cigarette smoke exposure and likely contribute to the high mutation burden observed in smoking-related cancers. It stands to reason that lung epithelium would have a robust DNA repair capacity to counter the DNA damage elicited by cigarette smoking, and early research demonstrated the importance of DNA repair in lung carcinogenesis (31, 32). This repair capacity can explain the rapid resistance to cancer therapeutic modalities that induce DNA damage including two frequently used Pt-based agents, cisplatin and carboplatin, and ionizing radiation. Recent advances in our understanding of how cells, both normal and cancerous, respond to DNA damage stress has identified a number of unique vulnerabilities that can be exploited for effective therapy to treat cancer. Our retrospective and cellular data strongly suggest that RPA plays an important role in treating this disease. This premise is supported by the clear single-agent anticancer activity observed with our newly formulated RPAi and combined suggests that inhibition of RPA will have a significant impact on cancer therapy in this difficult to treat disease.

DATA AVAILABILITY STATEMENT

The original contributions presented in the study are included in the article/supplementary material. Further inquiries can be directed to the corresponding authors.

ETHICS STATEMENT

The animal study was reviewed and approved by IACUC-Indiana University.

AUTHOR CONTRIBUTIONS

PV-C contributed cellular studies. NG contributed chemical synthesis. EE, JH, and SP contributed DNA fiber analysis data. All authors contributed to the article and approved the submitted version.

FUNDING

This work was supported by NIH grant R01 CA257430 and the Tom and Julie Wood Family Foundation (J.J.T.). Additional studies were supported by NIH grant RO1CA229535 (S.M.P.), NICHD P50HD090215 (K.E.P), P30CA082709 awarded to the Indiana University Simon Comprehensive Cancer Center (K.E.P), and the Indiana University Grand Challenge–Precision Health Initiative (K.E.P).

REFERENCES

1. Lord CJ, Tutt AN, Ashworth A. Synthetic Lethality and Cancer Therapy: Lessons Learned From the Development of PARP Inhibitors. *Annu Rev Med* (2015) 66:455–70. doi: 10.1146/annurev-med-050913-022545
2. Chabanon RM, Rouanne M, Lord CJ, Soria JC, Pasero P, Postel-Vinay S. Targeting the DNA Damage Response in Immuno-Oncology: Developments and Opportunities. *Nat Rev Cancer* (2021) 21:701–17. doi: 10.1038/s41568-021-00386-6
3. Gavande NS, VanderVere-Carozza PS, Hinshaw HD, Jalal SI, Sears CR, Pawelczak KS, et al. DNA Repair Targeted Therapy: The Past or Future of Cancer Treatment? *Pharmacol Ther* (2016) 160:65–83. doi: 10.1016/j.pharmthera.2016.02.003
4. Toledo LI, Altmeyer M, Rask MB, Lukas C, Larsen DH, Povlsen LK, et al. ATR Prohibits Replication Catastrophe by Preventing Global Exhaustion of RPA. *Cell* (2013) 155:1088–103. doi: 10.1016/j.cell.2013.10.043
5. Toledo L, Neelsen KJ, Lukas J. Replication Catastrophe: When a Checkpoint Fails Because of Exhaustion. *Mol Cell* (2017) 66:735–49. doi: 10.1016/j.molcel.2017.05.001
6. Shuck SC, Turchi JJ. Targeted Inhibition of Replication Protein A Reveals Cytotoxic Activity, Synergy With Chemotherapeutic DNA-Damaging Agents, and Insight Into Cellular Function. *Cancer Res* (2010) 70:3189–98. doi: 10.1158/0008-5472.CAN-09-3422
7. Anciano Granadillo VJ, Earley JN, Shuck SC, Georgiadis MM, Fitch RW, Turchi JJ. Targeting the OB-Folds of Replication Protein A With Small Molecules. *J Nucleic Acids* (2010) 2010:304035. doi: 10.4061/2010/304035
8. Mishra AK, Dormi SS, Turchi AM, Woods DS, Turchi JJ. Chemical Inhibitor Targeting the Replication Protein A-DNA Interaction Increases the Efficacy of Pt-Based Chemotherapy in Lung and Ovarian Cancer. *Biochem Pharmacol* (2015) 93:25–33. doi: 10.1016/j.bcp.2014.10.013
9. Gavande NS, VanderVere-Carozza PS, Pawelczak KS, Vernon TL, Jordan MR, Turchi JJ. Structure-Guided Optimization of Replication Protein A (RPA)-DNA Interaction Inhibitors. *ACS Med Chem Lett* (2020) 11:1118–24. doi: 10.1021/acsmedchemlett.9b00440
10. Gavande NS, VanderVere-Carozza PS, Pawelczak KS, Mendoza-Munoz P, Vernon TL, Hanakahi LA, et al. Discovery and Development of Novel DNA-PK Inhibitors by Targeting the Unique Ku-DNA Interaction. *Nucleic Acids Res* (2020) 48:11536–50. doi: 10.1093/nar/gkaa934
11. Nieminuszczy J, Schwab RA, Niedzwiedz W. The DNA Fibre Technique - Tracking Helicases at Work. *Methods* (2016) 108:92–8. doi: 10.1016/j.ymeth.2016.04.019
12. Petermann E, Orta ML, Issaeva N, Schultz N, Helleday T. Hydroxyurea-Stalled Replication Forks Become Progressively Inactivated and Require Two Different RAD51-Mediated Pathways for Restart and Repair. *Mol Cell* (2010) 37:492–502. doi: 10.1016/j.molcel.2010.01.021
13. Cong K, Peng M, Kousholt AN, Lee WTC, Lee S, Nayak S, et al. Replication Gaps are a Key Determinant of PARP Inhibitor Synthetic Lethality With BRCA Deficiency. *Mol Cell* (2021) 81:3128–44. doi: 10.1016/j.molcel.2021.06.011
14. VanderVere-Carozza P, Pawelczak KS, Gavande NS, Jalal S, Pollok KE, Ekinci E, et al. Chemical Exhaustion of RPA in Cancer Treatment. *BioRxIV* (2020). doi: 10.1101/2020.11.30.404640
15. Yap TA, Krebs MG, Postel-Vinay S, El-Khouiery A, Soria JC, Lopez J, et al. Ceralasertib (AZD6738), an Oral ATR Kinase Inhibitor, in Combination With Carboplatin in Patients With Advanced Solid Tumors: A Phase I Study. *Clin Cancer Res* (2021). doi: 10.1158/1078-0432.CCR-21-1032

16. Tan CS, Kumarakulasinghe NB, Huang YQ, Ang YLE, Choo JR, Goh BC, et al. Third Generation EGFR TKIs: Current Data and Future Directions. *Mol Cancer* (2018) 17:29. doi: 10.1186/s12943-018-0778-0
17. Arora S, Heyza J, Zhang H, Kalman-Maltese V, Tillison K, Floyd AM, et al. Identification of Small Molecule Inhibitors of ERCC1-XPF That Inhibit DNA Repair and Potentiate Cisplatin Efficacy in Cancer Cells. *Oncotarget* (2016) 7:75104–17. doi: 10.18632/oncotarget.12072
18. Exell JC, Thompson MJ, Finger LD, Shaw SJ, Debreczeni J, Ward TA, et al. Cellularly Active N-Hydroxyurea FEN1 Inhibitors Block Substrate Entry to the Active Site. *Nat Chem Biol* (2016) 12:815–21. doi: 10.1038/nchembio.2148
19. Gavande NS, VanderVere-Carozza P, Mishra AK, Vernon TL, Pawelczak KS, Turchi JJ. Design and Structure-Guided Development of Novel Inhibitors of the Xeroderma Pigmentosum Group A (XPA) Protein-DNA Interaction. *J Med Chem* (2017) 60:8055–70. doi: 10.1021/acs.jmedchem.7b00780
20. Gavande NS, VanderVere-Carozza PS, Pawelczak KS, Vernon TL, Jordan MR, Turchi JJ. Structure-Guided Optimization of Replication Protein A (RPA)–DNA Interaction Inhibitors. *ACS Med Chem Lett* (2020). doi: 10.1021/acsmedchemlett.9b00440
21. Pawelczak KS, Gavande NS, VanderVere-Carozza PS, Turchi JJ. Modulating DNA Repair Pathways to Improve Precision Genome Engineering. *ACS Chem Biol* (2018) 13:389–96. doi: 10.1021/acschembio.7b00777
22. Neher TM, Shuck SC, Liu J, Zhang JT, Turchi JJ. Identification of Novel Small Molecule Inhibitors of the XPA Protein Using in Silico Based Screening. *ACS Chem Biol* (2010) 5:953–65. doi: 10.1021/cb1000444
23. Neher TM, Bodenmiller D, Fitch RW, Jalal SI, Turchi JJ. Novel Irreversible Small Molecule Inhibitors of Replication Protein A Display Single-Agent Activity and Synergize With Cisplatin. *Mol Cancer Ther* (2011) 10:1796–806. doi: 10.1158/1535-7163.MCT-11-0303
24. Haring SJ, Mason AC, Binz SK, Wold MS. Cellular Functions of Human RPA1. Multiple Roles of Domains in Replication, Repair, and Checkpoints. *J Biol Chem* (2008) 283:19095–111. doi: 10.1074/jbc.M800881200
25. Hanzlikova H, Kalasova I, Demin AA, Pennicott LE, Cihlarova Z, Caldecott KW. The Importance of Poly(ADP-Ribose) Polymerase as a Sensor of Unligated Okazaki Fragments During DNA Replication. *Mol Cell* (2018) 71:319–31. doi: 10.1016/j.molcel.2018.06.004
26. Cong K, Peng M, Kousholt AN, Lee WTC, Lee S, Nayak S, et al. Replication Gaps are a Key Determinant of PARP Inhibitor Synthetic Lethality With BRCA Deficiency. *Mol Cell* (2021) 81:3227. doi: 10.1016/j.molcel.2021.07.015
27. Levidou G, Gakiopoulou H, Kavantzas N, Saetta AA, Karlou M, Pavlopoulos P, et al. Prognostic Significance of Replication Protein A (RPA) Expression Levels in Bladder Urothelial Carcinoma. *BJU Int* (2011) 108:E59–65. doi: 10.1111/j.1464-410X.2010.09828.x
28. Levidou G, Ventouri K, Nonni A, Gakiopoulou H, Bamias A, Sotiropoulou M, et al. Replication Protein A in Nonearly Ovarian Adenocarcinomas: Correlation With MCM-2, MCM-5, Ki-67 Index and Prognostic Significance. *Int J Gynecol Pathol* (2012) 31:319–27. doi: 10.1097/PGP.0b013e31823ef92e
29. Givalos N, Gakiopoulou H, Skliri M, Bousboukea K, Konstantinidou AE, Korkolopoulou P, et al. Replication Protein A is an Independent Prognostic Indicator With Potential Therapeutic Implications in Colon Cancer. *Mod Pathol* (2007) 20:159–66. doi: 10.1038/modpathol.3800719
30. Simon GR. Individualizing Chemotherapy for non-Small Cell Lung Cancer (NSCLC) in the Adjuvant and Advanced Setting: Current Status and Future Directions. *Curr Treat Options Oncol* (2008) 9:300–12. doi: 10.1007/s11864-008-0075-z
31. Shen H, Spitz MR, Qiao Y, Guo Z, Wang LE, Bosken CH, et al. Smoking, DNA Repair Capacity and Risk of Nonsmall Cell Lung Cancer. *Int J Cancer* (2003) 107:84–8. doi: 10.1002/ijc.11346
32. Wei Q, Cheng L, Amos CI, Wang LE, Guo Z, Hong WK, et al. Repair of Tobacco Carcinogen-Induced DNA Adducts and Lung Cancer Risk: A Molecular Epidemiologic Study. *J Natl Cancer Inst* (2000) 92:1764–72. doi: 10.1093/jnci/92.21.1764

Conflict of Interest: Author JT is a shareholder and founder and KP is a shareholder and employed by NERx BioSciences.

The remaining authors declare that the research was conducted in the absence of any commercial or financial relationships that could be construed as a potential conflict of interest.

Publisher's Note: All claims expressed in this article are solely those of the authors and do not necessarily represent those of their affiliated organizations, or those of the publisher, the editors and the reviewers. Any product that may be evaluated in this article, or claim that may be made by its manufacturer, is not guaranteed or endorsed by the publisher.

frontiers in Oncology

BRIEF RESEARCH REPORT
published: 10 March 2022
doi: 10.3389/fonc.2022.852859

Chemical Biology Screening Identifies a Vulnerability to Checkpoint Kinase Inhibitors in TSC2-Deficient Renal Angiomyolipomas

*Robert M. Vaughan[1], Jennifer J. Kordich[2], Chun-Yuan Chan[2], Nanda K. Sasi[3], Stephanie L. Celano[2,4], Kellie A. Sisson[2], Megan Van Baren[2], Matthew G. Kortus[2], Dean J. Aguiar[5], Katie R. Martin[2,4] and Jeffrey P. MacKeigan[1,2,4]**

[1] Pediatrics and Human Development, College of Human Medicine, Michigan State University, Grand Rapids, MI, United States, [2] Center for Cancer & Cell Biology, Van Andel Research Institute, Grand Rapids, MI, United States, [3] Graduate Program in Genetics, Michigan State University, East Lansing, MI, United States, [4] Obstetrics, Gynecology, and Reproductive Biology, College of Human Medicine, Michigan State University, Grand Rapids, MI, United States, [5] Preclinical Research, Tuberous Sclerosis Complex (TSC) Alliance, Silver Springs, MD, United States

OPEN ACCESS

Edited by:
John Turchi,
Indiana University Bloomington,
United States

Reviewed by:
Sanjeevani Arora,
Fox Chase Cancer Center,
United States
Matthias P. Wymann,
University of Basel, Switzerland

***Correspondence:**
Jeffrey P. MacKeigan
mackeig1@msu.edu

Specialty section:
This article was submitted to Cancer Molecular Targets and Therapeutics, a section of the journal Frontiers in Oncology

Received: 11 January 2022
Accepted: 14 February 2022
Published: 10 March 2022

Citation:
Vaughan RM, Kordich JJ, Chan C-Y, Sasi NK, Celano SL, Sisson KA, Van Baren M, Kortus MG, Aguiar DJ, Martin KR and MacKeigan JP (2022) Chemical Biology Screening Identifies a Vulnerability to Checkpoint Kinase Inhibitors in TSC2-Deficient Renal Angiomyolipomas. Front. Oncol. 12:852859. doi: 10.3389/fonc.2022.852859

The tuberous sclerosis complex (TSC) is a rare genetic syndrome and multisystem disease resulting in tumor formation in major organs. A molecular hallmark of TSC is a dysregulation of the mammalian target of rapamycin (mTOR) through loss-of-function mutations in either tumor suppressor *TSC1* or *TSC2*. Here, we sought to identify drug vulnerabilities conferred by TSC2 tumor-suppressor loss through cell-based chemical biology screening. Our small-molecule chemical screens reveal a sensitivity to inhibitors of checkpoint kinase 1/2 (CHK1/2), regulators of cell cycle, and DNA damage response, in both *in vitro* and *in vivo* models of TSC2-deficient renal angiomyolipoma (RA) tumors. Further, we performed transcriptional profiling on TSC2-deficient RA cell models and discovered that these recapitulate some of the features from TSC patient kidney tumors compared to normal kidneys. Taken together, our study provides a connection between mTOR-dependent tumor growth and CHK1/2, highlighting the importance of CHK1/2 inhibition as a potential antitumor strategy in TSC2-deficient tumors.

Keywords: Chk1/2, CHEK1/2, TSC2, tuberous sclerosis complex, mTOR, checkpoint kinase inhibitors, AZD7762, tumor xenografts

INTRODUCTION

The tuberous sclerosis complex (TSC) is a multisystem disease genetically characterized by a loss of function in either of the two tumor suppressors, *TSC1* (hamartin) or *TSC2* (tuberin) (1, 2). We recently used comprehensive genomic profiling of TSC patient tumors and found that ~85% carried mutant *TSC2*, ~12% had mutant *TSC1*, and ~3% had no identified mutation in either *TSC* gene (3). Loss of TSC1 or TSC2 results in benign tumor formation in various organs (4), including subependymal nodules (SEN), subependymal giant cell astrocytomas (SEGA) and cortical tubers

of the brain, smooth muscle tissue and cystic changes in the lungs (lymphangioleiomyomatosis, LAM), skin fibromas and angiofibromas, and cardiac rhabdomyomas in infants (5, 6). The kidney is the most common location for lesions in TSC patients, with up to 80% of patients developing renal cysts and angiomyolipoma (RA). RA tumors are associated with spontaneous hemorrhage and require lifelong surveillance (7). Further, the multisystem and numerous organ manifestations can be associated with severe morbidity and potentially death with kidney disease as the highest cause of mortality in TSC patients (8).

Loss of TSC1 or TSC2 leads to constitutive activation of the mammalian target of rapamycin (mTOR) (9), a master regulator of nutrient and energy status in cells. This permits aberrant cell division and growth. Accordingly, TSC tumors show dramatic therapeutic sensitivity to rapamycin (sirolimus) or other rapamycin analogs (rapalogs). However, while sirolimus is effective against various TSC-based tumor lesions, this allosteric mTOR inhibitor is primarily cytostatic, and tumors regrow upon cessation of therapy (10, 11). Furthermore, rapamycin treatment in patients is associated with a decrease in angiomyolipoma volume of ~50%, and unfortunately, these benefits are reversed after treatment is withdrawn (10, 12, 13). However, rapamycin side effects are mild to moderate, and after continuous treatment for 3 years, efficacy was maintained without new or additional significant side effects (14). Due to this cytostatic effect and favorable safety profile, most patients may require a lifelong treatment regimen of rapamycin (15). Therefore, identifying additional therapeutic options for TSC patients that would sensitize TSC2-deficient angiomyolipoma cells might be preferable over lifelong therapy. Here, we sought to identify new TSC2-dependent vulnerabilities using chemical biology approaches and validation in mouse models.

MATERIALS AND METHODS

Cell Culture

621-102 (TSC2-deficient) and 621-103 (TSC2-rescued) were previously generated (16) by stable expression of either an empty vector or *TSC2* in the E6/E7 and hTERT immortalized renal angiomyolipoma 621-101 cells (17). 621-102 and 621-103 cells were maintained in DMEM with 10% FBS. UMB1949 cells were originally isolated from a renal angiomyolipoma and immortalized *via* SV40 large T antigen and hTERT introduction (18). 105K cells were derived from a renal tumor from a *Tsc2*$^{+/-}$ mouse (19). 621-102, 621-103, and UMB1949 were purchased from ATCC and maintained in DMEM (high glucose) with 10% FBS and 250 U/ml penicillin–streptomycin at 37°C with 5% CO_2. 105K cells were maintained in DMEM with 10% FBS and penicillin (100 U/ml) and streptomycin (100 µg/ml). For nutrient depletion experiments, cells were plated in complete media (10% FBS). The next day, cells were washed once with PBS and then starved overnight in media with either full media (10% FBS, with nutrients) or starvation media (0.1% FBS, without nutrients).

Reagents and Antibodies

LY2603618, AZD7762, and rapamycin were purchased from Selleck Chemicals. Antibodies used in Western blotting were TSC2 (Cell Signaling Technologies [CST] #4308), pS6K-T389 (CST #9205), pS6-S235/236 (CST #4858), α-tubulin (CST #2144), CHK1 (CST #2360), pCHK1-S296 (CST #90178), and pCHK1-S345 (CST #2348).

Chemical Compound Screens

Cell viability assays using a luminescent CellTiter-Glo (Promega) assay were optimized to achieve at least two population doublings in 384-well plates after plating in full media conditions; the result was 700 cells/well and growth time of 72 h for 621-102/621-103. Each of the 384-well screening plates contained positive control compounds, an allosteric mTOR inhibitor (50 nM rapamycin), and cell death control (1 µM staurosporine). All results presented as viability relative to vehicle (DMSO-treated) cells on a per plate basis. The primary screen (621-102 vs. 621-103) included 480 compounds (selected from SelleckChem L1100) at six different concentrations (**Supplemental Table 1**). Validation dose–response curves were generated at 72 h. For the secondary screen (**Supplemental Table 2**), 458 compounds from the primary screen passed quality control and were screened against 621-102 in our optimized growth conditions (DMEM + 0.1% FBS) where 621-103 would not grow (reflective of functional TSC2). The top compounds for relative viability reduction in 621-102 were included (n = 88) in the follow-up screen in UMB1949 and 621-102 cells in 0.1% FBS growth conditions. With the 88 compounds, we performed 10-point dose–response curves in both TSC2-deficient cell lines and calculated the EC_{50} values on the CellTiter-Glo data (**Supplemental Table 3**). The EC_{50} values were calculated in GraphPad Prism using the non-linear fit of [inhibitor] vs. response (three parameters), and the best-fit data are presented.

siRNA Knockdown

For siRNA knockdown, 2,500 cells were plated in 96-well plates and treated with 25 nM siRNA from Qiagen (AllStars Negative Control, Qiagen SI03650318; AllStars Cell Death Control, Qiagen SI04381048; CHEK1 equimolar pool of SI02660007, SI00299859, SI00605094, SI00287658; or CHEK2 equimolar pool of SI02224271, SI02655422, SI02224264) in siLentFect (Bio-Rad, Hercules, CA, USA) and CellTiter-Glo (CTG, Promega, Madison, WI, USA) was performed 72 h later. Negative and positive controls, including transfection controls, were used to determine Relative Cell Viability (%) with CHK1 and CHK2 knockdown.

UMB1949 Cell Line Tumorgraft Models

All animal studies were performed in accordance with recommendations of the AAALAC and received institutional IACUC approvals. Prior to establishing cell line tumorgraft models, UMB1949 cells were found negative for mouse hepatitis virus, mouse parvovirus, minute virus of mice, Theiler's murine encephalomyelitis virus GDVII, *M. pulmonis*, and *mycoplasma* (IDEXX BioResearch, Westbrook, ME, USA). UMB1949 cells (5×10^6) were subcutaneously injected into the right flank of female NSG (NOD *scid* gamma) mice until tumors

formed, at which point mice were euthanized and tumors aseptically harvested. The resected tumors were then subdivided to allot material for both cryopreservation and subsequent propagation *in vivo* (<3 mm in size). Tumor specimens were placed into transfer media [RPMI 1640 media (Invitrogen, Carlsbad, CA, USA), 10% fetal bovine serum (Mediatech, Manassas, VA, USA), 1% penicillin/streptomycin (Invitrogen), and 50 units/ml heparin (Sigma, St. Louis, MO, USA)]. Tumor specimens were moved into individual petri dishes of sterile phosphate-buffered saline (Invitrogen, Carlsbad, CA, USA) and separated into <3-mm fragments. Each mouse was treated with the analgesic ketoprofen (5 mg/kg body weight) with betadine (Purdue Products LP, Stamford, CO, USA) being used to sterilize the right flank prior to surgery. While under isoflurane anesthesia, a subcutaneous pocket was subsequently created, and the tumor fragment was inserted prior to closing with surgical staples. Postoperative care included daily animal monitoring for overall health and tumor growth. Tumor volumes were measured by calipers in three dimensions and calculated using the following equation: (½ × length × depth × height). Measurements were taken once weekly when tumor volumes ≤ 100 mm^3 and three times weekly when > 100 mm^3. In parallel with these measurements, weekly body weights were also recorded. Treatments were initiated when tumorgraft volume was 400 ± 25 mm^3. AZD7762 was dissolved (5 mg/ml) in vehicle (11.3% 2-hydroxypropyl-b-cyclodextrin in PBS) and diluted (1 mg/ml) prior to injection at 12.5 mg/kg. For sacrifice, mice were anesthetized with i.p. injection overdose of avertin, followed by perfusion with 10 ml of PBS and removal of subcutaneous tumor into either 4% paraformaldehyde followed by washes in increasing concentration of ethanol to a final of 70%, or into isopentane on dry ice for freezing and long-term storage.

105K Xenografts

Seven- to eight-week-old female BALB/c nude mice (Janvier Labs, Le Genest-Saint-Isle, France) were injected subcutaneously into the right flank with 2×10^6 105K *Tsc2* null cells (19) in 150 µl of DMEM/Matrigel (1:1) by Porsolt SAS (Le Genest-Saint-Isle, France). When the tumors reached 100 mm^3, treatment group mice (n = 14) were administered either vehicle (2% ethanol, 5% Tween-80, 5% PEG400 in PBS) or AZD7762 (12.5 kg/kg, 1×/day) *via* intraperitoneal injection for 28 days total.

Cystadenoma Mouse Model

A/J $Tsc2^{+/-}$ mice (20) were maintained through the TSC Alliance Preclinical Consortium by the Van Andel Research Institute. Groups (n = 10) of 8-month-old mice (five male and five female) were treated for 28 days with either AZD7762 or vehicle (12.5 mg/kg, 1×/day, in 5% PEG400, 5% Tween-80, 2% ethanol in PBS). After 28 days, animals were euthanized, and both kidneys were collected for histology. Kidneys were embedded in paraffin, split parasagittal, and serial 5 micron-thick sections were obtained 100 microns apart. Slides were processed on the Discovery Ultra platform (Ventana, Oro Valley, AZ, USA) and imaged using the ScanScope XT digital pathology slide scanner (Aperio, Sausalito, CA, USA) at ×20 magnification. Histological analysis was performed by PsychoGenics Inc. (Paramus, NJ). Dystrophic areas were manually outlined, and the cell content was measured by Image-Pro Premier (v3.2). Lesions were classified as cysts (0%–25%) or cystadenomas (25%–90%).

Immunoblotting

Cells were lysed in ice-cold lysis buffer (10 mM KPO_4, 1 mM EDTA, 5 mM EGTA, 10 mM $MgCl_2$, 25 mM beta-glycerolphosphate, 50 mM NaF, 1 mM Na_3VO_4, 0.5% NP40, 0.1% Brij35, 0.1% sodium deoxycholate, 1 mM DTT, and 1× protease inhibitors (Sigma)). Tumor lysates were prepared by resuspending the pellets in RIPA buffer (150 mM NaCl, 1% NP-40, 0.5% sodium deoxycholate, 0.1% SDS, 50 mM Tris–HCl, pH 8) containing protease inhibitors (100 µM PMSF, 1 mM benzamidine, 2.5 µg/ml pepstatin A, 10 µg/ml leupeptin, and 10 µg/ml aprotinin) and phosphatase inhibitors (1 mM each of NaF, Na_3VO_4, and $Na_2P_2O_7$). Equal amounts of proteins were subjected to SDS-PAGE and transferred to nitrocellulose membranes. Membranes were blocked overnight at 4°C with 5% nonfat milk in TBS-T, followed by incubation in primary and secondary antibodies (1 h at RT, 2% milk in TBS-T). Proteins were detected by enhanced chemiluminescence.

RNA Isolation

The specific method for RNA isolations was indicated in Martin et al. (3). DNA and RNA were simultaneously isolated using a modified version of the method described in Pena-Llopis and Brugarolas (21). Tissues were lysed and homogenized using mirVana kit lysis buffer (Ambion), a micropestle, and QIAshredder columns (Qiagen, Hilden, Germany). DNA was isolated (targeted TSC2 sequencing) using AllPrep columns (Qiagen), while flow-throughs were used to isolate RNA using an acid phenol–chloroform extraction and the mirVana kit (Ambion). RNA integrity was confirmed using a Bioanalyzer 2100 (Agilent, Santa Clara, CA, USA). RNA concentrations were determined using a Qubit 2.0 fluorometer (Invitrogen).

RNA Sequencing and Differential Gene Expression Analysis

RNA sequencing of the UMB1949 and 621-102 cell lines was performed under identical published methods of our previous study (3). For RNA sequencing (GSE #189969), polyA-enriched libraries were sequenced with 100-bp paired end reads, aligned to hg19 genome build, and normalized to counts per million (CPM) (**Supplemental Table 3**). The patient RA tumor samples and normal kidney were from Martin et al. (2017) (3). For differential gene expression (DEG) analysis, mitochondrial genes were excluded; the remaining genes were ranked (high to low) by the absolute difference in $\log_2$ CPM between the average of the normal kidneys and the average of the RA tumors. CIBERSORT was performed as previously described (3), using the latest version 1.05 (3).

Statistical Analyses

Data are presented as mean ± standard error of the mean (s.e.m.) or mean ± standard deviation (s.d.), as indicated. For all animal

models, data are presented as mean ± 95% confidence interval. The EC_{50} calculations represent the best-fit data after fitting to a three-parameter dose–response curve in GraphPad Prism. A one-way ANOVA was performed to measure differences of the histological lesion types.

RESULTS AND DISCUSSION

To identify therapeutic vulnerabilities in TSC2-deficient tumors, we used a pair of isogenic cell lines derived from a renal angiomyolipoma (RA) cell line 621-101 that were either TSC2-deficient (621-102, control) or TSC2-rescued (621-103, *TSC2* expression) (**Figure 1A**) (16). First, we performed chemical compound screens in each cell line to identify compounds that compromised cell viability greater in the TSC2-deficient setting when compared to the TSC2-rescued cells (**Figure 1** and **Supplemental Table 1**). We used a molecularly targeted library consisting of 480 compounds from a collection of diverse, active, cell-permeable small-molecule inhibitors from preclinical research and clinical trials, including kinase inhibitors, natural products, and chemotherapeutic agents, screened at six concentrations (0.1 nM to 10 μM) for 72-h treatments (**Supplemental Table 1**). Next, we generated six-point dose–response curves for each molecularly targeted compound to generate cellular half maximal effective concentration (EC_{50}) values and prioritized compounds that were effective (reduced cell viability > 60% at any concentration) and particularly potent in TSC2-deficient cells (EC_{50} < 1 μM). By plotting EC_{50} values in TSC2-deficient versus TSC2-rescued cells (**Figure 1B**), we identified two compounds targeting the serine/threonine-protein checkpoint kinase 1 and 2 (CHK1 and CHK2), LY2603618 and AZD7762, as selective for TSC2-deficient cells, which were selected for additional interrogation. AZD7762 is equally potent against CHK1 and CHK2, and generally with good selectivity (>10-fold) against 164 kinases. Kinases with <10-fold selectivity were in the same family of kinases as CHK1/2, the CAM kinases, and some non-receptor tyrosine kinases (22). For LY2603618, CHK1 maintained >100-fold selectivity over the next target (PDK1) tested, and >1,500-fold selectivity over CHK2 (23). Dose–response curves for these inhibitors displayed >17-fold and

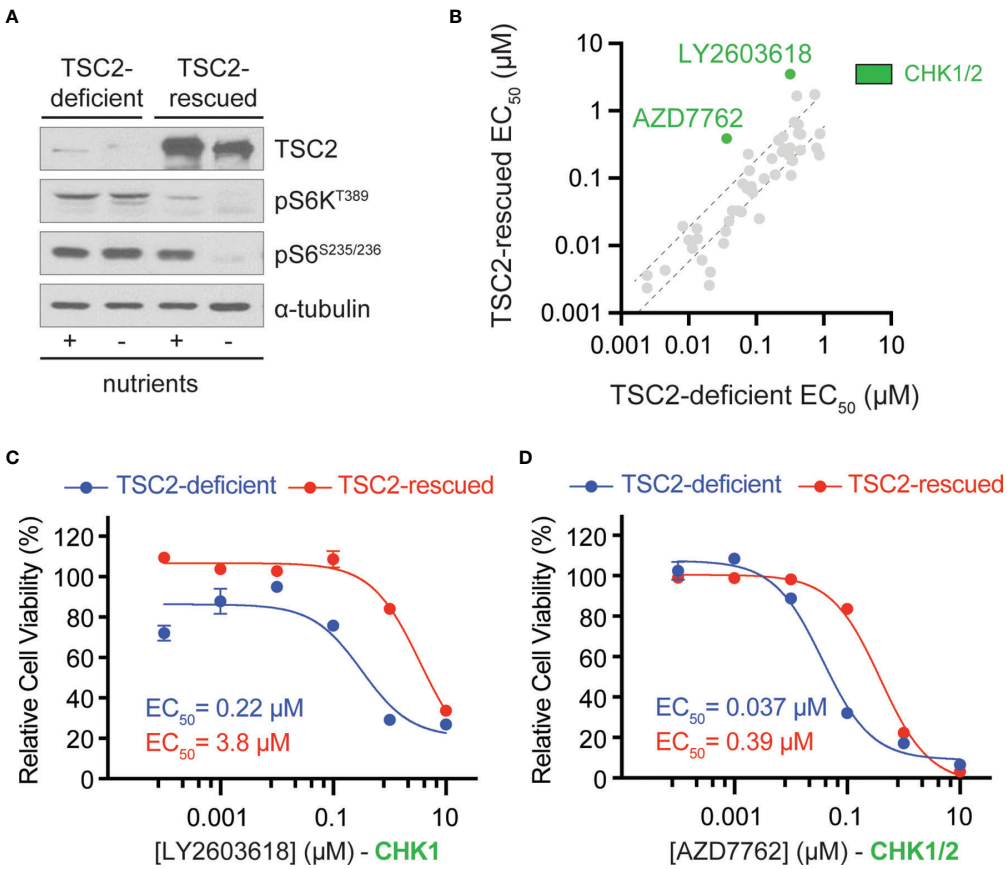

FIGURE 1 | Chemical compound screen identifies sensitivity to checkpoint kinase inhibition in TSC2-deficient cells. **(A)** Western blots from TSC2-deficient (621-102) or TSC2-rescued (621-103) cells cultured with (+) or without (-) nutrients. **(B)** Scatter plot of EC_{50} values after chemical compound screens in TSC2-deficient (x-axis) vs. TSC2-rescued (y-axis) cells with >60% reduction in viability and an EC_{50} value <1 μM in TSC2-deficient cells; dashed black lines represent the 99% confidence interval for the linear regression. CHK1/2, checkpoint kinase 1/2, inhibitors (green). **(C, D)** Dose–response curves for the indicated CHK inhibitors LY2603628 **(C)** and AZD7762 **(D)** in TSC2-deficient (blue) or TSC2-rescued cells (red) after 72 h; data are presented as mean ± s.e.m (n = 3).

>10-fold reductions in EC_{50} dependent on TSC2 status for LY2603618 and AZD7762, respectively (**Figures 1C, D**). Notably, TSC2-deficient cells treated with the dual CHK1/2 inhibitor, AZD7762 (**Figure 1D**), have a more potent and complete cellular EC_{50} when compared to the more selective CHK1 inhibitor, LY2693618 (**Figure 1C**), suggesting that CHK1/2 inhibition may be more effective at reducing the viability of TSC2-deficient cells. We note that AZD7762, while selective for CHK1/2, may be eliciting increased toxicity through off-target kinase engagement (22). Specifically, AZD7762 (EC_{50} = 37 nM) was 6-fold more potent for TSC2-deficient cells than LY2603618 (EC_{50} = 220 nM), and thus, we decided to pursue dual CHK1/2 inhibition in a TSC2-deficient setting.

To validate the primary chemical screen from 621-102 cells, we extended to a second patient-derived TSC cell line, UMB1949. We performed ten-point dose–response curves with AZD7762 in both TSC2-deficient cell lines, UMB1949 and 621-102. AZD7762 inhibited the growth of UMB1949 cells (EC_{50} = 33 nM) with a similar potency as 621-102 cells (**Figure 2A**). To validate that the inhibitory effects on viability were, in fact, due to CHK1 or CHK2 engagement, we used siRNA gene knockdown of CHK1 or CHK2 in the aforementioned cell lines (**Figure 2B**). While CHK1 knockdown resulted in a ~35% reduction in viability after 72 h, knockdown of CHK2 reduced viability up to 65%, consistent with increased potency of the dual CHK1/2 inhibitor AZD7762 relative to the CHK1-selective LY2603618. Given the role of TSC2 as a negative regulator of mTORC1 in response to various cellular stresses (24), including growth factor deprivation, we wanted to explore media conditions that allowed for cell growth and proliferation in a TSC2-deficient setting (**Supplemental Figure 1A**). In response to serum-restricted culture media (0.1% FBS), TSC2-deficient cells proliferated and responded to rapamycin treatment, while the TSC2-rescued cells were arrested and were unresponsive to rapamycin treatment (**Supplemental Figure 1B**) (25). Under these optimized growth conditions, we performed a secondary chemical screen in the TSC2-deficient 621-102 cells with a ten-point dose–response to acquire EC_{50} measurements (**Supplemental Table 2**). Notably, the rapalog everolimus was a potent inhibitor (**Supplemental Figure 1C**) as were both CHK inhibitors, LY2603618 and AZD7762 (**Supplemental Figure 1D**).

To expand the repertoire of potent compounds against TSC2-deficient cells, the top eighty-eight most potent (EC_{50}) compounds

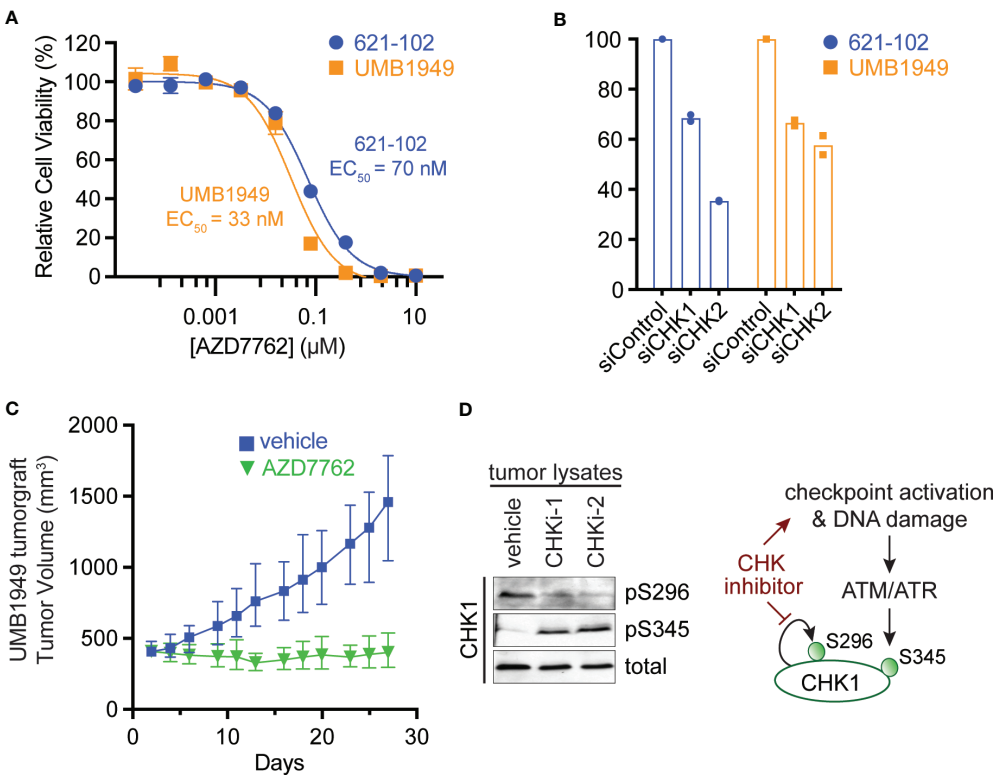

FIGURE 2 | Antitumor efficacy of CHK1/2 inhibitors in patient-derived TSC2-deficient tumors. **(A)** Dose–response curves for AZD7762 in 621-102 or UMB1949 cell lines after 72 h of treatment. Data are presented as mean ± s.e.m. (n = 3) after normalization to control, and the best fit EC_{50} is indicated. **(B)** Relative viability measurements of 621-102 or UMB1949 cells 72 h after siRNA knockdown of either CHK1 or CHK2. **(C)** UMB1949 cell line tumorgraft tumor volume in NSG mice. After tumors reached 400 ± 25 mm^3 in volume, mice were treated (i.p. injection) 5× per week with either vehicle (n = 9) or AZD7762 (12.5 mg/kg, n = 9); data presented as mean ± 95% confidence interval. **(D)** Western blot of tumor lysates from UMB1949 tumografts treated with either vehicle or AZD7762. Lysates were probed for phospho-markers of CHK1 (pS296 and pS345) and total CHK1 used as loading control; CHKi-1 and CHKi-2 indicate two AZD7762-treated tumors from panel **(C)**.

with >60% reduction in viability were selected from the secondary chemical screen in 621-102 cells, as described above (**Supplemental Table 2**). Next, we performed a follow-up compound screen in both the 621-102 and UMB1949 cell lines with ten-point dose responses to report EC_{50} measurements (**Supplemental Table 3**). Under the limited serum and growth factor conditions, both CHK inhibitors were among the most potent compounds tested, maintaining EC_{50} < 7 nM for UMB1949 cells and EC_{50} < 3 nM for 621-102 (**Supplemental Figures 1D–F**). The general overview of the chemical screens performed is shown in **Supplemental Figure 1G**.

To test the effects of the dual CHK1/2 inhibitor, AZD7762, on tumor growth, we turned to *in vivo* mouse models. We first established a cell line tumorgraft model of the patient-derived UMB1949 in NSG (NOD *scid* gamma) mice. Next, we treated mice with either vehicle or AZD7762 (12.5 mg/kg, 5× weekly, for 28 days) and measured tumor volume (**Figure 2C**). AZD7762 treatment caused a significant reduction in UMB1949 TSC2-deficient tumor size compared with the tumor volume of the vehicle control. Strikingly, the growth delay, calculated at the days required to reach tumor volume of 500 mm^3, was not achieved in the AZD7762 treatment group over the 28 days of treatment, while the control group reached 500 mm^3 on day five. This indicates complete tumor stasis with CHK1/2 inhibition, as mice were enrolled to begin drug treatment when tumors reached 400 mm^3, and final tumor measurements did not reach starting tumor volumes with 0% tumor growth in the AZD7762-treated group. As expected, tumor lysates from AZD7762-treated mice showed decreased CHK1 serine 296 auto-phosphorylation (pS296), confirming *in vivo* CHK1 target inhibition (**Figure 2D**). In addition, increased CHK1 serine 345 phosphorylation (pS345) by ATM/ATR indicates strong checkpoint activation, replication stress, or DNA damage response by CHK1 inhibition (**Figure 2D**).

The patient-derived UMB1949 cell line represents an additional cellular model of TSC with loss of TSC2 (**Figure 3A**), originally isolated from a male TSC patient with renal angiolipoma (18). Interestingly, we uncovered that UMB1949 cells reported by Lim et al. (18) were derived from a TSC patient that was part of our Martin et al. genomic profiling study (08-RA1) (3), which contained the same pathogenic frameshift deletion in TSC2 (**Figure 3A**). UMB1949 cell line identity matched to patient 08-RA1 was confirmed by rare variant analysis with minor allele frequency (MAF) < 0.01 in our exome data (3). To further establish a molecular understanding for the *in vitro* and *in vivo* models tested above, RNA-sequencing (**Supplemental Table 4**) was performed on UMB1949 and 621-102 cell lines and compared to our existing transcriptional landscape data for both normal kidney (NK) and RA tumors (3). When examining the top 500 differentially expressed genes (DEG) between normal kidneys and RA tumors, the transcriptional profiles of the two cell lines resembled the patient tumors (**Figure 3B**). In addition, cell-type deconvolution software (26) found adipose tissue and smooth muscle signatures shared between the cell models and patient angiomyolipomas, while expanded fetal kidney signatures were prominent in the cell lines (**Figure 3C**), perhaps due to the immortalization and effect, excess growth factors, or nutrients in cell culture media. Importantly, each cell line contained signatures of blood vessels, smooth muscle, and adipose tissue, the defining features of renal angiomyolipomas.

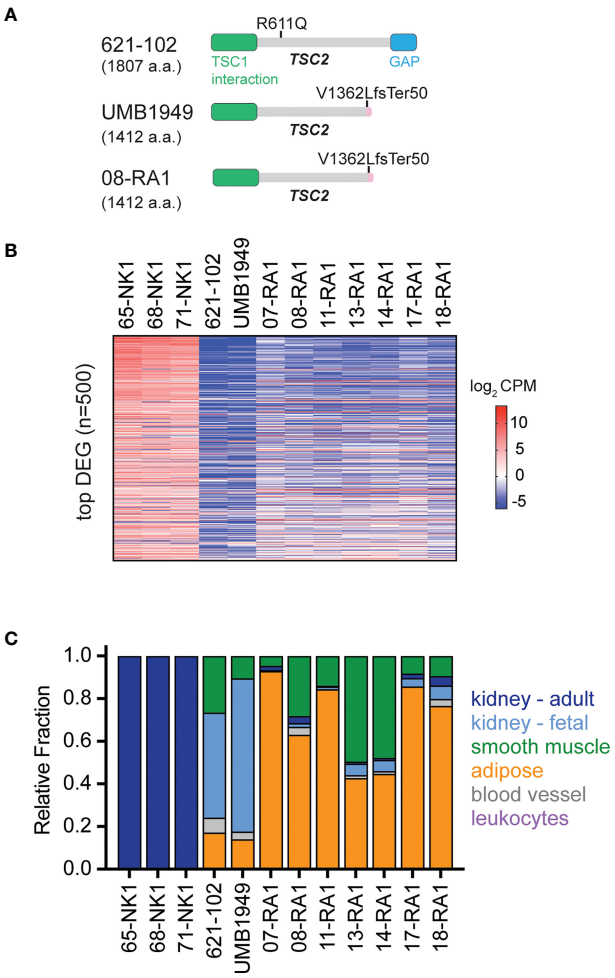

FIGURE 3 | Molecular characterization of TSC cellular models. **(A)** Schematic for TSC2 protein structure in TSC2-deficient cell lines (621-102 and UMB1949) or 08-RA1 patient renal angiolipoma (RA) tumor; GAP, GTPase-activating protein. TSC2 deletion in patient-derived UMB1949 and renal angiomyolipoma 08-RA1. **(B)** Top 500 most differentially expressed genes (DEG), sorted high (top) to low (bottom) across the indicated samples and colored by log2 CPM according to the indicated scale. **(C)** The relative fraction of gene signatures estimated by CIBERSORT (gray, blood vessel; green, smooth muscle; orange, adipose; light blue, fetal kidney; dark blue, adult kidney; leukocytes purple).

We further evaluated CHK1/2 inhibition in a second mouse TSC model (27), in which 105K cells, a Tsc2-deficient cystadenoma cell line, derived from a renal tumor from a $Tsc2^{+/-}$ mouse (19). Tsc2-deficient 105K cells were engrafted subcutaneously into BALB/c-nu immunodeficient mice, and again, mice treated with AZD7762 had a significant reduction in tumor volume relative to vehicle-treated mice (**Figure 4A**). In addition, complete tumor stasis with CHK1/2 inhibition was

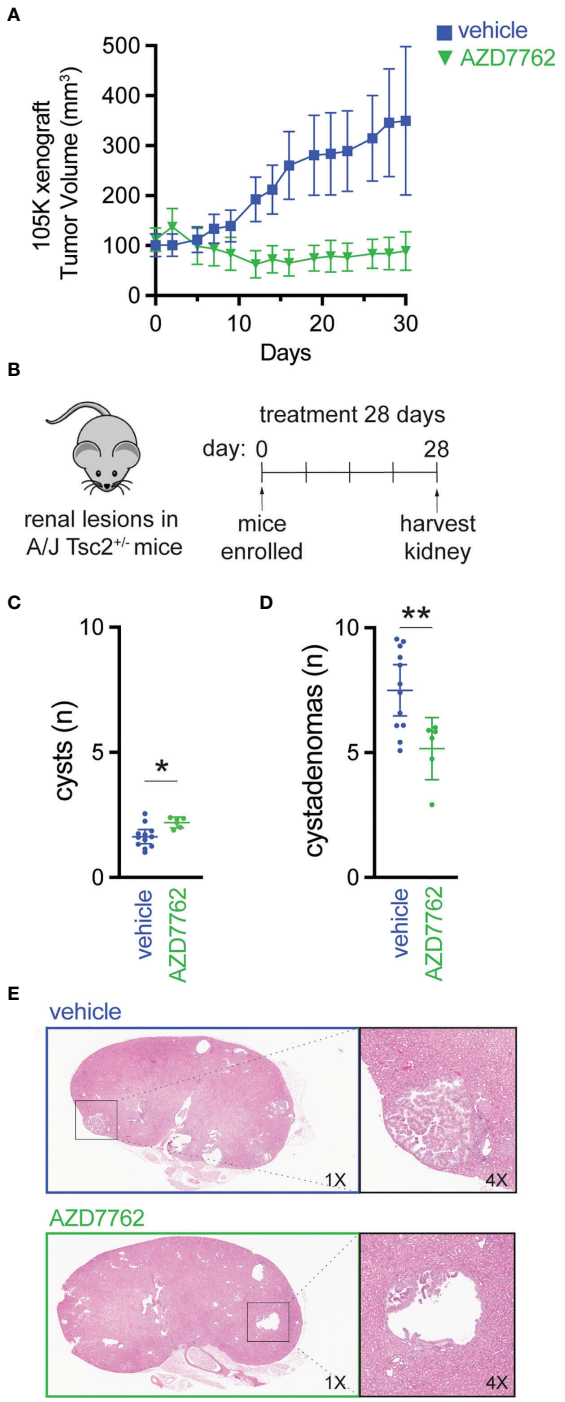

FIGURE 4 | Checkpoint kinase inhibition as an effective antitumor strategy in preclinical tumor models of TSC2 loss. **(A)** Tumor volume of 105K xenografts in BALB/c nude mice treated once daily for 28 days with either vehicle (n = 14) or AZD7762 (12.5 mg/kg, n = 14); data presented as mean ± 95% confidence interval. **(B–D)** Eight-month-old A/J *Tsc2*$^{+/-}$ mice were treated daily with either vehicle (n = 10) or AZD7762 (12.5 mg/kg, n = 10) for 28 days; each treatment group had five male and five female mice. Data presented as mean ± 95% confidence interval and analyzed by one way ANOVA (*p < 0.05; **p < 0.01). **(E)** H&E-stained tissue of kidney sections from each indicated treatment group showing large cystadenoma lesion (vehicle) and cleared cyst (AZD7762).

again observed, as mice were enrolled to begin drug treatment when tumors reached 100 mm^3 and final tumor measurements at 30 days did not reach starting tumor volumes. The AZD7762-treated mice had a >20% reduction in tumor volume as compared to the vehicle treated group with a >300% increase in tumor volume.

Next, we treated an A/J mouse model with heterozygous germline deletion of *Tsc2* (*A/J Tsc2*$^{+/-}$ mice) that spontaneously develops kidney pathology with age (20). In this model, tumors develop and progress from cysts to cystadenomas, and the severity of kidney cystadenomas increases with age. At 8 months of age, the age at which these mice have high tumor burden, *A/J Tsc2*$^{+/-}$ mice received AZD7762 or vehicle for 28 days (**Figure 4B**). After treatment, we harvested both left and right kidneys and performed histological analysis of cysts and cystadenomas to quantify overall cyst and tumor burden. Representative H&E-stained kidney sections used to quantify cysts and cystadenomas after treatment are shown (**Figure 4E**). Lesions were classified as cysts (0% < cell content < 25%) or cystadenomas (25% < cell content < 90%). AZD7762 treatment resulted in a 32% decrease in cystadenomas (**Figure 4D**) and a reduction in the progression from cyst to cystadenomas, as evidenced by the modest increase in the number of cysts (**Figure 4C**).

Here, we presented multiple chemical compound screens in TSC2-deficient cells as compared to TSC2-rescued cells. CHK inhibitors were potent inhibitors under all screening conditions tested, in particular in the restricted growth conditions that reveal the tumor-promoting properties of TSC2 loss. The antitumor potential of the dual CHK1/2 inhibitor, AZD7762, was demonstrated in three different animal models of TSC2-deficient tumors. The second-generation CHK inhibitor (prexasertib) is currently in clinical trials for various human cancers and appears to have mitigated toxicity concerns associated with the first-generation CHK inhibitor (28). Our data support further exploration of CHK inhibition in mTOR-driven pathologies and suggest a mechanistic connection between DNA damage response and mTOR signaling. Indeed, a growing body of evidence links mTORC1 activation to DNA damage repair (29–31). Consistent with these data, we previously reported a low mutational burden in TSC2-deficient patient tumors (3), suggesting efficient DNA repair mechanisms and perhaps a therapeutic vulnerability in tumors lacking functional TSC2.

DATA AVAILABILITY STATEMENT

The datasets presented in this study can be found in online repositories. The names of the repository/repositories and accession number(s) can be found in the article/**Supplementary Material**.

ETHICS STATEMENT

The animal studies were reviewed and approved by Porsolt's Ethical Committee and Van Andel Institute Review Committee.

AUTHOR CONTRIBUTIONS

Designing research studies: KM., JM, DA. Conducting experiments: KM, JK, KS, C-YC, NS, MB, MK. Acquiring data: KM, RV, JM. Analyzing data: KM, RV, NS, JM, DA. Providing reagents: DA. Writing the manuscript: RV, KM, JM. Acquisition of funding: RV, JM, DA. All authors contributed to the article and approved the submitted version.

FUNDING

RV (K00CA245821) and JM (R21CA263133) have research support from the National Cancer Institute. This work was supported by grants and funding from the Michigan Strategic Fund, Tuberous Sclerosis Complex Alliance, Blue Cross Blue Shield of Michigan Foundation, and individual donors.

ACKNOWLEDGMENTS

We thank team members from PsychoGenics, Porsolt, and the MacKeigan Lab for their helpful discussions.

SUPPLEMENTARY MATERIAL

The Supplementary Material for this article can be found online at: https://www.frontiersin.org/articles/10.3389/fonc.2022.852859/full#supplementary-material

REFERENCES

1. Dabora SL, Jozwiak S, Franz DN, Roberts PS, Nieto A, Chung J, et al. Mutational Analysis in a Cohort of 224 Tuberous Sclerosis Patients Indicates Increased Severity of TSC2, Compared With TSC1, Disease in Multiple Organs. *Am J Hum Genet* (2001) 68:64–80. doi: 10.1086/316951
2. Tyburczy ME, Dies KA, Glass J, Camposano S, Chekaluk Y, Thorner AR, et al. Mosaic and Intronic Mutations in TSC1/TSC2 Explain the Majority of TSC Patients With No Mutation Identified by Conventional Testing. *PloS Genet* (2015) 11:e1005637. doi: 10.1371/journal.pgen.1005637
3. Martin KR, Zhou W, Bowman MJ, Shih J, Au KS, Dittenhafer-Reed KE, et al. The Genomic Landscape of Tuberous Sclerosis Complex. *Nat Commun* (2017) 8:15816. doi: 10.1038/ncomms15816
4. McKusick VA. Mendelian Inheritance in Man and its Online Version, OMIM (2007) (Accessed August 31, 2021).
5. Crino PB, Nathanson KL, Henske EP. The Tuberous Sclerosis Complex. *N Engl J Med* (2006) 355:1345–56. doi: 10.1056/NEJMra055323
6. MacKeigan JP, Krueger DA. Differentiating the mTOR Inhibitors Everolimus and Sirolimus in the Treatment of Tuberous Sclerosis Complex. *Neuro Oncol* (2015) 17:1550–9. doi: 10.1093/neuonc/nov152
7. Brakemeier S, Bachmann F, Budde K. Treatment of Renal Angiomyolipoma in Tuberous Sclerosis Complex (TSC) Patients. *Pediatr Nephrol* (2017) 32:1137–44. doi: 10.1007/s00467-016-3474-6
8. Eijkemans MJC, van der Wal W, Reijnders LJ, Roes KCB, van Waalwijk van Doorn-Khosrovani SB, Pelletier C, et al. Long-Term Follow-Up Assessing Renal Angiomyolipoma Treatment Patterns, Morbidity, and Mortality: An Observational Study in Tuberous Sclerosis Complex Patients in the Netherlands. *Am J Kidney Dis* (2015) 66:638–45. doi: 10.1053/j.ajkd.2015.05.016
9. Inoki K, Li Y, Zhu T, Wu J, Guan K-L. TSC2 Is Phosphorylated and Inhibited by Akt and Suppresses mTOR Signalling. *Nat Cell Biol* (2002) 4:648–57. doi: 10.1038/ncb839
10. Bissler JJ, McCormack FX, Young LR, Elwing JM, Chuck G, Leonard JM, et al. Sirolimus for Angiomyolipoma in Tuberous Sclerosis Complex or Lymphangioleiomyomatosis. *N Engl J Med* (2008) 358:140–51. doi: 10.1056/NEJMoa063564
11. McCormack FX, Inoue Y, Moss J, Singer LG, Strange C, Nakata K, et al. Efficacy and Safety of Sirolimus in Lymphangioleiomyomatosis. *N Engl J Med* (2011) 364:1595–606. doi: 10.1056/NEJMoa1100391
12. Krueger DA, Care MM, Holland K, Agricola K, Tudor C, Mangeshkar P, et al. Everolimus for Subependymal Giant-Cell Astrocytomas in Tuberous Sclerosis. *N Engl J Med* (2010) 363:1801–11. doi: 10.1056/NEJMoa1001671
13. Franz DN, Belousova E, Sparagana S, Bebin EM, Frost M, Kuperman R, et al. Efficacy and Safety of Everolimus for Subependymal Giant Cell Astrocytomas Associated With Tuberous Sclerosis Complex (EXIST-1): A Multicentre, Randomised, Placebo-Controlled Phase 3 Trial. *Lancet* (2013) 381:125–32. doi: 10.1016/S0140-6736(12)61134-9
14. Krueger DA, Care MM, Agricola K, Tudor C, Mays M, Franz DN. Everolimus Long-Term Safety and Efficacy in Subependymal Giant Cell Astrocytoma. *Neurology* (2013) 80:574–80. doi: 10.1212/WNL.0b013e3182815428
15. Valianou M, Filippidou N, Johnson DL, Vogel P, Zhang EY, Liu X, et al. Rapalog Resistance Is Associated With Mesenchymal-Type Changes in Tsc2-Null Cells. *Sci Rep* (2019) 9:3015. doi: 10.1038/s41598-019-39418-5
16. Hong F, Larrea MD, Doughty C, Kwiatkowski DJ, Squillace R, Slingerland JM. mTOR-Raptor Binds and Activates SGK1 to Regulate P27 Phosphorylation. *Mol Cell* (2008) 30:701–11. doi: 10.1016/j.molcel.2008.04.027
17. Yu J, Astrinidis A, Howard S, Henske EP. Estradiol and Tamoxifen Stimulate LAM-Associated Angiomyolipoma Cell Growth and Activate Both Genomic and Nongenomic Signaling Pathways. *Am J Physiol Lung Cell Mol Physiol* (2004) 286:L694–700. doi: 10.1152/ajplung.00204.2003
18. Lim SD, Stallcup W, Lefkove B, Govindarajan B, Au KS, Northrup H, et al. Expression of the Neural Stem Cell Markers NG2 and L1 in Human Angiomyolipoma: Are Angiomyolipomas Neoplasms of Stem Cells? *Mol Med* (2007) 13:160–5. doi: 10.2119/2006-00070.Lim
19. Parkhitko AA, Priolo C, Coloff JL, Yun J, Wu JJ, Mizumura K, et al. Autophagy-Dependent Metabolic Reprogramming Sensitizes TSC2-Deficient Cells to the Antimetabolite 6-Aminonicotinamide. *Mol Cancer Res* (2014) 12:48–57. doi: 10.1158/1541-7786.MCR-13-0258-T
20. Woodrum C, Nobil A, Dabora SL. Comparison of Three Rapamycin Dosing Schedules in A/J Tsc2+/- Mice and Improved Survival With Angiogenesis Inhibitor or Asparaginase Treatment in Mice with Subcutaneous Tuberous Sclerosis Related Tumors. *J Transl Med* (2010) 8:14. doi: 10.1186/1479-5876-8-14
21. Peña-Llopis S, Brugarolas J. Simultaneous Isolation of High-Quality DNA, RNA, miRNA and Proteins From Tissues for Genomic Applications. *Nat Protoc* (2013) 8:2240–55. doi: 10.1038/nprot.2013.141
22. Zabludoff SD, Deng C, Grondine MR, Sheehy AM, Ashwell S, Caleb BL, et al. AZD7762, A Novel Checkpoint Kinase Inhibitor, Drives Checkpoint Abrogation and Potentiates DNA-Targeted Therapies. *Mol Cancer Ther* (2008) 7:2955–66. doi: 10.1158/1535-7163.MCT-08-0492
23. King C, Diaz H, Barnard D, Barda D, Clawson D, Blosser W, et al. Characterization and Preclinical Development of LY2603618: A Selective and Potent Chk1 Inhibitor. *Invest New Drugs* (2014) 32:213–26. doi: 10.1007/s10637-013-0036-7
24. Demetriades C, Plescher M, Teleman AA. Lysosomal Recruitment of TSC2 is a Universal Response to Cellular Stress. *Nat Commun* (2016) 7:10662. doi: 10.1038/ncomms10662
25. Zhang H, Cicchetti G, Onda H, Koon HB, Asrican K, Bajraszewski N, et al. Loss of Tsc1/Tsc2 Activates mTOR and Disrupts PI3K-Akt Signaling Through Downregulation of PDGFR. *J Clin Invest* (2003) 112:1223–33. doi: 10.1172/JCI17222
26. Newman AM, Liu CL, Green MR, Gentles AJ, Feng W, Xu Y, et al. Robust Enumeration of Cell Subsets From Tissue Expression Profiles. *Nat Methods* (2015) 12:453–7. doi: 10.1038/nmeth.3337
27. Liu H-J, Lizotte PH, Du H, Speranza MC, Lam HC, Vaughan S, et al. TSC2-Deficient Tumors Have Evidence of T Cell Exhaustion and Respond to Anti–PD-1/Anti–CTLA-4 Immunotherapy. *JCI Insight* (2018) 3(8):e98674. doi: 10.1172/jci.insight.98674
28. Sausville E, Lorusso P, Carducci M, Carter J, Quinn MF, Malburg L, et al. Phase I Dose-Escalation Study of AZD7762, A Checkpoint Kinase Inhibitor,

in Combination With Gemcitabine in US Patients With Advanced Solid Tumors. *Cancer Chemother Pharmacol* (2014) 73:539–49. doi: 10.1007/s00280-014-2380-5
29. Silvera D, Ernlund A, Arju R, Connolly E, Volta V, Wang J, et al. mTORC1 and -2 Coordinate Transcriptional and Translational Reprogramming in Resistance to DNA Damage and Replicative Stress in Breast Cancer Cells. *Mol Cell Biol* (2017) 37:e00577–16. doi: 10.1128/MCB.00577-16
30. Xie X, Hu H, Tong X, Li L, Liu X, Chen M, et al. The mTOR-S6K Pathway Links Growth Signalling to DNA Damage Response by Targeting RNF168. *Nat Cell Biol* (2018) 20:320–31. doi: 10.1038/s41556-017-0033-8
31. Ma Y, Vassetzky Y, Dokudovskaya S. mTORC1 Pathway in DNA Damage Response. *Biochim Biophys Acta Mol Cell Res* (2018) 1865:1293–311. doi: 10.1016/j.bbamcr.2018.06.011

Conflict of Interest: JM has consulting agreements with Merck, research support from Erasca, and scholarly activity and support from Translational Genomics Research Institute (non-profit organization). JK's current affiliation is with AbbVie. The remaining authors declare that the research was conducted in the absence of any commercial or financial relationships that could be construed as a potential conflict of interest.

Publisher's Note: All claims expressed in this article are solely those of the authors and do not necessarily represent those of their affiliated organizations, or those of the publisher, the editors and the reviewers. Any product that may be evaluated in this article, or claim that may be made by its manufacturer, is not guaranteed or endorsed by the publisher.

frontiers in Oncology

ORIGINAL RESEARCH
published: 16 March 2022
doi: 10.3389/fonc.2022.837980

Nuclear Receptor PXR Confers Irradiation Resistance by Promoting DNA Damage Response Through Stabilization of ATF3

Xiaxia Niu[1†], Hongmei Cui[1†], Xinsheng Gu[2*], Ting Wu[1], Min Sun[3], Changlong Zhou[1] and Mei Ma[1]*

[1] Institute of Toxicology, School of Public Health, Lanzhou University, Lanzhou, China, [2] College of Basic Medical Sciences, Hubei University of Medicine, Shiyan, China, [3] Department of General Surgery, Taihe Hospital, Hubei University of Medicine, Shiyan, China

Low response rate to radiotherapy remains a problem for liver and colorectal cancer patients due to inappropriate DNA damage response in tumors. Here, we report that pregnane X receptor (PXR) contributes to irradiation (IR) resistance by promoting activating transcription factor 3 (ATF3)-mediated ataxia-telangiectasia-mutated protein (ATM) activation. PXR stabilized ATF3 protein by blocking its ubiquitination. PXR–ATF3 interaction is required for regulating ATF3, as one mutant of lysine (K) 42R of ATF3 lost binding with PXR and abolished PXR-reduced ubiquitination of ATF3. On the other hand, threonine (T) 432A of PXR lost binding with ATF3 and further compromised ATM activation. Moreover, the PXR–ATF3 interaction increases ATF3 stabilization through disrupting ATF3–murine double minute 2 (MDM2) interaction and negatively regulating MDM2 protein expression. PXR enhanced MDM2 auto-ubiquitination and shortened its half-life, therefore compromising the MDM2-mediated degradation of ATF3 protein. Structurally, both ATF3 and PXR bind to the RING domain of MDM2, and on the other hand, MDM2 binds with PXR on the DNA-binding domain (DBD), which contains zinc finger sequence. Zinc finger sequence is well known for nuclear receptor peroxisome proliferator-activated receptor-γ (PPARγ) playing E3 ligase activity to degrade nuclear factor κB (NFκB)/p65. However, whether zinc-RING sequence grants E3 ligase activity to PXR remains elusive. Taken together, these results provide a novel mechanism that PXR contributes to IR resistance by promoting ATF3-mediated ATM activation through stabilization of ATF3. Our result suggests that targeting PXR may sensitize liver and colon cancer cells to IR therapy.

Keywords: irradiation resistance, DNA damage response, PXR, ATF3, MDM2, stabilization, ubiquitination

OPEN ACCESS

Edited by:
Katherine Pawelczak, NERx Biosciences, United States

Reviewed by:
Shilpa Singh, Virginia Commonwealth University, United States
Kishore Chiruvella, University of North Carolina at Chapel Hill, United States

****Correspondence:***
Hongmei Cui
cuihm@lzu.edu.cn
Xinsheng Gu
gu.xinsheng@gmail.com

†These authors have contributed equally to this work

Specialty section:
This article was submitted to Cancer Molecular Targets and Therapeutics, a section of the journal Frontiers in Oncology

Received: *17 December 2021*
Accepted: *10 February 2022*
Published: *16 March 2022*

Citation:
Niu X, Cui H, Gu X, Wu T, Sun M, Zhou C and Ma M (2022) Nuclear Receptor PXR Confers Irradiation Resistance by Promoting DNA Damage Response Through Stabilization of ATF3. Front. Oncol. 12:837980. doi: 10.3389/fonc.2022.837980

INTRODUCTION

Adjuvant or neoadjuvant radiotherapy is applied to treat approximately 50% of all cancers. The rate of pathological complete responses to radiotherapy remains very low (1). Only 12.2% of patients with rectal cancer achieve pathological complete responses after neoadjuvant chemoradiation therapy (2). Resistance to irradiation (IR) therapy occurs in 70%–96% of patients with gastrointestinal cancer, which has become a pressing issue to be solved in order to achieve high rates of pathological complete responses of cancer therapy. Unfortunately, so far, there is no agent that can function as a radiosensitizer to be used in gastrointestinal cancer therapy in the clinic (1).

Cancer cells have been found to employ several mechanisms related to the tumor and the surrounding microenvironment to resist IR damage. Such mechanisms include altered cell cycles, evolving a hypoxia microenvironment, survival from oxidative stress, evading apoptosis, altered DNA damage response (DDR) and enhanced DNA repair, remodeling of cellular energetic system, and acquisition of radioresistant capability (1). Among these mechanisms, DDR is an initiator step to resist radiotherapy for cancer cells and the first step to recover from radioactive damage for healthy cells.

The DDR is a highly organized and coordinated process in eukaryotes to survive DNA damage. This process starts from sensing the aberrant DNA structures induced by genotoxic chemicals and IR, then the signals are transduced and executed to promote survival of organisms. Ataxia-telangiectasia-mutated protein (ATM) is one of the master transducers of DNA damage signal to orchestrate a large network of cellular processes to maintain genomic integrity upon activation. ATM is a kinase that phosphorylates itself and downstream effectors, such as p53 and checkpoint kinase 2 (Chk2), thus arresting cell cycle, allowing for DNA repair or apoptosis. The ATM-Chk2-cell division cycle 25A (Cdc25A)-cyclin-dependent kinase 2 (Cdk2) pathway acts as a genomic integrity checkpoint and guards against radioresistant DNA synthesis (3). ATM phosphorylates and stabilizes zinc (Zn) finger E-box binding homeobox 1(ZEB1) in response to DNA damage, subsequently, ZEB1 interacts with USP7 and enhances its ability to deubiquitylate and stabilize CHK1, thereby promoting CHK1-mediated homologous recombination-dependent DNA repair and resistance to IR in breast cancer cells (4). ATM has become a promising target to develop sensitizers for cancer radiotherapy and chemotherapy.

Activating transcription factor 3 (ATF3) belongs to ATF/cAMP-responsive element-binding protein (CREB) family (5). ATF3 mainly functions as a tumor suppressor, and its expression is induced under stress conditions (6). Previously, researchers reported that ATF3 stabilizes "genome guardian" p53 by blocking murine double minute 2 (MDM2)-mediated ubiquitination, and a cancer-derived ATF3 mutant (R88G) devoid of ubiquitination failed to prevent p53 from MDM2-mediated degradation and thus was unable to activate DDR (7, 8). Additionally, ATF3 is involved in DDR by regulating ATM activation (9, 10). ATF3 promotes acetylation and activation of ATM through recruiting USP7 to Tat-interactive protein 60 (Tip60) that is a MYST histone acetyltransferase (HAT), thus stabilizing Tip60 and facilitating acetylation and phosphorylation of ATM (10). It has been shown that ATF3 promotes resistance of breast cancer to chemotherapy (11, 12) and radiotherapy (13).

MDM2 is an E3 ubiquitin ligase that carries out the final step in the ubiquitination cascade, catalyzing transfer of ubiquitin from an E2 enzyme to form a covalent bond with a substrate lysine (14–16). ATF3 is one of the substrates of MDM2 and degraded through MDM2-mediated ubiquitin–proteasome pathway (17).

Pregnane X receptor (PXR, NR1I2, SXR) belongs to the nuclear receptor superfamily and is mainly expressed in normal liver, small intestine, colon, duodenum, and gall bladder tissues (18). PXR is involved in the metabolism of a broad spectrum of endogenous and xenobiotic compounds, including more than 50% of clinical drugs through coordinately regulating the expression of phase I and phase II drug-metabolizing enzymes (19–21). In addition, PXR is also involved in carcinogenesis, glucose metabolism, and inflammation response (19). Interaction between PXR and PRMT1 promotes translocation of PRMT1 from nuclei to cytoplasm, and interaction between PXR and YAP mediates liver size and regeneration (22, 23). Our previous studies have revealed that PXR plays an important role in protecting hepatocellular carcinoma HepG2 cells against DNA damage induced by benzo[a]pyrene (BaP), a representative genetic toxicant of polycyclic aromatic hydrocarbons (PAHs), probably through a coordinated regulation of genes involved in BaP metabolism (24, 25). These studies suggest that PXR protects liver cancer cells from DNA damage stress. We hypothesized that PXR may also protect cancer cells from DNA damage induced by IR and confers resistance of these cells to IR.

In this study, we investigated the role and the mechanism of PXR in the protection of liver and colon cancer cells from IR-induced DDR. We have found that PXR confers resistance of liver and colon cancer cells to IR-induced DNA damage stress through stabilization of ATF3. In this pathway, PXR promotes ATM activation through ATF3. PXR stabilizes ATF3 against MDM2-mediated ubiquitination through both disrupting MDM2–ATF3 interaction and negatively regulating MDM2 expression level. Our findings provided a clue to overcome resistance of liver and colon cancers to IR therapy by targeting PXR.

MATERIALS AND METHODS

Plasmids

Flag-ATF3 and GST-ATF3, HA-ubiquitin, pCG-ATF3 were kindly provided by Dr. Chunhong Yan (Augusta University) and Dr. Tsonwin Hai (Ohio State University). GST-PXR, GST-PXR (1-107), and GST-PXR (107-434) were kindly presented by Dr. Yanan Tian (Texas A&M University). pCDNA3-MDM2 (Plasmid #16233) and Myc3-HDM2 (Plasmid #20935) were purchased from Addgene (Watertown, MA, USA). The primers used to develop GST-ATF3 truncated protein upon

request. PXR protein was purchased from ProteinOne (Rockville, MD, USA). All site-directed mutations of PXR or ATF3 constructs were generated using Quick Change Site-Directed Mutagenesis Kit (Agilent, Santa Clara, CA, USA).

Cell Culture and Colony Formation Assays

Colon cancer LS180 cells and liver cancer HepG2-C3A cells were obtained from ATCC and cultured in EMEM supplemented with 10% FBS, 100 units/ml penicillin, and 100 μg/ml streptomycin. Cells were verified to be mycoplasma-free by using Mycoplasma Detection Kit (R&D Systems). To generate PXR-knockout (KO) cell line, PXR CRISPR/Cas9 KO plasmid (sc-400824-KO-2) and PXR HDR plasmid (sc-400824-HDR-2) were co-transfected using Lipofectamine 2000 (Invitrogen) according to the manufacturer's instruction. Here, 2 μg/ml puromycin was used to screen the PXR-KO single clones. For colony formation assays, 1,000 cells were seeded in 6-well plates and were exposed to 0, 10, and 30 Gy of IR, and surviving colonies were fixed with 10% formalin and stained with 0.1% crystal violet 8 days later. Stained colonies were dissolved with buffer containing SDS, and absorbance was recorded at 490 nm using a microplate reader.

Neutral Comet Assay

Radiated cells were trypsinized, centrifuged for 2 min at 300×g, and resuspended in PBS at 2×10^4/ml. Cell suspensions were then mixed with 1% of low-melting point agarose at 1:3 (V/V) and layered on a microscope slide precoated with 1% agarose gel. Cells in gels were lysed with the neutral lysis buffer (2 M NaCl, 30 mM EDTA, 10 mM Tris-HCl, pH 8.5, 1% N-laurylsarcosine, 1% Triton X-100) at 4°C for 1 h. After rinsing 3 times with the TBE buffer (90 mM Tris, 90 mM boric acid, 2 mM EDTA, pH 8.5) at room temperature for 30 min, slides were submerged in TBE for electrophoresis at 20 V for 25 min. Slides were then rinsed, neutralized in distilled water, dipped in ethanol, and dried. Slides were stained using 2.5 μg/ml of ethidium bromide in distilled water for 20 min and observed under a fluorescence microscope. At least 100 comet images from each slide were analyzed using the CASP software (http://casplab.com/).

Western Blotting

Cells were lysed in modified radioimmunoprecipitation assay (RIPA) containing 50 mm Tris-HCl (pH 7.4), 150 mm NaCl, 1% Nonidet P-40, 0.1% SDS, 0.5% sodium deoxycholate, 1 mm EDTA, and proteinase inhibitor mixtures. The proteins were resolved in 10%–12% SDS-PAGE gels and detected using the desired antibodies. The antibodies and the dilution ratios are as follows: ATF3 (sc-44C3a, 1:1000), PXR (sc-48340, 1:1000), and HA antibody (sc-805, 1:200) were purchased from Santa Cruz Biotechnology, Inc. (Dallas, TX, USA). MDM2 (4B11, 1:500) was purchased from EMD Millipore (Billerica, MA, USA); anti-mouse IgG VeriBlot for IP secondary antibody (HRP) (ab131368) and anti-Phosphor-(Ser/Thr) Phe antibody (ab17464, 1:1000) were purchased from Abcam (Cambridge, MA, USA). FLAG (F3165, 1:4000) and actin (A5441, 1:5000) were purchased from MilliporeSigma (St. Louis, MO, USA). The p-Ser1981 ATM (#5883, 1:1,000) and p-H2AX (#2557, 1:1000) were purchased from Cell Signaling (Danvers, MA, USA).

Quantitative RT-PCR

Total RNA was extracted from cells using TRIzol (Invitrogen, Carlsbad, CA, USA), reverse-transcribed using the SuperScript® VILO™ cDNA Synthesis Kit (Thermo Fisher Scientific Inc. NYSE: TMO), and subjected to real-time PCR assays using SYBR Green reagents (Qiagen, Venlo, Netherlands). The sequences of the primers were as follows: GAPDH, 5'-AACGGATTTGGTCGTATTGGG-3' and 5'-CCTGGAAGATGGTGATGGGATT-3'; ATF3, 5'-GTGCCGAAACAAGAAGAAGG-3' and 5'-TCTGAGCCTTCAGTTCAGCA-3'; PXR, 5'-GGCCACTGGCTATCACTTCAA-3' and 5'-TTCATGGCCCTCCTGAAAA-3'.

SiRNA Knockdown

The PXR and MDM2 siRNA SMARTpool were purchased from Dharmacon (Thermo Fisher Scientific Inc. NYSE: TMO). Double knockdown of PXR and MDM2 or ATF3 expression was carried out using RNAiMAX (Invitrogen, Carlsbad, CA, USA) following the manufacturer's protocols. Briefly, HepG2-C3A and LS180 cells were transfected with 100 pM SiPXR, Si MDM2, SiATF3, or SiLuc as control for 48 h and aliquoted for further run of knockdown. After 72 h, cells were harvested and subjected to Western blotting assays.

In Vitro GST-Pulldown Assays

In this study, 1 μg GST or GST fusion proteins immobilized on glutathione-agarose from MilliporeSigma (St. Louis, MO, USA) were incubated with *in vitro*-translated proteins (5 μl) (TnT® Quick Coupled Transcription/Translation Systems, L1170, Promega, Madison, WI, USA) or recombinant proteins (50–100 ng) (ProteinOne, Rockville, MD, USA) in a buffer containing 20 mM Tris-HCl, pH 8.0, 100 mM NaCl, 2 mM EDTA, 2 mM DTT, 5% glycerol, and 0.4% NP-40 at 4°C overnight, followed by extensive washes with a similar buffer containing 150 mM NaCl. Bound proteins in the beads were eluted by boiling in the SDS-PAGE loading buffer and detected by Western blotting or fluorography using a desired antibody.

In Vivo Co-Immunoprecipitation Assays

Cell lysates (1–2 mg) were incubated with 20 μl protein A/protein G agarose beads (Cat #: IP05, Millipore) in RIPA buffer (50 mM Tris-HCl, pH 7.4, 100 mM NaCl, 1% NP-40, 0.1% SDS, 0.5% sodium deoxycholate, and 1 mM EDTA) at 4°C overnight for precleaning. After centrifugation, the supernatants were transferred to incubate with another 20 μl of protein A/protein G agarose beads (Millipore) together with 1 μg corresponding antibody in RIPA buffer at 4°C for 5 h. After extensive washes with RIPA buffer containing 150 mM NaCl, bound proteins in the beads were eluted by boiling in the SDS-PAGE loading buffer and detected by Western blotting or fluorography using a desired antibody.

In Vivo Ubiquitination Assays and *In Vitro* Ubiquitination Assays

The *in vivo* ubiquitination assay was performed according to the published method (10). Briefly, H1299 cells were transfected

with FLAG-ATF3 and HA-ubiquitin with or without MDM2 or PXR and treated with 5 μM of MG132 overnight and then lysed in the FLAG lysis buffer (50 mM Tris-HCl, pH 7.9, 137 mM NaCl, 10 mM NaF, 1 mM EDTA, 1% Triton X-100, 0.2% sarkosyl, and 10% glycerol). Cell lysates (1–2 mg) were incubated with 20 μl of anti-FLAG M2 affinity gel (Sigma) at 4°C overnight. After extensive washes, agarose gels were loaded on spin columns (Affymetrix), and bound FLAG-ATF3 was eluted with 20 μl of FLAG peptide at a final concentration of 0.1 mg/ml. ATF3 ubiquitination was determined by Western blotting using the hemagglutinin (HA) antibody.

The *in vitro* ubiquitination assay was performed using a human MDM2/HDM2 Ubiquitin Ligase Kit (K-200B) by following the manufacturer's instructions with modifications. Briefly, *in vitro* translated ATF3 (TnT® Quick Coupled Transcription/Translation Systems, L1170) was incubated with E1, E2, and GST-MDM2, ubiquitin with buffer containing 50 mM Tris-HCl, pH 8.0, 50 mM NaCl, 1 mM EDTA, 5% glycerol, 10 mM fresh DTT on ice for 2 h and then add with or without PXR recombinant protein (ProteinOne, Rockville, MD) at 37°C for another 2 h. Polyubiquitinated proteins were detected using ATF3 antibody or FK-1 (ENZO) after resolving in SDS-PAGE.

Immunofluorescence Staining

Tissue array that incorporated 50 pairs of human colon adenocarcinoma tissue and adjacent non-tumor tissue sample (D100Co01) from Bioaitech (China) was used to stain the protein expression of PXR (sc-48340, 1: 100) and MDM2 (4B11, 1: 100). Briefly, the tissue array was permeabilized with 0.1% Triton X-100 in PBS solution, and then the array was incubated with the indicated antibody overnight at 4°C, followed by incubation with immunofluorescence second antibody (A32728 and A32742, respectively, Invitrogen) at room temperature for 1 h. The array was washed three times with PBS and sealed with mounting media containing DAPI (Vector Labs, Burlingame, CA, USA; H-2000). The photographs were scanned with 3DHISTECH (PANNORAMIC DESK/MIDI/250/1000, Hungary) and analyzed by ImageJ software.

Statistical Analysis

Data were analyzed using Prism Software 5.0 (GraphPad Software, Inc.). The statistical significance ($p < 0.05$) was evaluated by Student's t test and one-way ANOVA.

RESULTS

PXR Physically Interacted With ATF3

Given that ATF3 is quite critical in regulating Tip60 and p53-mediated DDR (7, 10), we want to explore whether PXR binds to ATF3. GST-pulldown assays showed that immobilized GST-ATF3 directly pulled down PXR protein *in vitro*. This was specific since GST alone did not pull down PXR (**Figure 1A**). In order to investigate whether the interaction between PXR and ATF3 occurs endogenously, we performed *in vivo* reciprocal co-immunoprecipitation (co-IP) assays using H1299 cells transiently co-transfected with PXR and/or ATF3 plasmid. The results showed that ATF3 antibody but not IgG precipitated PXR in H1299 cells transfected with both ATF3 and PXR (**Figure 1B**). Since PXR protein was only expressed in the liver cancer HepG2-C3A cells and colon adenocarcinoma LS180 cells (**Supplementary Figure S1A**), we then generated PXR KO of HepG2-C3A and LS180 cells. We found that PXR antibody precipitated ATF3 in wild-type LS180 cells but not in PXR-KO LS180 cells (**Figure 1C**). These results suggested that PXR physically interacted with ATF3. Because ATF3 expression alters largely under DNA damage treatments (7), we also determined whether the DNA damage condition affects the interaction between ATF3 and PXR. We then subjected LS180 cells to γ-IR and incubated cell lysates with GST-ATF3 and carried out the endogenous GST-pulldown assay. The results showed that PXR also interacted with ATF3 upon IR (**Figure 1D**, **Supplementary Figure S1B**); furthermore, like the ATF3–Tip60 interaction (7), the binding between PXR and ATF3 was altered neither by time extension after IR treatment nor by DNA damage treatment, such as IR, doxorubicin (DOX), or camptothecin (CPT) (**Figure 1D** and **Supplementary Figure S1B**).

PXR Increases ATF3 Stability by Blocking Ubiquitination

ATF3 protein has a very short half-life, and its protein stability can be altered (17). We then want to know whether PXR can affect the protein stability of ATF3. Results of co-expression with a fixed amount of ATF3 and different doses of PXR expression plasmids showed that the ATF3 protein levels were increased in association with increments of the doses of PXR plasmid (**Figure 2A**). KO of PXR decreased ATF3 expression (**Figure 2B**). The regulation of ATF3 by PXR does not likely occur in the transcriptional level, as there were no significant differences in the ATF3 mRNA levels between the wild-type and the screened PXR-KO clones (**Figure 2B**). Furthermore, this effect is not clone specific, as we transfected HepG2-C3A and LS180 wild-type cells with siRNAs targeting PXR, and the results confirmed that knockdown of PXR resulted in downregulation of ATF3 (**Supplementary Figure S2B**). PXR indeed extended the half-life of endogenous ATF3 protein (**Figure 2C**). These results have suggested that PXR stabilizes ATF3 at the protein level. It has been shown that ATF3 is susceptible to undergo ubiquitination, then proteolytic degradation (17, 26, 27); we next investigate whether ubiquitination of ATF3 is regulated by PXR. Since ATF3 can work as a ubiquitin trapper and FLAG antibody can precipitate ubiquitinated ATF3 (8), we transfected FLAG-ATF3, HA-ubiquitin, with or without PXR, and found that PXR indeed decreased ubiquitination of ATF3 in a dose-dependent manner (**Figure 2D**, lane 5 vs. lane 4). And this effect was proteasome dependent, as ATF3 decreased when ubiquitin was added (**Supplementary Figure S2B**). Taken together, PXR increased ATF3 stability and extended ATF3 protein half-life by blocking its ubiquitination and degradation.

PXR–ATF3 Interaction Is Required for Regulating ATF3

We next want to figure out whether interactions between PXR and ATF3 are required for PXR-mediated regulation of ATF3. In order

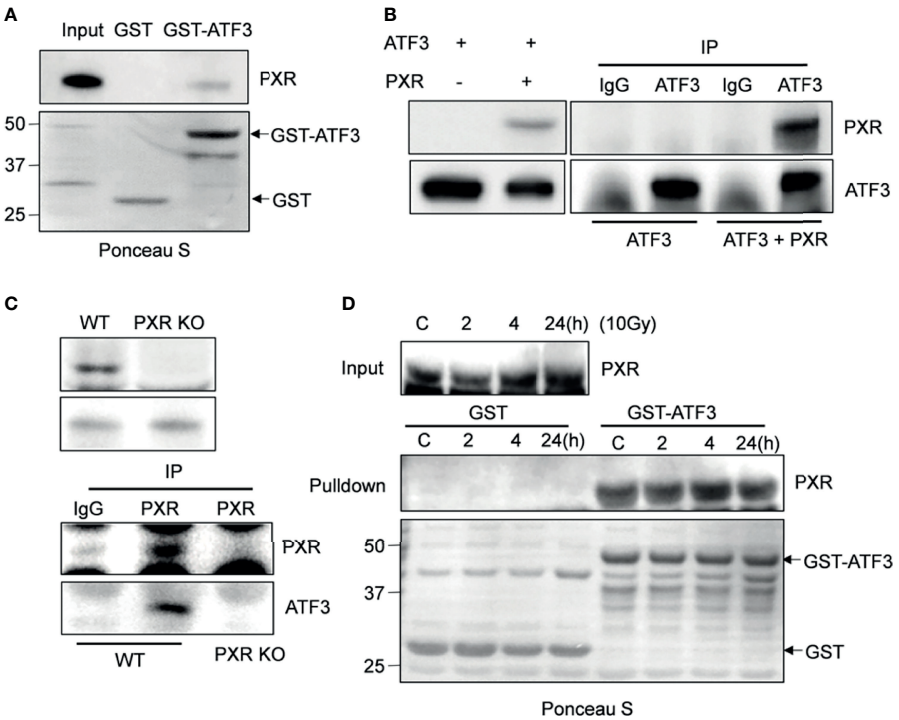

FIGURE 1 | PXR interacts with ATF3. **(A)** PXR interacted with GST-ATF3. 1 μg GST or GSTATF3 protein was immobilized onto 20 μl glutathione agarose beads, and then incubated with 5 μl *in vitro* translated PXR. GST-pulldown assay was performed. **(B)** Interaction between PXR and ATF3 revealed by reciprocal co-IP experiment. H1299 cells in 60 mm3 dish were co-transfected with 3 μg FLAG-PXR, and/or pCG-ATF3. The immunoprecipitation assay was performed using 1μg IgG antibody or ATF3 antibody. **(C)** Interaction between PXR and ATF3 confirmed by endogenous co-IP assay. 3 mg wild-type and PXR-knockout (KO) LS180 cells were harvested, and PXR antibody (sc-48403) was used for immunoprecipitation, HRP-labeled secondary antibody (ab131368) was used to develop signal. **(D)** Irradiation does not alter the binding of PXR to ATF3. LS180 cells were treated with 10 Gy of IR and harvested at different time points. 5 μl *in vitro* translated PXR was incubated with 1 μg immobilized GSTATF3 or GST as indicated for pulldown assays.

to gain this aim, we built several truncated constructs of ATF3 fused with GST agarose beads, incubated with *in vitro* translated PXR, and performed GST-pulldown assay. We found that full-length ATF3 except for leucine zipper (Zip) domain bound with PXR as a fragment of aa 1-79, aa 80-100, aa 141-181 was required for ATF3 to interact with PXR (**Figure 3A**). We therefore want to know whether there is an ATF3 binding-deficient lysine (K) residue that loses the ability to be ubiquitinated by PXR. Normally, lysine residue on the protein structure can be substrate to attach ubiquitination cascade (14), then we mutated 6 lysine residues on the binding region of ATF3 to arginine (R), performed FLAG-IP to test which mutant will lose the binding with PXR, and further abolished PXR-mediated regulation. Indeed, K42R mutation failed to pull down PXR (**Figure 3B**, lane 3 vs. lane 2). Furthermore, the FLAG-tagged ATF3 K42R mutation abolished PXR-mediated reduction of ubiquitination of ATF3 (**Figure 3C**, lane 4 vs. lane 3). The results suggested that the ATF3 K42 in a fragment of aa 1-79 was essential for PXR-inhibited ubiquitination of ATF3.

On the other hand, GST-pulldown assay revealed that partial ligand-binding domain of PXR (aa 300-434) was required for PXR to interact with ATF3 as a truncated fragment of aa 1-434, aa 1-420 but not aa 1-180, or aa1-300 pulled down ATF3 (**Figure 3D**). PXR protein structure is enriched with serine (S)/threonine (T) amino acid and defined as a phosphoprotein (28). Indeed, we observed that IR induced significant increases in the phosphorylation of S/T in PXR (**Figure 3E**). In order to identify which S/T sites are essential for PXR–ATF3 interaction, we mutated 12 S/T sites to alanine (A), which is located on aa 300-434 of PXR-binding region, and we found that the T432A mutant loses the ability to interact with ATF3 (**Figure 3F**, lane 13 vs. lane 2). In order to confirm that the phosphorylation of T432 is critical for ATF3-mediated ATM activation upon IR, we transfected the wild-type PXR or the PXR T432A mutant plasmid into the PXR-KO LS180 cells and then subjected cells to IR. The results demonstrated that the p-ATM level was significantly decreased in the PXR-KO LS180 cells transfected with the PXR T432A mutant plasmid compared with that of the wild-type PXR transfection (**Figure 3G**, lane 6 vs. lane 4), suggesting that the phosphorylation of PXR T432 was pivotal for ATF3-mediated ATM activation upon IR in colon cancer cells.

PXR Stabilized ATF3 by Counteracting MDM2-Catalyzed Ubiquitination of ATF3

Besides p53, ATF3 is a well-known substrate of E3 ligase MDM2, and MDM2 is responsible for the ubiquitination and degradation of ATF3 (17). This knowledge leads us to investigate whether PXR disrupts ATF3–MDM2 interaction, thus abrogating

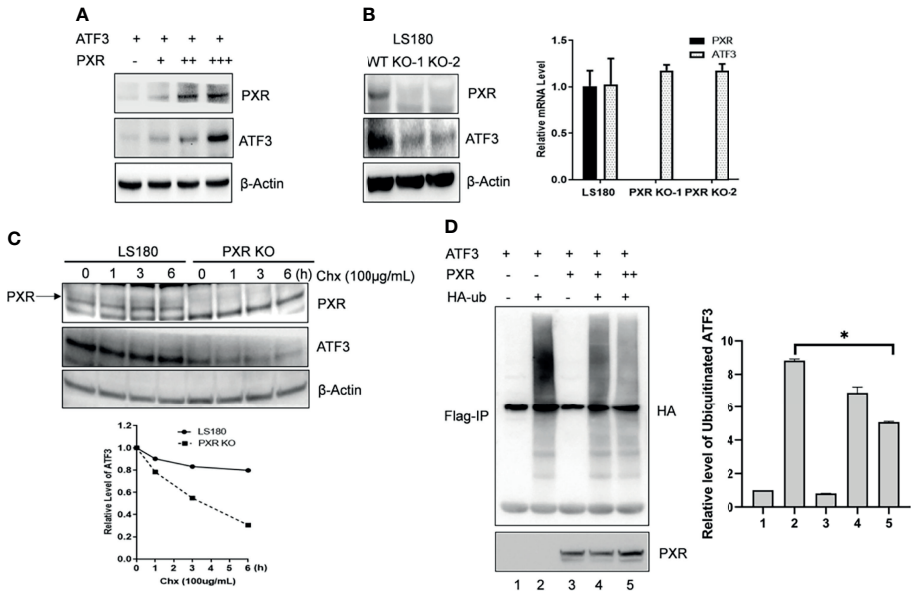

FIGURE 2 | PXR increased ATF3 stability by blocking its ubiquitination. **(A)** Co-transfection of PXR increased the ATF3 protein levels. H1299 cells were transfected with 0.2 μg FLAGATF3 and 0, 0.4, 0.8, or 3.2 μg PXR plasmids as indicated for 2 days. The protein levels were determined using Western blotting. **(B)** PXR regulates ATF3 in protein level. Two LS180 PXR KO clones (KO-1 and KO-2) and the wild-type cells were subjected for Western blotting and quantitative RT-PCR. **(C)** PXR stabilizes ATF3 protein. LS180 wild-type or PXR KO cells were treated with 100 μg/ml of cycloheximide (Chx), and lysed for Western blotting as indicated. Relative ATF3 levels were quantitated by densitometry and presented in the lower plot. **(D)** PXR decreased the ATF3 ubiquitination level. Lysates from H1299 cells transfected with 1μg FLAG-ATF3, 2μg HA-ubiquitin, and/or PXR plasmids (lane 3 and lane 4, 2μg; lane 5, 4ug) were subjected to immunoprecipitation assays using the FLAG agarose beads (Sigma) followed by SDS-PAGE. Ubiquitinated ATF3 were detected by HA antibody. *$p < 0.05$.

MDM2-mediated ubiquitination and stabilizing ATF3. To gain this aim, we incubated *in vitro* translated MDM2 with glutathione agarose beads conjugated with ATF3 overnight, added recombinant PXR to the system, and performed GST-pulldown assay. The results showed that ATF3 pulled down MDM2 as expected, and the amount of MDM2 bound with ATF3 was decreased by addition of recombinant PXR in a dose-dependent manner, suggesting that PXR indeed disrupted ATF3–MDM2 interaction *in vitro* (**Figure 4A**). Next, we want to clarify whether PXR increases ATF3 stability by blocking MDM2-catalyzed ATF3 ubiquitination. By applying FLAG-IP, we found that the ubiquitination levels of ATF3 were increased by MDM2, whereas PXR abolished MDM2-mediated ubiquitination (**Figure 4B**, lanes 5 vs. lane 4). By applying Western blotting, we found that the ATF3 protein levels were decreased by MDM2, while these were increased by addition of PXR (**Figure 4C**, lane 3 vs. lane 2, lane 5 vs. lane 4). Furthermore, we also performed *in vitro* ubiquitination assay, and the results demonstrated that the ATF3 ubiquitination levels were enhanced by MDM2 in a dose-dependent manner (**Figure 4D**, lane 2 and lane 4) as expected. More importantly, addition of PXR reduced the MDM2-mediated ATF3 ubiquitination (**Figure 4D**, lane 3 vs. lane 2 and lane 5 vs. lane 4). However, PXR is not an E3 ligase for ATF3, and it has no capability to induce ubiquitination of ATF3 (**Supplementary Figure S4E**, lane 6 vs. lane 3). Collectively, our results indicated that PXR suppressed MDM2-catalyzed ubiquitination of ATF3 *in vivo* and *in vitro*.

PXR Interacts With MDM2 and Negatively Regulates MDM2 Protein Expression

Interestingly, we noticed a diminished band of MDM2 when we co-transfected MDM2 with PXR plasmid together (**Figure 4B**, lane 5 vs. lane 4), which indicated that PXR might affect MDM2 expression level. To further understand this regulation, we analyzed 151 samples from The Cancer Genome Atlas rectum adenocarcinoma (TCGA-READ) database (portal.gdc.cancer.gov/) and found that the mRNA expression level of PXR negatively correlated with mRNA expression of MDM2 ($p < 0.05$) (**Figure 5A**). Immunofluorescence staining has revealed that PXR protein level is ubiquitously higher in human colon adenocarcinoma tissues than that in adjacent non-tumor tissues, whereas MDM2 protein expression has the opposite trend with PXR in tumor tissue vs. that in adjacent non-tumor tissues (**Figure 5B**). Indeed, PXR has physical binding with MDM2. By performing GST-pulldown assay, we found that MDM2 bound with PXR in the DNA-binding domain (DBD) (aa 1-107) (**Figure 5C** and **Supplementary Figure S4A**). Conversely, PXR binds with MDM2 on the RING domain (aa 431-491) (**Figure 5D** and **Supplementary Figure S4B**). The RING domain of MDM2 is essential for its E3 ligase activity. Coincidently, ATF3 also binds with MDM2 on this RING domain. The structure binding analysis provides the explanation that PXR structurally can interrupt the interaction between ATF3 and MDM2. In order to further address PXR-inhibited MDM2 expression, we detected the half-life of MDM2

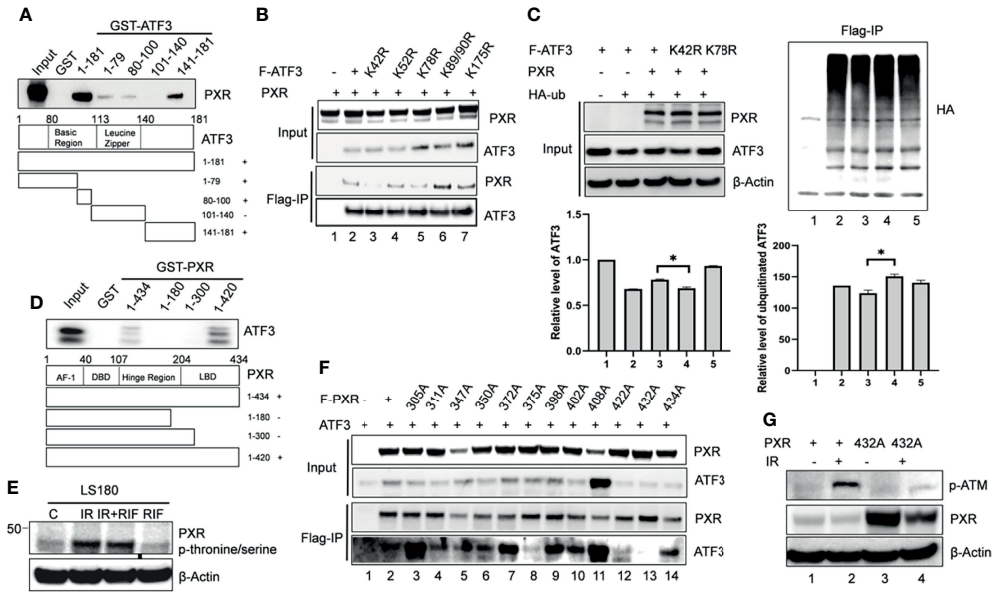

FIGURE 3 | The PXR-ATF3 interaction is required for ATF3 regulation. **(A)** Identification of ATF3 domains for PXR binding. 1 μg ATF3 truncated proteins fused to GST were immobilized onto glutathione agarose beads and incubated with 5 μl *in vitro* translated PXR for GST-pulldown assays. The pulled-down proteins were detected by Western blotting using the PXR antibody. **(B)** The ATF3 K42R mutation significantly reduced the binding between ATF3 and PXR. H1299 cells were transfected with 1.5 μg FLAG-ATF3 wild type or mutants, and 1.5 μg PXR as indicated for 2 days. FLAG-immunoprecipitation (IP) assays were performed using FLAG antibody to precipitate. **(C)** The ATF3 K42 was essential for ubiquitination of ATF3 regulated by PXR. H1299 cells were transfected with 1 μg FLAGATF3 wild type or mutants, and 2μg HA-ubiquitin, and/or 4 μg PXR as indicated for 2 days, and then subjected to FLAG-IP assays using FLAG antibody to precipitate *$p < 0.05$. **(D)** Mapping of PXR domains/regions for ATF3 binding. 1 μg PXR truncated proteins fused to GST were immobilized onto glutathione agarose beads and incubated with 5 μl *in vitro* translated ATF3 for GST-pulldown assays. The pulled-down proteins were detected by Western blotting using the ATF3 antibody. **(E)** Irradiation-induced significant increases in the phosphorylation of threonine/serine in PXR in colon cancer cells. LS180 cells were treated with 10 μM rifampicin (RIF) for 12 h, then radiated at a dose 10 Gy for 4h, PXR antibody was used to immunoprecipitate, then anti- Phosphor - (Ser/Thr) Phe antibody (ab17464) was used to blot. **(F)** The PXR T432A mutation significantly reduced the binding between ATF3 and PXR as determined by FLAG-IP. H1299 cells were transfected with 1 μg FLAG-PXR wild type or mutants, and 2μg HA-ubiquitin, and/or 1 μg ATF3 as indicated for 2 days, and then subjected to FLAG-IP assays using FLAG antibody to precipitate. **(G)** The PXR T432A mutation abolished ATM phosphorylation and activation induced by IR in colon cancer cells. LS180 PXR knockout cell was transfected with 1.5 ug PXR wildtype, or mutant for 2 days, and then subjected to 10 Gy of γ- irradiation and harvested after 24 h. The protein levels were determined by Western blotting using the indicated antibodies.

and ubiquitination of MDM2. Strikingly, the result showed that PXR reduced the MDM2 half-life in colon cancer cells (**Figure 5E**), and PXR increased endogenous ubiquitination of MDM2 (**Figure 5F**). MDM2 is an oncogene, and its auto-ubiquitination enhances its substrate ubiquitin ligase activity (29). In order to further confirm that PXR increases auto-ubiquitination of MDM2, we performed *in vitro* ubiquitination assays, incubated E1 and E2, and purified GST-MDM2 and recombinant PXR *in vitro* together. FK-1 antibody was used to detect polyubiquitination (7). The results showed that PXR indeed increased auto-ubiquitination of MDM2 in a dose-dependent manner (**Figure 5G**). In order to further confirm that PXR is an upstream regulator for MDM2, we transfected siRNA targeting PXR, and the results showed that PXR knockdown resulted in downregulation of ATF3 and upregulation of MDM2 (**Figure 5H**, lane 2 vs. lane 1, **Supplementary Figure S4C**). More importantly, it seems that PXR expression level is not altered by MDM2 (**Figure 5G**, lane 3 vs. lane 1), whereas MDM2 expression is dependent on PXR regulation (**Figure 5H**, lane 4 vs. lane 2). As a consequence, like ATF3, tumor suppressor p53, both of which are substrates of MDM2, also can be upregulated by PXR (**Supplementary Figure S4D**).

PXR Confers Irradiation-Induced DNA Damage Resistance Through Regulating ATF3

Previously, we proved that ATF3 promoted ATM activation upon IR treatment *via* USP14-Tip60 axis. Consistent with these results, IR-induced phosphorylation of ATM was dramatically suppressed in the PXR-KO cells where the ATF3 expression level was downregulated (**Figure 6A**, lanes 6–10 vs. lanes 1–5). Similarly, IR-induced phosphorylation of ATM substrates including H2AX was also repressed in the PXR-KO cells (**Figure 6A**). The suppression of ATM activation by PXR KO was not limited to LS180 cells, as similar observations were obtained in HepG2-C3A PXR-KO cells (**Supplementary Figure S5A**). Meanwhile, upregulated MDM2 followed PXR KO (**Figure 6A**). In line with this result, there are more colonies in the wild-type LS180 and HepG2-C3A cells after IR than those in PXR-KO cells (**Figure 6B**). Besides, the olive tail moments of the wild-type LS180 cells were much shorter than those of the PXR-

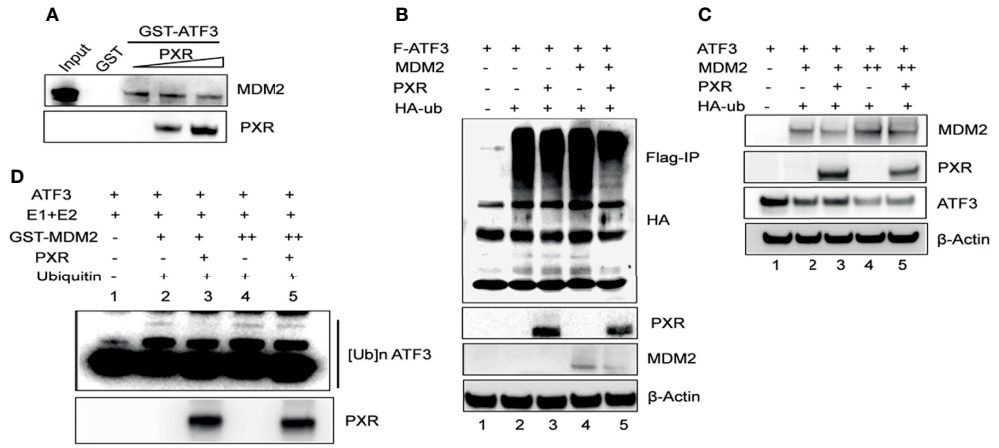

FIGURE 4 | PXR counteracts MDM2-mediated ubiquitination and stabilization of ATF3. **(A)** PXR disrupted ATF3-MDM2 interaction *in vitro*. *In vitro* translated MDM2 and GST-ATF3 were mixed and incubated for 4 h, then 0.5 μg or 1 μg recombinant PXR proteins were added and incubated at 4°C overnight. GST- pulldown assay was performed and the protein levels were determined by Western blotting using indicated antibodies. **(B)** PXR decreased MDM2-catalysed ubiquitination of ATF3. H1299 cells were transfected with 0.5 μg FLAG-ATF3, 2μg MDM2, HA-ubiquitin, and/or 3μg PXR plasmids. After cells were lysed, FLAG-IP assay was performed using FLAG antibody to precipitate and HA antibody to probe. **(C)** PXR counteracted MDM2-induced downregulation of ATF3. H1299 cells were transfected with 0.2μg ATF3, 0.8 μg PXR, and increasing amounts of MDM2 (+, 0.8μg; ++, 1.6μg) plasmids as indicated, and then lysed for Western blotting. **(D)** PXR protected ATF3 against MDM2-mediated ubiquitination *in vitro*. *In vitro* translated ATF3 incubated with E1, E2, and/or GSTMDM2 (E3) for 2h at 4°C, then mixed with or without 1μg recombinant PXR protein at 37°C for 2h. The protein levels were determined by Western blotting using indicated antibodies.

KO LS180 cells (**Figure 6C**). These results suggested that PXR promoted cell viability and conferred IR resistance through facilitating ATM activation of DNA damage response and repair in liver and colon cancer cells. In order to confirm that PXR promotes ATM signaling through regulating ATF3, we knocked down ATF3 expression by siRNA in both wild-type and PXR-KO LS180 cells and then determined IR-induced ATM activation. Consistent with our previous report, knockdown of ATF3 obviously compromised ATM activation (**Figure 6D** and **Supplementary Figure S5B**, lane 4 vs. lane 2), and KO of PXR indeed downregulated ATF3. Furthermore, KO of PXR induced much more suppression of ATM activation where ATF3 expression was further inhibited (**Figure 6D** and **Supplementary Figure S5B**, lane 8 vs. lane 4). Surprisingly, the basal level of phosphorylated ATM was almost abolished when ATF3 expression was knocked down in PXR-KO HepG2-C3A cells (**Supplementary Figure S5B**).

DISCUSSION

Resistance to IR therapy is a noxious problem in gastrointestinal cancer adjuvant or neoadjuvant radiotherapy. No radiosensitizer has been approved for use in gastrointestinal cancers (1). The rate of pathological complete responses to radiotherapy remains low (1). In the current study, our data reveal that PXR promotes viability and reduces DNA damage of liver and colon cancer cells after IR, providing a clue to overcoming radioresistance in liver and colon cancers where PXR is expressed by targeting PXR.

In the current study, our data have disclosed that PXR protects liver and colon cancer cells from IR-induced DNA damage through ATF3-mediated ATM activation. This is an extension for the mechanism by which PXR protects liver cancer HepG2 cells from DNA damage induced by genotoxicants such as BaP. PXR reduced BaP-induced DNA adduct formation through a coordinated regulation of genes involved in xenobiotic metabolism (24) and through inhibiting the BaP biotransformation (25). Ionized radiation directly causes lethal double-stranded DNA breaks, in which ATM is the master regulator of DNA damage response and repair (30). It is likely our data revealed a novel role of PXR in protecting cells against double-stranded DNA breaks, in addition to single-stranded DNA breaks and DNA adducts.

It has been shown that ATM activation is regulated by ATF3 in response to DNA damage stress (9, 10). As one of the key regulators of the DDR, ATF3 promotes DDR by facilitating ATM activation through increasing Tip60 HAT activity and determining cell fate by regulating p53 stabilization, thereby allowing appropriate cellular response to DNA damage (7, 10, 31). Despite many events that are regulated by ATF3 have been elucidated, little is known about how ATF3 activity is regulated. In the current study, we identified the nuclear receptor PXR as an ATF3 regulator. PXR interacts with ATF3 and increases ATF3 protein stability, thus facilitating DDR by promoting ATM activation. PXR is a well-known ligand-regulated transcription factor, and our current study shows that ATF3 protein levels are closely associated with PXR protein levels and PXR protein increases ATF3 protein levels but not the mRNA levels, suggesting that PXR regulates ATF3 at the protein levels. Furthermore, PXR increases ATF3 stability by blocking its ubiquitination. PXR increases ATF3 levels by counteracting MDM2-catalyzed ubiquitination of ATF3 *in vitro* and *in vivo*. Since ATF3 is a *bona fide* substrate of E3 ligase MDM2, MDM2 is the only E3 ligase so far known to degrade ATF3 (17), and ubiquitination is a proteasome-mediated pathway for

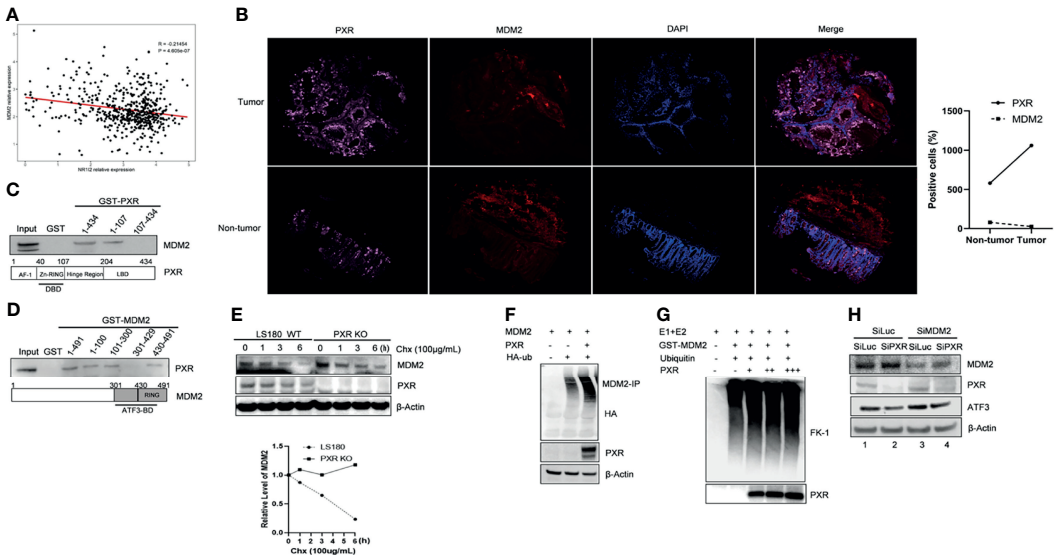

FIGURE 5 | PXR interacts with MDM2 and negatively regulate expression of MDM2. **(A)** mRNA expression of PXR negatively correlated with mRNA expression of MDM2. 151 colorectal samples from TCGA database were collected and analyzed the correlations between mRNA level of PXR and that of MDM2. **(B)** PXR, MDM2 immunofluorescence staining in matched samples of human colon adenocarcinoma tissue and adjacent non-tumor tissue. The right panel shows the statistics of positive staining cells. n = 50 for each group. **(C)** The DBD contains zinc-finger region of PXR physically interacted with MDM2. Truncated PXR were immobilized with GST and incubated with *in vitro* translated MDM2 and subjected with GST-pulldown to map the region of PXR binding with MDM2. **(D)** PXR physically interacted with MDM2 on the RING domain. Truncated MDM2 were immobilized with GST and incubated with *in vitro* translated PXR and subjected with GST-pulldown to map the region of MDM2 binding with PXR. **(E)** PXR reduced MDM2 protein half-life in colon cancer cells. LS180 wild-type and PXR knockout cells were treated with 100 μg/mL cycloheximide (CHX), harvested at different time point, and then Western blotting was performed to detect MDM2 half-life alteration. Relative MDM2 levels were quantitated by densitometry and presented in the right plot. **(F)** Ubiquitination of MDM2 was enhanced by addition of PXR. H1299 cells were transfected with 0.5 μg HDM2, 1 μg HA-ubiquitin, and/or 2 ug PXR plasmids, then MDM2-immunoprecipitation was performed with HA antibody to probe. **(G)** PXR increased polyubiquitination of MDM2 in a dose-dependent manner. E1, E2, and GST-MDM2 (E3) were incubated with ubiquitin for 3 h at 4°C, and 0.5 μg, 1 μg, 3 μg recombinant PXR was then added as indicated and incubated for another 3 h. The protein levels were determined by Western blotting. FK-1 antibody was used to detect polyubiquitination. **(H)** MDM2 inhibition by siRNA abolished knockdown of PXR mediated downregulation of ATF3 expression. LS180 cells were transfected with 20 nM SiLuc or SiMDM2 for 24 h and then transfected with 20 nM SiLuc or SiPXR for 48 h. Then cells were collected and lysed, and the PXR, MDM2 and ATF3 protein levels were determined using Western blotting.

protein degradation (32), it seems that PXR regulated ATF3 through modulating MDM2-mediated ATF3 protein ubiquitination and degradation, which are independent of its transcription activity. This is also a novel mechanism for PXR to function through protein–protein interaction and signaling crosstalk in the regulation of cellular function (19), in addition to being a transcription factor.

Strikingly, our data revealed that by binding with RING domain of MDM2, PXR decreased MDM2 protein expression, enhanced polyubiquitination of MDM2, and reduced MDM2 protein half-life (**Figure 5**). It has been reported that the nuclear receptor peroxisome proliferator-activated receptor-γ (PPARγ) exhibits the RING-finger E3 ligase activity and mediates degradation of MUC1-C oncoprotein (33) and nuclear factor κB (NF-κb)/p65 (34). Structurally, the RING-finger E3 ligase contains the Zn fingers of 40–60 residues that bind two atoms of Zn, which mediates protein–protein interactions (35–37). The basic pattern in Zn finger domain is CX (2) CX (9 to 39) CX (1 to 3) HX (2 to 3) CX (2) CX (4 to 48) CX (2) C. One of the characteristic structures of nuclear receptor superfamily is its conserved DBD, which contains Zn finger domain (36, 37). PPARγ contains two C4-type Zn finger domains in the DBD (38), in which a region between amino acid residues 139 and 198 (between the Znf1 and Znf2) is identified to be homologous to the RING domain, which mediated ubiquitination and degradation of NF-κB/p65 (34). Likewise, The DBD of human PXR also consists of two C4-type Zn finger domains in the DBD, CX2CX13CX2C (Zn finger I) and CX5CX9CX2C (Zn finger II) (39). However, whether the Zn fingers in the DBD of PXR contain the E3 ligase activity remains to be elusive.

MDM2 has several substrates including p53 and USP7 and regulates their protein turnover (7, 40). Accelerated MDM2 auto-degradation induced by DNA damage is required for p53 activation (41). Upon DNA damage, activated p53 and MDM2 form a negative feedback loop for a tight regulation of p53 activity. ATF3 is also a stabilizer for p53 by binding to C-terminal of p53 and blocking MDM2-mediated ubiquitination and degradation in response to DNA damage (7). Predictably, PXR might also stabilize p53 by blocking MDM2-mediated ubiquitination and stabilizing ATF3; indeed, we observed co-expression with PXR increased p53 expression (**Supplementary Figure S4D**). Taken together, PXR promoting ATM activation in response to DNA damage is a synergistic effect of upregulation of ATF3 and p53 and so on.

PXR has been shown to be expressed in a variety of cancers, such as breast, prostate, endometrial, ovarian, colon, liver, and gastric

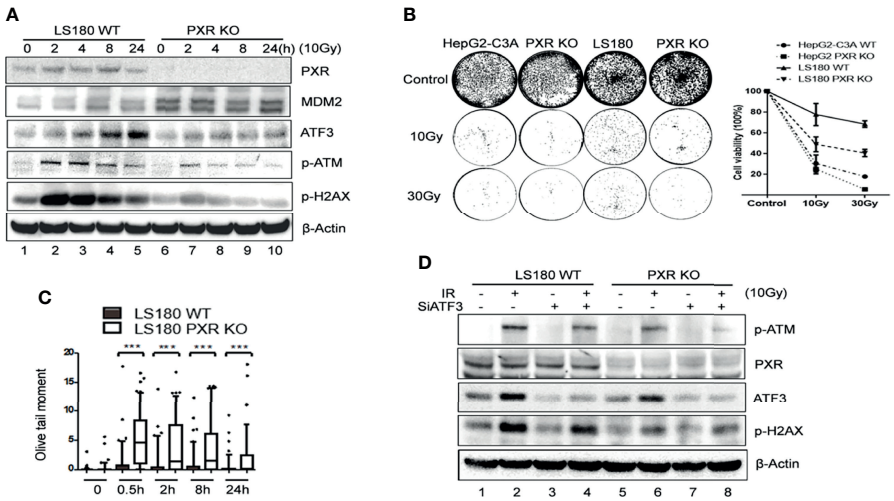

FIGURE 6 | Knockdown of PXR expression impaired ATM activation by IR. **(A)** IR-induced ATM activation and phosphorylation of downstream substrates were repressed in PXR knockout LS180 cells. Wildtype LS180 cells or PXR KO cells were irradiated (10 Gy), and then subjected to Western blotting using the indicated antibodies. **(B)** PXR promoted cell viability of LS180 cells against irradiation. Cells were irradiated and subjected to colony formation assay in 60-mm dishes in triplicate. The colonies in the well were counted by Image J and quantified in the right panel. DNA lesions were accumulated in PXR knockout LS180 cells after radiation. **(C)** PXR promoted DNA damage repair. Cells were radiated at a dose 10 Gy, and then used for neutral comet assays at the indicated time after radiation. ***$p < 0.001$, compared with the control, MannWhitney U-test. **(D)** PXR promotes ATM signaling through regulating ATF3. LS180 wildtype or PXR KO cells were transfected with 100 pmol ATF3 siRNA (siATF3) or control siRNA (siLuc) for 3 days, then subjected to 10 Gy of γ-radiation. The protein levels of PXR, ATF3, p-ATM, and p-H2AX were determined using Western blotting. Beta-actin was used as an internal control.

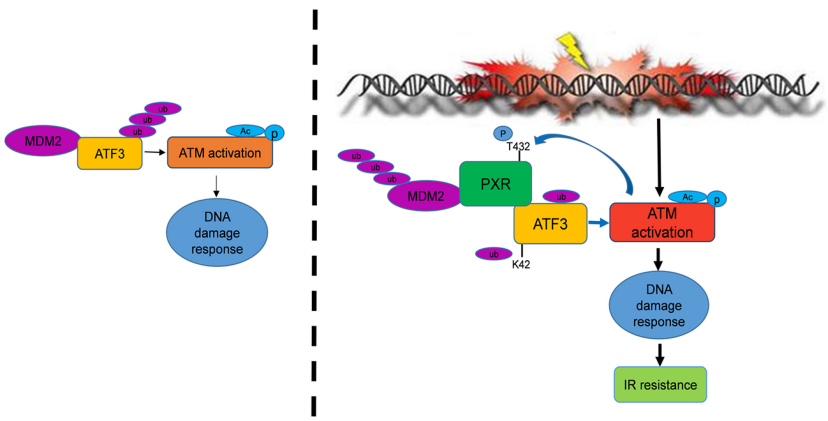

FIGURE 7 | PXR confers to IR resistance by promoting ATF3 stabilization. PXR stabilization of ATF3 protein contains two mechanisms: (1) PXR disrupts ATF3-MDM2 interaction, thus counteracts MDM2-mediated ubiquitination of ATF3. (2) PXR negatively regulates the expression of MDM2 and enhances its auto-ubiquitination and further reduces its half-life. PXR-ATF3 interaction is required for PXR-mediated stabilization of ATF3 as K42R of ATF3 lost binding with PXR and further abrogated PXR-mediated reduction of ATF3 ubiquitination. Furthermore, PXR-ATF3 interaction is also required for ATF3-mediated ATM activation as T432A mutant of PXR lost binding with ATF3, thus compromised ATF3-mediated ATM activation. Taken together, PXR promotes ATM activation and confers liver and colon cancer cell resistance to IR-induced DNA damage.

cancers. PXR regulates genes involved not only in drug metabolism (19–21) but also in proliferation, metastasis, apoptosis, anti-apoptosis, inflammation, and oxidative stress in cancers; PXR expression is correlated with drug resistance and prognosis of cancer (19, 42, 43). In the current study, our data showed that PXR promotes viability of liver and colon cancer cells upon IR treatment. We concluded that PXR plays an important role in its contribution of resistance to IR-induced damage in liver and colon cancer cells. Inhibition of PXR may be an important adjuvant therapy to increase radiosensitization in cancers, taking advantage of PXR-ATF3-ATM signaling pathway. Our data provide a rationale for clinical development of PXR antagonists for treating IR resistant to anticancer therapies that depend on promoting DNA damage response and repair (44). PXR antagonists ketoconazole,

fucoxanthin (FUC), and SPA70 were reviewed in reference (44). Pharmaceutical inhibition of PXR-ATF3-ATM pathway by PXR antagonists will sensitize cells to DNA damage and dampen the cell survival in a cancer cell that was treated with IR. Therefore, understanding the epigenetic regulation of ATF3 by PXR in tumors, such as deletion, mutation, or posttranslational modifications, may help to determine more effective therapeutic methods for cancer patients. The mechanisms documented here might also be implicated in other cancer types that depend on the PXR signaling pathway.

In summary, in the current study, we find that PXR confers resistance of liver and colon cancer cells to IR-induced DNA damage stress through stabilization of ATF3, thus promoting ATF3-mediated ATM activation. In this pathway, PXR promotes ATM activation through ATF3. PXR stabilizes ATF3 from MDM2-mediated ubiquitination through both disrupting MDM2–ATF3 interaction and negatively regulating MDM2 expression, promoting MDM2 ubiquitination and degradation (**Figure 7**). Collectively, our findings provide a clue to overcoming resistance of liver and colorectal cancer to IR therapy by targeting PXR.

DATA AVAILABILITY STATEMENT

The original contributions presented in the study are included in the article/**Supplementary Material**. Further inquiries can be directed to the corresponding authors.

AUTHOR CONTRIBUTIONS

HC designed and drafted the raw article. HC and XN performed most of the experiments. HC and XG reviewed and edited the article. TW, MS, CZ, and MM performed some of the experiments. All authors contributed to the article and approved the submitted version.

FUNDING

This work was supported by the initiative fund for faculty development from Lanzhou University (# 561119203).

ACKNOWLEDGMENTS

We thank Dr. Yanan Tian, Dr. Chunhong Yan, and Dr. Tsonwin Hai for providing plasmids.

SUPPLEMENTARY MATERIAL

The Supplementary Material for this article can be found online at: https://www.frontiersin.org/articles/10.3389/fonc.2022.837980/full#supplementary-material

REFERENCES

1. Buckley AM, Lynam-Lennon N, O'Neill H, O'Sullivan J. Targeting Hallmarks of Cancer to Enhance Radiosensitivity in Gastrointestinal Cancers. *Nat Rev Gastroenterol Hepatol* (2020) 17:298–313. doi: 10.1038/s41575-019-0247-2
2. van der Sluis FJ, Couwenberg AM, de Bock GH, Intven MPW, Reerink O, van Leeuwen BL, et al. Population-Based Study of Morbidity Risk Associated With Pathological Complete Response After Chemoradiotherapy for Rectal Cancer. *Br J Surg* (2020) 107:131–9. doi: 10.1002/bjs.11324
3. Falck J, Mailand N, Syljuasen RG, Bartek J, Lukas J. The ATM-Chk2-Cdc25A Checkpoint Pathway Guards Against Radioresistant DNA Synthesis. *Nature* (2001) 410:842–7. doi: 10.1038/35071124
4. Zhang P, Wei Y, Wang L, Debeb BG, Yuan Y, Zhang J, et al. ATM-Mediated Stabilization of ZEB1 Promotes DNA Damage Response and Radioresistance Through CHK1. *Nat Cell Biol* (2014) 16:864–75. doi: 10.1038/ncb3013
5. Hai T, Hartman MG. The Molecular Biology and Nomenclature of the Activating Transcription Factor/cAMP Responsive Element Binding Family of Transcription Factors: Activating Transcription Factor Proteins and Homeostasis. *Gene* (2001) 273:1–11. doi: 10.1016/S0378-1119(01)00551-0
6. Yan C, Boyd DD. ATF3 Regulates the Stability of P53: A Link to Cancer. *Cell Cycle* (2006) 5:926–9. doi: 10.4161/cc.5.9.2714
7. Yan C, Lu D, Hai T, Boyd DD. Activating Transcription Factor 3, a Stress Sensor, Activates P53 by Blocking its Ubiquitination. *EMBO J* (2005) 24:2425–35. doi: 10.1038/sj.emboj.7600712
8. Li X, Guo M, Cai L, Du T, Liu Y, Ding HF, et al. Competitive Ubiquitination Activates the Tumor Suppressor P53. *Cell Death Differ* (2020) 27:1807–18. doi: 10.1038/s41418-019-0463-x
9. Cui W, Sun M, Zhang S, Shen X, Galeva N, Williams TD, et al. A SUMO-Acetyl Switch in PXR Biology. *Biochim Biophys Acta* (2016) 1859:1170–82. doi: 10.1016/j.bbagrm.2016.02.008
10. Cui H, Guo M, Xu D, Ding ZC, Zhou G, Ding HF, et al. The Stress-Responsive Gene ATF3 Regulates the Histone Acetyltransferase Tip60. *Nat Commun* (2015) 6:6752. doi: 10.1038/ncomms7752
11. Borgoni S, Sofyali E, Soleimani M, Wilhelm H, Muller-Decker K, Will R, et al. Time-Resolved Profiling Reveals ATF3 as a Novel Mediator of Endocrine Resistance in Breast Cancer. *Cancers (Basel)* (2020) 12:2918. doi: 10.3390/cancers12102918
12. Kuroda J, Yamamoto M, Nagoshi H, Kobayashi T, Sasaki N, Shimura Y, et al. Targeting Activating Transcription Factor 3 by Galectin-9 Induces Apoptosis and Overcomes Various Types of Treatment Resistance in Chronic Myelogenous Leukemia. *Mol Cancer Res* (2010) 8:994–1001. doi: 10.1158/1541-7786.MCR-10-0040
13. Zhao W, Sun M, Li S, Chen Z, Geng D. Transcription Factor ATF3 Mediates the Radioresistance of Breast Cancer. *J Cell Mol Med* (2018) 22:4664–75. doi: 10.1111/jcmm.13688
14. Berndsen CE, Wolberger C. New Insights Into Ubiquitin E3 Ligase Mechanism. *Nat Struct Mol Biol* (2014) 21:301–7. doi: 10.1038/nsmb.2780
15. Sharma A, Trivedi AK. Regulation of Apoptosis by E3 Ubiquitin Ligases in Ubiquitin Proteasome System. *Cell Biol Int* (2020) 44:721–34. doi: 10.1002/cbin.11277
16. Zheng N, Shabek N. Ubiquitin Ligases: Structure, Function, and Regulation. *Annu Rev Biochem* (2017) 86:129–57. doi: 10.1146/annurev-biochem-060815-014922
17. Mo P, Wang H, Lu H, Boyd DD, Yan C. MDM2 Mediates Ubiquitination and Degradation of Activating Transcription Factor 3. *J Biol Chem* (2010) 285:26908–15. doi: 10.1074/jbc.M110.132597
18. Fagerberg L, Hallstrom BM, Oksvold P, Kampf C, Djureinovic D, Odeberg J, et al. Analysis of the Human Tissue-Specific Expression by Genome-Wide Integration of Transcriptomics and Antibody-Based Proteomics. *Mol Cell Proteomics* (2014) 13:397–406. doi: 10.1074/mcp.M113.035600
19. Oladimeji P, Cui H, Zhang C, Chen T. Regulation of PXR and CAR by Protein-Protein Interaction and Signaling Crosstalk. *Expert Opin Drug Metab Toxicol* (2016) 12:997–1010. doi: 10.1080/17425255.2016.1201069
20. Chen T. Nuclear Receptor Drug Discovery. *Curr Opin Chem Biol* (2008) 12:418–26. doi: 10.1016/j.cbpa.2008.07.001
21. Chen T. Overcoming Drug Resistance by Regulating Nuclear Receptors. *Adv Drug Deliv Rev* (2010) 62:1257–64. doi: 10.1016/j.addr.2010.07.008

22. Xie Y, Ke S, Ouyang N, He J, Xie W, Bedford MT, et al. Epigenetic Regulation of Transcriptional Activity of Pregnane X Receptor by Protein Arginine Methyltransferase 1. *J Biol Chem* (2009) 284:9199–205. doi: 10.1074/jbc.M806193200
23. Jiang Y, Feng D, Ma X, Fan S, Gao Y, Fu K, et al. Pregnane X Receptor Regulates Liver Size and Liver Cell Fate by Yes-Associated Protein Activation in Mice. *Hepatology (Baltimore Md)* (2019) 69:343–58. doi: 10.1002/hep.30131
24. Naspinski C, Gu X, Zhou GD, Mertens-Talcott SU, Donnelly KC, Tian Y. Pregnane X Receptor Protects HepG2 Cells From BaP-Induced DNA Damage. *Toxicol Sci* (2008) 104:67–73. doi: 10.1093/toxsci/kfn058
25. Cui H, Gu X, Chen J, Xie Y, Ke S, Wu J, et al. Pregnane X Receptor Regulates the AhR/Cyp1A1 Pathway and Protects Liver Cells From Benzo-[Alpha]-Pyrene-Induced DNA Damage. *Toxicol Lett* (2017) 275:67–76. doi: 10.1016/j.toxlet.2017.03.028
26. Wang CM, Yang WH. Loss of SUMOylation on ATF3 Inhibits Proliferation of Prostate Cancer Cells by Modulating CCND1/2 Activity. *Int J Mol Sci* (2013) 14:8367–80. doi: 10.3390/ijms14048367
27. Wang CM, Brennan VC, Gutierrez NM, Wang X, Wang L, Yang WH. SUMOylation of ATF3 Alters its Transcriptional Activity on Regulation of TP53 Gene. *J Cell Biochem* (2013) 114:589–98. doi: 10.1002/jcb.24396
28. Lichti-Kaiser K, Brobst D, Xu C, Staudinger JL. A Systematic Analysis of Predicted Phosphorylation Sites Within the Human Pregnane X Receptor Protein. *J Pharmacol Exp Ther* (2009) 331:65–76. doi: 10.1124/jpet.109.157180
29. Ranaweera RS, Yang X. Auto-Ubiquitination of Mdm2 Enhances its Substrate Ubiquitin Ligase Activity. *J Biol Chem* (2013) 288:18939–46. doi: 10.1074/jbc.M113.454470
30. Santivasi WL, Xia F. Ionizing Radiation-Induced DNA Damage, Response, and Repair. *Antioxid Redox Signal* (2014) 21:251–9. doi: 10.1089/ars.2013.5668
31. Cui H, Li X, Han C, Wang QE, Wang H, Ding HF, et al. The Stress-Responsive Gene ATF3 Mediates Dichotomous UV Responses by Regulating the Tip60 and P53 Proteins. *J Biol Chem* (2016) 291:10847–57. doi: 10.1074/jbc.M115.713099
32. Ciechanover A, Finley D, Varshavsky A. The Ubiquitin-Mediated Proteolytic Pathway and Mechanisms of Energy-Dependent Intracellular Protein Degradation. *J Cell Biochem* (1984) 24:27–53. doi: 10.1002/jcb.240240104
33. Hou Y, Gao J, Xu H, Xu Y, Zhang Z, Xu Q, et al. PPARgamma E3 Ubiquitin Ligase Regulates MUC1-C Oncoprotein Stability. *Oncogene* (2014) 33:5619–25. doi: 10.1038/onc.2013.504
34. Hou Y, Moreau F, Chadee K. PPARgamma is an E3 Ligase That Induces the Degradation of NFkappaB/P65. *Nat Commun* (2012) 3:1300. doi: 10.1038/ncomms2270
35. Borden KL, Freemont PS. The RING Finger Domain: A Recent Example of a Sequence-Structure Family. *Curr Opin Struct Biol* (1996) 6:395–401. doi: 10.1016/S0959-440X(96)80060-1
36. Porter BA, Ortiz MA, Bratslavsky G, Kotula L. Structure and Function of the Nuclear Receptor Superfamily and Current Targeted Therapies of Prostate Cancer. *Cancers (Basel)* (2019) 11:1852. doi: 10.3390/cancers11121852
37. Umesono K, Evans RM. Determinants of Target Gene Specificity for Steroid/Thyroid Hormone Receptors. *Cell* (1989) 57:1139–46. doi: 10.1016/0092-8674(89)90051-2
38. Schoonjans K, Staels B, Auwerx J. The Peroxisome Proliferator Activated Receptors (PPARS) and Their Effects on Lipid Metabolism and Adipocyte Differentiation. *Biochim Biophys Acta* (1996) 1302:93–109. doi: 10.1016/0005-2760(96)00066-5
39. Rana M, Dash AK, Ponnusamy K, Tyagi RK. Nuclear Localization Signal Region in Nuclear Receptor PXR Governs the Receptor Association With Mitotic Chromatin. *Chromosome Res* (2018) 26:255–76. doi: 10.1007/s10577-018-9583-2
40. Hu M, Gu L, Li M, Jeffrey PD, Gu W, Shi Y. Structural Basis of Competitive Recognition of P53 and MDM2 by HAUSP/USP7: Implications for the Regulation of the P53-MDM2 Pathway. *PloS Biol* (2006) 4:e27. doi: 10.1371/journal.pbio.0040027
41. Stommel JM, Wahl GM. Accelerated MDM2 Auto-Degradation Induced by DNA-Damage Kinases is Required for P53 Activation. *EMBO J* (2004) 23:1547–56. doi: 10.1038/sj.emboj.7600145
42. Qiao E, Ji M, Wu J, Ma R, Zhang X, He Y, et al. Expression of the PXR Gene in Various Types of Cancer and Drug Resistance. *Oncol Lett* (2013) 5:1093–100. doi: 10.3892/ol.2013.1149
43. Pondugula SR, Pavek P, Mani S. Pregnane X Receptor and Cancer: Context-Specificity is Key. *Nucl Receptor Res* (2016) 3:101198. doi: 10.11131/2016/101198
44. Niu X, Wu T, Li G, Gu X, Tian Y, Cui H. Insights Into the Critical Role of the PXR in Preventing Carcinogenesis and Chemotherapeutic Drug Resistance. *Int J Biol Sci* (2022) 18:742–59. doi: 10.7150/ijbs.68724

Conflict of Interest: The authors declare that the research was conducted in the absence of any commercial or financial relationships that could be construed as a potential conflict of interest

Publisher's Note: All claims expressed in this article are solely those of the authors and do not necessarily represent those of their affiliated organizations, or those of the publisher, the editors and the reviewers. Any product that may be evaluated in this article, or claim that may be made by its manufacturer, is not guaranteed or endorsed by the publisher.

frontiers in Oncology

ORIGINAL RESEARCH
published: 17 March 2022
doi: 10.3389/fonc.2022.819172

Modulation of ERCC1-XPF Heterodimerization Inhibition *via* Structural Modification of Small Molecule Inhibitor Side-Chains

Claudia Weilbeer[1†], David Jay[2†], James C. Donnelly[1], Francesco Gentile[3], Feridoun Karimi-Busheri[2], Xiaoyan Yang[2], Rajam S. Mani[2], Yaping Yu[4], Ahmed H. Elmenoufy[1,5], Khaled H. Barakat[6,7], Jack A. Tuszynski[2,3,7], Michael Weinfeld[2,7] and Frederick G. West[1,7*]*

[1] Department of Chemistry, University of Alberta, Edmonton, AB, Canada, [2] Department of Oncology, Cross Cancer Institute, University of Alberta, Edmonton, AB, Canada, [3] Department of Physics, University of Alberta, Edmonton, AB, Canada, [4] Centre for Genome Engineering, University of Calgary, Calgary, AB, Canada, [5] Department of Pharmaceutical Chemistry, College of Pharmacy, Misr University for Science and Technology, 6th of October City, Egypt, [6] Faculty of Pharmacy and Pharmaceutical Sciences, University of Alberta, Edmonton, AB, Canada, [7] Cancer Research Institute of Northern Alberta, University of Alberta, Edmonton, AB, Canada

Inhibition of DNA repair enzymes is an attractive target for increasing the efficacy of DNA damaging chemotherapies. The ERCC1-XPF heterodimer is a key endonuclease in numerous single and double strand break repair processes, and inhibition of the heterodimerization has previously been shown to sensitize cancer cells to DNA damage. In this work, the previously reported ERCC1-XPF inhibitor 4 was used as the starting point for an *in silico* study of further modifications of the piperazine side-chain. A selection of the best scoring hits from the *in silico* screen were synthesized using a late stage functionalization strategy which should allow for further iterations of this class of inhibitors to be readily synthesized. Of the synthesized compounds, compound 6 performed the best in the *in vitro* fluorescence based endonuclease assay. The success of compound 6 in inhibiting ERCC1-XPF endonuclease activity *in vitro* translated well to cell-based assays investigating the inhibition of nucleotide excision repair and disruption of heterodimerization. Subsequently compound 6 was shown to sensitize HCT-116 cancer cells to treatment with UVC, cyclophosphamide, and ionizing radiation. This work serves as an important step towards the synergistic use of DNA repair inhibitors with chemotherapeutic drugs.

Keywords: DNA repair, ERCC1-XPF small molecule inhibitors, computer aided drug design (CADD), proximity ligation assay, ionizing and UV irradiation

OPEN ACCESS

Edited by:
Jason Luke Parsons, University of Liverpool, United Kingdom

Reviewed by:
Olga Lavrik, Institute of Chemical Biology and Fundamental Medicine (RAS), Russia
Jung-Hyun Min, Baylor University, United States

***Correspondence:**
Michael Weinfeld
Michael.Weinfeld@albertahealthservices.ca
Frederick G. West
fwest@ualberta.ca

†These authors share first authorship

Specialty section:
This article was submitted to Cancer Molecular Targets and Therapeutics, a section of the journal Frontiers in Oncology

Received: *21 November 2021*
Accepted: *28 January 2022*
Published: *17 March 2022*

Citation:
Weilbeer C, Jay D, Donnelly JC, Gentile F, Karimi-Busheri F, Yang X, Mani RS, Yu Y, Elmenoufy AH, Barakat KH, Tuszynski JA, Weinfeld M and West FG (2022) Modulation of ERCC1-XPF Heterodimerization Inhibition via Structural Modification of Small Molecule Inhibitor Side-Chains. Front. Oncol. 12:819172. doi: 10.3389/fonc.2022.819172

INTRODUCTION

DNA damage has been implicated in causing cancer and other diseases related to aging (1). Processes that repair DNA damage and the proteins responsible for repair play an important role in preserving human genetic material and preventing these diseases (2–7). The heterodimer ERCC1-XPF is central to both global genome and transcription coupled nucleotide excision repair (NER), which removes bulky adducts and lesions in DNA (8–12), and in replication dependent and independent interstrand crosslink (ICL) repair (13–19). It has also been suggested that ERCC1-XPF plays minor roles in various other single (20, 21) and double (22–25) strand break repair processes.

Inhibition of DNA repair enzymes in the treatment of cancer has had some success; the approval of poly (ADP-ribose) polymerase (PARP) inhibitors to treat BRCA deficient cancers was a revolutionary step in exploiting synthetic lethality to afford enhanced selectivity in homologous recombination (HR) defective cancers. The development of PARP inhibition and the exploration of targeting other DNA repair enzymes in the treatment of cancers has been comprehensively reviewed (26–30). Inhibition of ERCC1-XPF is likely to increase the efficacy of DNA damaging therapies. Since cyclobutane pyrimidine dimers (CPD) and pyrimidine-pyrimidone (6–4) adducts are formed from UV radiation (31–34) and are repaired by NER, it follows that NER deficient cells will be more susceptible to treatment with UV (35, 36). The same can be said for damage caused by DNA crosslinking chemotherapeutic drugs, such as mitomycin C and cisplatin, which is removed by ICL repair (35, 37). Further evidence for the requirement for therapies that target ERCC1-XPF comes from recent (2015-present) systematic reviews and meta-analyses that conclude that high expression of ERCC1 and/or XPF in tumors leads to poor prognoses, and low expression of ERCC1 and/or XPF in tumors leads to improved prognoses in a wide variety of different cancer types (38–48).

ERCC1-XPF is an obligate heterodimer (49–51), in which the XPF protein is responsible for the endonuclease activity and the ERCC1 protein is involved in protein-protein and DNA-protein interactions (52, 53). The endonuclease activity of ERCC1-XPF and the stability of both proteins being reliant on their heterodimerization (53–55), and their interactions with other proteins while repairing DNA, presents multiple opportunities to inhibit the repair of damaged DNA. So far efforts have been made to inhibit the XPF active site, the interaction of ERCC1 with XPA, and the heterodimerization of ERCC1 and XPF.

Initially, Tsodikov and co-workers (56) were able to inhibit ERCC1-XPA dimerization with a XPA peptide fragment. This loss of ERCC1-XPA binding led to loss of NER, which was the first proof of principle that an inhibitor targeting an NER protein-protein interaction could lead to loss of NER. Following the success of the XPA peptide, Barakat et al. (57, 58) carried out virtual screening to identify potential ERCC1-XPA inhibitors; of the hit compounds 14 were tested for their ability to bind to ERCC1 and to sensitize HCT-116 and A549 cells to UVC radiation. One inhibitor was found to sensitize HCT-116 cells to UVC radiation and synergize with cisplatin in HCT-116 cells. Gentile et al. have since carried out larger *in silico* screening to identify ERCC1-XPA inhibitors (59). XPF active site inhibitors have also attracted interest (60–65). Several of these compounds were shown to be capable of sensitizing cancer cells to cisplatin (60, 61, 63, 64).

The inhibition of the heterodimerization of ERCC1 and XPF has been described as a "formidable target" (66); however, the instability of both proteins in the absence of heterodimerization (53–55) and the inability of incorrectly folded ERCC1-XPF to localize to the nucleus of damaged cells (67) makes it an attractive target to increase the susceptibility of tumor cells to DNA damaging chemotherapies. McNeil et al. (60) were able to identify an ERCC1-XPF inhibitor *via in silico*, surface plasmon resonance (SPR), and *in vivo* NER screening. This inhibitor was able to enhance the sensitivity of A375 human melanoma cells to cisplatin. Jordheim and co-workers (68) used binding energy decomposition analysis to identify three potential binding sites on XPF that could be inhibited. Of the residues studied the interaction of Phe293 of ERCC1 [previously identified as an important residue in ERCC1-XPF heterodimerization (52, 55)] with XPF had the largest contribution to the binding energy. As such, an *in silico* screen of inhibitors in that binding pocket in the C-terminal hairpin-helix-hairpin (HhH2) domain of XPF, and subsequent toxicity assay of the most promising hits identified inhibitors 1 and 2 (**Figure 1**). Compound 2 was later derivatized to 3, a prodrug which released cisplatin and 2 *in vivo*, that also inhibited DNA repair with some success (69). Compound 1 was shown to synergize with cisplatin and mitomycin C by interacting with ERCC1-XPF (68), and as such 1 was chosen as the basis for future inhibitors of ERCC1-XPF.

Following the successful inhibition of ERCC1-XPF and the synergy of compound 1 with chemotherapeutic drugs, Elmenoufy et al. (70) carried out *in silico* screening of inhibitors with differing piperazine substitutions, with the six best scoring entries being tested in an endonuclease assay. The most active compound (4, **Figure 1**) was then tested in HCT-116 cells and sensitized those cells to UVC radiation and cyclophosphamide treatment. Elmenoufy and co-workers (71) then investigated modifications of different sites on inhibitors 1 and 4. They found that inhibitor 5 (**Figure 1**) with the methyl group masking the phenolic OH removed led to an increase in activity, and sensitized HCT-116 cells to UVC radiation and cyclophosphamide treatment. Comprehensive molecular dynamics simulations were carried out on inhibitors 1 and 5 with a view to investigating further possible modifications to increase the efficacy of this class of inhibitors (72). Importantly, Ciniero et al. (73) were able to show that 5 sensitized HCT-116 and A549 cells to cisplatin and mitomycin C, they were also able to show, *via* a proximity ligation assay, that sensitization of A549 cells to cisplatin was due to inhibition of the heterodimerization of ERCC1-XPF.

The substantial reduction in IC_{50} in comparing compound 4 with the initial hit 1 showed that modification of the piperazine side-chain could have significant effects on activity. The importance of a tertiary amine moiety at the terminus of the side-chain was clear, but systematic structural variation would be necessary to determine the optimal linker and steric demand of the nitrogen substituents. We therefore conducted another round of *in silico* screening, with focus on this side chain.

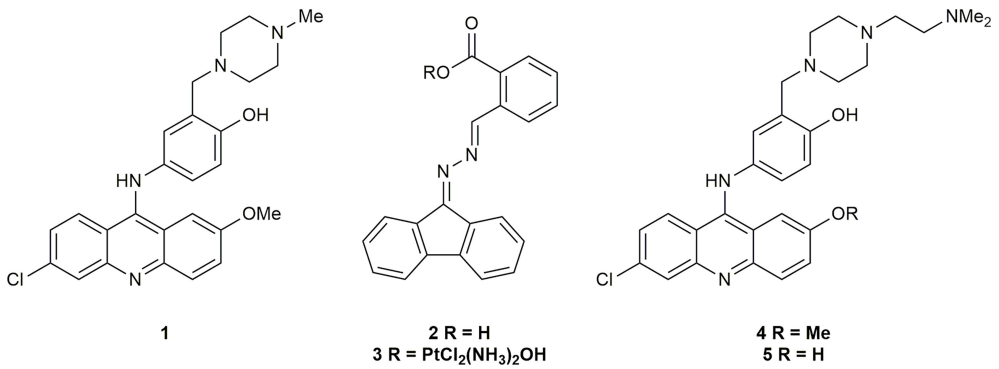

FIGURE 1 | Previously reported inhibitors of ERCC1-XPF heterodimerization.

These studies revealed a strong positive effect of diisopropyl substitution on the amino group, as shown in compound 6. Of the ten highest ranked hits (**Figure 2**) from the *in silico* screen, six were synthesized, including 6. Herein we report the design, synthesis, and biological evaluation of these novel inhibitors, among which 6 stands out as a promising hit.

MATERIALS AND METHODS

Overview of *In Silico* Design Strategy for ERCC1–XPF Inhibitors

Molecular Operating Environment (MOE) Dock's pharmacophore-assisted docking (74) was used in the initial step of the virtual screening procedure, using the same procedure previously described (72). 32 top-scoring compounds were selected, based on their Born Volume Integral/Weighted Surface Area (GBVI/WSA) docking score (75) and visual inspection of the docking poses, and average Mechanics/Generalized Born Surface Area (MM/GBSA) scores (76) were computed from 2-ns molecular dynamics simulations run as previously described (72). LogP values were calculated using the SlogP function in MOE (77).

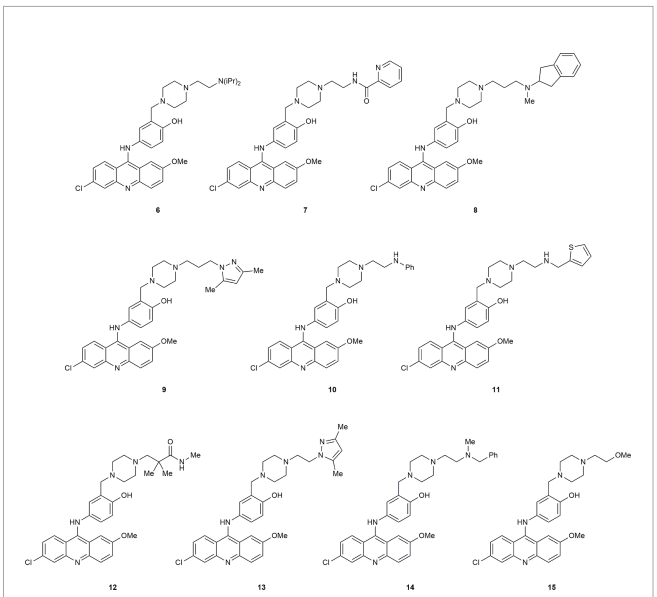

FIGURE 2 | Structures of compounds from *in silico* screening results.

Synthesis of ERCC1-XPF Inhibitors

Full experimental procedures and characterization data can be found in the supporting information.

Synthesis of 6, 10 and 11

A late-stage functionalization by reductive amination of intermediate 20 (**Scheme 1**) was employed in efforts to synthesize the inhibitors 6, 10, 11, 13, and 14. Synthesis began with a mono-alkylation of piperazine with the dimethyl acetal of bromoacetaldehyde to afford **16** in acceptable yield, which could be alkylated in excellent yield with 2-chloromethyl-4-nitrophenol to give 17 (**Scheme 1**). Compound 17 underwent reduction with Pd/C to generate 18, which could undergo a regioselective S_NAr reaction with 6,9-dichloro-2-methoxyacridine to provide 19, the dimethyl acetal of the required aldehyde 20. Treatment of 19 with BBr_3 afforded the desired intermediate 20. Reductive aminations with diisopropylamine, benzylamine, and 2-thiophenemethylamine were successful in affording the inhibitors 6, 10, and 11, respectively (**Scheme 1**). Unfortunately, reductive aminations with the amines required to synthesize 13, and 14 were unable to afford material of sufficient quantity and/or purity for biological testing.

Synthesis of 8

Starting from 3-chloropropionaldehyde diethyl acetal (later converted to the dimethyl acetal *in situ* during the S_NAr reaction), an analogous late-stage functionalization by reductive amination of intermediate 25 (**Scheme 2**) was employed to attempt to synthesize 8 and 9. The synthesis of compound 8 was successful, however, the synthesis of 9 was unsuccessful.

Synthesis of 12

The synthesis of 12 presented the unique challenge of the geminal dimethyl group in the linker (**Scheme 3**). Commercially available

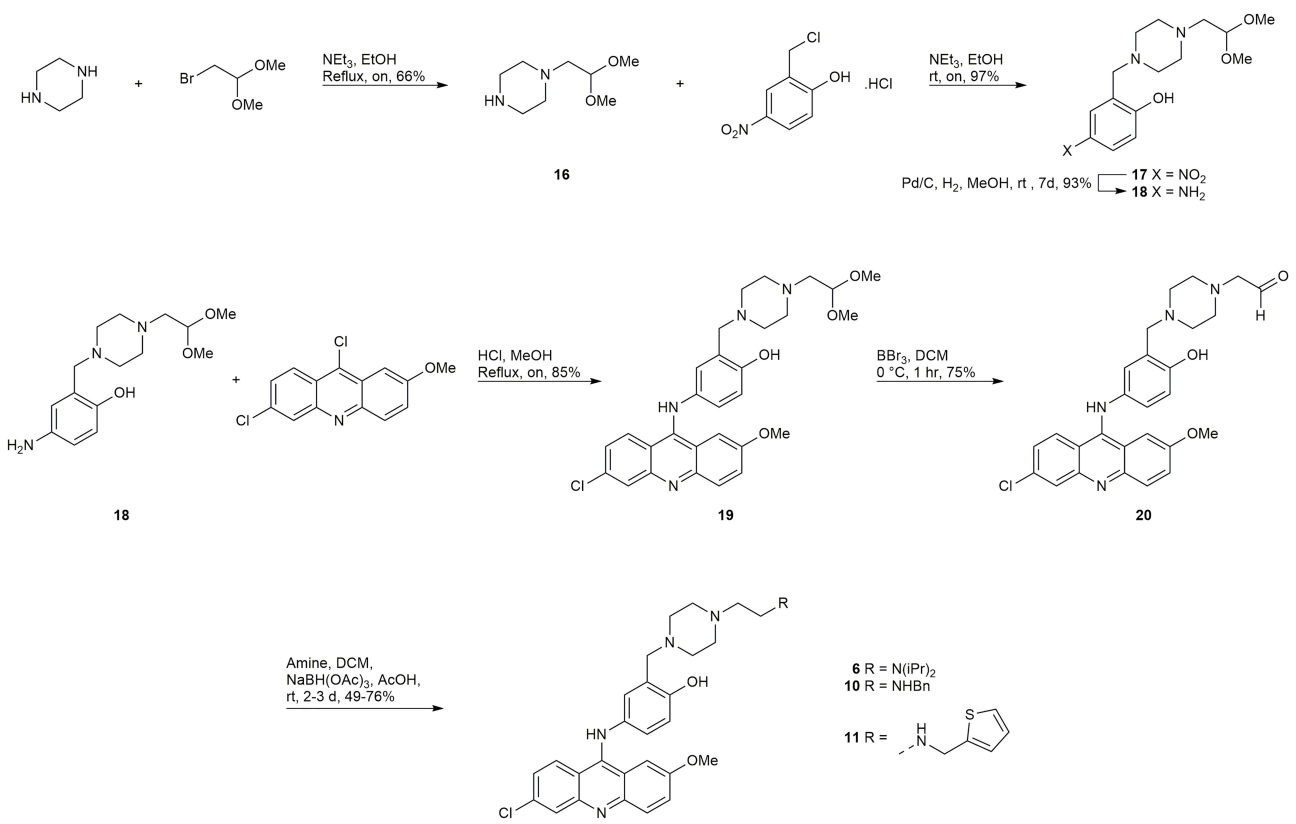

SCHEME 1 | Synthesis of 6, 10, and 11.

26 was subjected to the Swern modified Moffatt oxidation conditions to afford the aldehyde 27, which could undergo a reductive amination with the easily prepared amine 28 to afford intermediate 29. Compound 29 was a convenient intermediate to convert the methyl ester to the methyl amide *via* saponification, activation with $SOCl_2$, and amidation with methylamine to afford compound 31. Reduction of 31 to 32 and subsequent S_NAr reaction with 6,9-dichloro-2-methoxyacridine gave the desired inhibitor 12.

Synthesis of 15

The synthesis of 15 is depicted in **Scheme 4**. Boc protection and methylation of 1-(2-hydroxyethyl)piperazine afforded compound 33. The deprotection of 33 with TFA afforded the TFA salt 34, which could undergo a multicomponent reaction with acetaminophen and formaldehyde, and subsequent acid hydrolysis to afford the required amine 35. Compound 35 underwent a S_NAr reaction with 6,9-dichloro-2-methoxyacridine to give 15.

ERCC1-XPF Protein Preparation

Recombinant human ERCC1–XPF wild-type protein (containing polyhistidine (His-6) tags) was expressed from a bicistronic plasmid (kindly provided by Dr. Richard Wood, University of Texas MD Anderson Cancer Center, Smithville, TX) in the *E. coli* BL21(DE3) strain, Following previously described procedures (70, 78) the proteins extracted from *E. coli* were eluted from a ProBond Nickel-Chelating Resin (Thermo Fisher Scientific) and then a Hi-trap heparin column (GE Healthcare). Fractions containing ERCC1–XPF were dialyzed, concentrated, and stored at −80°C in 10 mM HEPES, pH 7.4, 2.5 mM β-mercaptoethanol, 0.01% CHAPS, 0.25 mM EDTA, 50% glycerol, and 25 mM NaCl. Based on polyacrylamide gel separation and Coomassie Blue staining, the final purity of the full-length ERCC1-XPF heterodimer was determined to be ~35%.

Microplate Fluorescence Incision Assay

We employed a previously described protocol (60, 70, 78) in which the incision of the stem–loop substrate [6-FAM-5′-CAGCGCTCGG(20T)CCGAGCGCTG-3′-dabcyl] (100 nM in 50 mM Tris-HCl, pH 8, 20 mM NaCl, 0.5 mM DDT, and 0.75 mM $MnCl_2$) mediated by ERCC1-XPF (25 ng) in a total volume of 20 μL at 25°C was monitored by fluorescence using a FLUOstar Optima fluorimeter (BMG Labtech) with Optima software and excitation and emission wavelengths of 485 and 520 nm, respectively, for 5.5 min. The final concentration of inhibitor in the reaction was 10 μM prepared from a 200 μM stock solution in DMSO. With a molecular weight of 151 KDa for the XPF-ERCC1 heterodimer, a concentration of 25 ng of

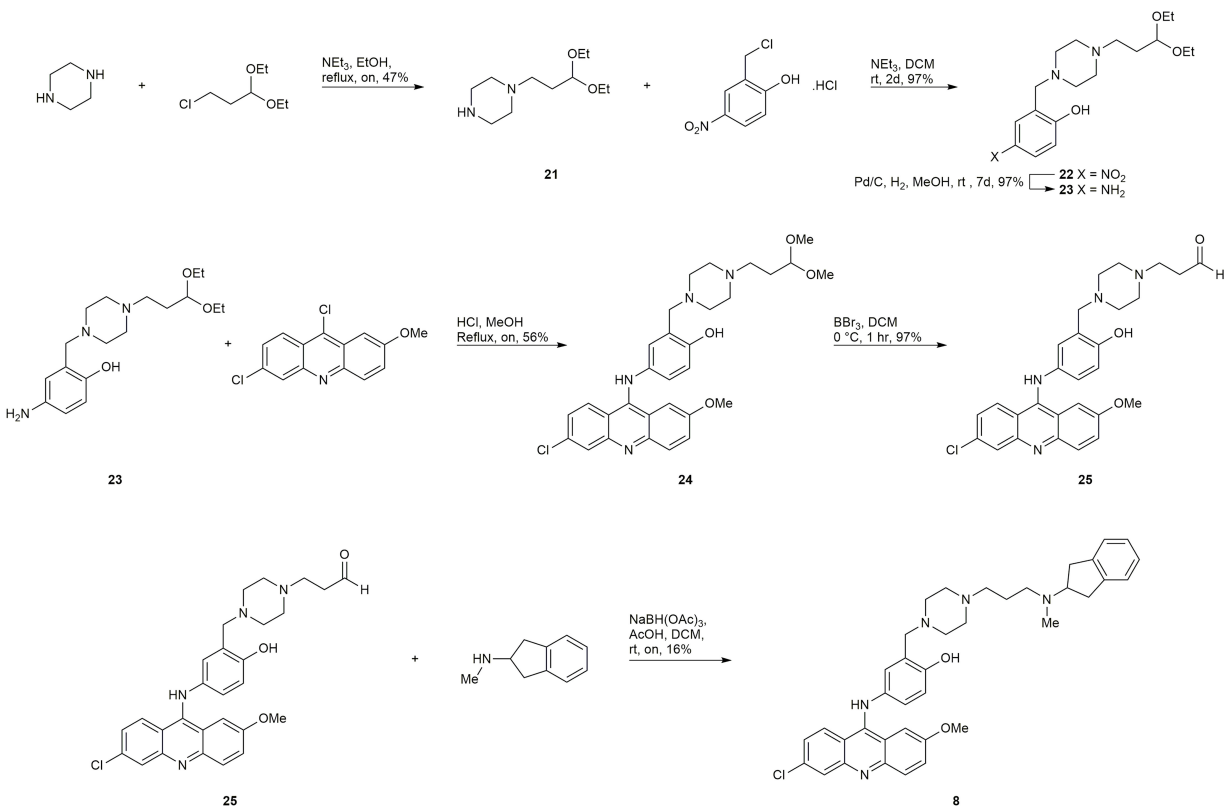

SCHEME 2 | Synthesis of 8.

protein in 20 µl reaction buffer and a purity of 35%, the molar concentration of the enzyme was estimated to be 2.9 nM. Data were plotted using Microsoft Excel 2016.

Steady State Fluorescence Assays

Steady-state fluorescence spectra were measured at room temperature on a PerkinElmer LS-55 spectrofluorometer (Freemont, CA) as previously described (70). In studying the effects of inhibitors on protein fluorescence intensities, additions to protein samples were made from inhibitor stock solutions in DMSO, keeping the protein dilution below 3%. Data were plotted using GraphPad Prism version 5.04 software (San Diego, California)

Cell Culture

Human HCT-116 colorectal cancer cells and A549 human lung cancer cells were purchased from the American Type Culture Collection (ATCC, Manassas, VA). Following expansion of the cell population immediately after arrival, aliquots were stored frozen in liquid nitrogen. Freshly thawed cells were used for each experiment. Cells were cultured in 1:1 DMEM/F12 media supplemented with 10% FBS, 50 units/mL penicillin, 50 µg/mL streptomycin, 2.5 mM l-glutamine, 0.1 mM nonessential amino acids, and 1 mM sodium pyruvate and maintained under 5% CO_2 in a humidifier incubator at 37°C. All cell culture supplies were purchased from Gibco/BRL through ThermoFisher Scientific (Mississauga, ON). Information on CRISPR deletion of XPF from HCT-116 cells can be found in the **Supplementary Information**.

Cellular Repair of Cyclobutane Pyrimidine Dimers

We followed the protocol of Mirzayans et al. (79) with minor modifications as previously described (70). Inhibitor compounds were dissolved in DMSO and applied to a final DMSO concentration of 0.2% in media and 0.2% DMSO was used as the vehicle control. Mouse anti-thymine dimer monoclonal antibody (cat. no. MC-062, Kamiya Biomedical Company, Seattle, WA) was used for the immunofluorescence following UVC irradiation of the cells and fluorescent microscopic evaluation and measurement of fluorescence intensity were performed using MetaXpress, version 6.2.1.704, software (Molecular Devices, Sunnyvale, California). Data were plotted using GraphPad Prism version 5.04 software.

Proximity Ligation Assay

A previously published protocol (73) was followed with minor modifications. Briefly, 3 x 10^4 A549 cells were seeded in each well of an 8-well Chamber Slide system (Ibidi. Fitchburg, WI) and allowed to adhere overnight. The cells were then treated with the inhibitor (2 µM prepared from a 1 mM stock in DMSO) or vehicle control (0.2% DMSO) and incubated for 24 h. Samples

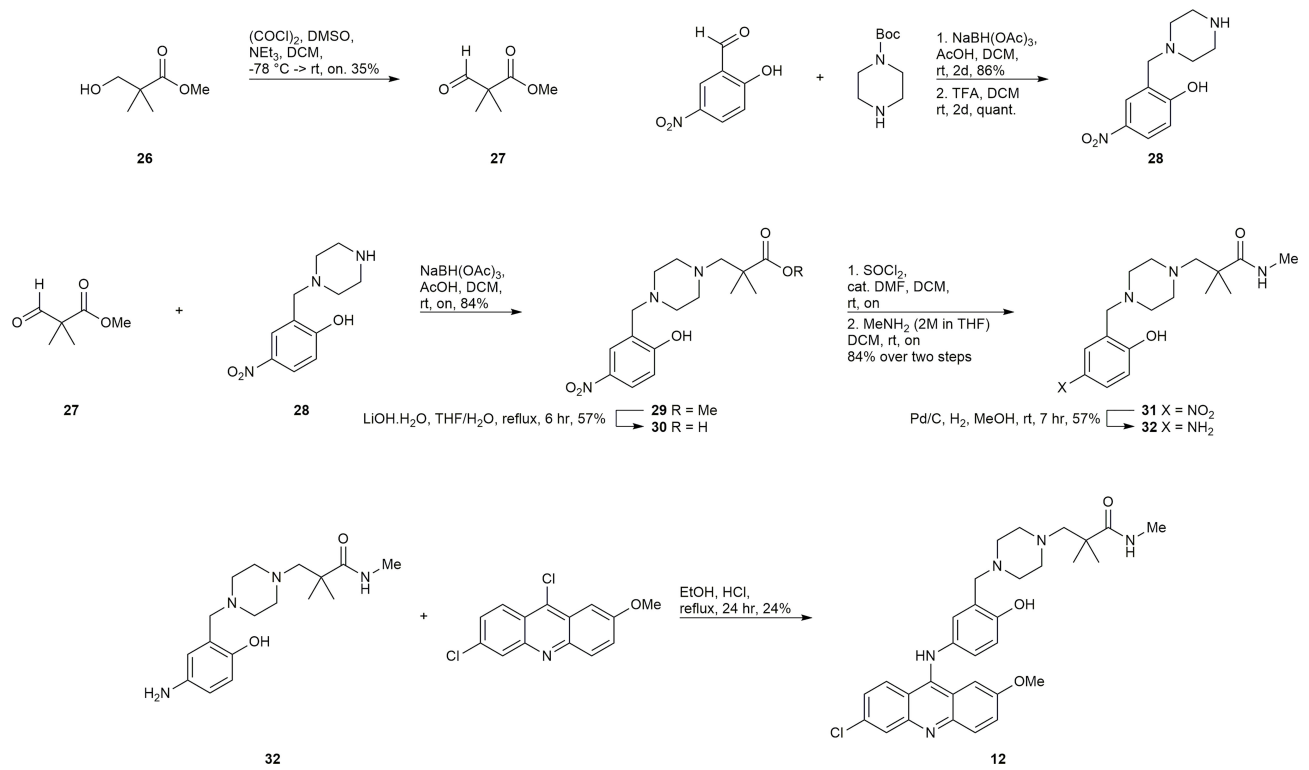

SCHEME 3 | Synthesis of 12.

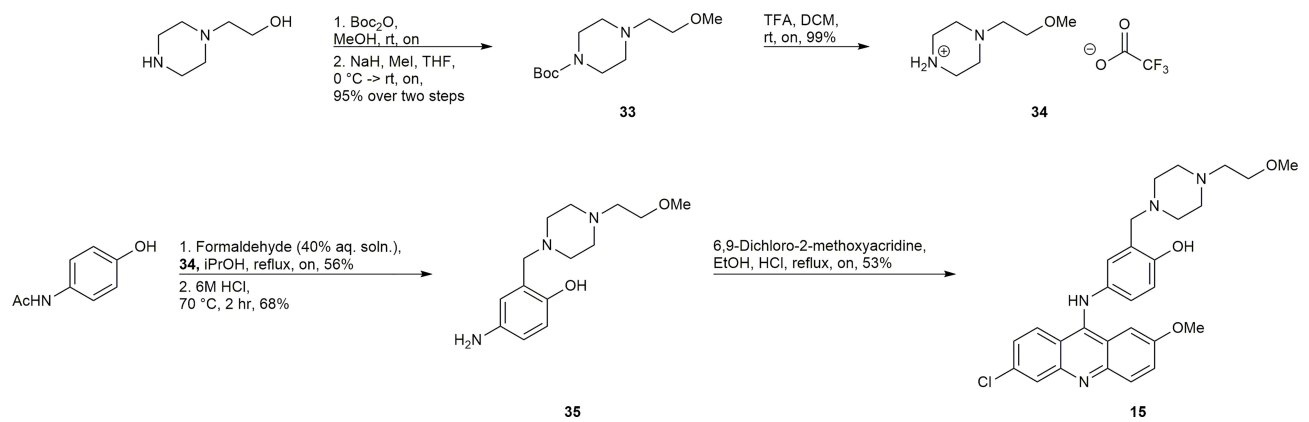

SCHEME 4 | Synthesis of 15.

were fixed and processed for protein proximity ligation analysis (PLA) by the Duolink PLA assay kit (Sigma-Aldrich, Oakville, ON) using an ERCC1 antibody (A73368-100, 1/100; EpiGentek, Farmingdale, NY) and an XPF antibody (LS-C173159, 1/100; LifeSpan BioSciences, Seattle, WA). Nuclei were then stained with DAPI and the samples visualized using a laser scanning confocal microscope (ZEISS LSM710, Germany). Images of the interaction of ERCC1 and XPF represented as red dots were analyzed using IMARIS 9.7 software (Oxford Instruments). Results are expressed as mean values from at least three experiments conducted independently in duplicate. We confirmed that the addition of only one antibody, either ERCC1 or XPF did not elicit any signal nor did the use of a HCT 116 cell line deficient in XPF expression (data not shown).

Clonogenic Survival Assays

UV Treatment

HCT-116 cells (100–800 cells depending on the UV dose) were plated in triplicate in 60-mm Petri dishes in DMEM/F12 medium. Following overnight attachment of the cells in a humidified atmosphere containing 5% CO_2 at 37°C, the cells were treated with 0.5 μM compound 6 or 10 in DMSO (as described in section 2.7) for 4 h before the medium was removed, and the cells exposed to increasing doses (0–10 J/m^2) of UV-C radiation. The cells were then cultured for a further 24 h in the presence of inhibitor and then for an additional 9 days in the absence of inhibitor to allow for colony formation. Colonies were stained with crystal violet and counted using a Colcount instrument (Oxford Optronix, Abingdon UK) to facilitate determination of plating efficiency and surviving fraction. Data were plotted using GraphPad Prism version 5.04 software.

Cyclophosphamide Treatment

A similar protocol was followed to that described above for the UV treatment. Cells were treated with 0.5 μM compound **6** or compound 10 in DMSO for 4 h followed by addition of increasing doses of cyclophosphamide (0–300 μM) and further incubation for 24 h. The medium was then replaced with drug and inhibitor-free fresh medium. After incubation for another 9 days to allow for colony formation, the plates were stained with crystal violet, colonies were counted, and plating efficiency and surviving fraction were calculated. Data were plotted using GraphPad Prism version 5.04. software.

Treatment With Ionizing Radiation

The effectiveness of compound 6 for sensitization of cells to ionizing radiation was also assessed using the clonogenic survival assay. Briefly, 200-3000 of HCT-116 cells (depending on the radiation dose) were seeded and after 24 hours the cells were pretreated with 0.5 or 1 μM of compound 6 in DMSO for 4 hours followed by exposure to increasing doses of γ-radiation (^{60}Co Gammacell; Atomic Energy of Canada Limited, Ottawa) from 0 to 8 Gy (at a dose rate of 0.8 Gy/min) and kept for an additional 24 hours in inhibitor-containing medium. The medium was then replaced with fresh medium without the compound, and the plates were incubated at 37°C for 9 more days before staining and determining the number of colonies. Data were plotted using GraphPad Prism version 5.04 software.

Pharmacokinetic Assessment

The ADME (absorption, distribution, metabolism, and excretion) profile of our lead compound 6 was determined by standard protocols carried out by WuXi AppTec (Shanghai) Co (https://www.wuxiapptec.com/). The following tests were conducted: distribution coefficient (log *D* at pH 7.4), aqueous solubility (Kinetic), metabolic stability in human liver microsomes and cryopreserved human hepatocytes, bidirectional permeability in Caco-2 cells, serum protein binding, and cytochrome P450 (CYP) inhibition (CYP1A2, CYP2C9, CYP2C19, CYP2D6, and CYP3A4-M).

RESULTS

Identification of Piperazine Side-Chain Modifications *via In Silico* Screening

Our initial computational screening of modifications to the piperazine side chain revealed 32 hits. These 32 hits were subjected to molecular dynamics simulations; the compounds with the lowest computed binding affinities can be found in **Table 1**. It is clear from the relative scores for 1 and 4 (-17.78 and -13.12 kcal/mol, respectively) that the calculated binding affinity does not necessarily correlate to *in vivo* efficacy, however, the standout calculated binding affinity of -32.47 kcal/mol strongly suggested that 6 would be an effective inhibitor of ERCC1-XPF. Compounds 7-15 (**Figure 2**) all had similar calculated binding affinities to compounds 1 and 4, which suggested that those compounds would inhibit ERCC1-XPF to a degree similar to that of the parent compounds.

Inhibition of ERCC1-XPF Endonuclease Activity

An *in vitro* fluorescence-based assay was used to assess the ability of the synthesized compounds to inhibit the endonuclease activity of ERCC1-XPF. This assay has been previously described (60, 70, 78) and makes use of a stem-loop DNA substrate with a 5'-FAM fluorescent dye, and a 3'-dabcyl quencher. When ERCC1-XPF can cleave the DNA substrate, a 5'-FAM containing molecule is liberated from the stem-loop (and the quencher) and the fluorescence of the solution increases. The increase of the fluorescence of the solution can be observed in **Figure 3A**, in the absence of any inhibitor. To determine the influence of the inhibitory compounds, the protein was preincubated for 10 minutes with 10 μM of each inhibitor prior to addition of the substrate. It can be observed that while the synthesized inhibitors 8, 10, 11, 12, and 15 showed a decrease in fluorescence intensity when compared to the control, indicating some inhibition of ERCC1-XPF endonuclease activity, they were unable to improve on the inhibition shown by 4 (**Figure 3A**). However, in keeping with our computational

TABLE 1 | *In silico* screening results: Average binding energies were calculated over a molecular dynamics trajectory using MM/GBSA method; cLog P values were determined in MOE using an empirical method based on single atom contributions.

Compound	MM/GBSA [kcal/mol]	cLog P
6	-32.47	5.58
7	-18.75	5.71
8	-17.63	4.54
9	-16.80	5.64
10	-16.19	7.0
11	-15.42	5.97
12	-15.15	4.24
13	-14.52	5.25
14	-13.32	4.45
15	-13.27	4.11
1	-17.78	4.10
4	-13.12	2.61

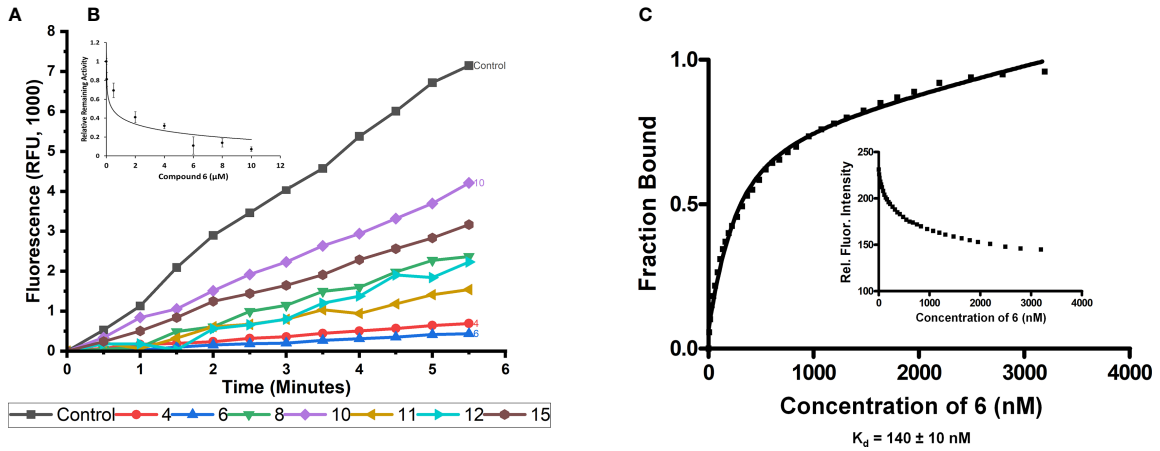

FIGURE 3 | *In vitro* inhibition of ERCC1-XPF endonuclease activity and binding of compound 6 to ERCC1-XPF. **(A)** ERCC1-XPF mediated cleavage of the stem-loop DNA substrate, in which the FAM signal is quenched, releases the fluorescently tagged octanucleotide. A representative tracing of the effect of the different compounds (10 μM each) on the incision activity is shown. The inset **(B)** shows the initial velocities (slopes) obtained as indicated in **(A)** normalized by its value in the absence of compound, *vs.* its value in the presence of increasing micro molar concentrations of compound 6. The bars represent the S.D. of three different measurements for each point (R^2 = 0.96). **(C)** Binding affinity (Kd) measurement between ERCC1-XPF complex and compound 6. Representative plot of ERCC1-XPF fluorescence quenching *vs* concentration of compound 6 to determine unimodal binding pattern (R^2 = 0.98). Protein fluorescence was excited at 295 nm, and changes in fluorescence intensity were monitored at the emission maximum (330 nm). The Kd value of 140 ± 10 nM was determined from three independent plots.

predictions, compound 6 showed increased inhibition of ERCC1-XPF endonuclease activity relative to 4 and decreased the activity of ERCC1-XPF by 94% at 5.5 minutes (**Figure 3A**, **Supplementary Figure 1**).

Different concentrations of compound 6 were plotted against the relative remaining activity of the enzyme. From this plot (**Figure 3B**) an IC_{50} of 0.167 +/- 0.028 μM was calculated for compound 6.

Compound 6 Binding to ERCC1-XPF

Investigation of the binding of compound 6 to ERCC1-XPF was carried out *via* intrinsic fluorescence spectroscopy. The tryptophan residues of ERCC1-XPF were irradiated at 295 nm and the emission at 330 nm was monitored. Upon addition of compound 6 quenching of the intrinsic fluorescence of the protein was observed, consistent with ligand binding to a protein. The binding affinity was determined by plotting emission at 330 nm against increasing concentration of compound 6 (**Figure 3C**). Nonlinear regression of the results was carried out, as previously described (70, 80), to calculate a K_d of 140 +/- 10 nM.

Inhibition of Cellular NER

Immunofluorescent detection of cyclobutane pyrimidine dimers (CPD) generated in the DNA of HCT-116 cells after exposure to UVC radiation was used to measure NER. Our observations that approximately 80% of CPD were removed 24 hours post irradiation in the absence of any inhibitors mirrors previous observations (70, 79). Addition of 2 μM 10 as a negative control showed no significant effect on CPD removal (**Figure 4**). Addition of 2 μM 6 inhibited the removal of CPD to approximately 67% (**Figure 4**), showing that 6 caused significant inhibition of NER in a cell-based setting.

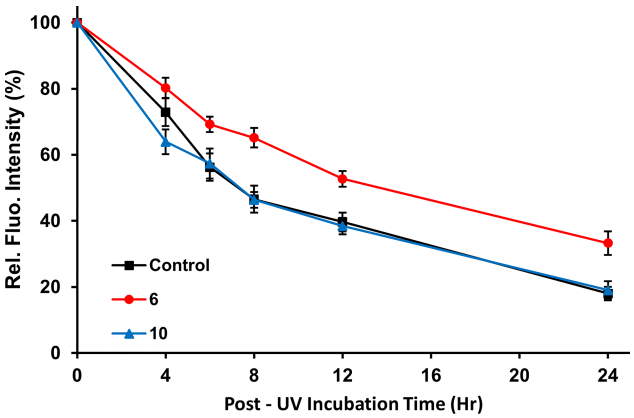

FIGURE 4 | Inhibition of cellular NER. Immunofluorescence images were obtained at various time points to monitor the removal of CPDs from UVC-irradiated HCT-116 cells treated with vehicle only (control), compound 10 (2 μM; negative control), or compound 6 (2 μM). Plot shows the normalized fluorescence intensity of the cells based on quantitation of fluorescence from 100 cells randomly selected per time point. Error bars indicate the S.E.M. The measured intensities of cells treated with the active inhibitor, compound 6 were significantly different from the non-inhibitory negative control, compound 10, at time points from 4 to 24 h post-irradiation ($p < 0.005$, Student's t-test) indicating that compound 6 slows the removal of CPD.

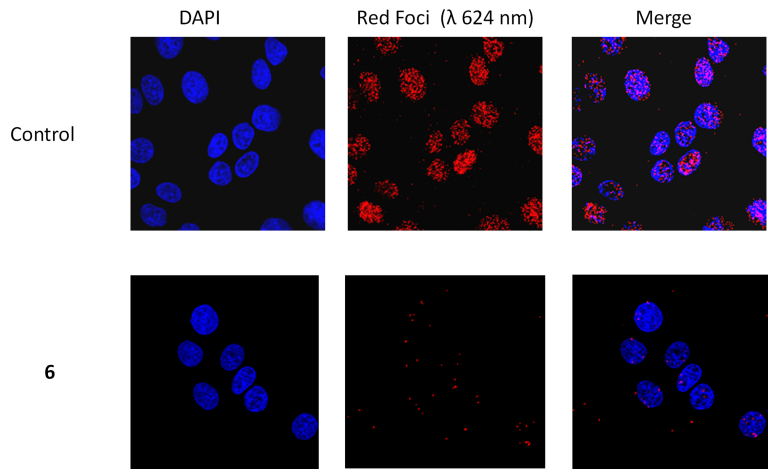

FIGURE 5 | Representative PLA images of A549 cells exposed to 2 μM compound 6 or the equivalent amount of DMSO vehicle (1 μl/ml, Control). Images were obtained at 40X magnification. ERCC1-XPF complexes appear as red dots, and cellular nuclei are shown in blue after DAPI staining.

Inhibition of the Heterodimerization of ERCC1 and XPF

To confirm that compound **6** was able to disrupt the interaction between subunits in the ERCC1-XPF heterodimer in cells, we performed PLA using A549 lung cancer cells exposed to 2 μM compound 6 or DMSO vehicle for 24 h. (**Figure 5**). In the presence of vehicle (0.2% DMSO) alone we observed an average of 75.7 ± 15.4 foci per cell whereas in the presence of compound 6 only an average of 3.1 ± 2.6 foci per cell were detected. The few red dots observed outside of the nuclei may be derived from disrupted nuclear membrane integrity or compromised membrane permeability which may occur during the experiment at multiple points (i.e. cell culture, washing of cells, trypsinization, cell manipulation, etc.). They may also arise from heterodimers that have not been translocated to the nucleus after protein synthesis. To rule out the possibility that compound 6 caused a reduction in the levels of ERCC1 or XPF, we compared the levels of the proteins in untreated cells and cells treated with compounds 4 and 6 and observed no significant differences (**Supplementary Figure 2**). These data extend the inhibitory observations of compound 6 on ERCC1-XPF from a cell free model to intact cells.

Sensitization of HCT-116 Cells to DNA Damaging Agents

HCT-116 cells were incubated with media containing a non-toxic concentration of 6 or 10 (**Supplementary Figure 3**) prior to exposure to the DNA damaging agents.

Sensitization to UVC Radiation

Compound 6 was tested for its ability to sensitize HCT-116 cells to UVC radiation. At the non-toxic concentration of 0.5 μM, 6 sensitized cells to UVC radiation (**Figure 6A**). Compound 10 was used as a negative control at the same concentrations and

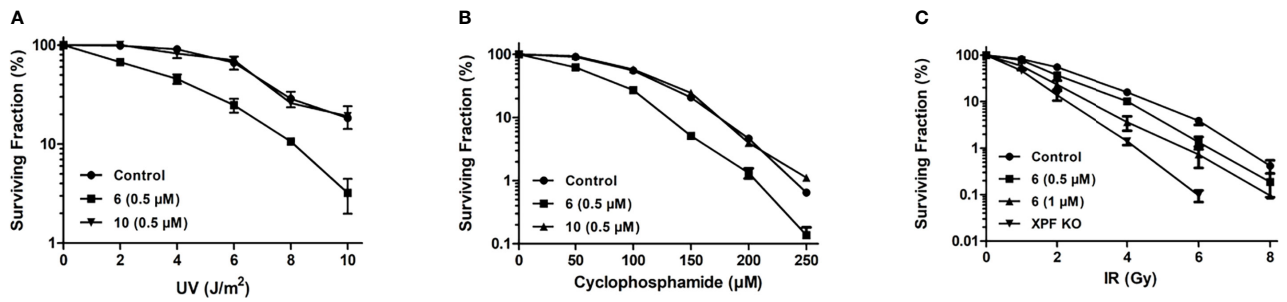

FIGURE 6 | Sensitization of HCT-116 cells to DNA damaging agents as determined by clonogenic survival assay. **(A)** Survival of HCT-116 cells exposed to increasing doses of 254 nm UV radiation and treated with 0.5 μM compound 6 or 10 **(B)** Survival of HCT-116 cells exposed to increasing doses of cyclophosphamide and treated with 0.5 μM compound 6 or 10. **(C)** Survival of HCT-116 cells exposed to increasing doses of ionizing radiation and treated with 0.5 and 1 μM compound 6. The radiosensitivity of HCT-116 XPF knockout cells (70) is provided for comparison.

showed no sensitization of HCT-116 to UVC radiation, as expected (**Figure 6A**).

Sensitization to Cyclophosphamide

Compounds 6 and 10 (negative control) were tested for their ability to sensitize HCT-116 cells to the DNA crosslinking agent cyclophosphamide (**Figure 6B**). HCT-116 cells were treated with 0.5 μM 6 or 1.0 μM 10 before being exposed to increasing concentrations of cyclophosphamide. Compound 6 sensitized the cells to cyclophosphamide, with almost no cells surviving at 250 μM cyclophosphamide. Compound 10 showed no significant sensitization of HCT-116 cells to cyclophosphamide.

Sensitization to Ionizing Radiation

HCT-116 cells were exposed to increasing intensities of ionizing radiation to establish the baseline sensitivity of HCT-116 cells to ionizing radiation. HCT-116 derived XPF knockout cells were exposed to increasing intensities of ionizing radiation to provide a theoretical maximal sensitization of HCT-116 cells to ionizing radiation. Addition of 0.5 and 1 μM 6 sensitized HCT-116 cells in a dose-dependent manner (**Figure 6C**).

ADME

Further investigation of the pharmacokinetics of compound 6 was carried out by WuXi AppTec (Shanghai) Co by performing absorption, distribution, metabolism, and excretion (ADME) measurements. The screening included distribution coefficient (log D), solubility, cell permeability, serum protein binding, CYP inhibition, and microsomal and hepatocyte stability (**Table 2**). The compound has a log D at pH 7.4 of 3.95 and a low to moderate metabolic stability as determined by both liver microsome and hepatocyte assays. The results show that 6 is a moderate inhibitor of CYP1A2, CYP2D6, and CYP 3A4-M and weak inhibitor of CYP2C9 and CYP2C19.

DISCUSSION

Our previous studies (70) made it clear that significant improvements in IC_{50} could be realized by modifying the piperazine side chain of 1, although it was originally unclear if the improvement of IC_{50} could be attributed to simply increased steric bulk in that area, the addition of a heteroatom, or any other interactions with the ERCC1-XPF interface. To interrogate the key interactions and to investigate what further changes could be made to this site we carried out an MOE pharmacaphore-assisted docking experiment to identify compounds with modifications in this area that could improve upon the binding observed with 4. The top 32 scoring compounds were selected based on their GBVI/WSA score and MM/GBSA scores were calculated; from these MM/GBSA scores (top ten in **Table 1**) there was a standout performer in compound 6 with significantly lower binding energy than any of the other hits.

We then set out to synthesize the top ten performing inhibitors for *in vitro* testing. Of the top ten inhibitors from the *in silico* screen six compounds were successfully synthesized, including the top performing compound 6. These six compounds were tested in an *in vitro* endonuclease assay to assess their ability to inhibit the endonuclease activity of ERCC1-XPF (**Figure 3A**); surprisingly, compounds 8, 10, 11, 12, and 15 were unable to improve on the inhibition shown by the parent compound 4 despite having similar or lower calculated GBSA scores. However, the top scoring compound 6 did show a modest increase in inhibition over the parent compound 4, and a lowering of calculated IC_{50} from 0.33 μM for 4 (70) to 0.17 μM for 6 (**Figure 3A**).

To first test if the increased inhibition of endonuclease activity would translate to activity in cells we tested the ability of 6 to inhibit the removal of UV induced CPD in cells. As expected, compound 6 was able to slow the removal of CPD by ERCC1-XPF at a concentration of 2 μM, whereas our negative control compound 10 at the same concentration was unable to slow the removal of CPD *vs* the control (**Figure 4**). Interestingly, the inhibition of the removal of CPD was slightly less effective using 2 μM concentration of compound 6 than the same concentration of compound 4 (67% and 60% (70) CPD removal after 24 hours, respectively). Despite the slightly reduced inhibition of CPD removal as compared to compound 4, the inhibition of CPD removal observed with compound 6 provided strong evidence that 6 inhibited cellular NER and would likely be able to sensitize cells to DNA damaging chemotherapies with similar efficacy as that observed with compound 4.

TABLE 2 | Pharmacokinetic profile of compounds **4** and **6**.

Screening Test	Compound	Results				
LogD at pH 7.4	Compound 6	3.95				
	Compound 4	2.86				
Metabolic stability in human liver microsomes	Compound 6	376.2 (mL/min/kg)				
	Compound 4	44.0 (mL/min/kg)				
Metabolic stability in cryopreserved human hepatocytes	Compound 6	33.5 (mL/min/kg), $T^{1/2}$ 114.9 (min)				
	Compound 4	48.8 (mL/min/kg), $T^{1/2}$ 79.0 (min)				
Permeability	Compound 6	27.51				
(Efflux Ratio)	Compound 4	8.92				
Inhibition of cytochrome P450	Compound 6	CYP1A2	CYP2C9	CYP2C19	CYP2D6	CYP3A4-M
(IC_{50})		6.51 μM	33.4 μM	10.8 μM	2.92 μM	1.9 μM
	Compound 4	CYP1A2	CYP2C9	CYP2C19	CYP2D6	CYP3A4-M
		6.40 μM	>50 μM	>50 μM	16.0 μM	37.1 μM

Before carrying out sensitization studies we attempted to gather evidence that the inhibition of cellular NER was a result of compound 6 binding to ERCC1-XPF and inhibiting the heterodimerization. Fluorescence spectroscopy revealed a dose dependent quenching of the intrinsic fluorescence of ERCC1-XPF tryptophan residues (**Figure 3C**) providing strong evidence of compound 6 binding directly to ERCC1-XPF. However, the calculated K_d of 140 nM from the intrinsic fluorescence spectroscopy indicates slightly weaker binding of compound 6 to ERCC1-XPF than the K_d of 100 nM calculated for compound 4 (70), which runs contrary to what was expected from the computational results. The confounding results from the computational screening and the binding affinity means that we may need to re-evaluate our calculated mode of binding in future work to build a more accurate computational model. Nonetheless, the calculated K_d, as well as inhibition of endonuclease activity, and inhibition of cellular NER provided strong evidence that compound 6 could be an effective inhibitor of ERCC1-XPF.

The PLA results also provided further evidence that compound 6 inhibits DNA repair by inhibiting the heterodimerization of ERCC1 and XPF. In the A549 cells there is clear interaction between ERCC1 and XPF at the site of DAPI stained DNA (**Figure 5**), with an average of 76 foci per cell. However, when media containing 2 μM concentration of compound 6 is added the number of foci per cell drops to an average of 3 per cell, showing a clear disruption of ERCC1-XPF heterodimerization (**Figure 5**). This result is in keeping with the PLA results previously observed for 1, 4, and 5 (73), where this series of inhibitors showed clear inhibition of the interaction between ERCC1 and XPF when A549 cells were treated with 20 μM cisplatin and 1 μM concentrations of the inhibitors. However, only compound 5 showed any significant disruption of ERCC1-XPF heterodimerization on A549 not treated with cisplatin in those experiments. At this juncture it is difficult to make direct comparisons between these results and those obtained by Ciniero et al. (73) due to the large difference in the foci per cell of the A549 control cells and the different concentrations of inhibitors used between the experiments (2 μM and 1 μM, respectively). Despite the differences in details of experimental methodology, it is clear that compound 6 has a profound impact on the heterodimerization of ERCC1 and XPF, which provides further evidence for our hypothesized mode of inhibition.

We then tested the ability of compound 6 to sensitize cells to DNA damaging agents. Since compound 6 had already been shown to inhibit removal of UV-induced CPD, sensitization of HCT-116 cells to UVC radiation was the obvious starting point. At a concentration of 0.5 μM, compound 6 sensitized HCT-116 cells to UVC radiation as expected, with the negative control 10 showing no sensitization (**Figure 6A**). For example, at 4 J/m^2 91% of the untreated cells survived but <50% of cells treated with 0.5 μM compound 6 survived. By comparison, 1.0 μM compound 4 reduced survival of HCT-116 cells to ~ 50% under the same conditions (70). This sensitization of cells to UVC radiation is a promising sign that HCT-116 cells can be made more sensitive to treatments that cause DNA damage that is repaired by NER, allowing for more effective treatments at lower doses.

Following the successful sensitization of HCT-116 cells to UVC radiation we wished to investigate the sensitization of HCT-116 cells to the DNA crosslinking agent cyclophosphamide. Successful sensitization of cancer cells to cyclophosphamide would imply that 6 inhibited cellular ICL as well as NER, lending credence to the notion that compound 6 was indeed inhibiting NER by inhibiting the endonuclease activity of ERCC1-XPF and not *via* inhibition of another protein involved in NER. Compound 6 sensitized HCT-116 cells to cyclophosphamide, with 10 again showing no sensitization (**Figure 6B**). Notably, at the lowest dosage of cyclophosphamide (50 μM) only 62% of the HCT-116 cells treated with 0.5 μM of 6 survived, in contrast to the 91.5% that survived when treated with cyclophosphamide alone, and at 250 μM cyclophosphamide there were almost no surviving HCT-116 cells when treated with 0.5 μM compound 6. Elmenoufy and co-workers (70) had previously reported much more modest sensitization of HCT-116 cells to 50 μM concentration of cyclophosphamide (about 75% cell survival) with double the concentration of compound 4 (i.e.,1 μM). This increase in the potentiation of cyclophosphamide activity by compound 6 offers support to the notion that inhibition of ERCC1-XPF could allow lowering of the effective doses of cytotoxic DNA-targeting drugs such as cyclophosphamide, which is known to have a plethora of negative side effects (81–87).

Following the outcome of compound 6 in sensitizing HCT-116 cells to DNA therapies that cause DNA damage that is repaired by NER and ICL, we turned our attention to cells damaged by cobalt-60 γ-rays. Previous studies have indicated that ERCC1-XPF deficient mammalian cells display enhanced sensitivity to ionizing radiation and reduced DSB repair (24, 88, 89). In agreement with these earlier findings, our CRISPR-mediated XPF knockout cells were shown to be significantly more sensitive to ionizing radiation than the control HCT-116 cells (**Figure 6C**). We therefore treated HCT-116 cells with 0.5 and 1 μM concentrations of compound 6 before exposure to increasing doses of ionizing radiation. Compound 6 sensitized HCT-116 cells to ionizing radiation in a dose dependent manner (**Figure 6C**). Importantly, sensitization was observed even at the typical clinical dose of 2 Gy (90) with both 0.5 and 1 μM concentrations of 6. Our data clearly indicate a potential role for targeting ERCC1-XPF to enhance radiotherapy.

The ADME results (**Table 2**) when compared with the previous ADME screening of parent hit compound 1, and first and second generation compounds 4 (70) and 5 (71) indicated fairly similar responses to compound 4. However, two differences in the ADME data between compounds 6 and 4 may have a possible bearing on the lower sensitization capacity seen with compound 4 relative compound 6. First, compound 6 inhibits cytochromes 2C19, 2D6 and 3A4-M, much more effectively than compound 4. It is therefore feasible that compound 4 is metabolized more rapidly in HCT116 cells than compound 6. Similarly, if the clearance from human hepatocytes reflects the clearance from HCT116 cells, it is noticeable that compound 4 is cleared more rapidly than compound 6 ($T^{1/2}$ = 79 *vs* 114.9 min), which would imply lower cellular retention of active compound 4 *vs* 6. These possibilities will need to be further explored.

In conclusion, we used a computer aided drug design strategy to identify potential inhibitors of ERCC1-XPF based on the modification of the piperazine side-chain of the previously reported inhibitor 4. Of the compounds screened, compound 6 was the best performing compound by a wide margin. Six of the 10 best performing compounds were synthesized and subjected to *in vitro* testing to inhibit the endonuclease activity of ERCC1-XPF. Compound 6 was the best performing of the synthesized inhibitors *in vitro* and was subsequently shown to inhibit NER in cells. Our binding studies and PLA provided further evidence that the observed inhibition was due to the inhibition of the heterodimerization of ERCC1 and XPF. Compound 6 was then shown to sensitize HCT-116 cells to UVC radiation, cyclophosphamide, and ionizing radiation; proving that it is a promising candidate to be used alongside existing DNA damaging therapies. Furthermore, we have found that variation of the piperazine side-chain is well tolerated and does not interfere with what we believe to be the key binding between the binding pocket in the HhH2 domain of XPF and the aminophenol substituted acridine moieties found in 1, 4, 5, and 6. This discovery allows for further functionalization at this site and the potential for the introduction of moieties to improve the binding affinity and pharmacokinetic properties of this series of inhibitors.

DATA AVAILABILITY STATEMENT

The datasets presented in this study can be found in online repositories. The names of the repository/repositories and accession number(s) can be found in the article/**Supplementary Material**.

AUTHOR CONTRIBUTIONS

CW synthesized and characterized all the compounds. DJ expressed and purified ERCC1-XPF protein, carried out the *in vitro* endonuclease assays, and the PLA. JD wrote the manuscript. FG carried out the computational studies. FK-B and XY carried out cell culturing, UV dimer repair assays, and clonogenic survival assays. RM conducted the binding affinity study. YY provided the XPF knockout cells. KB and JT supervised FG in designing the computational studies. AE contributed to compound design and interpretation of assay results. MW supervised XY and co-wrote and edited the manuscript. FW supervised CW, JD and AE and co-wrote and edited the manuscript. All authors contributed to the article and approved the submitted version.

FUNDING

This work was supported by grants funded by the Alberta Cancer Foundation Transformative Program Project (26603) and the Alberta Cure Cancer Foundation. We also acknowledge the support of the Savard Family Lung Research Fund. JD was supported by the La Vie En Rose Scholarship for Fundamental Breast Cancer Research. FG was supported by an Alberta Innovates graduate student scholarship and a Novartis Pharmaceuticals Canada Inc. graduate scholarship. The funder was not involved in the study design, collection, analysis, interpretation of data, the writing of this article or the decision to submit it for publication.

ACKNOWLEDGMENTS

We acknowledge the technical assistance of Dr. Xuejun Sun from the Cell Imaging Facility at the Cross Cancer Institute.

SUPPLEMENTARY MATERIAL

The Supplementary Material for this article can be found online at: https://www.frontiersin.org/articles/10.3389/fonc.2022.819172/full#supplementary-material

REFERENCES

1. Hoeijmakers JHJ. DNA Damage, Aging, and Cancer. *N Engl J Med* (2009) 361:1475–85. doi: 10.1056/NEJMra0804615
2. Sancar A, Lindsey-Boltz LA, Ünsal-Kaçmaz K, Linn S. Molecular Mechanisms of Mammalian DNA Repair and the DNA Damage Checkpoints. *Annu Rev Biochem* (2004) 73:39–85. doi: 10.1146/annurev.biochem.73.011303.073723
3. Jackson SP, Bartek J. The DNA-Damage Response in Human Biology and Disease. *Nature* (2009) 461:1071–8. doi: 10.1038/nature08467
4. Ciccia A, Elledge SJ. The DNA Damage Response: Making It Safe to Play With Knives. *Mol Cell* (2010) 40:179–204. doi: 10.1016/j.molcel.2010.09.019
5. Pearl LH, Schierz AC, Ward SE, Al-Lazikani B, G Pearl FM. Therapeutic Opportunities Within the DNA Damage Response. *Nature Reviews Cancer* (2015) 15(3):166–80. doi: 10.1038/nrc3891
6. Chatterjee N, Walker GC. Mechanisms of DNA Damage, Repair, and Mutagenesis. *Environ Mol Mutagen* (2017) 58:235–63. doi: 10.1002/em.22087
7. Huang R, Zhou PK. DNA Damage Repair: Historical Perspectives, Mechanistic Pathways and Clinical Translation for Targeted Cancer Therapy. *Signal Transduct Target Ther* (2021) 6:254. doi: 10.1038/s41392-021-00648-7
8. Park CH, Sancar A. Formation of a Ternary Complex by Human XPA, ERCC1, and ERCC4(XPF) Excision Repair Proteins. *Proc Natl Acad Sci USA* (1994) 91:5017–21. doi: 10.1073/pnas.91.11.5017
9. Gillet LCJ, Schärer OD. Molecular Mechanisms of Mammalian Global Genome Nucleotide Excision Repair. *Chem Rev* (2006) 106:253–76. doi: 10.1021/cr040483f
10. Kirschner K, Melton DW. Multiple Roles of the ERCC1-XPF Endonuclease in DNA Repair and Resistance to Anticancer Drugs. *Anticancer Res* (2010) 30:3223–32.
11. Marteijn JA, Lans H, Vermeulen W, Hoeijmakers JHJ. Understanding Nucleotide Excision Repair and its Roles in Cancer and Ageing. *Nat Rev Mol Cell Biol* (2014) 15:465–81. doi: 10.1038/nrm3822
12. Gregersen LH, Svejstrup JQ. The Cellular Response to Transcription-Blocking DNA Damage. *Trends Biochem Sci* (2018) 43:327–41. doi: 10.1016/j.tibs.2018.02.010
13. Bhagwat N, Olsen AL, Wang AT, Hanada K, Stuckert P, Kanaar R, et al. XPF-ERCC1 Participates in the Fanconi Anemia Pathway of Cross-Link Repair. *Mol Cell Biol* (2009) 29:6427–37. doi: 10.1128/mcb.00086-09
14. Williams HL, Gottesman ME, Gautier J. Replication-Independent Repair of DNA Interstrand Crosslinks. *Mol Cell* (2012) 47:140–7. doi: 10.1016/j.molcel.2012.05.001

15. Kottemann MC, Smogorzewska A. Fanconi Anaemia and the Repair of Watson and Crick DNA Crosslinks. *Nature* (2013) 493:356–63. doi: 10.1038/nature11863
16. Williams HL, Gottesman ME, Gautier J. The Differences Between ICL Repair During and Outside of S Phase. *Trends Biochem Sci* (2013) 38:386–93. doi: 10.1016/j.tibs.2013.05.004
17. Klein Douwel D, Hoogenboom WS, Boonen RA, Knipscheer P. Recruitment and Positioning Determine the Specific Role of the XPF - ERCC 1 Endonuclease in Interstrand Crosslink Repair. *EMBO J* (2017) 36:2034–46. doi: 10.15252/embj.201695223
18. Abdullah UB, McGouran JF, Brolih S, Ptchelkine D, El-Sagheer AH, Brown T, et al. RPA Activates the XPF - ERCC 1 Endonuclease to Initiate Processing of DNA Interstrand Crosslinks. *EMBO J* (2017) 36:2047–60. doi: 10.15252/embj.201796664
19. Seol JH, Holland C, Li X, Kim C, Li F, Medina-Rivera M, et al. Distinct Roles of XPF-ERCC1 and Rad1-Rad10-Saw1 in Replication-Coupled and Uncoupled Inter-Strand Crosslink Repair. *Nat Commun* (2018) 9:1–13. doi: 10.1038/s41467-018-04327-0
20. Caldecott KW. Single-Strand Break Repair and Genetic Disease. *Nat Rev Genet* (2008) 9:619–31. doi: 10.1038/nrg2380
21. Takahata C, Masuda Y, Takedachi A, Tanaka K, Iwai S, Kuraoka I. Repair Synthesis Step Involving ERCC1-XPF Participates in DNA Repair of the Top1-DNA Damage Complex. *Carcinogenesis* (2015) 36:841–51. doi: 10.1093/carcin/bgv078
22. Bennardo N, Cheng A, Huang N, Stark JM. Alternative-NHEJ is a Mechanistically Distinct Pathway of Mammalian Chromosome Break Repair. *PloS Genet* (2008) 4:e1000110. doi: 10.1371/journal.pgen.1000110
23. Al-minawi AZ, Saleh-gohari N, Helleday T. The ERCC1/XPF Endonuclease is Required for Efficient Single-Strand Annealing and Gene Conversion in Mammalian Cells. *Nucleic Acids Res* (2008) 36:1–9. doi: 10.1093/nar/gkm888
24. Ahmad A, Robinson AR, Duensing A, van Drunen E, Beverloo HB, Weisberg DB, et al. ERCC1-XPF Endonuclease Facilitates DNA Double-Strand Break Repair. *Mol Cell Biol* (2008) 28:5082–92. doi: 10.1128/mcb.00293-08
25. Mao Z, Bozzella M, Seluanov A, Gorbunova V. DNA Repair by Nonhomologous End Joining and Homologous Recombination During Cell Cycle in Human Cells. *Cell Cycle* (2008) 7:2902–6. doi: 10.4161/cc.7.18.6679
26. O'Connor MJ. Targeting the DNA Damage Response in Cancer. *Mol Cell* (2015) 60:547–60. doi: 10.1016/j.molcel.2015.10.040
27. Hengel SR, Spies MA, Spies M. Small-Molecule Inhibitors Targeting DNA Repair and DNA Repair Deficiency in Research and Cancer Therapy. *Cell Chem Biol* (2017) 24:1101–19. doi: 10.1016/j.chembiol.2017.08.027
28. Brown JS, O'Carrigan B, Jackson SP, Yap TA. Targeting DNA Repair in Cancer: Beyond PARP Inhibitors. *Cancer Discovery* (2017) 7:20–37. doi: 10.1158/2159-8290.CD-16-0860
29. Cleary JM, Aguirre AJ, Shapiro GI, D'Andrea AD. Biomarker-Guided Development of DNA Repair Inhibitors. *Mol Cell* (2020) 78:1070–85. doi: 10.1016/j.molcel.2020.04.035
30. McPherson KS, Korzhnev DM. Targeting Protein-Protein Interactions in the DNA Damage Response Pathways for Cancer Chemotherapy. *RSC Chem Biol* (2021) 2:1167–95. doi: 10.1039/d1cb00101a
31. Setlow RB. Cyclobutane-Type Pyrimidine Dimers in Polynucleotides. *Science (80-)* (1966) 153:379–86. doi: 10.1126/science.153.3734.379
32. Löber G, Kittler L. Selected Topics in Photochemistry of Nucleic Acids, Recent Results and Perspectives. *Photochem Photobiol* (1977) 25:215–33. doi: 10.1111/j.1751-1097.1977.tb06902.x
33. Brash DE, Haseltine WA. UV-Induced Mutation Hotspots Occur at DNA Damage Hotspots. *Nature* (1982) 298:189–92. doi: 10.1038/298189a0
34. Glickman BW, Schaaper RM, Haseltine WA, Dunn RL, Brash DE. The C-C (6-4) UV Photoproduct is Mutagenic in Escherichia coli. *Proc Natl Acad Sci USA* (1986) 83:6945–9. doi: 10.1073/pnas.83.18.6945
35. Yagi T, Katsuya A, Koyano A, Takebe H. Sensitivity of Group F Xeroderma Pigmentosum Cells to UV and Mitomycin C Relative to Levels of XPF and ERCC1 Overexpression. *Mutagenesis* (1998) 13:595–9. doi: 10.1093/mutage/13.6.595
36. Dunkern TR, Fritz G, Kaina B. Ultraviolet Light-Induced DNA Damage Triggers Apoptosis in Nucleotide Excision Repair-Deficient Cells *via* Bcl-2 Decline and Caspase-3/-8 Activation. *Oncogene* (2001) 20:6026–38. doi: 10.1038/sj.onc.1204754
37. Heyza JR, Lei W, Watza D, Zhang H, Chen W, Back JB, et al. Identification and Characterization of Synthetic Viability With ERCC1 Deficiency in Response to Interstrand Crosslinks in Lung Cancer. *Clin Cancer Res* (2019) 25:2523–36. doi: 10.1158/1078-0432.CCR-18-3094
38. Zhou CX, Zhao JH. Systematic Review on the Association Between ERCC1 Rs3212986 and ERCC2 Rs13181 Polymorphisms and Glioma Risk. *Genet Mol Res* (2015) 14:2868–75. doi: 10.4238/2015.March.31.17
39. Xuelei M, Jingwen H, Wei D, Hongyu Z, Jing Z, Changle S, et al. ERCC1 Plays an Important Role in Predicting Survival Outcomes and Treatment Response for Patients With HNSCC: A Meta-Analysis. *Oral Oncol* (2015) 51:483–92. doi: 10.1016/j.oraloncology.2015.02.094
40. Zhang C, Gao S, Hou J. ERCC1 Expression and Platinum Chemosensitivity in Patients With Ovarian Cancer: A Meta-Analysis. *Int J Biol Markers* (2020) 35:12–9. doi: 10.1177/1724600820963396
41. Gao Y, Liu D. The Roles of Excision Repair Cross-Complementation Group1 in Objective Response After Cisplatin-Based Concurrent Chemoradiotherapy and Survival in Head and Neck Cancers: A Systematic Review and Meta-Analysis. *Oral Oncol* (2015) 51:570–7. doi: 10.1016/j.oraloncology.2015.03.009
42. Song P, Yin Q, Lu M, Fu B, Wang B, Zhao Q. Prognostic Value of Excision Repair Cross-Complementation Group 1 Expression in Gastric Cancer: A Meta-Analysis. *Exp Ther Med* (2015) 9:1393–400. doi: 10.3892/etm.2015.2284
43. Bišof V, Zajc Petranović M, Rakušić Z, Samardžić KR, Juretić A. The Prognostic and Predictive Value of Excision Repair Cross-Complementation Group 1 (ERCC1) Protein in 1288 Patients With Head and Neck Squamous Cell Carcinoma Treated With Platinum-Based Therapy: A Meta-Analysis. *Eur Arch Oto Rhino Laryngol* (2016) 273:2305–17. doi: 10.1007/s00405-015-3710-x
44. Urun Y, Leow JJ, Fay AP, Albiges L, Choueiri TK, Bellmunt J. ERCC1 as a Prognostic Factor for Survival in Patients With Advanced Urothelial Cancer Treated With Platinum Based Chemotherapy: A Systematic Review and Meta-Analysis. *Crit Rev Oncol Hematol* (2017) 120:120–6. doi: 10.1016/j.critrevonc.2017.10.012
45. Zhu J, Ji S, Hu Q, Chen Q, Liu Z, Wu J, et al. The Prognostic Value of Excission Repair Cross-Complementation Group One Enzyme Expression in Locally Advanced Cervical Carcinoma Patients Treated With Cisplatin–Based Treatment: A Meta–Analysis. *Int J Gynecol Cancer* (2019) 29:35–41. doi: 10.1136/ijgc-2018-000027
46. Wu J, Li R, Chen X, Chen C, Chen H, Ma B. Meta-Analysis of Excision Repair Cross Complementary Gene 1 (ERCC1) Expression and Platinum Chemosensitivity in Patients With Ovarian Cancer. *Ann Palliat Med* (2020) 9:3428–35. doi: 10.21037/apm-20-1634
47. Li G, Cheng D. Meta-Analysis of ERCC1 Protein Expression and Platinum Chemosensitivity in Non-Small-Cell Lung Cancer. *Evidence-Based Complement Altern Med* (2020) 2020:1–8. doi: 10.1155/2020/7376568
48. Wang Y, Li J, Shen C, Wu Y, Che G. Clinical Role of Excision Repair Cross-Complementing 1 Gene Expression in Resected Esophageal Squamous Cell Carcinoma: A Meta-Analysis. *Dig Dis Sci* (2020) 65:2264–71. doi: 10.1007/s10620-019-05941-8
49. Van Vuuren AJ, Appeldoorn E, Odijk H, Yasui A, Jaspers NGJ, Bootsma D, et al. Evidence for a Repair Enzyme Complex Involving ERCC1 and Complementing Activities of ERCC4, ERCC11 and Xeroderma Pigmentosum Group F. *EMBO J* (1993) 12:3693–701. doi: 10.1002/j.1460-2075.1993.tb06044.x
50. Biggerstaff M, Szymkowski DE, Wood RD. Co-Correction of the ERCC1, ERCC4 and Xeroderma Pigmentosum Group F DNA Repair Defects *In Vitro*. *EMBO J* (1993) 12:3685–92. doi: 10.1002/j.1460-2075.1993.tb06043.x
51. Sijbers AM, van der Spek P, Odijk H, van den Berg J, van Duin M, Westerveld A, et al. Mutational Analysis of the Human Nucleotide Excision Repair Gene ERCC1. *Nucleic Acids Res* (1996) 24:3370–80. doi: 10.1093/nar/24.17.3370
52. de Laat WL, Appeldoorn E, Jaspers NGJ, Hoeijmakers JHJ. DNA Structural Elements Required for ERCC1-XPF Endonuclease Activity. *J Biol Chem* (1998) 273:7835–42. doi: 10.1074/jbc.273.14.7835
53. Gaillard P-HHL, Wood RD. Activity of Individual ERCC1 and XPF Subunits in DNA Nucleotide Excision Repair. *Nucleic Acids Res* (2001) 29:872–9. doi: 10.1093/nar/29.4.872

54. Choi YJ, Ryu KS, Ko YM, Chae YK, Pelton JG, Wemmer DE, et al. Biophysical Characterization of the Interaction Domains and Mapping of the Contact Residues in the XPF-ERCC1 Complex. *J Biol Chem* (2005) 280:28644–52. doi: 10.1074/jbc.M501083200
55. Tripsianes K, Folkers G, Ab E, Das D, Odijk H, Jaspers NGJ, et al. The Structure of the Human ERCC1/XPF Interaction Domains Reveals a Complementary Role for the Two Proteins in Nucleotide Excision Repair. *Struct (Cambridge MA United States)* (2005) 13:1849–58. doi: 10.1016/j.str.2005.08.014
56. Tsodikov OV, Ivanov D, Orelli B, Staresincic L, Shoshani I, Oberman R, et al. Structural Basis for the Recruitment of ERCC1-XPF to Nucleotide Excision Repair Complexes by XPA. *EMBO J* (2007) 26:4768–76. doi: 10.1038/sj.emboj.7601894
57. Barakat KH, Torin Huzil J, Luchko T, Jordheim L, Dumontet C, Tuszynski J. Characterization of an Inhibitory Dynamic Pharmacophore for the ERCC1-XPA Interaction Using a Combined Molecular Dynamics and Virtual Screening Approach. *J Mol Graph Model* (2009) 28:113–30. doi: 10.1016/j.jmgm.2009.04.009
58. Barakat KH, Jordheim LP, Perez-Pineiro R, Wishart D, Dumontet C, Tuszynski JA. Virtual Screening and Biological Evaluation of Inhibitors Targeting the XPA-ERCC1 Interaction. *PloS One* (2012) 7:e51329. doi: 10.1371/journal.pone.0051329
59. Gentile F, Tuszynski JA, Barakat KH. New Design of Nucleotide Excision Repair (NER) Inhibitors for Combination Cancer Therapy. *J Mol Graph Model* (2016) 65:71–82. doi: 10.1016/j.jmgm.2016.02.010
60. McNeil EM, Astell KR, Ritchie A-M, Shave S, Houston DR, Bakrania P, et al. Inhibition of the ERCC1–XPF Structure-Specific Endonuclease to Overcome Cancer Chemoresistance. *DNA Repair (Amst)* (2015) 31:19–28. doi: 10.1016/j.dnarep.2015.04.002
61. Chapman TM, Gillen KJ, Wallace C, Lee MT, Bakrania P, Khurana P, et al. Catechols and 3-Hydroxypyridones as Inhibitors of the DNA Repair Complex ERCC1-XPF. *Bioorganic Med Chem Lett* (2015) 25:4097–103. doi: 10.1016/j.bmcl.2015.08.031
62. Chapman TM, Wallace C, Gillen KJ, Bakrania P, Khurana P, Coombs PJ, et al. N-Hydroxyimides and Hydroxypyrimidinones as Inhibitors of the DNA Repair Complex ERCC1-XPF. *Bioorganic Med Chem Lett* (2015) 25:4104–8. doi: 10.1016/j.bmcl.2015.08.024
63. Arora S, Heyza J, Zhang H, Kalman-Maltese V, Tillison K, Floyd AM, et al. Identification of Small Molecule Inhibitors of ERCC1-XPF That Inhibit DNA Repair and Potentiate Cisplatin Efficacy in Cancer Cells. *Oncotarget* (2016) 7:75104–17. doi: 10.18632/oncotarget.12072
64. Heyza J, Arora S, Zhang H, Conner K, Lei W, Floyd A, et al. Targeting the DNA Repair Endonuclease ERCC1-XPF With Green Tea Polyphenol Epigallocatechin-3-Gallate (EGCG) and Its Prodrug to Enhance Cisplatin Efficacy in Human Cancer Cells. *Nutrients* (2018) 10:1644. doi: 10.3390/nu10111644
65. Gentile F, Barakat K, Tuszynski J. Computational Characterization of Small Molecules Binding to the Human XPF Active Site and Virtual Screening to Identify Potential New DNA Repair Inhibitors Targeting the ERCC1-XPF Endonuclease. *Int J Mol Sci* (2018) 19:1328. doi: 10.3390/ijms19051328
66. McNeil EM, Melton DW. DNA Repair Endonuclease ERCC1-XPF as a Novel Therapeutic Target to Overcome Chemoresistance in Cancer Therapy. *Nucleic Acids Res* (2012) 40:9990–10004. doi: 10.1093/nar/gks818
67. Ahmad A, Enzlin JH, Bhagwat NR, Wijgers N, Raams A, Appledoorn E, et al. Mislocalization of XPF-ERCC1 Nuclease Contributes to Reduced DNA Repair in XP-F Patients. *PloS Genet* (2010) 6:1000871. doi: 10.1371/journal.pgen.1000871
68. Jordheim LP, Barakat KH, Heinrich-Balard L, Matera E-L, Cros-Perrial E, Bouledrak K, et al. Small Molecule Inhibitors of ERCC1-XPF Protein-Protein Interaction Synergize Alkylating Agents in Cancer Cells. *Mol Pharmacol* (2013) 84:12–24. doi: 10.1124/mol.112.082347
69. Wang Z, Xu Z, Zhu G. A Platinum(IV) Anticancer Prodrug Targeting Nucleotide Excision Repair To Overcome Cisplatin Resistance. *Angew Chemie - Int Ed* (2016) 55:15564–8. doi: 10.1002/anie.201608936
70. Elmenoufy AH, Gentile F, Jay D, Karimi-Busheri F, Yang X, Soueidan OM, et al. Targeting DNA Repair in Tumor Cells *via* Inhibition of ERCC1–XPF. *J Med Chem* (2019) 62:7684–96. doi: 10.1021/acs.jmedchem.9b00326
71. Elmenoufy AH, Gentile F, Jay D, Karimi-Busheri F, Yang X, Soueidan OM, et al. Design, Synthesis and *In Vitro* Cell-Free/Cell-Based Biological Evaluations of Novel ERCC1-XPF Inhibitors Targeting DNA Repair Pathway. *Eur J Med Chem* (2020) 204:112658. doi: 10.1016/j.ejmech.2020.112658
72. Gentile F, Elmenoufy AH, Ciniero G, Jay D, Karimi-Busheri F, Barakat KH, et al. Computer-Aided Drug Design of Small Molecule Inhibitors of the ERCC1-XPF Protein–Protein Interaction. *Chem Biol Drug Des* (2020) 95:460–71. doi: 10.1111/cbdd.13660
73. Ciniero G, Elmenoufy AH, Gentile F, Weinfeld M, Deriu MA, West FG, et al. Enhancing the Activity of Platinum-Based Drugs by Improved Inhibitors of ERCC1–XPF-Mediated DNA Repair. *Cancer Chemother Pharmacol* (2021) 87:259–67. doi: 10.1007/s00280-020-04213-x
74. *Molecular Operating Environment 2019 (MOE 2019)* (2019). Available at: http://www.chemcomp.com (Accessed February 2, 2019).
75. Labute P. The Generalized Born/volume Integral Implicit Solvent Model: Estimation of the Free Energy of Hydration Using London Dispersion Instead of Atomic Surface Area. *J Comput Chem* (2008) 29:1693–8. doi: 10.1002/jcc.20933
76. Genheden S, Ryde U. The MM/PBSA and MM/GBSA Methods to Estimate Ligand-Binding Affinities. *Expert Opin Drug Discovery* (2015) 10:449–61. doi: 10.1517/17460441.2015.1032936
77. Wildman SA, Crippen GM. Prediction of Physicochemical Parameters by Atomic Contributions. *J Chem Inf Comput Sci* (1999) 39:868–73. doi: 10.1021/ci990307l
78. Bowles M, Lally J, Fadden AJ, Mouilleron S, Hammonds T, Mcdonald NQ. Fluorescence-Based Incision Assay for Human XPF-ERCC1 Activity Identifies Important Elements of DNA Junction Recognition. *Nucleic Acids Res* (2012) 40:e101. doi: 10.1093/nar/gks284
79. Mirzayans R, Pollock S, Scott A, Gao CQ, Murray D. Metabolic Labeling of Human Cells With Tritiated Nucleosides Results in Activation of the ATM-Dependent P53 Signaling Pathway and Acceleration of DNA Repair. *Oncogene* (2003) 22:5562–71. doi: 10.1038/sj.onc.1206514
80. Mani RS, Karimi-Busheri F, Fanta M, Caldecott KW, Cass CE, Weinfeld M. Biophysical Characterization of Human XRCC1 and its Binding to Damaged and Undamaged DNA. *Biochemistry* (2004) 43:16505–14. doi: 10.1021/bi048615m
81. Solomon J. Cyclophosphamide. *JAMA* (1963) 183:165. doi: 10.1001/jama.1963.03700030041009
82. Martin F, Lauwerys B, Lefèbvre C, Devogelaer JP, Houssiau FA. Side-Effects of Intravenous Cyclophosphamide Pulse Therapy. *Lupus* (1997) 6:254–7. doi: 10.1177/096120339700600307
83. Huong DLT, Amoura Z, Duhaut P, Sbai A, Costedoat N, Wechsler B, et al. Risk of Ovarian Failure and Fertility After Intravenous Cyclophosphamide. A Study in 84 Patients. *J Rheumatol* (2002) 29:2571–6.
84. Appel GB, Contreras G, Dooley MA, Ginzler EM, Isenberg D, Jayne D, et al. Mycophenolate Mofetil Versus Cyclophosphamide for Induction Treatment of Lupus Nephritis. *J Am Soc Nephrol* (2009) 20:1103–12. doi: 10.1681/ASN.2008101028
85. Jones RB, Cohen Tervaert JW, Hauser T, Luqmani R, Morgan MD, Peh CA, et al. Rituximab Versus Cyclophosphamide in ANCA-Associated Renal Vasculitis. *N Engl J Med* (2010) 363:211–20. doi: 10.1056/NEJMoa0909169
86. Baba S, Katsumata Y, Kawaguchi Y, Gono T, Sugiura T, Kanno T, et al. Association Between Low-Dose Pulsed Intravenous Cyclophosphamide Therapy and Amenorrhea in Patients With Systemic Lupus Erythematosus: A Case-Control Study. *BMC Womens Health* (2011) 11:28. doi: 10.1186/1472-6874-11-28
87. Harward LE, Mitchell K, Pieper C, Copland S, Criscione-Schreiber LG, Clowse MEB. The Impact of Cyclophosphamide on Menstruation and Pregnancy in Women With Rheumatologic Disease. *Lupus* (2013) 22:81–6. doi: 10.1177/0961203312468624
88. Wood RD, Burki HJ, Hughes M, Poley A. Radiation-Induced Lethality and Mutation in a Repair-Deficient CHO Cell Line. *Int J Radiat Biol* (1983) 43:207–13. doi: 10.1080/09553008314550241
89. Murray D, Macann A, Hanson J, Rosenberg E. ERCC1/ERCC4 5′-Endonuclease Activity as a Determinant of Hypoxic Cell Radiosensitivity. *Int J Radiat Biol* (1996) 69:319–27. doi: 10.1080/095530096145878

90. Durante M, Orecchia R, Loeffler JS. Charged-Particle Therapy in Cancer: Clinical Uses and Future Perspectives. *Nat Rev Clin Oncol* (2017) 14:483–95. doi: 10.1038/nrclinonc.2017.30

Conflict of Interest: The authors declare that the research was conducted in the absence of any commercial or financial relationships that could be construed as a potential conflict of interest.

Publisher's Note: All claims expressed in this article are solely those of the authors and do not necessarily represent those of their affiliated organizations, or those of the publisher, the editors and the reviewers. Any product that may be evaluated in this article, or claim that may be made by its manufacturer, is not guaranteed or endorsed by the publisher.

frontiers in Oncology

ORIGINAL RESEARCH
published: 24 March 2022
doi: 10.3389/fonc.2022.826617

RelA Is an Essential Target for Enhancing Cellular Responses to the DNA Repair/Ref-1 Redox Signaling Protein and Restoring Perturbated Cellular Redox Homeostasis in Mouse PDAC Cells

Mahmut Mijit[1], Randall Wireman[1], Lee Armstrong[1], Silpa Gampala[1], Zonera Hassan[2], Christian Schneeweis[2], Guenter Schneider[3], Chi Zhang[4,5,6], Melissa L. Fishel[1,7,8†] and Mark R. Kelley[1,7,8,9†]*

[1] Department of Pediatrics, Herman B Wells Center for Pediatric Research, Indiana University School of Medicine, Indianapolis, IN, United States, [2] Department of Clinic and Polyclinic for Internal Medicine II, Klinikum rechts der Isar, Technical University of Munich, Munich, Germany, [3] Department of General, Visceral and Pediatric Surgery, University Medical Center Göttingen, Göttingen, Germany, [4] Department of Medical and Molecular Genetics, Indiana University School of Medicine, Indianapolis, IN, United States, [5] Department of Biohealth Informatics, Indiana University-Purdue University (IUPUI), Indianapolis, IN, United States, [6] Indiana University Melvin and Bren Simon Comprehensive Cancer Center, Indiana University School of Medicine, Indianapolis, IN, United States, [7] Department of Pharmacology and Toxicology, Indiana University School of Medicine, Indianapolis, IN, United States, [8] Department of Biochemistry and Molecular Biology, Indiana University School of Medicine, Indianapolis, IN, United States, [9] Indiana University Melvin and Bren Simon Comprehensive Cancer Center, Indiana University, Indianapolis, IN, United States

OPEN ACCESS

Edited by:
Michael Weinfeld,
University of Alberta, Canada

Reviewed by:
Dindial Ramotar,
Hamad bin Khalifa University, Qatar
Bruce Demple,
Stony Brook University, United States
Lynn Harrison,
Louisiana State University Health Shreveport, United States

***Correspondence:**
Mark R. Kelley
mkelley@iu.edu

†These authors share senior authorship

Specialty section:
This article was submitted to Cancer Molecular Targets and Therapeutics, a section of the journal Frontiers in Oncology

Received: 01 December 2021
Accepted: 22 February 2022
Published: 24 March 2022

Citation:
Mijit M, Wireman R, Armstrong L, Gampala S, Hassan Z, Schneeweis C, Schneider G, Zhang C, Fishel ML and Kelley MR (2022) RelA Is an Essential Target for Enhancing Cellular Responses to the DNA Repair/Ref-1 Redox Signaling Protein and Restoring Perturbated Cellular Redox Homeostasis in Mouse PDAC Cells. Front. Oncol. 12:826617. doi: 10.3389/fonc.2022.826617

Pancreatic ductal adenocarcinoma (PDAC) is one of the deadliest cancers with a poor response to current treatment regimens. The multifunctional DNA repair-redox signaling protein Ref-1 has a redox signaling function that activates several transcriptional factors (TFs) including NF-κB (RelA), STAT3, AP-1. These have been implicated in signaling in PDAC and associated with cancer progression and therapy resistance. Numerous studies have shown a role for RelA in PDAC inflammatory responses and therapy resistance, little is known as to how these inflammatory responses are modulated through Ref-1 redox signaling pathways during pancreatic pathogenesis. RelA and STAT3 are two major targets of Ref-1 and are important in PDAC pathogenesis. To decipher the mechanistic role of RelA in response to Ref-1 inhibition, we used PDAC cells (KC3590) from a genetically engineered *Kras*^{G12D}-driven mouse model that also is functionally deficient for RelA (Parent/Vector) or KC3590 cells with fully functional RelA added back (clone 13; C13). We demonstrated that RelA deficient cells are more resistant to Ref-1 redox inhibitors APX3330, APX2009, and APX2014, and their sensitivity is restored in the RelA proficient cells. Knockdown of STAT3 did not change cellular sensitivity to Ref-1 redox inhibitors in either cell type. Gene expression analysis demonstrated that Ref-1 inhibitors significantly decreased IL-8, FOSB, and c-Jun when functional RelA is present. We also demonstrated that PRDX1, a known Ref-1 redox modulator, contributes to Ref-1 inhibitor cellular response. Knockdown of PRDX1 when functional RelA is present resulted

in dramatically increased PDAC killing in response to Ref-1 inhibitors. The enhanced cell killing was not due to increased intracellular ROS production. Although Ref-1 inhibition decreased the NADP/NADPH ratio in the cells, the addition of PRDX1 knockdown did not further this redox imbalance. This data suggests that the mechanism of cell killing following Ref-1 inhibition is at least partially mediated through RelA and not STAT3. Further imbalancing of the redox signaling through disruption of the PRDX1-Ref-1 interaction may have therapeutic implications. Our data further support a pivotal role of RelA in mediating Ref-1 redox signaling in PDAC cells with the *Kras*^{G12D} genotype and provide novel therapeutic strategies to combat PDAC drug resistance.

Keywords: pancreatic ductal adenocarcinoma (PDAC), Ape1, transcriptional factors, relA, DNA repair, redox signaling, PRDX1, STAT3

INTRODUCTION

Pancreatic ductal adenocarcinoma (PDAC) is one of the deadliest cancers due to poor response to current treatment regimens and lack of markers for early diagnostics, resulting in a 5-year overall survival of around 10% (1). Kras mutation is the most dominant oncogenic transformation in PDAC mutational profile confirmed in ∼90% of cases (2). The oncogenic Kras mutation leads to alteration of signaling pathways that are associated with the progression and metastasis of PDAC and is the main contributor of therapy recalcitrance (3).

Inflammation and remodeling of the local tumor microenvironment (TME) are key cellular events that exacerbate progression of PDAC. Aberrant Kras signaling activates several inflammatory signaling pathways, e.g., NF-κB, AP-1, IL-6/STAT3 signaling, that are constitutively active in PDAC and highly expressed in PDAC and its TME (4). Kras^{G12D} induces IL-1α expression *via* AP-1 activation, leading to NF-κB activation in tumor cells (5). Elevated levels of cytokines and chemokines are also observed in PDAC and correlated with the enhanced NF-κB signaling (6). Inhibition of NF-κB signaling in cancer-associated fibroblasts (CAFs), a major constituent of the TME, abolished its tumor-promoting effects, suggesting that NF-κB is critically involved in PDAC and the TME (7). Increasing evidence demonstrates that activated NF-κB partners with other signaling molecules, such as STAT3 and HIF-1α, and induces chemoresistance to gemcitabine and platinum agents, first line therapeutic regimens for PDAC (8–10). Consequently, the main challenge from the perspective of cancer treatment is identifying key molecular players that mediate cellular responses and are effective on PDAC cells with the activated Kras genotype.

Apurinic/apyrimidinic endonuclease-1/redox factor-1 (APE1/Ref-1 or Ref-1) is a multifunctional protein active in DNA repair, redox-signaling (reduction/oxidation) control, and transcriptional regulatory activities (11). Ref-1 functions in DNA base excision repair (BER) by virtue of its endonuclease activity and responds to oxidative and alkylation DNA damage lesions. Ref-1 is also involved in redox signaling through a thiol exchange reaction (12, 13). The Ref-1 redox activity reduces critical cysteine residues on transcription factors (TFs), such as RelA (subunit of NF-κB), AP-1, HIF-1α, STAT3 leading to transcription factor activation. Activation TFs that are regulated by Ref-1 have been implicated in tumor growth and proliferation, metastasis, metabolism, and survival of tumor cells as well as signaling within the TME (14). Ref-1 redox activity can be regulated by direct interactions with other proteins such as Peroxiredoxin 1 (PRDX1) or thioredoxin 1 (TRX1) and constitute the PRDX1/Ref-1/TRX1 redox regulatory cycle in cells (15, 16). For example, the redox interactions between NF-κB, PRDX1 and Ref-1 are responsible for overproduction of inflammatory cytokine, IL-8 (15). Several *in vitro* studies demonstrated significant inhibition of DNA binding activity of RelA and its altered subcellular localization when cells were challenged with small molecules (APX3330, APX2009, and APX2014) that target the redox signaling function of Ref-1 (17–19). The latter two are more potent second-generation Ref-1 redox inhibitors (20). Blocking the redox activity of Ref-1 using APX3330 results in inhibition of TNF-α-induced activation of IL-8 production in human cancer cell lines (17). However, the relationship of PRDX1-Ref-1 and subsequent RelA activation has not been rigorously explored beyond initial studies.

Previous work reported that RelA possesses dual functional roles during pancreatic oncogenesis, by promoting tumor suppression through regulation of inflammatory cytokines or facilitating proliferation of transformed tumor cells and tumor progression through bypassing senescence (21). However, the mechanistic details of how redox signaling regulates RelA-driven cellular proinflammatory events that drive therapy resistance or exploiting these events in cancer treatment remain to be investigated. In the present study, we focused on the cellular inflammatory responses of Ref-1 redox signaling inhibition in a murine PDAC *in vitro* model. Specifically, we wanted to investigate the relationship of RelA-dependent cellular responses to Ref-1 redox signaling inhibition and further identify other possible associated molecular targets or signaling pathways that may enhance cellular sensitivity to Ref-1 redox signaling inhibition. The model used is a mouse PDAC cell line generated from a Kras^{G12D}-driven mouse model that also is functionally deficient for RelA (KC3590: Parent/Vector) (22). A fully functional RelA was added back to these KC3590 cells

creating two clones (C13/C15) (23). We used these KC3590 cell lines to examine the roles of known Ref-1 target, RelA and known interacting protein of Ref-1, peroxidredoxin 1 PRDX1 and their effects on cellular sensitivity, ROS, and redox state *via* NADPH/NADP ratio to Ref-1 inhibitors. Our data demonstrate an essential involvement of Ref-1 redox signaling in RelA-driven cellular responses in PDAC cells with the $Kras^{G12D}$ genotype such that targeting Ref-1 may be a promising strategy to improve acquired resistance in PDAC chemotherapy.

MATERIAL AND METHOD

Cell Culture and Cell Lines

We used KC3590, a mouse PDAC cell line that was established from $Ptf1a^{Cre/+}$;$LSL\text{-}Kras^{G12D/+}$;$p65^{loxP/loxP}$ mice, with RelA truncation at exon (7-10). This truncation only codes for part of the Rel homology domain and the nuclear localization site and is inactive (22). Thus, KC3590 Parent and Vector lines express non-functional RelA (hereafter referred to as Parent or Vector). KC3590 cells were transfected with pcDNA3-Flag-RelA (prepared by Dr. Smale) (23) and are referred to as Clone #13 (C13) and Clone #15 (C15). PDAC mouse cell lines referred to as KC6075, KC8442, KC2259, KC53631, KC9091, KC5671, KC5559, KC5748 were isolated from tumors in mice that carry a Pdx1-Cre recombinase oncogenic $Kras^{G12D}$ mutation. All cell lines were maintained at 37°C in 5% CO_2 and grown in Dulbecco's Modified Eagle's Medium (DMEM, Invitrogen, Carlsbad, CA, USA) with 10% Fetal Bovine Serum (FBS) (Atlanta Biologicals, Minneapolis, MN, USA). The cell lines were authenticated by STTR analysis and tested negative for mycoplasma contamination.

Ref-1 Inhibitors

Small molecule inhibitors were prepared and used as previously described (24). Ref-1 redox signaling was inhibited using APX3330, APX2009, and APX2014 (Apexian Pharmaceuticals; Indianapolis, IN). RN7-58 (Apexian Pharmaceuticals) was used as a negative control and is structurally similar but does not inhibit Ref-1 redox signaling activity (25). APE1 repair inhibitor III (ARi3) (EMD Chemicals, CA, USA) was used as an inhibitor of the endonuclease activity of Ref-1 (26, 27).

Cell Viability and APE1 Redox Inhibitors Cytotoxicity

Cell proliferation and viability were measured with alamarBlue Cell Viability assay (Invitrogen, Eugene, USA) as previously described (25). Briefly, cancer cell lines were seeded at 2000 cells/well in 96-well tissue culture plates and their growth rates monitored. Cell viability was measured 48 hours after treatment and response was normalized to a non-treated (media only or vehicle) control. At least three replicates were performed.

siRNA Transfections

Targeted mRNA knock-down was optimized for each cell line and verified by Western blot (>80% knockdown) as previously reported (28). Cells were transfected by lipofectamine RNAiMax (Invitrogen, CA, USA) with PRDX1 (SR405074, OriGene Technologies, MD, USA), RelA (SR417160, OriGene Technologies, MD, USA), STAT3 (SR427487, OriGene Technologies, MD, USA), and universal scrambled control (SCR) (SR30004, OriGene Technologies, MD, USA) siRNAs.

After 24 hours post-transfection, cells were re-plated into 96-well plates for assessing Ref-1 inhibitors cytotoxicity.

RNA Isolation, Reverse Transcription, and Real-Time Quantitative PCR (qRT-PCR)

Cells were collected and processed for RNA extraction according to the manufacturer's protocol (Qiagen, Hilden, Germany, USA). The RNA concentrations were determined using a NanoDrop (Thermo Fisher, MA, USA). Subsequently, 1µg of RNA/25-µl reaction mix was reverse-transcribed to cDNA using random hexamers and MultiScribe reverse transcriptase (Applied Biosystems, Foster City, CA). qRT-PCR was performed in 96-well plates, with a final volume of 20 µL/well using the SYBR Green PCR kit (Applied Biosystems, Foster City, CA, USA) on the CFX96 real-time PCR detection system (BioRad, Hercules, CA, USA). Primers for indicated genes are commercially available (OriGene, Technologies, MD, USA) and primers sequence are shown in supplemental data (**Supplemental Data: Table S1**). qRT-PCR cycling conditions were 1 min at 95°C, 10 min at 95°C, 15 s at 95°C and 1 min at 60 °C for 40 cycles. Relative changes in mRNA expression levels were assessed by the $2^{-\Delta\Delta CT}$ method, and changes in mRNA expression of the target gene were normalized to that of RPL6 gene, as previously published (25, 29).

Total Protein Extraction and Western Blotting Analysis

Whole extracts from control and treated cells were obtained in 1% SDS extraction buffer supplemented with protease inhibitors (Santa Cruz Biotechnology, TX, USA). Briefly, cell extract was heated at 95°C for 5min, then sonicated (4 pulses, 4 cycle) to shear the DNA in the samples. Total protein concentration was determined by using the DC Protein Assay Kit (Bio-Rad Laboratories, CA, USA), and bovine serum albumin (BSA) (Bio-Techne, MN, USA) as the standard. Denatured samples (25–40 µg) were subjected to SDS-PAGE and proteins were transferred onto nitrocellulose membranes by electrophoretic transfer. Non-specific binding sites were blocked at room temperature for 1h with 5% (w/v) Blotting-Grade Blocker (Bio-Rad Laboratories, CA, USA) in Tris-buffer saline (Boston BioProducts, MA, USA) containing 0.05% (v/v) Tween-20 (Thermo Fisher, MA, USA) (TBS-T). Membranes were incubated overnight with the primary antibodies, anti-PRDX1(66820-1, Protientech), anti-STAT3 (CS-9139, Cell signaling), anti-Ref-1 (13B8E5C2, Novus Biologicals), anti-RelA (sc-8008, Santa Cruz) and anti-Vinculin (CP74-100, Millipore) diluted in TBS-T (1:1000), and then, with the peroxidase-conjugated secondary antibody (1706516, Bio-Rad Laboratories, CA, USA) for 1 h. Signal was then captured by using Bio-Rad ChemiDoc imager, and band intensities were analyzed by densitometry on Image Lab software (Bio-Rad

Laboratories, CA, USA). Vinculin expression was used as loading controls and used for data normalization.

Intracellular ROS Assays

KC3590 cells were transfected with target siRNA (PRDX1) as described above. Cells were collected at 24 hours post transfection and seeded at 10,000-12,000 cells/well in 96-well plates. At 48 hours post transfection (80-90% confluency), cells were treated with Ref-1 redox inhibitors, APX3330, APX2009, APX2014, as well as vehicle (DMSO) and media controls; all constituted in Opti-MEM (ThermoFisher, MA, USA) and treated for 2 hours at 37°C, 5% CO_2. CellROX® Green Reagent (Molecular Probes, Oregon, USA) was added to the drug media to a final concentration of 5 μM and incubated with reagent for 30 minutes. Next, media was removed, and one PBS wash was performed. ROS fluorescence was detected at 485/528nm excitation/emission (BioTek Synergy H4).

NADP/NADPH Assay

NADPH to NADP ratio in KC3590 cells was measured using NADP/NADPH Assay Kit from Abcam (Abcam, Inc, Cambridge, UK). Assay was performed as per manufacturer's protocol. Briefly, after treatment with Vehicle control or APX2009, 4×10^6 cells were lysed using 400 μL extraction buffer for cytoplasmic NADPH/NADP. Samples were sheared and passed through DNA spin columns. 150 μL of extracted samples were heated to 60 °C for 30 min to decompose NADP leaving NADPH and the remaining sample was used for total NADP (NADPt). 50 μL of standard or sample was used per well. 100 μL of Reaction Mix was added and incubated for 5 min at room temperature followed by addition of 10 μL of NADPH Developer per well. The readings were taken at OD_{450nm}. NADPH/$NADP^+$ was calculated as NADPH/NADP + ratio = NADPH/(NADPt—NADPH). The measured NADP and NADPH levels were calculated by comparison with a standard curve.

Statistics

All the experiments were performed at least three independent times. The obtained data were expressed as 'Mean + Standard Error'. Significance was calculated as per either One-way ANOVA or two-way ANOVA multiple comparisons wherever applicable using Graph Pad Prism Version 9. The difference was considered statistically significant when p-value < 0.05. For qRT-PCR, analysis of covariance models (ANCOVA) was performed to test the Ct difference of each target gene value between treatment with APX3330, APX2009 and vehicle (DMSO) after standardization by reference gene (RPL6) (29). A p-value of at least < 0.05 was considered statistically significant.

RESULTS

Re-Expression of RelA Renders Tumor Cells Sensitive to Ref-1 Inhibitors

Initially, we investigated how various murine PDAC tumor cells driven by $Kras^{G12D}$ mutation would respond to Ref-1 inhibition. A panel of cell lines established from the *Kras*^{G12D}; Pdx1-Cre (KC) mice were screened for sensitivity to APX3330, APX2009, and APX2014 and ranked based on inhibitor sensitivity (**Supplemental Data: Table S2**). We demonstrated that there are significant differences ($p<0.001$) in cell viability between the most resistant cell line (KC6075) and the most sensitive cell line (KC5748) when cells were challenged with indicated concentrations of Ref-1 inhibitors, APX3330 (25, 50, 75μM), APX2009 (3.1, 6.25, 12.5 μM) and APX2014 (6.25, 12.5, 25μM) (**Supplemental Data: Figure S1**).

To investigate Ref-1's regulation of RelA in PDAC cells, matched RelA deficient and proficient KC lines were utilized. Blockade of NF-κB/RelA signaling is important due to its role in driving differential sensitivity to chemotherapy agents, such as gemcitabine during PDAC oncogenesis. To examine the mechanistic role of RelA in response to Ref-1 inhibition, KC3590 cell lines were treated with APX3330, APX2009, APX2014. We found that KC3590 RelA-deficient cells (Parent, Vector) were 1.7-2.5–fold more resistant to Ref-1 inhibitors than RelA-proficient cells (C13, C15) (**Figures 1A–C**). EC_{50}s of Ref-1 inhibitors in KC3590 cells are shown in **Table 1**. In contrast, we did not observe any significant cellular sensitivity when KC3590 cells were treated with Ref-1 inactive redox inhibitor analog, RN7-58 (**Figure 1D**) or with ARi3, an inhibitor of Ref-1 endonuclease activity (**Figure 1E**). Overall, RelA deficient cells demonstrated two-fold more resistance to Ref-1 inhibitors, and their sensitivities were restored in cells expressing functional RelA. This suggests that at least some of the cell killing following Ref-1 inhibition is mediated through RelA and on-target effects of the APX compounds as the effects of the inhibitors are more dramatic in cells that are RelA proficient.

Ref-1 Inhibitors Suppress Inflammatory Responses *via* RelA Mediated Pathways

As an indicator of RelA activity, we assessed the levels of three genes (IL-8, FOSB, and c-Jun) in the RelA deficient and proficient KC lines after treatment with Ref-1 inhibitors (30). IL-8 is a well-established RelA target gene while FOSB and c-Jun are components of the AP-1 family of proteins, a transcriptional target of Ref-1. The AP-1 and RelA TFs have also been shown to crosstalk and influence expression of various AP-1 family members (30). Single cell RNA sequencing data from human PDAC cells revealed that FOSB and c-Jun were strongly downregulated with Ref-1 knockdown (**Supplementary Figure S3**). To investigate the interplay with Ref-1, AP-1, and RelA and these genes in response to Ref-1 inhibitors, we assessed Il-8, FOSB, and c-Jun mRNA levels both in RelA-proficient and deficient cells following Ref-1 inhibitor treatment.

As we expected, there is a significant decrease in endogenous IL-8 levels in the RelA-deficient line compared to the cells with RelA added back (Vector-DMSO vs C13-DMSO, $p<0.01$). IL-8 mRNA levels were significantly decreased in response to APX3330 and APX2009 in both Vector and C13 cells with respect to DMSO controls ($p<0.05$, **Figure 2A**). However, the effects were even more dramatic in Vector as IL-8 levels were minimally detectable following Ref-1 inhibition in RelA-deficient

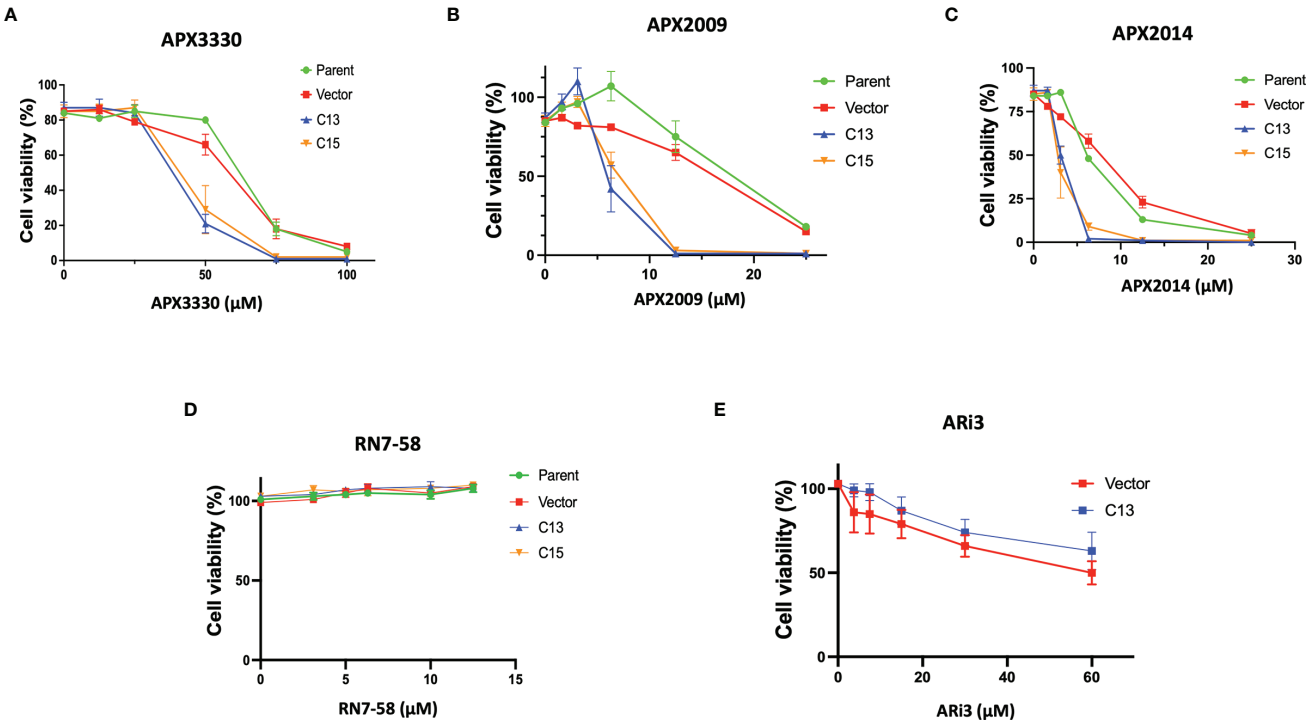

FIGURE 1 | Re-expression of RelA renders tumor cells sensitive to Ref-1 inhibitors. KC3590 cells that underwent functional deletion of RelA (Parent and Vector) and KC3590 clone lines that express functional RelA (C13, C15) were challenged with different concentrations of APX3330 **(A)**, APX2009 **(B)** and APX2014 **(C)**, RN7-58 **(D)**, ARi3 **(E)** for 48 hours. Cytotoxicity was measured by Alamar blue (4 hr incubation) at 590 nm. Error bars represent standard error (N = 3). Statistical differences between EC_{50}s of Ref-1 inhibitors in KC3590 cells are provided in **Table 1**.

lines (p<0.001 vs Vector DMSO). Interestingly, IL-8 expression is not solely dependent on RelA as we observed some expression in the RelA-deficient cells (Vector DMSO), and yet blockade of Ref-1 signaling in these cells was able to almost completely abrogate the expression of IL-8 (Vector APX3330 and Vector APX2009), suggesting that the other TFs regulating its expression are also under Ref-1 redox control.

Surprisingly, the basal levels of both FOSB and c-Jun were much higher (~4-fold) in RelA-deficient lines (Vector DMSO vs C13 DMSO, p<0.05) (**Figures 2B, C**). Treatment with APX3330 and APX2009 resulted in strong upregulation of FOSB in RelA-deficient cells (Vector DMSO vs Vector APX, p<0.001), however in cells with functional RelA, Ref-1 inhibition largely abrogated this induction (Vector APX3330 vs C13 APX3330, p<0.001; Vector APX2009 vs C13 APX2009, p<0.001). Similar results were observed for c-Jun except that treatment with APX3330 could block the induction of c-Jun in the Vector control cells (Vector DMSO vs Vector APX3330, p<0.001).This data suggests that RelA signaling may be promoting transcription of a repressor or there is dysregulation of the AP-1 –RelA crosstalk resulting in loss of a negative feedback loop.

STAT3 Is Not a Primary Target Determining Cellular Sensitivity to Ref-1 Inhibitors in Murine PDAC $Kras^{G12D}$ Cells

PDAC pathways are significantly altered when Ref-1 expression is decreased including the STAT3 signaling pathway (14). We previously demonstrated the synergistic effects of dual targeting Ref-1/STAT3 axis in PDAC *in vivo* xenograft model and in KPC tumor cells (13). Therefore, we expanded our investigations to examine if other TFs that are regulated by Ref-1, such as STAT3 also contribute to the sensitivity of cells that are driven by Kras and yet do not express functional RelA. In these studies, STAT3 levels were reduced using siRNA in the KC3590 cell line series to evaluate the cellular sensitivity to Ref-1 inhibitors.

TABLE 1 | EC_{50} (μM) summary table of APX3330, APX2009, APX2014 cytotoxicity assays in KC3590 lines.

EC_{50} μM	Parent	Vector	C13	C15
APX3330	60.8 (± 1.5)	52.9 (± 5.3)	*36.2 (± 2.3)	*39.3 (± 5.7)
APX2009	16.8 (± 1.9)	13.7 (± 1.1)	***##6.6 (± 0.1)	**##6.6 (± 0.2)
APX2014	6.0 (±0.3)	6.0 (±0.9)	***###3.0 (± 0.1)	***###2.8 (± 0.4)

$^{*}p < 0.05$, $^{**}p < 0.001$, $^{***}p < 0.0001$ vs Parent line; $^{\#\#}p < 0.001$, $^{\#\#\#}p < 0.0001$ vs Vector line, One-way ANOVA (N = 3).

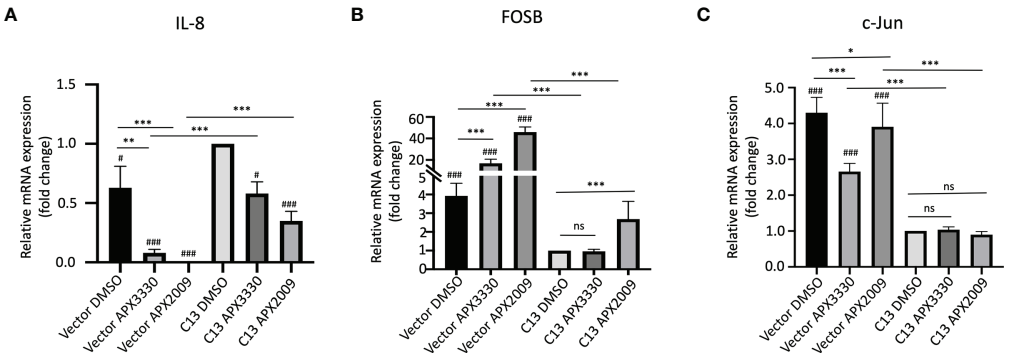

FIGURE 2 | Ref-1 inhibitors suppress inflammatory responses *via* RelA mediated pathways. KC3590 cells that are RelA deficient (Vector) and clone with functional RelA add back (C13) were challenged with Ref-1 inhibitors, APX3330 (60 μM Vector; 30 μM C13), APX2009 (16 μM Vector; 6 μM C13) based on their EC50 for 24 hours. The effects of Ref-1 inhibitors on mRNA expression levels of IL-8, FOSB, c-Jun was assessed with qPCR (Figure **(A–C)**, respectively). Six independent experiments were performed (n = 6). Hashtag "#" is comparing to C13 DMSO, $^{\#}p < 0.05$, $^{\#\#\#}p < 0.0001$; $^{*}p < 0.05$, $^{**}p < 0.01$, $^{***}p < 0.0001$, ANCOVA, N=6. "ns", not significant.

Upon STAT3 knockdown in both Vector and C13 cells (**Figure 3A**), the cellular response was identical following treatment with APX3330 and APX2009, with slight enhancement of APX2014 in the RelA-proficient cells, despite STAT3 knockdown of greater than 90% (**Figures 3B–D**). Minimal cell killing was observed in any of the conditions when cells were challenged with inactive analogue RN7-58 (**Figure 3E**). These results suggest that STAT3 minimally

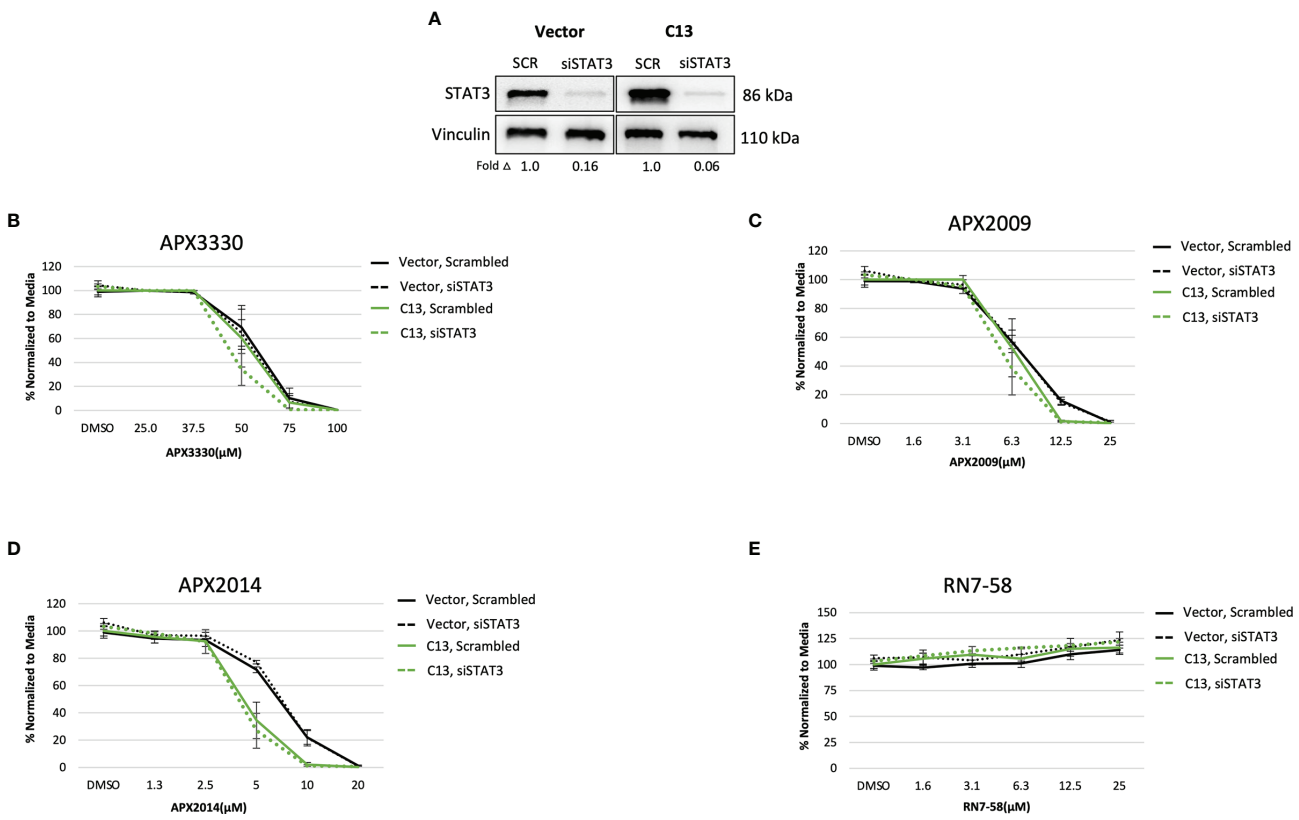

FIGURE 3 | STAT3 is not a primary target altering cellular sensitivity to Ref-1 inhibitors in murine PDAC $Kras^{G12D}$ cells. **(A)** STAT3 was knocked down in KC3590 cells that are RelA deficient (Vector) and clone with functional RelA add back (C13) and knockdown efficiency was assessed by Western bot. Vinculin was used as loading control. The cells were challenged for 48 hours with **(B)** APX3330, **(C)** APX2009, **(D)** APX2014, and **(E)** RN7-58. Cytotoxicity was measured by alamarBlue. At least three independent experiments were performed (N = 3).

contributes to the cellular sensitivity to Ref-1 redox inhibition in this PDAC cell model; i.e. functional RelA is driving the response to Ref-1 inhibitors.

Targeting the PRDX1/Ref-1 Axis Enhanced Cellular Sensitivity to Ref-1 Inhibition

Previous studies demonstrated signaling interactions between PRDX1 and Ref-1 that led to changes in IL-8 levels, presumably through RelA (15). Thus, we wanted to determine if perturbation of PRDX1, an oxidizer of Ref-1, could alter cellular responses to Ref-1 redox inhibitors observed in the KC3590 cell. Again using siRNA, PRDX1 levels were reduced to greater than 80% in both Vector and C13 lines (**Figure 4A**). Upon PRDX1 knockdown, dramatic enhancement of cellular sensitivity to APX3330, APX2009, and APX2014, in both Vector and C13 cells was observed in comparison to scrambled controls (**Figures 4B–D**). Surprisingly, the enhancement in cellular sensitivity was nearly 2-fold more in RelA-proficient cells compared to the RelA-deficient cells, demonstrating RelA-dependent effects on cellular responses to Ref-1 redox signaling inhibition and imbalance of redox homeostasis through knockdown of PRDX1. We did not observe any differential cell killing when Vector and C13 cell lines were challenged with an inactive analog RN7-58, confirming inhibitor specificity (**Figure 4E**). These results clearly indicate that PRDX1 is a key mediator impacting cellular sensitivity to Ref-1 redox inhibition, and these cellular responses are much more effective in the presence of functional RelA.

Targeting PRDX1/Ref-1 Redox Cycling With Ref-1 Inhibition and Its Impact on Cellular Redox Homeostasis

Two potential mechanisms that could explain the dramatic results on cell growth in **Figure 4** as well as relate to Ref-1/PRDX1/RelA signaling are generation of reactive oxygen species (ROS) and changes in redox status of the cell. To determine whether intracellular ROS production may be a part of the mechanism of RelA-driven differential cellular responses to Ref-1 inhibitors, we measured ROS levels, specifically superoxide and/or hydroxyl radicals, after PRDX1 knockdown and Ref-1 inhibitor treatment in KC3590 cells. Consistent with our previous findings, Ref-1 inhibition *via* APX3330, APX2009, or APX2014 generated significant amounts of ROS in the Vector lines, regardless of the levels of PRDX1 compared to vehicle

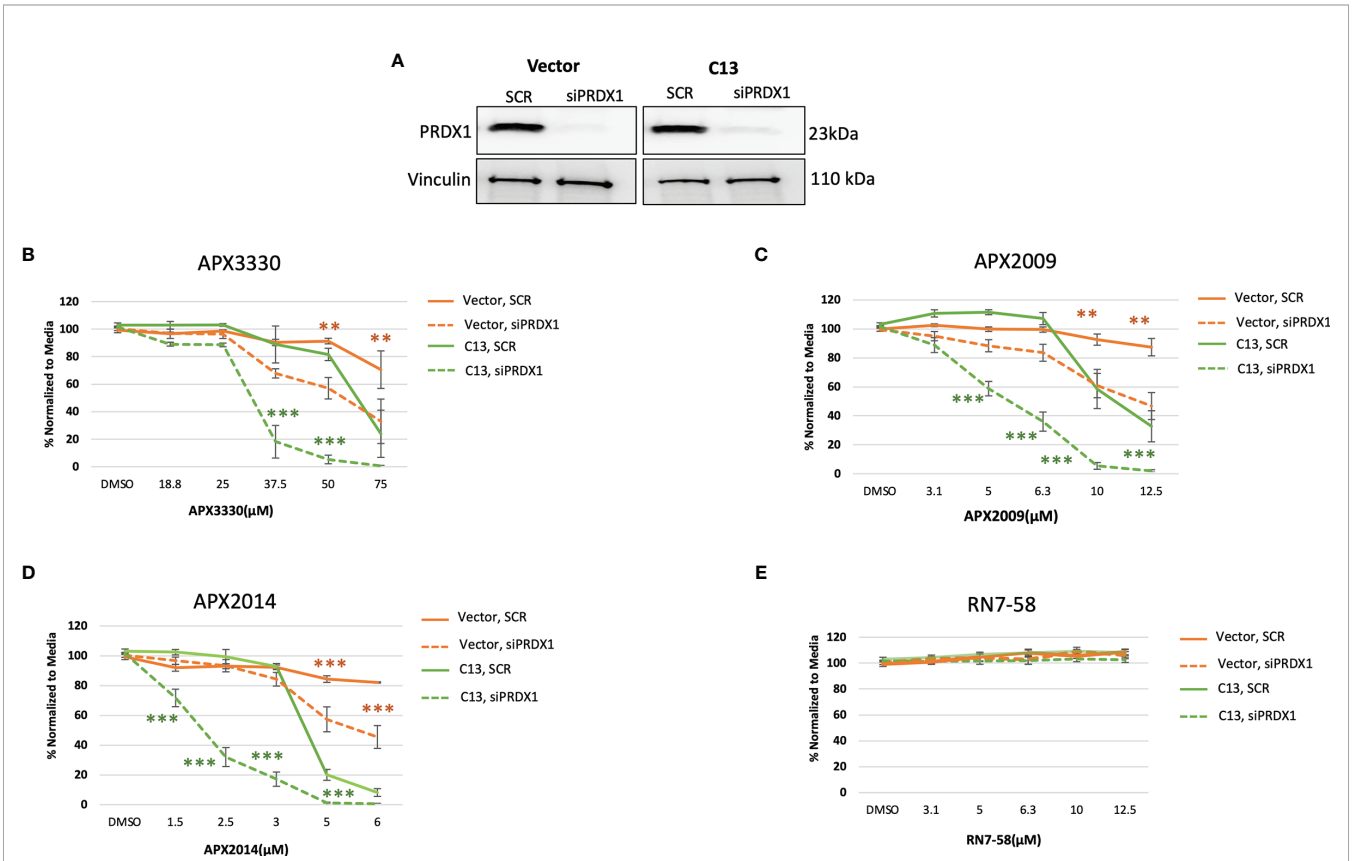

FIGURE 4 | PRDX1 is an effective target enhancing cellular sensitivity to Ref-1 inhibitors in mouse PDAC cells. **(A)** PRDX1 knockdown efficiency in KC3590 Vector and C13 cell lines were greater than 80% comparing to scrambled control (SCR). Vinculin was used as loading control. **(B–D)** The cytotoxicity of Ref-1 inhibitors, APX3330, APX2009, APX2014 upon the condition of PRDX1 knockdown both in Vector and C13 were assessed. **(E)** cytotoxicity of RN7-58 was also evaluated along with Ref-1 inhibitors. Two-way ANOVA, **p < 0.01, ***p < 0.001. At least three independent experiments were performed (N = 3).

controls (**Figures 5A, B**). Similar effects were observed with APX3330 and APX2009 in RelA-proficient cells, except following treatment with APX2014. There is a trend that there is increased ROS with APX2014 in the RelA-proficient cells, but it did not reach significance (**Figure 5C**). Importantly, the reduced expression of PRDX1 did not result in changes in ROS levels in untreated or treated Vector or C13 cells, which could be due to the species of ROS detected with the CellRox green assay. This data does show that superoxide and/or hydroxyl radical generation are not driving the large increase in cell killing seen with PRDX1 knockdown and Ref-1 inhibition in RelA-proficient cells.

To investigate the redox imbalance induced by Ref-1 inhibitors and PRDX1 knockdown and the link to RelA function in the cells, we assessed NADPH/NADP ratios following APX2009 treatment in cells with reduced expression of PRDX1. KC3590 cells treated with Ref-1 inhibitor, APX2009 display markedly reduced levels of NADPH as observed from the NADPH/NADP ratio in both Vector and C13 (**Figure 5D**). This indicates a more oxidized environment as expected after blocking Ref-1 redox function (25). Although Ref-1 inhibition resulted in a shift in the redox status of the cell, neither PRDX1 nor RelA expression altered this result. Again selective knockdown of PRDX1 is insufficient to change the generic redox balance in this matched cell line *in vitro* model pointing toward another mechanism of enhancement of cell killing in the KC3590 RelA-proficient cells.

DISCUSSION

Our studies described here investigate the RelA-driven cellular responses to Ref-1 redox inhibition through Ref-1/PRDX1 redox signaling in mouse PDAC cells. RelA has been implicated in driving resistance to treatments such as radiation and Gemcitabine. In one study, transiently silenced RelA increased Gemcitabine-induced cell killing (31), while in another study selective knockdown of RelA in combination with pyruvate dehydrogenase kinase (PDK1/2) enhanced radiation sensitivity of pancreatic cancer cells (32). RelA activity is regulated in many ways including redox regulation by Ref-1 (19, 33). Ref-1's activation of transcription factors such as RelA can be influenced by PRDX1, a peroxidase in the Ref-1/TRX1 redox cycling pathway (15). Results presented here demonstrate our novel observation that pancreatic cancer cells become more sensitive to Ref-1 redox inhibition when PRDX1 expression is decreased and when RelA is present in the cells indicating a novel interplay between PRDX1, Ref-1, and RelA.

In these studies, we used a murine PDAC cell line KC3590 with $Kras^{G12D}$ and a truncated RelA gene with missing exons 7-10 (KC) (**Supplementary Figure 2**). Exons 7-10 encode Rel homology domain (RHD), which is essential for dimerization of RelA, nuclear translocation, and DNA binding (22) (21). KC3590 cells were transfected with pcDNA3-Flag-RelA (clones C13 and C15) to have matched lines that express functional RelA and non-functional RelA. Due to Ref-1's redox regulation of

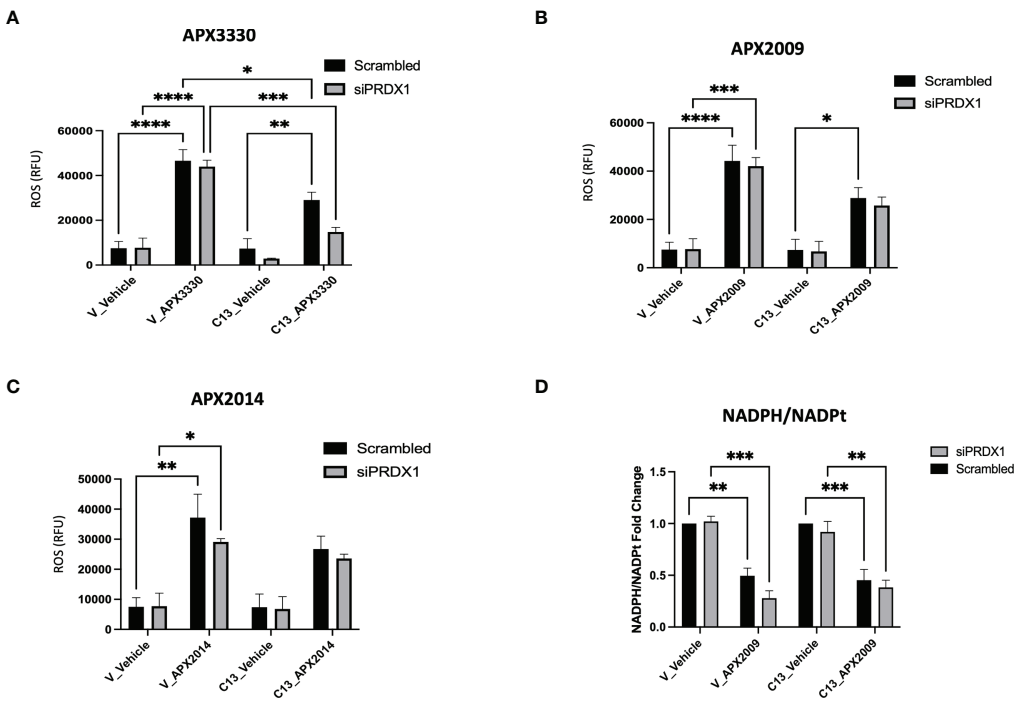

FIGURE 5 | Effects of RelA on cellular redox imbalances caused by Ref-1 inhibitors in PDAC cells. **(A–C)** intracellular ROS levels were measured upon PRDX1 knockdown cells at 48 hours post-transfection and following 2 hours of Ref-1 inhibitor treatment with APX3330 (75 μM), APX2009 (20 μM), APX2014 (20 μM). These experiments were repeated four times (N=4), and then compared by Two-way ANOVA of *p < 0.05, **p < 0.01, ***P < 0.001, ****p < 0.0001. **(D)** NADPH/NADPt ratio in PRDX1 knockdown cells (1nM/48h) was assessed following APX2009 treatment (12.5μM/5h). two-way ANOVA, **p < 0.01, ***p < 0.001, N=3.

NF-κB, these lines were used as an important tool to interrogate the cells' response to established Ref-1 inhibitor APX3330 as well as new analogs. APX3330, as well as the second-generation analogues APX2009 and APX2014 have been shown to be specific for Ref-1, directly targeting and interacting with the protein and not the downstream TFs (13, 34–39). This specificity has also been validated using another analogue of the APX compounds, RN7-58 which is similar in structure and came from the same structure-activity relationship (SAR) studies but is inactive in blocking Ref-1 redox activity (40, 41). As shown in **Figures 1A–C**, we demonstrated that RelA functionally deficient cells were more resistant to Ref-1 inhibitors APX3330, APX2009, and APX2014 and ranked in the top three Ref-1 inhibitor-resistant phenotype along with KC6075 (**Supplementary Table 2**). However, KC3590 cells with RelA added back were found to be significantly more sensitive to all three Ref-1 inhibitors. Accordingly, KC3590 C13 and C15 cells were in the top three Ref-1-inhibitor sensitive lines and ranked along with KC5748. These data support that our Ref-1 redox inhibitors are indeed hitting predicted downstream targets of Ref-1 i.e., NF-κB/RelA and that at least part of the mechanism of cell killing is mediated through RelA. Furthermore, we confirmed that the RelA-dependent differential cellular responses were lost when treated with a Ref-1 endonuclease specific inhibitor ARi3 (APE1/Ref-1 DNA Repair Inhibitor III). Additionally, an inactive analog of the APX redox inhibitor compounds, RN7-58 demonstrated no differential response or activity (**Figure 1D**). These findings once again underscore that the redox function of Ref-1 and subsequent regulation of RelA, but not the DNA repair function, plays a crucial role in driving cellular responses to Ref-1 redox inhibition in this particular cell model.

We also looked at another transcription factor that is under Ref-1 redox control, STAT3, to determine whether its expression correlates with the cytotoxicity response to Ref-1 redox inhibitors. Interestingly, we did not observe any differential cellular responses in cells with STAT3 knocked down when challenged with the Ref-1 redox inhibitors (**Figure 3**). In our previous studies, dual targeting of STAT3 with STAT3 inhibitors, Ruxolitinib or Napabucasin, along with Ref-1 redox inhibitors significantly increased cell killing in multiple PDAC cell lines (28). Additionally, we demonstrated that KPC cells (*LSL-Kras*$^{G12D/+}$*;LSL-Trp53*$^{R172H/+}$*;Pdx-1-Cre*) that lack expression of IL-6 and thereby reduced STAT3 signaling are very sensitive to the effects of Ref-1 redox inhibition. These cells have a mutated p53 while the murine PDAC cells used here do not. It is possible that p53 is important in the response to Ref-1 inhibition as p53 is also a redox target of Ref-1. These data also suggest a much more complex interplay between the genetic makeup of the tumors and the response to targeted agents – a focus of future studies. These differences support the well-established heterogeneity that exists in pancreatic cancer. Regardless, the results presented here support the rationale that RelA, but not STAT3, is a primary target in determining mouse PDAC cellular responses to Ref-1 redox inhibition in this Kras^{G12D} model.

Several *in vitro* studies reported that targeting redox activity of Ref-1 by APX3330 blocks activation of inflammatory modulators, such as RelA, IL-8 in human cancer lines (15, 19). We hypothesized that RelA deficient and proficient cells would demonstrate differential inflammatory responses to Ref-1 inhibitors. Indeed, IL-8 gene expression was significantly reduced in the RelA-deficient cells compared to proficient and in response to Ref-1 inhibitor treatments in both cell lines (**Figure 2A**). However, additional TFs must regulate IL-8 in these cells because IL-8 was still detectable in the deficient cells. IL-8 has been reported to be regulated by both NF-κB and AP-1 which could explain the lack of expression of IL-8 in the RelA-deficient cells following treatment with APX3330 and APX2009 (42). This data supports RelA driving IL-8 expression and that Ref-1 inhibition can block the activity of RelA and the other potential TFs that regulate IL-8 leading to very dramatic decreases in IL-8.

Additionally, we found 4-fold increased expression of FOSB and c-Jun mRNA levels in the Vector, RelA deficient cells compared to cells expressing RelA, C13 (**Figures 2B, C**), suggesting that RelA drives the expression of a repressor of FOSB and c-Jun or perturbation of some unknown feedback loop. The levels of FOSB were dramatically increased (20-40-fold) in response to Ref-1 redox inhibitors compared to Vector untreated control (**Figure 2B**). Studies have demonstrated that high expression AP-1 family proteins are involved in resistance to therapy to anti-cancer agents (43, 44). Higher expression of FOSB and c-Jun levels correlated to resistance to Ref-1 redox inhibitors as well. We also showed that in the presence of functional RelA, Ref-1 inhibitors at least in part restored FOSB and c-Jun mRNA expression to the control levels observed in C13 untreated cells (**Figures 2B, C**). These findings revealed that the added back functional RelA suppressed FOSB as well as c-Jun mRNA levels and may play a role in the sensitization of cells to Ref-1 redox inhibitors. As with the IL-8 data, AP-1 family members may also be playing a role in this response to Ref-1 inhibitors. AP-1 and NF-κB TFs can crosstalk and influence expression of various AP-1 family members (30).

Additionally, we learned that PRDX1 is playing an important role in the cellular response to Ref-1 inhibitors. Upon knocking down PRDX1, KC3590 cells were much more sensitive to Ref-1 redox inhibitors. Interestingly, the effects were significantly stronger when functional RelA was present in the cells (**Figure 4**). To dissect the role of RelA in Ref-1/PRDX-1 redox signaling, we examined ROS levels in response to Ref-1 inhibition. Indeed, we observed higher levels of ROS with Ref-1 inhibitor treatments, as we previously reported in human PDAC cells (28). Although PRDX1 levels did not influence ROS levels in either RelA-deficient or -proficient lines, RelA-deficient lines tended to have higher amounts of ROS in response to Ref-1 inhibitors when comparing to RelA-proficient lines. This difference was more prominent with APX3330, a quinone-based structure, compared to APX2009 and APX2014 which are naphthoquinone (**Figures 5A–C**). One caveat to this study is that the ROS assay that was utilized will not detect all forms of ROS so there is the possibility that PRDX1/Ref-1/RelA axis is altering a different ROS species that was not detected in the CellRox green assay. Moreover, we found a significant reduction in NADPH/

NADP ratios with APX2009 in both RelA-proficient and -deficient cell lines indicative of a shift in redox balance toward a more oxidized state. Surprisingly, reducing expression of PRDX1 was insufficient to alter the generic redox balance (**Figure 5D**). Future work will delineate more specific details of redox mechanism of Ref-1/PRDX1/2 axis in the cellular response to Ref-1 inhibition. These studies will further delineate the relationship of cellular redox cycling pathways and their role in regulating Ref-1 redox activity as well as potential translational significance. APX3330 has been in over 300 patients in clinical trials spanning diseases from hepatitis to oncology and currently enrolled in a phase II trial in diabetic retinopathy and diabetic macular edema. In all of the trials to date, it has demonstrated a strong safety profile.

Although many studies have shown a role for NF-kB/RelA in PDAC inflammatory responses and therapy resistance, little is known as to how these inflammatory responses are modulated through redox signaling pathways in PDAC and its impact on sensitivity to PDAC treatment regimens. While the role of Ref-1 and NF-κB and Ref-1's redox signaling inhibition has been supported in other inflammatory model systems, as observed in the conversion of preleukemia to leukemia (45), inflammatory bowel disease (46), and retinal indications (47), the uniqueness of these studies is the use of a genetically modified murine KC cell model with functional mutation of NF-kB/RelA. This system was used to directly investigate RelA-mediated differential sensitivity to Ref-1 redox inhibitors and the regulation of inflammatory cytokines in response to Ref-1 redox signaling inhibition. We also uncovered dramatic enhancement in cell killing in response to Ref-1 redox inhibitors when PRDX1/Ref-1 redox cycling was blocked, especially in presence of RelA. This study has provided an insight into interactions between PRDX1/Ref-1 redox signaling and its inhibition by specific APX drugs which will further advance our push for new therapeutic strategies and improve anticancer drug efficacy in PDAC.

DATA AVAILABILITY STATEMENT

The raw data supporting the conclusions of this article will be made available by the authors, without undue reservation.

AUTHOR CONTRIBUTIONS

MM performed experiments and led writing of the manuscript. RW performed experiments and assays, as well as contributed figures and to the writing and editing. LA performed some cellular cytotoxicity studies. SG performed assays and writing. ZH provided us with numerous cell lines, expertise, and experiments. CS performed analysis as well as cells and editing. GS provided us with cells and expertise. CZ provided bioinformatic analysis. MF provided expertise, experimental design, and writing/editing. MK provided expertise, experimental design, analysis and writing/editing of manuscript. All authors contributed to the article and approved the submitted version.

FUNDING

MK and MF were supported by grants from the National Institute of Health and National Cancer Institute R01CA167291 and R01CA254110. MK was also supported by NIH/NCI grants R01CA205166, R01CA231267, R01EY031939 and R01HL140961. MF was also supported by NIH/NCI grant U01HL143403, R01CA211098 and R01NF180045. MF and MK were additionally supported by the Riley Children's Foundation and the IU Simon Comprehensive Cancer Center, P30CA082709.

ACKNOWLEDGMENTS

We would like to thank Dr. Hassan, Dr. Schnessweis and Dr. Schneider for providing mouse PDAC KC lines and some initial studies in the various KC cell lines. Furthermore, we acknowledge APX2009 and APX2014, the second generation compounds that were gifted by Apexian Pharmaceuticals.

SUPPLEMENTARY MATERIAL

The Supplementary Material for this article can be found online at: https://www.frontiersin.org/articles/10.3389/fonc.2022.826617/full#supplementary-material

REFERENCES

1. Sarantis P, Koustas E, Papadimitropoulou A, Papavassiliou AG, Karamouzis MV. Pancreatic Ductal Adenocarcinoma: Treatment Hurdles, Tumor Microenvironment and Immunotherapy. *World J Gastrointest Oncol* (2020) 12(2):173–81. doi: 10.4251/wjgo.v12.i2.173
2. Ischenko I, D'Amico S, Rao M, Li J, Hayman MJ, Powers S, et al. KRAS Drives Immune Evasion in a Genetic Model of Pancreatic Cancer. *Nat Commun* (2021) 12(1):1482. doi: 10.1038/s41467-021-21736-w
3. Hu HF, Ye Z, Qin Y, Xu XW, Yu XJ, Zhuo QF, et al. Mutations in Key Driver Genes of Pancreatic Cancer: Molecularly Targeted Therapies and Other Clinical Implications. *Acta Pharmacol Sin* (2021) 42(11):1725–41. doi: 10.1038/s41401-020-00584-2
4. Silke J, O'Reilly LA. NF-κB and Pancreatic Cancer; Chapter and Verse. *Cancers (Basel)* (2021) 13(18):4510. doi: 10.3390/cancers13184510
5. Ling J, Kang Y, Zhao R, Xia Q, Lee DF, Chang Z, et al. KrasG12D-Induced IKK2/beta/NF-kappaB Activation by IL-1alpha and P62 Feedforward Loops Is Required for Development of Pancreatic Ductal Adenocarcinoma. *Cancer Cell* (2012) 21(1):105–20. doi: 10.1016/j.ccr.2011.12.006
6. Pramanik KC, Makena MR, Bhowmick K, Pandey MK. Advancement of NF-kappaB Signaling Pathway: A Novel Target in Pancreatic Cancer. *Int J Mol Sci* (2018) 19(12):3890. doi: 10.3390/ijms19123890
7. Wu F, Yang J, Liu J, Wang Y, Mu J, Zeng Q, et al. Signaling Pathways in Cancer-Associated Fibroblasts and Targeted Therapy for Cancer. *Signal Transduct Target Ther* (2021) 6(1):218. doi: 10.1038/s41392-021-00641-0
8. Grivennikov SI, Karin M. Dangerous Liaisons: STAT3 and NF-kappaB Collaboration and Crosstalk in Cancer. *Cytokine Growth Factor Rev* (2010) 21(1):11–9. doi: 10.1016/j.cytogfr.2009.11.005
9. Gujral TS, Kirschner MW. Hippo Pathway Mediates Resistance to Cytotoxic Drugs. *Proc Natl Acad Sci USA* (2017) 114(18):E3729–38. doi: 10.1073/pnas.1703096114
10. Gong J, Xie J, Bedolla R, Rivas P, Chakravarthy D, Freeman JW, et al. Combined Targeting of STAT3/NF-κb/COX-2/EP4 for Effective Management

of Pancreatic Cancer. *Clin Cancer Res* (2014) 20(5):1259–73. doi: 10.1158/1078-0432.CCR-13-1664
11. Curtis Heisel JY, Mijiti M, Charizanis K, Brigell M, Corson TW, Kelley MR. APE1/Ref-1 as a Novel Target for Retinal Diseases. *J Cell Signaling* (2021) 2 (2):133–8. doi: 10.33696/Signaling.2.044
12. Kelley M, Georgiadis M, Fishel M. APE1/Ref-1Role in Redox Signaling: Translational Applications of Targeting the Redox Function of the DNA Repair/Redox Protein APE1/Ref-1. *Curr Mol Pharmacol* (2012) 5(1):36–53. doi: 10.2174/1874467211205010036
13. Caston RA, Gampala S, Armstrong L, Messmann RA, Fishel ML, Kelley MR. The Multifunctional APE1 DNA Repair–Redox Signaling Protein as a Drug Target in Human Disease. *Drug Discovery Today* (2021) 26(1):218–28. doi: 10.1016/j.drudis.2020.10.015
14. Gampala S, Caston RA, Fishel ML, Kelley MR. Basic, Translational and Clinical Relevance of the DNA Repair and Redox Signaling Protein APE1 in Human Diseases. In: *DNA Damage, DNA Repair and Disease* MLRS Dizdaroglu. Ed. Cambridge, UK: Royal Society of Chemistry (2020) 2:286–318.
15. Nassour H, Wang Z, Saad A, Papaluca A, Brosseau N, Affar EB, et al. Peroxiredoxin 1 Interacts With and Blocks the Redox Factor APE1 From Activating Interleukin-8 Expression. *Sci Rep* (2016) 6:29389. doi: 10.1038/srep29389
16. Ando K, Hirao S, Kabe Y, Ogura Y, Sato I, Yamaguchi Y, et al. A New APE1/Ref-1-Dependent Pathway Leading to Reduction of NF-κb and AP-1, and Activation of Their DNA-Binding Activity. *Nucleic Acids Res* (2008) 36 (13):4327–36. doi: 10.1093/nar/gkn416
17. Cesaratto L, Codarin E, Vascotto C, Leonardi A, Kelley MR, Tiribelli C, et al. Specific Inhibition of the Redox Activity of Ape1/Ref-1 by E3330 Blocks Tnf-Alpha-Induced Activation of IL-8 Production in Liver Cancer Cell Lines. *PloS One* (2013) 8(8):e70909. doi: 10.1371/journal.pone.0070909
18. McIlwain DW, Fishel ML, Boos A, Kelley MR, Jerde TJ. APE1/Ref-1 Redox-Specific Inhibition Decreases Survivin Protein Levels and Induces Cell Cycle Arrest in Prostate Cancer Cells. *Oncotarget* (2018) 9(13):10962–77. doi: 10.18632/oncotarget.23493
19. Oliveira TT, Fontes-Dantas FL, de Medeiros Oliveira RK, Pinheiro DML, Coutinho LG, da Silva VL, et al. Chemical Inhibition of Apurinic-Apyrimidinic Endonuclease 1 Redox and DNA Repair Functions Affects the Inflammatory Response *via* Different But Overlapping Mechanisms. *Front Cell Dev Biol* (2021) 9:731588. doi: 10.3389/fcell.2021.731588
20. Gampala S, Shah F, Zhang C, Rhodes SD, Babb O, Grimard M, et al. Exploring Transcriptional Regulators Ref-1 and STAT3 as Therapeutic Targets in Malignant Peripheral Nerve Sheath Tumours. *Br J Cancer* (2021) 124 (9):1566–80. doi: 10.1038/s41416-021-01270-8
21. Lesina M, Wormann SM, Morton J, Diakopoulos KN, Korneeva O, Wimmer M, et al. RelA Regulates CXCL1/CXCR2-Dependent Oncogene-Induced Senescence in Murine Kras-Driven Pancreatic Carcinogenesis. *J Clin Invest* (2016) 126(8):2919–32. doi: 10.1172/JCI86477
22. Algül H, Treiber M, Lesina M, Nakhai H, Saur D, Geisler F, et al. Pancreas-Specific RelA/p65 Truncation Increases Susceptibility of Acini to Inflammation-Associated Cell Death Following Cerulein Pancreatitis. *J Clin Invest* (2007) 117(6):1490–501. doi: 10.1172/JCI29882
23. Conradt L, Henrich A, Wirth M, Reichert M, Lesina M, Algül H, et al. Mdm2 Inhibitors Synergize With Topoisomerase II Inhibitors to Induce P53-Independent Pancreatic Cancer Cell Death. *Int J Cancer* (2013) 132 (10):2248–57. doi: 10.1002/ijc.27916
24. Shah F, Goossens E, Atallah NM, Grimard M, Kelley MR, Fishel ML. APE1/Ref-1 Knockdown in Pancreatic Ductal Adenocarcinoma - Characterizing Gene Expression Changes and Identifying Novel Pathways Using Single-Cell RNA Sequencing. *Mol Oncol* (2017) 11(12):1711–32. doi: 10.1002/1878-0261.12138
25. Gampala S, Shah F, Lu X, Moon H-R, Babb O, Umesh Ganesh N, et al. Ref-1 Redox Activity Alters Cancer Cell Metabolism in Pancreatic Cancer: Exploiting This Novel Finding as a Potential Target. *J Exp Clin Cancer Res* (2021) 40(1):251. doi: 10.1186/s13046-021-02046-x
26. Wilson DM3rd, Simeonov A. Small Molecule Inhibitors of DNA Repair Nuclease Activities of APE1. *Cell Mol Life Sci* (2010) 67(21):3621–31. doi: 10.1007/s00018-010-0488-2
27. Rai G, Vyjayanti VN, Dorjsuren D, Simeonov A, Jadhav A, Wilson DM3rd, et al. Synthesis, Biological Evaluation, and Structure-Activity Relationships of a Novel Class of Apurinic/Apyrimidinic Endonuclease 1 Inhibitors. *J Med Chem* (2012) 55(7):3101–12. doi: 10.1021/jm201537d
28. Caston RA, Shah F, Starcher CL, Wireman R, Babb O, Grimard M, et al. Combined Inhibition of Ref-1 and STAT3 Leads to Synergistic Tumour Inhibition in Multiple Cancers Using 3D and *In Vivo* Tumour Co-Culture Models. *J Cell Mol Med* (2021) 25(2):784–800. doi: 10.1111/jcmm.16132
29. Fishel ML, Wu X, Devlin CM, Logsdon DP, Jiang Y, Luo M, et al. Apurinic/apyrimidinic Endonuclease/Redox Factor-1 (APE1/Ref-1) Redox Function Negatively Regulates NRF2. *J Biol Chem* (2015) 290(5):3057–68. doi: 10.1074/jbc.M114.621995
30. Fujioka S, Niu J, Schmidt C, Sclabas GM, Peng B, Uwagawa T, et al. NF-kappaB and AP-1 Connection: Mechanism of NF-kappaB-Dependent Regulation of AP-1 Activity. *Mol Cell Biol* (2004) 24(17):7806–19. doi: 10.1128/MCB.24.17.7806-7819.2004
31. Pan X, Arumugam T, Yamamoto T, Levin PA, Ramachandran V, Ji B, et al. Nuclear factor-kappaB P65/relA Silencing Induces Apoptosis and Increases Gemcitabine Effectiveness in a Subset of Pancreatic Cancer Cells. *Clin Cancer Res* (2008) 14(24):8143–51. doi: 10.1158/1078-0432.CCR-08-1539
32. Mendonca M, Chin-Sinex H, Erdwin R, Townsend D, Tenbarge M. Determining If Double Gene Knockdown of P65 and PDK2 Increases Cytotoxicity and Radiation Sensitivity of Pancreatic Cancer Cells. *Proc IMPRS* (2018) 1(1). doi: 10.18060/22794
33. Jedinak A, Dudhgaonkar S, Kelley MR, Sliva D. Apurinic/Apyrimidinic Endonuclease 1 Regulates Inflammatory Response in Macrophages. *Anticancer Res* (2011) 31(2):379–85.
34. Luo M, Delaplane S, Jiang A, Reed A, He Y, Fishel M, et al. Role of the Multifunctional DNA Repair and Redox Signaling Protein Ape1/Ref-1 in Cancer and Endothelial Cells: Small-Molecule Inhibition of the Redox Function of Ape1. *Antioxid Redox Signal* (2008) 10(11):1853–67. doi: 10.1089/ars.2008.2120
35. Nyland RL, Luo M, Kelley MR, Borch RF. Design and Synthesis of Novel Quinone Inhibitors Targeted to the Redox Function of Apurinic/Apyrimidinic Endonuclease 1/Redox Enhancing Factor-1 (Ape1/Ref-1). *J Med Chem* (2010) 53(3):1200–10. doi: 10.1021/jm9014857
36. Kelley MR, Luo M, Reed A, Su D, Delaplane S, Borch RF, et al. Functional Analysis of New and Novel Analogs of E3330 That Block the Redox Signaling Activity of the Multifunctional AP Endonuclease/Redox Signaling Enzyme APE1/Ref-1. *Antioxid Redox Signal* (2011) 14(8):1387–401. doi: 10.1089/ars.2010.3410
37. Sardar Pasha SPB, Sishtla K, Sulaiman RS, Park B, Shetty T, Shah F, et al. Ref-1/APE1 Inhibition With Novel Small Molecules Blocks Ocular Neovascularization. *J Pharmacol Exp Ther* (2018) 367(1):108–18. doi: 10.1124/jpet.118.248088
38. Luo M, Zhang J, He H, Su D, Chen Q, Gross ML, et al. Characterization of the Redox Activity and Disulfide Bond Formation in Apurinic/Apyrimidinic Endonuclease. *Biochemistry* (2012) 51(2):695–705. doi: 10.1021/bi201034z
39. Zhang J, Luo M, Marasco D, Logsdon D, LaFavers KA, Chen Q, et al. Inhibition of Apurinic/Apyrimidinic Endonuclease I's Redox Activity Revisited. *Biochemistry* (2013) 52(17):2955–66. doi: 10.1021/bi400179m
40. Fishel ML, Wu X, Devlin CM, Logsdon DP, Jiang Y, Luo M, et al. Apurinic/Apyrimidinic Endonuclease/Redox Factor-1 (APE1/Ref-1) Redox Function Negatively Regulates NRF2. *J Biol Chem* (2014) 290(5):3057–68. doi: 10.1074/jbc.M114.621995
41. Fishel ML, Xia H, McGeown J, McIlwain DW, Elbanna M, Craft AA, et al. Anti-Tumor Activity and Mechanistic Characterization of APE1/Ref-1 Inhibitors in Bladder Cancer. *Mol Cancer Ther* (2019) 18(11):1947–60. doi: 10.1158/1535-7163.MCT-18-1166
42. Roebuck KA. Regulation of Interleukin-8 Gene Expression. *J Interferon Cytokine Res* (1999) 19(5):429–38. doi: 10.1089/107999099313866
43. Wang Y, Wan GH, Wu YM, Wang HS, Wang HF, Zhang G, et al. AP-1 Confers Resistance to Anti-Cancer Therapy by Activating XIAP. *Oncotarget* (2018) 9(18):14124–37. doi: 10.18632/oncotarget.23897
44. Brennan A, Leech JT, Kad NM, Mason JM. Selective Antagonism of Cjun for Cancer Therapy. *J Exp Clin Cancer Res* (2020) 39(1):184. doi: 10.1186/s13046-020-01686-9
45. Cai Z, Kotzin JJ, Ramdas B, Chen S, Nelanuthala S, Palam LR, et al. Inhibition of Inflammatory Signaling in Tet2 Mutant Preleukemic Cells Mitigates Stress-Induced Abnormalities and Clonal Hematopoiesis. *Cell Stem Cell* (2018) 23 (6):833–849.e835. doi: 10.1016/j.stem.2018.10.013
46. Sahakian L, Filippone RT, Stavely R, Robinson AM, Yan XS, Abalo R, et al. Inhibition of APE1/Ref-1 Redox Signaling Alleviates Intestinal Dysfunction and Damage to Myenteric Neurons in a Mouse Model of Spontaneous Chronic Colitis. *Inflammatory Bowel Dis* (2020) 27(3):388–406. doi: 10.1093/ibd/izaa161

47. Hartman GD, Lambert-Cheatham NA, Kelley MR, Corson TW. Inhibition of APE1/Ref-1 for Neovascular Eye Diseases: From Biology to Therapy. *Int J Mol Sci* (2021) 22(19):10279. doi: 10.3390/ijms221910279

Conflict of Interest: MK has licensed APX3330 through Indiana University Research and Technology Corporation to Apexian Pharmaceuticals LLC.

The remaining authors declare that the research was conducted in the absence of any commercial or financial relationships that could be construed as a potential conflict of interest.

Publisher's Note: All claims expressed in this article are solely those of the authors and do not necessarily represent those of their affiliated organizations, or those of the publisher, the editors and the reviewers. Any product that may be evaluated in this article, or claim that may be made by its manufacturer, is not guaranteed or endorsed by the publisher.

frontiers | Frontiers in Oncology

REVIEW
published: 06 April 2022
doi: 10.3389/fonc.2022.850883

Recent Advances in the Development of Non-PIKKs Targeting Small Molecule Inhibitors of DNA Double-Strand Break Repair

Jeremy M. Kelm[1†], Amirreza Samarbakhsh[1†], Athira Pillai[1], Pamela S. VanderVere-Carozza[2], Hariprasad Aruri[1], Deepti S. Pandey[1], Katherine S. Pawelczak[3], John J. Turchi[2,3,4] and Navnath S. Gavande[1,5]*

[1] Department of Pharmaceutical Sciences, Eugene Applebaum College of Pharmacy and Health Sciences, Wayne State University, Detroit, MI, United States, [2] Department of Medicine, Indiana University School of Medicine, Indianapolis, IN, United States, [3] NERx Biosciences, Indianapolis, IN, United States, [4] Department of Biochemistry and Molecular Biology, Indiana University School of Medicine, Indianapolis, IN, United States, [5] Molecular Therapeutics Program, Barbara Ann Karmanos Cancer Institute, Wayne State University School of Medicine, Detroit, MI, United States

OPEN ACCESS

Edited by:
Maria Felice Brizzi,
University of Turin, Italy

Reviewed by:
Roopa Thapar,
Rice University, United States
Noritaka Adachi,
Yokohama City University, Japan

***Correspondence:**
Navnath S. Gavande
ngavande@wayne.edu;
orcid.org/0000-0002-2413-0235

[†]These authors have contributed equally to this work

Specialty section:
This article was submitted to Cancer Molecular Targets and Therapeutics, a section of the journal Frontiers in Oncology

Received: 08 January 2022
Accepted: 22 February 2022
Published: 06 April 2022

Citation:
Kelm JM, Samarbakhsh A, Pillai A, VanderVere-Carozza PS, Aruri H, Pandey D, Pawelczak KS, Turchi JJ and Gavande NS (2022) Recent Advances in the Development of Non-PIKKs Targeting Small Molecule Inhibitors of DNA Double-Strand Break Repair. Front. Oncol. 12:850883. doi: 10.3389/fonc.2022.850883

The vast majority of cancer patients receive DNA-damaging drugs or ionizing radiation (IR) during their course of treatment, yet the efficacy of these therapies is tempered by DNA repair and DNA damage response (DDR) pathways. Aberrations in DNA repair and the DDR are observed in many cancer subtypes and can promote *de novo* carcinogenesis, genomic instability, and ensuing resistance to current cancer therapy. Additionally, stalled or collapsed DNA replication forks present a unique challenge to the double-strand DNA break (DSB) repair system. Of the various inducible DNA lesions, DSBs are the most lethal and thus desirable in the setting of cancer treatment. In mammalian cells, DSBs are typically repaired by the error prone non-homologous end joining pathway (NHEJ) or the high-fidelity homology directed repair (HDR) pathway. Targeting DSB repair pathways using small molecular inhibitors offers a promising mechanism to synergize DNA-damaging drugs and IR while selective inhibition of the NHEJ pathway can induce synthetic lethality in HDR-deficient cancer subtypes. Selective inhibitors of the NHEJ pathway and alternative DSB-repair pathways may also see future use in precision genome editing to direct repair of resulting DSBs created by the HDR pathway. In this review, we highlight the recent advances in the development of inhibitors of the non-phosphatidylinositol 3-kinase-related kinases (non-PIKKs) members of the NHEJ, HDR and minor backup SSA and alt-NHEJ DSB-repair pathways. The inhibitors described within this review target the non-PIKKs mediators of DSB repair including Ku70/80, Artemis, DNA Ligase IV, XRCC4, MRN complex, RPA, RAD51, RAD52, ERCC1-XPF, helicases, and DNA polymerase θ. While the DDR PIKKs remain intensely pursued as therapeutic targets, small

molecule inhibition of non-PIKKs represents an emerging opportunity in drug discovery that offers considerable potential to impact cancer treatment.

Keywords: DNA repair and DNA damage response (DDR), DNA double-strand break (DSB) repair, non-PIKKs inhibitors, non-homologous end joining (NHEJ), homology directed repair (HDR), single-strand annealing (SSA), polymerase theta-mediated end joining (TMEJ), synthetic lethality

INTRODUCTION

DSB Repair Pathways

DNA double-strand breaks (DSB)s are considered the most lethal of all DNA lesions. DSBs may be induced by various exogenous and endogenous factors, such as ionizing or ultraviolet radiation, genotoxic chemicals/chemotherapeutic agents, replication errors or collapsed replication forks, reactive oxygen species (ROS), free radicals, V(D)J recombination and abortive enzymatic activity (1–4). Unrepaired DSBs can lead to cell death, as persistent DSBs can trigger apoptosis (5–7). Moreover, misrepair or inaccurate repair of DSBs can lead to pathological genomic alterations resulting in senescence, loss of heterozygosity or chromosomal translocations which can ultimately result in oncogenesis (8). Interestingly, DSBs are routinely generated in the process of V(D)J recombination in naïve B- and T-lymphocytes to generate a diverse array of immunoglobulins and T-cell receptors, and the role of DSB repair in these processes has recently been reviewed (9). Aside from posing risk for cancer, DSBs are implicated in premature aging, and DSB repair capacity generally declines with age (10). In mammalian cells, the majority of DSBs are repaired *via* non-homologous end joining (NHEJ) or the homology directed repair (HDR)/homologous recombination (HR) pathways (**Figure 1**). In addition to NHEJ and HDR, less frequently involved or backup pathways including single-strand annealing (SSA) and alternative NHEJ (alt-NHEJ) also contribute to DSB repair (11–13). Alt-NHEJ is also called microhomology-mediated end joining (MMEJ) and more recently referred to as polymerase theta-mediated end joining (TMEJ) as recently reviewed by Ramsden et al. (14). Canonical or classical NHEJ is the predominant pathway in human cells and is active throughout the cell cycle, rapidly repairing up to ∼80% of all DSBs (15, 16). HDR is a much slower DSB repair process and is restricted exclusively to S and G2 phases of the cell cycle due to the requirement for a homologous DNA sequence or availability of sister chromatid as a template for the repair process (3).

Figure 1 (left) depicts the various steps in the NHEJ repair pathway, and these can be summarized into four specific steps which include: (i) DNA termini recognition by Ku70/80; (ii) bridging of the two DNA ends also known as formation of the synaptic complex; (iii) DNA end processing, and finally (iv) DNA ligation (16–20). Following the induction of DSB by exogenous sources like ionizing radiation (IR) or chemotherapeutics, the NHEJ pathway is initiated by the binding of the heterodimeric Ku70/80 to the end of DNA break which recruits DNA-dependent protein kinase catalytic subunits (DNA-PKcs) to form the DNA-PK holoenzyme (DNA-PK). The DNA-PKcs serine/threonine protein kinase activity is activated once bound to a DNA terminus in the presence of Ku70/80. The formation of the DNA-PK complex stabilizes the two DNA ends at the site of the break by forming a synaptic complex that holds the two DNA termini together (21, 22). DNA-PK catalyzes both autophosphorylation and phosphorylation of other target proteins including Ku70/80, Artemis, polynucleotide kinase 3′-phosphatase (PNKP) and XRCC4. When required, DNA end processing relies on the kinase activity of DNA-PKcs, endonuclease cleavage activity of Artemis, nucleotide addition and modification by DNA polymerases (Pol X family polymerases such as pol λ and pol μ), tyrosyl-DNA phosphodiesterase (TDP), and PNKP. Finally, the DNA Ligase IV/XRCC4/XLF complex is recruited to DNA termini and catalyzes ligation of the DNA DSB.

The HDR pathway is depicted in stepwise fashion in **Figure 1** (right) and can be summarized as: (i) binding of the MRN complex to each of the damaged dsDNA ends; (ii) end resection by the MRN complex, CtIP, EXO1, BLM and stabilization of the ssDNA overhangs by RPA binding; (iii) RAD51 displacement of RPA and formation of the Holliday junction with a homologous sequence; and (iv) resolution of the Holliday junction. The MRN complex (MRE11-RAD50-NBS1) is crucial for recognition of homologous sequences, performing end resections to generate ssDNA tails and nucleofilament formation by Replication Protein A (RPA) which is eventually replaced by RAD51. BRCA1 and BRCA2 also facilitate RAD51 filament nucleation. After recruitment of RAD51, a homology search can now be performed that when successful allows invasion of the non-resected strand into the homologous template and resulting D-loop formation of the displaced template strand. Capture of the D-loop by the broken dsDNA produces a Holliday junction that is later resolved by endonuclease activity, completing HDR. The distinct independent pathways that can operate to complete the HDR repair pathway are reviewed elsewhere (23, 24). Decades of investigation have established the importance of NHEJ, HDR, TMEJ and SSA pathways, the roles of the various factors/proteins involved in these pathways and how these factors coordinate and regulate distinct steps of these pathways at the molecular level. More detailed descriptions of these pathways can be found in recent reviews (11, 14, 16, 25, 26).

It is worth mentioning that a prerequisite to repair of DSBs is that the lesion is accessible which typically requires histone modifications and reorganization of chromatin (27). Acetylation of histones promotes DNA unraveling by electronegative repulsion which enables the DNA repair machinery access to the DSB. Targeting histone deacetylases (HDACs) with small molecule drugs or through promoting their degradation by inhibition of the deubiquitinase conferring HDAC stability are other strategies to enhance radiosensitivity

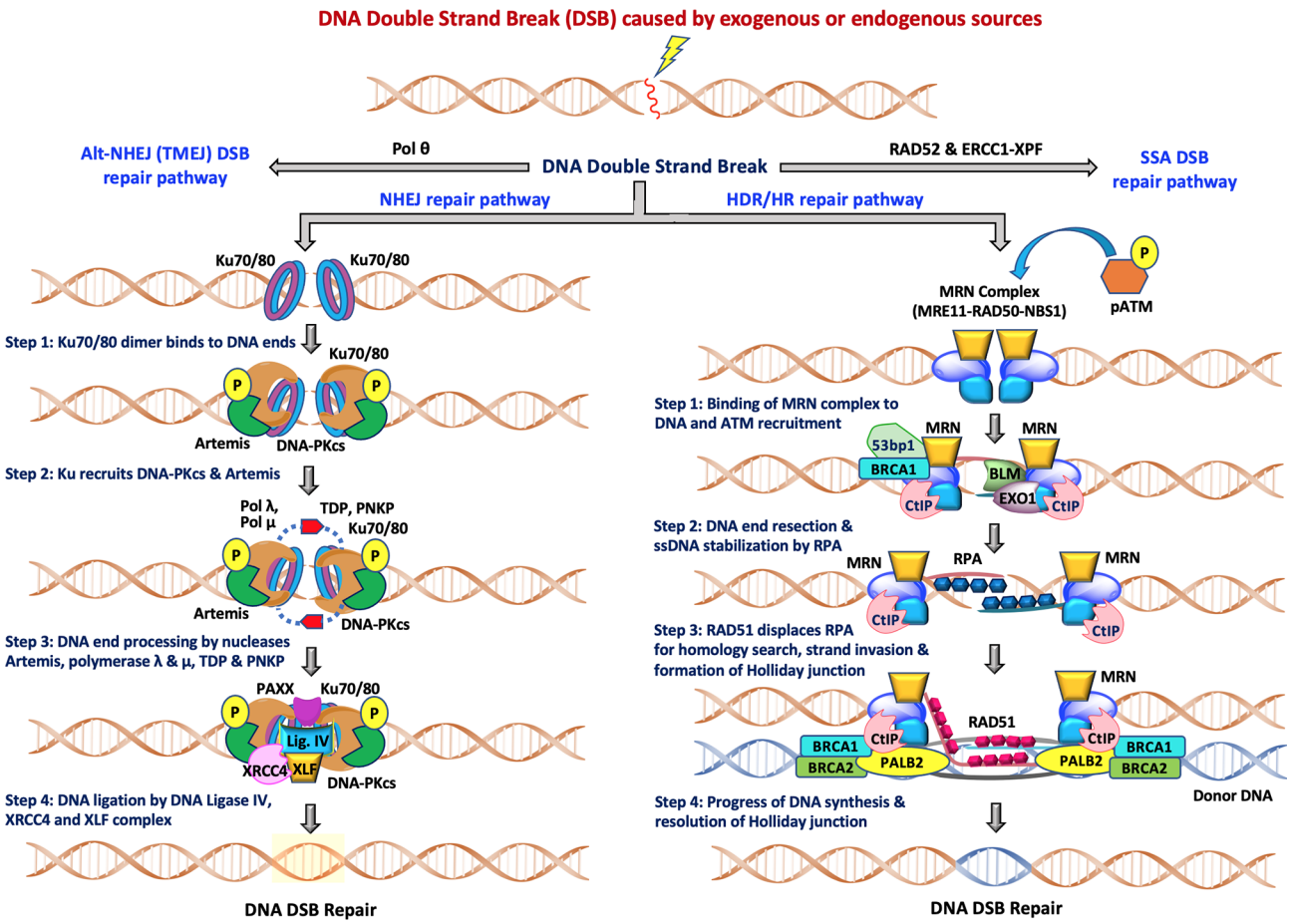

FIGURE 1 | The two major pathways of DNA double-strand break repair: During NHEJ, the DNA double strand sites are initially recognized by heterodimeric Ku70/80. This is followed by recruitment of DNA-PKcs and Artemis, DNA end processing by Artemis, polymerase λ and μ, TDP and PNKP and finally ligation of DSB breaks by Ligase IV/XRCC4/XLF complex for completion of the repair pathway. The other accessory proteins like APLF, PAXX and XLF also participate in the repair functions. During HDR/HR, DSBs are recognized and resected by the MRN complex to generate a 3' overhang. BRCA2/RAD51, along with other RAD51 paralogs, binds to the RPA coated ssDNA tails after which RAD51 replaces RPA in a BRCA1-and BRCA2-dependent process, forming a presynaptic filament. Upon strand invasion, D-loop formation and DNA repair synthesis can be resolved through Holliday junction, after which distinct independent pathways can operate to complete the HDR repair pathway. NHEJ is available throughout interphase while HDR is restricted to S/G2 phases of the cell cycle.

(28, 29). To complicate matters further, the chromatin state must be returned to the pre-existing state after DSB repair.

Telomeres are repetitive DNA elements that protect chromosomal termini and prevent their false recognition as DSBs which could activate a deleterious DDR such as NHEJ-mediated chromosomal fusion or cyclization (30, 31). DDR activation and maintenance at telomeres depends on the biogenesis and functions of the site-specific small non-coding RNAs, also known as DNA damage response RNAs (DDRNAs) (32). Telomeres shorten with cell division during replicative senescence (due to the end-replication problem). Excessive telomeric erosion has been shown to contribute to a persistent DDR and have been implicated in the ageing process and disease development alongside with a host of lifestyle factors, stresses, and environmental exposures (33). The maintenance of telomere homeostasis is critical for chromosome stability in proliferating cancer cells which usually have higher telomerase activity compared to normal cells (34). In general, cancer cells maintain telomeres at shorter lengths compared to normal cells. Besides preventing chromosome shortening, telomerase also intervenes to thwart the DSB response through protein-protein interactions with specialized telomere-binding proteins. There are several proteins involved in the DSB response which are also localized to telomeres and participate in telomere homeostasis (34). For example, the Ku protein has been demonstrated to be localized to telomeres and serves to protect the telomere against fusions. Particularly, depletion of the Ku heterodimer leads to severe telomere erosion and loss of cell viability (35, 36). Overall, telomerase has been an attractive target for the development of effective cancer therapeutics as it has shown overexpression in the majority of human cancers. The anti-telomerase therapeutics can provide selective destruction of

cancer cells while noncancerous cells are predominantly spared owing to telomerase silencing in most normal somatic cells (37).

RecQ and MCM (Minichromosome Maintenance) helicases, a family of DNA unwinding enzymes, play important roles in genomic stability through diverse roles in DNA recombination, replication and repair (38, 39). RecQ proteins can function both at early and late stages during repair of DSB. In addition, RecQ helicase proteins BLM (Bloom syndrome) and WRN (Werner syndrome) are also involved in telomere homeostasis as well as the processing and re-initiation of stalled replication forks (40, 41). The CMG helicase complex composed of three replication factors (Cdc45/Mcm2-7/GINS) is required to unwind dsDNA to generate the ssDNA template during DNA replication (42). A stalled replication forks by MCM helicases can lead to a DSB as well as chromosomal rearrangements, which can eventually recruit RecQ proteins for repair due to their functional connections (39, 43). Targeting these helicases has immense importance in developing new therapeutics against various cancers.

The recent advances in the field of the mitochondrial DNA damage response (mtDDR) warrant consideration of the nonnuclear genome in the development of inhibitors of non-PIKKs in DSB repair, as several non-PIKKs are now implicated in the mtDDR (44–46). In humans, mitochondria contain a polyploid genome comprised of a heterogenous mixture of ~16.5 kbp circular DNA chromosomes. Consistent with endosymbiotic ancestry from proteobacteria, the mitochondrial DNA (mtDNA) replication, transcription, and DDR machinery includes gene products evolutionary derived from eukarya, bacteria, and T7-like bacteriophages (47). mtDNA replication, transcription, and damage repair occur independently of their nuclear counterparts. The maternally inherited mitochondrial genome includes 37 genes encoding all required mitochondrial tRNAs and rRNAs and 13 core proteins of complexes I, III, IV, and V of the electron transport chain (ETC).

mtDNA is subjected to damage by the same sources as nuclear DNA, although the proximity of mtDNA to the ETC complexes heightens the risk for ROS-induced DNA damage. Aberrations of mtDNA including mutations or deletions are associated with the development of diseases including Kearns-Sayre syndrome, Pearson syndrome, cancer, aging, Alzheimer's disease, and diabetes among others (44–46). Unlike the nucleus, there appears to be no role for classical NHEJ in the mitochondria where DSBs are predominantly repaired by the alt-NHEJ pathway. Mitochondrial alt-NHEJ proceeds independent of Ku70/80 and is dependent on Ligase III and MRE11 among others (48). DNA polymerase θ also appears to play a role in mitochondrial alt-NHEJ but in an error-prone manner unlike in the nucleus where fidelity is high (49, 50). Besides alt-NHEJ there is now mounting evidence to suggest that HDR may also repair DSBs in mtDNA, although possibly with nuances and a requirement for additional proteins. Four-way junctions and HDR mediators RAD51, RAD51C, XRCC3, and MRE11 have been detected in the mitochondria, and functional assays have demonstrated DSB repair in mitochondria consistent with HDR (51–54). Unrepaired mtDNA may be compensated for by undamaged mitochondrial chromosomes or trigger mitochondrial translesion synthesis, fusion, fission, or mitophagy to manage or purge the damaged mtDNA (44). There is evidence to suggest that mtDNA damage is sufficient to induce apoptosis or enhanced immunogenicity independent of nuclear DNA damage (55–58). Given the roles of non-PIKKs in the mtDDR, inhibitors should be assessed for their effects on mitochondrial HDR and alt-NHEJ. In similar fashion, the proapoptotic and immunogenic effects seen with targeted mtDNA damage highlights a potential for mitochondrial-selective anticancer drugs.

The innate immune response to cancer is favored by heightened DNA damage such as by unrepaired DSBs, although the adaptive immune response effectors B cells and T cells require intact DSB repair to repair the DSBs they routinely generate in V(D)J recombination. Accordingly, the strategy for targeting DSB repair in cancer will need to balance these opposing effects on the immune system. A precondition to repairing DSBs is access to the lesion by the DDR machinery through chromatin modification, and inhibition of HDACs may provide a way to block DSB repair upstream of DDR effector scaffolding at the damaged site.

An emerging area of research within the field of DNA damage and repair is the role of non-coding RNAs (ncRNAs) in the DDR to DSBs which has recently been reviewed (59–61). ncRNAs are classified as being either long ncRNAs (lncRNAs) or short ncRNAs (sncRNAs) depending on whether length exceeds 200 nucleotides. A subclass of lncRNAs is damage-induced lncRNAs (dilncRNAs), which are transcribed bidirectionally from DSBs after the arrival of the MRN complex and promote HDR by localizing RAD51, BRCA1, and BRCA2 to the lesion (59, 60). Micro RNAs (miRNAs), a subclass of sncRNAs, are typically derived from RNases such as DICER or Drosha and in the DDR regulate gene expression post-transcriptionally to select the DSB repair pathway employed, induce cell cycle arrest, and promote apoptosis where indicated (61). More broadly, ncRNAs are thought to serve as an alert to the presence of DSBs, to recruit DDR effectors to the lesion, and to temporarily bridge the broken ends in proximity, among other functions (59, 60). However, an improved understanding of ncRNAs in DSB repairs may produce additional opportunities for RNA-targeted therapeutic intervention. Overall, the multifunctional role of DNA repair and DDR pathways increases the complexity and difficulty of targeting DNA repair pathways for a positive clinical outcome.

Biological Impacts of DSB Repair in Cancer

DNA repair pathways play a central role in protecting cells against genomic instability and mutations. Moreover, DNA repair pathways play a multifaceted role in cancer onset, progression, metastasis, and ultimately on clinical outcome of cancer therapeutic strategies. Aberrations of DNA repair proteins or genes can predispose the cells to carcinogenesis and this vulnerability can be therapeutically exploited to preferentially kill tumor cells. The relative functionalities of the DNA repair and DNA damage response (DDR) pathways, whether defective, deficient, or hyperactive, as well as the

ability of cancer therapeutics to inhibit or activate DNA repair, all can influence a patient's response to therapy (5, 62, 63). The upregulated DNA repair and DDR activity can promote disease progression and make cancer cells resistant to the treatment or cause post-treatment relapse.

Many well-known anticancer chemotherapeutics and IR impart their clinical efficacy by inducing DNA damage. DNA damaging agents such as etoposide, bleomycin, doxorubicin and IR (radiotherapy) exert their therapeutic efficacy by inducing DNA DSBs. Approximately 50% of all cancer patients worldwide with common epithelial malignancies (including lung, prostate, breast, colon, head and neck, and esophageal cancers) are subjected to radiation therapy as a component of their treatment regimen. Radiotherapy is very cost effective and in combination with other medical treatments has contributed to improved long-term survival in subsets of cancer patients. Despite advanced technical improvements and the fact that radiotherapy is one of the most effective forms of cancer treatment, many patients still suffer from detrimental locally recurrent disease or long-term chronic side effects after radiotherapy due to being treated with higher doses of radiation (64–66). Most importantly, radiotherapy and DNA damaging chemotherapeutics often lead to poor clinical response due to the development of intrinsic or extrinsic resistance. There are multiple factors involved in IR and drug resistance, among them increased capacity of DNA DSB repair is one of the major primary concerns, and in many cases, resistance to therapy is an adaptive response linked to hyperactive DSB repair mechanisms (64, 67). The overexpression or loss of function due to polymorphisms, mutations of core and processing NHEJ proteins such as Ku70/80, DNA-PKcs, Ligase IV/XRCC4, and HDR proteins such as MRN, BRCA1/2 and RAD51 have been implicated in reduced therapeutic efficacy of IR and DNA damaging chemotherapeutics. Research within cancer genomics, proteomics, and metabolomics has led to a deeper understanding of the molecular mechanisms driving the development of resistance. In response to DNA damage, the affected cells recruit functional proteins to initiate the DSB repair pathway that enhances the DNA lesion repair which ultimately leads to drug resistance.

The targeted inhibition of repair pathways is a novel and effective strategy to induce persistent DSBs and increase apoptosis of cancer cells. This strategy is particularly promising in the setting of combination therapy with DSB-inducing treatments such as radiotherapy or radiomimetic drugs or in combination with other DNA damaging drugs. However, where unrepaired DSBs fail to directly induce cell death, induction of the innate immune response may ensue. The interplay of the DDR and the innate immune response has recently been reviewed (9). Cytosolic DNA arising from damaged nuclear or mitochondrial DNA is recognized as a pathogen- or damage-associated molecular pattern (PAMP/DAMP) and ultimately induces stimulator of interferon genes (STING)-dependent signaling. The resulting production of interferons enhances the cellular antitumor response by the immune system. Intriguingly, several of the non-PIKKs targeted by ligands reviewed here such as MRN complex, DNA ligase IV, and XRCC4 appear to have dual roles in stimulating the innate immune response aside from their classical roles in DSB repair.

As cancer cells frequently harbor defect in genes of a DNA repair pathway, they may be increasingly reliant on the remaining available pathways to repair DNA damage occurring endogenously or in response to treatment. Defects in DNA repair in cancer cells thus presents a vulnerability to exploit synthetical lethal interactions where noncancerous cells would remain resilient. In cancer treatment, this has been typified using PARP inhibitors in cancers that are HDR-deficient. The synthetic lethality approaches have provided novel mechanisms to specifically target cancer cells while noncancerous cells can tolerate or repair the damage which is anticipated to reduce toxicity associated with treatment. The availability of DNA repair inhibitors targeting a variety of DSB repair and DDR mediators will allow the strategy of synthetic lethal interactions to be more broadly applied clinically and with greater efficacy.

In this review, we focus specifically on recent advances in the development of non-PIKKs (PI3 kinase-like kinases) DSB repair targeted inhibitors that can be exploited for effective chemo- or radio-sensitization and to enhance the efficiency of precise genome editing as well. PIKKs such as ATM, ATR, and DNA-PK which are involved in DNA repair and DDR, have received considerable attention recently as pharmacological targets, and several inhibitors have risen to clinical trials. The progress pertaining to the development of these inhibitors is reviewed elsewhere (62, 68–70).

RECENT ADVANCES IN THE DEVELOPMENT OF NON-PIKKS DSB REPAIR INHIBITORS

The rare mutations and altered expression levels of key NHEJ and HDR proteins, mainly Ku70/80, DNA-PK, Artemis, Ligase IV, XRCC4, XLF, MRE11, RAD51, RPA and RAD52 can lead to predisposition to cancer, whereas increased capacity of DNA repair and DDR can be clinically exploited by targeting repair pathways to overcome resistance and enhance chemo- or radiosensitivity in cancer patients (5, 71–75). DNA repair inhibitors can be used to specifically target proteins involved in key steps of NHEJ, HDR, MMEJ and SSA as well as core or processing proteins involved in DDR signaling pathways. Developing drugs aimed at modulating DNA DSB repair activity are most likely to have a profound impact on the efficacy of radio- and chemotherapy. Therefore, targeting these key proteins in the DNA DSB repair pathways (**Figure 2**) has recently become a popular approach for potential cancer treatments.

INHIBITORS TARGETING NHEJ PATHWAY

Ku 70/80 Inhibitors

There has been considerable progress made in the development of DNA-PK inhibitors and several of them are in various stages

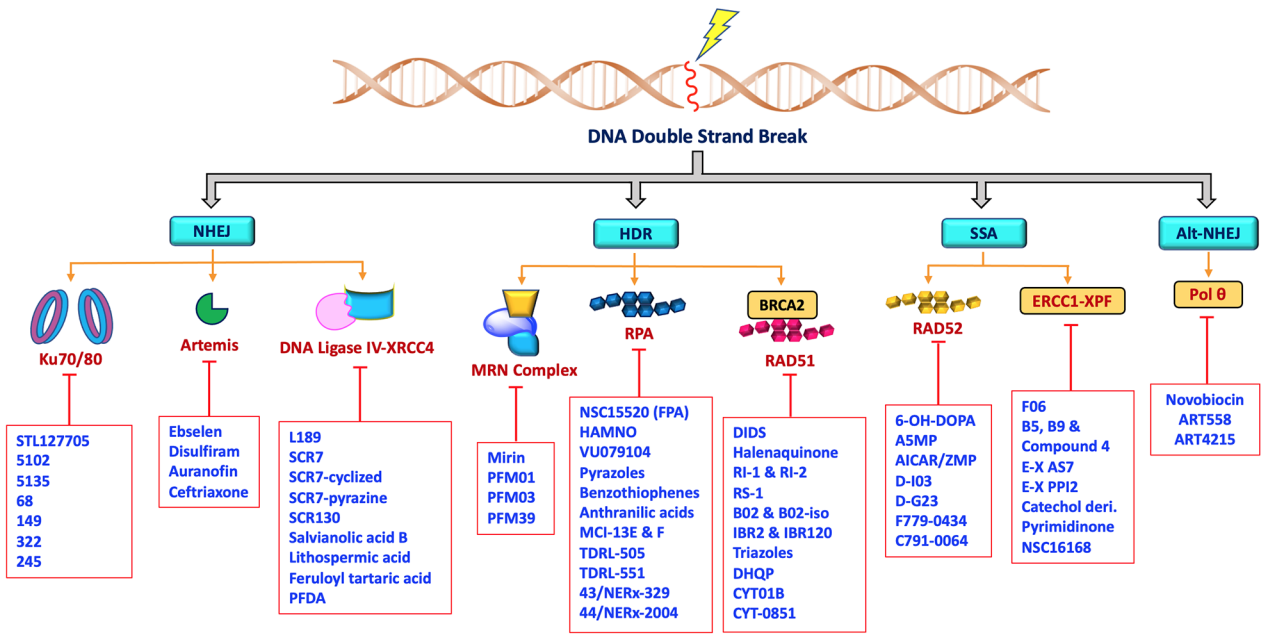

FIGURE 2 | Schematic representation showing non-PIKKs DSB repair inhibitors that target key/core and accessory proteins involved in DSB repair pathways.

of clinical trials (NCT02644278, NCT04172532, NCT03907969), but less attention has been placed on the upstream and most essential Ku70/80 heterodimer that recruits DNA-PKcs (68, 69). In the absence of heterodimeric Ku subunits, DNA-PKcs binding affinity to DNA DSB is significantly weak, resulting in halting of the repair process (76). DNA-PK has a unique mechanism of activation that requires binding to DNA termini, and this strong binding interaction is solely dependent on a protein-protein interaction with the Ku70/80 heterodimeric complex for the subsequent NHEJ activation (77, 78). Being the primary sensor and core regulator of this pathway, Ku is absolutely required for DNA DSBs repair by NHEJ (79–81). Inhibition of Ku subunits could therefore produce reduced DNA-PK and NHEJ activity. Therefore, Ku has a high potential for therapeutic outcomes in oncology.

Recent studies have demonstrated a significant increase in expression levels of Ku70 and Ku80 after chemo- and radiotherapy which correlates with poor prognosis in patients with rectal and cervical cancers (82–84). Further studies have also demonstrated that overexpression of Ku70/Ku80 is directly correlated with chemotherapy and radiotherapy resistance in various cancers (82). Previously, shRNA depletion of Ku70 or Ku80 produced cytotoxicity and radiosensitization in pancreatic cancer cells (85). In addition, Ku70 or Ku80 null cells exhibited enhanced chemo sensitization to DNA damaging agents including bleomycin, doxorubicin, and etoposide (86). Ku is also involved in several other DNA metabolism processes and in telomere maintenance (35, 36, 87). Despite the crucial role of Ku subunits early in the NHEJ pathway, there are currently a limited number of Ku70/80 inhibitors developed so far. In 2016, Weterings et al. identified STL127705 (compound L) (**Figure 3**) by computational screening of a commercial library that disrupts Ku-DNA binding activity in micro-molar range and has potential to sensitize cancer cells to IR (88). However, the ability of STL127705 to block NHEJ catalyzed DNA DSB repair is not documented to date.

Initially, our group identified arylalkyl esters of arylpyrazolone carboxylic acid derivatives, 5102 and 5135, through screening of a commercial library and both inhibitors displayed high potency in both Ku-DNA EMSA and DNA-PK kinase assays (**Figure 3**) (89). Retaining the core scaffold employed in 5102 and 5135, we recently further expanded our structure-guided synthetic chemistry efforts with the aim of improving Ku inhibitory potency, selectivity, and cellular activity while simultaneously improving solubility among other physicochemical properties (90). The structure activity relationship (SAR) from this study showed that an amide moiety increased both the solubility and the inhibition of Ku-DNA interaction by 4-fold over the ester group. Compounds 68, 149, 322 and 245 exhibited a high potency and specificity towards Ku and DNA-PK. Moreover, these compounds also showed improved chemical properties including solubility and stability. These Ku-DNA binding inhibitors (Ku-DBi's) directly interact with Ku and inhibit *in vitro* NHEJ, cellular NHEJ, and potentiate the cellular activity of radiomimetic agents and IR. Further analysis demonstrated that Ku-null cells are insensitive to Ku-DBi's however, Ku-DBi's potentiate cellular sensitivity to DSB-inducing agents in cancer cells. Molecular docking studies indicated that compounds 149 and 245 possess high affinity towards the Ku binding site (**Figure 4**). Inhibiting Ku interactions with DNA ends can efficiently block NHEJ catalyzed

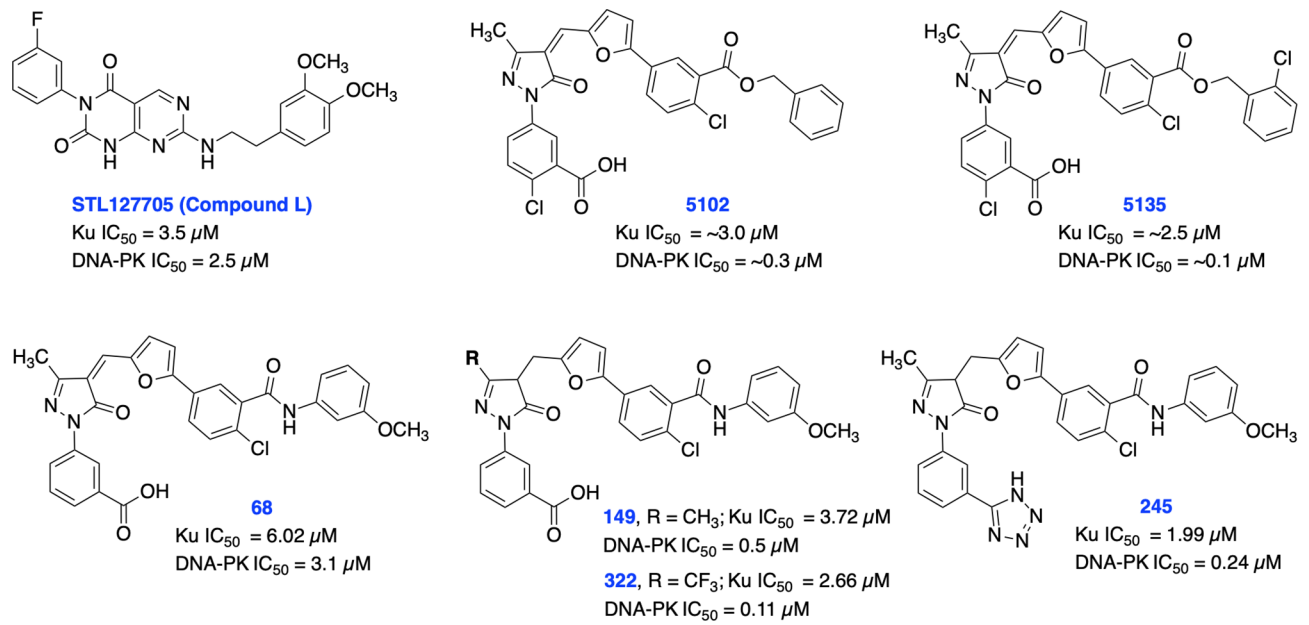

FIGURE 3 | Small molecule inhibitors of Ku70/80 and their respective IC50 values for disruption of DNA-binding by Ku70/80 and DNA-PK activity.

repair which is anticipated to increase efficiency of HDR-mediated recombination events. Therefore, we performed CRISPR-Cas9-mediated genome editing in the presence of Ku-DBi 245 where we observed a 6-fold increase in HDR mediated insertion at a DSB at the target site compared to the controls (90). These data suggests that Ku-DBi's could be effective to reduce off-target, potentially mutagenic events that have hampered CRISPR mediated therapeutic applications.

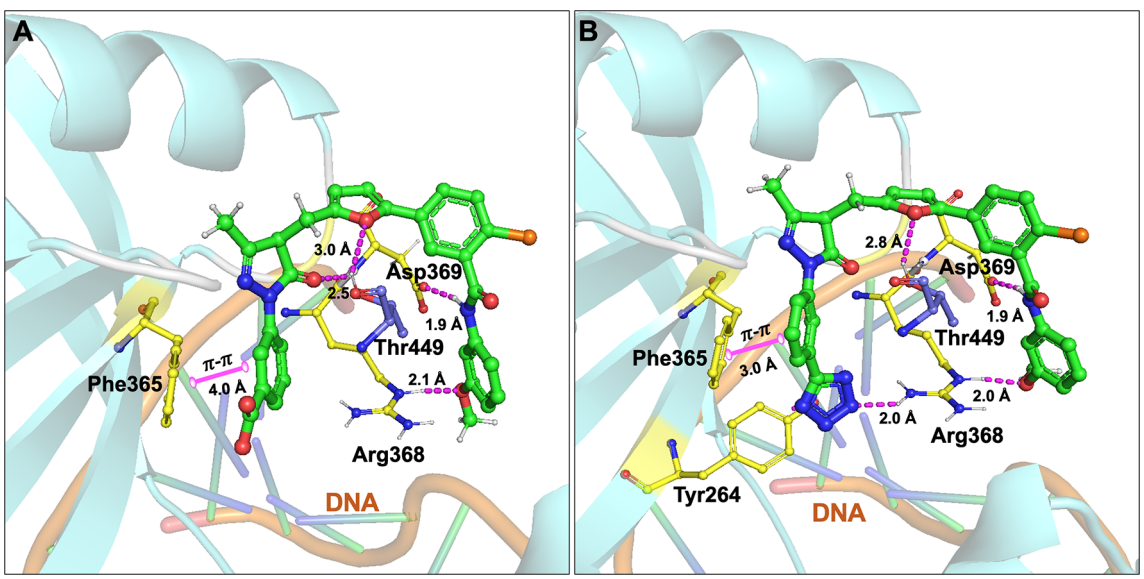

FIGURE 4 | Molecular interactions of **(A)** compound 149 and **(B)** 245 (all in green carbon) with Ku70/80 heterodimer (key amino acids are shown in yellow carbon (Ku70), blue carbon (Ku80) and cartoon is shown in cyan color). Interaction with amino acid side chains is indicated with the dashed magenta lines and π – π stacking interactions are shown in solid magenta dumbbell. The DNA helical structure is depicted in greenish blue sticks and light orange cartoon. Interaction distances indicated in Å.

Further development of Ku70/80 inhibitors has a considerable potential to impact cancer therapy as well as precise genome editing.

Artemis Inhibitors

Artemis is a structure specific endonuclease with critical roles in DSB repair by NHEJ, in the development of B- and T- lymphocytes *via* cleaving a hairpin intermediate during V(D)J recombination and has also been implicated to play a role in the maintenance of genomic stability (91–94). Artemis was first reported after investigators implicated its deficiency in severe combined immunodeficiency (SCID) as causative for observed phenotypes in this disorder including impaired V(D)J recombination and enhanced IR sensitivity, supporting the mechanistic role of Artemis in these pathways. Mouse embryonic fibroblasts (MEFs) derived from Artemis defective mice have increased chromosomal abnormalities, suggesting a role for Artemis in genome stability maintenance (95). In NHEJ, DNA-PKcs undergo auto phosphorylation and activate the endonuclease activity of Artemis at DNA ends (93). Artemis' C-terminal region influences V(D)J recombination through its interactions with DNA Ligase IV and DNA-PKcs, suggesting that the Artemis-binding site on Ligase IV also has physiological relevance to potentially disrupting NHEJ complex formation (96, 97). Artemis is the main nuclease known to remove DNA single-strand overhangs and 3′-phosphoglycolate groups from DNA termini generated by IR with its endonuclease activity (98). It is well documented that IR-induced DSBs require Artemis for repair (94, 95, 99, 100).

Recently, Yosaatmadja et al. generated a model for Artemis DNA binding based on their zinc bound Artemis crystal structure and another recently reported structure of the Artemis catalytic domain (101, 102). This unique zinc-finger-like motif has not been reported in other metallo-β-lactamase (MBL) enzymes (the super family to which Artemis belongs) and presents a possible novel targeting location. Further, they have screened thiol reactive compounds using this unique zinc-finger like motif of Artemis and identified that ebselen and disulfiram are able to inhibit Artemis endonuclease activity in the low micro-molar range (IC_{50s} = 8.5 uM and 10.8 uM, respectively), while auranofin and ceftriaxone are less potent (IC_{50s} = 46 uM and 65 uM, respectively) (**Figure 5**).

The recent crystal structures of Artemis and these inhibitors provide useful information for structure-based design of inhibitors to generate more selective and potent Artemis inhibitors, either binding at the active site or the unique zinc finger motif of Artemis. The key roles of Artemis within DNA repair make it an attractive target for a variety of therapeutic avenues. Artemis inhibitors have the potential to be used as radiosensitizers in various tumor types, demonstrated biologically by the sensitivity to IR seen in SCID patients. Because of its clear role in DNA repair and genome stability, Artemis targeted inhibitors also have the potential to synergize well with other DDR targeted inhibitors. There is the potential for impacts on immune cell maturation with long term clinical Artemis inhibition which could result in compromised immune function, thus monitoring immune system function will be critical as Artemis targeted agents progress to the clinic.

DNA Ligase IV Inhibitors

After DNA end processing, the final step in NHEJ pathway is ligation which is a crucial step in the repair of DNA DSBs and is an attractive target for inhibition of the DSB repair pathway. This is demonstrated by various Ligase IV deficient mutants and knockout studies, that have been shown to have significantly reduced NHEJ activity (103–105). Upon activation of kinase activity by DNA-PKcs, Ku heterodimer translocates internally to make DSB ends accessible to a specific ligation complex, which is composed of DNA ligase IV and its partnering proteins, XRCC4 and XLF (106).

In 2008, Chen et al. identified a competitive and non-specific ligase inhibitor, L189 through a computational drug design strategy which showed equipotent inhibitory activity against Ligase I, III, and IV (**Figure 6**) (107). Raghavan and co-workers in 2012 developed SCR7, a derivative of L189, which was initially suggested to be more selective for Ligase IV (108). Further extensive structural analysis by Greco et al. revealed that parental SCR7 is nonspecific, only exists in the more stable cyclized SCR7 pyrazine form and failed to inhibit DNA ligase IV-dependent V(D)J recombination in a cell-based ligation assay (109). On the contrary, Raghavan and co-workers in 2018 showed both intramolecular cyclized SCR7 (SCR7-cyclized) and further oxidized product (SCR7-pyrazine) could inhibit

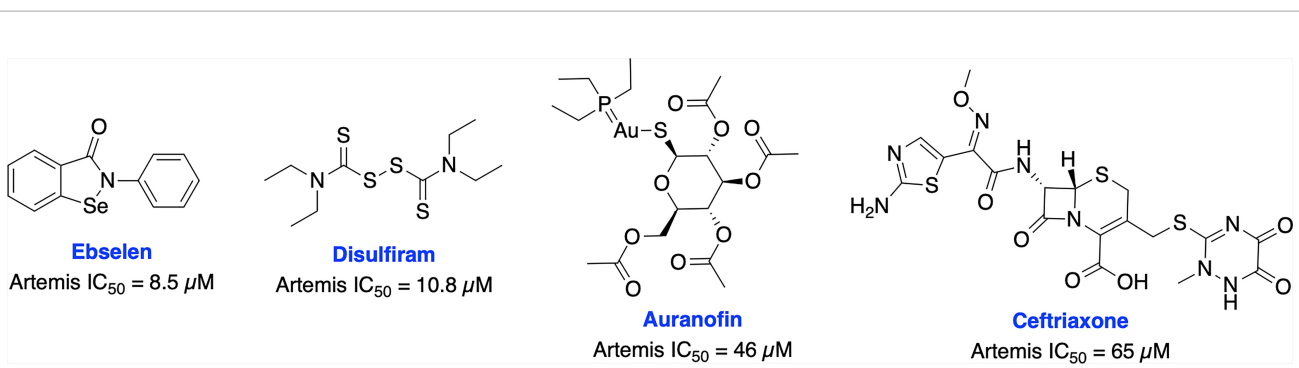

FIGURE 5 | Small molecule inhibitors targeting Artemis and their respective IC50 values for disruption of endonuclease activity.

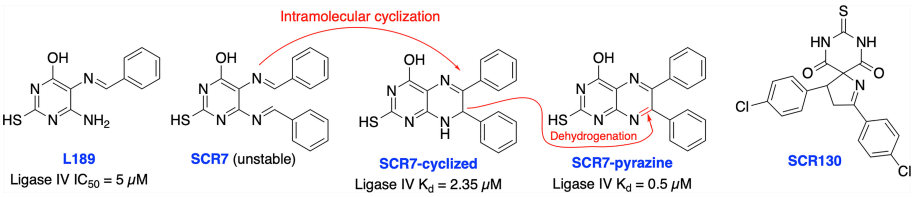

FIGURE 6 | Small molecule inhibitors targeting DNA Ligase IV and their IC50 values for either inhibition of Ligase IV adenylation or Ligase IV end-joining.

Ligase IV-mediated end joining and V(D)J recombination (110). Further studies showed that the SCR7-cyclized is Ligase IV specific and SCR7-pyrazine induced nonspecific cytotoxicity at higher concentrations in Ligase IV-null cells. Recently, Raghavan and co-workers developed a new ligase IV-specific inhibitor, SCR130, which exhibited 20-fold improved cytotoxicity compared to SCR7 and potentiated radiosensitivity in cancer cells (111). Furthermore, SCR7 produced enhanced HDR-mediated repair for CRISPR mediated genome editing by inhibiting NHEJ at lower concentrations (1 μM) (103), but cellular toxicity was observed with concentrations above 1 μM (104), suggesting that cell-dependent toxicity or off-target effects associated with the inhibitor (112). The higher IC_{50s} and inconsistent results could be explained by instability of parental SCR7 and its analogs. Given the conflicting results and unclear therapeutic and toxicological mechanisms of action, more research is required on this area. There is also a great need within medicinal chemistry to identify novel scaffolds apart from SCR7 to target Ligase IV as this will broaden the chemical space available to develop Ligase IV inhibitors.

XRCC4 Inhibitors

XRCC4 and its paralog, PAXX are responsible for the recruitment of other NHEJ factors to the damage site and XRCC4 is also a key regulator of DNA ligase IV activity in the NHEJ ligation step (17, 113–115). XRCC4 holds a potential to enhance chemo- and radiosensitivity of current therapeutics. Early attempts to inhibit XRCC4 resulted in the development of compounds salvianolic acid B, lithospermic acid, and 2-*O*-feruloyl tartaric acid (**Figure 7**); however, potential *in vitro* and *in vivo* effects of these agents is not documented to date (116). Recently, Liu et al. identified perfluorodecanoic acid (PFDA), a common persistent environmental pollutant, as a XRCC4 inhibitor which was able to sensitize gastric cancer cells to chemotherapy; however, mechanism of action, target engagement with XRCC4 and the toxicity profile of the inhibitor needed to be explored in more details (117).

INHIBITORS TARGETING HDR PATHWAY

MRN Complex (MRE11-RAD50-NBS1) Inhibitors

In case canonical NHEJ pathway fails to enact timely DNA repair, DSBs are subjected to end resection leading to the generation of 3′ ss-DNA that interfere with Ku recruitment and promote high-fidelity repair process by HDR (11, 118). Homologous recombination occurs between homologous DNA sequences through the MRN-RPA-RAD51 axis which facilitates

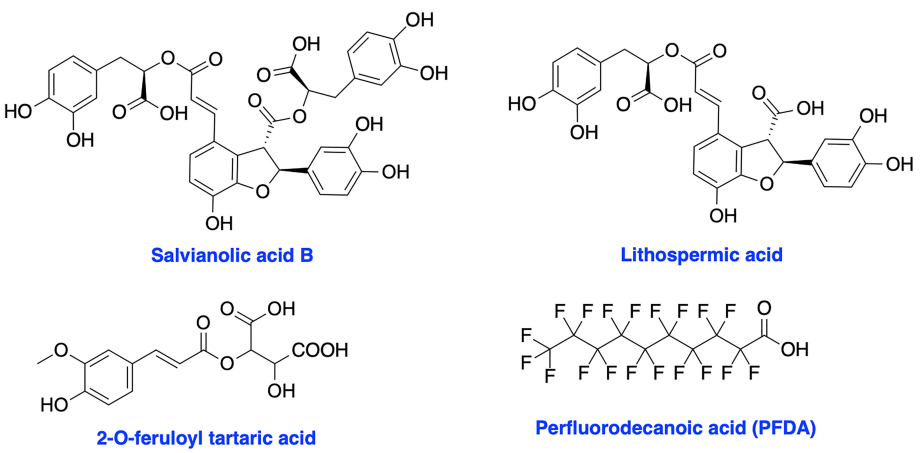

FIGURE 7 | Structures of XRCC4 inhibitors.

repair of the damaged sequence without loss of genetic information. The DSB recognition and DNA end resection are mediated by MRE11-RAD50-NBS1 (MRN) complex which further recruits and activates ATM kinase immediately after detection of DSB. Simultaneously, RPA mediates the recruitment of ATR/ATRIP (11, 119–121). An additional oncogenic role of the MRN complex involves promoting telomere lengthening *via* alternative telomere lengthening (ALT) by homologous recombination (122, 123). In this case, the chromosomal ends are first resected 5'→3' and then treated as broken ends for HDR. Additional mechanistic insight into HDR in response to telomeric DSBs and telomere lengthening has recently been reported (124).

The crucial role of the MRN complex in DSB repair and its potential as a target for cancer therapy has been widely explored in various types of cancers. The high-level expression of MRN complex is associated with chemo- and radio-resistance in breast cancer, glioblastoma and NSCLC as well as correlated with worse disease-free (DFS) and poor overall survival (OS) in rectal, prostate, gastric and NSCLC patients. However, the consequences of defects and/or altered expression level of MRN complex are still controversial with respect to its dual roles in tumorigenesis and prognosis (125–128).

Initial attempts to inhibit MRE11 resulted in Mirin as the first MRE11 inhibitor from high-throughput screening (HTS). Mirin blocks Mre11 exonuclease activity, prevents MRN-dependent ATM activation without affecting its kinase activity and abolishes the G2/M checkpoint and homology-dependent repair in mammalian cells (129). Mirin displayed inhibition of androgen-dependent transcription and growth of prostate cancer cells, MYCN-amplified neuroblastoma cells and enhanced chemosensitivity to DNA damaging agents in glioblastoma cells (130–132). Further structural modification of Mirin resulted in PFM01 and PFM03 as selective endonuclease inhibitors and PFM39 which selectively block the exonuclease activity of MRE11 (**Figure 8**), while their potential function in cancer therapy remains poorly explored (133). Further mechanistic studies revealed MRE11 exo- or endonuclease inhibitors confer distinct DSB repair mechanisms. Inhibition of endonuclease activity of MRE11 drives the cell to NHEJ repair pathway over HDR, while blocking the exonuclease activity of MRE11 results in a repair defect. These studies demonstrate the potential impact of targeting MRN complex for cancer therapy; however, the lack of HDR specificity and the broad spectrum of activity restricted further development of these inhibitors.

To date, there is no inhibitor developed targeting RAD50 and NBS1 despite their crucial role in MRN complex mediated repair pathway and targeting protein-protein interactions in the MRN complex could also provide a potential chemotherapeutic strategy.

RPA Inhibitors

Replication protein A (RPA) is the major human single stranded DNA (ssDNA)-binding protein and plays critical roles in a variety of DNA metabolic pathways including DNA replication, repair, recombination, checkpoint activation and DDR. RPA interacts with several functional proteins to regulate DNA metabolism for the maintenance of genomic stability. RPA's integral and non-redundant roles in both nucleotide excision repair (NER) and homology directed repair (HDR) DNA repair pathways have been well studied. Beyond NER and HDR, RPA is involved in the process of replication fork reversal and other DNA maintenance pathways such as DNA mismatch repair (MMR) and base excision repair (BER) (134–137). In NER, the recognition and verification of bulky adduct DNA damage requires RPA in conjunction with XPA while in HDR, RPA ssDNA-binding activity is required to promote RAD51 filament formation in preparation for strand invasion. RPA binding drives a chain of cooperative events that results in the recruitment of HDR repair proteins (including BRCA1 and BRCA2) at the site of DSB DNA damage. RPA acts as a key sensor to elicit cell cycle arrests at checkpoints and potentiate the activation of the ATR kinase mediated DNA damage signaling/DDR by following cellular exposure to genotoxic stresses (135, 138). Each of these roles requires binding of RPA to ssDNA, making the RPA-ssDNA interaction a promising target for cancer therapy. RPA has been shown to be over-expressed in several cancers including lung, ovarian, breast, colon, bladder, gastric, hepatic, and esophageal and these solid tumors may rely on RPA to mitigate the replication stress associated with these cancers (135, 139, 140).

RPA is a heterotrimeric complex consisting of 70 kDa (RPA70), 32 kDa (RPA32), and 14 kDa (RPA14) subunits (141). The 70 kDa subunit contains the two major high affinity ssDNA binding domains A and B, in addition to domains C and F. The F-domain located on the N-terminal of the 70 kDa subunit (RPA70N) of RPA does not bind ssDNA with high affinity; however, it is involved in a series of protein–protein interactions. The development of small molecule inhibitors of RPA has been pursued by either targeting the (i) N-terminal region of the 70 kDa subunit (RPA70N) to disrupt its interactions with key DDR proteins or (ii) the DNA-binding A and B domains of RPA to prevent binding of ssDNA. Early attempts to develop N-terminal RPA70N targeted inhibitors resulted in NSC15520 (Fumaropimaric acid, FPA) and HAMNO (**Figure 9**); however, their further progress is restricted due to limited cellular uptake, specificity, or metabolic instability (142–144). Fesik and co-workers exploited fragment-based NMR, HTS screening approaches, and further structure-based optimization efforts which led to the discovery of nanomolar or sub micromolar stapled helix peptides, thiazolothienopyrimidinone- (VU079104), anthranilic acid-, chlorobenzothiophene-, pyrazole-based inhibitors targeting RPA70-N-terminal domain (62, 137, 145). High binding affinity, good *in vitro* potency and cellular uptake observed with some of these inhibitors suggest potential for further development, albeit neither cellular activity nor specificity is documented to date.

Recent advances in the development of inhibitors targeting protein-DNA interactions hold considerable promise and opened an entirely new class of 'druggable' targets for therapeutic intervention. Earlier, we identified isoborneol haloacetate MCI13E and MCI13F as potent RPA inhibitors

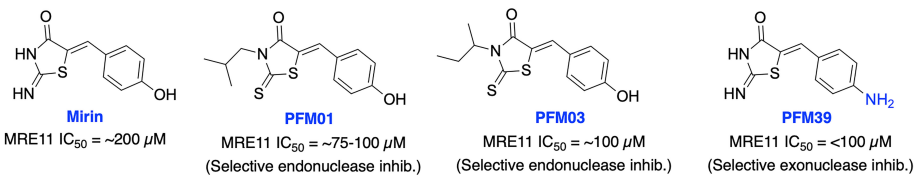

FIGURE 8 | Small molecule inhibitors targeting MRE11 with their respective IC50 values for inhibition of nuclease activity.

and biochemical analysis revealed an irreversible mechanism of inhibition involving covalent modification of RPA with these inhibitors. MCI13E showed cytotoxicity, induced apoptosis and demonstrated synergy with cisplatin in lung cancer cell line models (62, 146). Toward identifying reversible inhibitors of the RPA-DNA interactions, we identified TDRL-505 through HTS screening using a fluorescence polarization-based assay (147, 148). Further SAR studies with TDRL-505 scaffold generated several analogs and among them TDRL-551 was identified as the most potent compound (149). This proof-of-concept study identified that both inhibitors were capable of blocking the RPA-DNA interaction, resulting in cell cycle arrest, cytotoxicity, and increased the efficacy of the chemotherapeutic drugs cisplatin and etoposide *in vitro*. Moreover, TDRL-551 displays modest single agent activity in lung and ovarian cancer cell lines and synergy in combination with cisplatin and etoposide. Recently, we performed systematic structural modification of TDRL-551 in our laboratory by utilizing a structure-based drug design strategy and identified a series of novel chemical inhibitors (43/NERx-329, 44/NERx-2004 and 45-46) with improved RPA inhibitory potency, solubility, and cellular uptake for preclinical settings (150). Moreover, NERx-329 exhibited single agent activity in a broad spectrum of cancer cells, synergism with DNA damaging agents (cisplatin, etoposide and bleomycin) and DDR inhibitors (BMN673, NU7441 and VE821) in lung cancer cells and single agent anticancer activity in lung cancer xenograft models. DNA fiber analysis showed degradation of replication forks upon stalling and RPA exhaustion by NERx-329 and other known DDR inhibitors (151). Overall, a multifaceted role of RPA mediated DNA damage repair through NER, DSB repair through HDR, DNA damage signaling/DDR, replication fork dynamics and its interaction with other proteins holds the potential to fine tune the pathway and it's response to chemotherapy or radiotherapy induced DNA damage toward maximizing efficacy, overcoming resistance, and reducing the toxicities associated with existing cancer therapeutics.

RAD51 Inhibitors

RAD51 is essential for promoting the HDR pathway as RAD51 binds to ssDNA by displacing RPA with the help of BRCA2 and other accessory factors to allow homology search and strand invasion.

Both RAD51 and RPA also are essential regulators of replication forks stability including in regulating fork restart and reversal through management of ssDNA. RAD51 and RPA function early in the processing of stalled forks, before the formation of a DSB, to facilitate fork reversal and protection that help maintain genome stability during DNA replication (152, 153, 136). RAD51 overexpression is observed in several cancers, including pancreatic, soft tissue sarcoma, breast, NSCLC, prostate cancer, glioblastoma and leukemia (152). Overexpression of RAD51 enhanced DNA repair HDR activity and helps cancer cells to survive and develop resistance to DNA damaging agents (154, 155). Depletion of RAD51 expression or inhibition heightened sensitivity to DSB inducing agents including IR in various cancer cells. Therefore, developing RAD51 inhibitors could lead to persistent DNA damage, G2/M arrest, apoptosis in the cancer cells and overcome resistance associated with current DSB inducing agents. Additionally, making HDR-proficient tumor cells HR-deficient by inhibiting RAD51 could prove useful in restoring synthetic lethality in tumors that have developed resistance with PARP inhibitors (PARPi).

Currently, several RAD51 inhibitors have been developed to further exploit the HDR pathway as a therapeutic target for cancer therapy. RAD51 has been explored as a pharmacological target in two different ways, first, in cancers known to overexpress RAD51, compounds with single-agent activity have been described that exploit overexpression by inducing formation of toxic RAD51 complexes on undamaged DNA. The second of which is as a component of combination therapy where disruption of RAD51's ssDNA binding activity synergizes DNA damaging therapies. Ishida et al. identified DIDS as a competitive RAD51 inhibitor that prevents RAD51-ssDNA and RAD51-dsDNA binding, RAD51-mediated strand exchange and homologous pairing (**Figure 10**). However, the elevated human cell toxicity of DIDS has restricted its further development (156). A natural compound, halenaquinone was identified through an extensive screen of marine sponge extracts which directly inhibit RAD51-dsDNA binding, but it does not alter RAD51 affinity for ssDNA (157). Furthermore, halenaquinone-treated cells showed a reduction of IR induced RAD51 foci formation at DSB sites probably by preventing the DNA homologous pairing step of the HDR pathway. Chloromaleimide derivative RI-1 was identified as a potent RAD51 inhibitor and its biochemical analysis revealed an irreversible mechanism of inhibition involving covalent modification of the thiol group on the C319 residue of human RAD51 (158). In order to avoid off-target effects associated with covalent inhibitors and improve metabolic stability of the compound in biological systems, the reversible

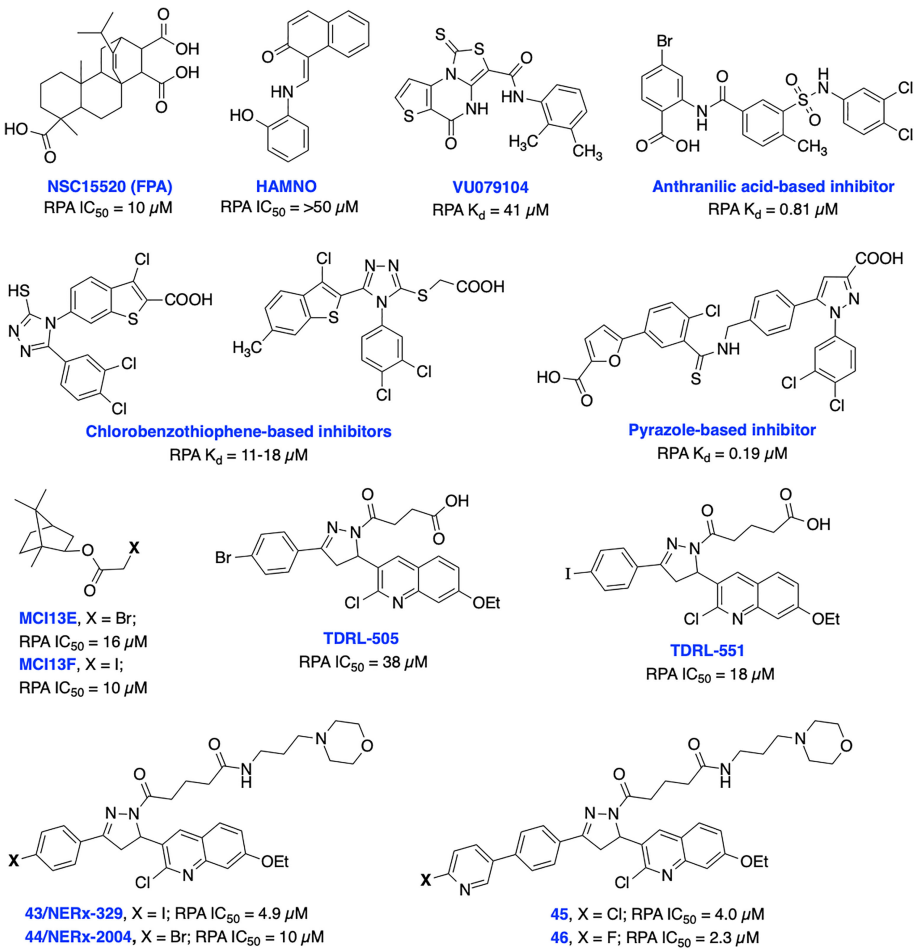

FIGURE 9 | Small molecule inhibitors targeting RPA N-terminal protein-protein interactions and RPA-DNA interactions with their respective Kd/IC50 values.

RAD51 inhibitor RI-2 was developed by introducing an aromatic ring at maleimide ring. RI-2 displayed a 6-fold decrease in potency compared to RI-1 and specifically inhibited HDR efficiency and sensitize human cancer cells to mitomycin C (MMC)-induced synthetic lethality (159).

The small molecule RS-1 was developed as an allosteric effector to exploit overexpression of RAD51 activity by further stimulating the formation of toxic RAD51 complexes on undamaged chromatin as a potential cancer therapy (160, 161). RS-1 was able to stimulate binding of RAD51 to ssDNA and dsDNA and enhanced recombination activities of RAD51 by locking its active conformation, without affecting ATP hydrolysis. RS-1 demonstrated a single agent activity in tumor cell lines which have more ssDNA due to increased replication, that leads to cytotoxicity while sparing normal cells (162). RS-1 also showed significant anticancer activity in a prostate cancer xenograft animal model (161). RS-1 exhibited inconsistent HDR efficiency in CRISPR/Cas9 precision genome editing in various other organisms and cell types (163, 164), suggesting that either different species may respond differently, or RAD51 may not be the most reliable target for improving precision genome engineering applications. Mazin and co-workers identified B02 as a highly specific RAD51 inhibitor that directly binds to RAD51, increases sensitivity to IR and several DNA damaging agents including etoposide and doxorubicin by inducing DSBs and subsequent blocking of HDR repair (154, 165, 166). Recently, they have carried out further structural analysis of B02 and identified B02-iso and *p*-I-B02-iso as substantially stronger inhibitors of RAD51 and HDR than the parent compound. B02-iso significantly increased the sensitivity of BRCA-proficient triple-negative breast cancer (TNBC) MDA-MB-231 cells to the PARPi, olaparib through synthetic lethality (167).

Zhu et al. targeted protein–protein interaction sites of RAD51 by developing IBR2 which disrupts the RAD51-BRCA interaction and RAD51 multimerization and enhances proteasomal degradation of RAD51 (168). Further structural optimization of IBR2 generated the stereo selective inhibitor IBR20 which also disrupts RAD51 multimerization, impairs HDR activity and increases cytotoxic activity in a variety of

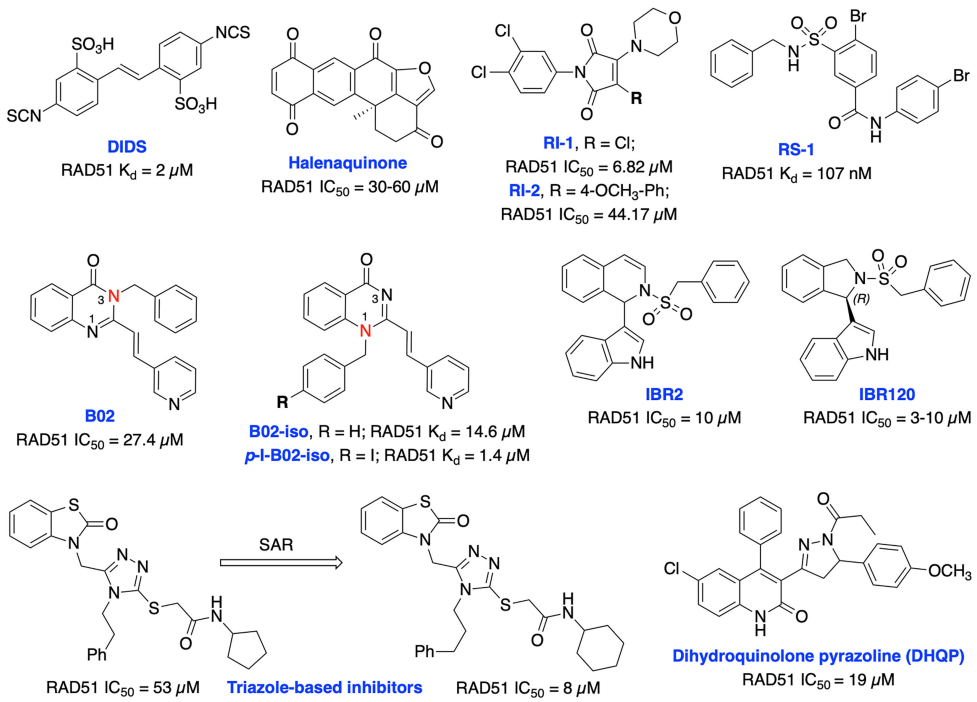

FIGURE 10 | Small molecule inhibitors targeting RAD51 with their respective Kd/IC50 values for either disruption of RAD51 binding or RAD51 mediated D-loop formation.

cancer cell lines (169). Utilizing high throughput docking and further SAR optimization, Cavalli and co-workers identified a series of triazoles that mimic BRCA2 mutations by disrupting the RAD51-BRCA2 interaction. Further, these compounds inhibited DSB repair and exhibited synergy with olaparib in pancreatic cancer cells with functional BRCA2 (170, 171). Recently, the same research group identified a dihydroquinolone pyrazoline (DHQP)-based inhibitor which also disrupted the RAD51-BRCA2 interaction, inhibited HDR activity and showed synergy with olaparib in pancreatic cancer to trigger synthetic lethality (172). However, further structural optimization is needed to improve potency, solubility, cytotoxicity and true synthetic lethality outcome of both triazole- and DHQP-based inhibitors. The fatty acid nitroalkene 10-nitro-octadec-9-enoic acid (OA-NO_2) inhibited RAD51-ABL1 complex formation by alkylating RAD51 Cys-319 residue and decreased HDR activity. It also increased the sensitivity of doxorubicin, olaparib, IR and cisplatin in TNBC cells (68, 173). CYT01B and CYT-0851 (structures are not disclosed), are orally bioavailable small molecule RAD51 inhibitors, being developed by Cyteir Therapeutics. Both inhibitors blocked HDR activity and have demonstrated anticancer activity in cells expressing activation-induced cytidine deaminase (AID), a protein that promotes formation of DSBs. Preclinical data showed synergy with PARP and ATR inhibitors in various models, suggesting these inhibitors have the ability to overcome resistance of PARPi (174, 175). CYT-0851 is currently in Phase 1/2 clinical trials demonstrated promising antitumor activity *in vitro* and *in vivo* models across different tumor types including both hematologic malignancies and solid tumors (NCT03997968, https://clinicaltrials.gov/ct2/show/NCT03997968).

The development of either RAD51 inhibitors or modulators can be safe and effective for clinical use and it is an exciting approach for cancer therapy.

INHIBITORS TARGETING SSA AND ALT-NHEJ (TMEJ) PATHWAYS

SSA is a RAD51-independent DSB repair pathway which joins two homologous repetitive sequences oriented in the same direction through annealing. SSA shares DNA end resection and RPA displacement steps with HDR to reveal complementary homologous sequences. RAD52 is the central protein for SSA which is recruited to anneal each ssDNA with two repetitive sequences. After the annealing step, the sequences between the homologous repeats are flanked out on either side. These flanked ends are then cleaved off by nucleases, preferentially by ERCC1/XPF endonuclease and finally the ssDNA gap is closed by ligation (11, 176).

Alt-NHEJ (MMEJ/TMEJ) utilizes short microhomologies to join the two DNA strands. PARP1 is involved in promoting DNA end synapsis and recruiting the DNA polymerase θ (Pol θ) to DSB ends. Pol θ eventually stabilizes microhomology-mediated joints between the two DNA ends and flaps

extending from these joints are cleaved off by either ERCC1-XPF or Flap endonuclease 1 (FEN1), followed by a ligation step (5). However, both SSA and alt-NHEJ DSB repair pathways serve primarily as backup pathways in mammalian cells which are deficient of either NHEJ or HDR pathways.

RAD52 Inhibitors

RAD52 plays essential roles in homology dependent DSB repair. RAD52 binds to ssDNA, promotes DNA annealing in the SSA pathway while it interacts with RAD51 to modulate its DNA strand-exchange activity in the HDR pathway. In addition, RAD52 protects stalled replication forks from degradation (177–180). RAD52-mediated annealing of large regions of a homologous sequence, independent of RAD51-mediated strand invasion is key for the SSA (181). The N-terminal region of RAD52 is involved in the oligomeric ring formation leading to RAD52-ssDNA binding (182). The ring structure is crucial during different repair pathways by promoting annealing of complementary DNA strands. RAD52 also has a second DNA binding site that binds to dsDNA (183). Several studies demonstrated that unlike normal cells, RAD52 is required for the survival of cancer cells with loss-of-function mutation in genes such as BRCA1, BRCA2, PALB2, and RAD51 paralogs (184–186). Therefore, this differential effect facilitates RAD52 as a promising target to trigger synthetic lethality in BRCA-deficient tumor cells without affecting normal cells.

To date, there have been several RAD52 inhibitors identified by various research groups (**Figure 11**) (179). Chandramouly et al. identified 6-OH-DOPA as a specific inhibitor to RAD52 ring structure formation through HTS. Notably, 6-OH-DOPA disrupts the heptamer and undecamer ring of truncated RAD52 (residues 1-209) into dimers (187), leading to abolished recruitment of RAD52 to ssDNA damage sites. 6-OH DOPA disrupted the association of ssDNA with RAD52 and consistently inhibited SSA in cells while having a minimal effect on HR and NHEJ in BRCA-proficient cells while increased level of apoptosis and DNA damage observed in BRCA1/2-deficient cells. In addition, 6-OH DOPA selectively halted proliferation of BRCA1/2 deficient TNBC cells, pancreatic cancer cells and patient-derived AML and CML cells. Another study reported Adenosine 5'-monophosphate (A5MP), its mimics 5-aminoimidazole-4-carboxamide ribonucleotide (AICAR) and 5' phosphate (ZMP) as RAD52 inhibitors through virtual computer screening of FDA and NCI drug libraries (188). All three inhibitors inhibited RAD52-ssDNA binding, while cell permeable AICAR disrupted SSA repair and reduced cisplatin-induced RAD52-ssDNA foci formation in BRCA1-deficient leukemic cells. Both A5MP and AICAR exerted anti-tumor activity against BRCA-deficient cancer cells by triggering synthetic lethality. Huang et al. identified 17 putative inhibitors of RAD52 through HTS. Among these, D-G09 and D-I03 showed exquisite selectivity against RAD51 and anticancer activity in BRCA1/2 deficient pancreas, ovarian, and TNBC cells with no effect in BRCA1/2 proficient cells (189). Further biochemical studies confirmed that both inhibitors bind directly to RAD52, impairs its ssDNA-annealing activity and DNA pairing activity of RAD52 (D-loop formation) in the sub-micromolar range. D-I03 showed no significant effect on cisplatin-induced RAD51 foci formation although this compound significantly reduced level of SSA repair without influencing HDR indicating specific targeting of RAD52. In addition, structurally distinct compounds, D-G23, D-I05 and D-K17 also inhibited RAD52 ssDNA annealing, DNA pairing activities of RAD52 and preferentially inhibited at least two BRCA1/2-defficient cell lines.

Li et al. identified several RAD52 inhibitors through virtual HTS and docking studies with top compounds F779-0434 and C791-0064 inhibiting RAD52-ssDNA association and disrupting single strand annealing activity of RAD52, respectively and inducing synthetic lethality by suppressing the proliferation of BRCA2-deficient cancer cells at high concentrations (190, 191). Hengel et al. identified natural products (−)-epigallocatechin, epigallocatechin-3-monogallate and NP-004255 (RAD52 IC_{50s} = 1.8, 0.277 and 1.5 μM, respectively) as potent inhibitors of RAD52 by utilizing HTS and FRET-based assays. Both (−)-epigallocatechin and epigallocatechin-3-monogallate inhibited DSB repair and significantly reduced proliferation of BRCA2 and MUS81 deficient cells under conditions of replication stress (192).

While clearly in the developmental stages, each of the RAD52 inhibitors could offer potential for further development of effective treatment to improve therapeutic outcome of BRCA deficient malignancies in combination with PARPi.

ERCC1-XPF Inhibitors

The structure-specific heterodimeric endonuclease ERCC1-XPF complex is primarily involved in NER but has roles in SSA and alt-NHEJ mediated DSB repair as well as interstrand cross-link (ICL) repair pathways due to its unique catalytic incision properties (193, 194). ERCC1 regulates DNA-protein and protein-protein interactions and is catalytically inactive while XPF which contains an inactive helicase-like motif, is involved in protein-protein interactions and DNA binding, and provides the endonuclease activity. The overexpression of ERCC1-XPF has been linked with poor responses to chemotherapy in various cancers including NSCLC, squamous cell carcinoma, ovarian cancer and melanoma while low ERCC1-XPF expression observed in testicular cancer has extended overall survival of cancer patients (195, 196). Further, ERCC1 deficient melanoma cells exhibited around 10-fold more sensitivity to cisplatin than ERCC1-proficient cells and in a xenograft mouse model as well (197). ERCC1-XPF became an interesting target to investigate in order to overcome resistance to chemotherapeutic agents due to its involvement in multiple key repair pathways.

The heterodimerization and localization of ERCC1 and XPF is required to constitute a functional and stable complex and essential for endonuclease activity. ERCC1-XPF interaction through their double helix–hairpin–helix (HhH2) domains is an essential requirement to stabilize ERCC1-XPF complex to promote catalytic activity (198, 199). Therefore, several research groups are targeting ERCC1-XPF HhH2 domain protein-protein interaction to develop novel inhibitors to increase sensitivity of existing therapies whose DNA-damaging effects are primarily repaired by ERCC1-XPF-dependent pathways.

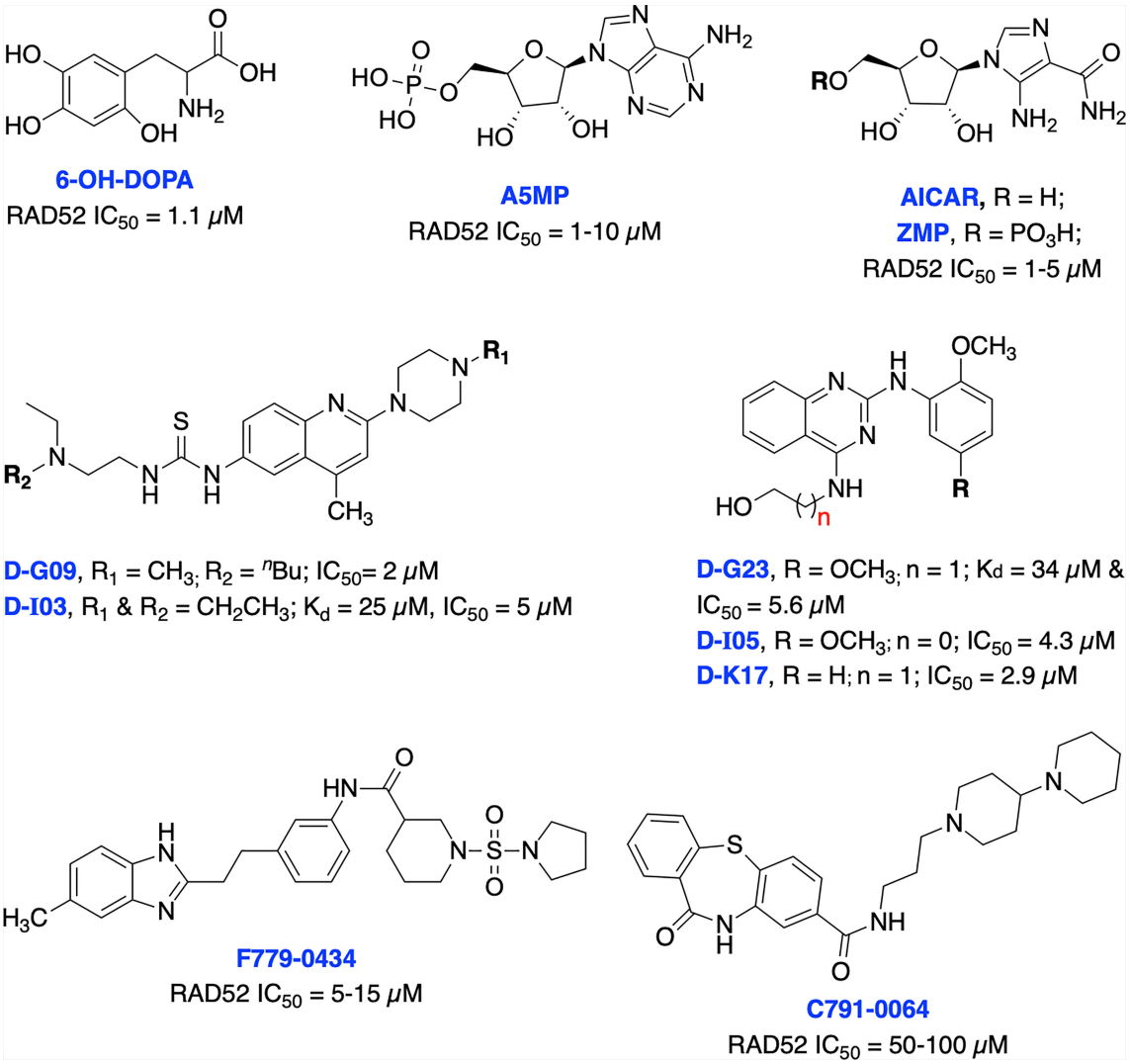

FIGURE 11 | Small molecule inhibitors targeting RAD52 with their respective Kd/IC50 values for either RAD52 binding or ssDNA annealing activity.

Jordheim et al. identified F06/NERI02 (NSC130813) through *in silico* screening, as a small molecule inhibitor targeting ERCC1-XPF heterodimerization and demonstrated modest affinity for XPF and sensitized cancer cells to MMC and cisplatin (**Figure 12**) (200). In addition, F06 exhibited a synergy with PARPi olaparib in BRCA1-deficient breast cancer cells. However, suboptimal potency, toxicity and off-target effects of F06 restricted further biochemical and cellular studies (62). Recently, West and co-workers rationally modified the structure of F06 by utilizing computer-aided drug design (CADD) to identify potential binding interactions and further SAR studies to improve inhibition of ERCC1-XPF endonuclease activity. The lead compounds B5/B9 and compound 4 showed 3-fold improvement in inhibition activity compared to F06. The sensitivity to UV radiation and cyclophosphamide also increased significantly in reducing proliferation of metastatic colorectal cancer (201–203). Moreover, compound 4 showed lower lipophilicity and greater metabolic stability which makes this compound an interesting candidate for further advancement. McNeil et al. targeted three sites of the ERCC1-XPF HhH2 domain to identify possible inhibitors for the heterodimer by utilizing an *in silico* screening approach (204). They identified E–X AS7 which binds to ERCC1-XPF through a metal-based interaction, inhibits NER in low micromolar concentrations and specifically increases the cisplatin sensitivity of NER-proficient human and mouse cells. E-X PPI2 inhibited the NER activity in melanoma cells, showed marginal sensitivity to cisplatin treatment but caused significant reduction in the level of ERCC1-XPF heterodimer levels in ovarian cancer cells. However, the medium-high micromolar range binding affinity (Kd) and inhibitory potency (IC_{50}) makes these compounds unsuitable for further studies. A

series of highly potent and selective catechols, hydroxylimides/hydroxy pyrimidinones have been identified as ERCC1-XPF inhibitors through *in silico* HTS and SAR approach (205, 206). Most of the compounds from these series showed good selectivity for ERCC1-XPF against FEN-1 and DNase I; however, potential *in vitro* and *in vivo* effects of these compounds are not documented yet. Patrick and co-workers targeted the active site on the XPF nuclease domain and identified NSC16168 as a potent ERCC1-XPF inhibitor by performing a HTS using the NCI-DTP (National Cancer Institute Developmental Therapeutics Program) diversity database. NSC16168 significantly enhanced cisplatin antitumor activity in a lung cancer xenograft model (207).

Overall efforts resulted in several potent ERCC1-XPF endonuclease inhibitors which are capable to diminish NER activity and enhance the cytotoxicity of platinum-based chemotherapeutics although these inhibitors are not explored in targeting DSB repair and its defects for cancer therapy. Moreover, the lack of structural insights, selectivity against other endonucleases and most importantly limited utilization of these inhibitors in targeting DSB repair restricts their further advancement into the clinic.

DNA Polymerase Theta (Pol θ) Inhibitors

Pol θ (*gene* name, *PolQ*) belongs to the error-prone A family of DNA polymerases and is a critical component of the alt-NHEJ (MMEJ or TMEJ) repair pathway of resected DSBs. Biochemical and mechanistic studies have shown that the helicase domain of Pol θ displaces RPA bound to the ssDNA overhang and facilitates joining of short microhomologies to the two DNA strands that flank a DSB. The polymerase domain of Pol θ initiates DNA synthesis to fill in the DNA gaps, prior to the ligation step employed by DNA Ligase I or III. In addition, Pol θ also plays an important role in joining unprotected telomeres in alt-NHEJ pathway (14, 208–211). Alt-NHEJ serves as an essential backup pathway to repair DSBs when HDR and NHEJ pathways are compromised in cancer cells such as germline *BRCA*-gene deficient cancer cells. Recently, Pol θ emerged as a new promising drug target to trigger the synthetic lethality between loss of the PolQ gene and deficiencies in DSB DNA repair-related tumor suppressor genes including BRCA1/2, ATM and FANCD2 for the treatment of HDR-deficient tumors (212–214). The expression of Pol θ is particularly high in subtypes of breast and ovarian cancers featuring loss of HDR activity and Pol θ-depletion reduced the survival of HR-deficient cancer cells in the presence of PARPi, cisplatin, or MMC (214). Pol θ overexpression also found in other cancers, including stomach, lung and colon (215). In addition, the higher expression of Pol θ is correlated with shorter relapse-free survival compared to patients with relatively lower expression of Pol θ. Feng et al. employed CRISPR-based genetic screening and identified 140 genes that are synthetically lethal with Pol θ, highlighting the impact of Pol θ inhibitor for cancer therapy (216).

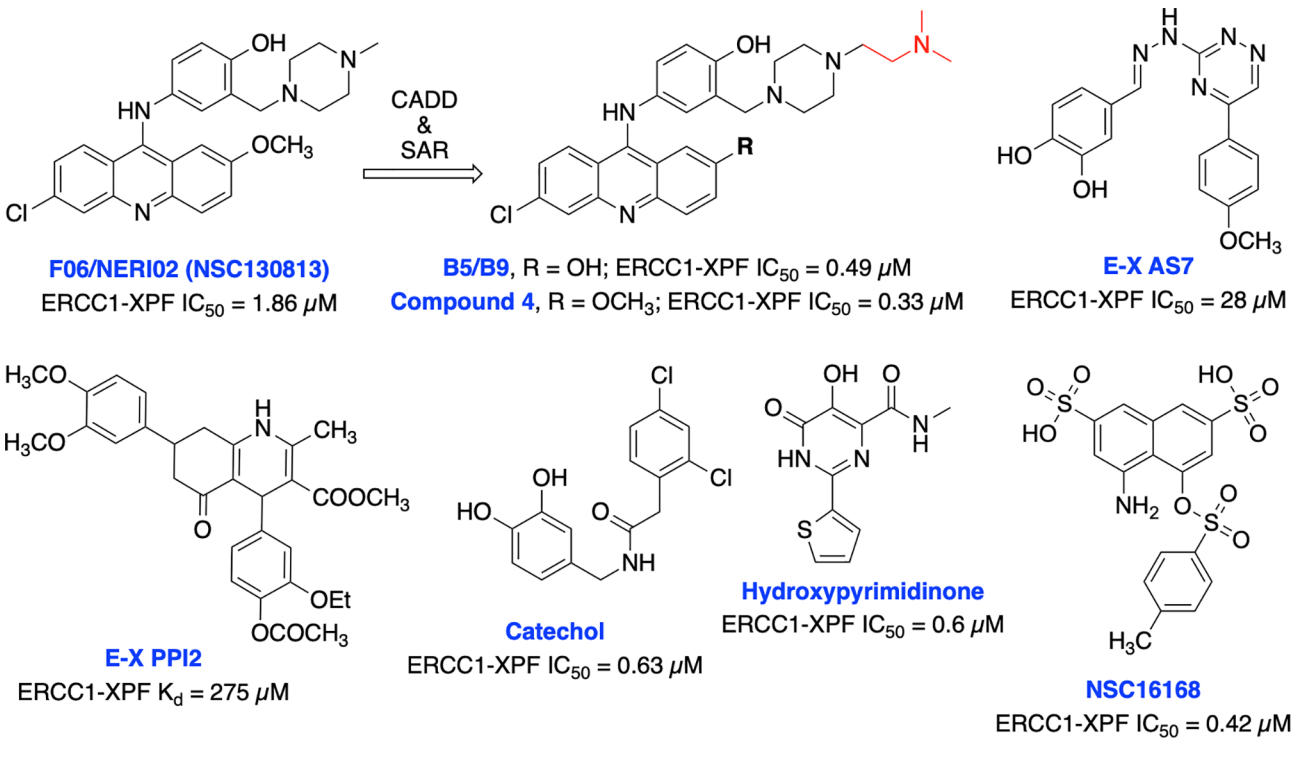

FIGURE 12 | Small molecule inhibitors targeting ERCC1-XPF with their respective Kd/IC50 values for inhibition of ERCC1-XPF endonuclease activity.

Recently, Zhou et al. identified antibiotic novobiocin (NVB) as a specific potent inhibitor of human Pol θ (**Figure 13**) which inhibited alt-NHEJ repair and selectively killed HDR-deficient (both BRCA1- and BRCA2-deficient) cells over wild-type cells and significantly enhanced the cytotoxic effect of PARPi in HDR-deficient tumor cells in cellular as well as in xenograft and PDX mouse models (217). Most importantly NVB also killed HDR-deficient, PARPi-resistant tumor cells. Artios Pharma in collaboration with the Institute of Cancer Research (UK) identified ART558 as a highly potent and specific small molecule Pol θ inhibitor (213). ART558 exhibited not only *BRCA*-gene synthetic lethality, but also targets cells with PARPi resistance caused by defects in 53BP1/Shieldin DNA repair complex. There is a possibility that Pol θ inhibitors might be a more suitable treatment option than PARPi for combination with existing DNA-damaging chemotherapies. Several biopharmaceutical companies are currently pursuing Pol θ as a therapeutic target and the first orally bioavailable Pol θ inhibitor ART4215 (structure is not disclosed) is currently in Phase 1/2 clinical trials where it is being investigated as a monotherapy and in combination with PARPi talazoparib in patients with advanced or metastatic solid tumors (NCT04991480, https://clinicaltrials.gov/ct2/show/NCT04991480).

RecQ and MCM Helicases Inhibitors

It is well established that RecQ helicases play an important role in DSB repair and the maintenance of genome stability. However, a direct or passive role of each RecQ helicase's enzymatic activity in NHEJ, HDR, TMEJ and SSA mediated DSB repair pathway is yet to be elucidated (43). RecQ proteins are highly conserved from bacteria to humans, and the reduced RecQ helicases activity is associated with cancer predisposition, metastasis and premature aging. In contrast, overexpression of RecQ helicases may promote carcinogenesis and RecQ helicases are highly upregulated in various cancers (218, 219). Aggarwal et al. identified NSC 19630 and NSC 617145 (**Figure 14**) as WRN inhibitors through HTS of the National Cancer Institute (NCI) diversity set of compounds. Both NSC compounds dramatically impaired growth and proliferation, induced apoptosis in a WRN-dependent manner, and DSBs and chromosomal abnormalities in cellular models (220, 221). However, the presence of the maleimide group in both compounds may restrict their further development due to its propensity for non-specific covalent interactions. The same group recently identified several non-specific reversible and irreversible helicase inhibitors through HTS using a larger library of approximately 350,000 small molecules (222). Several studies identified WRN synthetic lethal vulnerability in cancers with microsatellite instability (218, 223, 224), suggesting specific WRN inhibitors hold great potential to target microsatellite instability tumors to enable a clear stratification path in the clinic.

BLM helicase plays a multifaceted role in HDR pathway as it is required for the early phase of the pathway to stimulate resection of DSB ends or displacement of the invading strand of DNA displacement loops as well as at the terminal steps in dissolution of double Holliday junctions (43). Nguyen et al. identified the first BLM inhibitor by utilizing HTS and further structural optimization efforts yielding ML216 and compound 33 as potent inhibitors of the DNA unwinding activity of both BLM and WRN (225, 226). ML216 exhibited cellular induction of sister chromatid exchanges and demonstrated selective antiproliferative activity in BLM-positive cells but not those lacking BLM. However, further preclinical studies may be restricted due to poor selectivity, solubility, and cell permeability of these inhibitors. Recently, Yin et al. identified isaindigotone derivatives as novel BLM helicase inhibitors that disrupted the recruitment of BLM at DNA DSB sites. BLM inhibition by their lead compound promoted accumulation of RAD51, regulated HDR repair, and synergized cytotoxicity of cisplatin and the RAD51 inhibitor, RI-1 (227). BLM and other helicases are attractive targets for the development of cancer therapeutics which rely on synthetic lethality effects for targeting tumors with preexisting DNA repair deficiencies. Minichromosome maintenance (MCM) complex is a family of six proteins 2-7 (MCM2-7) that are activated by forming a holo-helicase CMG complex with Cdc45 and the hetero-tetrameric GINS complex (Cdc45-MCM2-7-GINS). CMG complex is cell-cycle regulated and responsible for unwinding DNA forks during DNA replication. MCM2-7 proteins have essential roles in DNA replication particularly under replicative stress where they activate dormant replication origins which allows for continued genome replication in spite of replication stress. Increased levels of MCM2-7 protein expression have been observed in a variety of cancers (39, 42). Initially, Simon et al. identified ciprofloxacin which preferentially inhibits MCM2-7 at higher concentrations than its normal therapeutic range (228). However, most recently inhibition of MCM2-7 activity by ciprofloxacin significantly delayed neuroendocrine prostate cancer (NEPC) cell growth and migration *in vitro*, exhibited potent anti-tumor effects in an NEPC xenograft model, and partially reversed neuroendocrine features (229). Alshahrani et al. identified UEFS99, UEFS137 and UEFS428 as MCM7 inhibitors from the natural compounds databases using *in silico* computational screening, however further *in vitro* and *in vivo* studies are needed to validate target engagement (230). A furanonaphthoquinone-based small molecule, AS4583 was identified as an MCM2 inhibitor through phenotypic screening and target deconvolution (231). Further mechanistic studies revealed that AS4583 inhibited cell-cycle progression and reduced DNA replication by inducing proteasomal degradation of MCM complex which ultimately contributed to the death of NSCLC cells. Subsequently, structural optimization of AS4583 led to compound RJ-LC-07-48 which showed greater potency in drug-resistant NSCLC cells and in mice bearing H1975 tumor xenografts. Overall, MCM complex can serve as a potential target for cancer therapy. Further exploration of design, screening and medicinal chemistry efforts are needed to develop MCM2-7 complex-specific inhibitors for better clinical outcomes.

DSB REPAIR INHIBITORS FOR COMBINATION THERAPY, INDUCTION OF SYNTHETIC LETHALITY AND PRECISION GENOME EDITING

While there remain no FDA approved inhibitors of non-PIKKs within the DSB repair pathways, the future applications of such

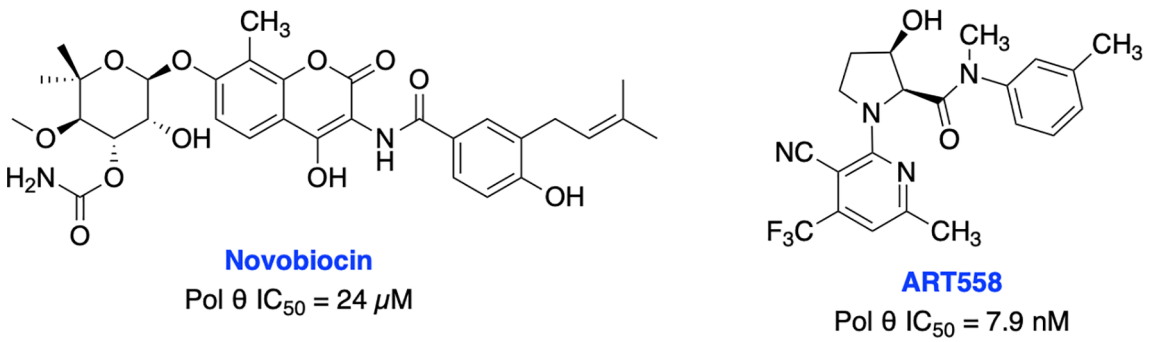

FIGURE 13 | Small molecule inhibitors targeting Pol θ with their respective IC50 values for inhibition of polymerase activity.

compounds may include use within combination chemotherapy regimens, as chemo- or radiosensitizers, induction of synthetic lethality in HDR-deficient cancer subtypes, and as an adjuvant therapy in precision genome editing. As described in the above corresponding sections, each of the non-PIKK pharmacological targets, whether involve directly or indirectly mediate repair of DSBs induced by either DNA damaging agents or IR, and combination therapy with either DNA damaging agents or IR has been the natural step towards maximizing synergistic efficacy, overcoming resistance, and reducing the toxicities associated with existing chemo- and radiotherapy. Provided that the preponderance of cancer patients receives DNA-damaging drugs or IR and later experience disease progression, the therapeutic potential for agents that augment the response to such therapies is large.

Synthetic lethality refers to any scenario whereby loss of two gene products produces cellular death, but loss of either individually is non-lethal. In the setting of cancer treatment, synthetic lethality is a term usually used in reference to disruption of the repair of DNA nicks in HDR-deficient cancers which yields DSBs that are repaired by error-prone pathways resulting in cell death or senescence (232). The clinically available PARP inhibitors (PARPis) olaparib, rucaparib, talazoparib, and niraparib operate by this mechanism and are frequently employed in cancers where HDR-deficiency is conferred by BRCA mutations. PARPis remain the sole class of approved anticancer drugs capable of exploiting this unique vulnerability. However, more than 40% patients with BRCA mutations fail to respond to PARPis and resistance mechanisms have been described indicating new classes of medications capable of inducing synthetic lethality are needed (233). Two particularly noteworthy non-PIKKs targets within the DSB repair pathways whose inhibition have been probed for synthetic lethality in the setting of PARPi resistance include DNA polymerase θ and RAD52. The activity of DNA polymerase θ offers an escape pathway beyond NHEJ *via* alt-NHEJ in the setting of BRCA

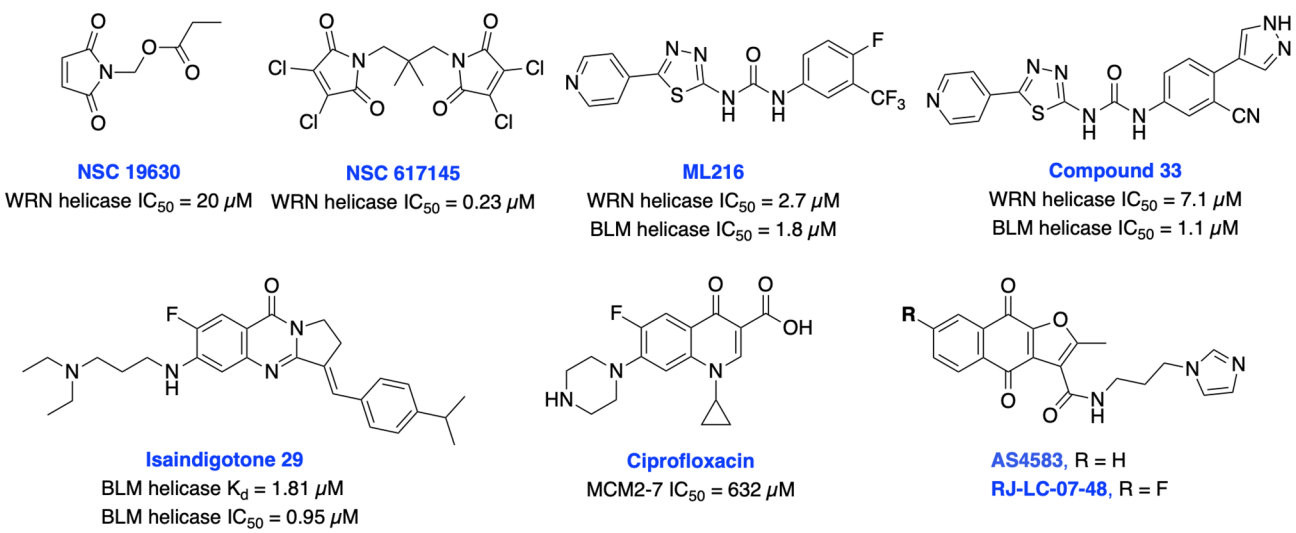

FIGURE 14 | Small molecule inhibitors targeting WRN, BLM and MCM helicases with their respective IC_{50} values.

mutations (70, 208). An siRNA knockdown of DNA polymerase θ produces synthetic lethality in BRCA2 mutation variants (214) and the aforementioned DNA polymerase θ inhibitor ART558 retains preclinical efficacy even in the presence of 53bp1 mutations which are known to confer PARPi resistance (213). The RAD52 deficiency leads to loss of a compensatory DNA repair pathway resulting in genomic instability and persistent cell death in BRCA1/2-deficient cells. Intriguingly, RAD52 is thought to be capable of orchestrating HDR even in BRCA1/2 mutants and thus may also play a role in PARPi resistance. Targeting RAD52 for the induction of synthetic lethality could potentially improve the therapeutic outcome of BRCA-deficient malignancies treated with PARPi and restrict the emergence of drug-induced toxicity to normal tissues (179, 208).

CRISPR-Cas9 genome editing offers the possibility to prevent, treat, or even cure human diseases that are initiated by or maintained by genetic aberrations (234). Notwithstanding other barriers to the clinical application of CRISPR-Cas9 for genome editing such as selective delivery and the requirement for protospacer adjacent motifs (PAM) at the targeted region of a locus, a major challenge this platform faces is management of the DSBs created both on-target and off-target (235, 236). Provided that HDR is only available in the G2/S phases of the cell cycle because of the requirement for a sister chromatid, the predominant NHEJ pathway must be regulated in precision genome editing to preempt chromosomal rearrangements and large indels. DNA DSB repair inhibitors could help in enhancing precision genome editing as well as improving the safety of gene targeting. NHEJ inhibitors and HDR modulators can be exploited to increase the current efficiency of nuclease-based HDR mediated gene editing alongside CRISPR towards the more precise HDR mediated repair while decreasing inaccurate integration events. However, specificity, efficacy and toxicity associated with DSB repair inhibitors targeting NHEJ pathway restricted utilization of these inhibitors in CRISPR-Cas9 genome editing (89, 103, 104). Future availability of an arsenal of DSB-repair inhibitors capable of directing DSB repair by HDR will foster the arrival of precision genome editing within clinical practice.

We have summarized a list of targeted proteins and their respective inhibitors, mechanism of their action, binding affinity or *in vitro* potency, indication along with cellular activity and their phase of development in **Table 1**.

CONCLUSIONS

DSBs are the most lethal of all DNA lesions and the cadre of proteins that respond to repair of DSBs represent a diverse array of proteins and enzymes of which a small portion are in fact kinases. Combinational therapy of DSB repair inhibitors with existing DSB inducing agents has been the most effective strategy. Careful consideration of the sequence of combination drug administration and optimizing drug scheduling will likely be needed to optimize synergistic effects of combination therapy while sparing normal cells. DSB repair deficiency and mutation can increase the immunogenicity of cancers and combination of

TABLE 1 | A summary of non-PIKKs DSB Repair inhibitors.

Targeted Protein and Inhibitors	Mechanism of Action and *In vitro* potency	Cellular Activity	Phase of Development
Ku70/80			
STL127705 (Compound L)	• Disrupts Ku-DNA binding activity and inhibits DNA-PK enzymatic activity. Ku IC_{50} = 3.5 μM DNA-PK IC_{50} = 2.5 μM	• Single agent activity and radiosensitivity in glioblastoma and prostate epithelial cancer cells. IC_{50} = 20-35 μM	Pre-Clinical
5102	• Disrupts Ku-DNA binding activity and inhibits DNA-PK enzymatic activity. Ku IC_{50} = ~3.0 μM DNA-PK IC_{50} = ~0.3 μM	NR	Pre-Clinical
5135	• Disrupts Ku-DNA binding activity and inhibits DNA-PK enzymatic activity. Ku IC_{50} = ~2.5 μM DNA-PK IC_{50} = ~0.1 μM	NR	Pre-Clinical
68	• Disrupts Ku-DNA binding activity and inhibits DNA-PK enzymatic activity. Ku IC_{50} = 6.02 μM DNA-PK IC_{50} = 3.1 μM	• Inhibits cellular NHEJ activity. • Potentiates the cellular activity of bleomycin.	Pre-Clinical
149	• Disrupts Ku-DNA binding activity and inhibits DNA-PK enzymatic activity. Inhibits *in vitro* NHEJ. Ku IC_{50} = 3.72 μM DNA-PK IC_{50} = 0.5 μM	• Inhibits cellular NHEJ activity.	Pre-Clinical

(Continued)

TABLE 1 | Continued

Targeted Protein and Inhibitors	Mechanism of Action and *In vitro* potency	Cellular Activity	Phase of Development
322	• Disrupts Ku-DNA binding activity and inhibits DNA-PK enzymatic activity. Ku IC_{50} = 2.66 μM DNA-PK IC_{50} = 0.11 μM	• Inhibits cellular NHEJ activity. • Potentiates the cellular activity of etoposide and IR in lung cancer cells.	Pre-Clinical
245	• Disrupts Ku-DNA binding activity and inhibits DNA-PK enzymatic activity. Ku IC_{50} = 1.99 μM DNA-PK IC_{50} = 0.24 μM	• Inhibits cellular NHEJ activity. • Potentiate the cellular activity of bleomycin and IR in lung cancer cells. • Shows modulation of CRISPR/cas9 mediated gene insertion.	Pre-Clinical
Artemis			
Ebselen	• Interacts with zinc finger motif of Artemis and inhibit its endonuclease activity IC_{50} = 8.5 μM	NR	Pre-Clinical
Disulfiram	• Interacts with zinc finger motif of Artemis and inhibit its endonuclease activity IC_{50} = 10.8 μM	NR	Pre-Clinical
Auranofin	• Interacts with zinc finger motif of Artemis and inhibit its endonuclease activity IC_{50} = 46 μM	NR	Pre-Clinical
Ceftriaxone	• Interacts with zinc finger motif of Artemis and inhibit its endonuclease activity IC_{50} = 65 μM	NR	Pre-Clinical
DNA Ligase IV			
L189	• Binds in DNA-binding pocket of the DBD. • Inhibits DNA ligases I, III, and IV in DNA joining assay. Ligase I IC_{50} = 5 μM, Ligase III IC_{50} = 9 μM, Ligase IV IC_{50} = 5 μM	• Single agent activity and radiosensitivity in colon and breast cancer cells. IC_{50} = 20-35 μM	Pre-Clinical
SCR7-cyclized and SCR7-pyrazine	• Inhibit Ligase IV-mediated end joining and V(D)J recombination. • Blocks NHEJ in a Ligase IV-dependent manner. SCR7-cyclized K_d = 2.35 μM SCR7-pyrazine K_d = 0.5 μM	• Single agent activity in leukemic, cervical, breast cancer cells and radiosensitivity in cervical cancer cells. IC_{50} = 50-250 μM	Pre-Clinical
SCR130	• Inhibits Ligase IV-mediated end joining in concentration dependent manner Ligase IV IC^{50} = NR	• Single agent activity and radiosensitivity in leukemic and cervical cancer cells. IC_{50} = 2-14 μM	Pre-Clinical
MRE11			
Mirin	• Binds in the active site of MRE11 and blocks DNA phosphate backbone rotation which selectively blocks Mre11 exonuclease activity. • Inhibits the MRN-dependent activation of ATM without affecting its kinase activity (IC_{50} = 66 μM). MRE11 IC_{50} = ~200 μM	• Abolishes the G2/M checkpoint and HDR DNA repair in human cells. • Inhibits dsDNA end resection in A549 cells. • Single agent activity in neuroblastoma, glioblastoma, prostate cancer cells and chemosensitivity to DNA damaging agents in glioblastoma cells. IC_{50} = 15-72 μM	Pre-Clinical
PFM01 and PFM03	• Binds near the dimer interface by blocking ssDNA-binding and selectively blocks Mre11 endonuclease activity. MRE11 IC_{50} = ~75-100 μM	• Prevents dsDNA end resection in A549 cells (IC_{50} = 50-75 μM).	Pre-Clinical
PFM39	• Binds in the active site similar to Mirin and selectively blocks Mre11 exonuclease activity MRE11 IC_{50} = < 100 μM	• Prevents dsDNA end resection in A549 cells (IC_{50} = 50-75 μM).	Pre-Clinical
RPA			
NSC15520 (FPA)	• Disrupts RPA DBD-F (N-terminal RPA70N) interactions with Rad9 and p53. • Inhibits RPA dsDNA binding, and helix destabilization activity without affecting ssDNA binding activity. RPA IC_{50} = 10 μM	NR	Pre-Clinical
HAMNO	• Disrupts RPA DBD-F (N-terminal RPA70N) interactions with Rad9 • Prevents DBD-F-dependent unwinding of DNA	• Single agent activity in head and neck and glioblastoma cancer cells, sensitizes head and neck cancer cells to etoposide and glioblastoma cancer stem-like cells to IR. IC_{50} = 5-33 μM	Pre-Clinical

(Continued)

TABLE 1 | Continued

Targeted Protein and Inhibitors	Mechanism of Action and *In vitro* potency	Cellular Activity	Phase of Development
	by RPA but does not prevent RPA ssDNA binding RPA IC_{50} = >50 μM		
VU079104	• Binds in basic cleft of N-terminal RPA70N • Inhibits the interaction of RPA70N with the peptide binding motif derived from ATRIP RPA K_d = 41 μM	NR	Pre-Clinical
Anthranilic acid-based inhibitors	• Binds to N-terminal RPA70N RPA K_d = 0.81 μM	NR	Pre-Clinical
Chlorobenzothiophene-and Pyrazole-based inhibitors	• Binds in basic cleft of N-terminal RPA70N and displaces the binding of an ATRIP-derived peptide to RPA. RPA K_d = 0.19-18 μM	NR	Pre-Clinical
MCI13E and MCI13F (Irreversible inhibitors)	• Covalently binds with DBD A and B of RPA. RPA IC_{50} = 10-16 μM	• Single agent activity in lung and ovarian cancer cells and synergism with cisplatin in lung cancer cells. IC_{50} = 1-5 μM	Pre-Clinical
TDRL-505 and TDRL-551	• Inhibits DNA-binding activity of RPA targeting DBD-A and DBD-B in the 70-kDa subunit of RPA RPA IC_{50} = 18-38 μM	• Single agent activity in lung and ovarian cancer cells and synergism with cisplatin and etoposide in lung cancer cells and xenograft model. IC_{50} = 25-30 μM	Pre-Clinical
43/NERx-329 and 44/NERx-2004	• Inhibits DNA-binding activity of RPA targeting DBD-A and DBD-B in the 70-kDa subunit of RPA RPA IC_{50} = 4.9-10 μM	• 43/NERx-329 shows degradation of replication forks upon stalling and RPA exhaustion, single agent activity in a broad spectrum of cancer cells and synergism with cisplatin, etoposide, bleomycin, BMN673, NU7441 and VE821 in lung cancer cells. IC_{50} = 3-10 μM	Pre-Clinical
RAD51			
DIDS	• Directly binds to RAD51 and inhibits both RAD51-ssDNA and RAD51-dsDNA binding. • Inhibits the RAD51-mediated strand exchange and homologous pairing in the absence of RPA. RAD51 K_d = 2 μM	NR	Pre-Clinical
Halenaquinone	• Specifically inhibits the RAD51-dsDNA binding. RAD51 IC_{50} = 30-60 μM	NR	Pre-Clinical
RI-1 (Irreversible inhibitor)	• Inhibits RAD51 binding to ssDNA by covalently modifying C319 thiol group of RAD51 • Inhibits D-loop formation of RAD51. IC_{50} = 6.82 μM	• Inhibits HR DNA repair and disrupts DNA damage induced RAD51 foci formation. • Sensitizes osteosarcoma, cervical, and breast cancer cells to MMC by triggering synthetic lethality. IC_{50} = 20-40 μM	Pre-Clinical
RI-2	• Reversibly Inhibits RAD51 binding to ssDNA. IC_{50} = 44.17 μM	• Inhibits HR DNA repair and sensitizes HEK293 cells to MMC by triggering synthetic lethality. LD_{50} = 70 μM	Pre-Clinical
RS-1	• Enhances binding of RAD51 to ssDNA and dsDNA. • Enhances recombination activities of RAD51 by locking its active conformation, without affecting ATP hydrolysis. RAD51 K_d = 107 nM	• Enhances HR activity, D-loop formation and the formation of toxic RAD51 complexes on undamaged chromatin. • Leads to the accumulation of RAD51 foci in prostate cancer cells but not in normal cells which is independent of DNA damage. • Enhances cellular resistance to cisplatin at ~7.5 μM.	Pre-Clinical
B02	• Specifically binds to RAD51 and disrupts binding of dsDNA to RAD51-ssDNA Filament. RAD51 IC_{50} = 27.4 μM	• Inhibits DSB-induced HR DNA repair and RAD51 foci formation induced by DNA damage. • Enhances sensitivity of cancer cells to IR, MMC, cisplatin, etoposide and topotecan. • Significantly increases sensitivity of doxorubicin in myeloma cells and MMS in combination with PARPi in MEF cells by triggering synthetic lethality.	Pre-Clinical
B02-iso and *p*-I-B02-iso	• Binds within the dimerization interface of a RAD51 filament. B02-iso RAD51 K_d = 14.6 μM *p*-I-B02-iso RAD51 K_d = 1.4 μM	• Inhibits HR DNA repair and RAD51 foci formation in cancer cells induced by DNA damage. • Single agent activity in TNBC cells and enhances the sensitivity of BRCA-proficient TNBC cells to the PARPi, olaparib through synthetic lethality. • Enhances radiosensitivity in combination with olaparib in	Pre-Clinical

(Continued)

TABLE 1 | Continued

Targeted Protein and Inhibitors	Mechanism of Action and *In vitro* potency	Cellular Activity	Phase of Development
		different cancer cells by inducing synthetic lethality. IC_{50} = 2.6-11.9 μM	
IBR2	• Directly binds to RAD51, disrupts the RAD51-BRCA interaction and RAD51 multimerization. RAD_{51} IC_{50} = 10 μM	• Specifically inhibits RAD51-mediated HR, diminishes IR-induced RAD51 foci and enhances proteasomal degradation of RAD51. • Single agent activity and enhances chemosensitivity to receptor tyrosine kinase and microtubule inhibitors in a broad spectrum of cancer cells by inducing synthetic lethality. • Overcomes CML drug resistance. IC_{50} = 12-16 μM	Pre-Clinical
IBR120	• Directly binds to RAD51, disrupts the RAD51-BRCA interaction and RAD51 multimerization. RAD_{51} IC_{50} = 3-10 μM	• Inhibits HR DNA repair and single agent activity in a broad spectrum of cancer cells. IC_{50} = 3-9.5 μM	Pre-Clinical
Triazole-based inhibitors	• Disrupts the RAD51-BRCA2 interaction and mimics the effect of BRCA2 mutation. RAD51 IC_{50} = 8-53 μM	• Inhibits HR DNA repair and increases the formation of DSBs in combination with olaparib. • Enhances the sensitivity of pancreatic cancer cells to olaparib by inducing synthetic lethality to the functional BRCA2. IC_{50} = 20-30 μM	Pre-Clinical
Dihydroquinolone pyrazoline (DHQP)	• Disrupts the RAD51-BRCA2 interaction and mimics the effect of BRCA2 mutation. RAD51 IC_{50} = 19 μM	• Inhibits HR DNA repair, reduces RAD51 foci formation induced by DNA damage. and synergizes with olaparib in pancreatic cancer cells to trigger synthetic lethality. IC_{50} = 20-30 μM	Pre-Clinical
CYT01B and CYT-0851	• Directly binds to RAD51 and disrupts RAD51 focus formation which reduces the nuclear concentration of RAD51 and promotes RAD51 protein degradation.	• Inhibits HR activity and anticancer activity in cells expressing activation-induced cytidine deaminase (AID), a protein that promotes formation of DSBs. • Shows synergy with cisplatin, PARP and ATR inhibitors in various cancer cells by inducing synthetic lethality. IC_{50} = 20 nM-5 μM	**CYT-0851** in phase 1/2 clinical trials for hematologic malignancies and advanced solid tumors. (NCT03997968)
RAD52			
6-OH-DOPA	• Disrupts the association of ssDNA with RAD52 and RAD52 oligomers. RAD52 IC_{50} = 1.1 μM	• Inhibits RAD52 foci induced by cisplatin and inhibits SSA with minimal effect on HR and NHEJ in BRCA-proficient cells. • Single agent activity in BRCA1/2 deficient TNBC cells, pancreatic cancer cells and patient-derived AML and CML cells through synthetic lethality. IC_{50} = 5-75 μM	Pre-Clinical
A5MP, AICAR and AICAR 5'-phosphate (ZMP)	• Disrupts the RAD52-ssDNA interaction A5MP RAD52 IC_{50} = 1-10 μM AICAR & ZMP RAD52 IC_{50} = 1-5 μM	• AICAR reduces RAD52 foci formation and inhibits SSA activity. • AICAR reduces growth of BRCA1-mutated breast and BRCA2-mutated pancreatic cancer cells by inducing synthetic lethality. IC_{50} = 2-20 μM	Pre-Clinical
D-G09 and D-I03	• D-G09 and D-I03 bind directly to RAD52, impairs RAD52 ssDNA-annealing activity (IC_{50} = 2 and 5 μM, respectively) and DNA pairing activity (D-loop formation) with IC_{50} = 14 and 8 μM, respectively.	• D-I03 significantly reduces level of SSA repair without influencing HDR and shows no effect on cisplatin-induced RAD51 foci formation. • D-G09 and D-I03 shows anticancer activity in BRCA1/2 deficient leukemic, pancreas, ovarian, and TNBC cells by inducing synthetic lethality. IC_{50} = 2.5-16 μM	Pre-Clinical
D-G23, D-I05 and D-K17	• Bind directly to RAD52, impairs RAD52 ssDNA-annealing activity (IC_{50} = 2.9-5.6 μM) and DNA pairing activity (D-loop formation) with IC_{50} = 4.8-7.2 μM.	• Shows anticancer activity in BRCA1/2-defficient cancer cells through synthetic lethality. IC_{50} = 9-26 μM	Pre-Clinical
F779-0434 and C791-0064	• F779-0434 inhibits RAD52-ssDNA association (IC_{50} = 5-15 μM) and C791-0064 disrupting single strand annealing activity of RAD52 (IC_{50} = 50-100 μM).	• Shows anticancer activity in BRCA1/2-defficient pancreatic cancer cells through synthetic lethality. IC_{50} = 5-80 μM	Pre-Clinical
ERCC1-XPF			
F06/NERI02 (NSC130813)	• Interacts with the XPF double helix–hairpin –helix (HhH2) domain to disrupt ERCC1-XPF heterodimerization.	• Inhibits the interaction between XPF and ERCC1 in lung cancer cells. • Single agent activity and chemosensitivity to MMC and cisplatin in lung and colorectal cancer cells and radiosensitivity	Pre-Clinical

(Continued)

TABLE 1 | Continued

Targeted Protein and Inhibitors	Mechanism of Action and *In vitro* potency	Cellular Activity	Phase of Development
	• Inhibits ERCC1-XPF endonuclease activity. ERCC1-XPF IC_{50} = 1.86 μM	in lung cancer cells. • Shows synergy in BRCA1-defficient breast cancer cells by inducing synthetic lethality. IC_{50} = 0.79-3 μM	
B5/B9 and Compound 4	• Binds in the subunit interaction domain of ERCC1–XPF. • Inhibits ERCC1-XPF endonuclease activity. • B5/B9 ERCC1-XPF IC_{50} = 0.49 μM Compound 4 ERCC1-XPF IC_{50} = 0.33 μM	• Both compounds inhibit the removal of bulky DNA lesions, such as cyclobutane pyrimidine dimers (CPDs) in UV-irradiated cells. • Both compounds enhance the sensitivity of colorectal cancer cells to UV radiation and cyclophosphamide. B5/B9 IC_{50} = ~17 μM Compound 4 IC_{50} = 3.5-6 μM	Pre-Clinical
E-X AS7 and E-X PPI2	• Interacts with the XPF double helix–hairpin –helix (HhH2) domain to disrupt ERCC1-XPF heterodimerization. • Inhibits ERCC1-XPF endonuclease activity. E-X AS7 ERCC1-XPF IC_{50} = 28 μM E-X PPI2 ERCC1-XPF K_d = 275 μM	• Inhibit NER and enhance the sensitivity of NER-proficient melanoma cells to cisplatin. • E-X PPI2 reduces ERCC1-XPF heterodimer levels in ovarian cancer cells. E-X PPI2 IC_{50} = 20 μM	Pre-Clinical
Catechol and Hydroxy-pyrimidinone	• Inhibit ERCC1-XPF endonuclease activity and show selectivity for ERCC1-XPF against FEN-1 and DNase. ERCC1-XPF IC_{50} = 0.6 μM	• Catechol inhibits NER activity and enhances the sensitivity of melanoma cells to cisplatin.	Pre-Clinical
NSC16168	• Inhibits ERCC1-XPF endonuclease activity and DNA binding ability of ERCC1-XPF. ERCC1-XPF IC_{50} = 0.42 μM	• Potentiates cisplatin efficacy in lung cancer cells and xenograft model.	Pre-Clinical
Pol θ			
Novobiocin	• Binds to the Pol θ ATPase domain and inhibits its ATPase activity. Pol θ IC_{50} = 24 μM	• Inhibits the TMEJ activity in cells and induces excessive DSB end resection and RAD51 foci. • Inhibits HDR-deficient (BRCA1- and BRCA2) breast and ovarian tumors in GEMM, xenograft and PDX models. • Enhances the cytotoxic effect of PARPi in HDR-deficient tumor cells, xenograft and PDX models and overcomes acquired PARPi resistance in HR-deficient ovarian cancer PDX model by triggering synthetic lethality. IC_{50} = 25-50 μM	Pre-Clinical
ART558 and ART4215	• Inhibit Pol θ polymerase activity and Pol θ-mediated DNA DSB repair. ART558 Pol θ IC_{50} = 7.9 nM	• ART558 elicits DNA damage and synthetic lethality in BRCA1- or BRCA2- deficient cancer cells, xenograft model and enhances the effects of a PARPi in BRCA deficient cancer cells. • Induces synthetic lethality in PARPi resistance cells with defects in the Shieldin complex. IC_{50} = 0.5-1.5 μM	**ART4215** in phase 1/2 clinical trials as a monotherapy and in combination with PARPi, talazoparib for advanced or metastatic solid tumors. (NCT04991480)
RecQ and MCM helicases			
NSC 19630 and NSC 617145	• Inhibit WRN helicase activity but not its nuclease activity. NSC 19630 IC_{50} = 20 μM NSC 617145IC_{50} = 0.23 μM	• Both compounds show single agent activity and accumulation of DSBs and formation of stalled replication forks. • NSC 19630 sensitizes cells to G-quadruplex-binding compound telomestatin, or PARP inhibitor by inducing synthetic lethality. • NSC 617145 induces WRN binding to chromatin and proteasomal degradation, enhances Fanconi Anemia (FA) mutated cells activity to MMC and activates ATM by inducing synthetic lethality. IC_{50} = 2-5 μM	Pre-Clinical
ML216 and Compound 33	• Inhibit helicase activity, DNA unwinding activity of both BLM and WRN and disrupt the DNA binding activity of BLM. ML216 WRN IC50 = 2.7 μM and BLM IC_{50} = 1.8 μM. Compound 33 WRN IC_{50} = 7.1 μM and BLM IC_{50} = 1.1 μM	• ML216 enhances sister chromatid exchange, single agent activity and sensitivity to aphidicolin in BLM expressing cells.	Pre-Clinical

(Continued)

TABLE 1 | Continued

Targeted Protein and Inhibitors	Mechanism of Action and *In vitro* potency	Cellular Activity	Phase of Development
Isaindigotone 29	• Inhibits BLM helicase activity and disrupts the recruitment of BLM at DNA DSB sites. BLM IC_{50} = 0.95 μM	• Induces DNA damage, promotes the accumulation of RAD51 at DNA DSB sites and regulates HR in cells. • Single agent activity in a broad spectrum of cancer cells and enhances the sensitivity of colorectal cancer cells to RAD51 inhibitor, RI-1 and cisplatin by inducing synthetic lethality. IC_{50} = 2-25 μM	Pre-Clinical
AS4583 and RJ-LC-07-48	• Bind to the N-terminal portion of MCM2	• AS4583 inhibits the formation of the DNA replication fork by disrupting MCM complex in lung cancer cells. • AS4583 promotes ubiquitination of MCM2–7 and their degradation in lung cancer cells. • Shows single agent anticancer activity in a broad spectrum of cancer cells as well as in tyrosine kinase inhibitor (TKI)-sensitive and TKI-resistant lung cancer cells and in xenograft model. IC_{50} = 0.02-1 μM	Pre-Clinical

NR, Not Reported; DBD, DNA binding domain; NER, Nucleotide Excision Repair; GEMM, genetically-engineered mouse model; PDX, patient-derived xenograft.

selective DSB repair inhibitors with immunotherapy could be a useful strategy in treating subsets of cancer patients. The identification of useful synthetic lethal interactions to enhance the sensitivity to widely prescribed chemotherapeutics is expected to allow more selective and efficient tumor killing with reduced toxicity. However, stratification of clinically relevant biomarkers along with extensive medicinal chemistry efforts are needed to develop novel compounds that can be exploited to discover synthetic lethal interactions with other DNA repair and DDR genes.

In the last two decades, our understanding of DSB repair pathways has improved dramatically, however, development of small molecule inhibitors targeting these repair pathways are only now being pursued in earnest and recent high-resolution protein structures of many of these putative targets can enhance these efforts. Even though, there is still an urgent need for rapid expansion of DNA repair targeted agents to move from the lab to the clinic through drug discovery and development efforts. The interdependencies between DNA repair pathways can lead to potential druggable vulnerabilities but may increase the mutagenic lesions in surviving cells and drug resistance to DSB inhibitors so a cautious approach is warranted. Thus, development of potent and selective inhibitors for each of the DSB repair proteins accompanied by robust clinical trials will have new treatment modalities for a wide range of tumors and ultimately confer benefit to human health.

AUTHOR CONTRIBUTIONS

All authors listed have made a substantial and direct contribution to the work. All authors have given approval to the final version of the manuscript.

FUNDING

This work is supported by NIH grant R01 CA247370 (JT and NG), Wayne State University Start-up funds (NG) and the Tom and Julie Wood Family Foundation (JT).

ACKNOWLEDGMENTS

We thank Dr. Diana Ainembabazi and Olusayo Ogunyemi for critical reading and comments on the manuscript. We apologize to authors whose work could not be cited due to space limitations.

REFERENCES

1. Ray U, Raghavan SC. Inhibitors of DNA Double-Strand Break Repair at the Crossroads of Cancer Therapy and Genome Editing. *Biochem Pharmacol* (2020) 182:114195.
2. Mehta A, Haber JE. Sources of DNA Double-Strand Breaks and Models of Recombinational DNA Repair. *Cold Spring Harb Perspect Biol* (2014) 6:1–17.
3. Chapman JR, Taylor MR, Boulton SJ. Playing the End Game: DNA Double Strand Break Repair Pathway Choice. *Mol Cell* (2012) 47:497–510.
4. O'Driscoll M, Jeggo PA. The Role of Double-Strand Break Repair-Insights From Human Genetics. *Nat Rev Genet* (2006) 7:45–54.
5. Trenner A, Sartori AA. Harnessing DNA Double-Strand Break Repair for Cancer Treatment. *Front Oncol* (2019) 9:1388. doi: 10.3389/FONC.2019.01388
6. Jeggo PA, Löbrich M. DNA Double-Strand Breaks: Their Cellular and Clinical Impact? *Oncogene* (2007) 26:7717–9. doi: 10.1038/sj.onc.1210868
7. Helleday T, Lo J, van Gent DC, Engelward BP. DNA Double-Strand Break Repair: From Mechanistic Understanding to Cancer Treatment. *DNA Repair (Amst)* (2007) 6:923–35. doi: 10.1016/j.dnarep.2007.02.006
8. Bunting SF, Nussenzweig A. End Joining, Translocations and Cancer. *Nat Rev Cancer* (2013) 13:443–54.
9. Ye Z, Shi Y, Lees-Miller SP, Tainer JA. Function and Molecular Mechanism of the DNA Damage Response in Immunity and Cancer Immunotherapy. *Front Immunol* (2021) 12:797880–0.
10. Gorbunova V, Seluanov A. DNA Double Strand Break Repair, Aging and the Chromatin Connection. *Mutat Res - Fundam Mol Mech Mutagenesis* (2016) 788:2–6.

11. Scully R, Panday A, Elango R, Willis NA. DNA Double-Strand Break Repair-Pathway Choice in Somatic Mammalian Cells. *Nat Rev Mol Cell Biol* (2019) 20:698–714.
12. Sfeir A, Symington LS. Microhomology-Mediated End Joining: A Back-Up Survival Mechanism or Dedicated Pathway? *Trends Biochem Sci* (2015) 40:701–14.
13. Bhargava R, Onyango DO, Stark JM. Regulation of Single-Strand Annealing and its Role in Genome Maintenance. *Trends Genet* (2016) 32:566–75.
14. Ramsden DA, Carvajal-Garcia J, Gupta GP. Mechanism, Cellular Functions and Cancer Roles of Polymerase-Theta-Mediated DNA End Joining. *Nat Rev Mol Cell Biol* (2021) 23:125–40. doi: 10.1038/s41580-021-00405-2. ahead of print.
15. Karanam K, Kafri R, Loewer A, Lahav G. Quantitative Live Cell Imaging Reveals a Gradual Shift DNA Repair Mechanisms and a Maximal Use of HR in Mid S Phase. *Mol Cell* (2012) 47:320–29.
16. Stinson BM, Loparo JJ. Repair of DNA Double-Strand Breaks by the Nonhomologous End Joining Pathway. *Annu Rev Biochem* (2021) 90:137–64.
17. Chang HHY, Pannunzio NR, Adachi N, Lieber MR. Non-Homologous DNA End Joining and Alternative Pathways to Double-Strand Break Repair. *Nat Rev Mol Cell Biol* (2017) 18:495–506.
18. Pawelczak KS, Bennett SM, Turchi JJ. Coordination of DNA-PK Activation and Nuclease Processing of DNA Termini in NHEJ. *Antioxid Redox Signal* (2011) 14:2531–43.
19. Pawelczak KS, Turchi JJ. A Mechanism for DNA-PK Activation Requiring Unique Contributions From Each Strand of a DNA Terminus and Implications for Microhomology-Mediated Nonhomologous DNA End Joining. *Nucleic Acids Res* (2008) 36:4022–31.
20. Pawelczak KS, Andrews BJ, Turchi JJ. Differential Activation of DNA-PK Based on DNA Strand Orientation and Sequence Bias. *Nucleic Acids Res* (2005) 33:152–61.
21. Hammel M, Tainer JA. X-Ray Scattering Reveals Disordered Linkers and Dynamic Interfaces in Complexes and Mechanisms for DNA Double-Strand Break Repair Impacting Cell and Cancer Biology. *Protein Sci* (2021) 30:1735–56. doi: 10.1002/pro.4133
22. Zhao B, Watanabe G, Morten MJ, Reid DA, Rothenberg E, Lieber MR. The Essential Elements for the Noncovalent Association of Two DNA Ends During NHEJ Synapsis. *Nat Commun* (2019) 10:3588. doi: 10.1038/s41467-019-11507-z
23. San Filippo J, Sung P, Klein H. Mechanism of Eukaryotic Homologous Recombination. *Annu Rev Biochem* (2008) 77:229–57.
24. Li X, Heyer W-D. Homologous Recombination in DNA Repair and DNA Damage Tolerance. *Cell Res* (2008) 18:99–113.
25. Zhao B, Rothenberg E, Ramsden DA, Lieber MR. The Molecular Basis and Disease Relevance of non-Homologous DNA End Joining. *Nat Rev Mol Cell Biol* (2020) 12:765–81. doi: 10.1038/s41580-020-00297-8
26. Huang R, Zhou PK. DNA Damage Repair: Historical Perspectives, Mechanistic Pathways and Clinical Translation for Targeted Cancer Therapy. *Signal Transduct Target Ther* (2021) 6:254. doi: 10.1038/s41392-021-00648-7
27. Kumar R, Horikoshi N, Singh M, Gupta A, Misra HS, Albuquerque K. Chromatin Modifications and the DNA Damage Response to Ionizing Radiation. *Front Oncol* (2013) 2012:2:214–214.
28. Camphausen K, Tofilon PJ. Inhibition of Histone Deacetylation: A Strategy for Tumor Radiosensitization. *J Clin Oncol* (2007) 25:4051–6.
29. Hu C, Zhang M, Moses N, Hu C, Polin L, Chen W. The USP10-HDAC6 Axis Confers Cisplatin Resistance in non-Small Cell Lung Cancer Lacking Wild-Type P53. *Cell Death Dis* (2020) 11:328. doi: 10.1038/s41419-020-2519-8
30. Jafri MA, Ansari SA, Alqahtani MH, Shay JW. Roles of Telomeres and Telomerase in Cancer, and Advances in Telomerase-Targeted Therapies. *Genome Med* (2016) 8:69. doi: 10.1186/s13073-016-0324-x
31. Marcand S. How do Telomeres and NHEJ Coexist? *Mol Cell Oncol* (2014) 1 (3):1–6. doi: 10.4161/23723548.2014.963438
32. Rossiello F, Aguado J, Sepe S, Iannelli F, Nguyen Q, Pitchiaya S, et al. DNA Damage Response Inhibition at Dysfunctional Telomeres by Modulation of Telomeric DNA Damage Response RNAs. *Nat Commun* (2017) 8:13980. doi: 10.1038/ncomms13980
33. Nelson CB, Alturki TM, Luxton JJ, Taylor LE, Maranon DG, Muraki K, et al. Telomeric Double Strand Breaks in G1 Human Cells Facilitate Formation of 5' C-Rich Overhangs and Recruitment of TERRA. *Front Genet* (2021) 12:644803:644803. doi: 10.3389/fgene.2021.644803
34. Galli M, Frigerio C, Longhese MP, Clerici M. The Regulation of the DNA Damage Response at Telomeres: Focus on Kinases. *Biochem Soc Trans* (2021) 49(2):933–43. doi: 10.1042/BST20200856
35. Sui J, Zhang S, Chen BPC. DNA-Dependent Protein Kinase in Telomere Maintenance and Protection. *Cell Mol Biol Lett* (2020) 25:2. doi: 10.1186/s11658-020-0199-0
36. Wang Y, Ghosh G, Hendrickson EA. Ku86 Represses Lethal Telomere Deletion Events in Human Somatic Cells. *Proc Natl Acad Sci USA* (2009) 106:12430–5. doi: 10.1073/pnas.0903362106
37. Guterres AN, Villanueva J. Targeting Telomerase for Cancer Therapy. *Oncogene* (2020) 39:5811–24. doi: 10.1038/s41388-020-01405-w
38. Bochman ML. Roles of DNA Helicases in the Maintenance of Genome Integrity. *Mol Cell Oncol* (2014) 1(3):1–9. doi: 10.4161/23723548.2014.963429
39. Daniel DC, Dagdanova AV, Johnson EM. The MCM and RecQ Helicase Families: Ancient Roles in DNA Replication and Genomic Stability Lead to Distinct Roles in Human Disease. In: *The Mechanisms of DNA Replication*. London, United Kingdom:IntechOpen (2013). doi: 10.5772/52961
40. Suhasini AN, Brosh RM Jr. Fanconi Anemia and Bloom's Syndrome Crosstalk Through FANCJ-BLM Helicase Interaction. *Trends Genet* (2012) 28:7–13. doi: 10.1016/j.tig.2011.09.003
41. Bernstein KA, Gangloff S, Rothstein R. The RecQ DNA Helicases in DNA Repair. *Annu Rev Genet* (2010) 44:393–417. doi: 10.1146/annurev-genet-102209-163602
42. Seo YS, Kang YH. The Human Replicative Helicase, the CMG Complex, as a Target for Anti-Cancer Therapy. *Front Mol Biosci* (2018) 5:26. doi: 10.3389/fmolb.2018.00026
43. Lu H, Davis AJ. Human RecQ Helicases in DNA Double-Strand Break Repair. *Front Cell Dev Biol* (2021) 9:640755:640755. doi: 10.3389/fcell.2021.640755
44. Rong Z, Tu P, Xu P, Sun Y, Yu F, Tu N, et al. The Mitochondrial Response to DNA Damage. *Front Cell Dev Biol* (2021) 9:669379–9.
45. Dahal S, Raghavan SC. Mitochondrial Genome Stability in Human: Understanding the Role of DNA Repair Pathways. *Biochem J* (2021) 478:1179–97.
46. Yasukawa T, Kang D. An Overview of Mammalian Mitochondrial DNA Replication Mechanisms. *J Biochem (Tokyo)* (2018) 164:183–93.
47. Shutt TE, Gray MW. Bacteriophage Origins of Mitochondrial Replication and Transcription Proteins. *Trends Genet* (2006) 22:90–5.
48. Tadi SK, Sebastian R, Dahal S, Babu RK, Choudhary B, Raghavan SC. Microhomology-Mediated End Joining is the Principal Mediator of Double-Strand Break Repair During Mitochondrial DNA Lesions. *Mol Biol Cell* (2016) 27:223–35.
49. Wisnovsky S, Sack T, Pagliarini DJ, Laposa RR, Kelley SO. DNA Polymerase θ Increases Mutational Rates in Mitochondrial DNA. *ACS Chem Biol* (2018) 13:900–8.
50. Krasich R, Copeland WC. DNA Polymerases in the Mitochondria: A Critical Review of the Evidence. *Front Biosci - Landmark* (2017) 22:692–709.
51. Dahal S, Dubey S, Raghavan SC. Homologous Recombination-Mediated Repair of DNA Double-Strand Breaks Operates in Mammalian Mitochondria. *Cell Mol Life Sci: CMLS* (2017) 2018:75:1641–1655.
52. Mishra A, Saxena S, Kaushal A, Nagaraju G. RAD51C/XRCC3 Facilitates Mitochondrial DNA Replication and Maintains Integrity of the Mitochondrial Genome. *Mol Cell Biol* (2018) 2017:38.
53. Sage JM, Gildemeister OS, Knight KL. Discovery of a Novel Function for Human Rad51: Maintenance of the Mitochondrial Genome. *J Biol Chem* (2010) 285:18984–90.
54. Pohjoismäki JLO, Goffart S, Tyynismaa H, Wilcox S, Ide T, Kang D. Human Heart Mitochondrial DNA Is Organized in Complex Catenated Networks Containing Abundant Four-Way Junctions and Replication Forks. *J Biol Chem* (2009) 284:21446–57.
55. Tann AW, Boldogh I, Meiss G, Qian W, Van Houten B, Mitra S. Apoptosis Induced by Persistent Single-Strand Breaks in Mitochondrial Genome:

Critical Role of EXOG (5'-EXO/endonuclease) in Their Repair. *J Biol Chem* (2011) 286(37):31975–83. doi: 10.1074/jbc.M110.215715
56. Yamazaki T, Kirchmair A, Sato A, Buqué A, Rybstein M, Petroni G. Mitochondrial DNA Drives Abscopal Responses to Radiation That are Inhibited by Autophagy. *Nat Immunol* (2020) 21:1160–71.
57. Buondonno I, Gazzano E, Jean SR, Audrito V, Kopecka J, Fenelli M. Mitochondria-Targeted Doxorubicin: A New Therapeutic Strategy Against Doxorubicin-Resistant Osteosarcoma. *Mol Cancer Ther* (2016) 15:2640–52.
58. West AP, Khoury-Hanold W, Staron M, Tal MC, Pineda CM, Lang SM. Mitochondrial DNA Stress Primes the Antiviral Innate Immune Response. *Nat (London)* (2015) 520:553–7.
59. Durut N, Mittelsten Scheid O. The Role of Noncoding RNAs in Double-Strand Break Repair. *Front Plant Sci* (2019) 10:1155–5.
60. Statello L, Guo C, Chen L, Huarte M. Gene Regulation by Long non-Coding RNAs and its Biological Functions. *Nat Rev Mol Cell Biol* (2021) 2020:22:96–118.
61. Chowdhury D, Choi YE, Brault ME. DNA DAMAGE - OPINION Charity Begins at Home: non-Coding RNA Functions in DNA Repair. *Nat Rev Mol Cell Biol* (2013) 14:181–9.
62. Gavande NS, VanderVere-Carozza PS, Hinshaw HD, Jalal SI, Sears CR, Pawelczak KS, et al. DNA Repair Targeted Therapy: The Past or Future of Cancer Treatment? *Pharmacol Ther* (2016) 160:65–83.
63. Helleday T, Petermann E, Lundin C, Hodgson B, Sharma RA. DNA Repair Pathways as Targets for Cancer Therapy. *Nat Rev Cancer* (2008) 8:193–204.
64. Begg AC, Stewart FA, Vens C. Strategies to Improve Radiotherapy With Targeted Drugs. *Nat Rev Cancer* (2011) 11:239–53.
65. Sciubba JJ, Goldenberg D. Oral Complications of Radiotherapy. *Lancet Oncol* (2006) 7:175–83.
66. Barnett GC, West CML, Dunning AM, Elliott RM, Coles CE, Pharoah PDP, et al. Normal Tissue Reactions to Radiotherapy: Towards Tailoring Treatment Dose by Genotype. *Nat Rev Cancer* (2009) 9:134–42.
67. Jeggo P, Lavin MF. Cellular Radiosensitivity: How Much Better do We Understand it? *Int J Radiat Biol* (2009) 85:1061–81.
68. Myers SH, Ortega JA, Cavalli A. Synthetic Lethality Through the Lens of Medicinal Chemistry. *J Med Chem* (2020) 63:14151–83. doi: 10.1021/acs.jmedchem.0c00766
69. Suwen H, Zi H, Frédéric L, Carmen G, Xiang-Yang Y, Tian X. Small Molecule DNA-PK Inhibitors as Potential Cancer Therapy: A Patent Review (2010–Present). *Expert Opin Ther Pat* (2021) 31:435–52. doi: 10.1080/13543776.2021.1866540
70. Brown JS, O'Carrigan B, Jackson SP, Yap TA. Targeting DNA Repair in Cancer: Beyond PARP Inhibitors. *Cancer Discovery* (2017) 7:20–37. doi: 10.1158/2159-8290.CD-16-0860
71. Woodbine L, Gennery AR, Jeggo PA. The Clinical Impact of Deficiency in DNA non-Homologous End-Joining. *DNA Repair* (2014) 16:84–96. doi: 10.1016/j.dnarep.2014.02.011
72. Van der Burg M, IJspeert H, Verkaik NS, Turul T, Wiegant WW, Morotomi-Yano K, et al. A DNA-PKcs Mutation in a Radiosensitive T-B- SCID Patient Inhibits Artemis Activation and Nonhomologous End-Joining. *J Clin Invest* (2009) 119:91–8. doi: 10.1172/JCI37141
73. Buck D, Malivert L, de Chasseval R, Barraud A, Fondanèche MC, Sanal O, et al. Cernunnos, a Novel Nonhomologous End-Joining Factor, is Mutated in Human Immunodeficiency With Microcephaly. *Cell* (2006) 124:287–99. doi: 10.1016/j.cell.2005.12.030
74. Marangoni E, Foray N, O'Driscoll M, Douc-Rasy S, Bernier J, Bourhis J, et al. A Ku80 Fragment With Dominant Negative Activity Imparts a Radiosensitive Phenotype to CHO-K1 Cells. *Nucleic Acids Res* (2000) 28:4778–82. doi: 10.1093/nar/28.23.4778
75. Riballo E, Critchlow SE, Teo SH, Doherty AJ, Priestley A, Broughton B, et al. Identification of a Defect in DNA Ligase IV in a Radiosensitive Leukaemia Patient. *Curr Biol* (1999) 9:699–702. doi: 10.1016/s0960-9822(99)80311-x
76. Downs JA, Jackson SP. A Means to a DNA End: The Many Roles of Ku. *Nat Rev Mol Cell Biol* (2004) 5:367–78.
77. Walker JR, Corpina RA, Goldberg J. Structure of the Ku Heterodimer Bound to DNA and its Implications for Double-Strand Break Repair. *Nature* (2001) 412:607–14.
78. Bennett SM, Woods DS, Pawelczak KS, Turchi JJ. Multiple Protein-Protein Interactions Within the DNA-PK Complex are Mediated by the C-Terminus of Ku 80. *Int J Biochem Mol Biol* (2012) 3:36–45.
79. Fell VL, Schild-Poulter C. The Ku Heterodimer: Function in DNA Repair and Beyond. *Mutat Res* (2015) 763:15–29.
80. Kragelund BB, Weterings E, Hartmann-Petersen R, Keijzers G. The Ku70/80 Ring in Non Homologous End-Joining: Easy to Slip on Hard to Remove. *Front Biosci (Landmark Ed)* (2016) 21:514–27.
81. Osipovich O, Duhe RJ, Hasty P, Durum SK, Muegge K. Defining Functional Domains of Ku80: DNA End Binding and Survival After Radiation. *Biochem Biophys Res Commun* (1999) 261:802–7.
82. Baptistella AR, Landemberger MC, Dias MVS, Giudice FS, Rodrigues BR, Da Silva PPCE. Rab5C Enhances Resistance to Ionizing Radiation in Rectal Cancer. *J Mol Med (Berl)* (2019) 97:855–69.
83. Pucci S, Polidoro C, Joubert A, Mastrangeli F, Tolu B, Benassi M. Ku70, Ku80, and Sclusterin: A Cluster of Predicting Factors for Response to Neoadjuvant Chemoradiation Therapy in Patients With Locally Advanced Rectal Cancer. *Int J Radiat Oncol Biol Phys* (2017) 97:381–8.
84. Beskow C, Skikuniene J, Holgersson A, Nilsson B, Lewensohn R, Kanter L, et al. Radioresistant Cervical Cancer Shows Upregulation of the NHEJ Proteins DNA-PKcs, Ku70 and Ku86. *Br J Cancer* (2009) 101:816–221.
85. Li YH, Wang X, Pan Y, Lee DH, Chowdhury D, Kimmelman AC. Inhibition of non-Homologous End Joining Repair Impairs Pancreatic Cancer Growth and Enhances Radiation Response. *PloS One* (2012) 7:e39588.
86. Kim SH, Kim D, Han JS, Jeong CS, Chung BS, Kang CD. Ku Autoantigen Affects the Susceptibility to Anticancer Drugs. *Cancer Res* (1999) 59:4012–7.
87. Zahid S, Seif El Dahan M, Iehl F, Fernandez-Varela P, Le Du MH, Ropars V, et al. The Multifaceted Roles of Ku70/80. *Int J Mol Sci* (2021) 22:1–23. doi: 10.3390/ijms22084134
88. Weterings E, Gallegos AC, Dominick LN, Cooke LS, Bartels TN, Vagner J, et al. A Novel Small Molecule Inhibitor of the DNA Repair Protein Ku70/80. *DNA Repair (Amst)* (2016) 43:98–106. doi: 10.1016/j.dnarep.2016.03.014
89. Pawelczak KS, Gavande NS, VanderVere-Carozza PS, Turchi JJ. Modulating DNA Repair Pathways to Improve Precision Genome Engineering. *ACS Chem Biol* (2018) 13:389–96. doi: 10.1021/acschembio.7b00777
90. Gavande NS, VanderVere-Carozza PS, Pawelczak KS, Mendoza-Munoz P, Vernon TL, Hanakahi LA, et al. Discovery and Development of Novel DNA-PK Inhibitors by Targeting the Unique Ku-DNA Interaction. *Nucleic Acids Res* (2020) 48:11536–50. doi: 10.1093/nar/gkaa934
91. Pannunzio NR, Watanabe G, Lieber MR. Nonhomologous DNA End-Joining for Repair of DNA Double-Strand Breaks. *J Bio Chem* (2018) 293:10512–23.
92. Löbrich M, Jeggo P. A Process of Resection-Dependent Nonhomologous End Joining Involving the Goddess Artemis. *Trends Biochem Sci* (2017) 9:690–701. doi: 10.1016/j.tibs.2017.06.011
93. Gu J, Li S, Zhang X, Wang LC, Niewolik D, Schwarz K, et al. DNA-PKcs Regulates a Single-Stranded DNA Endonuclease Activity of Artemis. *DNA Repair (Amst)* (2010) 9:429–37.
94. Moshous D, Callebaut I, De Chasseval R, Corneo B, Cavazzana-Calvo M, Le Deist F, et al. Artemis, a Novel DNA Double-Strand Break Repair/V(D)J Recombination Protein, is Mutated in Human Severe Combined Immune Deficiency. *Cell* (2001) 105:177–86.
95. Rooney S, Alt FW, Lombard D, Whitlow S, Eckersdorff M, Fleming J, et al. Defective DNA Repair and Increased Genomic Instability in Artemis-Deficient Murine Cells. *J Exp Med* (2003) 197:553–65. doi: 10.1084/jem.20021891
96. Ochi T, Gu X, Blundell TL. Structure of the Catalytic Region of DNA Ligase IV in Complex With an Artemis Fragment Sheds Light on Double-Strand Break Repair. *Structure* (2013) 21:672–9. doi: 10.1016/j.str.2013.02.014
97. Malu S, De Ioannes P, Kozlov M, Greene M, Francis D, Hanna M, et al. Artemis C-Terminal Region Facilitates V(D)J Recombination Through its Interactions With DNA Ligase IV and DNA-PKcs. *J Exp Med* (2012) 209:955–63. doi: 10.1084/jem.20111437
98. Povirk LF, Zhou T, Zhou R, Cowan MJ, Yannone SM. Processing of 3'-Phosphoglycolate-Terminated DNA Double Strand Breaks by Artemis Nuclease. *J Biol Chem* (2007) 282:3547–58.

99. Riballo E, Kühne M, Rief M, Doherty A, Smith GCM, Recio MJ. A Pathway of Double-Strand Break Rejoining Dependent Upon ATM, Artemis, and Proteins Locating to γ-H2AX Foci. *Mol Cell* (2004) 16:715–24.
100. Kurosawa A, Koyama H, Takayama S, Miki K, Ayusawa D, Fujii M. The Requirement of Artemis in Double-Strand Break Repair Depends on the Type of DNA Damage. *DNA Cell Biol* (2008) 27:55–61.
101. Yosaatmadja Y, Baddock HT, Newman JA, Bielinski M, Gavard AE, Mukhopadhyay SMM, et al. Structural and Mechanistic Insights Into the Artemis Endonuclease and Strategies for its Inhibition. *Nucleic Acids Res* (2021) 49:9310–26. doi: 10.1093/nar/gkab693
102. Karim MF, Liu S, Laciak AR, Volk L, Koszelak-Rosenblum M, Lieber MR, et al. Structural Analysis of the Catalytic Domain of Artemis Endonuclease/SNM1C Reveals Distinct Structural Features. *J Biol Chem* (2020) 295:12368–77. doi: 10.1074/jbc.RA120.014136
103. Chu VT, Weber T, Wefers B, Wurst W, Sander S, Rajewsky K, et al. Increasing the Efficiency of Homology-Directed Repair for CRISPR-Cas9-Induced Precise Gene Editing in Mammalian Cells. *Nat Biotechnol* (2015) 32:543–8. doi: 10.1038/nbt.3198
104. Maruyama T, Dougan SK, Truttmann MC, Bilate AM, Ingram JR, Ploegh HL. Increasing the Efficiency of Precise Genome Editing With CRISPR-Cas9 by Inhibition of Nonhomologous End Joining. *Nat Biotechnol* (2015) 33:538–42. doi: 10.1038/nbt.3190
105. Adachi N, Ishino T, Ishii Y, Takeda S, Koyama H. DNA Ligase IV-Deficient Cells are More Resistant to Ionizing Radiation in the Absence of Ku70: Implications for DNA Double-Strand Break Repair. *Proc Natl Acad Sci USA* (2001) 98:12109–13. doi: 10.1073/pnas.201271098
106. Davis AJ, Chen DJ. DNA Double Strand Break Repair *via* non-Homologous End-Joining. *Transl Cancer Res* (2013) 2:130–43.
107. Chen X, Zhong S, Zhu X, Dziegielewska B, Ellenberger T, Wilson GM, et al. Rational Design of Human DNA Ligase Inhibitors That Target Cellular DNA Replication and Repair. *Cancer Res* (2008) 68:3169–77. doi: 10.1158/0008-5472.CAN-07-6636
108. Srivastava M, Nambiar M, Sharma S, Karki SS, Goldsmith G, Hegde M, et al. An Inhibitor of Nonhomologous End-Joining Abrogates Double-Strand Break Repair and Impedes Cancer Progression. *Cell* (2012) 151:1474–87.
109. Greco GE, Matsumoto Y, Brooks RC, Lu Z, Lieber MR, Tomkinson AE. SCR7 is Neither a Selective Nor a Potent Inhibitor of Human DNA Ligase Iv. *DNA Repair* (2016) 43:18–23.
110. Vartak SV, Swarup HA, Gopalakrishnan V, Gopinatha VK, Ropars V, Nambiar M, et al. Autocyclized and Oxidized Forms of SCR7 Induce Cancer Cell Death by Inhibiting Nonhomologous DNA End Joining in a Ligase IV Dependent Manner. *FEBS J* (2018) 285:3959–76.
111. Ray U, Raul SK, Gopinatha VK, Ghosh D, Rangappa KS, Mantelingu K, et al. Identification and Characterization of Novel SCR7-Based Small-Molecule Inhibitor of DNA End-Joining, SCR130 and its Relevance in Cancer Therapeutics. *Mol Carcinog* (2020) 59:618–28.
112. Ray U, Raghavan SC. Modulation of DNA Double-Strand Break Repair as a Strategy to Improve Precise Genome Editing. *Oncogene* (2020) 39:6393–405. doi: 10.1038/s41388-020-01445-2
113. Koike M, Yutoku Y, Koike A. Establishment of Hamster Cell Lines With EGFP-Tagged Human XRCC4 and Protection From Low-Dose X-Ray Radiation. *J Vet Med Sci* (2012) 74:1269–75. doi: 10.1292/jvms.12-0112
114. Ochi T, Blackford AN, Coates J, Jhujh S, Mehmood S, Tamura N, et al. DNA Repair. PAXX, a Paralog of XRCC4 and XLF, Interacts With Ku to Promote DNA Double-Strand Break Repair. *Science* (2015) 347:185–8.
115. Costantini S, Woodbine L, Andreoli L, Jeggo PA, Vindigni A. Interaction of the Ku Heterodimer With the DNA Ligase IV/Xrcc4 Complex and its Regulation by DNA-Pk. *DNA Repair* (2007) 6:712–22.
116. Sun MF, Chen HY, Tsai FJ, Lui SH, Chen CY, Chen CY. Search for Novel Remedies to Augment Radiation Resistance of Inhabitants of Fukushima and Chernobyl Disasters: Identifying DNA Repair Protein XRCC4 Inhibitors. *J Biomol Struct Dyn* (2011) 29:325–37. doi: 10.1080/07391102.2011.10507388
117. Liu F, Fan Z, Song N, Han M, Yan M, Guo LH, et al. XRCC4, Which is Inhibited by PFDA, Regulates DNA Damage Repair and Cell Chemosensitivity. *J Cell Biochem* (2019) 120:12665–76. doi: 10.1002/jcb.28534
118. Jeggo PA, Löbrich M. How Cancer Cells Hijack DNA Double-Strand Break Repair Pathways to Gain Genomic Instability. *Biochem J* (2015) 471:1–11. doi: 10.1042/BJ20150582
119. Zhao F, Kim W, Kloeber JA, Lou Z. DNA End Resection and its Role in DNA Replication and DSB Repair Choice in Mammalian Cells. *Exp Mol Med* (2020) 52:1705–14. doi: 10.1038/s12276-020-00519-1
120. Kopa P, Macieja A, Galita G, Witczak ZJ, Poplawski T. DNA Double Strand Breaks Repair Inhibitors: Relevance as Potential New Anticancer Therapeutics. *Curr Med Chem* (2019) 26:1483–93. doi: 10.2174/0929867325666180214113154
121. Lee JH, Paull TT. ATM Activation by DNA Double-Strand Breaks Through the Mre11-Rad50-Nbs1 Complex. *Science* (2005) 308:551–4. doi: 10.1126/science.1108297
122. Zhang J, Zou L. Alternative Lengthening of Telomeres: From Molecular Mechanisms to Therapeutic Outlooks. *Cell Biosci* (2020) 10:30–0.
123. Reddel RR, Cesare AJ. Alternative Lengthening of Telomeres: Models, Mechanisms and Implications. *Nat Rev Genet* (2010) 11:319–30.
124. Nelson CB, Alturki TM, Luxton JJ, Taylor LE, Maranon DG, Muraki K. Telomeric Double Strand Breaks in G1 Human Cells Facilitate Formation of 5′ C-Rich Overhangs and Recruitment of TERRA. *Front Genet* (2021) 12:644803–3.
125. Wang YY, Hung AC, Lo S, Hsieh YC, Yuan SF. MRE11 as a Molecular Signature and Therapeutic Target for Cancer Treatment With Radiotherapy. *Cancer Lett* (2021) 28:514:1–11. doi: 10.1016/j.canlet.2021.05.013
126. Bian L, Meng Y, Zhang M, Li D. MRE11-RAD50-NBS1 Complex Alterations and DNA Damage Response: Implications for Cancer Treatment. *Mol Cancer* (2019) 18:169. doi: 10.1186/s12943-019-1100-5
127. Wang J, Xu WH, Wei Y, Zhu Y, Qin XJ, Zhang HL. Elevated MRE11 Expression Associated With Progression and Poor Outcome in Prostate Cancer. *J Cancer* (2019) 10:4333–40. doi: 10.7150/jca.31454
128. Cheng L, Wu Q, Huang Z, Guryanova OA, Huang Q, Shou W, et al. L1CAM Regulates DNA Damage Checkpoint Response of Glioblastoma Stem Cells Through Nbs1. *EMBO J* (2011) 30:800–13.
129. Dupré A, Boyer-Chatenet L, Sattler RM, Modi AP, Lee JH, Nicolette ML, et al. A Forward Chemical Genetic Screen Reveals an Inhibitor of the Mre11-Rad50-Nbs1 Complex. *Nat Chem Biol* (2008) 4:119–25. doi: 10.1038/nchembio.63
130. Jividen K, Kedzierska KZ, Yang CS, Szlachta K, Ratan A, Paschal BM. Genomic Analysis of DNA Repair Genes and Androgen Signaling in Prostate Cancer. *BMC Cancer* (2018) 18:960. doi: 10.1186/s12885-018-4848-x
131. Petroni M, Sardina F, Infante P, Bartolazzi A, Locatelli E, Fabretti F, et al. MRE11 Inhibition Highlights a Replication Stress-Dependent Vulnerability of MYCN-Driven Tumors. *Cell Death Dis* (2018) 9:895. doi: 10.1038/s41419-018-0924-z
132. Berte N, Piée-Staffa A, Piecha N, Wang M, Borgmann K, Kaina B, et al. Targeting Homologous Recombination by Pharmacological Inhibitors Enhances the Killing Response of Glioblastoma Cells Treated With Alkylating Drugs. *Mol Cancer Ther* (2016) 15:2665–78. doi: 10.1158/1535-7163.MCT-16-0176
133. Shibata A, Moiani D, Arvai AS, Perry J, Harding SM, Genois MM, et al. DNA Double-Strand Break Repair Pathway Choice is Directed by Distinct MRE11 Nuclease Activities. *Mol Cell* (2014) 53:7–18. doi: 10.1016/j.molcel.2013.11.003
134. Par S, Vaides S, VanderVere-Carozza PS, Pawelczak KS, Stewart J, Turchi JJ. OB-Folds and Genome Maintenance: Targeting Protein-DNA Interactions for Cancer Therapy. *Cancers (Basel)* (2021) 13:3346. doi: 10.3390/cancers13133346
135. Dueva R, Iliakis G. Replication Protein A: A Multifunctional Protein With Roles in DNA Replication, Repair and Beyond. *NAR Cancer* (2020) 2:1–24. doi: 10.1093/narcan/zcaa022
136. Bhat KP, Cortez D. RPA and RAD51: Fork Reversal, Fork Protection, and Genome Stability. *Nat Struct Mol Biol* (2018) 25:446–53. doi: 10.1038/s41594-018-0075-z
137. Gavande NS, VanderVere-Carozza PS, Pawelczak KS, Turchi JJ. Targeting the Nucleotide Excision Repair Pathway for Therapeutic Applications. In: M Kelley, editor. *DNA Repair in Cancer Therapy: Molecular Targets and Clinical Applications*. Amsterdam, The Netherlands: Elsevier Academic Press (2016). p. 135–50.
138. Maréchal A, Zou L. RPA-Coated Single-Stranded DNA as a Platform for Post-Translational Modifications in the DNA Damage Response. *Cell Res* (2015) 25:9–23. doi: 10.1038/cr.2014.147

139. Jekimovs C, Bolderson E, Suraweera A, Adams M, O'Byrne KJ, Richard DJ. Chemotherapeutic Compounds Targeting the DNA Double-Strand Break Repair Pathways: The Good, the Bad, and the Promising. *Front Oncol* (2014) 4:86. doi: 10.3389/fonc.2014.00086
140. Planchard D, Domont J, Taranchon E, Monnet I, Tredaniel J, Caliandro R, et al. The NER Proteins are Differentially Expressed in Ever Smokers and in Never Smokers With Lung Adenocarcinoma. *Ann Oncol* (2009) 20:1257–63. doi: 10.1093/annonc/mdn785
141. Fan J, Pavletich NP. Structure and Conformational Change of a Replication Protein A Heterotrimer Bound to ssDNA. *Genes Dev* (2012) 26:2337–47. doi: 10.1101/gad.194787.112
142. Glanzer JG, Liu S, Oakley GG. Small Molecule Inhibitor of the RPA70 N-Terminal Protein Interaction Domain Discovered Using in Silico and *In Vitro* Methods. *Bioorg Med Chem* (2011) 19:2589–95. doi: 10.1016/j.bmc.2011.03.012
143. Glanzer JG, Carnes KA, Soto P, Liu S, Parkhurst LJ, Oakley GG. A Small Molecule Directly Inhibits the P53 Transactivation Domain From Binding to Replication Protein a. *Nucleic Acids Res* (2013) 41:2047–59. doi: 10.1093/nar/gks1291
144. Glanzer JG, Liu S, Wang L, Mosel A, Peng A, Oakley GG. RPA Inhibition Increases Replication Stress and Suppresses Tumor Growth. *Cancer Res* (2014) 74:5165–72. doi: 10.1158/0008-5472.CAN-14-0306
145. Patrone JD, Waterson AG, Fesik SW. Recent Advancements in the Discovery of Protein-Protein Interaction Inhibitors of Replication Protein a. *Medchemcomm* (2016) 8:259–67. doi: 10.1039/c6md00460a
146. Neher TM, Bodenmiller D, Fitch RW, Jalal SI, Turchi JJ. Novel Irreversible Small Molecule Inhibitors of Replication Protein A Display Single-Agent Activity and Synergize With Cisplatin. *Mol Cancer Ther* (2011) 10:1796–806. doi: 10.1158/1535-7163.MCT-11-0303
147. Shuck SC, Turchi JJ. Targeted Inhibition of Replication Protein A Reveals Cytotoxic Activity, Synergy With Chemotherapeutic DNA-Damaging Agents, and Insight Into Cellular Function. *Cancer Res* (2010) 70:3189–98. doi: 10.1158/0008-5472.CAN-09-3422
148. Andrews BJ, Turchi JJ. Development of a High-Throughput Screen for Inhibitors of Replication Protein A and its Role in Nucleotide Excision Repair. *Mol Cancer Ther* (2004) 3:385–91.
149. Mishra AK, Dormi SS, Turchi AM, Woods DS, Turchi JJ. Chemical Inhibitor Targeting the Replication Protein A-DNA Interaction Increases the Efficacy of Pt-Based Chemotherapy in Lung and Ovarian Cancer. *Biochem Pharmacol* (2015) 93:25–33. doi: 10.1016/j.bcp.2014.10.013
150. Gavande NS, VanderVere-Carozza PS, Pawelczak KS, Vernon TL, Jordan MR, Turchi JJ. Structure-Guided Optimization of Replication Protein A (RPA)-DNA Interaction Inhibitors. *ACS Med Chem Lett* (2020) 11:1118–24. doi: 10.1021/acsmedchemlett.9b00440
151. VanderVere-Carozza PS, Gavande NS, Jalal SI, Pollok KE, Ekinci KE, Heyza J, et al. *In Vivo* Targeting Replication Protein A for Cancer Therapy. *Front Oncol* (2022) 12:1–13. doi: 10.3389/fonc.2022.826655. Article in Press.
152. Laurini E, Marson D, Fermeglia A, Aulic S, Fermeglia M, Pricl S. Role of Rad51 and DNA Repair in Cancer: A Molecular Perspective. *Pharmacol Ther* (2020) 208:107492. doi: 10.1016/j.pharmthera.2020.107492
153. Bhattacharya S, Srinivasan K, Abdisalaam S, Su F, Raj P, Dozmorov I, et al. RAD51 Interconnects Between DNA Replication, DNA Repair and Immunity. *Nucleic Acids Res* (2017) 45:4590–605. doi: 10.1093/nar/gkx126
154. Grundy MK, Buckanovich RJ, Bernstein KA. Regulation and Pharmacological Targeting of RAD51 in Cancer. *NAR Cancer* (2020) 2:1–14. doi: 10.1093/narcan/zcaa024
155. Makino E, Fröhlich LM, Sinnberg T, Kosnopfel C, Sauer B, Garbe C, et al. Targeting Rad51 as a Strategy for the Treatment of Melanoma Cells Resistant to MAPK Pathway Inhibition. *Cell Death Dis* (2020) 11:581. doi: 10.1038/s41419-020-2702-y
156. Ishida T, Takizawa Y, Kainuma T, Inoue J, Mikawa T, Shibata T, et al. DIDS, a Chemical Compound That Inhibits RAD51-Mediated Homologous Pairing and Strand Exchange. *Nucleic Acids Res* (2009) 37:3367–76. doi: 10.1093/nar/gkp200
157. Takaku M, Kainuma T, Ishida-Takaku T, Ishigami S, Suzuki H, Tashiro S, et al. Halenaquinone, a Chemical Compound That Specifically Inhibits the Secondary DNA Binding of RAD51. *Genes Cells* (2011) 16:427–36. doi: 10.1111/j.1365-2443.2011.01494.x
158. Budke B, Logan HL, Kalin JH, Zelivianskaia AS, Cameron McGuire W, Miller LL, et al. RI-1: A Chemical Inhibitor of RAD51 That Disrupts Homologous Recombination in Human Cells. *Nucleic Acids Res* (2012) 40:7347–57. doi: 10.1093/nar/gks353
159. Budke B, Kalin JH, Pawlowski M, Zelivianskaia AS, Wu M, Kozikowski AP, et al. An Optimized RAD51 Inhibitor That Disrupts Homologous Recombination Without Requiring Michael Acceptor Reactivity. *J Med Chem* (2013) 56(1):254–63. doi: 10.1021/jm301565b
160. Jayathilaka K, Sheridan SD, Bold TD, Bochenska K, Logan HL, Weichselbaum RR, et al. A Chemical Compound That Stimulates the Human Homologous Recombination Protein Rad51. *Proc Natl Acad Sci USA* (2008) 105:15848–53. doi: 10.1073/pnas.0808046105
161. Mason JM, Logan HL, Budke B, Wu M, Pawlowski M, Weichselbaum RR, et al. The RAD51-Stimulatory Compound RS-1 can Exploit the RAD51 Overexpression That Exists in Cancer Cells and Tumors. *Cancer Res* (2014) 74:3546–55. doi: 10.1158/0008-5472.CAN-13-3220
162. Mason JM, Dusad K, Wright WD, Grubb J, Budke B, Heyer WD, et al. RAD54 Family Translocases Counter Genotoxic Effects of RAD51 in Human Tumor Cells. *Nucleic Acids Res* (2015) 43:3180–96. doi: 10.1093/nar/gkv175
163. Song J, Yang D, Xu J, Zhu T, Chen YE, Zhang J. RS-1 Enhances CRISPR/Cas9- and TALEN-Mediated Knock-In Efficiency. *Nat Commun* (2016) 7:10548. doi: 10.1038/ncomms10548
164. Zhang JP, Li XL, Li GH, Chen W, Arakaki C, Botimer GD, et al. Efficient Precise Knocking With a Double Cut HDR Donor After CRISPR/Cas9-Mediated Double-Stranded DNA Cleavage. *Genome Biol* (2017) 18:35. doi: 10.1186/s13059-017-1164-8
165. Huang F, Motlekar NA, Burgwin CM, Napper AD, Diamond SL, Mazin AV. Identification of Specific Inhibitors of Human RAD51 Recombinase Using High-Throughput Screening. *ACS Chem Biol* (2011) 6:628–35. doi: 10.1021/cb100428c
166. Alagpulinsa DA, Ayyadevara S, Shmookler Reis RJ. A Small-Molecule Inhibitor of RAD51 Reduces Homologous Recombination and Sensitizes Multiple Myeloma Cells to Doxorubicin. *Front Oncol* (2014) 4:289. doi: 10.3389/fonc.2014.00289
167. Shkundina IS, Gall AA, Dick A, Cocklin S, Mazin AV. New RAD51 Inhibitors to Target Homologous Recombination in Human Cells. *Genes (Basel)* (2021) 12:920. doi: 10.3390/genes12060920
168. Zhu J, Zhou L, Wu G, Konig H, Lin X, Li G, et al. A Novel Small Molecule RAD51 Inactivator Overcomes Imatinib-Resistance in Chronic Myeloid Leukaemia. *EMBO Mol Med* (2013) 5:353–65. doi: 10.1002/emmm.201201760
169. Zhu J, Chen H, Guo XE, Qiu XL, Hu CM, Chamberlin AR, et al. Synthesis, Molecular Modeling, and Biological Evaluation of Novel RAD51 Inhibitors. *Eur J Med Chem* (2015) 96:196–208. doi: 10.1016/j.ejmech.2015.04.021
170. Roberti M, Schipani F, Bagnolini G, Milano D, Giacomini E, Falchi F, et al. Rad51/BRCA2 Disruptors Inhibit Homologous Recombination and Synergize With Olaparib in Pancreatic Cancer Cells. *Eur J Med Chem* (2019) 165:80–92. doi: 10.1016/j.ejmech.2019.01.008
171. Falchi F, Giacomini E, Masini T, Boutard N, Di Ianni L, Manerba M, et al. Synthetic Lethality Triggered by Combining Olaparib With BRCA2-Rad51 Disruptors. *ACS Chem Biol* (2017) 12:2491–7. doi: 10.1021/acschembio.7b00707
172. Bagnolini G, Milano D, Manerba M, Schipani F, Ortega JA, Gioia D, et al. Synthetic Lethality in Pancreatic Cancer: Discovery of a New RAD51-BRCA2 Small Molecule Disruptor That Inhibits Homologous Recombination and Synergizes With Olaparib. *J Med Chem* (2020) 63:2588–619. doi: 10.1021/acs.jmedchem.9b01526
173. Asan A, Skoko JJ, Woodcock CC, Wingert BM, Woodcock SR, Normolle D, et al. Electrophilic Fatty Acids Impair RAD51 Function and Potentiate the Effects of DNA-Damaging Agents on Growth of Triple-Negative Breast Cells. *J Biol Chem* (2019) 294:397–404. doi: 10.1074/jbc.AC118.005899
174. Maclay T, Day M, Mills K. Abstract 363: CYT01B, a Novel RAD51 Inhibitor, Acts Synergistically With PARP Inhibitors. *Cancer Res* (2019) 79:363.
175. Lynch RC, Bendell JC, Advani RJ, Falchook GS, Munster PN, Patel MR. First-In-Human Phase I/II Study of CYT-0851, a First-In-Class Inhibitor of RAD51-Mediated Homologous Recombination in Patients With Advanced Solid and Hematologic Cancers. *J Clin Oncol* (2021) 39:3006–6.
176. Shinohara A, Shinohara M, Ohta T, Matsuda S, Ogawa T. Rad52 Forms Ring Structures and Co-Operates With RPA in Single-Strand DNA Annealing. *Genes Cells* (1998) 3:145–56. doi: 10.1046/j.1365-2443.1998.00176.x

177. Rossi MJ, DiDomenico SF, Patel M, Mazin AV. RAD52: Paradigm of Synthetic Lethality and New Developments. *Front Genet* (2021) 12:780293. doi: 10.3389/fgene.2021.780293
178. Nogueira A, Fernandes M, Catarino R, Medeiros R. *RAD52* Functions in Homologous Recombination and Its Importance on Genomic Integrity Maintenance and Cancer Therapy. *Cancers (Basel)* (2019) 11:1622. doi: 10.3390/cancers11111622
179. Toma M, Sullivan-Reed K, Śliwiński T, Skorski T. RAD52 as a Potential Target for Synthetic Lethality-Based Anticancer Therapies. *Cancers (Basel)* (2019) 11:1561. doi: 10.3390/cancers11101561
180. Malacaria E, Pugliese GM, Honda M, Marabitti V, Aiello FA, Spies M, et al. Rad52 Prevents Excessive Replication Fork Reversal and Protects From Nascent Strand Degradation. *Nat Commun* (2019) 10:1412. doi: 10.1038/s41467-019-09196-9
181. Wu Y, Kantake N, Sugiyama T, Kowalczykowski SC. Rad51 Protein Controls Rad52-Mediated DNA Annealing. *J Biol Chem* (2008) 283:14883–92. doi: 10.1074/jbc.M801097200
182. Velic D, Couturier AM, Ferreira MT, Rodrigue A, Poirier GG, Fleury F, et al. DNA Damage Signalling and Repair Inhibitors: The Long-Sought-After Achilles' Heel of Cancer. *Biomolecules* (2015) 5:3204–59. doi: 10.3390/biom5043204
183. Kagawa W, Kagawa A, Saito K, Ikawa S, Shibata T, Kurumizaka H, et al. Identification of a Second DNA Binding Site in the Human Rad52 Protein. *J Biol Chem* (2008) 283:24264–73. doi: 10.1074/jbc.M802204200
184. Lok BH, Carley AC, Tchang B, Powell SN. RAD52 Inactivation is Synthetically Lethal With Deficiencies in BRCA1 and PALB2 in Addition to BRCA2 Through RAD51-Mediated Homologous Recombination. *Oncogene* (2013) 32:3552–8. doi: 10.1038/onc.2012.391
185. Feng Z, Scott SP, Bussen W, Sharma GG, Guo G, Pandita TK, et al. Rad52 Inactivation is Synthetically Lethal With BRCA2 Deficiency. *Proc Natl Acad Sci USA* (2011) 108:686–91. doi: 10.1073/pnas.1010959107
186. Chun J, Buechelmaier ES, Powell SN. Rad51 Paralog Complexes BCDX2 and CX3 Act at Different Stages in the BRCA1-BRCA2-Dependent Homologous Recombination Pathway. *Mol Cell Biol* (2013) 33:387–95. doi: 10.1128/MCB.00465-12
187. Chandramouly G, McDevitt S, Sullivan K, Kent T, Luz A, Glickman JF, et al. Small-Molecule Disruption of RAD52 Rings as a Mechanism for Precision Medicine in BRCA-Deficient Cancers. *Chem Biol* (2015) 22:1491–504. doi: 10.1016/j.chembiol.2015.10.003
188. Sullivan K, Cramer-Morales K, McElroy DL, Ostrov DA, Haas K, Childers W, et al. Identification of a Small Molecule Inhibitor of RAD52 by Structure-Based Selection. *PloS One* (2016) 11:e0147230. doi: 10.1371/journal.pone.0147230
189. Huang F, Goyal N, Sullivan K, Hanamshet K, Patel M, Mazina OM, et al. Targeting BRCA1- and BRCA2-Deficient Cells With RAD52 Small Molecule Inhibitors. *Nucleic Acids Res* (2016) 44:4189–99. doi: 10.1093/nar/gkw087
190. Li J, Yang Q, Zhang Y, Huang K, Sun R, Zhao Q. Compound F779-0434 Causes Synthetic Lethality in BRCA2-Deficient Cancer Cells by Disrupting RAD52–SsDNA Association. *RSC Adv* (2018) 8:18859–69. doi: 10.1039/C8RA01919C
191. Yang Q, Li Y, Sun R, Li J. Identification of a RAD52 Inhibitor Inducing Synthetic Lethality in BRCA2-Deficient Cancer Cells. *Front Pharmacol* (2021) 12:637825. doi: 10.3389/fphar.2021.637825
192. Hengel SR, Malacaria E, Folly da Silva Constantino L, Bain FE, Diaz A, Koch BG, et al. Small-Molecule Inhibitors Identify the RAD52-ssDNA Interaction as Critical for Recovery From Replication Stress and for Survival of BRCA2 Deficient Cells. *Elife* (2016) 5:e14740. doi: 10.7554/eLife.14740
193. Faridounnia M, Folkers GE, Boelens R. Function and Interactions of ERCC1-XPF in DNA Damage Response. *Molecules* (2018) 23:3205. doi: 10.3390/molecules23123205
194. Ahmad A, Robinson AR, Duensing A, van Drunen E, Beverloo HB, Weisberg DB, et al. ERCC1-XPF Endonuclease Facilitates DNA Double-Strand Break Repair. *Mol Cell Biol* (2008) 28:5082–92. doi: 10.1128/MCB.00293-08
195. McNeil EM, Melton DW. DNA Repair Endonuclease ERCC1-XPF as a Novel Therapeutic Target to Overcome Chemoresistance in Cancer Therapy. *Nucleic Acids Res* (2012) 40:9990–10004. doi: 10.1093/nar/gks818
196. Bowden NA. Nucleotide Excision Repair: Why is it Not Used to Predict Response to Platinum-Based Chemotherapy? *Cancer Lett* (2014) 346:163–71. doi: 10.1016/j.canlet.2014.01.005
197. Song L, Ritchie AM, McNeil EM, Li W, Melton DW. Identification of DNA Repair Gene Ercc1 as a Novel Target in Melanoma. *Pigment Cell Melanoma Res* (2011) 24:966–71. doi: 10.1111/j.1755-148X.2011.00882.x
198. Tsodikov OV, Enzlin JH, Schärer OD, Ellenberger T. Crystal Structure and DNA Binding Functions of ERCC1, a Subunit of the DNA Structure-Specific Endonuclease XPF-Ercc1. *Proc Natl Acad Sci USA* (2005) 102:11236–41. doi: 10.1073/pnas.0504341102
199. Tripsianes K, Folkers G, Ab E, Das D, Odijk H, Jaspers NG, et al. The Structure of the Human ERCC1/XPF Interaction Domains Reveals a Complementary Role for the Two Proteins in Nucleotide Excision Repair. *Structure* (2005) 13:1849–58. doi: 10.1016/j.str.2005.08.014
200. Jordheim LP, Barakat KH, Heinrich-Balard L, Matera EL, Cros-Perrial E, Bouledrak K, et al. Small Molecule Inhibitors of ERCC1-XPF Protein-Protein Interaction Synergize Alkylating Agents in Cancer Cells. *Mol Pharmacol* (2013) 84:12–24. doi: 10.1124/mol.112.082347
201. Elmenoufy AH, Gentile F, Jay D, Karimi-Busheri F, Yang X, Soueidan OM, et al. Targeting DNA Repair in Tumor Cells *via* Inhibition of ERCC1-XPF. *J Med Chem* (2019) 62:7684–96. doi: 10.1021/acs.jmedchem.9b00326
202. Gentile F, Elmenoufy AH, Ciniero G, Jay D, Karimi-Busheri F, Barakat KH, et al. Computer-Aided Drug Design of Small Molecule Inhibitors of the ERCC1-XPF Protein-Protein Interaction. *Chem Biol Drug Des* (2020) 95:460–71. doi: 10.1111/cbdd.13660
203. Elmenoufy AH, Gentile F, Jay D, Karimi-Busheri F, Yang X, Soueidan OM, et al. Design, Synthesis and In Vitro Cell-Free/Cell-Based Biological Evaluations of Novel ERCC1-XPF Inhibitors Targeting DNA Repair Pathway. *Eur J Med Chem* (2020) 204:112658. doi: 10.1016/j.ejmech.2020.112658
204. McNeil EM, Astell KR, Ritchie AM, Shave S, Houston DR, Bakrania P, et al. Inhibition of the ERCC1-XPF Structure-Specific Endonuclease to Overcome Cancer Chemoresistance. *DNA Repair (Amst)* (2015) 31:19–28. doi: 10.1016/j.dnarep.2015.04.002
205. Chapman TM, Gillen KJ, Wallace C, Lee MT, Bakrania P, Khurana P, et al. Catechols and 3-Hydroxypyridones as Inhibitors of the DNA Repair Complex ERCC1-XPF. *Bioorg Med Chem Lett* (2015) 19:4097–103. doi: 10.1016/j.bmcl.2015.08.031
206. Chapman TM, Wallace C, Gillen KJ, Bakrania P, Khurana P, Coombs PJ, et al. N-Hydroxyimides and Hydroxypyrimidinones as Inhibitors of the DNA Repair Complex ERCC1-XPF. *Bioorg Med Chem Lett* (2015) 25:4104–8. doi: 10.1016/j.bmcl.2015.08.024
207. Arora S, Heyza J, Zhang H, Kalman-Maltese V, Tillison K, Floyd AM, et al. Identification of Small Molecule Inhibitors of ERCC1-XPF That Inhibit DNA Repair and Potentiate Cisplatin Efficacy in Cancer Cells. *Oncotarget* (2016) 7:75104–17. doi: 10.18632/oncotarget.12072
208. Patel PS, Algouneh A, Hakem R. Exploiting Synthetic Lethality to Target BRCA1/2-Deficient Tumors: Where We Stand. *Oncogene* (2021) 40:3001–14. doi: 10.1038/s41388-021-01744-2
209. Carvajal-Garcia J, Cho JE, Carvajal-Garcia P, Feng W, Wood RD, Sekelsky J, et al. Mechanistic Basis for Microhomology Identification and Genome Scarring by Polymerase Theta. *Proc Natl Acad Sci USA* (2020) 117(15):8476–85. doi: 10.1073/pnas.1921791117
210. Seol JH, Shim EY, Lee SE. Microhomology-Mediated End Joining: Good, Bad and Ugly. *Mutat Res* (2018) 809:81–7. doi: 10.1016/j.mrfmmm.2017.07.002
211. Kent T, Chandramouly G, McDevitt SM, Ozdemir AY, Pomerantz RT. Mechanism of Microhomology-Mediated End-Joining Promoted by Human DNA Polymerase θ. *Nat Struct Mol Biol* (2015) 22:230–7. doi: 10.1038/nsmb.2961
212. Higgins GS, Boulton SJ. Beyond PARP-Polθ as an Anticancer Target. *Science* (2018) 359:1217–8. doi: 10.1126/science.aar5149
213. Zatreanu D, Robinson HMR, Alkhatib O, Boursier M, Finch H, Geo L, et al. Polθ Inhibitors Elicit BRCA-Gene Synthetic Lethality and Target PARP Inhibitor Resistance. *Nat Commun* (2021) 12:3636. doi: 10.1038/s41467-021-23463-8
214. Ceccaldi R, Liu JC, Amunugama R, Hajdu I, Primack B, Petalcorin MI, et al. Homologous-Recombination-Deficient Tumours are Dependent on Polθ-Mediated Repair. *Nature* (2015) 518:258–62. doi: 10.1038/nature14184
215. Wood RD, Doublié S. DNA Polymerase θ (POLQ), Double-Strand Break Repair, and Cancer. *DNA Repair (Amst)* (2016) 44:22–32. doi: 10.1016/j.dnarep.2016.05.003

216. Feng W, Simpson DA, Carvajal-Garcia J, Price BA, Kumar RJ, Mose LE, et al. Genetic Determinants of Cellular Addiction to DNA Polymerase Theta. *Nat Commun* (2019) 10:4286. doi: 10.1038/s41467-019-12234-1
217. Zhou J, Gelot C, Pantelidou C, Li A, Yücel H, Davis RE, et al. A First-In-Class Polymerase Theta Inhibitor Selectively Targets Homologous-Recombination-Deficient Tumors. *Nat Cancer* (2021) 2:598–610. doi: 10.1038/s43018-021-00203-x
218. Newman JA, Gileadi O. RecQ Helicases in DNA Repair and Cancer Targets. *Essays Biochem* (2020) 64:819–30. doi: 10.1042/EBC20200012
219. Kaiser S, Sauer F, Kisker C. The Structural and Functional Characterization of Human RecQ4 Reveals Insights Into its Helicase Mechanism. *Nat Commun* (2017) 8:15907. doi: 10.1038/ncomms15907
220. Aggarwal M, Sommers JA, Shoemaker RH, Brosh RMJr.. Inhibition of Helicase Activity by a Small Molecule Impairs Werner Syndrome Helicase (WRN) Function in the Cellular Response to DNA Damage or Replication Stress. *Proc Natl Acad Sci U.S.A.* (2011) 108:1525–30. doi: 10.1073/pnas.1006423108
221. Aggarwal M, Banerjee T, Sommers JA, Iannascoli C, Pichierri P, Shoemaker RH, et al. Werner Syndrome Helicase has a Critical Role in DNA Damage Responses in the Absence of a Functional Fanconi Anemia Pathway. *Cancer Res* (2013) 73(17):5497–507. doi: 10.1158/0008-5472.CAN-12-2975
222. Sommers JA, Kulikowicz T, Croteau DL, Dexheimer T, Dorjsuren D, Jadhav A, et al. A High-Throughput Screen to Identify Novel Small Molecule Inhibitors of the Werner Syndrome Helicase-Nuclease (WRN). *PloS One* (2019) 14(1):1–23. doi: 10.1371/journal.pone.0210525
223. Picco G, Cattaneo CM, van Vliet EJ, Crisafulli G, Rospo G, Consonni S. Werner Helicase Is a Synthetic-Lethal Vulnerability in Mismatch Repair-Deficient Colorectal Cancer Refractory to Targeted Therapies, Chemotherapy, and Immunotherapy. *Cancer Discovery* (2021) 11:1923–37. doi: 10.1158/2159-8290.CD-20-1508
224. Chan EM, Shibue T, McFarland JM, Gaeta B, Ghandi M, Dumont N. WRN Helicase is a Synthetic Lethal Target in Microsatellite Unstable Cancers. *Nature* (2019) 568:551–6. doi: 10.1038/s41586-019-1102-x
225. Nguyen GH, Dexheimer TS, Rosenthal AS, Chu WK, Singh DK, Mosedale G, et al. A Small Molecule Inhibitor of the BLM Helicase Modulates Chromosome Stability in Human Cells. *Chem Biol* (2013) 20:55–62. doi: 10.1016/j.chembiol.2012.10.016
226. Rosenthal AS, Dexheimer TS, Gileadi O, Nguyen GH, Chu WK, Hickson ID, et al. Synthesis and SAR Studies of 5-(Pyridin-4-Yl)-1,3,4-Thiadiazol-2-Amine Derivatives as Potent Inhibitors of Bloom Helicase. *Bioorg Med Chem Lett* (2013) 23:5660–6. doi: 10.1016/j.bmcl.2013.08.025
227. Yin QK, Wang CX, Wang YQ, Guo QL, Zhang ZL, Ou TM, et al. Discovery of Isaindigotone Derivatives as Novel Bloom's Syndrome Protein (BLM) Helicase Inhibitors That Disrupt the BLM/DNA Interactions and Regulate the Homologous Recombination Repair. *J Med Chem* (2019) 62:3147–62. doi: 10.1021/acs.jmedchem.9b00083
228. Simon N, Bochman ML, Seguin S, Brodsky JL, Seibel WL, Schwacha A. Ciprofloxacin is an Inhibitor of the Mcm2-7 Replicative Helicase. *Biosci Rep* (2013) 33:783–95. doi: 10.1042/BSR20130083
229. Hsu EC, Shen M, Aslan M, Liu S, Kumar M, Garcia-Marques F, et al. MCM2-7 Complex is a Novel Druggable Target for Neuroendocrine Prostate Cancer. *Sci Rep* (2021) 11:13305. doi: 10.1038/s41598-021-92552-x
230. Alshahrani MY, Alshahrani KM, Tasleem M, Akeel A, Almeleebia TM, Ahmad I, et al. Computational Screening of Natural Compounds for Identification of Potential Anti-Cancer Agents Targeting MCM7 Protein. *Molecules* (2021) 26(19):5878. doi: 10.3390/molecules26195878
231. Lin CY, Wu HY, Hsu YL, Cheng TR, Liu JH, Huang RJ, et al. Suppression of Drug-Resistant Non-Small-Cell Lung Cancer With Inhibitors Targeting Minichromosomal Maintenance Protein. *J Med Chem* (2020) 63:3172–87. doi: 10.1021/acs.jmedchem.9b01783
232. O'Neil NJ, Bailey ML, Hieter P. Synthetic Lethality and Cancer. *Nat Rev Genet* (2017) 18:613–23. doi: 10.1038/nrg.2017.47
233. Li H, Liu ZY, Wu N, Chen YC, Cheng Q, Wang J. PARP Inhibitor Resistance: The Underlying Mechanisms and Clinical Implications. *Mol Cancer* (2020) 19:107. doi: 10.1186/s12943-020-01227-0
234. Li H, Yang Y, Hong W, Huang M, Wu M, Zhao X. Applications of Genome Editing Technology in the Targeted Therapy of Human Diseases: Mechanisms, Advances and Prospects. *Signal Transduct Target Ther* (2020) 5:1. doi: 10.1038/s41392-019-0089-y
235. Liu M, Zhang W, Xin C, Yin J, Shang Y, Ai C, et al. Global Detection of DNA Repair Outcomes Induced by CRISPR-Cas9. *Nucleic Acids Res* (2021) 49 (15):8732–42. doi: 10.1093/nar/gkab686
236. Fu Y, Foden JA, Khayter C, Maeder ML, Reyon D, Joung JK, et al. High-Frequency Off-Target Mutagenesis Induced by CRISPR-Cas Nucleases in Human Cells. *Nat Biotechnol* (2013) 31:822–6. doi: 10.1038/nbt.2623

Conflict of Interest: KSP is a Vice-President of Research and JJT is a cofounder and CSO of NERx Biosciences.

The remaining authors declare that the research was conducted in the absence of any commercial or financial relationships that could be construed as a potential conflict of interest.

Publisher's Note: All claims expressed in this article are solely those of the authors and do not necessarily represent those of their affiliated organizations, or those of the publisher, the editors and the reviewers. Any product that may be evaluated in this article, or claim that may be made by its manufacturer, is not guaranteed or endorsed by the publisher.

frontiers | Frontiers in Oncology

REVIEW
published: 21 April 2022
doi: 10.3389/fonc.2022.846965

Xeroderma Pigmentosum Complementation Group C (XPC): Emerging Roles in Non-Dermatologic Malignancies

Nawar Al Nasrallah[1], *Benjamin M. Wiese*[1] *and Catherine R. Sears*[1,2]*

[1] Division of Pulmonary, Critical Care, Sleep and Occupational Medicine, Department of Medicine, Indiana University School of Medicine, Indianapolis, IN, United States, [2] Division of Pulmonary Medicine, Richard L. Roudebush Veterans Affairs Medical Center, Indianapolis, IN, United States

Xeroderma pigmentosum complementation group C (XPC) is a DNA damage recognition protein essential for initiation of global-genomic nucleotide excision repair (GG-NER). Humans carrying germline mutations in the *XPC* gene exhibit strong susceptibility to skin cancer due to defective removal *via* GG-NER of genotoxic, solar UV-induced dipyrimidine photoproducts. However, XPC is increasingly recognized as important for protection against non-dermatologic cancers, not only through its role in GG-NER, but also by participating in other DNA repair pathways, in the DNA damage response and in transcriptional regulation. Additionally, XPC expression levels and polymorphisms likely impact development and may serve as predictive and therapeutic biomarkers in a number of these non-dermatologic cancers. Here we review the existing literature, focusing on the role of XPC in non-dermatologic cancer development, progression, and treatment response, and highlight possible future applications of XPC as a prognostic and therapeutic biomarker.

Keywords: nucleotide excision repair (NER), base excision repair (BER), lung cancer, biomarker, bladder cancer, chemotherapy, xeroderma pigmentosum (XP)

OPEN ACCESS

Edited by:
Michael Weinfeld, University of Alberta, Canada

Reviewed by:
Elliot Drobetsky, Université de Montréal, Canada
Bennett Van Houten, University of Pittsburgh, United States

***Correspondence:**
Catherine R. Sears
crufatto@iu.edu

Specialty section:
This article was submitted to Cancer Molecular Targets and Therapeutics, a section of the journal Frontiers in Oncology

Received: *31 December 2021*
Accepted: *09 March 2022*
Published: *21 April 2022*

Citation:
Nasrallah NA, Wiese BM and Sears CR (2022) Xeroderma Pigmentosum Complementation Group C (XPC): Emerging Roles in Non-Dermatologic Malignancies. Front. Oncol. 12:846965. doi: 10.3389/fonc.2022.846965

INTRODUCTION

Genomic instability from altered DNA repair processes is a hallmark of cancer, playing an important role in both tumor development and treatment response (1). Importantly, the therapeutic efficacy of many chemotherapy drugs and radiation relies on the induction of DNA damage as a means of selectively eliminating rapidly proliferating tumor cells. (2).

Daily DNA damage comes from a variety of different sources exogenous to the cell, such as ultraviolet (UV) light, tobacco smoking, and other chemicals, as well as endogenous sources such as oxidative stress caused by normal cellular metabolism (3). The nucleotide excision repair (NER) pathway is the primary DNA repair pathway involved in repair of bulky, helix distorting intrastrand DNA crosslinks caused by UV or platinum chemotherapeutics, as well as bulky monoadducts induced by environmental carcinogens including B[*a*]P-7,8-dihydrodiol-9,10-epoxide (BPDE) and

aflatoxin B1 (AFB1). Much of our understanding of NER comes from studying the repair of UV-induced lesions, such as pyrimidine-pyrimidone (6-4) photoproduct (6–4PPs) and cyclobutane pyrimidine dimers (CPDs), for which NER serves as the primary repair pathway (4). Critical to its role in cancer therapeutic response, NER is the primary repair pathway for 1,2-d(GpG) and 1,3-d(GpTpG) intrastrand platinum crosslinking lesions, the predominant DNA adducts produced by the commonly used chemotherapeutic drugs cisplatin and carboplatin (5). The NER pathway consists of 4 essential steps: recognition, incision/excision, re-synthesis, and ligation (2). Differing in the mechanism of DNA damage recognition, NER is divided into two subpathways: global genomic NER (GG-NER) and transcription-coupled NER (TC-NER). Both NER subpathways repair helix-destabilizing DNA lesions, with TC-NER rapidly repairing damage in actively transcribed genes. TC-NER is initiated when the RNA polymerase II complex is physically stalled at the site of a DNA damaging lesion; this subsequently triggers recruitment of CSB and coordinated recruitment of other TC-NER recognition proteins including CSA, XAB2, UVSSA, USP7 and others (6, 7). Initiated by the xeroderma pigmentosum group C (XPC) complex, GG-NER recognizes helix-distorting lesions anywhere throughout the genome but is primarily responsible for the slower repair of damage on non-transcribed portions (8, 9). Following damage recognition, subsequent NER repair then progresses identically between both NER subpathways. XPC is critical to damage recognition and initiation of GG-NER, but dispensable for TC-NER (9).

There is a clear and established association between defective NER and tumor development, as illustrated by the rare autosomal recessive congenital syndrome xeroderma pigmentosum (XP). XP patients are characterized by defective nucleotide excision repair (NER) of sunlight-induced dipyrimidine photoproducts (10). Depending on the mutated NER protein, XP patients present with a spectrum of disease, which consists of various neurological degenerative disorders and even developmental defects, but all XP patients present with extreme photosensitivity and a strong predisposition to skin cancer (10, 11). Those with a mutation in XPC (XP-C), a common cause of XP in Europe, the United States and North Africa, present with classical XP skin manifestations, including photosensitivity and early dermatologic malignancies, without neurological or developmental defects (11, 12). Indeed, both non-melanomatous skin cancers and melanomas develop more often (10,000 and 2,000-fold increased incidence) and at a much younger age in XP compared to non-XP populations, with a median age at diagnosis of 9 and 22 years respectively (13). Importantly, although XP patients most commonly die of skin cancers or of progressive neurologic diseases, internal malignancies are frequently described in XP patients, with a 39-year prospective cohort study finding internal cancers as the cause of death in 17%, highlighting an important role of NER in non-dermatologic malignancies as well (13, 14).

XPC is increasingly recognized as an important player in solid organ cancer development and response to cancer therapeutics, both through its canonical role in GG-NER and through other repair pathways. Here we review the most recent updates on the role of XPC in non-dermatologic malignancies.

XPC ROLE IN DNA REPAIR

XPC in GG-NER

XPC is essential to GG-NER, serving as the primary initiating factor. XPC scans the genome in a 5'-to-3' directionality until it detects strand distortion caused by DNA damaging lesions, binding the opposite strand in a sequence-independent manner (8, 15, 16). The XPC protein *in vivo* is found in a heterodimeric form with RAD23B (human orthologue HR23B) which further stimulates XPC's role in NER repair (17). Centrin2 forms a heterotrimer with XPC/HR23B, which has been found to augment binding to DNA damage sites (18). While the XPC complex is typically sufficient to identify NER-repaired DNA lesions, some minimally strand-distorting lesions, such as UV-induced CPD, require recognition by DDB2 and DDB1, which then recruit XPC to the damage site (7).

After the initial recognition of a helix distorting lesion by either XPC or RNA polymerase II, NER proceeds in a stepwise sequence that involves recruitment of several proteins. Transcription factor IIH complex (TFIIH) partially unwinds the DNA duplex at the site of DNA damage, creating an opened bubble (16, 19). TFIIH further coordinates repair by interacting with XPA, stabilizing the bubble along with the single stranded binding protein RPA, and finally engaging with the nuclease (XPF/ERCC1) that makes an incision 5' of the lesion. Subsequent repair involves coordination of repair synthesis by DNA polymerases δ, ϵ or κ, subsequent incision 3' of the DNA lesion by XPG to remove the damaged strand, and finally repair of the nick by DNA ligases. Several excellent reviews are available which expand upon and provide excellent graphical representation of the steps involved in NER (7, 16, 20).

A number of recent studies highlight that post-translational modifications of XPC, including polyubiquitination, SUMOylation and phosphorylation, likely impact XPC efficiency to detect DNA damage and initiate NER (21–25). Polyubiquitination of XPC appears to aid in repair of UV-damaged DNA, by allowing XPC to replace DDB1/DDB2 proteins and in promoting XPC binding to the site of DNA damage (21, 25). Tight control of XPC ubiquitination is likely required to ensure DNA repair and may be dysregulated in human cancers. For instance, overexpression of ubiquitin ligases, such as Cullin-RING ubiquitin ligase 4 A (CUL4A), is common in cigarette smoke-related lung cancer, and inversely correlates to XPC expression (26). SUMOylation of XPC appears to stabilize the protein, preventing proteasome degradation and enhancing GG-NER in the setting of UV-induced DNA damage (22). XPC phosphorylation is closely regulated after DNA damage, with phosphorylation at serine 982 likely mediated by the DNA damage response proteins ATM and ATR, and dephosphorylation mediated by wild-type p53-induced phosphatase 1 (WIP1) (27, 28). Following UVB exposure, serine/threonine casein kinase 2 (CK2) phosphorylates XPC at serine 94, leading to recruitment of ubiquitinated XPC and downstream NER factors to DNA damage sites (24). Phosphorylation of XPC at serine

892 seems to decrease repair of UVB-induced DNA damage, including CPD and 6-4PP, while serine 94 phosphorylation promotes GG-NER repair (24). However, whether these modifications impact the role of XPC on other repair pathways, or how they affect XPC's role in repair of DNA damage from other sources, such as cisplatin, is not well-studied. Further, modification of other proteins may impact XPC function. For instance, histone acetylation may decrease NER through attenuated XPC interaction at sites of DNA damage (23). These modifications, which regulate XPC function in GG-NER repair and the downstream DNA damage response, are likely to impact cancer risk and response to therapy, although this specific link requires more study.

XPC in Other DNA Repair Processes

It is important to note the mounting evidence highlighting an important link between the role of XPC in DNA repair, DNA damage response and transcriptional regulation and cancer development. These are summarized in **Figure 1**. In particular, the impact of XPC DNA damage repair extends beyond its canonical role in GG-NER. XPC may play a role as a more global DNA damage sensor. Recent *in vitro* studies have elucidated a role of Rad4, the yeast homolog of XPC, in the recognition and repair of multiple contiguous mismatched base pairs (29). Specifically, *in vitro* binding and conformational studies suggest that Rad4/XPC interacts with the nucleotides directly across from the mismatched bases (on the complementary strand), leading to subsequent unwinding, DNA bending, and flipping out of the mismatched nucleotides and stabilization of this conformation to allow for subsequent DNA repair (29, 30). These studies suggest a mechanism by which XPC acts as a universal DNA damage sensor, recognizing sites of DNA distortion and binding in a lesion-agnostic fashion ("non-specific binding"). Indeed, recent studies suggest that the Rad4/XPC-DNA binding leads to different conformational changes based on the lesion type, such that XPC bound at the site of UV-induced DNA damage ("specific binding") facilitates recruitment and initiation of NER while "non-specific" binding to minimally strand-distorting lesions facilitates non-NER repair (29, 30). Extensive structural analysis has been done to understand sequence and structural changes of DNA lesions sensitive and resistant to Rad4/XPC binding and subsequent GG-NER efficiency (31).

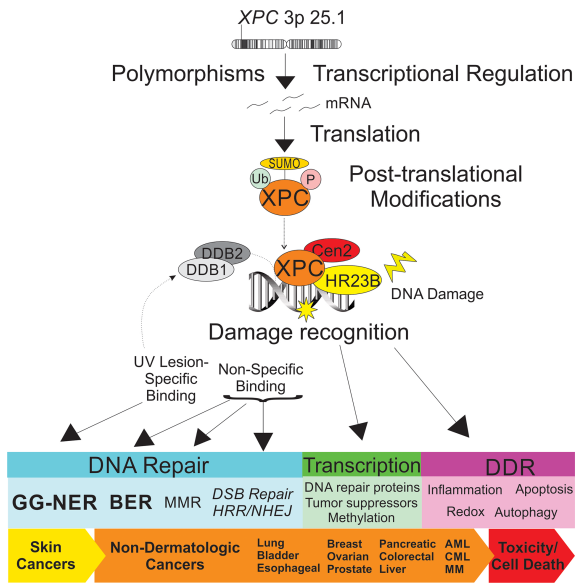

FIGURE 1 | Schematic representation of the impact of XPC in dermatologic and non-dermatologic malignancies. Both *XPC* mutations and transcriptional regulation of *XPC* expression levels are described as impacting risk of the cancer development and response to treatment. Post-translational modifications of XPC include ubiquitination, SUMOylation and phosphorylation, which impact XPC expression levels and XPC function. XPC is a versatile DNA damage sensor, leading to differing binding affinities and DNA-XPC conformational changes for UV-induced DNA damage ("specific binding", in concert with the UV-DDB complex, leading to GG-NER) and other DNA damage ("non-specific binding", leading to other DNA repair pathways). Differential response of XPC to DNA damage leads to classical GG-NER or alternate DNA repair, altered transcriptional regulation, and DNA damage response ultimately impacting cancer risk and tumor cell toxicity. XPC, xeroderma pigmentosum group c; Ub, ubiquitin; SUMO, small ubiquitin-like modifier; P, phosphorylation site; DDB1, DNA damage-binding 1; DDB2, DNA damage binding 2; Cen2, centrin 2; HR23B, human UV excision repair protein RAD23; GG-NER, global genomic nucleotide excision repair; BER, base excision repair; MMR, mismatch repair; DSB, double strand break; HRR, homologous recombination repair; DDR, DNA damage response; AML, acute myeloid leukemia; CML, chronic myeloid leukemia; MM, multiple myeloma.

Mounting evidence points to a role of XPC in base excision repair (BER). BER is the primary repair mechanism of small, base modifications that do not distort the DNA helical structure. Fibroblasts obtained from XP-C patients displayed increased oxidative DNA damage after UVB-irradiation compared to fibroblasts without an *XPC* defect. These UV-treated *XPC* deficient fibroblasts had decreased gene expression of a number of factors involved in BER, including *OGG1*, *MYH*, *APE1*, *LIG3*, *XRCC1*, and *Polβ*, and this correlated with decreased protein expression in three BER-glycosylases: OGG1, MYH, and APE1 (32). Likewise, *XPC* deficient fibroblast cell lines show lower levels of *APE1* and *OGG1* mRNA compared to *XPC* proficient cells, however transiently complementing these cells with XPC only augmented the level and function of OGG1 but not APE1, suggesting a differential impact of XPC on OGG1 glycosylase activity (33). Numerous *in vitro* studies support a role of XPC in augmenting BER activity, particularly through augmentation of the glycosylase activities of OGG1, SMUG1, 3-methyladenine DNA glycosylase (MPG) and thymine DNA glycosylase (TDG) (34–37). XPC may also augment BER through DNA damage recognition. Interestingly, live cell imaging studies show a rapid recruitment of both cockayne syndrome protein B (CSB, involved in TC-NER) and XPC to the BER-repaired 8-dihydro-8-oxodeoxyguanosine (8-OHdG) DNA lesion, suggesting a role of XPC in early recognition of BER-repaired lesions, even though these do not cause significant strand distortion (38). This may be further explained by the recent finding that DDB2 rapidly localizes to 8-OHdG lesions, preceding and augmenting XPC and subsequent OGG1 recruitment (39). This role of DDB2 in recruiting XPC to minimally helix-distorting lesions is similar to that modeled in GG-NER repair. Interestingly, this recent study suggested a specific role of XPC and DDB2 in augmenting OGG1-mediated BER repair

of 8-OHdG lesions in non-transcribed, heavily chromatin-bound genomic regions, which differed from the mechanism observed for repair of 8-OHdG lesions in actively transcribed regions, which ultimately involved recruitment of XPA by OGG1 but was independent of XPC and DDB2 (39). *In vivo* studies further support a supportive role of XPC in BER. *Xpc* deficient mice had increased oxidative stress and mutation load over time with treatment with pro-oxidant agents, which was not observed in *Xpa* deficient and wild type mice (40). However, there was a comparable increase of 8-OHdG lesions by liquid chromatography electrospray tandem mass spectrometry in the uterus of both *Xpc* deficient and *Xpc* proficient mice after treatment with equine estrogen, suggesting the effect may be specific to the damaging agent, duration of treatment or tissue-specific (41). Urethane-treated *Xpc*-/- mice developed an increase in lung adenocarcinomas compared to their wild-type counterparts, but treatment with the anti-oxidant N-acetylcysteine (NAC) decreased tumor development, further supporting a link between XPC, oxidative damage and cancer development (42). Although modified base recognition and augmentation of BER glycosylase and APE1 endonuclease activity have all been proposed, exactly how XPC is involved in BER of oxidized DNA lesions and the subsequent cancer development remain areas of active research.

Mismatched DNA nucleotides, particularly those occurring during replication, are repaired by DNA mismatch repair (MMR). In humans, deficient MMR, through both sporadic and inherited genetic disease, is linked to aging and cancer by promoting genomic instability (43, 44). In particular, defective MMR leads to Lynch syndrome, characterized by a high lifetime risk of colon and other cancer, and MMR defects are associated with ~10-20% of sporadic colon cancers (45, 46). Increasingly, cooperative and possibly overlapping roles of both MMR and NER proteins have been implicated in the recognition and repair of some DNA interstrand crosslinks (ICLs), one of the most cytotoxic types of DNA damage. ICLs are caused by a number of environmental toxins as well as commonly used chemotherapeutic agents, including cisplatin, carboplatin and oxaliplatin commonly used to treat solid-organ tumors (47). Repair of these lesions requires cooperation between different DNA repair pathways, including the Fanconi anemia (FA), NER, homologous recombination repair (HRR) and translesion synthesis (TLS) pathways (47). XPC, along with other NER proteins, were found to be essential for repair of site-specific ICLs caused by psoralen and mitomycin C *in vitro* using a host-cell reactivation assay (48). Further, both the MMR and NER pathways have been implicated in the repair of triplex-forming oligonucleotide (TFO)-directed psoralen ICLs (Tdp-ICLs) (49–52). Specifically, in MSH2-deficient human cell-free extracts, both binding by the XPC complex and repair of Tdp-ICLs were decreased, further highlighting a cooperative role between NER and MMR ICL repair (53, 54). Additionally, two NER protein complexes, XPC-Rad23B and XPA-RPA can bind psoralen ICLs in cells and *in vitro*, forming a complex with the MMR complex MutSβ, without which cell toxicity to psoralen increases (55). Further evidence of a connection between XPC and MMR is evidenced in cisplatin-treated *XPC* deficient cells, in which altered expression was noted in three MMR genes: *MLH1*, *MSH2*, and *MSH6* (56). Cells deficient in *Xpa* and *Msh2* are less sensitive to UV-induced cellular toxicity compared to *Xpa*-/- cells with normal *Msh2* expression, suggesting a role of MSH2 in the DNA damage response but not necessarily in NER repair of UV-induced DNA damage (57). Finally, combined defects in NER and MMR have been associated with increased UV-induced skin cancers. Combined *Xpa* and *Msh2* deficiencies in mice are associated with an increase in UV-induced skin cancers, and similarly *Xpc*-/-; *Msh2*-/- mice developed UV-induced skin cancers earlier than their wild-type counterparts or those deficient in either *Xpc* or *Msh2* alone, suggesting cooperative but non-overlapping roles in UV-induced DNA damage repair (57, 58). An XPC-deficient lymphoblastoid cell line modified by acquired tolerance to the MMR-dependent chemical N-methyl-N-nitrosourea (MNU) exhibited decreased MSH6 expression and MMR efficiency (59). These XPC-deficient, MSH6-low cells effectively repaired UV- and cisplatin-induced lesions by TC-NER, suggesting that the previously observed MMR-NER interactions may rest in interactions with proteins involved in GG-NER, particularly in cancer development. Of interest, the authors of this study noted unusual difficulty in producing MMR deficient variants in two XPC-deficient lymphoblastoid cell lines, further suggesting possible yet still undefined interactions between XPC and MMR functions. Overall, these findings suggest that XPC may cooperate with MMR proteins in the identification and repair of strand-distorting configurations of mismatched nucleotides and ICLs and may serve a role in regulation of the MMR pathway for some types of DNA damage, impacting of mutagenesis.

Additionally, XPC may play a role in DNA double strand break (DSB) repair. Long-term *XPC* knock-down in HeLa cells was associated with increased sensitivity to the chemotherapeutic drug, etoposide, the cytotoxicity of which is dependent on replication-induced DSB; gamma-irradiation of these cells lead to cell cycle alterations without altered clonogenic survival (60). Furthermore, the increased somatic and germ line mutation rates, as measured by expanded simple tandem repeat (ESTR), were increased in *Xpc* deficient mice exposed to whole body irradiation (61). More direct evaluation of NHEJ activity *in vitro* using Manley extracts from *XPC* knock-down HeLa cells showed a capacity of NHEJ rejoining with linear but not circular DNA (60). XPC deficiency has also been associated with inhibition of BRCA1 expression on bladder cancer cells treated with cisplatin, resulting in accumulation of DNA damage and pointing to a potential indirect role of XPC in homologous recombination or, more likely, replication-induced double strand breaks (62). Overall, this suggests a complex, likely indirect role of XPC in the repair of multiple types of DNA damage.

The impact of XPC in DNA damage is not solely associated with its roles in DNA repair but has been implicated in altered downstream DNA damage response (**Figure 1**). For instance, at sites of UV-induced DNA damage, XPC attracts and physically interacts with Ataxia telangiectasia- and Rad3- related (ATR) and Ataxia telangiectasia mutated (ATM) proteins, two kinases important in DNA damage- and replication stress-induced

checkpoint activations. Both DDB2 and XPC facilitate ATR and ATM phosphorylation and subsequent activation, leading to phosphoactivation of ATR- and ATM- substrates involved in cell cycle regulation (including Chk1 and Chk2) (63). Additionally, XPC facilitates ATR- and ATM- recruitment to sites of DNA damage as well as two proteins, BRCA1 and RAD51, known to be involved in replication and HRR (63). XPC has been implicated in enhancing DNA damage–induced apoptosis through inhibition of caspase-2 transcription (64), and both increased apoptosis and altered autophagy are observed in cells exposed to carcinogenic cigarette smoke and arsenic trioxide *in vitro* and *in vivo* (65, 66). Independent of DNA damage, *XPC* silencing and overexpression in mouse and human embryonic stem cell models support a role of XPC in global DNA demethylation through augmentation of TDG avidity (37, 67). XPC may have an even broader role on transcriptional regulation through coordination with other transcription factors and has been linked with regulation of a number of genes, including tumor suppressor genes, even in the absence of DNA damage (37, 68, 69). XPC involvement in the DNA damage response may also impact cell redox homeostasis and also in local inflammation. For instance, silencing of XPC in arsenic trioxide-treated human glioma cells was associated with decreased anti-oxidant factors and subsequent increase in oxidative damage, including 8-OHdG (65). Melis and colleagues described the glutathione anti-oxidant response as deficient in *Xpc*-/- mice, and most recently, Mori and colleagues describe a redox imbalance due to compromised mitochondrial function and reduced glutathione peroxidase activity (70, 71). Lung fibroblasts exposed to both the carcinogen BPDE and to the chemotherapeutic drug cisplatin produced higher levels of the pro-inflammatory, tumor promoting cytokine interleukin-6 (IL-6) through the p38-SAPK pathway (72). As the local tumor immune response is increasingly recognized as critical to solid organ cancer development, the role of XPC in local tumor microenvironment, including immune escape, warrants further investigation.

XPC IN HEMATOLOGIC CANCERS

The role of XPC in hematopoietic malignancy has been explored over the last several years, both in mouse models and observations in various patient populations. XPC deficient mice (*Xpc*-/-) have a significantly higher frequency of spontaneous mutations in the *hprt* gene in splenic T lymphocytes as compared to *Xpa*-/- and *Csb*-/- mice; this was also enhanced with aging (73). Similarly, long-term exposure to paraquat in *Xpc*-/- mice leads to an increase in lymphoid hyperplasia (40). XPC deficient mice had hypocellular bone marrow associated with a 10-fold increased sensitivity to carboplatin and decreased cell and overall mouse survival as compared to wild type mice, suggesting an important role of XPC in hematopoietic cell response to treatment with platinum-containing drugs (74). Importantly, these studies suggest that XPC expression may impact bone marrow suppression and altered hematopoiesis, common treatment-limiting adverse events associated with platinum-based chemotherapeutic agents.

Alterations in DNA repair processes, including those associated with *XPC* deficiency, have been linked to hematologic malignancies in a human population (75). While overshadowed by the recognition of skin malignancies early after identification of the XP phenotype, early case reports include pediatric and young adult XP-C patients who develop hematologic malignancies (14). More recent studies have shown an increased propensity for hematologic malignancies and sarcomas in populations of individuals with xeroderma pigmentosum deficient in XPC (XP-C). Individuals with XP-C are at an increased risk of leukemia and other hematologic malignancies, as well as alterations in genotoxic effects due to treatment of these cancers (76, 77). Sarasin et al. examined a cohort of 161 patients with XP-C and found that 13 of these individuals developed either overt myelodysplastic syndrome (MDS) or acute myeloid leukemia (AML) with a median age of 22 years at diagnosis (**Table 1**). This finding of MDS/AML was specific for the most common homozygous frameshift *XPC* mutation delTG (c.1643_1644delTG; p.Val548Ala>fsX25) and has not been observed with an increased frequency in other XP patients (77). Similarly, a cohort of 117 individuals with XP-C were followed from 1971 to 2018 and four patients were found to develop hematologic malignancies, including MDS, acute leukemias and high grade lymphoma (110). More recently, a shared mutational profile was identified by whole genome sequencing in leukemias from six XP-C patients, which differed from the mutational patterns in non-XP-C spontaneous AML samples and corresponded to a pattern described with altered GG-NER (111). Single nucleotide polymorphisms (SNPs) of the *XPC* gene have been studied in a number of malignancies, many of which may modify disease risk, prognosis or alter treatment response (**Figure 2**). Of these, several have been studied in leukemias (**Table 1**). In AML treated with induction chemotherapy, the *XPC* Ala499Val SNP was associated with lower overall disease-free survival, particularly when combined with an *XPD* codon 751 AC/CC polymorphism (78), and two *XPC* SNPs (Ala499Val and Lys939Gln) were associated with variable responses to imatinib in BCR-ABL driven chronic myelogenous leukemia (CML) (79). In regard to tolerating induction chemotherapy or hematopoietic stem cell transplantation in the setting of XPC abnormalities, there is little data.

Recently, the NER pathway has been studied in the setting of multiple myeloma (MM) due to the reliance on alkylating agents in the treatment of this malignancy; DNA damage caused by alkylating agents are typically repaired by NER. Dumontet et al. found that SNPs in multiple genes, including *XPC*, were associated with longer time to progression- in individuals treated with vincristine-adriamycin-dexamethasone followed by high dose melphalan and stem cell transplantation (80). Similarly, inhibition of the NER pathway in multiple myeloma increases the sensitivity to alkylating agents and overcomes resistance to these alkylating agents (113). Though XPC has not been explicitly implicated in these latter studies, it warrants

TABLE 1 | Summary of clinical studies evaluating *XPC* polymorphisms and epigenetic alterations by malignancy.

Malignancy	*XPC* mutation or SNP	Clinical association	Study name and size
AML AML/MDS	*XPC* polymorphism Ala499Val (rs2228000)	*XPC* Ala499Val was associated with lower overall disease-free survival in AML patient treated with induction chemotherapy	(78) 170 adult de-novo AML patients with intermediate cytogenetics treated with induction chemotherapy
	c.1643-1644 delTG *XPC* mutation	Increased risk for developing MDS or AML	(77) 161 patients with XP-C from 142 consanguineous North African families living in France
CML	*XPC* polymorphisms 499C and 939A	Both 499C and 939A wild-type haplotype associated with improved response to imatinib.	(79) 92 Caucasian patients with BCR-ABL-positive CML in five Spanish Institutions.
Multiple Myeloma	*XPC* polymorphism 939A>C (Lys939Gln) (rs2228001)	*XPC* Lys939Gln was associated with freedom from progression (FFP) in patients receiving high-dose melphalan (HDM)	(80) 169 MM patients from France and Canada who underwent treatment with HDM and stem cell transplant.
Lung cancer	*XPC* polymorphism PAT+/+ variant	*XPC* PAT +/+ was associated with an increased risk for lung cancer	(81) Hospital-based case-control study of 359 newly diagnosed lung cancer and matched 375 control subjects in Northern Spain.
	XPC Lys939Gln polymorphisms (rs2228001)	Heterozygous carriers of the C-allele and homozygous carriers had higher risk of lung cancer in the youngest available age interval (50–55 years)	(82) Danish study included 265 lung cancer cases and 272 control individuals.
	XPC Polymorphisms Lys939Gln and Ala499Val (rs2228001, rs2228000)	*XPC* 939Gln/Gln and 939Lys/Gln both were associated with increased risk of lung cancer with low penetrance. *XPC* 499Val increased total cancer risk (OR1.15), but not specifically the lung cancer.	(83) Meta-analysis that included 33 published case–control studies
	XPC Polymorphism Lys939Gln (rs2228001)	Females carrying *XPC* 939Gln/Gln vs. *XPC* 939Lys/Gln. 939Gln/Gln had significantly increased risk of lung cancer as well as other females and males with several combination of polymorphisms in *XPC*, *XPD* (Lys751Gln), *hOGG1* (Ser326Cys) and *XRCC1* (Arg399Gln)	(84) Case-Control study of 382 patients with lung cancer and 379 healthy controls of Caucasian Slovaks race/ethnicity.
	XPC polymorphisms (Lys939Gln, Ala499Val, and PAT) (rs2228001, rs2228000)	Homozygous Gln939Gln genotype was associated with significantly increased risk of lung cancer in Asian population PAT -/- genotype significantly reduced susceptibility to lung cancer in Caucasian population *XPC* Ala499Val polymorphism was not associated with lung cancer risk.	(85) Meta-analysis of 14 studies including 5647 lung cancer cases and 6908 controls
	XPC Lys939Gln polymorphism (rs2228001)	*XPC* Lys939Gln was associated with higher lung cancer susceptibility (OR 1.28)	(86) Polymorphism stratified meta-analysis, 16 studies of cancers with 5581 cases and 6351 controls (5 studies specific for lung cancer)
	XPC polymorphism rs2733533	XPC rs2733533 associated with lung cancer susceptibility, the combination of genotype A carriers and heavy smokers (≥30 pack-year) had a 13.32-fold risk of lung cancer compared with the C/C genotype and no smoking.	(87) Case control study of 265 lung cancer patients and 301 healthy controls
	XPC polymorphisms Lys939Gln, Ala499Val (rs2228001, rs2228000)	Neither SNP altered response to platinum-based chemotherapy.	(88) Meta-analysis of 1,615 patients from 10 studies for the rs2228001 and 858 samples from six studies for rs2228000.
Prostate Cancer (PC)	*XPC* polymorphisms PAT, Lys939Gln (rs2228001)	PAT (insertion/insertion) genotype increases the risk of developing PC, *XPC* Lys939Gln and *XPC*-PAT variants (Lys/Gln + PAT D/D) were protected against PC development compared to controls.	(89) Study in Tunisian population included 110 PC patients compared to 266 matched control men.
	XPC PAT polymorphism	*XPC* PAT+/+ subjects genotype exhibited a significantly increased risk for PC, smokers with PAT+/– or PAT+/+ had a higher risk for PC.	(90) 202 subjects with prostate cancer and 221 healthy controls in a Chinese Han population.
	NER polymorphisms, *XPC* intron 11 C>A (rs3729587)	*XPC* intron11 C/A polymorphism was associated with an increased risk of prostate cancer.	(91) Hospital-based cohort consisted of 152 patients with prostate cancer and 142 male controls.

(Continued)

TABLE 1 | Continued

Malignancy	*XPC* mutation or SNP	Clinical association	Study name and size
	XPC polymorphism (Lys939Gln, PAT) (rs2228001)	*XPC* PAT deletion/insertion (D/I) and insertion/insertion (I/I) could decrease the risk of PC	(92) Iranian cohort including 154 prostate cancer patients and 205 Benign Prostate Hyperplasia (BPH) controls
Ovarian Cancer	*XPC* polymorphisms Ala299Val and Lys939Gln (s2228000 and rs2228001)	*XPC* Ala299Val was associated with reduced risk of ovarian cancer *XPC* Lys939Gln increased risk of ovarian cancer	(93) Chinese cohort, 89 ovarian cancer patients 356 cancer-free women
	XPC polymorphisms rs3731108, rs1124303 and PAT	*XPC* SNP rs3731108 (AG)/AA versus the GG genotype, SNP rs1124303 (GT)/GG genotype versus TT genotype and PAT (-/+)/(-/-) genotype versus the (+/+) genotype were associated with a prolonged PFS	(94) 139 patients with stage III and IV papillary serous ovarian cancer who underwent primary cytoreductive surgery followed by platinum-based chemotherapy.
Bladder Cancer (BC)	*XPC* Ala499Val polymorphism (rs2228000)	Ala499Val showed an increased overall cancer risk (OR 1.15), and specifically for BC in the simple genetic model	(83) meta-analysis that included 33 published case–control studies
	XPC polymorphisms (rs2228000)	*XPC* Ala499Val associated with increased BC susceptibility (OR 1.33)	(86) Polymorphism stratified meta-analysis, 11 published case-control studies of cancer with 5581 cases and 6351 controls
	XPC Ala499Val polymorphism (rs2228000)	Associated with risk of XPC Ala499Val associated with increased by 3 different calculations (allelic contrast, OR 1.11; homozygote comparison, OR 1.35; recessive genetic model, OR 1.36)	(95) Meta-analysis of 13 case-control studies, 4,927 bladder cancer cases and 5185 controls
	XPC polymorphisms Lys939Gln, Ala499Val, PAT (s2228000, rs2228001, PAT)	Multiple models showing increased BC susceptibility with *XPC* Lys939Gln, Ala499Val and PAT-/+ polymorphisms. Suggested polymorphism risk stratification may differ based on Asian vs Caucasian populations.	(96) Meta-analysis, 14 case-control BC studies, 10 Lys939Gln (3,934 cases, 4,269 controls), 5 Ala499Val (2,113 cases, 2,249 controls), 7 PAT-/+ (2,834 cases, 3,048 controls)
	XPC polymorphisms Lys939Gln, Ala499Val, PAT (s2228000, rs2228001)	Suggested increased bladder cancer risk with Ala499Val but not Lys939Gln. Lys939Gln bladder cancer risk appeared related to tobacco smoking or chewing (OR 2.23 and 2.4)	(97) Meta-analysis, 18 case-control BC studies, 7 studies Ala499Val (2893 cases, 3056 controls), 11 studies Lys939Gln (5064 cases, 5208 controls)
	Rare *XPC* polymorphisms (rs121965091, rs121965090)	4 of 5 novel *XPC* variants (Phe302Ser, Arg393Trp, c*156G>A, c.2251-37C>A) associated with increased BC odds (OR 3.1 for having 1+ variant)	(98) Case-control, 771 BC cases and 800 controls
	XPC mRNA and protein expression	Low XPC expression associated with increased BC recurrence and decreased survival	(99) mRNA: 79 BC patients, IHC: 219 BC patients. Relapse at 2 years, survival at time of publication (min-3 years, max 12 years)
Pancreatic cancer	*XPC* polymorphism PAT	PAT +/+ genotype could protect against pancreatic carcinogenesis.	(100) Study included 101 incident cases with pancreatic cancer and 337 controls
	XPC tagging SNPs rs2470353, rs2607775, rs2228000, rs3731114 and rs3729587.	For rs2470353, pancreatic cancer risk was increased in subjects with GC and GC+CC gene types Compared with the GG gene type. For rs2607775 the CG and CG+GG gene types were associated with increased pancreatic cancer risk compared with the CC gene type. CCC haplotype of rs2228000, rs3731114 and rs3729587 associated with an increased pancreatic cancer risk	(101) Study included 205 pancreatic cancer cases and 230 controls.
Esophageal cancer	Genetic variants of *XPA* in 50UTR and *XPC* at K939Q (rs2228001)	*XPA* 50UTR A/G and *XPC* K939Q C/C genotypes associated with a higher risk of mortality after treatment compared with wild-type homozygous genotypes especially in the population treated with esophagectomy and undergoing concurrent neoadjuvant chemoradiotherapy.	(102) 501 patients with esophageal squamous cell carcinoma (ESCC).
	XPC PAT polymorphism	*XPC* PAT -/+ genotype associated with decreased esophageal cancer risk	(103) 387 White esophageal patients and 462 White controls matched
	Multiple SNP panel, included *XPC* polymorphisms 499CC and 939AC+CC	5-polymorphism panel (*MTHFR* 677TT, *MDR1*2677GT, *GSTP1* 114CC, *XPC* 499CC, *XPC* 939AC+CC) that has a 79% sensitivity and 85.4% specificity of predicting 5 years PFS. They were associated to shorter RFS and in a univariate analysis.	(104) 124 patients receiving neoadjuvant chemoradiation treatment for locally advanced esophageal cancer

(Continued)

TABLE 1 | Continued

Malignancy	*XPC* mutation or SNP	Clinical association	Study name and size
Colorectal Cancer and Adenomas (CRC)	*XPC* SNPs (various) (rs2228001)	Haplotype *XPC* A499V independently protective from smoking-associated risk of CRC	(105) 772 subjects with left-sided advanced adenoma vs 777 Controls.
	XPC mRNA and protein expression	High XPC expression might be predictive of survival in CRC	(106) 167 patients with colorectal cancer
Breast Cancer	*XPC* polymorphisms K939Q (rs2228001) and rs2733532	rs2228001–A > C and rs2733532–C > T are associated with an increased risk for breast cancer development	(107) 493 breast cancer cases and 387 controls
	XPC polymorphisms Lys939Gln and PAT (rs2228001)	PAT -/+ is associated with an increased risk of breast cancer Combined genotypes 939AC/PAT+/+ and 939CC/PAT+/+ are associated with an increased risk of breast cancer.	(108) 200 women diagnosed with breast cancer as cases and 200 ethnically matched healthy controls
Hepatocellular Carcinoma	*XPC* polymorphism Lys939Gln (rs2228001)	Lys939Gln allele differed in HCC risk, with risk of *XPC*-GG > *XPC*-LG > *XPC*-LL. Heterozygous *XPC* 939LG and/or homozygous *XPC* 939GG, compared to homozygous *XPC* 939LL was associated with shorter overall survival	(109) 1156 HCC cases and 1402 controls without liver disease

RFS, relapse free survival; PFS, progression free survival; PC, prostate cancer; BC, bladder cancer.

further investigation given the role of the NER pathway and reliance on alkylating agents in multiple myeloma.

XPC IN SOLID CANCERS

Lung Cancer

Lung cancer is characterized by some of the highest levels of genomic diversity, and alterations in DNA repair pathways, including NER, have been proposed to play a role in lung cancer development (114, 115). Although dominated by dermatologic malignancies, early series of XP-C patients reveal cases of bronchogenic lung carcinomas (14, 116). Germline mutations causing XP-C are rare, however, more common *XPC* polymorphisms and variations in gene expression have been studied in lung cancer (**Table 1**). In the most common subset of lung cancers, non-small cell lung cancer (NSCLC), decreased tumor *XPC* mRNA level has been associated with poor outcomes (117).

Numerous studies associate various *XPC* SNP polymorphisms with lung cancer development, which, among other factors, may be influenced by gender and cigarette smoking status (**Table 1**) (81–87), and many *XPC* polymorphisms have been found to functionally modulate DNA repair capacity (118). It is likely that epigenetic regulation leads to decreased *XPC* gene expression. Decreased *XPC* mRNA expression has been identified in human specimens from lung adenocarcinoma and lung squamous cell carcinoma, the two most common NSCLC histologic subtypes (119–121). Pre-clinical studies support epigenetic regulation of *XPC* with different environmental exposures, possibly due to promoter hypermethylation or histone-related transcriptional regulation (122). For instance, exposure of C57Bl/6 mice to 6 months of cigarette smoke led to decreased *Xpc* mRNA expression without altered expression of other studied BER and NER genes, including *Xpa* and *Ogg1* (66). XPC protein expression is decreased in lung fibroblast and bronchial epithelial cell lines treated in culture with cigarette smoke extract, but not other NER proteins including XPA, and may be due to protein turnover by ubiquitination (123). Tight control of XPC ubiquitination is likely required to ensure DNA repair but may be dysregulated in human cancers, including lung cancers, which have been shown to have high levels of ubiquitin ligases, such as Cullin-RING ubiquitin ligase 4 A (CUL4A), overexpression of which is common in cigarette smoke-related lung cancer, and which is inversely proportionate to *XPC* expression (26). Additionally, murine exposure to side-stream smoke (up to 4 months) and nicotine-containing e-cigarette vape (12 weeks) led to increased DNA adduct formation and decreased *Xpc* and *Ogg1* mRNA expression in the lungs (124, 125). Importantly, these studies also show decreased *in vitro* BER and NER repair using lysates from e-cigarette vape exposed mouse lungs, correlating decreased gene expression to decreased repair function.

The strongest evidence supporting a critical role of XPC in lung cancer comes from translational animal studies. Two mouse models of global *Xpc* deficiency have been created, both of which are associated with complete loss of functional XPC and cause characteristic skin cancers with exposure to UV light (126, 127). Increased DNA damage has been observed in the lungs of *Xpc* deficient mice upon exposure to oxidizing agents, but not in mice deficient in another NER protein, *Xpa*, although both show increased mutational frequency in the liver (40, 128). Exposure to urban air pollution led to increased lung inflammation and DNA damage in *Xpc* deficient mice (129). Mice homozygous deficient in *Xpc* develop lung tumors (primarily adenomas) with advanced age (16-17 months), although development of adenocarcinomas were rare without a co-existing loss of another tumor suppressor gene (130). However, exposure of *Xpc* deficient mice to chronic cigarette smoke and carcinogens, including urethane, MCA-BHT, 2-acetylaminofluorene (AAF) and NOH-AAF leads to lung adenocarcinoma development (42, 131), and with advanced age and chronic cigarette smoke, *Xpc* deficient mouse lungs develop an increase in lung compliance and alveolar rarefication similar to that seen in emphysema, a lung disease which predisposes to lung cancer (66). Importantly, mice heterozygous in *Xpc* (*Xpc*+/-) exposed to the carcinogen, urethane, developed an

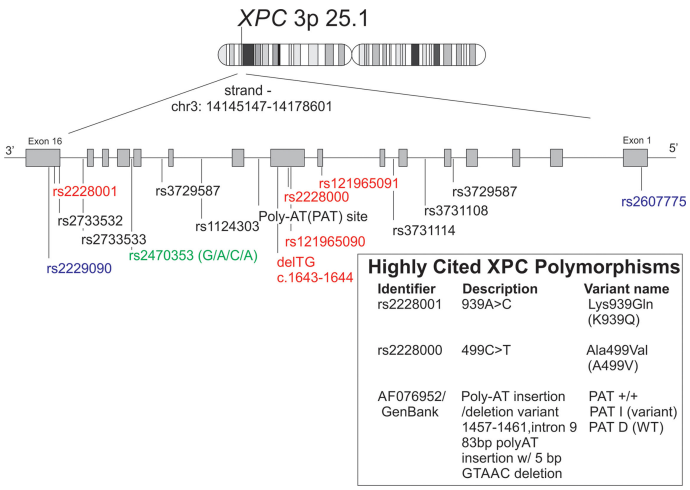

FIGURE 2 | Schematic representation of *XPC* polymorphisms discussed in this manuscript along with alternate names/identifiers for the *XPC* polymorphisms most commonly studied in non-dermatologic cancers. Reference XPC gene (chr 3:p25.1) with polymorphisms was reproduced using the GRCh38 (hg38) sequencing using the UCSC genome browser tool. [(112) http://genome.ucsc.edu. *Accessed 1/30/22*]. Red = missense mutations, blue = 5' or 3' UTR variants, green = upstream of transcript variant.

intermediate number of lung tumors when to compared to urethane-treated *Xpc* deficient and proficient littermate mice, suggesting a gene-dose effect and further supporting a role for intermediate levels of XPC expression, either through polymorphisms or epigenetic regulation, in lung cancer development (42).

Other more recently proposed mechanisms for XPC involvement in NSCLC development include regulation of cell proliferation and migration, and transcriptional regulation of p53. For instance, XPC, complexed with HR23B, impacts p53 transcriptional regulation of MMP1, low expression of which was associated with increased tumor size and metastasis (132). Cui and colleagues studied the impact of XPC on NSCLC cell lines *in vitro*, finding that *XPC* knock-down led to increased NSCLC cell growth and migration due to decreased surface e-cadherin expression through regulation of the SNAIL pathway (133). Although strong evidence supports an important role of XPC in lung cancer development, more research is needed to understand the link between alterations in XPC expression levels and XPC function on lung carcinogenesis and oncogenic development of characteristic genomic and transcriptomic alterations.

Prostate Cancer

Prostate cancer (PC) is the most common malignancy in males (134), and *XPC* polymorphisms have been correlated to an increased risk of PC development in several studies (**Table 1**). For instance, the *XPC* polymorphism, *XPC* PAT (PAT I/I genotype) was associated with an increased odds of prostate cancer, associated with a 3.83-fold increased risk in a Tunisian population. In contrast, other *XPC* polymorphisms, including those heterozygous for Lys939Gln (939Lys/Gln) along with the PAT D/D haplotype are considered protective of prostate cancer (89). One more study reported an increased risk of developing PC in those with the *XPC* PAT polymorphism (PAT +/+ or PAT +/-) along with tobacco smoking in a Chinese population (90). Other studies have shown varied increases in PC risk with other *XPC* polymorphisms (91, 135) (**Table 1**). It does not appear that *XPC* polymorphisms are associated with more advanced disease in PC, and similarly, studies did not find an association between *XPC* gene polymorphisms and Gleason score (a measure of histologic PC staging which correlates to prognosis) (89, 92). However, using TCGA data, low *XPC* expression was associated with worse overall survival in PC, similar to analyses in many other solid organ tumors (135). These studies suggest that *XPC* polymorphisms may serve as a tool to identify those at the highest risk for developing PC, which can help in targeting high and low-risk individuals to appropriate screening and clinical evaluations.

Ovarian Cancer

Like other solid organ tumors, *XPC* polymorphisms have been identified as one factor that may increase or decrease the risk of ovarian cancer as summarized in **Table 1**. Along with SNPs in two other NER proteins, XRCC1 and XRCC2, the *XPC* Ala499Val polymorphism was found to correlate to a decreased odds of ovarian cancer (OR 0.35) while the *XPC* Lys939Gln polymorphism was associated with an increased risk of ovarian cancer (OR 1.72) in a dominant genetic model (93). *XPC* polymorphisms may also serve as a biomarker in response to platinum-based chemotherapies as some specific SNP polymorphisms were associated with prolonged progression-free survival (PFS) (94). Going further, in ovarian cancer, overexpression of the eukaryotic translation initiation factor 3a (eIF3a) was associated with decreased response to cisplatin through downregulating *XPC* mRNA expression (136). This further supports an important role of XPC in predicting response

to platinum-based chemotherapy through its canonical involvement in GG-NER.

Bladder Cancer

As with several other cancers, DNA damage due to carcinogen exposure, including cigarette smoking, is strongly associated with bladder cancer. In this, as in several other cancers, *XPC* polymorphisms were associated with low penetrance susceptibility to bladder cancer (**Table 1**) (83, 86, 95–97). Several rare *XPC* mutations, identified in patients with bladder cancer, were studied *in vitro* and were associated with decreased XPC mRNA and protein expression (98). Supporting their likely role in bladder cancer development, XPC mRNA and protein expression is decreased in bladder cancer tumors and may portend a worse prognosis (99, 137, 138). A variable impact of factors such as cigarette smoking have been correlated to XPC expression in bladder cancers, and more recently, studies have suggested a role of both promoter hypermethylation and histone deacetylation by HDACs in regulation of *XPC* mRNA expression in bladder cancer (138, 139), the latter of which is supported by previously studies reporting SIRT-1 deacetylase regulation of XPC expression in other (skin) cancers (140). Overall, these studies support a role of XPC expression in variable risk and outcomes of bladder cancer, although the exact mechanisms of epigenetic regulation, and the specific mechanisms by which risk is altered in low XPC, remains less clear.

Pancreatic Cancer

XPC may play a role as a risk factor for developing pancreatic cancer. As summarized in **Table 1**, some *XPC* polymorphisms have been described as increasing pancreatic cancer risk, particularly in smokers with the rs2470353 and rs2607775 variants (101). However, one study suggested a protective role of the *XPC*-PAT polymorphism (PAT +/+) in pancreatic cancer risk (100). Other studies suggested a role for genetic variants of other NER associated proteins, including ERCC1, but not necessarily XPC as a risk factor for developing pancreatic cancer (141). None-the-less, the specific role of NER, and specifically of XPC expression and epigenetic regulation, still need to be further explored in pancreatic cancer development.

Other Solid Organ Cancers

In esophageal cancer XPC may play a role as a risk factor for developing malignancy. *XPC* genetic variants, specifically the *XPC* K939Q C/C genotypes were found to be associated with a higher mortality after treatment compared with patients with a wild-type homozygous genotype; particularly in those who were post-treatment with esophagectomy or neoadjuvant chemoradiation (102). Another polymorphism, *XPC* PAT +/+, was associated with decreased risk for esophageal cancer (103). The prognostic value of XPC is further supported by having two *XPC* polymorphisms, *XPC* 499CC and *XPC* 939AC+CC (939 Lys and Gln), as part of a 5-polymorphism panel (high risk genotype) that has a 79% sensitivity and 85.4% specificity of predicting 5 years progression free survival (104), indicating a potential prognostic role of *XPC* polymorphisms in esophageal cancer risk.

XPC may also play a role as a risk factor for other cancers including advanced colorectal cancer. The *XPC* polymorphism Ala499Val was found to play a protective role in developing advanced colorectal adenomas in smokers (105), and others have suggested a protective role of higher *XPC* mRNA and protein expression levels on colorectal survival, possibly related to an improved response to chemoradiation (106). A recent case-control association study using tissue from 493 breast cancer and 387 control cases suggested an association between two *XPC* polymorphisms, rs2228001-A>C (Lys939Gln) and rs2733532-C>T, with an increased odds of breast cancer (107), and another study with 200 cases and controls suggested an association between the *XPC* PAT+ allele and higher odds of breast cancer (108).

Finally, some evidence supports a role of XPC in liver (hepatocellular) carcinoma development. In a case-control study of hepatocellular carcinoma HCC related to aflatoxin B1 exposure, *XPC* polymorphism codon 939Gln allele, whether heterozygous (*XPC*-LG) or homozygous (*XPC*-GG), is associated with increased risk of HCC; these genotype variants correlated with decreased XPC tumor protein expression by IHC as well as a shorter overall survival (109).

XPC AS TUMOR SUPPRESSOR AND AN EMERGING BIOMARKER OF CANCER DEVELOPMENT

Numerous cancers are associated with decreased *XPC* expression, but the mechanism by which this occurs is less clear. The *XPC* gene, along with several other tumor suppressor genes, is located on chromosome 3p, a frequently site of chromosomal deletion in human tumors (130, 142). However, various modes of transcriptional regulation have been implicated in altered tumor *XPC* expression as well, and *XPC* expression may be altered in cells outside of the tumor itself. While studies have suggested decreased *XPC* expression in NSCLC tumor cells compared to surrounding lung (119), in 21 patients with NSCLC in which blood, tumor and lung tissue were collected, *XPC* mRNA expression was found to strongly correlate between blood and NSCLC tumor tissue, supporting the potential use of a minimally invasive blood draw as a prognostic and therapeutic biomarker (143).

The impact of low *XPC* mRNA expression may extend beyond alterations in DNA damage response and repair. Interestingly, XPC deficiency may also cause a mutational hot spot in the tumor suppressor p53 when treated with UV light, mediated by non-dipyrimidine base damage (144). Furthermore, there is evidence that XPC regulates a p53 post-ubiquitylation event and that XPC deficiency compromises p53 degradation, which may play a role in developing malignancy (145). These later two studies were performed in skin fibroblast cells and *in vitro* cell culture models, and whether XPC is involved in p53 regulation and mutations in other malignancies has not been well studied. In addition to its role in a number of DNA repair pathways, XPC has been implicated in transcriptional regulation both in response and independent of DNA damage. In the setting of DNA damage, studies have supported E2F1 transcriptional regulation of XPC expression

(146). Recently, XPC itself has been implicated in post-translational histone modification and recruitment of transcription factors such as E2F1 to gene promoter sites independent of its regulatory role in DNA repair (69). High expression of *miRNA-346*, commonly elevated in NSCLC and other cancers, was associated with lower *XPC* mRNA and protein expression, indicating another potential mechanism for XPC downregulation in human cancers (147).

XPC AS A BIOMARKER OF RESPONSE TO THERAPY

In addition to *XPC* polymorphisms and expression levels as potential biomarkers associated with risk for many malignancies, XPC may predict disease progression. In patients with NSCLC, low tumor *XPC* mRNA expression is associated with advanced stage at diagnosis and an increased rate of cancer relapse after treatment in never-smokers (148). Similarly in colorectal cancer, increased *XPC* expression was associated with longer 5 year survival in treated patients compared to patients with low *XPC* expression (106). *XPC* polymorphisms have been described as predicting response to platinum-based chemotherapy. For instance, DNA samples from whole blood cells showed that *XPC* rs2229090 GC/CC genotypes were associated with longer progressive free survival compared to the AA and GG genotypes (149). These findings are consistent with translational and *in vitro* studies inversely linking *XPC* mRNA expression with response to cisplatin, particularly in lung adenocarcinoma where cisplatin chemotherapy treatment remains a mainstay in locally advanced disease (150). However, a link between *XPC* polymorphisms and response to cisplatin therapy has not been clearly shown, with a recent meta-analysis (88). High mutational burden has been associated with improved response to the immune checkpoint inhibitors. Typically, angiosarcomas have poor response to immunotherapy, but a recent report highlights an angiosarcomas that developed in an XP-C patient which had the features suggestive of a good response to immunotherapy and ultimately benefitted from a good response to the immune checkpoint inhibitor pembrolizumab (151). This report provides a preliminary but intriguing potential link between XPC, high tumor mutation burden and response to immunotherapies.

In the last few years, more attention has been paid to targeting DNA repair as a modality to augment cancer therapy. For instance, in a micro-RNA (miR) screen of prostate cancer, *miR-890*, which directly inhibited transcription of *XPC* along with other DNA repair proteins, led to increased sensitivity to ionizing radiation, although further mechanistic testing indicated that IR-sensitization by *miR-890* persisted in *XPC* knock-down cells, suggesting an indirect role of XPC in double-strand break repair and overlapping gene-functionality in IR-sensitization (152). However, most studies show a predictive role in response to chemotherapies, especially platinum-based agents, which cause DNA lesions that are primarily repaired by NER, requiring XPC for recognition (2). Since increased NER repair could mean increased resistance to platinum-based therapy, inhibiting XPC could be a viable option to overcome platinum resistance in cancer cells. For instance modulation of XPC by hyperthermia or by treatment with sodium arenite was found to suppress XPC-induced cisplatin toxicity and sensitize tumors to platinum based therapy in a mouse ovarian cancer xenograft model (153). However, others have found a seemingly contradictory impact of histone deacetylase (HDAC) inhibitors in bladder cancer, showing a correlation between HDAC inhibition, increased XPC expression and higher cisplatin-induced activation of the pro-apoptotic protein, caspase 3 (139). Additionally, it is unclear if described decreases in XPC expression are in cancer cells alone or found in other cells within the tumor microenvironment, such as fibroblasts, in which XPC inhibition could be expected to decrease the tumor promoting cytokine IL-6 (72). On the other hand, this inhibition may help to sensitize tumor cells to other therapies due to the involvement of XPC in other DNA repair pathways and in checkpoint activation. Future studies should explore XPC targeting by small molecular inhibitors to investigate these possibilities, especially given conflicting data regarding XPC expression levels and therapeutic response to chemotherapeutic agents.

CONCLUSION

XPC is increasingly recognized as playing an important role in the development of non-dermatologic malignancies. Decreased *XPC* mRNA and protein expression has been described in a number of cancers, with gene polymorphisms, deletions, and transcriptional regulation all active areas of research in the regulation of XPC expression. Additionally, research supports a role of XPC in the prognosis and treatment response in several of these cancers. Although XPC's essential role in the recognition of bulky DNA lesions and subsequent activation of GG-NER, when altered, is a leading mechanism for development of UV-induced dermatologic malignancies and in modifications of cancer response to chemotherapies including cisplatin, recent data support a non-canonical role of XPC in DNA damage response and repair mechanisms, tumor suppressor transcriptional regulation, and in the development of non-dermatologic malignancies. Future studies would benefit from studying XPC as a biomarker of cancer prognosis and response to treatment in non-dermatologic malignancies.

AUTHOR CONTRIBUTIONS

Conceptualization, NN and CRS. Writing—original draft preparation, NN, BMW and CRS. Writing—review and editing, NN and CRS. Funding acquisition, CRS. All authors have read and agreed to the published version of the manuscript.

FUNDING

This work was funded by the U.S. Department of Veterans Affairs BLR&D, Merit Review grant I01-BX005353 to CRS and in part by the National Institutes of Health, U.S.A. T32HL091816 to BMW.

REFERENCES

1. Hanahan D, Weinberg RA. Hallmarks of Cancer: The Next Generation. *Cell* (2011) 144:646–74. doi: 10.1016/j.cell.2011.02.013
2. Gavande NS, Vandervere-Carozza PS, Hinshaw HD, Jalal SI, Sears CR, Pawelczak KS, et al. DNA Repair Targeted Therapy: The Past or Future of Cancer Treatment? *Pharmacol Ther* (2016) 160:65–83. doi: 10.1016/j.pharmthera.2016.02.003
3. Jalal S, Earley JN, Turchi JJ. DNA Repair: From Genome Maintenance to Biomarker and Therapeutic Target. *Clin Cancer Res* (2011) 17:6973–84. doi: 10.1158/1078-0432.CCR-11-0761
4. Nemzow L, Lubin A, Zhang L, Gong F. XPC: Going Where No DNA Damage Sensor has Gone Before. *DNA Repair (Amst)* (2015) 36:19–27. doi: 10.1016/j.dnarep.2015.09.004
5. Zamble DB, Mu D, Reardon JT, Sancar A, Lippard SJ. Repair of Cisplatin-DNA Adducts by the Mammalian Excision Nuclease. *Biochemistry* (1996) 35:10004–13. doi: 10.1021/bi960453+
6. Fousteri M, Mullenders LH. Transcription-Coupled Nucleotide Excision Repair in Mammalian Cells: Molecular Mechanisms and Biological Effects. *Cell Res* (2008) 18:73–84. doi: 10.1038/cr.2008.6
7. Spivak G. Nucleotide Excision Repair in Humans. *DNA Repair (Amst)* (2015) 36:13–8. doi: 10.1016/j.dnarep.2015.09.003
8. Shell SM, Hawkins EK, Tsai MS, Hlaing AS, Rizzo CJ, Chazin WJ. Xeroderma Pigmentosum Complementation Group C Protein (XPC) Serves as a General Sensor of Damaged DNA. *DNA Repair (Amst)* (2013) 12:947–53. doi: 10.1016/j.dnarep.2013.08.013
9. Zebian A, Shaito A, Mazurier F, Rezvani HR, Zibara K. XPC Beyond Nucleotide Excision Repair and Skin Cancers. *Mutat Res Rev Mutat Res* (2019) 782:108286. doi: 10.1016/j.mrrev.2019.108286
10. Lehmann AR, Mcgibbon D, Stefanini M. Xeroderma Pigmentosum. *Orphanet J Rare Dis* (2011) 6:70. doi: 10.1186/1750-1172-6-70
11. Digiovanna JJ, Kraemer KH. Shining a Light on Xeroderma Pigmentosum. *J Invest Dermatol* (2012) 132:785–96. doi: 10.1038/jid.2011.426
12. Chavanne F, Broughton BC, Pietra D, Nardo T, Browitt A, Lehmann AR, et al. Mutations in the *XPC* Gene in Families With Xeroderma Pigmentosum and Consequences at the Cell, Protein, and Transcript Levels. *Cancer Res* (2000) 60:1974–82.
13. Bradford PT, Goldstein AM, Tamura D, Khan SG, Ueda T, Boyle J, et al. Cancer and Neurologic Degeneration in Xeroderma Pigmentosum: Long Term Follow-Up Characterises the Role of DNA Repair. *J Med Genet* (2011) 48:168–76. doi: 10.1136/jmg.2010.083022
14. Kraemer KH, Lee MM, Scotto J. Xeroderma Pigmentosum: Cutaneous, Ocular, and Neurologic Abnormalities in 830 Published Cases. *Arch Dermatol* (1987) 123:241–50. doi: 10.1001/archderm.123.2.241
15. Sugasawa K, Akagi J, Nishi R, Iwai S, Hanaoka F. Two-Step Recognition of DNA Damage for Mammalian Nucleotide Excision Repair: Directional Binding of the XPC Complex and DNA Strand Scanning. *Mol Cell* (2009) 36:642–53. doi: 10.1016/j.molcel.2009.09.035
16. Mu H, Geacintov NE, Broyde S, Yeo JE, Scharer OD. Molecular Basis for Damage Recognition and Verification by XPC-RAD23B and TFIIH in Nucleotide Excision Repair. *DNA Repair (Amst)* (2018) 71:33–42. doi: 10.1016/j.dnarep.2018.08.005
17. Sugasawa K, Masutani C, Uchida A, Maekawa T, van der Spek PJ, Bootsma D, et al. HHR23B, a Human Rad23 Homolog, Stimulates XPC Protein in Nucleotide Excision Repair *In Vitro*. *Mol Cell Biol* (1996) 16:4852–61. doi: 10.1128/MCB.16.9.4852
18. Renaud E, Miccoli L, Zacal N, Biard DS, Craescu CT, Rainbow AJ, et al. Differential Contribution of XPC, RAD23A, RAD23B and CENTRIN 2 to the UV-Response in Human Cells. *DNA Repair* (2011) 10:835–47. doi: 10.1016/j.dnarep.2011.05.003
19. Friedberg EC. How Nucleotide Excision Repair Protects Against Cancer. *Nat Rev Cancer* (2001) 1:22–33. doi: 10.1038/35094000
20. Scharer OD. Nucleotide Excision Repair in Eukaryotes. *Cold Spring Harb Perspect Biol* (2013) 5:a012609. doi: 10.1101/cshperspect.a012609
21. Sugasawa K, Okuda Y, Saijo M, Nishi R, Matsuda N, Chu G, et al. UV-Induced Ubiquitylation of XPC Protein Mediated by UV-DDB-Ubiquitin Ligase Complex. *Cell* (2005) 121:387–400. doi: 10.1016/j.cell.2005.02.035
22. Wang QE, Zhu Q, Wani G, El-Mahdy MA, Li J, Wani AA. DNA Repair Factor XPC is Modified by SUMO-1 and Ubiquitin Following UV Irradiation. *Nucleic Acids Res* (2005) 33:4023–34. doi: 10.1093/nar/gki684
23. Kakumu E, Nakanishi S, Shiratori HM, Kato A, Kobayashi W, Machida S, et al. Xeroderma Pigmentosum Group C Protein Interacts With Histones: Regulation by Acetylated States of Histone H3. *Genes Cells* (2017) 22:310–27. doi: 10.1111/gtc.12479
24. Shah P, Zhao B, Qiang L, He YY. Phosphorylation of Xeroderma Pigmentosum Group C Regulates Ultraviolet-Induced DNA Damage Repair. *Nucleic Acids Res* (2018) 46:5050–60. doi: 10.1093/nar/gky239
25. Chauhan AK, Sun Y, Zhu Q, Wani AA. Timely Upstream Events Regulating Nucleotide Excision Repair by Ubiquitin-Proteasome System: Ubiquitin Guides the Way. *DNA Repair (Amst)* (2021) 103:103128. doi: 10.1016/j.dnarep.2021.103128
26. Jia L, Yan F, Cao W, Chen Z, Zheng H, Li H, et al. Dysregulation of CUL4A and CUL4B Ubiquitin Ligases in Lung Cancer. *J Biol Chem* (2017) 292:2966–78. doi: 10.1074/jbc.M116.765230
27. Matsuoka S, Ballif BA, Smoogorzewska A, Mcdonald ER, Hurov KE, Luo J, et al. ATM and ATR Substrate Analysis Reveals Extensive Protein Networks Responsive to DNA Damage. *Science* (2007) 316:5828. doi: 10.1126/science.1140321
28. Nguyen TA, Slattery SD, Moon SH, Darlington YF, Lu X, Donehower LA. The Oncogenic Phosphatase WIP1 Negatively Regulates Nucleotide Excision Repair. *DNA Repair (Amst)* (2010) 9:813–23. doi: 10.1016/j.dnarep.2010.04.005
29. Chakraborty S, Steinbach PJ, Paul D, Mu H, Broyde S, Min JH, et al. Enhanced Spontaneous DNA Twisting/Bending Fluctuations Unveiled by Fluorescence Lifetime Distributions Promote Mismatch Recognition by the Rad4 Nucleotide Excision Repair Complex. *Nucleic Acids Res* (2018) 46:1240–55. doi: 10.1093/nar/gkx1216
30. Panigrahi A, Vemuri H, Aggarwal M, Pitta K, Krishnan M. Sequence Specificity, Energetics and Mechanism of Mismatch Recognition by DNA Damage Sensing Protein Rad4/XPC. *Nucleic Acids Res* (2020) 48:2246–57. doi: 10.1093/nar/gkaa078
31. Geacintov NE, Broyde S. Repair-Resistant DNA Lesions. *Chem Res Toxicol* (2017) 30:1517–48. doi: 10.1021/acs.chemrestox.7b00128
32. Fayyad N, Kobaisi F, Beal D, Mahfouf W, Ged C, Morice-Picard F, et al. Xeroderma Pigmentosum C (XPC) Mutations in Primary Fibroblasts Impair Base Excision Repair Pathway and Increase Oxidative DNA Damage. *Front Genet* (2020) 11:561687. doi: 10.3389/fgene.2020.561687
33. De Melo JT, De Souza Timoteo AR, Lajus TB, Brandao JA, De Souza-Pinto NC, Menck CF, et al. XPC Deficiency Is Related to APE1 and OGG1 Expression and Function. *Mutat Res* (2016) 784-785:25–33. doi: 10.1016/j.mrfmmm.2016.01.004
34. Miao F, Bouziane M, Dammann R, Masutani C, Hanaoka F, Pfeifer G, et al. 3-Methyladenine-DNA Glycosylase (MPG Protein) Interacts With Human RAD23 Proteins. *J Biol Chem* (2000) 275:28433–8. doi: 10.1074/jbc.M001064200
35. Shimizu Y, Iwai S, Hanaoka F, Sugasawa K. Xeroderma Pigmentosum Group C Protein Interacts Physically and Functionally With Thymidine DNA Glycosylase. *EMBO J* (2003) 22:164–73. doi: 10.1093/emboj/cdg016
36. Parlanti E, D'errico M, Degan P, Calcagnile A, Zijno A, van der Pluijm I, et al. The Cross Talk Between Pathways in the Repair of 8-Oxo-7,8-Dihydroguanine in Mouse and Human Cells. *Free Radical Biol Med* (2012) 53:2171–7. doi: 10.1016/j.freeradbiomed.2012.08.593
37. Ho JJ, Cattoglio C, Mcswiggen DT, Tjian R, Fong YW. Regulation of DNA Demethylation by the XPC DNA Repair Complex in Somatic and Pluripotent Stem Cells. *Genes Dev* (2017) 31:830–44. doi: 10.1101/gad.295741.116
38. Menoni H, Hoeijmakers JH, Vermeulen W. Nucleotide Excision Repair-Initiating Proteins Bind to Oxidative DNA Lesions *In Vivo*. *J Cell Biol* (2012) 199:1037–46. doi: 10.1083/jcb.201205149
39. Kumar N, Theil AF, Roginskaya V, Ali Y, Calderon M, Watkins SC, et al. Global and Transcription-Coupled Repair of 8-oxoG is Initiated by Nucleotide Excision Repair Proteins. *Nat Commun* (2022) 13:974. doi: 10.1038/s41467-022-28642-9
40. Melis JP, Kuiper RV, Zwart E, Robinson J, Pennings JL, Van Oostrom CT, et al. Slow Accumulation of Mutations in Xpc Mice Upon Induction of

Oxidative Stress. *DNA Repair* (2013) 12:1081–6. doi: 10.1016/j.dnarep.2013.08.019
41. Okamoto Y, Chou PH, Kim SY, Suzuki N, Laxmi YR, Okamoto K, et al. Oxidative DNA Damage in XPC-Knockout and Its Wild Mice Treated With Equine Estrogen. *Chem Res Toxicol* (2008) 21:1120–4. doi: 10.1021/tx700428m
42. Zhou H, Saliba J, Sandusky GE, Sears CR. XPC Protects Against Smoking and Carcinogen-Induced Lung Adenocarcinoma. *Carcinogenesis* (2019) 40:403–11. doi: 10.1093/carcin/bgz003
43. Modrich P, Lahue R. Mismatch Repair in Replication Fidelity, Genetic Recombination, and Cancer Biology. *Annu Rev Biochem* (1996) 65:101–33. doi: 10.1146/annurev.bi.65.070196.000533
44. Kolodner RD, Marsischky GT. Eukaryotic DNA Mismatch Repair. *Curr Opin Genet Dev* (1999) 9:89–96. doi: 10.1016/S0959-437X(99)80013-6
45. Poynter JN, Siegmund KD, Weisenberger DJ, Long TI, Thibodeau SN, Lindor N, et al. Molecular Characterization of MSI-H Colorectal Cancer by MLHI Promoter Methylation, Immunohistochemistry, and Mismatch Repair Germline Mutation Screening. *Cancer Epidemiol Biomarkers Prev* (2008) 17:3208–15. doi: 10.1158/1055-9965.EPI-08-0512
46. Li X, Liu G, Wu W. Recent Advances in Lynch Syndrome. *Exp Hematol Oncol* (2021) 10:37. doi: 10.1186/s40164-021-00231-4
47. Deans AJ, West SC. DNA Interstrand Crosslink Repair and Cancer. *Nat Rev Cancer* (2011) 11:467–80. doi: 10.1038/nrc3088
48. Noll DM, Mason TM, Miller PS. Formation and Repair of Interstrand Cross-Links in DNA. *Chem Rev* (2006) 106:277–301. doi: 10.1021/cr040478b
49. Mchugh PJ, Spanswick VJ, Hartley JA. Repair of DNA Interstrand Crosslinks: Molecular Mechanisms and Clinical Relevance. *Lancet Oncol* (2001) 2:483–90. doi: 10.1016/S1470-2045(01)00454-5
50. Chen Z, Xu XS, Yang J, Wang G. Defining the Function of XPC Protein in Psoralen and Cisplatin-Mediated DNA Repair and Mutagenesis. *Carcinogenesis* (2003) 24:1111–21. doi: 10.1093/carcin/bgg051
51. Christensen LA, Finch RA, Booker AJ, Vasquez KM. Targeting Oncogenes to Improve Breast Cancer Chemotherapy. *Cancer Res* (2006) 66:4089–94. doi: 10.1158/0008-5472.CAN-05-4288
52. Jain A, Wang G, Vasquez KM. DNA Triple Helices: Biological Consequences and Therapeutic Potential. *Biochimie* (2008) 90:1117–30. doi: 10.1016/j.biochi.2008.02.011
53. Thoma BS, Wakasugi M, Christensen J, Reddy MC, Vasquez KM. Human XPC-Hhr23b Interacts With XPA-RPA in the Recognition of Triplex-Directed Psoralen DNA Interstrand Crosslinks. *Nucleic Acids Res* (2005) 33:2993–3001. doi: 10.1093/nar/gki610
54. Wu Q, Christensen LA, Legerski RJ, Vasquez KM. Mismatch Repair Participates in Error-Free Processing of DNA Interstrand Crosslinks in Human Cells. *EMBO Rep* (2005) 6:551–7. doi: 10.1038/sj.embor.7400418
55. Zhao J, Jain A, Iyer RR, Modrich PL, Vasquez KM. Mismatch Repair and Nucleotide Excision Repair Proteins Cooperate in the Recognition of DNA Interstrand Crosslinks. *Nucleic Acids Res* (2009) 37:4420–9. doi: 10.1093/nar/gkp399
56. Wang G, Chuang L, Zhang X, Colton S, Dombkowski A, Reiners J, Diakiw A, Xu XS. (2004). The Initiative Role of XPC Protein in Cisplatin DNA Damaging Treatment-Mediated Cell Cycle Regulation. *Nucleic Acids Res* 32(7):2231–40. doi: 10.1093/nar/gkh541
57. Yoshino M, Nakatsuru Y, Te Riele H, Hirota S, Kitamura Y, Tanaka K. Additive Roles of XPA and MSH2 Genes in UVB-Induced Skin Tumorigenesis in Mice. *DNA Repair (Amst)* (2002) 1(11):935–40. doi: 10.1016/S1568-7864(02)00144-1
58. Meira LB, Reis AMC, Cheo DL, Nahari D, Burns DK, Friedberg EC. Cancer Predisposition in Mutant Mice Defective in Multiple Genetic Pathways: Uncovering Important Genetic Interactions. *Mutat Res* (2001) 477:51–8. doi: 10.1016/S0027-5107(01)00097-5
59. Kobayashi K, O'driscoll M, Macpherson P, Mullenders L, Vreeswijk M, Karran P. XPC Lymphoblastoid Cells Defective in the Hmutsalpha DNA Mismatch Repair Complex Exhibit Normal Sensitivity to UVC Radiation and Normal Transcription-Coupled Excision Repair of DNA Cyclobutane Pyrimidine Dimers. *DNA Repair (Amst)* (2004) 3:649–57. doi: 10.1016/j.dnarep.2004.02.007
60. Despras E, Pfeiffer P, Salles B, Calsou P, Kuhfittig-Kulle S, Angulo JF, et al. Long-Term XPC Silencing Reduces DNA Double-Strand Break Repair. *Cancer Res* (2007) 67:2526–34. doi: 10.1158/0008-5472.CAN-06-3371
61. Miccoli L, Burr KL, Hickenbotham P, Friedberg EC, Angulo JF, Dubrova YE. The Combined Effects of Xeroderma Pigmentosum C Deficiency and Mutagens on Mutation Rates in the Mouse Germ Line. *Cancer Res* (2007) 67:4695–9. doi: 10.1158/0008-5472.CAN-06-3844
62. Wang H, Huang Y, Shi J, Zhi Y, Yuan F, Yu J, et al. XPC Deficiency Leads to Centrosome Amplification by Inhibiting BRCA1 Expression Upon Cisplatin-Mediated DNA Damage in Human Bladder Cancer. *Cancer Lett* (2019) 444:136–46. doi: 10.1016/j.canlet.2018.12.004
63. Ray A, Milum K, Battu A, Wani G, Wani AA. NER Initiation Factors, DDB2 and XPC, Regulate UV Radiation Response by Recruiting ATR and ATM Kinases to DNA Damage Sites. *DNA Repair (Amst)* (2013) 12:273–83. doi: 10.1016/j.dnarep.2013.01.003
64. Wang QE, Han C, Zhang B, Sabapathy K, Wani AA. Nucleotide Excision Repair Factor XPC Enhances DNA Damage-Induced Apoptosis by Downregulating the Antiapoptotic Short Isoform of Caspase-2. *Cancer Res* (2012) 72:666–75. doi: 10.1158/0008-5472.CAN-11-2774
65. Liu SY, Wen CY, Lee YJ, Lee TC. XPC Silencing Sensitizes Glioma Cells to Arsenic Trioxide *via* Increased Oxidative Damage. *Toxicol Sci* (2010) 116:183–93. doi: 10.1093/toxsci/kfq113
66. Sears CR, Zhou H, Justice MJ, Fisher AJ, Saliba J, Lamb I, et al. Xeroderma Pigmentosum Group C Deficiency Alters Cigarette Smoke DNA Damage Cell Fate and Accelerates Emphysema Development. *Am J Respir Cell Mol Biol* (2018) 58:402–11. doi: 10.1165/rcmb.2017-0251OC
67. Ito S, Yamane M, Ohtsuka S, Niwa H. The C-Terminal Region of Xpc Is Dispensable for the Transcriptional Activity of Oct3/4 in Mouse Embryonic Stem Cells. *FEBS Lett* (2014) 588:1128–35. doi: 10.1016/j.febslet.2014.02.033
68. Le May N, Mota-Fernandes D, Velez-Cruz R, Iltis I, Biard D, Egly JM. NER Factors Are Recruited to Active Promoters and Facilitate Chromatin Modification for Transcription in the Absence of Exogenous Genotoxic Attack. *Mol Cell* (2010) 38:54–66. doi: 10.1016/j.molcel.2010.03.004
69. Bidon B, Iltis I, Semer M, Nagy Z, Larnicol A, Cribier A, et al. XPC is an RNA Polymerase II Cofactor Recruiting ATAC to Promoters by Interacting With E2F1. *Nat Commun* (2018) 9:2610. doi: 10.1038/s41467-018-05010-0
70. Melis JP, Luijten M, Mullenders LH, Van Steeg H. The Role of XPC: Implications in Cancer and Oxidative DNA Damage. *Mutat Res* (2011) 728:107–17. doi: 10.1016/j.mrrev.2011.07.001
71. Mori MP, Costa RA, Soltys DT, Freire TS, Rossato FA, Amigo I, et al. Lack of XPC Leads to a Shift Between Respiratory Complexes I and II But Sensitizes Cells to Mitochondrial Stress. *Sci Rep* (2017) 7:155. doi: 10.1038/s41598-017-00130-x
72. Schreck I, Grico N, Hansjosten I, Marquardt C, Bormann S, Seidel A, et al. The Nucleotide Excision Repair Protein XPC Is Essential for Bulky DNA Adducts to Promote Interleukin-6 Expression *via* the Activation of P38-SAPK. *Oncogene* (2016) 35:908–18. doi: 10.1038/onc.2015.145
73. Wijnhoven SWP, Kool HJM, Mullenders LHF, Van Zeeland AA, Friedberg EC, van der Horst GTJ, et al. Age-Dependent Spontaneous Mutagenesis in Xpc Mice Defective in Nucleotide Excision Repair. *Oncogene* (2000) 19:5034–7. doi: 10.1038/sj.onc.1203844
74. Fischer JL, Kumar MA, Day TW, Hardy TM, Hamilton S, Besch-Williford C, et al. The Xpc Gene Markedly Affects Cell Survival in Mouse Bone Marrow. *Mutagenesis* (2009) 24:309–16. doi: 10.1093/mutage/gep011
75. Furutani E, Shimamura A. Germline Genetic Predisposition to Hematologic Malignancy. *J Clin Oncol* (2017) 35:1018–28. doi: 10.1200/JCO.2016.70.8644
76. El-Zein R, Monroy CM, Etzel CJ, Cortes AC, Xing Y, Collier AL, et al. Genetic Polymorphisms in DNA Repair Genes as Modulators of Hodgkin Disease Risk. *Cancer* (2009) 115:1651–9. doi: 10.1002/cncr.24205
77. Sarasin A, Quentin S, Droin N, Sahbatou M, Saada V, Auger N, et al. Familial Predisposition to TP53/complex Karyotype MDS and Leukemia in DNA Repair-Deficient Xeroderma Pigmentosum. *Blood* (2019) 133:2718–24. doi: 10.1182/blood-2019-01-895698
78. Strom SS, Estey E, Outschoorn UM, Garcia-Manero G. Acute Myeloid Leukemia Outcome: Role of Nucleotide Excision Repair Polymorphisms in Intermediate Risk Patients. *Leuk Lymphoma* (2010) 51:598–605. doi: 10.3109/10428190903582804
79. Guillem VM, Cervantes F, Martinez J, Alvarez-Larran A, Collado M, Camos M, et al. XPC Genetic Polymorphisms Correlate With the Response to Imatinib Treatment in Patients With Chronic Phase Chronic Myeloid Leukemia. *Am J Hematol* (2010) 85:482–6. doi: 10.1002/ajh.21726

80. Dumontet C, Landi S, Reiman T, Perry T, Plesa A, Bellini I, et al. Genetic Polymorphisms Associated With Outcome in Multiple Myeloma Patients Receiving High-Dose Melphalan. *Bone Marrow Transplant* (2010) 45:1316–24. doi: 10.1038/bmt.2009.335
81. Marin MS, Lopez-Cima MF, Garcia-Castro L, Pascual T, Marron MG, Tardon A. Poly (AT) Polymorphism in Intron 11 of the *XPC* DNA Repair Gene Enhances the Risk of Lung Cancer. *Cancer Epidemiol Biomarkers Prev* (2004) 13:1788–93. doi: 10.1158/1055-9965.1788.13.11
82. Vogel U, Overvad K, Wallin H, Tjonneland A, Nexo BA, Raaschou-Nielsen O. Combinations of Polymorphisms in XPD, XPC and XPA in Relation to Risk of Lung Cancer. *Cancer Lett* (2005) 222:67–74. doi: 10.1016/j.canlet.2004.11.016
83. Francisco G, Menezes PR, Eluf-Neto J, Chammas R. XPC Polymorphisms Play a Role in Tissue-Specific Carcinogenesis: A Meta-Analysis. *Eur J Hum Genet* (2008) 16:724–34. doi: 10.1038/ejhg.2008.6
84. Letkova L, Matakova T, Musak L, Sarlinova M, Krutakova M, Slovakova P, et al. DNA Repair Genes Polymorphism and Lung Cancer Risk With the Emphasis to Sex Differences. *Mol Biol Rep* (2013) 40:5261–73. doi: 10.1007/s11033-013-2626-z
85. Jin B, Dong Y, Zhang X, Wang H, Han B. Association of XPC Polymorphisms and Lung Cancer Risk: A Meta-Analysis. *PloS One* (2014) 9:e93937. doi: 10.1371/journal.pone.0093937
86. Qiu L, Wang Z, Shi X. Associations Between XPC Polymorphisms and Risk of Cancers: A Meta-Analysis. *Eur J Cancer* (2008) 44:2241–53. doi: 10.1016/j.ejca.2008.06.024
87. Mei C, Hou M, Guo S, Hua F, Zheng D, Xu F, et al. Polymorphisms in DNA Repair Genes of XRCC1, XPA, XPC, XPD and Associations With Lung Cancer Risk in Chinese People. *Thorac Cancer* (2014) 5:232–42. doi: 10.1111/1759-7714.12073
88. Xie C, Zhao J, Hua W, Tan P, Chen Y, Rui J, et al. Effect of XPC Polymorphisms on the Response to Platinum-Based Chemotherapy: A Meta-Analysis. *Onco Targets Ther* (2019) 12:3839–48. doi: 10.2147/OTT.S202617
89. Said R, Bougatef K, Setti Boubaker N, Jenni R, Derouiche A, Chebil M, et al. Polymorphisms in XPC Gene and Risk for Prostate Cancer. *Mol Biol Rep* (2019) 46:1117–25. doi: 10.1007/s11033-018-4572-2
90. Liu Y, Chen Z, Wei Q, Yuan F, Zhi Y, Song B, et al. Poly (AT) Polymorphism in the XPC Gene and Smoking Enhance the Risk of Prostate Cancer in a Low-Risk Chinese Population. *Cancer Genet* (2012) 205:205–11. doi: 10.1016/j.cancergen.2012.01.013
91. Yoshino Y, Takeuchi S, Katoh T, Kuroda Y. XPC Intron11 C/A Polymorphism as a Risk Factor for Prostate Cancer. *Environ Health Prev Med* (2016) 21:100–4. doi: 10.1007/s12199-015-0505-z
92. Kahnamouei SA, Narouie B, Sotoudeh M, Mollakouchekian MJ, Simforoosh N, Ziaee SA, et al. Association of XPC Gene Polymorphisms With Prostate Cancer Risk. *Clin Lab* (2016) 62:1009–15. doi: 10.7754/Clin.Lab.2015.150914
93. Zhao Z, Zhang A, Zhao Y, Xiang J, Yu D, Liang Z, et al. The Association of Polymorphisms in Nucleotide Excision Repair Genes With Ovarian Cancer Susceptibility. *Biosci Rep* (2018) 38:BSR20180114. doi: 10.1042/BSR20180114
94. Fleming ND, Agadjanian H, Nassanian H, Miller CW, Orsulic S, Karlan BY, et al. Xeroderma Pigmentosum Complementation Group C Single-Nucleotide Polymorphisms in the Nucleotide Excision Repair Pathway Correlate With Prolonged Progression-Free Survival in Advanced Ovarian Cancer. *Cancer* (2012) 118:689–97. doi: 10.1002/cncr.26329
95. Zhang Y, Wang X, Zhang W, Gong S. An Association Between XPC Lys939Gln Polymorphism and the Risk of Bladder Cancer: A Meta-Analysis. *Tumor Biol* (2013) 34:973–82. doi: 10.1007/s13277-012-0633-7
96. Dai Q-S, Hua R-X, Zeng R-F, Long J-T, Peng Z-W. XPC Gene Polymorphisms Contribute to Bladder Cancer Susceptibility: A Meta-Analysis. *Tumor Biol* (2014) 35:447–53. doi: 10.1007/s13277-013-1062-y
97. Sankhwar M, Sankhwar SN, Bansal SK, Gupta G, Rajender S. Polymorphisms in the XPC Gene Affect Urinary Bladder Cancer Risk: A Case-Control Study, Meta-Analyses and Trial Sequential Analyses. *Sci Rep* (2016) 6:27018. doi: 10.1038/srep27018
98. Qiao B, Ansari AH, Scott GB, Sak SC, Chambers PA, Elliott F, et al. *In Vitro* Functional Effects of XPC Gene Rare Variants From Bladder Cancer Patients. *Carcinogenesis* (2011) 32:516–21. doi: 10.1093/carcin/bgr005
99. Qiu J, Wang X, Meng X, Zheng Y, Li G, Ma J, et al. Attenuated NER Expressions of XPF and XPC Associated With Smoking Are Involved in the Recurrence of Bladder Cancer. *PloS One* (2014) 9:e115224. doi: 10.1371/journal.pone.0115224
100. Wang L, Lin DX, Lu XH, Miao XP, Li H. [Polymorphisms of the DNA Repair Genes XRCC1 and XPC: Relationship to Pancreatic Cancer Risk]. *Wei Sheng Yan Jiu* (2006) 35:534–6.
101. Liang XH, Yan D, Zhao JX, Ding W, Xu XJ, Wang XY. Interaction of Polymorphisms in Xeroderma Pigmentosum Group C With Cigarette Smoking and Pancreatic Cancer Risk. *Oncol Lett* (2018) 16:5631–8. doi: 10.3892/ol.2018.9350
102. Yang PW, Hsieh CY, Kuo FT, Huang PM, Hsu HH, Kuo SW, et al. The Survival Impact of XPA and XPC Genetic Polymorphisms on Patients With Esophageal Squamous Cell Carcinoma. *Ann Surg Oncol* (2013) 20:562–71. doi: 10.1245/s10434-012-2622-x
103. Pan J, Lin J, Izzo JG, Liu Y, Xing J, Huang M, et al. Genetic Susceptibility to Esophageal Cancer: The Role of the Nucleotide Excision Repair Pathway. *Carcinogenesis* (2009) 30:785–92. doi: 10.1093/carcin/bgp058
104. Gusella M, Giacopuzzi S, Bertolaso L, Zanoni A, Pezzolo E, Modena Y, et al. Genetic Prediction of Long-Term Survival After Neoadjuvant Chemoradiation in Locally Advanced Esophageal Cancer. *Pharmacogenomics J* (2017) 17:252–7. doi: 10.1038/tpj.2016.9
105. Huang WY, Berndt SI, Kang D, Chatterjee N, Chanock SJ, Yeager M, et al. Nucleotide Excision Repair Gene Polymorphisms and Risk of Advanced Colorectal Adenoma: XPC Polymorphisms Modify Smoking-Related Risk. *Cancer Epidemiol Biomarkers Prev* (2006) 15:306–11. doi: 10.1158/1055-9965.EPI-05-0751
106. Hu LB, Chen Y, Meng XD, Yu P, He X, Li J. Nucleotide Excision Repair Factor XPC Ameliorates Prognosis by Increasing the Susceptibility of Human Colorectal Cancer to Chemotherapy and Ionizing Radiation. *Front Oncol* (2018) 8:290. doi: 10.3389/fonc.2018.00290
107. Malik SS, Zia A, Rashid S, Mubarik S, Masood N, Hussain M, et al. XPC as Breast Cancer Susceptibility Gene: Evidence From Genetic Profiling, Statistical Inferences and Protein Structural Analysis. *Breast Cancer* (2020) 27:1168–76. doi: 10.1007/s12282-020-01121-z
108. Qazvini MG, Salehi Z, Mashayekhi F, Saedi HS. A33512C and Intronic Poly (AT) Insertion/Deletion (PAT-/+) Polymorphisms of the XPC Gene and Their Association With the Risk of Breast Cancer. *Clin Breast Cancer* (2020) 20:e771–7. doi: 10.1016/j.clbc.2020.05.014
109. Long XD, Ma Y, Zhou YF, Ma AM, Fu GH. Polymorphism in Xeroderma Pigmentosum Complementation Group C Codon 939 and Aflatoxin B1-Related Hepatocellular Carcinoma in the Guangxi Population. *Hepatology* (2010) 52:1301–9. doi: 10.1002/hep.23807
110. Oetjen KA, Levoska MA, Tamura D, Ito S, Douglas D, Khan SG, et al. Predisposition to Hematologic Malignancies in Patients With Xeroderma Pigmentosum. *Haematologia* (2020) 105:e146. doi: 10.3324/haematol.2019.223370
111. Yurchenko AA, Padioleau I, Matkarimov BT, Soulier J, Sarasin A, Nikolaev S. XPC Deficiency Increases Risk of Hematologic Malignancies Through Mutator Phenotype and Characteristic Mutational Signature. *Nat Commun* (2020) 11:5834. doi: 10.1038/s41467-020-19633-9
112. Kent WJ, Hsu F, Karolchik D, Kuhn RM, Clawson H, Trumbower H, Haussler D. Exploring relationships and mining data with the UCSC Gene Sorter. *Genome Res.* (2005) 15(5):737–41. doi: 10.1101/gr.3694705
113. Szalat R, Samur MK, Fulciniti M, Lopez M, Nanjappa P, Cleynen A, et al. Nucleotide Excision Repair Is a Potential Therapeutic Target in Multiple Myeloma. *Leukemia* (2018) 32:111–9. doi: 10.1038/leu.2017.182
114. Kandoth C, Mclellan MD, Vandin F, Ye K, Niu B, Lu C, et al. Mutational Landscape and Significance Across 12 Major Cancer Types. *Nature* (2013) 502:333–9. doi: 10.1038/nature12634
115. Sears CR. DNA Repair as an Emerging Target for COPD-Lung Cancer Overlap. *Respir Invest* (2019) 57:111–21. doi: 10.1016/j.resinv.2018.11.005
116. Kraemer KH, Lee MM, Scotto J. DNA Repair Protects Agains Cutaneous and Internal Neoplasia: Evidence From Xeroderma Pigmentosum. *Carcinogenesis* (1984) 5:511–4. doi: 10.1093/carcin/5.4.511
117. Wu YH, Cheng YW, Chang JT, Wu TC, Chen CY, Lee H. Reduced XPC Messenger RNA Level may Predict a Poor Outcome of Patients With Nonsmall Cell Lung Cancer. *Cancer* (2007) 110:215–23. doi: 10.1002/cncr.22743

118. Zhu Y, Yang H, Chen Q, Lin J, Grossman HB, Dinney CP, et al. Modulation of DNA Damage/DNA Repair Capacity by XPC Polymorphisms. *DNA Repair (Amst)* (2008) 7:141–8. doi: 10.1016/j.dnarep.2007.08.006
119. Stearman RS, Dwyer-Nield L, Zerbe L, Blaine SA, Chan Z, Bunn PA, et al. Analysis of Orthologous Gene Expression Between Human Pulmonary Adenocarcinoma and a Carcinogen-Induced Murine Model. *Am J Pathol* (2005) 167:1763–75. doi: 10.1016/S0002-9440(10)61257-6
120. Saviozzi S, Ceppi P, Novello S, Ghio P, Lo Iacono M, Borasio P, et al. Non-Small Cell Lung Cancer Exhibits Transcript Overexpression of Genes Associated With Homologous Recombination and DNA Replication Pathways. *Cancer Res* (2009) 69:3390–6. doi: 10.1158/0008-5472.CAN-08-2981
121. De Feraudy S, Ridd K, Richards LM, Kwok PY, Revet I, Oh D, et al. The DNA Damage-Binding Protein XPC Is a Frequent Target for Inactivation in Squamous Cell Carcinomas. *Am J Pathol* (2010) 177:555–62. doi: 10.2353/ajpath.2010.090925
122. Wu YH, Tsai Chang JH, Cheng YW, Wu TC, Chen CY, Lee H. Xeroderma Pigmentosum Group C Gene Expression Is Predominantly Regulated by Promoter Hypermethylation and Contributes to P53 Mutation in Lung Cancers. *Oncogene* (2007) 26:4761–73. doi: 10.1038/sj.onc.1210284
123. Holcomb N, Goswami M, Han SG, Clark S, Orren DK, Gairola CG, et al. Exposure of Human Lung Cells to Tobacco Smoke Condensate Inhibits the Nucleotide Excision Repair Pathway. *PloS One* (2016) 11:e0158858. doi: 10.1371/journal.pone.0158858
124. Lee H-W, Wang H-T, Weng M-W, Chin C, Huang W, Lepor H, et al. Cigarette Side-Stream Smoke Lung and Bladder Carcinogenesis: Inducing Mutagenic Acrolein-DNA Adducts, Inhibiting DNA Repair and Enhancing Anchorage-Independence-Growth Cell Transformation. *Oncotarget* (2015) 6:33226–36. doi: 10.18632/oncotarget.5429
125. Lee HW, Park SH, Weng MW, Wang HT, Huang WC, Lepor H, et al. E-Cigarette Smoke Damages DNA and Reduces Repair Activity in Mouse Lung, Heart, and Bladder as Well as in Human Lung and Bladder Cells. *Proc Natl Acad Sci USA* (2018) 115:E1560–9. doi: 10.1073/pnas.1718185115
126. Sands AT, Abuin A, Sanchez A, Conti CJ, Bradley A. High Susceptibility to Ultraviolet-Induced Carcinogenesis in Mice Lacking XPC. *Nature* (1995) 377:162–5. doi: 10.1038/377162a0
127. Friedberg EC, Bond JP, Burns DK, Cheo DL, Greenblatt MS, Meira LB, et al. Defective Nucleotide Excision Repair in XPC Mutant Mice and its Association With Cancer Predisposition. *Mutat Res* (2000) 459:99–108. doi: 10.1016/S0921-8777(99)00068-3
128. Melis JP, Wijnhoven SW, Beems RB, Roodbergen M, Van Den Berg J, Moon H, et al. Mouse Models for Xeroderma Pigmentosum Group A and Group C Show Divergent Cancer Phenotypes. *Cancer Res* (2008) 68:1347–53. doi: 10.1158/0008-5472.CAN-07-6067
129. De Oliveira Alves N, Martins Pereira G, Di Domenico M, Costanzo G, Benevenuto S, De Oliveira Fonoff AM, et al. Inflammation Response, Oxidative Stress and DNA Damage Caused by Urban Air Pollution Exposure Increase in the Lack of DNA Repair XPC Protein. *Environ Int* (2020) 145:106150. doi: 10.1016/j.envint.2020.106150
130. Hollander MC, Philburn RT, Patterson AD, Velasco-Miguel S, Friedberg EC, Linnoila RI, et al. Deletion of XPC Leads to Lung Tumors in Mice and Is Associated With Early Events in Human Lung Carcinogenesis. *Proc Natl Acad Sci USA* (2005) 102:13200–5. doi: 10.1073/pnas.0503133102
131. Cheo DL, Burns DK, Meira LB, Houle JF, Friedberg EC. Mutational Inactivation of the Xeroderma Pigmentosum Group C Gene Confers Predisposition to 2-Acetylaminofluorene-Induced Liver and Lung Cancer and to Spontaneous Testicular Cancer in *Trp53-/-* Mice. *Cancer Res* (1999) 59:771–5.
132. Wu YH, Wu TC, Liao JW, Yeh KT, Chen CY, Lee H. P53 Dysfunction by Xeroderma Pigmentosum Group C Defects Enhance Lung Adenocarcinoma Metastasis *via* Increased MMP1 Expression. *Cancer Res* (2010) 70:10422–32. doi: 10.1158/0008-5472.CAN-10-2615
133. Cui T, Srivastava AK, Han C, Yang L, Zhao R, Zou N, et al. XPC Inhibits NSCLC Cell Proliferation and Migration by Enhancing E-Cadherin Expression. *Oncotarget* (2015) 6:10060–72. doi: 10.18632/oncotarget.3542
134. Islami F, Ward EM, Sung H, Cronin KA, Tangka FKL, Sherman RL, et al. Annual Report to the Nation on the Status of Cancer, Part 1: National Cancer Statistics. *J Natl Cancer Inst* (2021) 113(12):1648-69. doi: 10.1093/jnci/djab131
135. Qin F, Gao SL, Xu K, Su QX, Zhang Z, Shi L, et al. XPC Exon15 Lys939Gln Variant Increase Susceptibility to Prostate Adenocarcinoma: Evidence Based on 4306 Patients and 4779 Controls. *Medicine (Baltimore)* (2020) 99:e21160. doi: 10.1097/MD.0000000000021160
136. Zhang Y, Yu JJ, Tian Y, Li ZZ, Zhang CY, Zhang SF, et al. Eif3a Improve Cisplatin Sensitivity in Ovarian Cancer by Regulating XPC and p27Kip1 Translation. *Oncotarget* (2015) 6:25441–51. doi: 10.18632/oncotarget.4555
137. Chen Z, Yang J, Wang G, Song B, Li J, Xu Z. Attenuated Expression of Xeroderma Pigmentosum Group C Is Associated With Critical Events in Human Bladder Cancer Carcinogenesis and Progression. *Cancer Res* (2007) 67:4578–85. doi: 10.1158/0008-5472.CAN-06-0877
138. Yang J, Xu Z, Li J, Zhang R, Zhang G, Ji H, et al. XPC Epigenetic Silence Coupled With P53 Alteration Has a Significant Impact on Bladder Cancer Outcome. *J Urol* (2010) 184:336–43. doi: 10.1016/j.juro.2010.03.044
139. Xu XS, Wang L, Abrams J, Wang G. Histone Deacetylases (HDACs) in XPC Gene Silencing and Bladder Cancer. *J Hematol Oncol* (2011) 4:17. doi: 10.1186/1756-8722-4-17
140. Ming M, Shea CR, Guo X, Li X, Soltani K, Han W, et al. Regulation of Global Genome Nucleotide Excision Repair by SIRT1 Through Xeroderma Pigmentosum C. *Proc Natl Acad Sci USA* (2010) 107:22623–8. doi: 10.1073/pnas.1010377108
141. Zhao F, Shang Y, Zeng C, Gao D, Li K. Association of Single Nucleotide Polymorphisms of DNA Repair Genes in NER Pathway and Susceptibility to Pancreatic Cancer. *Int J Clin Exp Pathol* (2015) 8:11579–86.
142. Zabarovsky ER, Lerman MI, Minna JD. Tumor Suppressor Genes on Chromosome 3p Involved in the Pathogenesis of Lung and Other Cancers. *Oncogene* (2002) 21:6915–35. doi: 10.1038/sj.onc.1205835
143. Schena M, Guarrera S, Buffoni L, Salvadori A, Voglino F, Allione A, et al. DNA Repair Gene Expression Level in Peripheral Blood and Tumour Tissue From Non-Small Cell Lung Cancer and Head and Neck Squamous Cell Cancer Patients. *DNA Repair (Amst)* (2012) 11:374–80. doi: 10.1016/j.dnarep.2012.01.003
144. Nahari D, Mcdaniel LD, Task LB, Daniel RL, Velasco-Miguel S, Friedberg EC. Mutations in the Trp53 Gene of UV-Irradiated Xpc Mutant Mice Suggest a Novel Xpc-Dependent DNA Repair Process. *DNA Repair* (2004) 3:379–86. doi: 10.1016/j.dnarep.2003.03.001
145. Krzeszinski JY, Choe V, Shao J, Bao X, Cheng H, Luo S, et al. XPC Promotes MDM2-Mediated Degradation of the P53 Tumor Suppressor. *Mol Biol Cell* (2014) 25:213–21. doi: 10.1091/mbc.e13-05-0293
146. Lin PS, Mcpherson LA, Chen AY, Sage J, Ford JM. The Role of the Retinoblastoma/E2F1 Tumor Suppressor Pathway in the Lesion Recognition Step of Nucleotide Excision Repair. *DNA Repair (Amst)* (2009) 8:795–802. doi: 10.1016/j.dnarep.2009.03.003
147. Sun C-C, Li S-J, Yuan Z-P, Li D-J. MicroRNA-346 Facilitates Cell Growth and Metastasis, and Supresses Cell Apoptosis in Human Non-Small Cell Lung Cancer by Regulation of XPC/ERK/Snail/E-Cadherin Pathway. *Aging* (2016) 8:2509–24. doi: 10.18632/aging.101080
148. Yeh KT, Wu YH, Lee MC, Wang L, Li CT, Chen CY, et al. XPC mRNA Level may Predict Relapse in Never-Smokers With Non-Small Cell Lung Cancers. *Ann Surg Oncol* (2012) 19:734–42. doi: 10.1245/s10434-011-1992-9
149. Zhang R, Jia M, Xue H, Xu Y, Wang M, Zhu M, et al. Genetic Variants in ERCC1 and XPC Predict Survival Outcome of non-Small Cell Lung Cancer Patients Treated With Platinum-Based Therapy. *Sci Rep* (2017) 7:10702. doi: 10.1038/s41598-017-10800-5
150. Lai TC, Chow KC, Fang HY, Cho HC, Chen CY, Lin TY, et al. Expression of Xeroderma Pigmentosum Complementation Group C Protein Predicts Cisplatin Resistance in Lung Adenocarcinoma Patients. *Oncol Rep* (2011) 25:1243–51. doi: 10.3892/or.2011.1184
151. Lehmann AR, Fassihi H. Molecular Analysis Directs the Prognosis, Management and Treatment of Patients With Xeroderma Pigmentosum. *DNA Repair (Amst)* (2020) 93:102907. doi: 10.1016/j.dnarep.2020.102907
152. Hatano K, Kumar B, Zhang Y, Coulter JB, Hedayati M, Mears B, et al. A Functional Screen Identifies miRNAs That Inhibit DNA Repair and Sensitize Prostate Cancer Cells to Ionizing Radiation. *Nucleic Acids Res* (2015) 43:4075–86. doi: 10.1093/nar/gkv273
153. Muenyi CS, States VA, Masters JH, Fan TW, Helm CW, States JC. Sodium Arsenite and Hyperthermia Modulate Cisplatin-DNA Damage Responses and Enhance Platinum Accumulation in Murine Metastatic Ovarian Cancer Xenograft After Hyperthermic Intraperitoneal Chemotherapy (HIPEC). *J Ovarian Res* (2011) 4:9. doi: 10.1186/1757-2215-4-9

Author Disclaimer: CRS is employed by the U.S. Department of Veterans Affairs. The contents of this manuscript do not represent the views of the U.S. Department of Veterans Affairs or the United States Government.

Conflict of Interest: CRS has served on Scientific and Medical Advisory Boards for Biodesix, Inc., bioAffinity Technologies, and as a scientific medical consultant for Bristol-Myers Squibb Company; these are not relevant to the topic of this manuscript.

The remaining authors declare that the research was conducted in the absence of any commercial or financial relationships that could be construed as a potential conflict of interest.

Publisher's Note: All claims expressed in this article are solely those of the authors and do not necessarily represent those of their affiliated organizations, or those of the publisher, the editors and the reviewers. Any product that may be evaluated in this article, or claim that may be made by its manufacturer, is not guaranteed or endorsed by the publisher.

frontiers | Frontiers in Oncology

ORIGINAL RESEARCH
published: 13 May 2022
doi: 10.3389/fonc.2022.885186

Targeting the Homologous Recombination Pathway in Cancer With a Novel Class of RAD51 Inhibitors

Peng Gu[1†], Liting Xue[1†], Chunyan Zhao[1], Wenjing Li[1], Zhen Jiang[1], Aiguo Liu[1], Tingting Li[1], Lu Liu[1], Markus Decker[1], Xiaoxuan Cheng[2], Wenqing Yang[1] and Renhong Tang[1]*

[1] State Key Laboratory of Translational Medicine and Innovative Drug Development, Jiangsu Simcere Pharmaceutical Co., Ltd., Nanjing, China, [2] High School Sophomore, Hangzhou Foreign Languages School, Hangzhou, China

OPEN ACCESS

Edited by:
John Turchi,
Indiana University Bloomington,
United States

Reviewed by:
Michael G. Kemp,
Wright State University, United States
Pamela L Mendoza-Munoz,
Purdue University Indianapolis,
United States

***Correspondence:**
Renhong Tang
renhong.tang@simceregroup.com

[†]These authors have contributed equally to this work and share first authorship

Specialty section:
This article was submitted to Cancer Molecular Targets and Therapeutics, a section of the journal Frontiers in Oncology

Received: 27 February 2022
Accepted: 29 March 2022
Published: 13 May 2022

Citation:
Gu P, Xue L, Zhao C, Li W, Jiang Z, Liu A, Li T, Liu L, Decker M, Cheng X, Yang W and Tang R (2022) Targeting the Homologous Recombination Pathway in Cancer With a Novel Class of RAD51 Inhibitors. Front. Oncol. 12:885186. doi: 10.3389/fonc.2022.885186

Targeting DNA damage response (DDR) pathway has been proposed as an approach for amplifying tumor-specific replicative lesions. RAD51 plays a central role in the DDR process, and thus represents a promising anti-tumor target. We here report the discovery of a series of next generation RAD51 inhibitors that can prevent RAD51 foci formation. The lead compounds dramatically impaired human cancer cell growth, induced cell cycle arrest in S-phase, and resulted in elevated γH2AX. Furthermore, cancer cells became sensitized to chemotherapy and other DDR inhibitors. Dosed either as a single agent or in combination with cisplatin, the compounds significantly inhibited tumor growth *in vivo*. By upregulating ATR-CHK1 signaling, the RAD51 inhibitors increased surface PD-L1 levels in various tumor cells, suggesting a potential combination of RAD51 inhibitors with PD-1/PD-L1 blockade. Overall, our findings provide the preclinical rationale to explore RAD51 inhibitors as monotherapy or in combination with chemotherapy, immunotherapy or DDR-targeting therapy in cancer treatment.

Keywords: Keywords: RAD51, small molecule inhibitor, DNA damage response, homologous recombination, synthetic lethality

INTRODUCTION

The DNA damage response (DDR) is a complex mechanism for DNA damage detection and repair while unrepaired DNA lesions may result in cell death. Genomic instability caused by dysregulation of DDR is one of the major hallmarks of cancer (1). Targeting the DDR in cancers has therefore garnered much attention in recent years yielding novel therapeutic interventions. Most prominently, poly (ADP-ribose) polymerase (PARP) inhibitors such as olaparib have demonstrated clinical benefit in several human cancers (2). Beyond PARP inhibitors, compounds targeting protein kinases involved in activating ATM, ATR and DNA-PK, are currently in clinical trials for hematologic and solid tumors (3).

Homologous recombination (HR) is a central pathway that repairs DNA double-strand breaks (DSBs) caused by endogenous replication stresses and exogenous agents such as ionizing radiation

and genotoxic compounds. The DNA replication stress caused by oncogene activation is an important cause of genomic instability in tumorigenesis (4). The HR repair begins with the recruitment of the MRN complex (Mre11, Rad50 and Nbs1) to the DSB site, followed by ATM recruitment and activation (5). Once activated, ATM orchestrates DSB repair by phosphorylating H2AX on Ser139, referred to as γH2AX, and downstream proteins such as 53BP1 and RAD50. In addition, ATR and DNA-PK kinases are also involved in the DDR by interacting with the DNA binding co-activator complex RPA-ATRIP and XRCC6/XRCC5, respectively. The principle role of RAD51, a homologue of *E. coli* RecA, in the HR pathway is well established (6, 7). The RAD51 recombinase assembles at the resected DNA ends of the DSB to form the nucleoprotein filament. Subsequently, the RAD51 filament searches and invades the homologous region in the sister chromatid to form a displacement loop called a D-loop, followed by gap-filling DNA synthesis and ligation to complete the repair. RAD51 filament formation is controlled by several mediators including BRCA2, RAD52 and RAD51 paralogues (8). Importantly, RAD51 deficient cells lead to genomic instability, as RAD51 depletion in chicken cells resulted in chromosome aberrations and cell lethality (9).

RAD51 overexpression is observed in several human malignancies, including pancreatic adenocarcinoma, non-small-cell lung cancer and breast cancer (10). In addition, it is reported that the overexpression of RAD51 confers resistance to PARP inhibitors in triple negative breast cancer cells (11). Moreover, RAD51 foci formation correlates with resistance to PARP inhibitor in breast cancer patients with germline BRCA mutations (12). As such, RAD51 is emerging as an attractive therapeutic target for restoring synthetic lethality in tumors that have developed resistance to PARP inhibitors. The importance of RAD51 in DNA DSB repair is illustrated by studies showing that increased expression of RAD51 and other HR-associated genes in tumor cells is associated with resistance to radiotherapies or chemotherapies that induce DNA damage (13, 14), implying that targeting RAD51 may improve the efficacy of DNA-damaging agents such as irradiation or chemotherapy. Indeed, there has been intense interest in developing small molecule RAD51 inhibitors. First generation RAD51 inhibitors such as B02, RI-1, RI-2 and IBR2 (15), were limited by a poor potency of growth inhibition, displaying micromolar inhibition concentrations (IC_{50}) in cellular assay (16). We thus set out to identify a highly potent RAD51 inhibitor with good clinical development ability. Moreover, small molecules that specifically target RAD51 could be used as a powerful tool to further understand the role of RAD51 in DNA repair and beyond.

Here we describe the identification and characterization of next-generation orally bioavailable inhibitors against RAD51 with antiproliferative activities in both *in vitro* and *in vivo* models. Of note, a patent application disclosing structures of the compounds described herein has been submitted. We show that the inhibitor's antiproliferative effect can be explained by a mechanism of reduced RAD51 nuclear accumulation and RAD51 degradation by the ubiquitin-proteasome pathway. Oral dosing demonstrated dose-dependent anti-tumor activity and a combination benefit with cisplatin in mice implanted with Daudi xenografts. On the basis of these findings, we propose the preclinical rationale to target RAD51 in Burkitt's lymphoma patients. In addition, we identify the RAD51 inhibitor as a potential synthetic lethal partner for other DDR inhibitors extending the applicability of our identified compound to other tumor types. Furthermore, our findings suggest that RAD51 inhibition may increase the effectiveness of immunotherapy.

MATERIALS AND METHODS

Cell Lines and Culture

A full list of cell lines, their origins, cell growth media and assay media used in this study can be found in **Supplementary Table 1**. All cells were cultured in 5% CO_2 humidified atmosphere at 37°C.

Cellular Thermal Shift Assay

For the cell lysate CETSA experiments, Z138 cells were harvested and washed with PBS supplemented with protease and phosphatase inhibitor tablets. The cell suspensions were freeze-thawed three times using liquid nitrogen. The soluble fraction was separated by centrifugation at 20000g for 20 min at 4°C. Then cell lysate was divided into several aliquots for different compounds or temperatures treatment. After 10-30 min incubation at room temperature (RT) with compounds, cell lysates were heated at indicated temperatures for 3 min followed by cooling for 3 min at RT. The appropriate temperatures were determined in preliminary CETSA experiments (data no shown). The heated lysates were centrifuged at 20000g for 20 min at 4°C and supernatants were transferred to new microtubes and subjected to western blot analysis.

Immunofluorescence Staining

Cells were seeded on coverslips which were pre-coated with poly-L-lysine (Sigma-Aldrich). After the drug treatment, cells were fixed with 4% paraformaldehyde on ice for 20 min, followed by 3 washes with cold PBS. Fixed cells were permeabilized by 0.25% Triton X-100 for 10 min on ice and blocked by 5% FBS in PBS for 1 hour at RT. For staining, blocking buffer was removed and primary antibodies were diluted in 5% FBS and then incubated with cells overnight at 4°C. Coverslips were washed with PBS for 3 times and then incubated with 5% FBS containing Alexa Fluor® secondary antibodies at RT for 1 hour. After washing with PBS for 3 times, coverslips were mounted on glass slides with anti-fade fluorescence mounting medium. Images were acquired with an inverted fluorescent microscope (Nikon Eclipse Ti2-U) and processed with Adobe Photoshop CC 2018. For RAD51 foci quantification, cells with more than 10 foci were counted as positive and at least 300 cells per experiment were scored for the presence of foci. Each experiment was repeated 3 times independently.

Immunofluorescence Histochemistry

To measure γH2AX foci formation *in vivo*, after the drug treatment, mice with Daudi xenograft were euthanized and the tumors were dissected and washed briefly with cold PBS, then fixed overnight in 10 ml of fresh neutral buffered formalin (10%). The tissues were gradually dehydrated with 20% and 30% sucrose solutions until tissue sinks. Dehydrated issues were transferred to OCT (Optimum cutting temperature compound) chamber and surround with OCT, dissected into 10um thickness. The slices were fixed 40 min with cool acetone, then equilibrated with PBS for 10 min and blocked by incubation in PBS containing 0.1% Triton X-100, 0.5% Tween-20 (PBSTT) supplemented with 4% (w/v) BSA and 4% goat serum for 2 h at room temperature. For staining, slides were then incubated with rabbit monoclonal anti-γH2AX antibody in PBSTT containing 4% (w/v) BSA and 4% goat serum overnight at 4°C. The sections were washed 3 times for 5 min each in PBSTT and then incubated with anti-rabbit Alexa Fluor® 488 antibody in PBSTT for 2 h at room temperature. Nuclei were counterstained with DAPI in mounting media (Abcam). γH2AX foci were visualized under Nikon ECLIIPSE Ni-U microscope with 40× objective. Images were processed with Adobe Photoshop CC 2018.

Western Blot

After compounds treatment at indicated time points, cells were washed with PBS and lysed by RIPA lysis buffer (ThermoFisher) supplemented with protease and phosphatase inhibitor tablets. Cell lysate were cleared by centrifugation at 12000g for 10 min. Protein concentration were measured by BCA protein assay kit (ThermoFisher) and equal amount of protein samples were separated by 4–15% Mini-PROTEAN® TGX™ Precast Protein Gels (Bio-Rad) and transferred by Trans-Blot® Turbo™ System (Bio-Rad). Membranes were blocked with 5% non-fat milk or BSA in Tris Buffered Saline with 0.05% Tween-20 (TBS-T) and incubated with primary antibody overnight at 4°C. Membranes were then washed with TBS-T and incubated with HRP-conjugated secondary antibody for 1 hour at RT. Antibody signals were detected by incubating membrane with SuperSignal™ West Dura Extended Duration Substrate (ThermoFisher). Images were acquired by Sapphire Biomolecular Imager (Azure biosystems) and processed using Adobe Photoshop CC 2018. Relative protein amount was measured by calculating the pixel intensity using ImageJ (National Institute of Health). Immunoblots presented in all figures are representatives of at least three independent experiments. Antibodies used in this study can be found in **Supplementary Table 2**.

Cell Growth Inhibition Assay

Cells were seeded in opaque-walled 96-well microplates at appropriate densities according to the growth curves (data no shown). On the following day cells were dosed with compounds. After 7 days treatments, cells viability was measured by adding 30μL CellTiter-Glo reagent (Promega) and incubated for 10 min at RT. Luminescence was measured by Envision plate reader (Perkin Elmer). For synergy analysis, the survival rates of the cells upon different treatment combinations were calculated based on the luminescence and analyzed by Combenefit software. The bliss independence model was used to analyzed the interaction between two tested articles to determine if the interaction between those two tested articles was synergistic, independent or antagonistic.

Cell Cycle Analysis

Cells were fixed with 70% ethanol and then washed with PBS for 3 times (5 min each), after the fixation, they were stained with 150 μL PI/RNase Staining Buffer incubated 15 min at RT in the dark. DNA content were determined using a FACS Canto II flow cytometer (BD Biosciences).

Apoptosis Assay

For analysis of apoptosis, treated cells were stained with PE Annexin V Apoptosis Detection Kit I (BD) in accordance with the manufacturer's instructions. Flow cytometry data were acquired using a FACS Canto II flow cytometer (BD Bioscience) and analyzed using FACS Diva software (BD Bioscience).

γH2AX Analysis

Cells treated with compounds or cisplatin were harvested at indicated time points, fixed with IC Fix buffer overnight and permeabilized with True-Phos™ Perm Buffer (BioLegend) for 1 h at -20°C. After washed with PBS for 3 times (5 min each), cells were stained with anti-γH2AX (phospho S139) antibody for 1 h at 4°C. Cells were then washed and incubated with Alexa Fluor® secondary antibody for 1 h at 4°C. The fluorescence was determined by flow cytometry (BD Biosciences) and analyzed using FACS Diva software (BD Biosciences).

Flow Cytometric Analysis of Cell Surface PD-L1

To evaluate cell surface PD-L1 levels, cells were suspended in 100 μL of cell staining buffer and incubated with PE anti-human CD274 (PD-L1) antibody at 4°C for 30 min. Then cells were washed in PBS for 3 times (5 min each). Flow cytometry data were acquired using a FACS Canto II flow cytometer (BD Biosciences) and analyzed using FACS Diva software (BD Biosciences).

In Vivo Studies

Daudi xenograft mouse model was established by subcutaneously implantation of 10^7 cells into the female BABL/c nude mice at the age of 6-8 weeks. When tumors reached approximately 100-120 mm^3, the mice were randomly grouped into five groups (n=6) and treated with vehicle control orally every day, 30 mg/kg or 100 mg/kg Cpd-4 orally every day, 2 mg/kg Cisplatin intraperitoneally every week, or combination of 30 mg/kg Cpd-4 and 2 mg/kg Cisplatin. Cpd-4 was formulated in in 30% PEG400 (Sigma) and 70% 10% vitamin E TPGS (Sigma) in water. Cisplatin was reconstituted in normal saline. Cpd-4 was administrated starting from Day 0 and Cisplatin was administrated starting from on Day1. Cisplatin was

administrated 4 hours after the treatment of Cpd-4 at day 1, 8 and 15. Tumor volume was monitored twice a week.

The long diameter (a) and the short diameter (b) of the tumor were measured using caliper and the tumor volume (v was calculated using the following formula:

$$V = 0.5 \times a \times b^2$$

Tumor growth inhibition was calculated using the formula:

$$\mathrm{TGI}(\%) = \frac{(1 - (V_t(\text{treatment group}) - V_0(\text{treatment group}))}{V_t(\text{vehicle group}) - V_0(\text{vehicle group}))} \times 100\%$$

V_0 is the tumor volume of the animal when treatment starts; $v_t$is the tumor volume of the animal someday after treatment. The statistics of tumor volume was analyzed by two-way ANOVA followed by Tukey's multiple comparisons test using GraphPad Prism 8.0.

T-Cell Killing Assay

MDA-MB-231 cells were seeded in 96-well plates. On the following day, cells were treated with DMSO or Cpd-4 for 48h. Human peripheral blood mononuclear cells (STEMCELL) were activated with 100 ng/mL CD3 antibody, 100 ng/mL CD28 antibody, and 10 ng/mL IL2 (BioLegend) and then cocultured with MDA-MB-231 cells at 10:1 ratio. The co-cultured cells were treated with or without PD-L1 antibody for 24h. Cell viability was measured by CellTiter-Glo reagent.

Statistical Analysis

Unless stated otherwise ordinary one-way ANOVA followed by Dunnett's multiple comparisons test using GraphPad Prism 8.0 was used to determine the significances of differences. *, P<0.05; **, P <0.01; ***, P <0.001; ****, P <0.0001. P-values of <0.05 were considered statistically significant and P-values of <0.1 were considered meaningful.

RESULTS

High RAD51 Expression Is Associated With Poor Clinical Outcome

Initially, we evaluated the significance of RAD51 as a potential therapeutic target by analyzing of public datasets with large sample sizes. The KM Plotter Online Tool (kmplot.com) (17) was used to associate RAD51 expression with clinical outcome for more than 1000 patients with breast or lung cancer. The analysis revealed that tumors with high RAD51 mRNA expression is significantly associated with poor outcome in both cancer types (**Figure 1A**). Further, high expression of RAD51 protein was also found to be significantly associated with shorter overall survival (OS) based on RPPA data retrieved from TCGA (**Figure 1B**). Overall, these data suggest that RAD51 overexpression is a negative prognostic marker and thus a promising therapeutic target.

Discovery and Mechanism of Action of a Novel Class of RAD51 Inhibitors

Up to now, there is only a limited number of useful inhibitors for RAD51. The widely used RAD51 inhibitor B02 inhibits DNA strand exchange activity (18, 19). However, it exhibits a relatively weak inhibitory potency regarding cell growth. We therefore aimed to identify a unique class of inhibitors with a novel molecular mechanism of action. To this end, we designed and synthesized about 100 diverse compounds in-house which were tested for their cellular potency and pharmacokinetics parameters to yield more drug-like inhibitors. Because Raji cells are characterized by genomic instability induced by c-MYC overexpression (16), this cell line was used for proliferation screening against normal WI-38 cells. This initial screening allowed the identification of five compounds, named as Cpd-1, Cpd-2, Cpd-3, Cpd-4, and Cpd-5, exhibiting potent antiproliferative effects in Raji cells with nanomolar IC_{50} values

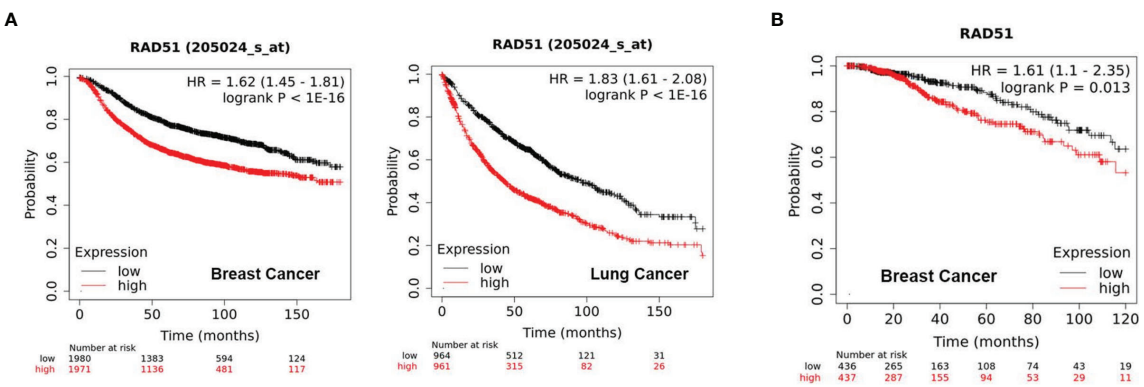

FIGURE 1 | High RAD51 expression is associated with poor clinical outcome. **(A)** Kaplan-Meier Plots showing the probability of relapse-free survival (RFS) in breast cancer patients (n = 3951, left) and overall survival (OS) in lung cancer patients (n = 1925, right), who were stratified by the median of RAD51 gene expression. **(B)** Kaplan-Meier Plots showing the probability of OS in breast cancer patients (n = 873), who were stratified by the median of RAD51 protein expression. *P* value was calculated using the log-rank test.

which did not affect normal cell viability (IC_{50} > 10 μM) (**Figure 2A**). Since these compounds displayed similar cellular potency, they were used interchangeably in subsequent studies.

To investigate the mechanism of action of these novel RAD51 inhibitors, we performed different molecular assays. We first determined intracellular target engagement using the commonly used cellular thermal shift assay (CETSA) (20, 21). Here the RAD51 inhibitors induced a considerable destabilization of cellular RAD51 upon increased temperatures when compared to DMSO (**Figure 2B**). Furthermore, a concentration-dependent destabilization of RAD51 induced by compounds at 54°C was observed (**Figure 2B**). These results suggest a specific binding of the compound to RAD51 in cells and, thus, implicating RAD51 as a *bona fide* target of the newly developed compounds.

For HR-mediated DNA damage repair, RAD51 foci formation is a critical step and unrepaired DNA damage results in reduced cellular survival. To determine if the antiproliferative effect of identified small molecules was mediated *via* inhibition of RAD51 foci, we investigated the effect of RAD51 inhibitors on RAD51 foci formation and the DNA damage marker γH2AX following treatment with a DNA damaging agent. To this end, BRCA1 mutant HCC-1937 breast cancer cells were treated with either DMSO or the RAD51 inhibitor for 2 days before cisplatin treatment. The results demonstrated detectable levels of RAD51 foci in cultured cells without cisplatin (**Figure 2C**). As expected, exposure to cisplatin increased RAD51 foci formation (**Figure 2C**) in cells while treatment with the RAD51 inhibitor inhibited respective cisplatin-induced RAD51 foci formation (**Figure 2C**). Consistently the combination of RAD51 inhibitors with cisplatin led to an increase of γH2AX, indicative of an accumulation of DNA damage (**Figure 2C**). This result suggests that the inhibitor directly impaired the formation of RAD51 foci. We also performed a similar experiment using BRCA1 wildtype MDA-MB-468 breast cells. Comparing to BRCA1 mutant HCC-1937 cells, though cisplatin treatment induced less RAD51 foci formation and γH2AX increase, the RAD51 foci formation can also be inhibited upon RAD51 inhibitor treatment (**Figure S1**).

To investigate the mechanism of the attenuated RAD51 foci formation by RAD51 inhibition, we evaluated the effects of RAD51 inhibitors on RAD51 protein levels and its subcellular distribution. Western blot analysis revealed that the inhibitor treatment resulted in a concentration-dependent decrease in RAD51 protein levels in HCC-1937 cells (**Figure 2D**). We also determined that the nuclear localization of RAD51 was reduced after RAD51 inhibitor treatment both in the presence and the absence of cisplatin (**Figure 2E**). These findings suggest that the RAD51 inhibitor prevented the RAD51 foci formation, at least in part, by reducing nuclear accumulation and stability of RAD51. Furthermore, we found that RAD51 protein degradation induced by the RAD51 inhibitor can only be prevented when cells were treated with the proteasome inhibitor MG132, but not the lysosome inhibitor chloroquine (CQ) or E64 (**Figure 2F**), suggesting that the RAD51 inhibitor facilitates proteasomal degradation of RAD51 protein.

To investigate how these new compounds function differently from the RAD51 inhibitors currently in use, we performed docking simulations between RAD51 inhibitors and RAD51 protein. The binding mode of one representative RAD51 inhibitor Cpd-5 to RAD51 protein, as obtained by docking simulations, displays some points of interaction similar to those of the crystallographic BRC4-RAD51 complex (**Figure S2A**). Specifically, the docking model suggests that (i) the cyclopropane in a hydrophobic pocket outlined by the side chains of Tyr202, Ala203, Arg204, Leu214, Ala218 of RAD51; (ii) the NH group of the pyrazole-3-amine group forms hydrogen bonds interaction with the Gln217 of RAD51; the NH group of the methylcarbamate forms hydrogen bonds interaction with the Ala201 of RAD51. In addition, the model suggests that the pyrazole ring is likely to form the Π-Π interaction with the H210. By analyzing the electrostatic potential of RAD51 pockets and Cpd-5, we found that molecules can better form electrostatic complementarity with RAD51 pockets (**Figure S2B**). The chemical structures of our RAD51 inhibitors are illustrated (**Figure 2G**).

RAD51 Inhibition Attenuates Growth of Various Types of Tumor Cells and Induces Cell Cycle Arrest

Next, we examined the effects of the five identified compounds on the proliferation of 15 human tumor cell lines from four cancer types (**Figure 3A**). The most significant inhibition of cell growth was observed for lymphoma cell lines. Of the compounds tested, Daudi showed the most response to Cpd-5 (IC_{50} = 5 nM) and Cpd-4 (IC_{50} = 4 nM). Notably, compared with B02, this novel class of inhibitors can decrease the IC_{50} values by more than 100-fold in some of the cell lines. These data suggest that the newly identified RAD51 inhibitors have a broad antiproliferative activity against various types of cancer cells. Because PARP inhibitors are reported to exhibit increased sensitivity in cells with HR deficiency (22), we were interested to know the potential of olaparib sensitivity as a biomarker of response to RAD51 inhibitors. The 15 cell lines exhibited diverse sensitivity to olaparib, with IC_{50} values ranging from 0.134 μM to over 25 μM. However, we did not observe any significant correlation between sensitivity of cells to olaparib and RAD51 inhibitors, suggesting that response to olaparib does not appear to be a predictive biomarker for RAD51 inhibitor sensitivity in cancer cells. To evaluate the effects of RAD51 inhibitors on inducing DNA damage, we analyzed γH2AX expression and found a dose response for γ-H2AX following exposure to the RAD51 inhibitor Cpd-5 with statistically significant increase of γ-H2AX expression at 0.1 μM and above (P<0.01, **Figure 3B**). We further analyzed the effects of the RAD51 inhibitor on cell cycle progression and apoptosis by flow cytometry. This analysis showed that RAD51 inhibition caused a dose-dependent S-phase arrest of the cell cycle, consistent with its central role in HR, which occurs preferentially during S-phase. Similarly, statistically significant increase of cells in S-phase has been observed when Cpd-5 concentration was 0.1 μM and above (P<0.0001, **Figure 3C**). Additionally, Daudi cells exposed to

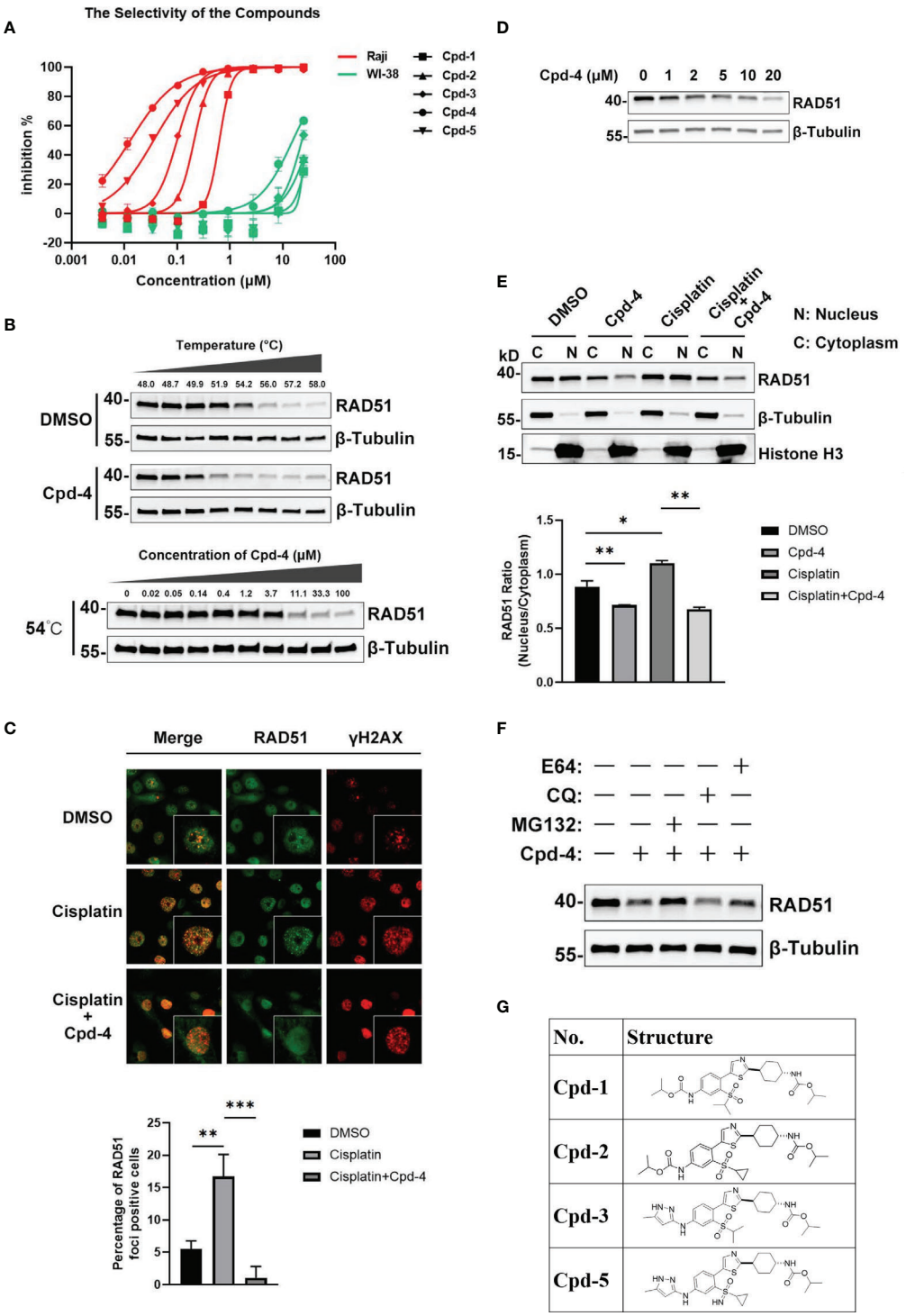

FIGURE 2 | Discovery and mechanism of action of a novel class of RAD51 inhibitors. **(A)** Representative dose response curve of a series of RAD51 inhibitors on Raji and WI-38 cell line generated in GraphPad Prism. **(B)** Comparison of thermo stability of endogenous RAD51 protein with or without the treatment of compounds. β-Tubulin served as the negative control. In the top panel, Z138 cells were treated with 20 μM Cpd-4. **(C)** Image analysis of DNA damage and repair marker upon the compound treatment. HCC1937 cells were treated with DMSO (upper and middle panels) or Cpd-4 (10μM, lower panel) for 2 days, then cells were exposed to cisplatin (10μM) for 2 h (middle and lower panels) and stained 5 h later. Quantification shows fraction of cells with ≥10 RAD51 foci. **(D)** Western blot analysis of endogenous RAD51 protein level in HCC-1937 cells after the treatment of compounds for 24 h. **(E)** Subcellular fraction of RAD51 protein in HCC-1937 cells were separated by using the NE-PER Nuclear Cytoplasmic Extraction Reagent Kit (Pierce) and analyzed by western blot. β-Tubulin and histone H3 were used as the cytoplasmic and nuclear markers, respectively. **(F)** Compounds treatment induced RAD51 protein degradation can be blocked by proteasome inhibitor (MG132) but not lysosome inhibitor (CQ or E64). All data represent mean ± SD based on at least three biological repeats. **(G)** Structures of representative compounds. *, P<0.05; **, P <0.01; ***, P <0.001.

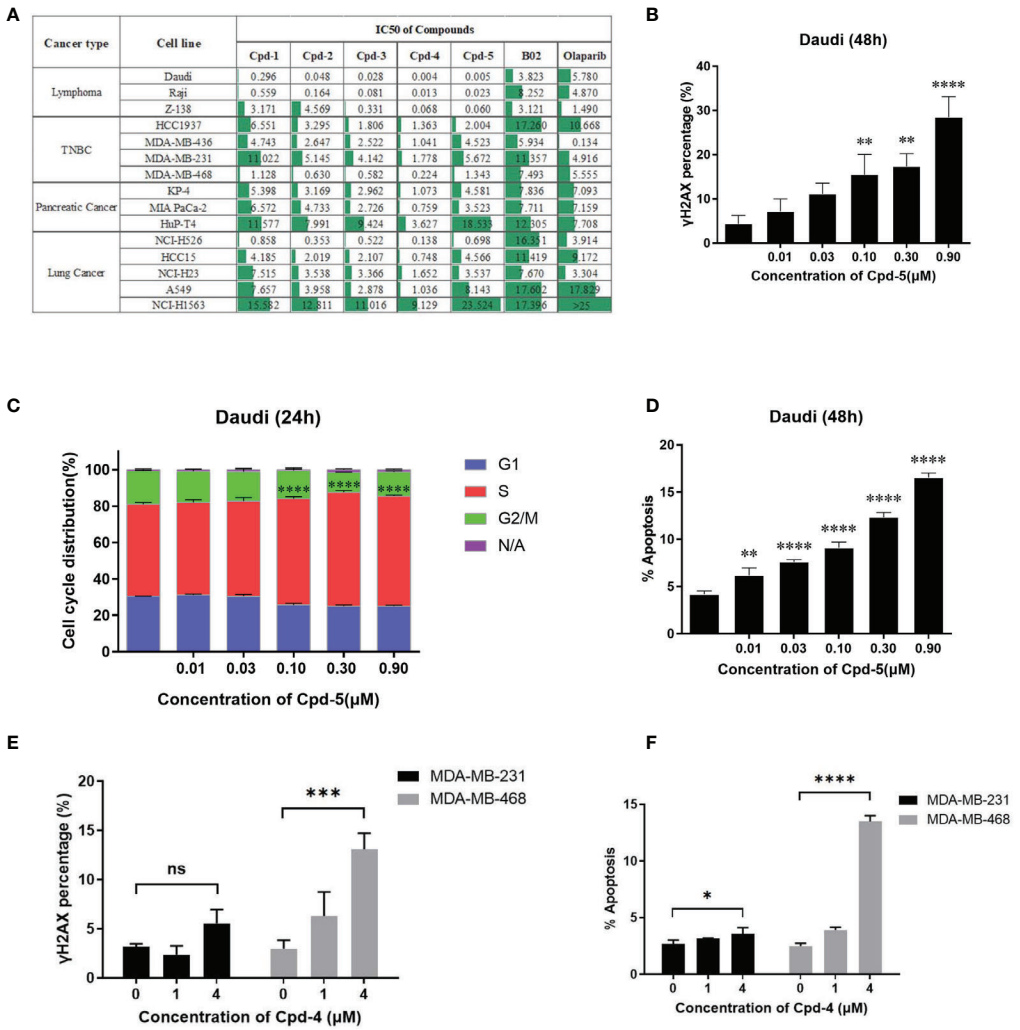

FIGURE 3 | RAD51 inhibition attenuates growth of various types of tumor cells and induces cell cycle arrest. **(A)** Estimated IC_{50} values (μM) of a series of RAD51 inhibitors and Olaparib on different cancer cell lines based on the four-parameter dose response curve generated in GraphPad prism. Data are representative of at least three independent experiments. **(B)** Dose-dependent γH2AX expression under compound treatment was analyzed by flow cytometry. Statistical analysis was performed comparing Cpd-5 treated cells with non-treated cells. **(C)** Cell cycle analysis of Daudi cells after compound treatment for 24 hours. Cells were stained with PI and images were analyzed by flow cytometry. N/A (non-assigned) represents cell populations where signal intensities exceeded the threshold to accurately determine the cell cycle phase. Statistical analysis was performed using percentage of cells in S-phase treated with Cpd-5 comparing with non-treated cells. **(D)** Induction of apoptosis in Daudi cells by compound treatment in a dose-dependent manner at 48 h. Statistical analysis was performed comparing Cpd-5 treated cells with non-treated cells. **(E)** Quantitative data from flow cytometry analysis showing percentage of γH2AX positive cells in MDA-MB-468 and MDA-MB-231 cell lines after compound treatment. **(F)** Analysis of apoptosis by flow cytometry in MDA-MB-468 and MDA-MB-231 cell lines following treatment with compounds for 48 h. All data presented with mean ± SD are based on at least three biological repeats. *, P<0.05; **, P <0.01; ***, P <0.001; ****, P <0.0001; NS, not significant.

escalating doses of the RAD51 inhibitor displayed a dose-dependent statistically significant increase in apoptosis (P<0.01, **Figure 3D**). Together, these data suggest that these next generation RAD51 inhibitors impaired cell growth through cell cycle arrest in S-phase and elevated apoptosis.

To further confirm that the difference in sensitivity of cells to the compound is due to the mechanism of action instead of off-target toxicity, two TNBC cell lines (MDA-MB-231 and MDA-MB-468) with a 10-fold difference in IC_{50} were selected for a comparison of DNA damage and apoptosis. At the same concentration of compound, the increase in γH2AX expression and apoptosis in MDA-MB-468 cells was greater than that in MDA-MB-231 cells (**Figures 3E, F**), accounting for the higher sensitivity of MDA-MB-468 cells to the RAD51 inhibitor.

RAD51 Inhibition Enhances the Anti-Tumor Effect of Chemotherapy Agents

Given the crucial role for RAD51 in repairing DSBs induced by chemotherapy, we explored whether RAD51 inhibition could

sensitize cancer cells to chemotherapeutic drugs. To this end, we detected γH2AX levels in cells by western blot as a measure of DNA damage. Daudi cells were incubated with RAD51 inhibitors for 72 h before a 2 h co-incubation with cisplatin or DMSO. We observed that the RAD51 inhibitors greatly potentiated cisplatin-induced DSBs, evidenced by the dramatic increase of γH2AX levels in cells treated with cisplatin in combination with RAD51 inhibitors compared with those treated only with cisplatin or RAD51 inhibitors (**Figure 4A**). Accordingly, we observed significantly improved cytotoxicity of the RAD51 inhibitor in combination with cisplatin as demonstrated by a 3.4-fold shift in IC_{50} (**Figure 4B**). Synergy analysis employing the Bliss model (Combenefit) revealed a strong synergy for the combination of RAD51 inhibitors and cisplatin (**Figure 4B**). Specifically, limited doses of RAD51 inhibitor (0.25 μM) and of cisplatin (0.63 μM) exerted only mild effects on cell viability on their own, whereas the combination of RAD51 inhibitor and cisplatin inhibited cell viability by 90%, demonstrating a strong synergistic effect (**Figure 4B**).

To further evaluate the synergistic effect of RAD51 inhibitors with cisplatin *in vivo*, BALB/c nude mice bearing Daudi tumors were treated with RAD51 inhibitor and/or cisplatin. The RAD51 inhibitor Cpd-4 alone showed dose-dependent anti-tumor efficacy, with TGIs of 34.3% and 85.6% at 30 mg/kg and 100 mg/kg, respectively. Cisplatin alone at 2 mg/kg did not show any significantly anti-tumor activity with TGI of 20.7%. Low dose combination treatment of Cpd-4 (30 mg/kg) and cisplatin (2 mg/kg) presented significantly better anti-tumor efficacy than either monotherapy with TGI of 86.2%, indicating a synergistic effect with acceptable tolerability (**Figures 4C, D**). Subsequent immunofluorescence histochemistry carried out on Daudi xenograft tissue indicated increased γH2AX expression in groups treated with Cpd-4, cisplatin or drug combination (**Figure 4E**) compared to vehicle group.

In addition to lymphoma, we also verified the synergistic effect of RAD51 inhibitors with cisplatin on solid tumor cells. Our results showed a strong combination effect of RAD51 inhibitors and cisplatin in A549 lung cancer cells (**Figure 4F**). Furthermore, we also investigated RAD51 inhibition in context of pancreatic cancer cell. In this tumor type, the microtubule-targeting agent Docetaxel combined with other DNA-damaging agents represents a first-line chemotherapeutic regimen. Although the underlying action remains largely unknown, it is proposed that microtubule-targeting agents cause cytoplasmic retention of DNA repair proteins, and thus enhance DNA damage (23). We postulated that inhibition of RAD51, a protein essential for DNA repair, would increase Docetaxel sensitivity. To test this hypothesis, we used two representative pancreatic cancer cell lines (KP-4 and MIA PaCa-2) and analyzed the effect of synergy. We observed that the combination of RAD51 inhibitors and Docetaxel displayed a strong synergy in both cell lines (**Figures 4G, H**). Collectively, these data demonstrate the potential clinical utility for RAD51 inhibitors in combination with chemotherapy.

RAD51 Inhibition Synergizes With DDR-Targeting Agents on Cell Proliferation

PARP family proteins are activated upon binding to damaged DNA and have crucial roles in detecting SSB, recruiting DDR machinery and stabilizing replication forks during repair (24). PARP inhibitors are approved therapies for a number of cancers including breast cancers, pancreatic adenocarcinoma and ovarian cancer that carry HR-related mutations based on the concept of synthetic lethality (25). Given the role of RAD51 in HR-mediated DNA damage repair, we further explored the synergistic effect of RAD51 inhibition with olaparib in Daudi and KP-4 cells. As shown in **Figure 5A**, a moderate synergy was observed in both cell lines. These synergy effects were further confirmed by γH2AX expression analysis (**Figure 5B**). Next, we explored the possibility of the combination of RAD51 inhibitor and other DDR-targeting agents. While the RAD51 inhibitors synergized with WEE1 inhibition, no apparent synergistic effect was observed when combined with ATRi or DNA-PKi in MDA-MB-436 breast cancer cells (**Figure 5C**). Previous studies reported that ATM was upregulated when ATR signaling was blocked (26), implying ATM compensation for ATR deficiency. Therefore, we investigated the synergy between RAD51 inhibition and ATRi in ATM-null cells. In the ATM-deficient NCI-H23 cells, the RAD51 inhibitor showed profound synergy with ATRi with regard to inhibition of cell proliferation (**Figure 5D**). Consistent with this, we found an activation of ATR signaling when RAD51 was inhibited in NCI-H23 cells (**Figure 5E**).

RAD51 Inhibition Induces PD-L1 Upregulation and Shows Potential for Combination With PD-L1 Immune Checkpoint Blockade

Double strand break (DSB) repair is sufficient to induce PD-L1 expression in cancer cells through ATR/Chk1 signaling axis (27). Because RAD51 inhibition induces DSBs as evidenced by an accumulation of γH2AX foci, we wanted to determine whether PD-L1 expression would be increased. The FACS analysis revealed that RAD51 inhibitor treatment increased PD-L1 expression in TNBC (MDA-MB-231), lung cancer (A549), pancreatic cancer (KP-4) and colon cancer (HCT 116) cell lines in a dose-dependent manner (**Figure 6A**).

Next, we analyzed whether RAD51 inhibition induced PD-L1 expression is mediated by ATR/Chk1/IRF-1 signaling. HCT 116 cells exposed to the RAD51 inhibitor displayed a 5-fold increase of PD-L1 expression compared with DMSO-treated cells (**Figure 6B**). Strikingly, the induction of PD-L1 expression upon RAD51 inhibition was significantly suppressed by a specific inhibitor of ATR or Chk1, suggesting that PD-L1 upregulation requires ATR-Chk1 signaling after RAD51 inhibition. To confirm the ATR activation, we measured ATR phosphorylation at Thr-1989 and Chk1 phosphorylation at Ser-345. RAD51 inhibitor treatment led to a dramatic increase in p-ATR and p-Chk1 levels (**Figure 6C**), consistent with what has been observed in NCI-H23 cells (**Figure 5E**). Previous studies

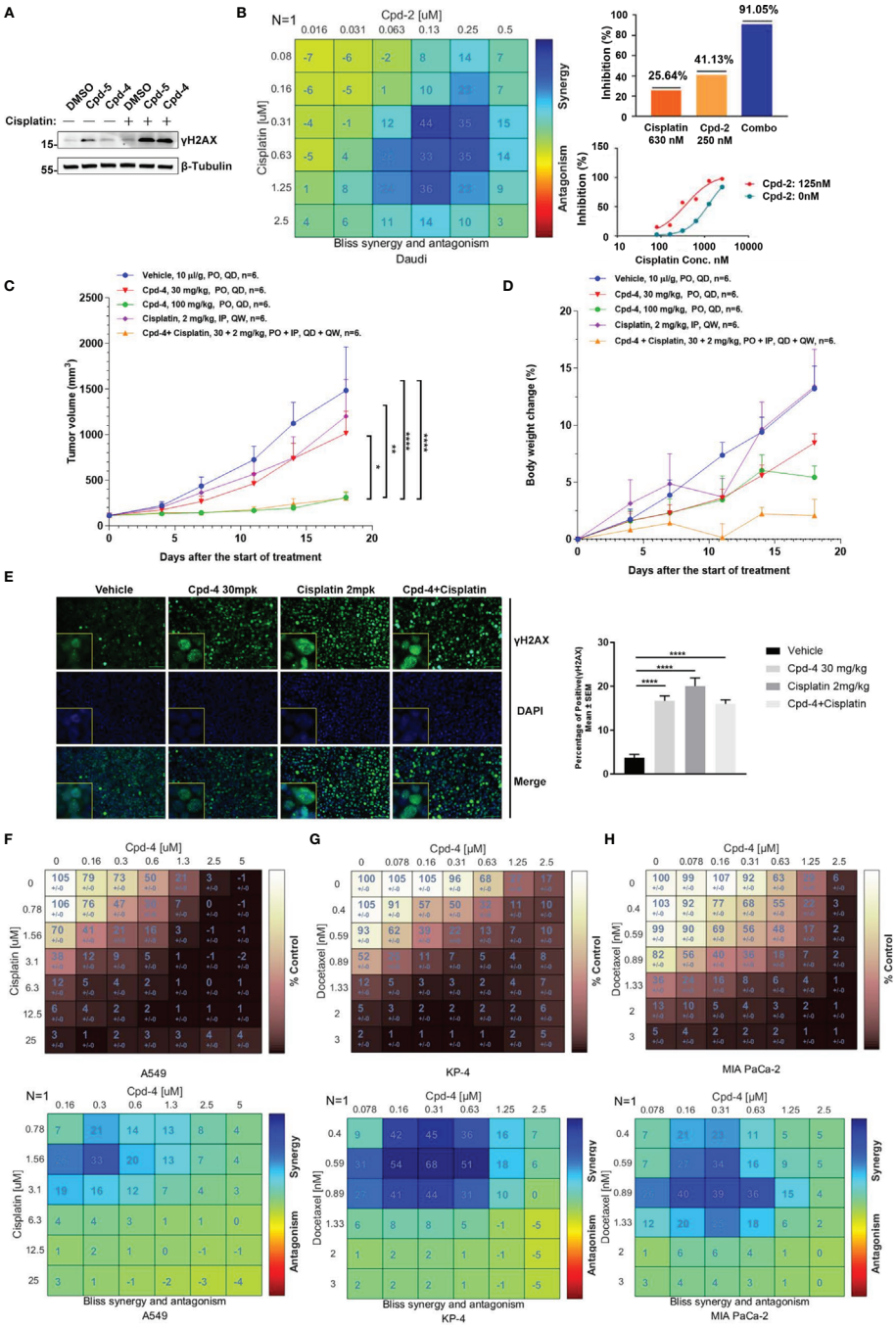

FIGURE 4 | RAD51 inhibition enhances the anti-tumor effect of chemotherapy agents. **(A)** Western blot analysis of γH2AX expression in cell lysate. Daudi cells were co-cultured with DMSO, Cpd-5 (50 nM) and Cpd-4 (25 nM) for 72 h, then cells were treated with 30 μM cisplatin for 2 h and recovered for 5 h. β-Tubulin served as loading control. **(B)** Synergy effect of compounds and cisplatin in Daudi cells. Cells were dosed with Cpd-2 and cisplatin in a 6×6 concentration grid in 96-well plate for 7 days. Cell viability was determined with CellTiter-Glo reagent. The experimental data were analyzed with bliss synergy model using the Combenefit software (left panel) and GraphPad Prism software (right panel). Data are representative of at least two independent experiments. **(C, D)** The anti-tumor effects of Cpd-4 and cisplatin in the Daudi xenograft mouse model. The Daudi tumor bearing female BALB/c nude mice were administrated with Cpd-4, cisplatin or combination and the tumor volume and the body weight change are graphed in **(C, D)**, respectively (N=6 for each group). The error bars represent Standard Error of Mean. PO, oral garage; QD, once daily; IP, intraperitoneal injection; QW, once a week. P value was calculated based on the tumor volume using two-way ANOVA. *, P<0.05; **, P <0.01; ****, P <0.0001. **(E)** γH2AX expression in tumor tissue analyzed by fluorescence histochemistry. For quantification, nuclei with ≥5 foci were counted as γH2AX-positive cells. A total of 4 field with >100 cells were counted in each mouse. Mean ± SEM. Scale bar, 100 μM. **(F)** Synergy analysis of compounds and cisplatin in A549 cell lines. Upper panel, cell viability. Lower panel, bliss synergy score. **(G, H)** Synergy effect of compounds and docetaxel in MIA PaCa-2 and KP-4 cell lines. Data are representative of at least two independent experiments.

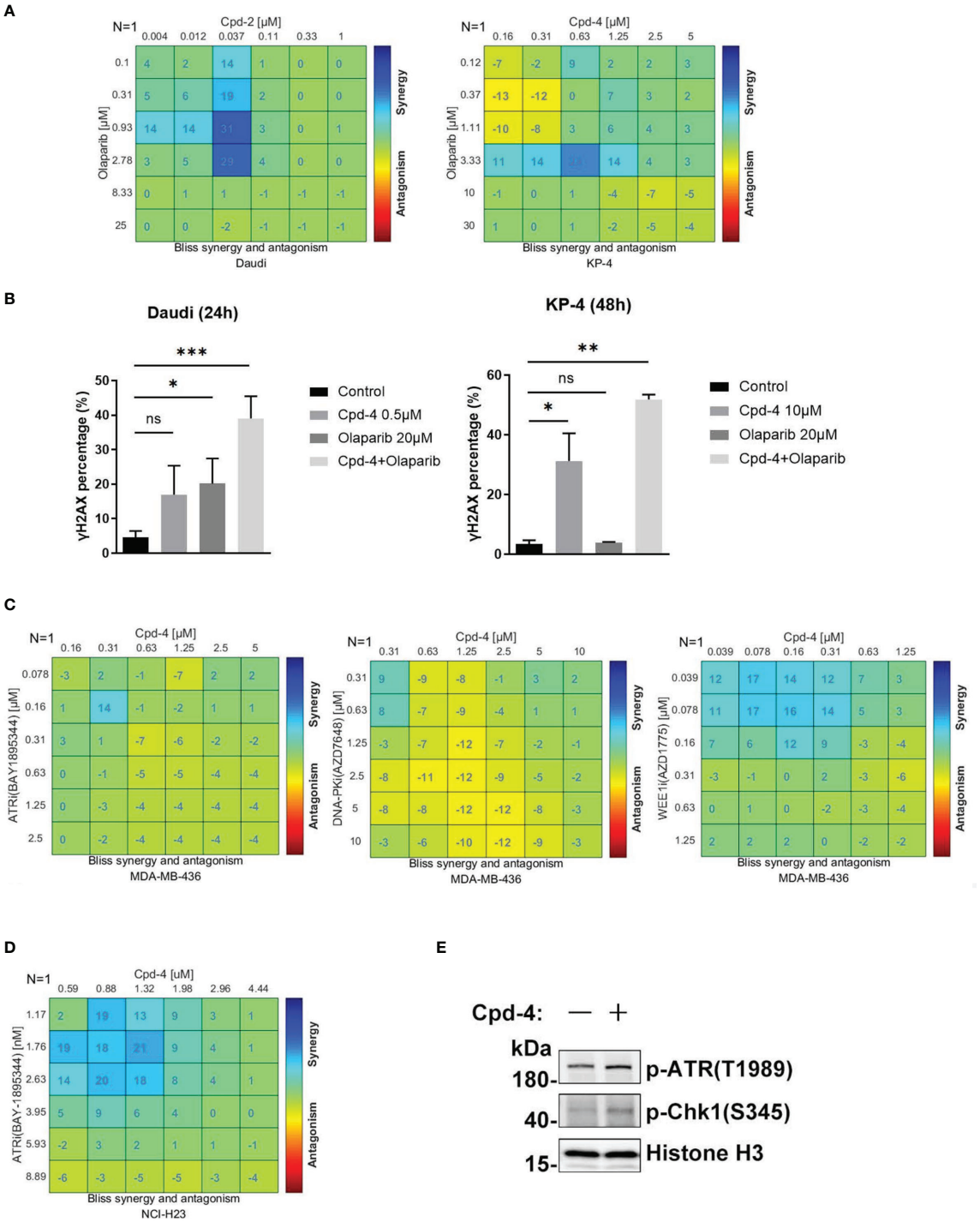

FIGURE 5 | RAD51 inhibition synergizes with DDR-targeting agents on cell proliferation. **(A)** Synergy effect of compounds and olaparib in Daudi and KP-4 cells. Cells were dosed with Cpd-4 and Olaparib in a 6×6 concentration grid in 96-well plate for 5-7 days. Cell viability was determined with CellTiter-Glo reagent. The experimental data were analyzed with bliss synergy model using the Combenefit software. Data are representative of at least two independent experiments. **(B)** γH2AX expression analyzed after cells exposed to drugs combination. Cells were treated with DMSO, Cpd-4, Olaparib or drug combination for 24 h (Daudi) or 48 h (KP-4), then cells were stained with γH2AX antibody and analyzed by flow cytometry. **(C)** Synergy analysis of compound and ATRi (BAY1895344), DNA-PKi (AZD7648) or WEE1i (AZD1775) combination in MDA-MB-436 cells. **(D)** Synergy analysis of compound and ATRi (BAY1895344) combination in NCI-H23 cell lines. **(E)** ATR-Chk1 signaling was up-regulated under the compound treatment in NCI-H23 cells. Cells were treated with DMSO or 10 μM Cpd-4 for 6 h before subjected to western blot analysis. *, P<0.05; **, P <0.01; ***, P <0.001, ns, not significant.

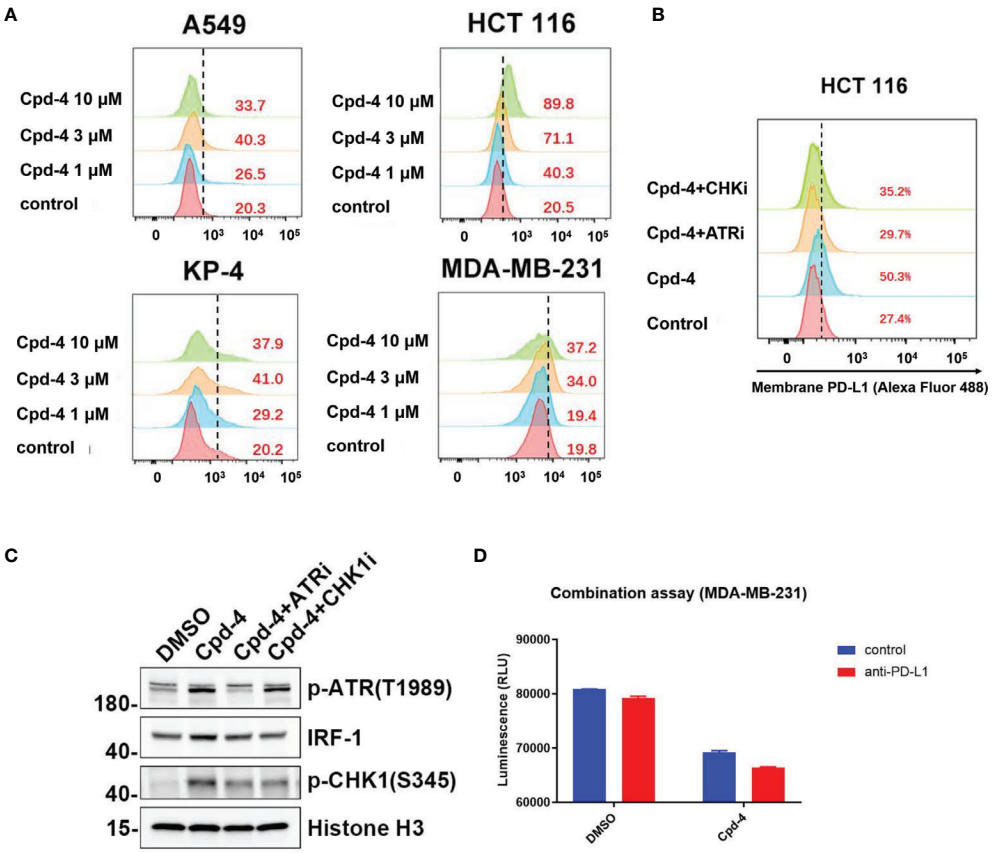

FIGURE 6 | RAD51 inhibition induces PD-L1 upregulation and shows potential for combination with PD-L1 immune checkpoint blockade. **(A)** RAD51 inhibitor upregulates PD-L1 expression in various cell lines. MDA-MB-231, A549, KP-4 and HCT 116 cells were treated with indicated concentration of Cpd-4 for 24 h, and cell surface PD-L1 was analyzed by flow cytometry. **(B)** RAD51 inhibition induced PD-L1 expression depends on the activity of ATR-Chk1 signaling. HCT 116 cells were treated with ATRi (AZD6738, 10 μM) or Chk1i (MK8776, 1 μM) inhibitor 1 h prior to RAD51 inhibitor (Cpd-4, 2 μM) treatment. Cell surface PD-L1 expression was examined after 24 hours. **(C)** ATR-Chk1 signaling promotes IRF-1 expression after RAD51 inhibition in HCT 116 cells. Cells were treated with DMSO, ATRi or CHKi for 2 hours and then treated with DMSO or Cpd-4 for 4 h. The levels of p-ATR, IRF1 and p-Chk1 were examined by western blot after indicated compound treatment. **(D)** Quantitation showing cell viability following treatment with Cpd-4 (10 μM), PD-L1 antibody (PD-L1 Ab; 10 mg/mL), or the combination cocultured with activated PBMCs for 72 hours. Cell viability were determined with CellTiter-Glo reagent.

reported that IRF-1 is a potential effector downstream of ATR-Chk1 signaling and modulates PD-L1 expression (27, 28). As expected, we found that the RAD51 inhibitor exposure resulted in an increase in levels of IRF-1, which could be suppressed by ATR or Chk1 inhibitor treatment (**Figure 6C**). Collectively, these findings show that RAD51 inhibition-mediated IRF1 upregulation, a downstream component of ATR/Chk1 signaling, is a critical mechanism underlying PD-L1 expression regulation in cancer cells.

RAD51 inhibition induced PD-L1 upregulation may result in increased binding of PD-1 and affect T-cell functions. We therefore tested T-cell killing in context of the combination of PD-L1 antibody and RAD51 inhibitor. The results showed that the combination of RAD51 inhibition and PD-L1 blockade was more effective than each agent alone in inducing T-cell killing (**Figure 6D**), suggesting potential for combination treatment of RAD51 inhibitors with PD-L1 immune checkpoint blockade.

DISCUSSION

Due to the prominent role of RAD51 to maintain the genomic stability, we set out to identify a small molecule that would inhibit its biological function as a strategy for cancer therapy. To accomplish this goal, we have screened about 100 diverse compounds synthesized in-house using an *in vitro* cell proliferation assay. Here we describe what is to our knowledge the first small molecule inhibitor of RAD51 with low-nanomolar IC_{50} values regarding antiproliferative effects *in vitro*. The RAD51 inhibitor Cpd-4, as a single agent, demonstrated dose-

dependent antitumor activity in a xenograft model. Corresponding increased levels of γH2AX in the excised tumors suggest that the antitumor effects were a direct consequence of HR disruption. Using CETSA, we found that the RAD51 protein got thermally destabilized upon addition of Cpd-4 inside cells, further supporting a specific RAD51 inhibitory activity of this compound. Mechanism of action analysis indicated that the novel inhibitor prevented RAD51 foci formation by altering the nucleocytoplasmic distribution and by acceleration of RAD51 degradation. Unlike this novel class of inhibitors, the older-generation RAD51 inhibitors have a different mechanism of action (29). For instance, B02 inhibits DNA strand exchange activity of RAD51, while IBR2 disrupts RAD51 oligomerization through inhibition of the BRC motif-RAD51 interaction (15). Regardless of the different mechanism of action, micromolar potencies of these compounds in human cells present significant obstacles for their potential clinical utility.

Our work also reveals a broad antiproliferative response of cancer cells originating from various organs by RAD51 inhibition. Hence, our identified inhibitors could be expected to be efficacious in various solid tumors. However, we show that various solid tumor cell lines differentially responded to RAD51 inhibition, with MDA-MB-468 and NCI-H526 being sensitive whereas MDA-MB-231 being less sensitive to RAD51 inhibition. This could be due to differences of their genetic backgrounds, among other factors. Indeed, increasing evidence illustrates that most synthetic lethal effects appear to be highly context-dependent, in other words the effects are only observed in one specific genetic background (30). As such, in PDAC cell lines, deletion of ATM was found to sensitize the cells to ATR inhibition (31). Future work will need to aim at overcoming the current challenge to identify which genetic backgrounds confer sensitivity to the RAD51 inhibition. To this end, further assessment of the efficacy of the inhibitor using solid human tumor xenografts is warranted.

Previous reports have demonstrated the abilities of the inhibitors targeting DDR proteins such as DNA-PK and ATR to sensitize cells to chemotherapeutic agents. For example, the selective DNA-PK inhibitor, AZD7648, enhanced doxorubicin efficacy in both xenograft and patient-derived xenograft (PDX) models (32). In addition, several ATR inhibitors in combination with chemotherapy reveal preclinical activities and have been advanced to clinical trials (34). This is consistent with a role for DDR kinases in repairing cytotoxic DNA damages. In agreement with this, our study showed that inhibition of RAD51 is synthetic lethal with cisplatin in Daudi cells and with Docetaxel in pancreatic cells. This synergistic effect was associated with DNA damage accumulation, as evidenced by elevated levels of γH2AX in respective cells (**Figure 4A**). Moreover, our data provide direct evidence that Cpd-4 and cisplatin combination enhanced antitumor efficacy *in vivo*, suggesting that a combination treatment could be beneficial in patients.

In order to make PARP inhibitors more efficacious, efforts are continuously ongoing to develop targets of DDR pathway that can be proposed for an enhancement of the cancer response through synthetic lethality. As reported previously, patients with HR-deficient tumors demonstrated therapeutic benefits to PARP inhibitors (35). Given the critical role of RAD51 in commencing HR in cases of DSBs, we hypothesize that RAD51 inhibition could create an HR-deficient phenotype that likely synergizes with PARP inhibitors. Consistent with this hypothesis, we demonstrate that RAD51 inhibitors combined with olaparib increased accumulation of DNA damage, producing a synergistic effect on cancer cell growth inhibition. In support of our results, inhibitors of ATR and DNK-PK kinases, the key players of the DDR, were shown to sensitize cancer cells to olaparib (32, 33). However, only a modest synergy between RAD51 inhibition and olaparib was observed, in contrast to a strong synergy with chemotherapy. Presumably, this might be due to lower base line levels of endogenous DSBs in the absence of DNA damage induction or due to bypass within the DDR machinery.

We further examined synergy of RAD51 inhibition with a number of inhibitors against DDR kinases that are currently under clinical evaluation. Our data showed that a weak synergy was observed with each inhibitor in the MDA-MB-436 cell line with the exception of the WEE1 inhibitor. The WEE1 inhibitor AZD1775 inhibits CDK1 phosphorylation, resulting in premature mitotic entry and cell death. The synergistic interaction between RAD51 and WEE1 inhibition probably reflects the importance of targeting both the cell cycle checkpoints and DSB repair pathways simultaneously. Another interesting observation is that the combination between RAD51 and ATR inhibition were more effective in the ATM-deficient H23 cell line model but, in contrast, little synergy in MDA-MB-436 cells with functional ATM. Our findings show that the RAD51 inhibitor increased ATR activation in H23 cells, as judged by phosphorylation of ATR and its downstream target Chk1, which is in line with another study suggesting that RAD51 inactivation increased sensitivity to ATR and Chk1 inhibition (36). Previously, ATR inhibitor was shown to induce ATM activation as a compensatory response (37). This provides an explanation for the little synergy observed in MDA-MB-436 cells with functional ATM. Further exploration of other genetic vulnerabilities that sensitize to the combination are warranted to extend therapeutic options.

High expression of PD-L1 on tumor cells is well known to suppress antitumor T-cell responses and correlate with clinical responses to PD-1 therapy in cancer patients. Regulation of PD-L1 expression by small molecule inhibitors has been demonstrated to alter the efficacy of PD-L1/PD-1 immunotherapy in mouse models. For example, HDAC3 inhibitors synergize with PD-L1 blockade to enhance tumor regression by transcriptionally upregulating PD-L1 expression (38). Furthermore, genomic instability involved in PD-L1 regulation has been reported. DSBs induced by ionizing radiation or treatment with DNA damaging agents has recently been shown to lead to an increase of PD-L1 expression in cancer cells *via* an ATM/ATR/Chk1-dependent mechanism (27).

Consistent with this report, we found that RAD51 inhibitors can increase surface PD-L1 levels in various tumor cells by activation of the ATR/Chk1 signaling and its downstream effector IRF1. A previous report suggested that IRF1 induction by STAT1/3 phosphorylation and its subsequent recruitment to the PD-L1 promoter by interferon gamma exposure is responsible for PD-L1 regulation (39), suggesting that the STATs-IRF1 pathway underlies the transcriptional upregulation of PD-L1. Such details should be further investigated to elucidate the mechanism by which DSBs trigger an IRF1 response to activate PD-L1 expression. Collectively, our findings reveal that RAD51 inhibition, leading to increased DNA DSBs, may be a rational strategy to be implemented in combination with PD-1 therapy to improve therapeutic outcome. Consistent with this notion, anti-PD-1 immune checkpoint blockade has recently been approved for the treatment of patients with microsatellite instability-high (MSI-H) or mismatch repair deficient (dMMR) colorectal cancer.

Overall, our findings establish that RAD51 inhibition could be used as a new prospect for cancer treatment with the potential to enhance the therapeutic window of many established therapeutic strategies across multiple cancer indications. We are optimizing those compounds to obtain a pre-clinical candidate RAD51 inhibitor which will be tested in future clinical studies.

DATA AVAILABILITY STATEMENT

The raw data supporting the conclusions of this article will be made available by the authors, without undue reservation.

ETHICS STATEMENT

The animal study was reviewed and approved by Institutional Animal Care and Use Committee of the WuXi AppTec.

AUTHOR CONTRIBUTIONS

PG and LX made equal contributions to this work. They conceived and coordinated the study, designed the experiments, carried out data analysis, and wrote the paper. WL, ZJ, AL, TL, LL and XC designed and performed the experiments. CZ, MD, WY, and RT coordinated the study and made scientific contributions. RT conceived and coordinated the study, designed the experiments, carried out the data analysis and data interpretation, and revised the paper. All authors reviewed the results and approved the final version of the manuscript.

ACKNOWLEDGMENTS

We thank Jinwen Shan for performing the work on docking simulation.

SUPPLEMENTARY MATERIAL

The Supplementary Material for this article can be found online at: https://www.frontiersin.org/articles/10.3389/fonc.2022.885186/full#supplementary-material

REFERENCES

1. Negrini S, Gorgoulis VG, Halazonetis TD. Genomic Instability—An Evolving Hallmark of Cancer. *Nat Rev Mol Cell Biol* (2010) 11(3):220–8. doi: 10.1038/nrm2858
2. Jiang X, Li W, Li X, Bai H, Zhang Z. Current Status and Future Prospects of Parp Inhibitor Clinical Trials in Ovarian Cancer. *Cancer Manage Res* (2019) 11:4371. doi: 10.2147/CMAR.S200524
3. Pilié PG, Tang C, Mills GB, Yap TA. State-of-the-Art Strategies for Targeting the DNA Damage Response in Cancer. *Nat Rev Clin Oncol* (2019) 16(2):81–104. doi: 10.1038/s41571-018-0114-z
4. Primo LM, Teixeira LK. DNA Replication Stress: Oncogenes in the Spotlight. *Genet Mol Biol* (2020) 43(1):1–14. doi: 10.1590/1678-4685gmb-2019-0138
5. Daley JM, Sung P. 53bp1, Brca1, and the Choice Between Recombination and End Joining at DNA Double-Strand Breaks. *Mol Cell Biol* (2014) 34(8):1380–8. doi: 10.1128/MCB.01639-13
6. Holthausen JT, Wyman C, Kanaar R. Regulation of DNA Strand Exchange in Homologous Recombination. *DNA Repair* (2010) 9(12):1264–72. doi: 10.1016/j.dnarep.2010.09.014
7. Rad51 Paralogs: Roles in DNA Damage Signalling, Recombinational Repair and Tumorigenesis. *Semin Cell Dev Biol* (2011) 22(8):898–905. doi: 10.1016/j.semcdb.2011.07.019
8. Fujimori A, Tachiiri S, Sonoda E, Thompson LH, Dhar PK, Hiraoka M, et al. Rad52 Partially Substitutes for the Rad51 Paralog Xrcc3 in Maintaining Chromosomal Integrity in Vertebrate Cells. *EMBO J* (2001) 20(19):5513–20. doi: 10.1093/emboj/20.19.5513
9. Sonoda E, Sasaki MS, Buerstedde JM, Bezzubova O, Shinohara A, Ogawa H, et al. Rad51-Deficient Vertebrate Cells Accumulate Chromosomal Breaks Prior to Cell Death. *EMBO J* (1998) 17(2):598–608. doi: 10.1093/emboj/17.2.598
10. Xu Y, Chen K, Cai Y, Cheng C, Zhang Z, Xu G. Overexpression of Rad51 Predicts Poor Prognosis and Silencing of Rad51 Increases Chemo-Sensitivity to Doxorubicin in Neuroblastoma. *Am J Trans Res* (2019) 11(9):5788.
11. Liu Y, Burness ML, Martin-Trevino R, Guy J, Bai S, Harouaka R, et al. Rad51 Mediates Resistance of Cancer Stem Cells to Parp Inhibition in Triple-Negative Breast Cancer. *Clin Cancer Res* (2017) 23(2):514–22. doi: 10.1158/1078-0432.CCR-15-1348
12. Cruz C, Castroviejo-Bermejo M, Gutierrez-Enriquez S, Llop-Guevara A, Ibrahim Y, Gris-Oliver A, et al. Rad51 Foci as a Functional Biomarker of Homologous Recombination Repair and Parp Inhibitor Resistance in Germline Brca-Mutated Breast Cancer. *Ann Oncol* (2018) 29(5):1203–10. doi: 10.1093/annonc/mdy099
13. Wang J, Che W, Wang W, Su G, Zhen T, Jiang Z. Cdkn3 Promotes Tumor Progression and Confers Cisplatin Resistance *Via* Rad51 in Esophageal Cancer. *Cancer Manage Res* (2019) 11:3253–64. doi: 10.2147/CMAR.S193793
14. Xu Z-Y, Loignon M, Han F-Y, Panasci L, Aloyz R. Xrcc3 Induces Cisplatin Resistance by Stimulation of Rad51-Related Recombinational Repair, S-Phase Checkpoint Activation, and Reduced Apoptosis. *J Pharmacol Exp Ther* (2005) 314(2):495–505. doi: 10.1124/jpet.105.084053
15. Murfuni I, Rass U. Targeting Homologous Recombination Repair in Cancer. *DNA Repair Cancer Ther Elsevier* (2016) 225–75. doi: 10.1016/B978-0-12-803582-5.00008-5
16. Hengel SR, Spies MA, Spies M. Small-Molecule Inhibitors Targeting DNA Repair and DNA Repair Deficiency in Research and Cancer Therapy. *Cell Chem Biol* (2017) 24(9):1101–19. doi: 10.1016/j.chembiol.2017.08.027

17. Győrffy B, Lanczky A, Eklund AC, Denkert C, Budczies J, Li Q, et al. An Online Survival Analysis Tool to Rapidly Assess the Effect of 22,277 Genes on Breast Cancer Prognosis Using Microarray Data of 1,809 Patients. *Breast Cancer Res Treat* (2010) 123(3):725–31. doi: 10.1007/s10549-009-0674-9
18. Huang F, Motlekar NA, Burgwin CM, Napper AD, Diamond SL, Mazin AV. Identification of Specific Inhibitors of Human Rad51 Recombinase Using High-Throughput Screening. *ACS Chem Biol* (2011) 6(6):628–35. doi: 10.1021/cb100428c
19. Huang F. Mazin AV. A Small Molecule Inhibitor of Human Rad51 Potentiates Breast Cancer Cell Killing by Therapeutic Agents in Mouse Xenografts. *PloS One* (2014) 9(6):e100993. doi: 10.1371/journal.pone.0100993
20. Jensen AJ, Molina DM, Lundbäck T. Cetsa: A Target Engagement Assay With Potential to Transform Drug Discovery. *Future med Chem* (2015) 7(8):975–8. doi: 10.4155/fmc.15.50
21. Molina DM, Jafari R, Ignatushchenko M, Seki T, Larsson EA, Dan C, et al. Monitoring Drug Target Engagement in Cells and Tissues Using the Cellular Thermal Shift Assay. *Science* (2013) 341(6141):84–7. doi: 10.1126/science.1233606
22. McCabe N, Turner NC, Lord CJ, Kluzek K, Białkowska A, Swift S, et al. Deficiency in the Repair of DNA Damage by Homologous Recombination and Sensitivity to Poly (Adp-Ribose) Polymerase Inhibition. *Cancer Res* (2006) 66 (16):8109–15. doi: 10.1158/0008-5472.CAN-06-0140
23. Poruchynsky MS, Komlodi-Pasztor E, Trostel S, Wilkerson J, Regairaz M, Pommier Y, et al. Microtubule-Targeting Agents Augment the Toxicity of DNA-Damaging Agents by Disrupting Intracellular Trafficking of DNA Repair Proteins. *Proc Natl Acad Sci* (2015) 112(5):1571–6. doi: 10.1073/pnas.1416418112
24. Lord CJ, Ashworth A. Parp Inhibitors: Synthetic Lethality in the Clinic. *Science* (2017) 355(6330):1152–8. doi: 10.1126/science.aam7344
25. Fong PC, Boss DS, Yap TA, Tutt A, Wu P, Mergui-Roelvink M, et al. Inhibition of Poly (Adp-Ribose) Polymerase in Tumors From Brca Mutation Carriers. *N Engl J Med* (2009) 361(2):123–34. doi: 10.1056/NEJMoa0900212
26. Cheng A, Zhao T, Tse K-H, Chow H-M, Cui Y, Jiang L, et al. Atm and Atr Play Complementary Roles in the Behavior of Excitatory and Inhibitory Vesicle Populations. *Proc Natl Acad Sci* (2018) 115(2):E292–301. doi: 10.1073/pnas.1716892115
27. Sato H, Niimi A, Yasuhara T, Permata TBM, Hagiwara Y, Isono M, et al. DNA Double-Strand Break Repair Pathway Regulates Pd-L1 Expression in Cancer Cells. *Nat Commun* (2017) 8(1):1–11. doi: 10.1038/s41467-017-01883-9
28. Yan Y, Zheng L, Du Q, Yan B, Geller DA. Interferon Regulatory Factor 1 (Irf–1) and Irf–2 Regulate Pd–L1 Expression in Hepatocellular Carcinoma (Hcc) Cells. *Cancer Immunol Immunother: CII* (2020) 69(9):1891–903. doi: 10.1007/s00262-020-02586-9
29. Grundy MK, Buckanovich RJ, Bernstein KA. Regulation and Pharmacological Targeting of Rad51 in Cancer. *NAR Cancer* (2020) 2(3):zcaa024. doi: 10.1093/narcan/zcaa024
30. Ryan CJ, Bajrami I, Lord CJ. Synthetic Lethality and Cancer–Penetrance as the Major Barrier. *Trends Cancer* (2018) 4(10):671–83. doi: 10.1016/j.trecan.2018.08.003
31. Dunlop CR, Wallez Y, Johnson TI, de Quirós Fernández SB, Durant ST, Cadogan EB, et al. Complete Loss of Atm Function Augments Replication Catastrophe Induced by Atr Inhibition and Gemcitabine in Pancreatic Cancer Models. *Br J Cancer* (2020) 123(9):1424–36. doi: 10.1038/s41416-020-1016-2
32. Lloyd RL, Wijnhoven PW, Ramos-Montoya A, Wilson Z, Illuzzi G, Falenta K, et al. Combined Parp and Atr Inhibition Potentiates Genome Instability and Cell Death in Atm-Deficient Cancer Cells. *Oncogene* (2020), 1–15. doi: 10.1038/s41388-020-1328-y
33. Fok JH, Ramos-Montoya A, Vazquez-Chantada M, Wijnhoven PW, Follia V, James N, et al. Azd7648 Is a Potent and Selective DNA-Pk Inhibitor That Enhances Radiation, Chemotherapy and Olaparib Activity. *Nat Commun* (2019) 10(1):1–15. doi: 10.1038/s41467-019-12836-9
34. Laroche-Clary A, Chaire V, Verbeke S, Algéo M-P, Malykh A, Le Loarer F, et al. Atr Inhibition Broadly Sensitizes Soft-Tissue Sarcoma Cells to Chemotherapy Independent of Alternative Lengthening Telomere (Alt) Status. *Sci Rep* (2020) 10(1):7488. doi: 10.1038/s41598-020-63294-z
35. Pilié PG, Gay CM, Byers LA, O'Connor MJ, Yap TA. Parp Inhibitors: Extending Benefit Beyond Brca-Mutant Cancers. *Clin Cancer Res* (2019) 25 (13):3759–71. doi: 10.1158/1078-0432.CCR-18-0968
36. Krajewska M, Fehrmann R, Schoonen P, Labib S, De Vries E, Franke L, et al. Atr Inhibition Preferentially Targets Homologous Recombination-Deficient Tumor Cells. *Oncogene* (2015) 34(26):3474–81. doi: 10.1038/onc.2014.276
37. Reaper PM, Griffiths MR, Long JM, Charrier J-D, MacCormick S, Charlton PA, et al. Selective Killing of Atm-Or P53-Deficient Cancer Cells Through Inhibition of Atr. *Nat Chem Biol* (2011) 7(7):428–30. doi: 10.1038/nchembio.573
38. Deng S, Hu Q, Zhang H, Yang F, Peng C, Huang C. Hdac3 Inhibition Upregulates Pd-L1 Expression in B-Cell Lymphomas and Augments the Efficacy of Anti–Pd-L1 Therapy. *Mol Cancer Ther* (2019) 18(5):900–8. doi: 10.1158/1535-7163.MCT-18-1068
39. Garcia-Diaz A, Shin DS, Moreno BH, Saco J, Escuin-Ordinas H, Rodriguez GA, et al. Interferon Receptor Signaling Pathways Regulating Pd-L1 and Pd-L2 Expression. *Cell Rep* (2017) 19(6):1189–201. doi: 10.1016/j.celrep.2017.04.031

Conflict of Interest: Authors PG, LX, CZ, WL, ZJ, AL, TL, LL, MD, WY, and RT were employed by Jiangsu Simcere Pharmaceutical Co., Ltd.

The remaining author declares that the research was conducted in the absence of any commercial or financial relationships that could be construed as a potential conflict of interest.

Publisher's Note: All claims expressed in this article are solely those of the authors and do not necessarily represent those of their affiliated organizations, or those of the publisher, the editors and the reviewers. Any product that may be evaluated in this article, or claim that may be made by its manufacturer, is not guaranteed or endorsed by the publisher.

Advantages of publishing in Frontiers

OPEN ACCESS
Articles are free to read for greatest visibility and readership

FAST PUBLICATION
Around 90 days from submission to decision

HIGH QUALITY PEER-REVIEW
Rigorous, collaborative, and constructive peer-review

TRANSPARENT PEER-REVIEW
Editors and reviewers acknowledged by name on published articles

Frontiers
Avenue du Tribunal-Fédéral 34
1005 Lausanne | Switzerland

Visit us: www.frontiersin.org
Contact us: frontiersin.org/about/contact

REPRODUCIBILITY OF RESEARCH
Support open data and methods to enhance research reproducibility

DIGITAL PUBLISHING
Articles designed for optimal readership across devices

FOLLOW US
@frontiersin

IMPACT METRICS
Advanced article metrics track visibility across digital media

EXTENSIVE PROMOTION
Marketing and promotion of impactful research

LOOP RESEARCH NETWORK
Our network increases your article's readership